

AFFDL-TR-71-62

VOLUME V

AD736824

Volume V. Wind Tunnel Test of a Powered Tilt-Rotor Performance Model

John P. Magee

Robert B. Taylor

Frank J. McHugh

Nelson Miller

Leon N. DeLarm

The Boeing Company, Vertol Division

Philadelphia, Pennsylvania

TECHNICAL REPORT AFFDL-TR-71-62, VOLUME V

October 1971

APPROVED FOR PUBLIC RELEASE

DISTRIBUTION UNLIMITED

Reproduced by
NATIONAL TECHNICAL
INFORMATION SERVICE
Springfield, Va 22151

Air Force Flight Dynamics Laboratory

Aeronautical Systems Division

Air Force Systems Command

Wright-Patterson Air Force Base, Ohio

**Best
Available
Copy**

NOTICE

When Government drawings, specifications, or other data are used for any purpose other than in connection with a definitely related Government procurement operation, the United States Government thereby incurs no responsibility nor any obligation whatsoever; and the fact that the government may have formulated, furnished, or in any way supplied the said drawings, specifications, or other data, is not to be regarded by implication or otherwise as in any manner licensing the holder or any other person or corporation, or conveying any rights or permission to manufacture, use, or sell any patented invention that may in any way be related thereto.

Copies of this report should not be returned unless return is required by security considerations, contractual obligations, or notice on a specific document.

UNCLASSIFIED

Security Classification

DOCUMENT CONTROL DATA - R&D

(Security classification of title, body of abstract and indexing annotation must be entered when the overall report is classified)

1 ORIGINATING ACTIVITY (Corporate author) The Boeing Company, Vertol Division Boeing Center, P.O. Box 16858 Philadelphia, Pa. 19142		2a REPORT SECURITY CLASSIFICATION Unclassified	
		2b GROUP	
3. REPORT TITLE VOLUME V. WIND TUNNEL TEST OF A POWERED TILT-ROTOR PERFORMANCE MODEL			
4 DESCRIPTIVE NOTES (Type of report and inclusive dates) Final Report, June to December 1970			
5 AUTHOR(S) (Last name, first name, initial) John P. Magee Nelson Miller Robert B. Taylor Leon N. Delarm Frank J. McHugh			
6. REPORT DATE October 1971		7a. TOTAL NO. OF PAGES 504	7b NO OF REFS 12
8a. CONTRACT OR GRANT NO. F33615-69-C-1577		9a. ORIGINATOR'S REPORT NUMBER(S) D213-10000-5	
b. PROJECT NO.			
c.		9b. OTHER REPORT NO(S) (Any other numbers that may be assigned this report)	
d.		AFFDL-TR-71-62, Volume V	
10. AVAILABILITY/LIMITATION NOTICES Approved for Public Release - Distribution Unlimited			
11 SUPPLEMENTARY NOTES		12. SPONSORING MILITARY ACTIVITY Air Force Flight Dynamics Laboratory Air Force Systems Command Wright-Patterson Air Force Base, Ohio	
13 ABSTRACT -Wind tunnel test data obtained with a full span, two prop, tilt rotor, powered model in the Boeing V/STOL wind tunnel are reported. Data were taken in hover, transition and cruise flight conditions and include performance, stability and control and blade loads information. The effects of the rotors, tail surfaces and airframe on the performance and stability are isolated as are the effects of the airframe on the rotors. The airframe and the rotors are not dynamically representative of the full scale aircraft but the rotors are flexible out of plane having a flap-wise natural frequency between 1.4 to 1.66 per rev and are still in-plane with a natural frequency between 1.7 and 2.0 per rev. Predicted rotor frequencies were verified, both static and rotating, and since they influence rotor response characteristics, correlation for stability and blade load data is included.			

DD FORM 1473
1 JAN 64

UNCLASSIFIED

Security Classification

UNCLASSIFIED

Security Classification

14 KEY WORDS	LINK A		LINK B		LINK C	
	ROLE	WT	ROLE	WT	ROLE	WT
Stowed Rotor Tilt Rotor Hover Transition Cruise Performance Stability Control Rotor Loads						

INSTRUCTIONS

1. **ORIGINATING ACTIVITY:** Enter the name and address of the contractor, subcontractor, grantee, Department of Defense activity or other organization (*corporate author*) issuing the report.

2a. **REPORT SECURITY CLASSIFICATION:** Enter the overall security classification of the report. Indicate whether "Restricted Data" is included. Marking is to be in accordance with appropriate security regulations.

2b. **GROUP:** Automatic downgrading is specified in DoD Directive 5200.10 and Armed Forces Industrial Manual. Enter the group number. Also, when applicable, show that optional markings have been used for Group 3 and Group 4 as authorized.

3. **REPORT TITLE:** Enter the complete report title in all capital letters. Titles in all cases should be unclassified. If a meaningful title cannot be selected without classification, show title classification in all capitals in parenthesis immediately following the title.

4. **DESCRIPTIVE NOTES:** If appropriate, enter the type of report, e.g., interim, progress, summary, annual, or final. Give the inclusive dates when a specific reporting period is covered.

5. **AUTHOR(S):** Enter the name(s) of author(s) as shown on or in the report. Enter last name, first name, middle initial. If military, show rank and branch of service. The name of the principal author is an absolute minimum requirement.

6. **REPORT DATE:** Enter the date of the report as day, month, year, or month, year. If more than one date appears on the report, use date of publication.

7a. **TOTAL NUMBER OF PAGES:** The total page count should follow normal pagination procedures, i.e., enter the number of pages containing information.

7b. **NUMBER OF REFERENCES:** Enter the total number of references cited in the report.

8a. **CONTRACT OR GRANT NUMBER:** If appropriate, enter the applicable number of the contract or grant under which the report was written.

8b, 8c, & 8d. **PROJECT NUMBER:** Enter the appropriate military department identification, such as project number, subproject number, system numbers, task number, etc.

9a. **ORIGINATOR'S REPORT NUMBER(S):** Enter the official report number by which the document will be identified and controlled by the originating activity. This number must be unique to this report.

9b. **OTHER REPORT NUMBER(S):** If the report has been assigned any other report numbers (*either by the originator or by the sponsor*), also enter this number(s).

10. **AVAILABILITY/LIMITATION NOTICES:** Enter any limitations on further dissemination of the report, other than those

imposed by security classification, using standard statements such as:

- (1) "Qualified requesters may obtain copies of this report from DDC."
- (2) "Foreign announcement and dissemination of this report by DDC is not authorized."
- (3) "U. S. Government agencies may obtain copies of this report directly from DDC. Other qualified DDC users shall request through _____."
- (4) "U. S. military agencies may obtain copies of this report directly from DDC. Other qualified users shall request through _____."
- (5) "All distribution of this report is controlled. Qualified DDC users shall request through _____."

If the report has been furnished to the Office of Technical Services, Department of Commerce, for sale to the public, indicate this fact and enter the price, if known.

11. **SUPPLEMENTARY NOTES:** Use for additional explanatory notes.

12. **SPONSORING MILITARY ACTIVITY:** Enter the name of the departmental project office or laboratory sponsoring (paying for) the research and development. Include address.

13. **ABSTRACT:** Enter an abstract giving a brief and factual summary of the document indicative of the report, even though it may also appear elsewhere in the body of the technical report. If additional space is required, a continuation sheet shall be attached.

It is highly desirable that the abstract of classified reports be unclassified. Each paragraph of the abstract shall end with an indication of the military security classification of the information in the paragraph, represented as (TS), (S), (C), or (U).

There is no limitation on the length of the abstract. However, the suggested length is from 150 to 225 words.

14. **KEY WORDS:** Key words are technically meaningful terms or short phrases that characterize a report and may be used as index entries for cataloging the report. Key words must be selected so that no security classification is required. Identifiers, such as equipment model designation, trade name, military project code name, geographic location, may be used as key words but will be followed by an indication of technical context. The assignment of links, rules, and weights is optional.

AFFDL-TR-71-62

VOLUME V

Volume V. Wind Tunnel Test of a Powered Tilt-Rotor Performance Model

John P. Magee

Robert B. Taylor

Frank J. McHugh

Nelson Miller

Leon N. DeLarm

The Boeing Company, Vertol Division

Philadelphia, Pennsylvania

TECHNICAL REPORT AFFDL-TR-71-62, VOLUME V

October 1971

APPROVED FOR PUBLIC RELEASE

DISTRIBUTION UNLIMITED

Air Force Flight Dynamics Laboratory

Aeronautical Systems Division

Air Force Systems Command

Wright-Patterson Air Force Base, Ohio

FOREWORD

This report was prepared by the Boeing Company, Vertol Division, Philadelphia, Pennsylvania, for the Air Force Flight Dynamics Laboratory, Wright-Patterson Air Force Base, Ohio, under Phase II of Contract F33615-69-C-1577. The contract objective is to develop design criteria and aerodynamic prediction techniques for the folding tilt rotor concept through a program of model testing and analysis.


The contract was administered by the Air Force Flight Dynamics Laboratory with Mr. Daniel E. Fraga (FV) as Project Engineer.

This report covers the period from June to December 1970.

The reports published under this contract for Design Studies and Model Tests of the Stowed Tilt Rotor Concept are:

Volume I	Parametric Design Studies
Volume II	Component Design Studies
Volume III	Performance Data for Parametric Study
Volume IV	Wind Tunnel Test of the Conversion Process of a Folding Tilt Rotor Aircraft Using a Semi-Span Unpowered Model
Volume V	Wind Tunnel Test of a Powered Tilt Rotor Performance Model
Volume VI	Wind Tunnel Test of a Powered Tilt Rotor Dynamic Model on a Simulated Free Flight Suspension System
Volume VII	Wind Tunnel Test of the Dynamics and Aerodynamics of Rotor Spinup, Stopping and Folding on a Semi-Span Folding Tilt Rotor Model
Volume VIII	Summary of Structural Design Criteria and Aerodynamic Prediction Techniques
Volume IX	Value Engineering Report

This report has been reviewed and is approved.


Ernest J. Cross, Jr.
Lt. Colonel, USAF
Chief, Prototype Division

ABSTRACT

Wind tunnel test data obtained with a full span, two prop, tilt rotor, powered model in the Boeing V/STOL wind tunnel are reported. Data were taken in hover, transition and cruise flight conditions and include performance, stability and control and blade loads information. The effects of the rotors, tail surfaces and airframe on the performance and stability are isolated as are the effects of the airframe on the rotors.

The airframe and the rotors are not dynamically representative of the full scale aircraft but the rotors are flexible out of plane having a flapwise natural frequency between 1.4 to 1.66 per rev and are stiff in-plane with a natural frequency between 1.7 and 2.0 per rev. Predicted rotor frequencies were verified, both static and rotating, and since they influence rotor response characteristics, correlation for stability and blade load data is included.

SUMMARY

A wind tunnel test (BVWT 062) of a 1/10 scale full span, tilt rotor, powered performance model, rotor diameter 5.5' and wing span 6.78' rotor center to center was conducted in the Boeing V/STOL tunnel. This test produced performance, stability and control, and rotor loads data in hover, transition and cruise flight to provide verification of aerodynamic prediction techniques and establish structural design criteria.

The report is divided into performance, stability and control and rotor loads sections and a brief summary of each section follows.

Performance

Total aircraft lift data in hover with leading edge umbrella flaps shows that a download of 5 percent of the aircraft thrust occurs out-of-ground effect for this configuration and is reduced as ground height is reduced.

Airframe lift data in the STOL mode IGE shows that the lift due to the ground cushion decreases with speed and vanishes when the downwash tucks under the aircraft.

Performance data were obtained in transition and cruise flight regimes for correlation with theory.

Stability and Control

Control moment data in hover show that adequate pitch and yaw control can be obtained with cyclic pitch control. The effects of ground proximity on control moments were found to be small for tests with one rotor. Tests with both rotors were prevented by motor failure. Twin rotors could give different results.

Rotor stability derivatives measured in transition show that the rotor contribution is large and destabilizing, and that wing and rotor stall now define the limits of the transition envelope.

Roll and yaw control in transition can be provided by the use of differential thrust and differential cyclic pitch. The required mixing for pure control based on test data and crossplots from test data are presented.

A comparison of the predicted isolated rotor pitching moment derivative and test data crossplotted to zero wing lift in cruise show good agreement and indicates a 50-percent increase in hub moment due to wing-rotor interference. The total model pitching moment derivative is unstable and this is predicted by the isolated rotor theory corrected for wing interference. The same methodology was used to compute the full-scale aircraft derivative which is shown to be stable because of the differences in model and full-scale rotor dynamics.

Rotor Loads

Rotor loads data were obtained in the hover, transition and cruise modes. The test objectives included the determination of rotating blade frequencies in the hover mode and the effect of various tilt rotor flight conditions on blade bending moments and rotor loads.

A coupled flap-lag frequency analysis was used to predict the rotating blade frequencies for the first flap and first lag bending modes and an uncoupled flap-lag-torsion frequency analysis was used to predict the first torsional frequency. Baffle test data substantiated the analysis.

Past prop-rotor and helicopter blade stall flutter inception data were used to predict the inception of stall flutter in hover at a collective pitch of 14 degrees. No stall flutter was found.

The effect of angle of attack on blade flap bending in cruise was predicted by the coupled flap-pitch uncoupled lag analysis and correlation of the test data with prediction is good. The hub moment due to angle of attack in cruise and the effect of wing flap deflection on blade flap bending in cruise were also predicted and the correlation with test is good.

Dynamics

Pre-test predictions of the modal frequencies and dampings were made prior to the 1/10-scale performance model wind tunnel test to insure structural integrity of the model during the test. The analyses used accounted for the dynamic interactions produced by rotor airframe coupling effects. During the test, baffles were used to determine blade frequencies at discrete rotor speeds. The measured blade flap frequencies are in excellent agreement with the predictions and the blade lag frequencies are slightly higher than predicted.

Step aircraft angles of attack were input into the model in cruise, transition and hover flight modes to determine the aircraft's susceptibility in whirl flutter modes to forcing functions of this type. Results of the test show the aircraft to be insensitive to this type of forcing function.

TABLE OF CONTENTS

	<u>PAGE</u>
1.0 INTRODUCTION	1
2.0 OBJECTIVES	2
3.0 TEST INSTALLATION	5
3.1 MODEL DESCRIPTION.	5
3.2 TUNNEL INSTALLATION	9
3.3 DATA REDUCTION.	10
4.0 PERFORMANCE.	21
4.1 HOVER PERFORMANCE.	27
4.1.1 Download & Flow Recirculation	27
4.1.2 Rotor Performance	28
4.1.3 Aircraft Performance	29
4.2 STOL PERFORMANCE.	40
4.2.1 Rotor Airframe Interactions	40
4.2.2 Rotor Performance	41
4.2.3 Aircraft Performance	41
4.3 TRANSITION PERFORMANCE	55
4.3.1 Rotor Airframe Interactions	55
4.3.2 Rotor Performance	56
4.3.3 Aircraft Performance	57

TABLE OF CONTENTS

	<u>PAGE</u>
4.4 CRUISE PERFORMANCE	71
4.4.1 Rotor Performance	71
4.4.2 Aircraft Performance	71
4.5 CONCLUSIONS	83
5.0 STABILITY AND CONTROL	84
5.1 HOVER STABILITY AND CONTROL	91
5.1.1 Rotor Stability Derivatives	91
5.1.2 Aircraft Stability Derivatives	91
5.1.3 Cyclic Pitch Control	91
5.1.4 Control Phasing	92
5.1.5 Ground Effect and Skittishness	93
5.2 STOL STABILITY	118
5.2.1 Rotor Stability Derivatives	118
5.2.2 Aircraft Stability Derivatives	119
5.3 TRANSITION STABILITY AND CONTROL	137
5.3.1 Rotor Stability Derivatives	137
5.3.2 Aircraft Stability Derivatives	142
5.3.3 Control Mixing	144
5.3.4 Attitude Effects on Control	145
5.4 CRUISE STABILITY	190
5.4.1 Rotor Stability Derivatives	190
5.4.2 Aircraft Stability Derivatives	197
5.5 CONCLUSIONS	258
6.0 ROTOR LOADS	259
6.1 BLADE FREQUENCY SUBSTANTIATION	267
6.1.1 First Flap Mode	267
6.1.2 First Lag Mode	269
6.1.3 First Torsional Mode	269

TABLE OF CONTENTS

	<u>PAGE</u>
6.2 HOVER BLADE LOADS	302
6.2.1 Effect of Cyclic Pitch	302
6.2.2 Stall Flutter	303
6.2.3 Rotor Height	304
6.2.4 Rotor-Rotor Interference	304
6.2.5 Low Forward Speed	305
6.3 HOVER HUB MOMENTS	339
6.3.1 Effect of Cyclic Pitch	339
6.4 TRANSITION BLADE LOADS	342
6.4.1 Attitude Effects	342
6.4.2 Effect of Cyclic Pitch	342
6.4.3 Stall Flutter	343
6.5 TRANSITION HUB MOMENTS	356
6.5.1 Attitude Effects	356
6.5.2 Effect of Cyclic Pitch	356
6.6 CRUISE BLADE LOADS	359
6.6.1 Attitude Effects	359
6.6.2 Effect of Wing Flap Deflection	360
6.7 CRUISE HUB MOMENTS	391
6.7.1 Attitude Effects	391
6.8 CONCLUSIONS	393
7.0 DYNAMICS	394
7.1 FREQUENCIES AND MODAL DAMPING	394
7.2 RESPONSE TO CHANGE IN ANGLE OF ATTACK	394
7.3 INFLUENCE OF FUSELAGE ANGLE OF ATTACK	395
7.4 CONCLUSIONS	396
8.0 CONCLUSIONS	406
9.0 RECOMMENDATIONS	408
10.0 REFERENCES	409

TABLE OF CONTENTS

	<u>PAGE</u>
APPENDICES	
A. ROTOR BLADE PHYSICAL PROPERTIES	410
B. STATIC DISTURBANCE TESTS	431
C. DEFLECTION TESTS	440
D. TEST RUN LOG	448

LIST OF ILLUSTRATIONS

<u>FIGURE NO.</u>	<u>TITLE</u>	<u>PAGE</u>
3-1	MODEL 160 1/10 SCALE POWERED TILT ROTOR WIND TUNNEL MODEL -- CRUISE MODE	12
3-2	MODEL 160 WIND TUNNEL MODEL - SIDE VIEW	13
3-3	MODEL 160 WIND TUNNEL MODEL - TOP VIEW	14
3-4	MODEL 160 WIND TUNNEL MODEL - FRONT VIEW	15
3-5	MODEL 160 WIND TUNNEL MODEL - TUFT GRID HOVER FLOW VISUALIZATION SET-UP	16
3-6	SKETCH OF ARRANGEMENT OF PIE-SHAPED BAFFLE	17
3-7	SKETCH OF MODEL INSTALLATION IN TEST SECTION	18
3-8	MODEL REFERENCE CENTER GEOMETRY	19
3-9	MODEL 160 WIND TUNNEL MODEL FORCE AND MOMENT SIGN CONVENTION	20
4-1	HOVER DOWNLOAD FROM FULL SCALE AND MODEL TESTS	22
4-2	EFFECT OF UMBRELLA AND FLAP ANGLE ON TOTAL AIRCRAFT HOVER PERFORMANCE	23
4-3	AIRFRAME LIFT VARIATION DURING IN-GROUND EFFECT TAKEOFF AT $h/D=0.39$ (ZERO WHEEL HEIGHT)	24
4-4	AIRCRAFT LIFT/PROPULSIVE FORCE VARIATION DURING TRANSITION AND CRUISE	25
4-5	AIRCRAFT LIFT/ROTOR POWER VARIATION DURING TRANSITION AND CRUISE	26
4-6	EFFECT OF UMBRELLA FLAP ANGLE ON AIRCRAFT HOVER DOWNLOAD/THRUST RATIO	30
4-7	EFFECT OF FLAP DEFLECTION ON AIRCRAFT HOVER DOWNLOAD/THRUST RATIO	31
4-8	EFFECT OF GROUND HEIGHT ON AIRCRAFT HOVER DOWNLOAD/THRUST RATIO	32
4-9	EFFECT OF FUSELAGE ANGLE OF ATTACK ON AIRCRAFT HOVER DOWNLOAD/THRUST RATIO	33

LIST OF ILLUSTRATIONS

<u>FIGURE NO.</u>	<u>TITLE</u>	<u>PAGE</u>
4-10	BLADE TIP VORTEX TRAJECTORIES AT h/D=0.39	34
4-11	BLADE TIP VORTEX TRAJECTORIES AT h/D=0.65	35
4-12	ISOLATED ROTOR HOVER PERFORMANCE (OUT OF GROUND EFFECT)	36
4-13	EFFECT OF UMBRELLA AND FLAP ANGLE ON ROTOR HOVER PERFORMANCE	37
4-14	ROTOR/ROTOR INTERFERENCE EFFECTS ON HOVER PERFORMANCE	38
4-15	EFFECT OF UMBRELLA AND FLAP ANGLE ON TOTAL AIRCRAFT HOVER PERFORMANCE	39
4-16	AIRFRAME LIFT VARIATION DURING IN-GROUND EFFECT TAKEOFF AT h/D=0.39	42
4-17	AIRCRAFT SLIPSTREAM THRUST COEFFICIENT VARIATION DURING IN-GROUND EFFECT TAKEOFF AT h/D=0.39	43
4-18	ROTOR THRUST VARIATION DURING IN-GROUND EFFECT TAKEOFF AT h/D=0.39	44
4-19	ROTOR POWER VARIATION DURING IN-GROUND EFFECT TAKEOFF AT h/D=0.39	45
4-20	ROTOR THRUST VARIATION DURING STOL CLIMB-OUT AT $V/V_T = 0.206$	46
4-21	ROTOR POWER VARIATION DURING STOL CLIMB-OUT AT $V/V_T = 0.206$	47
4-22	AIRCRAFT LIFT VARIATION DURING IN-GROUND EFFECT TAKEOFF AT h/D=0.39	48
4-23	AIRCRAFT PROPULSIVE FORCE VARIATION DURING IN-GROUND EFFECT TAKEOFF AT h/D=0.39	49
4-24	AIRCRAFT PROPULSIVE FORCES/LIFT VARIATION FOR IN-GROUND EFFECT TAKEOFF AT h/D=0.39	50

LIST OF ILLUSTRATIONS

<u>FIGURE NO.</u>	<u>TITLE</u>	<u>PAGE</u>
4-25	AIRCRAFT ROTOR POWER VARIATION DURING IN- GROUND EFFECT TAKEOFF AT $h/D=0.39$	51
4-26	AIRCRAFT LIFT VARIATION DURING STOL CLIMB OUT AT $V/V_T = 0.206$ $C_{TS} = 0.356$	52
4-27	AIRCRAFT PROPULSIVE FORCE VARIATION DURING STOL CLIMB OUT AT $V/V_T = 0.206$ $C_{TS} = 0.356$	53
4-28	AIRCRAFT ROTOR POWER VARIATION DURING STOL CLIMB OUT AT $V/V_T = 0.206$ $C_{TS} = 0.356$	54
4-29	CONTRIBUTION OF PROP/ROTOR AND HORIZONTAL TAIL TO AIRCRAFT LIFT AT $V/V_T = 0.206$ WITH $i_N = 70^\circ$	58
4-30	CONTRIBUTION OF PROP/ROTOR AND HORIZONTAL TAIL TO AIRCRAFT LIFT AT $V/V_T = 0.260$ WITH $i_N = 45^\circ$	59
4-31	ROTOR-AIRFRAME INTERACTION ON AIRCRAFT SIDE FORCE AT $V/V_T = 0.206$ WITH $i_N = 70^\circ$	60
4-32	ROTOR-AIRFRAME INTERACTION ON AIRCRAFT SIDE FORCE AT $V/V_T = 0.260$ WITH $i_N = 45^\circ$	61
4-33	ROTOR THRUST/ANGLE OF ATTACK VARIATION DURING TRANSITION	62
4-34	ROTOR THRUST/ANGLE OF ATTACK VARIATION DURING TRANSITION	63
4-35	ROTOR THRUST/POWER VARIATION DURING TRANSITION	64
4-36	ROTOR THRUST/POWER VARIATION DURING TRANSITION	65
4-37	ROTOR POWER/ANGLE OF ATTACK VARIATION DURING TRANSITION	66
4-38	ROTOR POWER/ANGLE OF ATTACK VARIATION DURING TRANSITION	67

LIST OF ILLUSTRATIONS

<u>FIGURE NO.</u>	<u>TITLE</u>	<u>PAGE</u>
4-39	AIRCRAFT LIFT/ANGLE OF ATTACK VARIATION DURING TRANSITION	68
4-40	AIRCRAFT LIFT/PROPULSIVE FORCE VARIATION DURING TRANSITION	69
4-41	AIRCRAFT LIFT/POWER REQUIRED VARIATION DURING TRANSITION	70
4-42	ROTOR THRUST/ANGLE OF ATTACK VARIATION IN CRUISE	73
4-43	ROTOR THRUST/ANGLE OF ATTACK VARIATION IN CRUISE	74
4-44	ROTOR POWER/ANGLE OF ATTACK VARIATION IN CRUISE	75
4-45	ROTOR POWER/ANGLE OF ATTACK VARIATION IN CRUISE	76
4-46	TOTAL AIRCRAFT LIFT/ANGLE OF ATTACK VARIATION IN CRUISE $i_N = 0$	77
4-47	TOTAL AIRCRAFT LIFT/PROPULSIVE FORCE VARIATION IN CRUISE $i_N = 0$	78
4-48	TOTAL AIRCRAFT LIFT/ROTOR POWER VARIATION IN CRUISE $i_N = 0^\circ$	79
4-49	AIRCRAFT LIFT/YAW ANGLE VARIATION AT $V/V_T = 0.382$	80
4-50	AIRCRAFT PROPULSIVE FORCE/YAW ANGLE VARIATION AT $V/V_T = 0.382$ $i_N = 0^\circ$	81
4-51	AIRCRAFT ROTOR POWER/YAW ANGLE VARIATION AT $V/V_T = 0.382$ $i_N = 30^\circ$	82
5-1	YAW CONTROL HOVER, OGE	85
5-2	ROTOR PITCHING MOMENT/ANGLE OF ATTACK VARIATION AT $V/V_T = 0.260$ WITH $i_N = 45^\circ$	86
5-3	CONTRIBUTION OF PROP/ROTORS AND HORIZONTAL TAIL TO AIRCRAFT PITCHING MOMENT AT $V/V_T = 0.26$ WITH $i_N = 45^\circ$	87

LIST OF ILLUSTRATIONS

<u>FIGURE NO.</u>	<u>TITLE</u>	<u>PAGE</u>
5-4	CONTROL MIXING DURING TRANSITION	88
5-5	INFLUENCE OF WING LIFT ON ROTOR PITCHING MOMENT AT $V/V_T=0.386$	89
5-6	CONTRIBUTION OF PROP/ROTORS AND HORIZONTAL TAIL TO AIRCRAFT PITCHING MOMENT AT $V/V_T = 0.386$	90
5-7	EFFECT OF ANGLE OF ATTACK ON ROTOR PITCHING MOMENT IN HOVER	96
5-8	EFFECT OF ANGLE OF ATTACK ON ROTOR NORMAL FORCE IN HOVER	97
5-9	EFFECT OF ANGLE OF ATTACK ON ROTOR NORMAL FORCE AND PITCHING MOMENT IN THE NEAR HOVER MODE AT $q=4$ psf	98
5-10	EFFECT OF ANGLE OF ATTACK ON AIRCRAFT LIFT IN THE NEAR HOVER MODE AT $q=4$ psf	99
5-11	EFFECT OF ANGLE OF ATTACK ON AIRCRAFT PITCHING MOMENT IN THE NEAR HOVER MODE AT $q=4$ psf	100
5-12	INPUT CYCLIC PITCH PHASE ANGLE GEOMETRY	101
5-13	EFFECT OF CYCLIC PITCH ON ROTOR FORCES	102
5-14	EFFECT OF CYCLIC PITCH ON ROTOR MOMENTS	103
5-15	EFFECT OF CYCLIC PITCH ON THRUST AND POWER	104
5-16	RESULTANT IN-PLANE FORCE AND HUB MOMENT DUE TO CYCLIC PITCH	105
5-17	HOVER CYCLIC PITCH PHASE ANGLE	106
5-18	PITCH CONTROL OVER, OGE	107
5-19	YAW CONTROL HOVER, OGE	108
5-20	EFFECT OF GROUND HEIGHT ON ALTERNATING AIRCRAFT MOMENTS IN HOVER	109

LIST OF ILLUSTRATIONS

<u>FIGURE NO.</u>	<u>TITLE</u>	<u>PAGE</u>
5-21	MODEL ALTERNATING MOMENTS IN TERMS OF DESIGN CONTROL POWER	110
5-22	EFFECT OF RPM DIFFERENCE (BEATING) ON AIRCRAFT LONG PERIOD FORCES AND MOMENTS . . .	111
5-23	EXAMPLE OF FUSELAGE BALANCE OSCILLOGRAPH TRACES	112
5-24	EFFECT OF ROTOR RPM ON ALTERNATING MODEL MOMENTS IN HOVER	113
5-25	ALTERNATING MODEL MOMENTS OBTAINED WITH ROTOR SHAFT IN LINE WITH CHORD	114
5-26	EFFECT OF TIME ON ALTERNATING ROLL MOMENT . . .	115
5-27	EFFECT OF TIME ON ALTERNATING YAW MOMENT . . .	116
5-28	HOVER TRIM MOMENTS PRODUCED BY ANGLE OF ATTACK WITH ROLL ANGLE VARIATION IN GROUND EFFECT . .	117
5-29	ROTOR PITCHING MOMENT VARIATION FOR IN-GROUND EFFECT TAKEOFF AT $h/D=0.39$ $i_N=70^\circ$	120
5-30	ROTOR NORMAL FORCE VARIATION FOR IN-GROUND EFFECT TAKEOFF AT $h/D=0.39$ $i_N=70^\circ$	121
5-31	ROTOR YAWING MOMENT VARIATION FOR IN-GROUND EFFECT TAKEOFF AT $h/D=0.39$ $i_N=70^\circ$	122
5-32	ROTOR SIDE FORCE VARIATION FOR IN-GROUND EFFECT TAKEOFF AT $h/D=0.39$ $i_N=70^\circ$	123
5-33	ROTOR YAWING MOMENT/YAW ANGLE VARIATION IN GROUND EFFECT AT $h/D=0.39$ AND $V/V_{T1}=0.206$. . .	124
5-34	ROTOR YAWING MOMENT/YAW ANGLE VARIATION IN GROUND EFFECT AT $h/D=0.39$ AND $V/V_{T1}=0.206$. . .	125
5-35	ROTOR SIDE FORCE/YAW ANGLE VARIATION IN GROUND EFFECT AT $h/D=0.39$ AND $V/V_{T1}=0.206$. . .	126

LIST OF ILLUSTRATIONS

<u>FIGURE NO.</u>	<u>TITLE</u>	<u>PAGE</u>
5-36	ROTOR PITCHING MOMENT/YAW ANGLE VARIATION IN GROUND EFFECT AT $h/D=0.39$ AND $V/V_T=0.206$. .	127
5-37	ROTOR NORMAL FORCE/YAW ANGLE VARIATION IN GROUND EFFECT AT $h/D=0.39$ AND $V/V_T=0.206$. . .	128
5-38	ROTOR PITCHING MOMENT VARIATION DURING STOL CLIMB OUT $V/V_T=0.206$	129
5-39	ROTOR NORMAL FORCE VARIATION DURING STOL CLIMB OUT $V/V_T=0.206$	130
5-40	ROTOR YAWING MOMENT VARIATION DURING STOL CLIMB OUT AT $V/V_T=0.206$	131
5-41	ROTOR SIDE FORCE VARIATION DURING STOL CLIMB OUT $V/V_T=0.206$	132
5-42	AIRCRAFT PITCHING MOMENT VARIATION FOR IN GROUND EFFECT TAKEOFF AT $h/D=0.39$	133
5-43	AIRCRAFT SIDE FORCE/YAW ANGLE VARIATION IN GROUND EFFECT AT $h/D=0.39$ AND $V/V_T=0.206$. . .	134
5-44	AIRCRAFT YAWING MOMENT/YAW ANGLE VARIATION IN GROUND EFFECT AT $h/D=0.39$ AND $V/V_T=0.206$. .	135
5-45	AIRCRAFT PITCHING MOMENT VARIATION DURING STOL CLIMB OUT $V/V_T=0.206$	136
5-46	ROTOR PITCHING MOMENT/ANGLE OF ATTACK VARIATION AT $V/V_T=0.206$ AND 0.234 WITH $i_N=70^\circ$	146
5-47	ROTOR PITCHING MOMENT/ANGLE OF ATTACK VARIATION AT $V/V_T=0.206$ AND 0.236 WITH $i_N=70^\circ$	147
5-48	ROTOR NORMAL FORCE/ANGLE OF ATTACK VARIATION VARIATION AT $V/V_T=0.206$ AND 0.234 WITH $i_N=70^\circ$	148
5-49	ROTOR NORMAL FORCE/ANGLE OF ATTACK VARIATION AT $V/V_T=0.206$ AND 0.234 WITH $i_N=70^\circ$	149

LIST OF ILLUSTRATIONS

<u>FIGURE NO.</u>	<u>TITLE</u>	<u>PAGE</u>
5-50	ROTOR YAWING MOMENT/ANGLE OF ATTACK VARIATION AT $V/V_T=0.206$ AND 0.234 WITH $i_N=70^\circ$	150
5-51	ROTOR YAWING MOMENT/ANGLE OF ATTACK VARIATION AT $V/V_T=0.206$ AND 0.234 WITH $i_N=70^\circ$	151
5-52	ROTOR SIDE FORCE/ANGLE OF ATTACK VARIATION AT $V/V_T=0.206$ AND 0.234 WITH $i_N=70^\circ$	152
5-53	ROTOR SIDE FORCE/ANGLE OF ATTACK VARIATION AT $V/V_T=0.206$ AND 0.234 WITH $i_N=70^\circ$	153
5-54	ROTOR PITCHING MOMENT/ANGLE OF ATTACK VARIATION AT $V/V_T=0.260$ WITH $i_N=45^\circ$	154
5-55	ROTOR NORMAL FORCE/ANGLE OF ATTACK VARIATION AT $V/V_T=0.260$ WITH $i_N=45^\circ$	155
5-56	ROTOR YAWING MOMENT/ANGLE OF ATTACK VARIATION AT $V/V_T=0.260$ WITH $i_N=45^\circ$	156
5-57	ROTOR YAWING MOMENT/ANGLE OF ATTACK VARIATION AT $V/V_T=0.260$ WITH $i_N=45^\circ$	157
5-58	ROTOR SIDE FORCE/ANGLE OF ATTACK VARIATION AT $V/V_T=0.260$ WITH $i_N=45^\circ$	158
5-59	ROTOR YAWING MOMENT/YAW ANGLE VARIATION AT $V/V_T=0.206$ WITH $i_N=70^\circ$	159
5-60	ROTOR YAWING MOMENT/YAW ANGLE VARIATION AT $V/V_T=0.206$ WITH $i_N=70^\circ$	160
5-61	ROTOR SIDE FORCE/YAW ANGLE VARIATION AT $V/V_T=0.206$ WITH $i_N=70^\circ$	161
5-62	ROTOR PITCHING MOMENT/YAW ANGLE VARIATION AT $V/V_T=0.206$ WITH $i_N=70^\circ$	162
5-63	ROTOR NORMAL FORCE/YAW ANGLE VARIATION AT $V/V_T=0.206$ WITH $i_N=70^\circ$	163

LIST OF ILLUSTRATIONS

<u>FIGURE NO.</u>	<u>TITLE</u>	<u>PAGE</u>
5-64	ROTOR YAWING MOMENT/YAW ANGLE VARIATION AT $V/V_T=0.260$ WITH $i_N=45^\circ$	164
5-65	ROTOR YAWING MOMENT/YAW ANGLE VARIATION AT $V/V_T=0.260$ WITH $i_N=45^\circ$	165
5-66	ROTOR SIDE FORCE/YAW ANGLE VARIATION AT $V/V_T=0.260$ WITH $i_N=45^\circ$	166
5-67	ROTOR PITCHING MOMENT/YAW ANGLE VARIATION AT $V/V_T=0.260$ WITH $i_N=45^\circ$	167
5-68	ROTOR NORMAL FORCE/YAW ANGLE VARIATION AT $V/V_T=0.260$ WITH $i_N=45^\circ$	168
5-69	IMPACT OF GROUND EFFECT ON ROTOR YAWING MOMENT AT $V/V_T=0.206$ WITH $i_N=70^\circ$	169
5-70	IMPACT OF GROUND EFFECT ON ROTOR SIDE FORCE AT $V/V_T=0.206$ WITH $i_N=70^\circ$	170
5-71	IMPACT OF GROUND EFFECT ON ROTOR SIDE FORCES AT $V/V_T=0.206$ WITH $i_N=70^\circ$	171
5-72	IMPACT OF GROUND EFFECT ON ROTOR PITCHING MOMENT AT $V/V_T=0.206$ $i_N=70^\circ$	172
5-73	IMPACT OF GROUND EFFECT ON ROTOR NORMAL FORCE AT $V/V_T=0.206$ WITH $i_N=70^\circ$	173
5-74	CONTRIBUTION OF PROP/ROTOR AND HORIZONTAL TAIL TO AIRCRAFT PITCHING MOMENT AT $V/V_T=$ 0.206 WITH $i_N=70^\circ$	174
5-75	CONTRIBUTION OF PROP/ROTORS AND HORIZONTAL TAIL TO AIRCRAFT PITCHING MOMENT AT $V/V_T=$ 0.26 WITH $i_N=45^\circ$	175

LIST OF ILLUSTRATIONS

<u>FIGURE NO.</u>	<u>TITLE</u>	<u>PAGE</u>
5-76	CONTRIBUTION OF PROP/ROTOR AND VERTICAL TAIL TO AIRCRAFT SIDE FORCE AT $V/V_T=0.206$ WITH $i_N=70^\circ$	176
5-77	CONTRIBUTION OF PROP/ROTORS AND VERTICAL TAIL TO AIRCRAFT YAWING AND MOMENT AT $V/V_T=0.206$ WITH $i_N=70^\circ$	177
5-78	CONTRIBUTION OF PROP/ROTOR AND VERTICAL TAIL TO AIRCRAFT SIDE FORCE AT $V/V_T=0.260$ WITH $i_N=45^\circ$	178
5-79	CONTRIBUTION OF PROP/ROTORS AND VERTICAL TAIL TO AIRCRAFT YAWING MOMENT AT $V/V_T=0.26$ WITH $i_N=45^\circ$	179
5-80	CONTROL MISSING DURING TRANSITION	180
5-81	VARIATION OF CYCLIC PHASE ANGLE WITH ADVANCE RATIO	181
5-82	VARIATION OF ROTOR CONTROL FORCES WITH ANGLE OF ATTACK IN TRANSITION	182
5-83	VARIATION OF ROTOR CONTROL MOMENTS WITH ANGLE OF ATTACK IN TRANSITION	183
5-84	VARIATION OF CYCLIC PHASE ANGLE WITH ANGLE OF ATTACK IN TRANSITION	184
5-85	VARIATION OF ROTOR CONTROL FORCES WITH YAW ANGLE IN TRANSITION	185
5-86	VARIATION OF ROTOR CONTROL MOMENTS WITH YAW ANGLE IN TRANSITION	186
5-87	VARIATION OF CYCLIC PHASE ANGLE WITH YAW ANGLE IN TRANSITION	187
5-88	VARIATION OF ROTOR CONTROL FORCES WITH ADVANCE RATIO	188
5-89	VARIATION OF ROTOR CONTROL MOMENTS WITH ADVANCE RATIO	189

LIST OF ILLUSTRATIONS

<u>FIGURE NO.</u>	<u>TITLE</u>	<u>PAGE</u>
5-90	INFLUENCE OF FLAP DEFLECTION ON AIRFRAME LIFT . .	203
5-91	ROTOR PITCHING MOMENT/ANGLE OF ATTACK VARIATION AT $V/V_T=0.386$ AND $\delta_F=0^\circ$	204
5-92	ROTOR PITCHING MOMENT/ANGLE OF ATTACK VARIATION AT $V/V_T=0.386$, $\delta_F=45^\circ$	205
5-93	ROTOR NORMAL FORCE/ANGLE OF ATTACK VARIATION AT $V/V_T=0.386$ $\delta_F=0^\circ$	206
5-94	ROTOR NORMAL FORCE/ANGLE OF ATTACK VARIATION AT $V/V_T=0.386$, $\delta_F=45^\circ$	207
5-95	ROTOR YAWING MOMENT/ANGLE OF ATTACK VARIATION AT $V/V_T=0.386$, $\delta_F=0^\circ$	208
5-96	ROTOR YAWING MOMENT/ANGLE OF ATTACK VARIATION AT $V/V_T=0.386$, $\delta_F=45^\circ$	209
5-97	ROTOR SIDE FORCE/ANGLE OF ATTACK VARIATION AT $V/V_T=0.386$, $\delta_F=0^\circ$	210
5-98	ROTOR SIDE FORCE/ANGLE OF ATTACK VARIATION AT $V/V_T=0.386$, $\delta_F=45^\circ$	211
5-99	ROTOR YAWING MOMENT/YAW ANGLE VARIATION AT $V/V_T=0.386$, $\delta_F=0^\circ$	212
5-100	ROTOR SIDE FORCE/YAW ANGLE VARIATION AT $V/V_T=0.386$, $\delta_F=0^\circ$	213
5-101	ROTOR PITCHING MOMENT/YAW ANGLE VARIATION AT $V/V_T=0.386$, $\delta_F=0^\circ$	214
5-102	ROTOR NORMAL FORCE/YAW ANGLE VARIATION AT $V/V_T=0.386$, $\delta_F=0^\circ$	215
5-103	INFLUENCE OF FLAP DEFLECTION ON ROTOR PITCHING MOMENT AT $V/V_T=0.386$	216
5-104	INFLUENCE OF WING LIFT ON ROTOR PITCHING MOMENT AT $V/V_T=0.386$	217

LIST OF ILLUSTRATIONS

<u>FIGURE NO.</u>	<u>TITLE</u>	<u>PAGE</u>
5-105	INFLUENCE OF WING LIFT ON ROTOR PITCHING MOMENT AT $V/V_T=0.386$	218
5-106	COMPARISON OF ROTOR MOMENT DERIVATIVES AT $V/V_T=0.386$	219
5-107	INFLUENCE OF FLAP DEFLECTION ON ROTOR NORMAL FORCE AT $V/V_T=0.386$	220
5-108	INFLUENCE OF WING ON ROTOR NORMAL FORCE AT $V/V_T=0.386$	221
5-109	INFLUENCE OF WING LIFT ON ROTOR NORMAL FORCE AT $V/V_T=0.386$	222
5-110	COMPARISON OF ROTOR FORCE DERIVATIVES $\partial C_N / \partial \alpha$ AND $\partial C_{SF} / \partial \psi$ AT $V/V_T=0.386$	223
5-111	INFLUENCE OF FLAP DEFLECTION ON ROTOR YAWING MOMENT AT $V/V_T=0.386$	224
5-112	INFLUENCE OF WING LIFT ON ROTOR YAWING MOMENT AT $V/V_T=0.386$	225
5-113	INFLUENCE OF WING LIFT ON ROTOR YAWING MOMENT AT $V/V_T=0.386$	226
5-114	COMPARISON OF ROTOR MOMENT DERIVATIVES $\partial C_{YM} / \partial \alpha$ AND $\partial C_{PM} / \partial \psi$ AT $V/V_T=0.386$	227
5-115	INFLUENCE OF FLAP DEFLECTION ON ROTOR SIDE FORCE AT $V/V_T=0.386$	228
5-116	INFLUENCE OF WING LIFT ON ROTOR SIDE FORCE AT $V/V_T=0.386$	229
5-117	INFLUENCE OF WING LIFT ON ROTOR SIDE FORCE AT $V/V_T=0.386$	230
5-118	COMPARISON OF ROTOR FORCE DERIVATIVES $\partial C_{SF} / \partial \alpha$ AND $\partial C_N / \partial \psi$ AT $V/V_T=0.386$	231

LIST OF ILLUSTRATIONS

<u>FIGURE NO.</u>	<u>TITLE</u>	<u>PAGE</u>
5-119	ROTOR PITCHING MOMENT/ANGLE OF ATTACK VARIATION AT $V/V = 0.57$, $\delta_F = 0^\circ$	232
5-120	ROTOR NORMAL FORCE/ANGLE OF ATTACK VARIATION AT $V/V = 0.57$, $\delta_F = 0^\circ$	233
5-121	ROTOR YAWING MOMENT/ANGLE OF ATTACK VARIATION $V/V_T = 0.57$, $\delta_F = 0^\circ$	234
5-122	ROTOR SIDE FORCE/ANGLE OF ATTACK VARIATION AT $V/V_T = 0.57$ $\delta_F = 0^\circ$	235
5-123	ROTOR/ROTOR INTERFERENCE EFFECTS ON CRUISE ROTOR CHARACTERISTICS, $V/V_T = 0.386$	236
5-124	ROTOR/ROTOR INTERFERENCE EFFECTS ON CRUISE ROTOR CHARACTERISTICS, $V/V_T = 0.386$	237
5-125	ROTOR/ROTOR INTERFERENCE EFFECTS ON CRUISE ROTOR CHARACTERISTICS, $V/V_T = 0.386$	238
5-126	ROTOR/ROTOR INTERFERENCE EFFECTS ON CRUISE ROTOR CHARACTERISTICS, $V/V_T = 0.386$	239
5-127	EFFECT OF SPEED ON ROTOR PITCHING MOMENT IN THE HELICOPTER MODE	240
5-128	EFFECT OF SPEED ON ROTOR NORMAL FORCE IN THE HELICOPTER MODE	241
5-129	AIRFRAME LIFT AND DRAG CHARACTERISTICS IN CRUISE WITH ROTORS REMOVED AND $i_c = 0^\circ$	242
5-130	CONTRIBUTION OF PROP/ROTORS AND HORIZONTAL TAIL TO AIRCRAFT LIFT WITH $\delta_F = 0^\circ$ AND $V/V_T =$ 0.386	243
5-131	CONTRIBUTION OF PROP/ROTORS AND HORIZONTAL TAIL TO AIRCRAFT LIFT WITH $\delta_F = 45^\circ$ AND $V/V_T =$ 0.386	244
5-132	CONTRIBUTION OF PROP/ROTORS AND HORIZONTAL TAIL TO AIRCRAFT LIFT WITH $\delta_F = 60^\circ$ AND $V/V_T = 0.386$	245

LIST OF ILLUSTRATIONS

<u>FIGURE NO.</u>	<u>TITLE</u>	<u>PAGE</u>
5-133	CONTRIBUTION OF PROP/ROTORS AND HORIZONTAL TAIL TO AIRCRAFT PITCHING MOMENT, $\delta_F=0^\circ$, $V/V_T=0.386$	246
5-134	CONTRIBUTION OF PROP/ROTORS AND HORIZONTAL TAIL TO AIRCRAFT PITCHING MOMENT, $\delta_F=45^\circ$, $V/V_T=0.386$	247
5-135	CONTRIBUTION OF PROP/ROTORS AND HORIZONTAL TAIL TO AIRCRAFT PITCHING MOMENT, $\delta_F=60^\circ$, $V/V_T=0.386$	248
5-136	CONTRIBUTION OF PROP/ROTOR AND VERTICAL TAIL TO AIRCRAFT SIDE FORCE, $\delta_F=0^\circ$, $V/V_T=0.382$	249
5-137	CONTRIBUTION OF PROP/ROTOR AND VERTICAL TAIL TO AIRCRAFT YAWING MOMENT, $\delta_F=0^\circ$, $V/V_T=0.382$	250
5-138	CONTRIBUTION OF PROP/ROTOR AND VERTICAL TAIL TO AIRCRAFT ROLLING MOMENT, $\delta_F=0^\circ$, $V/V_T=0.382$	251
5-139	COMPARISON OF ROTORS ON/ROTORS OFF PITCHING MOMENT WITH AND WITHOUT TAIL	252
5-140	EFFECT OF ROTORS ON HORIZONTAL TAIL CON- TRIBUTION TO AIRCRAFT PITCHING MOMENT	253
5-141	COMPARISON OF ROTORS ON/ROTORS OFF YAWING MOMENT WITH AND WITHOUT TAIL	254
5-142	EFFECT OF ROTORS ON VERTICAL TAIL CON- TRIBUTION TO AIRCRAFT YAWING MOMENT	255
5-143	CONTRIBUTION OF PROP/ROTORS AND HORIZONTAL TAIL TO AIRCRAFT PITCHING MOMENT AT $V/V_T=0.386$	256
5-144	RESPONSE RESULTING FROM 4° PITCH STEP IN THE CRUISE MODE	257

LIST OF ILLUSTRATIONS

<u>FIGURE NO.</u>	<u>TITLE</u>	<u>PAGE</u>
FIGURE 6-1	CORRELATION OF MEASURED AND PREDICTED BLADE FREQUENCIES	260
FIGURE 6-2	MEASURED AND PREDICTION BLADE LOADS PRODUCED BY CYCLIC PITCH IN HOVER AT $V_{TIP} = 750$ FPS AND $h/D = .39$	261
FIGURE 6-3	COMPARISON BETWEEN MEASURED AND CALCULATED STEADY HUB RPM FOR 3° CYCLIC AND $V=0$	262
FIGURE 6-4	MEASURED AND PREDICTED ALTERNATING FLAP BENDING PRODUCED BY AIRCRAFT ANGLE OF ATTACK IN CRUISE AT $\theta_{75}=30^\circ$, $V_{TIP}=570$ FPS AND $V_{TUNNEL} = 220$ FPS	263
FIGURE 6-5	MEASURED AND PREDICTED BLADE FLAP BENDING IN CRUISE FOR $\alpha=10^\circ$, $\theta_{75}=30^\circ$, $V_{TIP}=570$ FPS AND $V_{TUNNEL} = 220$ PFS	264
FIGURE 6-6	COMPARISON BETWEEN MEASURED AND CALCULATED STEADY HUB MOMENT VS AIRCRAFT ANGLE OF ATTACK FOR $i_N=0$ DEG, and $V=226$ FPS	265
FIGURE 6-7	MEASURED AND PREDICTED ALTERNATING FLAP BENDING PRODUCED BY WING FLAP INCIDENCE IN CRUISE AT $\theta_{75}=30^\circ$, $V_{TIP}= 570$ FPS, $V_{TUNNEL}=220$ FPS AND $\alpha=0$	266

LIST OF ILLUSTRATIONS

<u>FIGURE NO.</u>	<u>TITLE</u>	<u>PAGE</u>
6-8	PREDICTED AND MEASURED ROTOR BLADE NATURAL FREQUENCIES FOR $\theta_{.75}=15^\circ$	270
6-9	LEFT-HAND BLADE FLAP BENDING RESPONSE TO ONE-PER-REV BAFFLE FOR TEN DEGREES COLLECTIVE PITCH	271
6-10	LEFT-HAND BLADE FLAP BENDING RESPONSE TO TWO-PER-REV BAFFLE FOR TEN DEGREES COLLECTIVE PITCH	272
6-11	LEFT-HAND BLADE FLAP BENDING RESPONSE TO THREE-PER-REV BAFFLE FOR TEN DEGREES COLLECTIVE PITCH	273
6-12	LEFT-HAND BLADE FLAP BENDING RESPONSE TO FOUR-PER-REV BAFFLE FOR TEN DEGREES COLLECTIVE PITCH	274
6-13	RIGHT-HAND BLADE FLAP BENDING RESPONSE TO TWO-PER-REV BAFFLE FOR TEN DEGREES COLLECTIVE PITCH	275
6-14	RIGHT-HAND BLADE FLAP BENDING RESPONSE TO THREE-PER-REV BAFFLE FOR TEN DEGREES COLLECTIVE PITCH	276
6-15	RIGHT-HAND BLADE FLAP BENDING RESPONSE TO FOUR-PER-REV BAFFLE FOR TEN DEGREES COLLECTIVE PITCH	277
6-16	RIGHT-HAND BLADE FLAP BENDING HARMONIC RESPONSE TO ONE-PER-REV BAFFLE FOR TEN DEGREES COLLECTIVE PITCH	278
6-17	RIGHT-HAND BLADE FLAP BENDING HARMONIC RESPONSE TO TWO-PER-REV BAFFLE FOR TEN DEGREES COLLECTIVE PITCH	279
6-18	RIGHT-HAND BLADE FLAP BENDING HARMONIC RESPONSE TO THREE-PER-REV BAFFLE FOR TEN DEGREES COLLECTIVE PITCH	280
6-19	RIGHT-HAND BLADE FLAP BENDING HARMONIC RESPONSE TO FOUR-PER-REV BAFFLE FOR TEN DEGREES COLLECTIVE PITCH	281

LIST OF ILLUSTRATIONS

<u>FIGURE NO.</u>	<u>TITLE</u>	<u>PAGE</u>
6-20	LEFT-HAND BLADE CHORD BENDING RESPONSE TO ONE-PER-REV BAFFLE FOR TEN DEGREES COLLECTIVE PITCH	282
6-21	LEFT-HAND BLADE CHORD BENDING RESPONSE TO TWO-PER-REV BAFFLE FOR TEN DEGREEE COLLECTIVE PITCH	283
6-22	LEFT-HAND BLADE CHORD BENDING RESPONSE TO THREE-PER-REV BAFFLE FOR TEN DEGREES COLLECTIVE PITCH	284
6-23	LEFT-HAND BLADE CHORD BENDING RESPONSE TO FOUR-PER-REV BAFFLE FOR TEN DEGREES COLLECTIVE PITCH	285
6-24	RIGHT-HAND BLADE CHORD BENDING RESPONSE TO TWO-PER-REV BAFFLE FOR TEN DEGREES COLLECTIVE PITCH	286
6-25	RIGHT-HAND BLADE CHORD BENDING RESPONSE TO THREE-PER-REV BAFFLE FOR TEN DEGREES COLLECTIVE PITCH	287
6-26	RIGHT-HAND BLADE CHORD BENDING RESPONSE TO FOUR-PER-REV BAFFLE FOR TEN DEGREES COLLECTIVE PITCH	288
6-27	RIGHT-HAND BLADE CHORD BENDING HARMONIC RESPONSES TO ONE-PER-REV BAFFLE FOR TEN DEGREES COLLECTIVE PITCH	289
6-28	RIGHT-HAND BLADE CHORD BENDING HARMONIC RESPONSE TO TWO-PER-REV BAFFLE FOR TEN DEGREES COLLECTIVE PITCH	290
6-29	RIGHT-HAND BLADE CHORD BENDING HARMONIC RESPONSE TO THREE-PER-REV BAFFLE FOR TEN DEGREES COLLECTIVE PITCH	291
6-30	RIGHT-HAND BLADE CHORD BENDING HARMONIC RESPONSE TO FOUR-PER-REV BAFFLE FOR TEN DEGREES COLLECTIVE PITCH	292

LIST OF ILLUSTRATIONS

<u>FIGURE NO.</u>	<u>TITLE</u>	<u>PAGE</u>
6-31	PREDICTED AND MEASURED ROTOR BLADE TORSIONAL NATURAL FREQUENCY	293
6-32	LEFT ROTOR BLADE TORSIONAL RESPONSE TO TWO-PER-REV BAFFLE AT 1100 RPM	294
6-33	RIGHT-HAND BLADE TORSIONAL RESPONSE TO TWO-PER-REV BAFFLE FOR TEN DEGREES COLLECTIVE PITCH	295
6-34	RIGHT-HAND BLADE TORSIONAL RESPONSE TO THREE-PER-REV BAFFLE FOR TEN DEGREES COLLECTIVE PITCH	296
6-35	RIGHT-HAND BLADE TORSIONAL RESPONSE TO FOUR-PER-REV BAFFLE FOR TEN DEGREES COLLECTIVE PITCH	297
6-36	RIGHT-HAND BLADE TORSIONAL HARMONIC RESPONSE TO ONE-PER-REV BAFFLE FOR TEN DEGREES COLLECTIVE PITCH	298
6-37	RIGHT-HAND BLADE TORSIONAL HARMONIC RESPONSE TO TWO-PER-REV BAFFLE FOR TEN DEGREES COLLECTIVE PITCH	299
6-38	RIGHT-HAND BLADE TORSIONAL HARMONIC RESPONSE TO THREE-PER-REV BAFFLE FOR TEN DEGREES COLLECTIVE PITCH	300
6-39	RIGHT-HAND BLADE TORSIONAL HARMONIC RESPONSE TO FOUR-PER-REV BAFFLE FOR TEN DEGREES COLLECTIVE PITCH	301
6-40	ALTERNATING BLADE FLAP BENDING VS. ROTOR RPM IN HOVER	307
6-41	ALTERNATING BLADE CHORD BENDING VS. ROTOR RPM IN HOVER	308
6-42	ALTERNATING BLADE TORSION VS. RPM FOR $i_N=90$ DEG, $\theta_2=3$ DEG, AND $h/D=.39, 1.8$	309

LIST OF ILLUSTRATIONS

<u>FIGURE NO.</u>	<u>TITLE</u>	<u>PAGE</u>
6-43	MEASURED AND PREDICTED BLADE LOADS PRODUCED BY CYCLIC PITCH IN HOVER AT $V_{TIP}=750$ FPS AND $h/D=.39$	310
6-44	MEASURED AND PREDICTED BLADE LOADS PRODUCED BY CYCLIC PITCH IN HOVER AT $V_{TIP}=750$ FPS and $h/D=1.8$	311
6-45	LEFT ROTOR BLADE TORSIONAL WAVEFORM FOR $\theta_{75}=14^\circ$, 2300 RPM and $\frac{\omega\theta}{\Omega}=6.4$	312
6-46	ALTERNATING BLADE TORSION VS. RPM FOR $i_N=$ 70° AND $h/D=1.8$	313
6-47	ALTERNATING BLADE TORSION VS. RPM FOR $i_N=70$ DEG, AND $h/D=1.8$	314
6-48	ALTERNATING BLADE TORSION VS. ROTOR HEIGHT FOR $i_N=70^\circ$ AND 2180 RPM	315
6-49	RANGE OF ROTOR THRUST AND TIP SPEED WHERE STALL FLUTTER DID NOT OCCUR	316
6-50	ALTERNATING BLADE FLAP BENDING VS h/D FOR $i_N=90$ DEG	317
6-51	ALTERNATING BLADE CHORD BENDING VS. h/D FOR $i_N=90$ DEG	318
6-52	ALTERNATING BLADE TORSION VS. RPM FOR $i_N=90$ DEG	319
6-53	ALTERNATING BLADE FLAP BENDING VS. h/D FOR $i_N=90$ DEG	320
6-54	ALTERNATING BLADE CHORD BENDING VS. h/D FOR $i_N=90$ DEG	321
6-55	ALTERNATING BLADE TORSION VS. h/D FOR $i_N=90$ DEG	322
6-56	ALTERNATING BLADE FLAP BENDING VS. h/D FOR $i_N=90$ DEG	323

LIST OF ILLUSTRATIONS

<u>FIGURE NO.</u>	<u>TITLE</u>	<u>PAGE</u>
6-57	ALTERNATING BLADE CHORD BENDING VS. h/D FOR $i_N=90$ DEG	324
6-58	ALTERNATING BLADE TORSION VS. h/D FOR $i_N=90$ DEG	325
6-59	ALTERNATING BLADE FLAP BENDING VS. ROTOR HEIGHT FOR $i_N=70^\circ$ AND 2180 RPM	326
6-60	ALTERNATING BLADE CHORD BENDING VS. ROTOR HEIGHT FOR $i_N=70^\circ$ AND 2180 RPM	327
6-61	ALT FLAP BENDING VS. RPM FOR $i_N=90^\circ$, $\theta_{75}=10^\circ$ AND h/D=.39	328
6-62	ALT CHORD BENDING VS. RPM FOR $i_N=90^\circ$, $\theta_{75}=10^\circ$ AND h/D=.39	329
6-63	ALT FLAP BENDING VS. RPM FOR $i_N=90^\circ$, $\theta_{75}=10^\circ$ AND h/D=1.8	330
6-64	ALT CHORD BENDING VS. RPM FOR $i_N=90^\circ$, $\theta_{75}=10^\circ$ AND h/D=1.8	331
6-65	LEFT ROTOR MOMENT WAVEFORMS FOR $i_N=70^\circ$, V=60 FPS $\theta_{75}=14^\circ$, RPM=2180 AND h/D=0.39	332
6-66	ALTERNATING BLADE FLAP BENDING VS. VELOCITY FOR $i_N=70$ DEG, h/D=.39 AND 2180 RPM	333
6-67	ALTERNATING BLADE CHORD BENDING VS. VELOCITY FOR $i_N=70$ DEG, h/D=.39 AND 2180 RPM	334
6-68	ALTERNATING BLADE TORSION VS. VELOCITY FOR $i_N=70$ DEG, h/D=.39 AND 2180 RPM	335
6-69	ALTERNATING BLADE FLAP BENDING VS. VELOCITY FOR $i_N=70$ DEG, h/D=1.8 AND 2180 RPM	336
6-70	ALTERNATING BLADE CHORD BENDING VS. VELOCITY FOR $i_N=70$ DEG, h/D=1.8 AND 2180 RPM	337

LIST OF ILLUSTRATIONS

<u>FIGURE NO.</u>	<u>TITLE</u>	<u>PAGE</u>
6-71	ALTERNATING BLADE TORSION VS. VELOCITY FOR $i_N=70$ DEG, $h/D=1.8$ AND 2180 RPM	338
6-72	STEADY HUB MOMENT VS. RPM FOR 3° cyclic AND $V=0$	340
6-73	COMPARISON BETWEEN MEASURED AND CALCULATED STEADY HUB MOMENT VS. RPM FOR 3° CYCLIC AND $V=0$	341
6-74	LEFT ROTOR ALTERNATING FLAP BENDING VS. AIRCRAFT ANGLE OF ATTACK FOR $i_N=70$ DEG AND $V=116$ FPS	344
6-75	LEFT ROTOR ALTERNATING CHORD BENDING VS. AIRCRAFT ANGLE OF ATTACK FOR $i_N=70$ DEG, AND $V=116$ FPS	345
6-76	ALTERNATING BLADE FLAP BENDING VS. AIRCRAFT ANGLE OF ATTACK FOR $i_N=45$ DEG, $V=132$ FPS	346
6-77	ALTERNATING BLADE CHORD BENDING VS. AIRCRAFT ANGLE OF ATTACK FOR $i_N=45$ DEG, $V=132$ FPS	347
6-78	ALTERNATING BLADE FLAP BENDING VS. AIRCRAFT YAW ANGLE FOR $i_N=45$ DEG, $V=132$ FPS, AND $\alpha=0$ DEG	348
6-79	ALTERNATING BLADE CHORD BENDING VS. AIRCRAFT YAW ANGLE FOR $i_N=45$ DEG, $V=132$ FPS, AND $\alpha=0$ DEG	349
6-80	ALTERNATING BLADE FLAP BENDING VS. AIRCRAFT ANGLE OF ATTACK FOR $i_N=45$ DEG, $V=132$ FPS, AND $+3$ DEG CYCLIC	350
6-81	ALTERNATING BLADE FLAP BENDING VS. AIRCRAFT YAW ANGLE FOR $i_N=45$ DEG, $V=132$ FPS, $\alpha=0$ DEG, AND $+3$ DEG CYCLIC	351
6-82	ALTERNATING BLADE CHORD BENDING VS. AIRCRAFT YAW ANGLE FOR $i_N=45$ DEG, $V=132$ FPS, $\alpha=0$ DEG, AND $+3$ DEG CYCLIC	352
6-83	LIFT ROTOP ALTERNATING TORSION IN TRANSITION DUE TO STALL FLUTTER FOR $i_N=70$ DEG, $\theta_{75}=14$ DEG, $V_{TUNNEL}=116$ FPS, 1970 RPM	353

LIST OF ILLUSTRATIONS

<u>FIGURE NO.</u>	<u>TITLE</u>	<u>PAGE</u>
6-84	LEFT ROTOR TORSIONAL FIRST AND EIGHTH HARMONICS IN TRANSITION FOR $i_N=70$ DEG, $\theta_{75}=14$ DEG, $V_{TUNNEL}=116$ FPS, 1970 RPM	354
6-85	LEFT BLADE TORSIONAL WAVEFORM BEFORE AND AFTER STALL FLUTTER INCEPTION FOR $i_N=70$ DEG, $\theta_{75}=14$ DEG, $V_{TUNNEL}=116$ FPS AND 170 RPM	355
6-86	STEADY HUB MOMENT VS. AIRCRAFT ANGLE OF ATTACK FOR $i_N=45$ DEG, AND $V=132$ FPS	357
6-87	STEADY HUB MOMENT VS. AIRCRAFT ANGLE OF ATTACK FOR $i_N=45$ DEG, AND $V=133$ FPS	358
6-88	ALTERNATING BLADE FLAP BENDING VS. AIRCRAFT ANGLE OF ATTACK FOR $i_N=0$ DEG, $V=224$ FPS, AND 60 DEG WING FLAP INCIDENCE	361
6-89	ALTERNATING BLADE CHORD BENDING VS. AIRCRAFT ANGLE OF ATTACK FOR $i_N=0$ DEG, $V=224$ FPS, AND 60 DEG WING FLAP INCIDENCE	362
6-90	ALTERNATING BLADE TORSION VS. AIRCRAFT ANGLE OF ATTACK FOR $i_N=0$ DEG, $V=224$ FPS, AND 60 DEG WING FLAP INCIDENCE	363
6-91	ALTERNATING BLADE FLAP BENDING VS. AIRCRAFT ANGLE OF ATTACK FOR $i_N=0$ DEG, $V=225$ FPS, AND 45 DEG WING FLAP INCIDENCE	364
6-92	ALTERNATING BLADE CHORD BENDING VS. AIRCRAFT ANGLE OF ATTACK FOR $i_N=0$ DEG, $V=225$ FPS, AND 45 DEG WING FLAP INCIDENCE	365
6-93	ALTERNATING BLADE TORSION VS. AIRCRAFT ANGLE OF ATTACK FOR $i_N=0$ DEG, $V=225$ FPS, AND 45 DEG WING FLAP INCIDENCE	366
6-94	ALTERNATING BLADE FLAP BENDING VS. AIRCRAFT ANGLE OF ATTACK FOR $i_N=0$ DEG, $V=226$ FPS, AND 0 DEG WING FLAP INCIDENCE	367
6-95	ALTERNATING BLADE CHORD BENDING VS. AIRCRAFT ANGLE OF ATTACK FOR $i_N=0$ DEG, $V=226$ FPS, AND 0 DEG WING FLAP INCIDENCE	368
6-96	ALTERNATING BLADE FLAP BENDING VS. AIRCRAFT ANGLE OF ATTACK FOR $i_N=0$ DEG, $V=216$ FPS	369

LIST OF ILLUSTRATIONS

<u>FIGURE NO.</u>	<u>TITLE</u>	<u>PAGE</u>
6-97	ALTERNATING BLADE CHORD BENDING VS. AIRCRAFT ANGLE OF ATTACK FOR $i = 0$ DEG, $V=216$ FPS	370
6-98	ALTERNATING BLADE FLAP BENDING VS. AIRCRAFT ANGLE OF ATTACK FOR $i_N=0^\circ$, $V=226$ FPS, AND 2030 RPM	371
6-99	ALTERNATING BLADE CHORD BENDING VS. AIRCRAFT ANGLE OF ATTACK FOR $i_N=0^\circ$, $V=226$ FPS, AND 2030 RPM	372
6-100	ALTERNATING BLADE TORSION VS. AIRCRAFT ANGLE OF ATTACK FOR $i_N=0^\circ$, $V=226$ FPS, AND 2030 RPM	373
6-101	MEASURED AND PREDICTED ALTERNATING FLAP BENDING PRODUCED BY AIRCRAFT ANGLE OF ATTACK IN CRUISE AT $\theta_{75}=30^\circ$, $V_{TIP}=$ 570 FPS AND $V_{TUNNEL}= 220$ FPS	374
6-102	MEASURED AND PREDICTED BLADE FLAP BENDING IN CRUISE FOR $\alpha=10^\circ$, $\theta_{75}=30^\circ$, $V_{TIP}=570$ FPS AND $V_{TUNNEL}=220$ FPS	375
6-103	MEASURED AND PREDICTED ALTERNATING CHORD BENDING PRODUCED BY AIRCRAFT ANGLE OF ATTACK IN CRUISE AT $\theta_{75}=30^\circ$, $V_{TIP}=570$ FPS AND $V_{TUNNEL}=220$ FPS	376
6-104	ALTERNATING BLADE FLAP BENDING VS. AIRCRAFT YAW ANGLE FOR $i_N=0^\circ$, $V=215$ FPS, AND $\alpha=0$ DEG . .	377
6-105	ALTERNATING BLADE CHORD BENDING VS. AIRCRAFT YAW ANGLE FOR $i_N=0^\circ$, $V=215$ FPS, AND $\alpha=0$ DEG . .	378
6-106	ALTERNATING BLADE FLAP BENDING VS. AIRCRAFT YAW ANGLE FOR $i_N=0^\circ$, $V=226$ FPS, $\alpha=0$ DEG, AND 2030 RPM	379
6-107	ALTERNATING BLADE CHORD BENDING VS. AIRCRAFT YAW ANGLE FOR $i_N=0^\circ$, $V=226$ FPS, $\alpha=0$ DEG, AND 2030 RPM	380
6-108	ALTERNATING BLADE TORSION VS. AIRCRAFT YAW ANGLE FOR $i_N=0^\circ$, $V=226$ FPS, $\alpha=0$ DEG, AND 2030 RPM	381

LIST OF ILLUSTRATIONS

<u>FIGURE NO.</u>	<u>TITLE</u>	<u>PAGE</u>
6-109	ALTERNATING BLADE FLAP BENDING VS. AIRCRAFT YAW ANGLE FOR $i_N=0^\circ$, $V=226$ FPS, $\alpha=0$ DEG, 2040 RPM	382
6-110	ALTERNATING BLADE CHORD BENDING VS. AIRCRAFT YAW ANGLE FOR $i_N=0^\circ$, $V=226$ FPS, $\alpha=0$ DEG, AND 2040 RPM	383
6-111	ALTERNATING BLADE TORSION VS. AIRCRAFT YAW ANGLE FOR $i_N=0^\circ$, $V=226$ FPS, $\alpha=0$ DEG, AND 2040 RPM	384
6-112	ALTERNATING BLADE FLAP BENDING VS. WING FLAP DEFLECTION FOR $i_N=0$ DEG, $V=226$ FPS AND $\alpha=0$ DEG	385
6-113	ALTERNATING BLADE CHORD BENDING VS WING FLAP DEFLECTION FOR $i_N=0$ DEG, $V=226$ FPS AND $\alpha=0$ DEG	386
6-114	MEASURED AND PREDICTED ALTERNATING FLAP BENDING PRODUCED BY WING FLAP INCIDENCE IN CRUISE AT $\theta_{75}=30^\circ$, $V=570$ FPS, $V_{TUNNEL}=220$ FPS AND $\alpha=0$	387
6-115	MEASURED AND PREDICTED ALTERNATING FLAP BENDING PRODUCED BY WING FLAP INCIDENCE IN CRUISE AT $\theta_{75}=30^\circ$, $V_{TIP}=570$ FPS, $V_{TUNNEL}=220$ FPS AND $\alpha=0$	388
6-116	STEADY HUB MOMENT VS. AIRCRAFT ANGLE OF ATTACK FOR $i_N=0$ DEG, AND $V=226$ FPS	389
6-117	COMPARISON BETWEEN MEASURED AND CALCULATED STEADY HUB MOMENT VS. AIRCRAFT ANGLE OF ATTACK FOR $i_N=0$ DEG, AND $V=226$ FPS	390
6-118	STEADY HUB MOMENT VS. AIRCRAFT ANGLE OF ATTACK FOR $i_N=0$ DEG, AND $V=226$ FPS	392
7-1	PREDICTED MODAL FREQUENCIES VS. ROTOR SPEED (HOVER)	397
7-2	PREDICTED MODAL DAMPING VS. ROTOR SPEED (HOVER)	398

LIST OF ILLUSTRATIONS

<u>FIGURE NO.</u>	<u>TITLE</u>	<u>PAGE</u>
7-3	PREDICTED MODAL FREQUENCIES VS. EQUIVALENT FORWARD SPEED (CRUISE)	399
7-4	PREDICTED MODAL DAMPING VS. EQUIVALENT FORWARD SPEED (CRUISE)	400
7-5	STEP ANGLE OF ATTACK INPUT DURING CRUISE	401
7-6	STEP ANGLE OF ATTACK INPUT DURING 45° TRANSITION	402
7-7	STEP ANGLE OF ATTACK INPUT DURING HOVER	403
7-8	FUSELAGE BALANCE MOMENTS VS. FUSELAGE ANGLE OF ATTACK	404
7-9	FUSELAGE BALANCE MOMENTS VS. FUSELAGE ANGLE OF ATTACK	405
A-1	MODEL 160 ATKINS AND MERRILL BLADE TWIST	415
A-2	1/10 SCALE MODEL 160 CYCLIC PROP BLADE COUPLED FLAP AND CHORD NATURAL FREQUENCIES $K_{\beta}=K_{\delta}=250 \times 10^3$	416
A-3	MODEL 160 1/10 SCALE PROP BLADE TORSIONAL NATURAL FREQUENCY	417
A-4	FIRST MODE BENDING - DEFINITION OF VIRTUAL FLAP HINGE	418
A-5	STATIC BLADE DEFLECTION TEST SETUP	419
A-6	LEFT HAND BLADE SHEAR CENTER DETERMINATION	420
A-7	RIGHT HAND BLADE SHEAR CENTER DETERMINATION	421
A-8	LEFT HAND BLADE ELASTIC TWIST AT 3/4 RADIUS	422
A-9	RIGHT HAND BLADE ELASTIC TWIST AT 3/4 RADIUS	423
A-10	LEFT HAND BLADE PITCH FLAP COUPLING AT 3/4 RADIUS	424

LIST OF ILLUSTRATIONS

<u>FIGURE NO.</u>	<u>TITLE</u>	<u>PAGE</u>
A-11	RIGHT HAND BLADE PITCH FLAP COUPLING AT 3/4 RADIUS	425
A-12	LEFT HAND BLADE LAG ANGLE	426
A-13	RIGHT HAND BLADE LAG ANGLE	427
A-14	LEFT HAND BLADE PITCH LAG COUPLING AT 3/4 RADIUS	428
A-15	RIGHT HAND BLADE PITCH LAG COUPLING AT 3/4 RADIUS	429
B-1	SCHEMATIC OF MODEL - STING MODES	432
C-1	DEFINITION OF YAW DEFLECTION ANGLES DUE TO SIDE FORCE AND YAWING MOMENT LOADINGS	441
C-2	DEFINITION OF PITCH DEFLECTION ANGLES FOR NORMAL FORCE AND PITCH MOMENT LOADINGS	442

LIST OF TABLES

<u>TABLE</u>		<u>PAGE</u>
2-1	Objectives of Test Program II.....	4
3-1	Model Dimensions.....	6
3-2	Model Instrumentation	8
5-1	Transition Rotor Stability Derivatives	138
5-2	Cruise Rotor Stability Derivatives	191
A-1	1/10 Scale Model 160 Cyclic Blade Physical Properties.....	414
A-2	Test Data Summary for Blade Shear and Elastic Coupling Test	430
B-1	Static Disturbance Data - Right Hand Rotor Blade Data	433
B-2	Static Disturbance Data - Left Hand Rotor Blade Data	434
B-3	Fuselage Balance Moment Static	435
B-4	Fuselage Balance Force Static	436
B-5	Fuselage Balance Static Disturbance Data	437
B-6	Fuselage Balance Static Disturbance Data	438
B-7	Nacelle Balance Static Disturbance Data	439
C-1	Yaw Deflections due to Side Force Applied at Rotor Hub	443
C-2	Yaw Deflections due to Pure Yaw Moment Applied at the Rotor Hub	444
C-3	Pitch Deflection due to Normal Force Loading at the Rotor Hub	445
C-4	Pitch Deflection due to Pure Pitching Moment Applied at Rotor Hub	446
C-5	Roll Deflections	447

LIST OF SYMBOLS

<u>SYMBOL</u>		<u>UNITS</u>
A	Rotor Disc Area = πR^2	FT ²
a	Airfoil section lift curve slope	1/RAD
b	Wing span - number of rotor blades	FT
c	Wing chord - rotor blade chord	FT
C _D	Airframe drag = $\frac{D}{qS}$	-
ΔC_{HM_y}	Incremental hub moment coefficient = $\frac{\partial M}{\rho AV_T^2 R}$	-
ΔIF_y	Incremental inplane rotor force coefficient = $\frac{\partial F}{\rho AV_T^2}$	-
C _L	Aircraft lift coefficient = $\frac{L}{qS}$	-
C _{L_S}	Aircraft slipstream lift coefficient = $\frac{L}{q_S S}$	-
C _N	Rotor normal force coefficient = $\frac{NF}{\rho AV_T^2}$	-
C _p	Rotor power coefficient = $\frac{HP \times 550}{\rho AV_T^3} = \frac{Q}{\rho AV_T^2 R}$	-
C _{pA/C}	Aircraft power coefficient = $\frac{HP \times 550}{2\rho AV_T^3}$	-
ΔC_{PM}	Aircraft pitch control moment (about wing quarter chord) = $\frac{PM}{qSc}$	-
C _{SF}	Rotor side force coefficient = $\frac{SF}{\rho AV_T^2}$	-
C _{PM}	Rotor pitching moment coefficient = $\frac{PM}{\rho AV_T^2 R}$	-
C _{PM_S}	Aircraft slipstream pitching moment coefficient = $\frac{PM}{q_S S}$	-
C _{PM_{C/4}}	Aircraft pitching moment coefficient about wing quarter chord = $\frac{PM}{qSc}$	-

LIST OF SYMBOLS

<u>SYMBOL</u>		<u>UNITS</u>
$C_{SF_{A/C}}$	Aircraft side force coefficient $\frac{SF}{qS}$	-
C_T	Rotor thrust coefficient $\frac{T}{\rho AV_T^2}$	-
C_{TS}	Aircraft slipstream thrust coefficient $\frac{T}{q_s S}$	-
C_{YM}	Rotor yawing moment coefficient $\frac{YM}{\rho AV_T^2 R}$	-
ΔC_{YM}	Aircraft yaw control moment $\frac{\Delta YM}{qSb}$	-
$C_{R_{MAC}}$	Aircraft rolling $\frac{YM}{qSb}$	-
$C_{YM_{A/C}}$	Aircraft yawing moment $\frac{YM}{qSb}$	-
C_W	Gross weight coefficient $\frac{GW}{2\rho AV_T^2}$	-
C_X	Aircraft propulsive force coefficient $\frac{X}{qS}$	-
C_{X_S}	Aircraft slipstream propulsive force coefficient $\frac{X}{q_s S}$	-
D	Rotor diameter	FT
D	Airframe drag	LB
E	Modulus of elasticity (Young's Modulus)	LB/IN ²
ev	Virtual flap hinge location	IN
ΔF	Incremental inplane rotor force	LB
GJ	Blade torsional stiffness	LB-IN ²

LIST OF SYMBOLS

<u>SYMBOL</u>		<u>UNIT</u>
GW	Gross weight	LB
HP	Rotor horsepower	HP
h/D	Height to diameter ratio	-
I_F	Moment of inertia about flap hinge	LB-FT SEC ²
I_p	Moment of inertia - Polar	LB-FT SEC ²
h	Height of rotor disc above the ground	FT
i_N	Nacelle incidence	Deg
IGE	In ground effect	-
L	Lift	LB
ΔM	Incremental hub moment	FT.LB.
NF	Normal force	LB
OGE	Out of ground effect	-
PM	Pitching moment	FT.LB.
p	Per revolution	-
q	Freestream dynamic pressure $(1/2)\rho v^2$	LB/FT ²
Q	Rotor torque	FT.LB.
q_s	Slipstream dynamic pressure $q+T/A$	LB/FT ²
R	Rotor radius	FT
$M_{R,L}$	Rolling moment	FT.LB.
r	Radial location to a blade station	IN
SF	Side force	LB
S	Wing area	FT ²
T	Rotor thrust	LB

LIST OF SYMBOLS

<u>SYMBOL</u>		<u>UNITS</u>
V	Freestream velocity	FT/SEC
V _T	Rotor tip speed	FT/SEC
X	Aircraft propulsive force	LB
YM	Yawing moment	FT.LB.
α	Fuselage angle of attack	Deg
α_f	Fuselage pitch deflection	°/LB °/FT.LB.
α_{fs}	Fuselage and sting pitch deflection	°/LB °/FT.LB.
α_{fsw}	Fuselage, sting and wing pitch deflection	°/LB °/FT.LB.
α_{fswn}	Fuselage, sting, wing and rotor shaft pitch deflection	°/LB °/FT.LB.
α_n	Rotor shaft pitch deflection	°/LB °/FT.LB.
α_s	Sting pitch deflection	°/LB °/FT.LB.
α_w	Wing pitch deflection	°/LB °/FT.LB.
γ	Blade cyclic pitch	Deg
γ	Locke number $\frac{c_p a R^4}{I_F}$	-
δ_F	Trailing edge flap deflection	Deg
δ_u	Umbrella deflection	Deg
ϕ	Roll angle	Deg
ζ	Lag angle	Deg
$\theta_{.75}$	Rotor blade collective pitch at the three quarter radius	Deg
θ_2	Blade cyclic angle	Deg

LIST OF SYMBOLS

<u>SYMBOL</u>		<u>UNITS</u>
λ	Taper ration $\frac{\text{Tip Chord}}{\text{Root Chord}}$	-
μ	Advance ratio V/V_T	-
ψ	Fuselage yaw angle (rotor azimuth angle)	Deg
ψ_f	Fuselage yaw deflection	°/LB °/FT.LB.
ψ_{fs}	Fuselage and sting yaw deflection	°/LB °/FT.LB.
ψ_{sfn}	Nacelle, sting and fuselage yaw deflection	°/LB °/FT.LB.
ψ_n	Rotor shaft yaw deflection	°/LB °/FT.LB.
ψ_s	Sting yaw deflection	°/LB °/FT.LB.
ρ	Density of air	LB SEC /FT ⁴
σ	Rotor solidity $\frac{bCR}{R}$	-
Ω	Rotor angular velocity	
ω_B	First mode, flapwise blade natural frequency	RAD/SEC
ω_L	First mode. inplane blade natrual frequency	RAD/SEC

LIST OF DATA PLOTTING SYMBOLS

RUN	SYMBOL	RUN	SYMBOL	RUN	SYMBOL	RUN	SYMBOL
1-----	△	28-----	▲	55-----	▲	82-----	▲
2-----	□	29-----	■	56-----	◐	83-----	◐
3-----	▵	30-----	▴	57-----	▴	84-----	▴
4-----	○	31-----	●	58-----	◑	85-----	◑
5-----	◁	32-----	▵	59-----	◁	86-----	◁
6-----	○	33-----	●	60-----	◐	87-----	◐
7-----	◇	34-----	◆	61-----	◑	88-----	◑
8-----	▷	35-----	◐	62-----	▷	89-----	▷
9-----	□	36-----	■	63-----	◐	90-----	◐
10-----	▵	37-----	▴	64-----	▴	91-----	▴
11-----	◐	38-----	◑	65-----	◐	92-----	◐
12-----	◑	39-----	■	66-----	◑	93-----	◑
13-----	▽	40-----	▼	67-----	▽	94-----	▽
14-----	○	41-----	●	68-----	◐	95-----	◐
15-----	▽	42-----	▼	69-----	▽	96-----	▽
16-----	◇	43-----	◆	70-----	◑	97-----	◑
17-----	◁	44-----	◐	71-----	◁	98-----	◁
18-----	✱	45-----	✱	72-----	✱	99-----	✱
19-----	☆	46-----	★	73-----	☆	100-----	☆
20-----	◐	47-----	●	74-----	◐	101-----	◐
21-----	▷	48-----	►	75-----	▷	102-----	▷
22-----	△	49-----	▲	76-----	▲	103-----	▲
23-----	◐	50-----	■	77-----	◐	104-----	◐
24-----	▴	51-----	▴	78-----	▴	105-----	▴
25-----	◇	52-----	◆	79-----	◑	106-----	◑
26-----	▵	53-----	▴	80-----	▴	107-----	▴
27-----	◐	54-----	■	81-----	◐		

1.0 INTRODUCTION

The stowed tilt rotor aircraft hovers, executes transition and cruises at low speed in the same manner as a pure tilt-rotor aircraft. When the aircraft reaches conversion speed, the rotors are feathered and folded, propulsion being maintained by convertible fan engines. The Boeing Company is conducting a program of parametric design, analysis and wind tunnel testing to establish design criteria and aerodynamic prediction techniques for this concept under Contract Number F33615-69-C-1577 from USAF Flight Dynamics Laboratory. This program consists of two phases. Phase I studies (Reference 1) included the preliminary design of stowed tilt-rotor vehicles for (1) high-speed, long-range rescue, (2) capsule recovery, and (3) VTOL transport, and laid the ground work necessary to plan Phase II. Phase II consists of a series of four wind tunnel tests designed to provide experimental data on which to base design criteria and prediction methods and to verify preliminary design information.

This volume reports the second of the four test programs and describes investigations of performance, stability and control and blade loads in hover, transition and cruise. This test program was conducted using the Boeing powered tilt-rotor performance model in the 20'x20' Boeing V/STOL tunnel. The model is a transport aircraft configuration with 5.5-foot diameter rotors. The model rotors are not dynamically representative of the full scale aircraft; however, the blade properties have a large effect on blade loads, stability, control and aircraft performance. The effects of blade flexibility (Reference 3) must be considered in order to understand and scale these data to full-scale design points. In order to verify the rotor blade natural frequencies in both static and rotating cases, a unique test was performed using baffles to provide blade load excitation and identify blade resonances.

The instrumentation system was designed to allow rotor-airframe, airframe-rotor and tail effects to be isolated and the breakdown of aircraft forces and moments into component parts is shown. The nacelles of the model are oversize relative to the rest of the aircraft in order to enclose the electric motors. The model, provides performance, stability and control, blade loads and dynamics information for correlation with prediction techniques and extrapolation to full-scale design points using those techniques.

2.0 OBJECTIVES

This test program is aimed at producing wind tunnel data to verify calculation procedures for the performance, stability, control and blade loads of a stowed tilt-rotor aircraft in all of the rotor-driven flight modes. The test objectives are summarized in Table 2-1 and formulated more fully below.

Objective 1

- a. Define the natural frequencies of the model rotor blades.

Data was obtained from the "baffle" test reported in Section 7.1. This requirement is the result of the high sensitivity of blade loads, aircraft performance, stability and control to rotor flexibility (See Reference 2).

Objective 2

- a. Obtain the rotor wake flow visualization pictures for hover OGE and IGE.
- b. Determine whether there is any adverse yaw/roll coupling for hover IGE.
- c. Establish the configuration that maximizes aircraft performance in hover.
- d. Investigate hover skittishness.

Objective 2a, c are dealt with in Section 4.1.1, 4.1.3 respectively, and objective 2b and d in Section 5.1.3 and 5.1.5.

Objective 3

- a. Establish the wing and horizontal stall tail boundaries in transition and cruise flight.
- b. Determine whether these boundaries represent flight envelope limits due to (1) buffet, (2) moment nonlinearities.

Data concerning Objective 3a are given in Section 7 and 3b in Sections 4 and 5.

Objective 4

- a. Obtain blade load data in hover and transition to define and evaluate the prediction techniques.
- b. Determine effects of ground height and cyclic pitch on blade loads.

Data for these objectives are given in Sections 6.2 through 6.5.

Objective 5

- a. Determine the prop/rotor static stability derivatives in hover, transition and cruise.

Data is shown in Sections 5.1.1, 5.2.1, 5.3.1 and 5.4.1.

Objective 6

- a. Obtain force and power polars from hover through transition and cruise to be utilized as a basis for comparison with prediction methods.

Measured data are compared with predictions in Section 4.1.2.

Objective 7

- a. Determine the blade loads during rotor start-up in a 30-knot crosswind.
- b. Determine wing interference effects on blade loads.

Objective 7a is not answered by this test. Objective 7b is dealt with in Section 6.6.2.

Objective 8

- a. Define control moments due to cyclic pitch and differential thrust in hover and transition.
- b. Establish how these controls should be mixed and phased.

These objectives are answered by data given in Sections 5.1.3, 5.1.4 and 5.4.2.

Objective 9

- a. Determine the whirl flutter modal damping of this model.
- b. Determine the dynamic rotor stability derivatives.

Data obtained in Section 7.1 for Objective 9a; for 9b, Section 5.4.1

TABLE 2-1

OBJECTIVES OR TEST PROGRAM II

<u>TEST OBJECTIVES</u>	<u>CONTRACT REQM'T.</u>	<u>DATA OBTAINED</u>
1. ROTOR BLADE DYNAMICS SUBSTANTIATION (BAFFLES)	NO	YES
2. NEAR HOVER FLOW FIELD STUDIES A. FLOW RECIRCULATION B. ADVERSE YAW WITH ROLL AT 30 KNOTS IGE C. NEAR HOVER DOWNLOAD D. HOVER SKITTISHNESS	YES	YES
3. WING AND HORIZONTAL TAIL STALL BOUNDARIES A. BUFFET B. MOMENT NONLINEARITIES	YES	YES
4. STALL FLUTTER LOADS IN HOVER AND TRANSITION A. IGE VS OGE B. EFFECT OF CYCLIC PITCH	NO	YES
5. PROP/ROTOR STATIC STABILITY DERI- VATIVES A. HOVER (CYCLIC) B. TRANSITION C. CRUISE	YES	YES
6. PERFORMANCE	YES	YES
7. BLADE LOADS (OTHER THAN STALL FLUTTER) A. START-UP LOADS IN 30-KNOT CROSSWIND B. WING INTERFERENCE	NO NO	NO YES
8. ROTOR HUB VIBRATORY LOADS	NO	YES
9. CONTROL MOMENTS	YES	YES
10. ANGLE OF ATTACK STEPS TO EXCITE DYNAMICS A. WHIRL FLUTTER MODAL DAMPING B. DYNAMIC STABILITY DERIVATIVES	NO	YES

3.0 DESCRIPTION OF TEST INSTALLATION

3.1 MODEL DESCRIPTION

The 1/10-scale, powered aerodynamic model of the Boeing Model 160 tilt rotor aircraft, Figure 3-1 was used in this test. The model was originally built for the Boeing Company by Atkins and Merrill Corp. The primary structure of this model is steel and aluminum. Fuselage shell, nacelle fairings, fillets, etc. are constructed of wood and/or fiberglass. The model was designed to permit testing at dynamic pressures up to 125 PSF. Dimensions and sketches of the model are given in Table 3-1 and Figures 3.2 to 3.4.

The configuration of the model is that of a two-rotor, high-wing, monoplane transport aircraft with T-tail and wing-tip-mounted tilting nacelles. The wings are constant chord, constant thickness and untwisted. Manually adjustable leading edge umbrella flaps are provided for download reduction in hover. Remotely controlled trailing edge flaperons are provided for further download reduction and to increase lift in transition. The horizontal stabilator is designed to be remotely controllable but was fixed at zero degrees incidence for these tests. The vertical tail has a manually adjustable rudder that was set at zero degrees deflection for the test. Nacelle incidence is manually adjustable in 5-degree increments and was varied during the test.

The rotors are 5.5 feet in diameter with three fiberglass blades each. Elastomeric bearings are used for blade retention in the hub. The collective pitch of each blade is set manually by loosening the clamps and physically turning the elastomeric bearing in its seat. Small changes in collective pitch ($\pm 5^\circ$) can be obtained by changing the length of the pitch links. Cyclic pitch on the blade is obtained by means of a manually adjustable swashplate.

The blades were geometrically scaled from the full-scale Model 160 blade. The blades are flexible but do not match the stiffness characteristics of the full-scale blades. The model blades had a flapping frequency/RPM ratio of 1.46 at the RPM for full-scale hover tip speed (2600 RPM and 750 FPS, respectively). This is about 17% higher than the full scale flapping frequency ratio. Blade physical properties are discussed in greater detail in Appendix A. The results of a test to determine the blade shear center and the elastic coupling between vibratory modes are given in Appendix A.

Each rotor is powered by a 52 nominal HP Task motor driving through a transmission. At 2600 RPM, the maximum indicated output of these motors was 26 HP for continuous running or 38 HP for up to three minutes.

TABLE 3-1
MODEL DIMENSIONS

<u>Rotor</u>	
Number of Blades	3
Radius	2.750 ft
Solidity	.0857
Effective Disc Area	23.750 ft ²
Blade Area	2.034 ft ²
<u>Wing</u>	
Airfoil	NACA 634421 (Modified)
Span (Nacelle C _L to Nacelle C _L)	6.78 ft
Chord (Constant)	.858 ft
Area	5.85 ft ²
Aspect Ratio	7.93
Flap Chord Aft of Hinge	.206 ft
Flaperon Area Aft of Hinge Line	1.00 ft ² (.5 ft ² /flaperon)
Nacelle Pitch Axis	31% Chord
Wing Angle of Attack with Respect to Fuselage Waterline	2.5 deg
Upper Umbrella Chord	.150 ft
Lower Umbrella Chord	.137 ft
<u>Horizontal Tail</u>	
Airfoil	NACA 0015
Root Chord	.883 ft
Tip Chord	.616 ft
Span	3.14 ft
Area	2.355 ft ²
Aspect Ratio	4.20
<u>Vertical Tail</u>	
Airfoil	NACA 0015
Root Chord	1.215 ft
Tip Chord	.750 ft
Span	1.408 ft
Aspect Ratio	1.43

The instrumentation capabilities of the model are summarized in Table 3-2. Of this capability, only the fuselage pressure transducer and the horizontal stabilator pot were not used. The slip-ring capability was used to transfer strain gauge moment data. One blade on each rotor was instrumented with strain gauges at 32.5%R to give blade torsional moment. As a precaution, the motor and gearbox on each rotor were equipped with thermocouples to permit temperatures to be monitored.

Air flow patterns in hover were recorded with the aid of tuft grids (Figure 3-5) and high-speed moving pictures. Two grids below the wing and one grid above the wing consisted of wires strung between brackets installed at the wing tips and fuselage. Wool tufts were knotted and bonded on the wires. The grids below the wing were 5" apart with the forward grid located at the 17-percent chord position. The upper grid was located at 25 percent chord. Figure 3-5 shows the model with the tuft grids installed.

The blade frequency substantiation tests were performed in hover with piershaped baffles mounted under the rotor to give 1, 2, 3 and 4/rev excitation. A sketch of the test set-up is shown in Figure 3-6.

TABLE 3-2

MODEL INSTRUMENTATION

PARAMETER	TYPE SENSOR	LOCATION
<u>ROTOR FORCES AND MOMENTS</u>	6 Component Strain Gage Balances (2)	One in Each Nacelle
<u>MODEL FORCES AND MOMENTS</u>	6 Component Strain Gage Balance	Between Fuselage and Wind Tunnel Sting
<u>FUSELAGE PRESSURE FLUCTUATIONS</u>	Pressure Transducer	On Side of Fuselage Under Wing
<u>ROTOR RPM (2)</u>	Gear and Tachometer	One in Each Nacelle
<u>1-PER-REV INDICATOR</u>	Magnetic Pick-up	One in Each Nacelle
<u>WING FLAP DEFLECTION</u>	Potentiometer	Trailing Edge of Wing and in Fuselage
<u>HORIZONTAL STABILIZER DEFLECTION</u>	Potentiometer	In Vertical Stabilizer
<u>MODEL ATTITUDE</u>	Potentiometers	In Sting and Pendulum Pot in Fuselage
<u>SLIP RING CAPABILITY</u>	3 Data Channels per Rotor	Nacelle

3.2 TUNNEL INSTALLATION

The model was sting-mounted in the 20x20-foot test section of the Boeing-Vertol V/STOL Wind Tunnel, Figure 3-1. A variable bent/offset adapter was used which gave a bend in the sting in the pitch direction and offset the model 16.5 inches to the right of the tunnel centerline. The bend permitted a pitch range of -15° to $+30^{\circ}$ with the model in the center height of the tunnel. The offset permitted a sideslip range of -5° to $+15^{\circ}$ with minimum wall interference. Model height, pitch and yaw angle were controlled from the tunnel console while roll was manual. Figure 3-7 presents a sketch of the model mounted on the sting in the test section and defines the height of the model from the tunnel floor. Included on the figure is a tabulation of the rotor height/diameter ratio, rotor height and the associated Gilmore height reading utilized in the test program. The test section walls and ceiling were removed for the hover and low q tests to reduce flow recirculation effects. The tunnel floor was used as a fixed ground plane. The boundary layer on the tunnel floor, being approximately 5 inches thick, has no effect on the model since the bottom of the fuselage was 7 inches from the floor at the lowest height to diameter ratio tested. A closed test section was used for the transition and cruise tests.

3.3 DATA REDUCTION

Test data were collected or presented on three media:

- a. Steady-state model and tunnel data on computer output.
- b. Dynamic and static model data in digitized form on magnetic tape.
- c. Dynamic model data in analog form on oscillograph.

Output of all tunnel and model sensors after appropriate signal conditioning and sampling was processed by an IBM 1800 computer.

Balance data were corrected for interactions on the sensing elements and for weight tares to give the absolute values for the loads and moments at or around designated positions in the model.

The main model data were presented in reference to the 1/4 chord point and the nacelle data in reference to the intersection of the shaft axis and the rotorplane.

The absolute loads and moments were converted to coefficient form and referred to three standard wind tunnel axes systems and with respect to tunnel and slipstream dynamic pressure. Rotor coefficients, calculated from the nacelle balances, were expressed in body and wind axes only but also with respect to tunnel and slipstream dynamic pressure.

The model pitch angle was corrected for model normal force and pitching moment to eliminate the error introduced by sting and model deflections. The yaw data are not corrected - deflection data is included in Appendix C.

The dynamic data from the blade gauges and balances were digitized and stored on magnetic tape. Identification, with respect to run number and test conditions, was added for later retrieval and processing. During certain test conditions, ten parameters were selected for on-line dynamic printout. Maximum, minimum, alternating and steady values in combination with the azimuth angle where they occurred, were presented at the end of the static data output. All other dynamic data could be harmonically analyzed with an offline computer program.

Selected parameters were recorded on three oscillographs. Calibration factors were, in advance, established from direct calibrations or from voltage equivalents. A time and rotor speed reference was added to all oscillograph records. The data from these records were manually reduced and analyzed.

Aircraft moment data presented in this report are referred to the wing quarter chord. Figure 3-8 gives the model dimensions necessary to transfer moments and forces. The sign convention for positive forces and moments is shown in Figure 3-9.

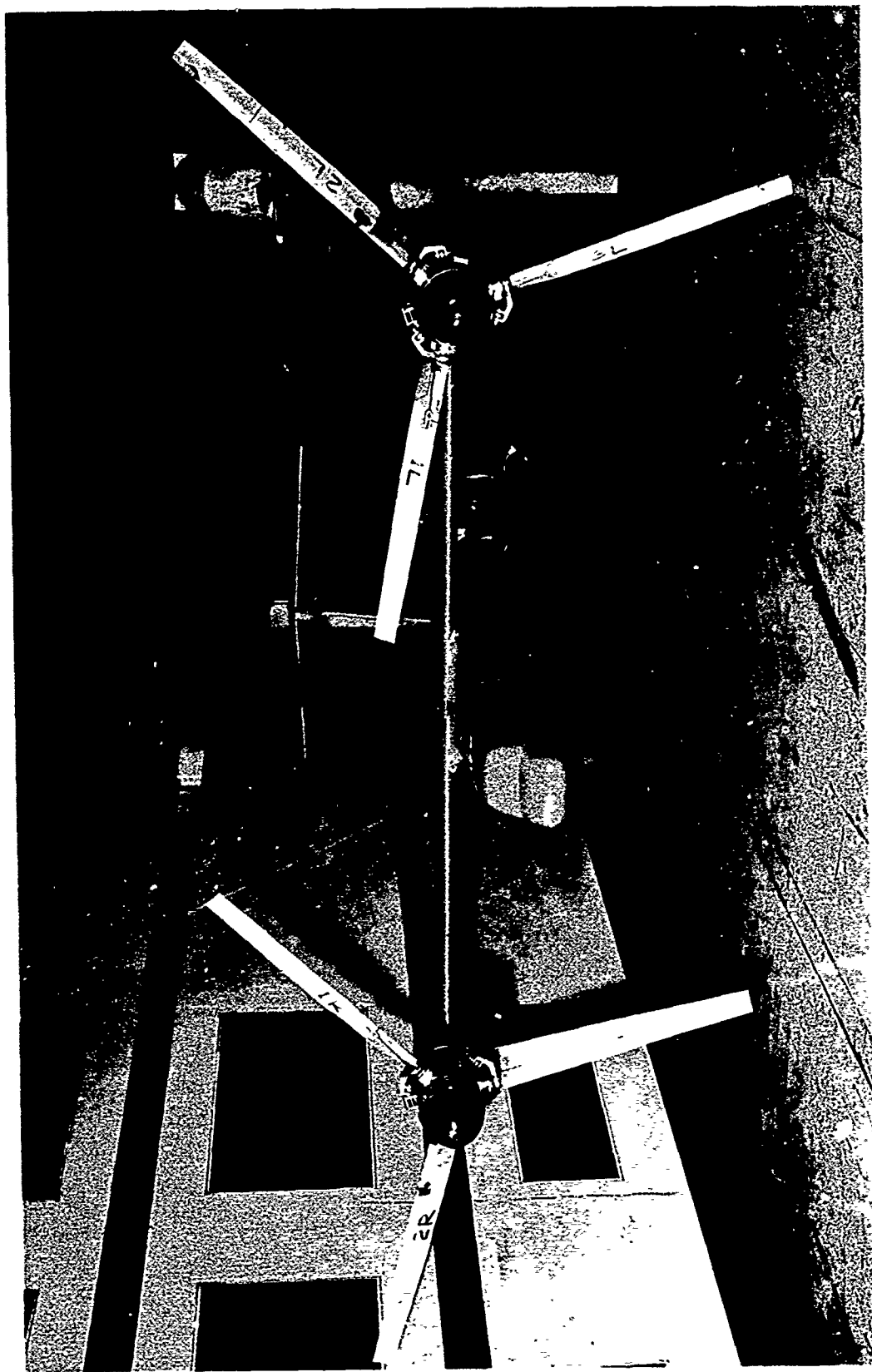


FIGURE 3-1 MODEL 160 1/10 SCALE POWERED TILT ROTOR
WIND TUNNEL MODEL CRUISE MODE

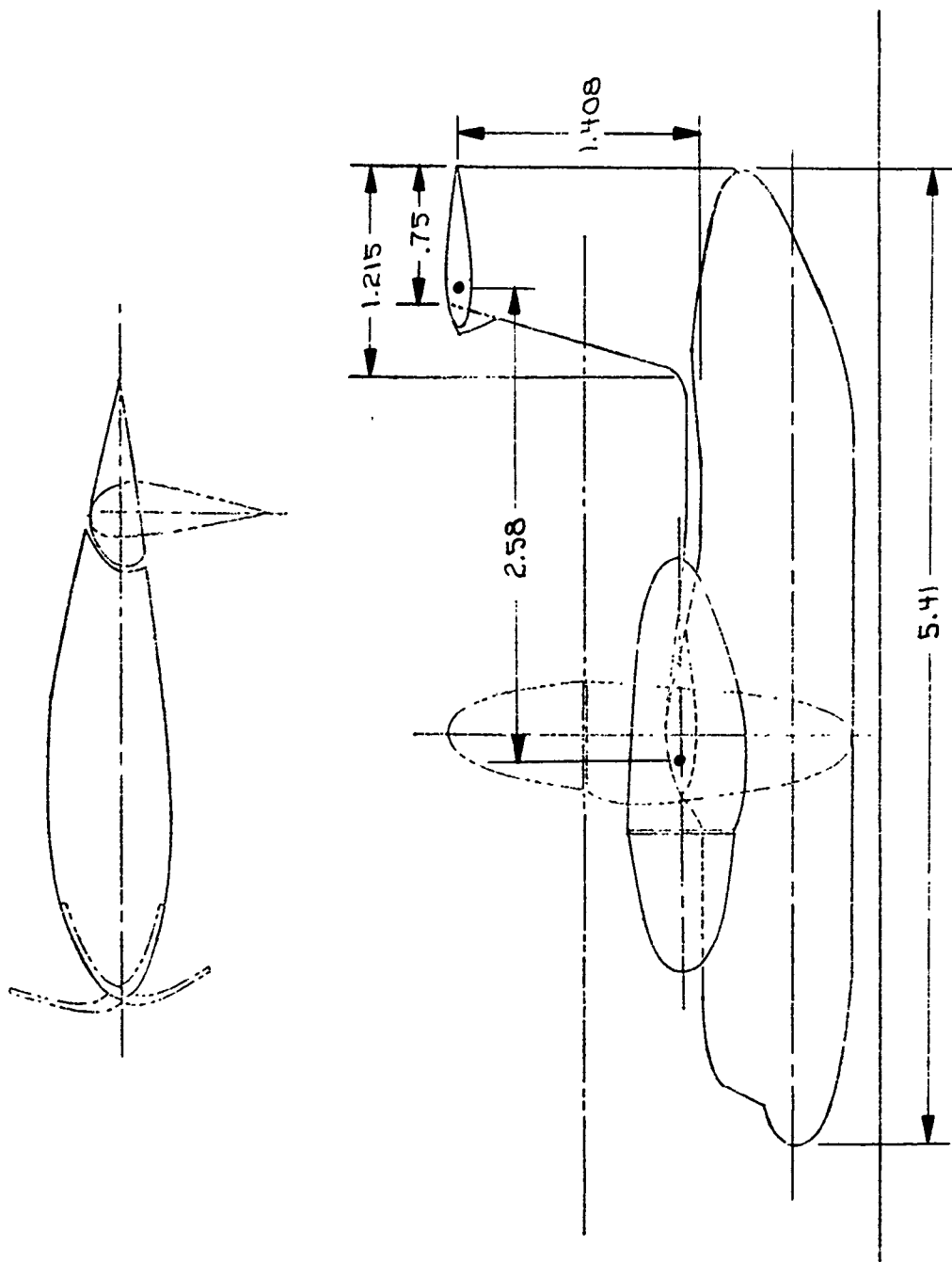


FIGURE 3-2 MODEL 160 WIND TUNNEL MODEL SIDE VIEW

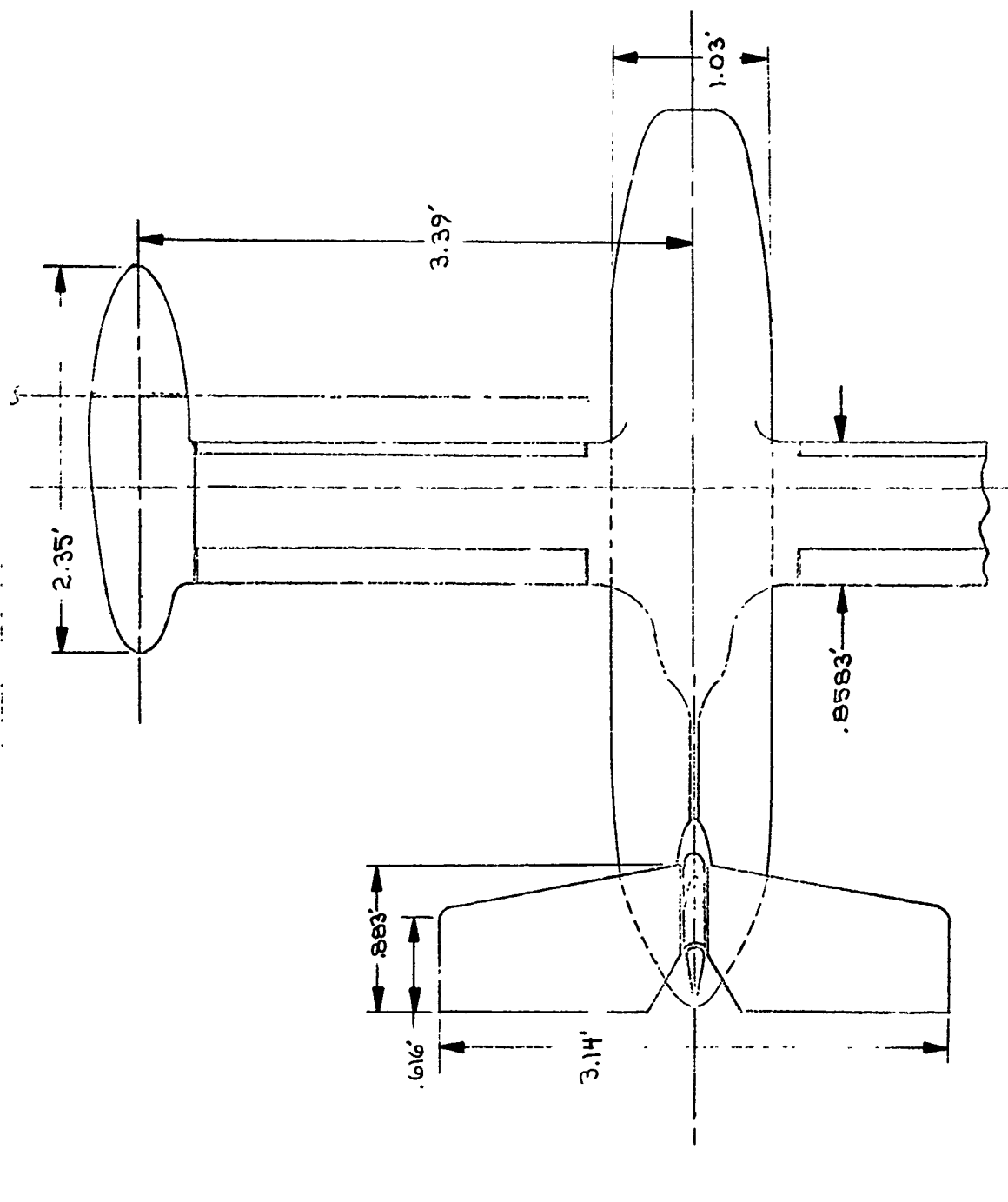


FIGURE 3-3 MODEL 160 WIND TUNNEL MODEL TOP VIEW

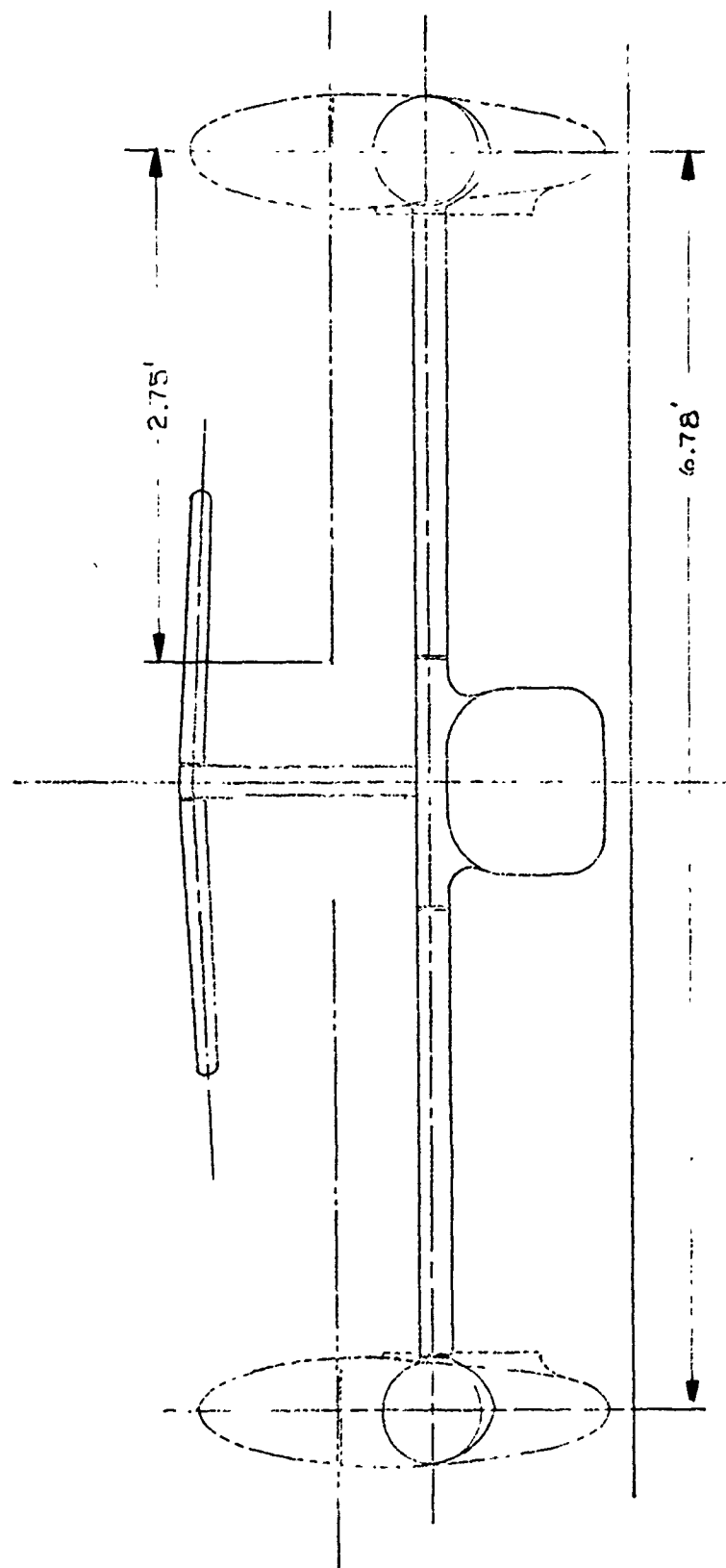


FIGURE 3-4 MODEL 160 WIND TUNNEL MODEL FRONT VIEW



FIGURE 3-5 MODEL 160 WIND TUNNEL - TUFT GRID HOVER
FLOW VISUALIZATION SET-UP

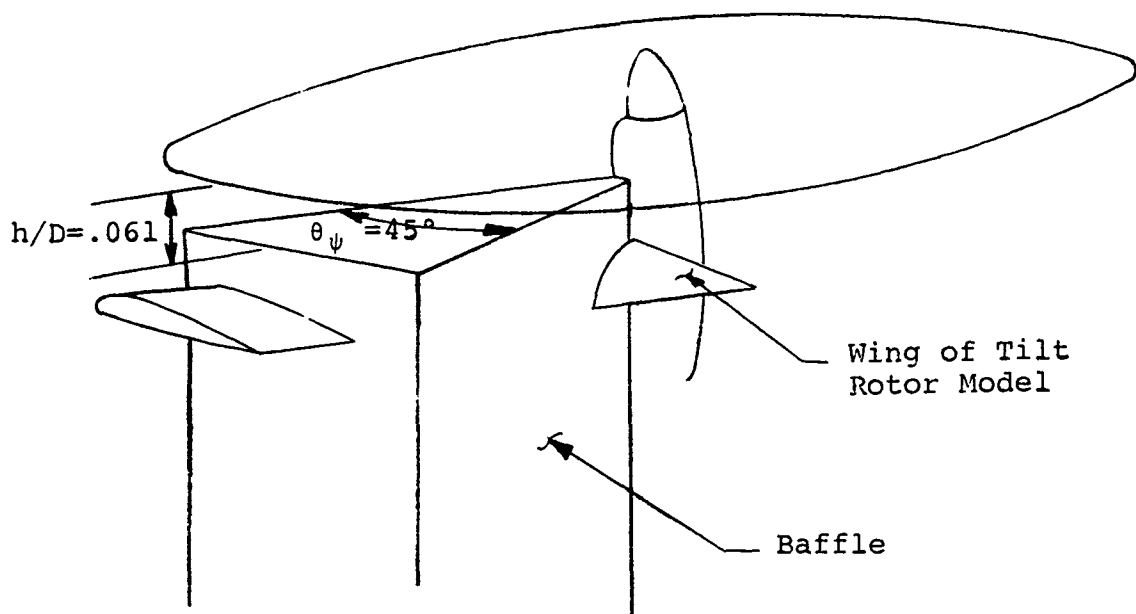


FIGURE 3-6 SKETCH OF ARRANGEMENT OF PIE-SHAPED BAFFLES

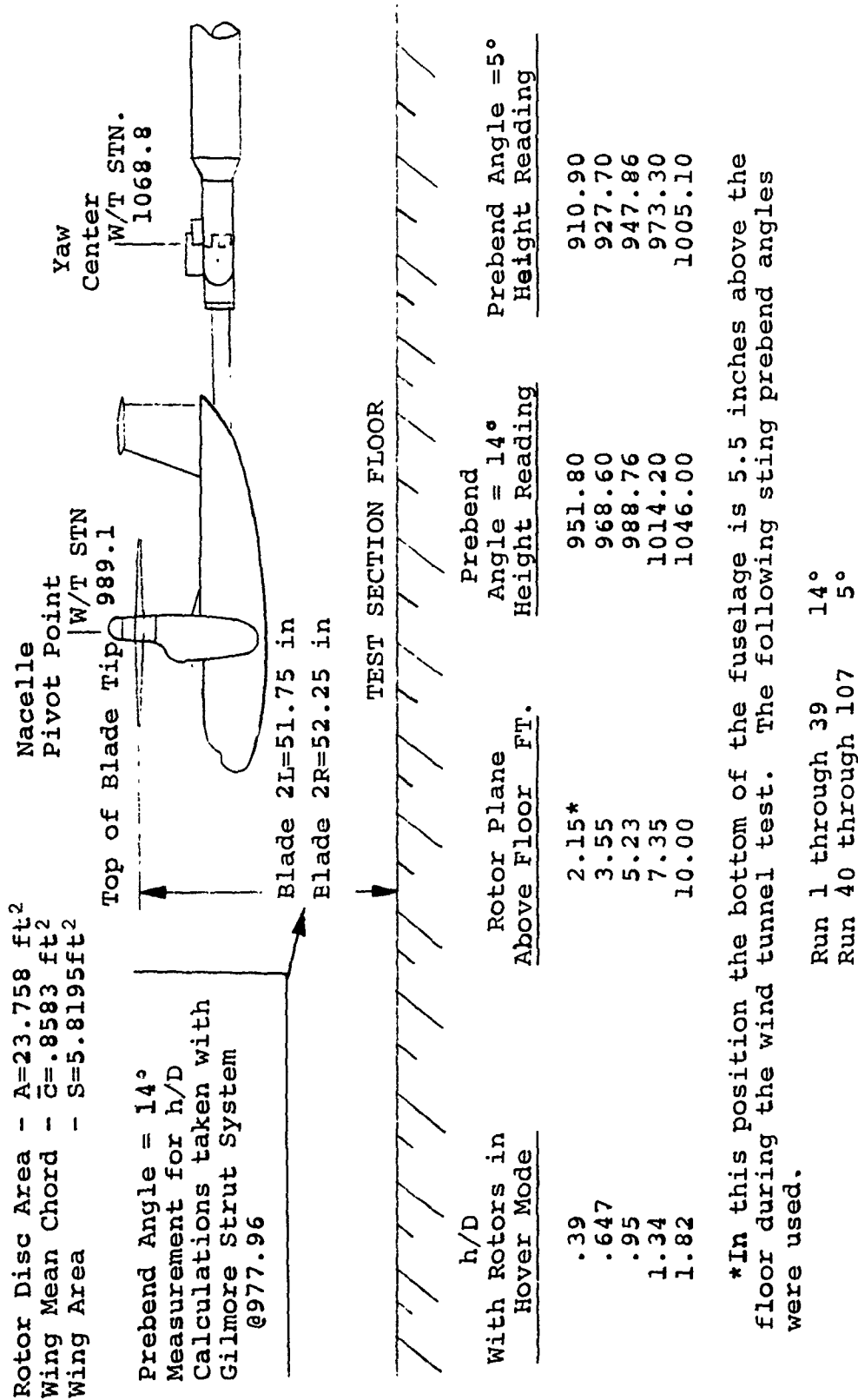


FIGURE 3-7 SKETCH OF MODEL INSTALLATION IN THE TEST SECTION

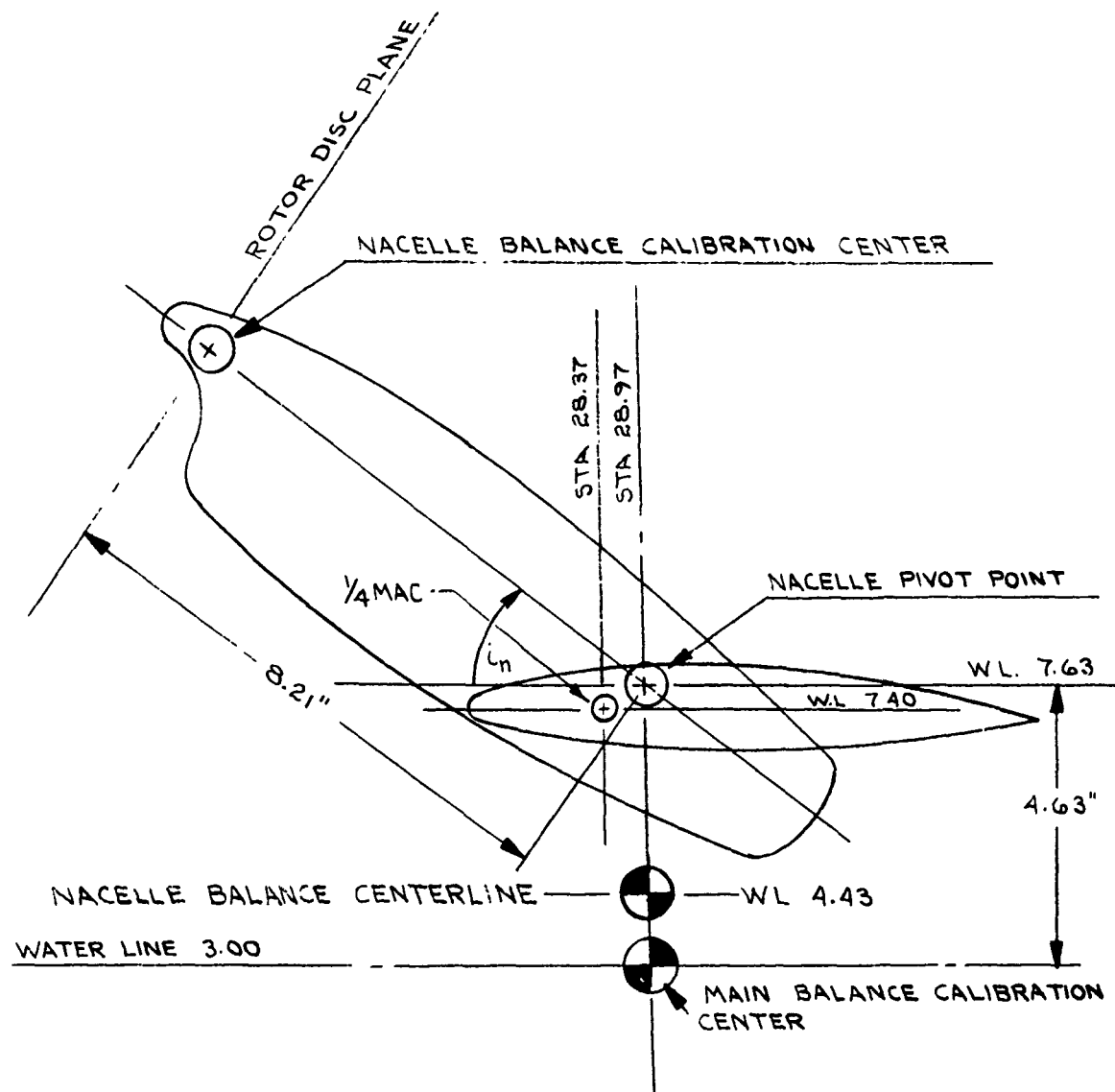


FIGURE 3-8 MODEL REFERENCE CENTER GEOMETRY

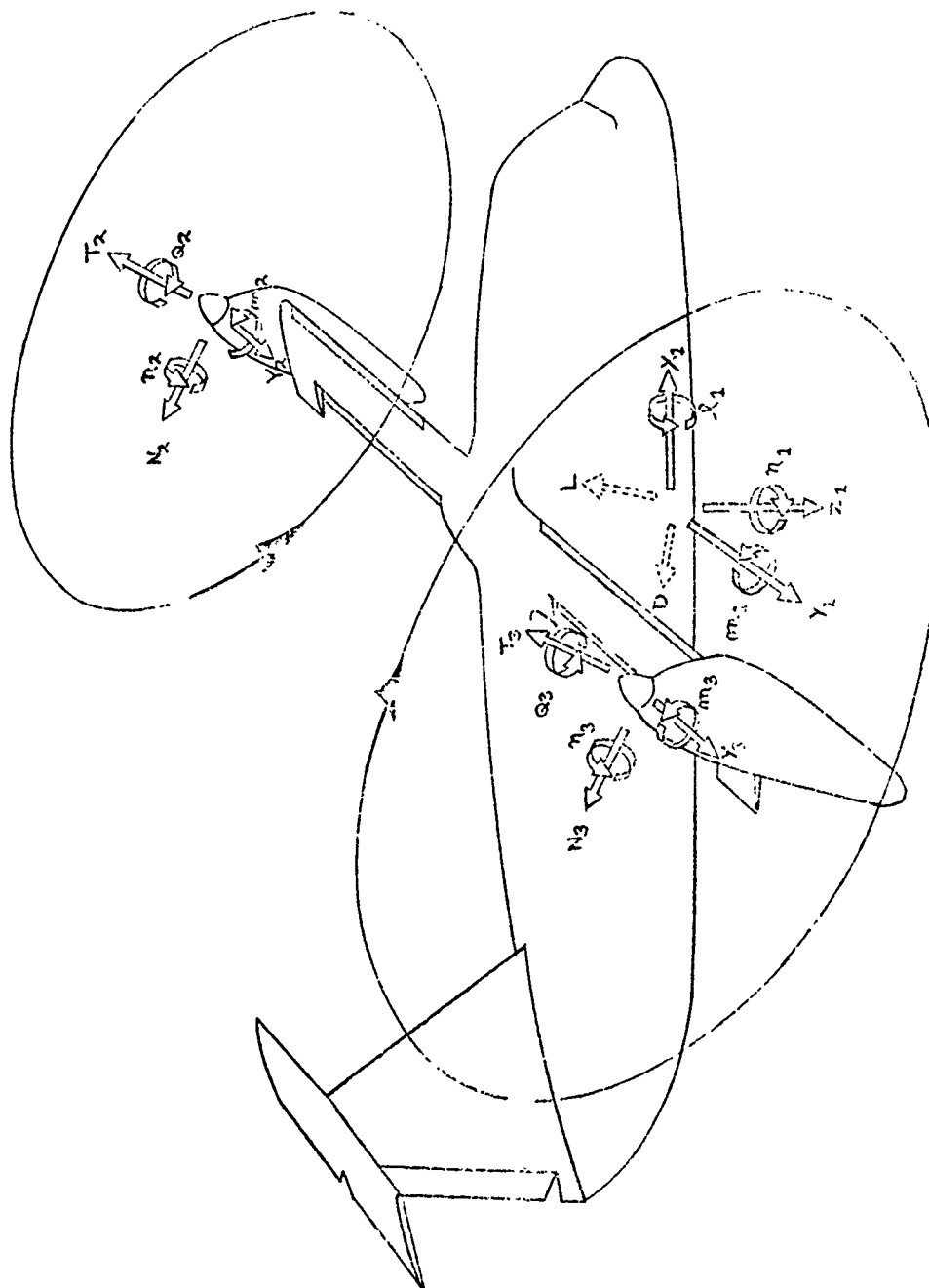


FIGURE 3-9 MODEL 160 WIND TUNNEL MODEL
FORCE AND MOMENT SIGN CONVENTION

4.0 PERFORMANCE

Tests were performed in hover, transition and cruise flight modes and a brief synopsis of the performance data obtained follows.

Total aircraft lift data in hover with and without umbrella flaps are shown in Figure 4-1 for various ground heights together with previous model test and full-scale data. A download of 5 percent of the aircraft thrust occurs out-of-ground effect for this configuration and is reduced as ground height is reduced. Flap and umbrella settings have no effect on the rotor performance; therefore, the minimum download configuration tested produced the best total aircraft performance (Figure 4-2).

Airframe lift data in the STOL mode IGE are shown in Figure 4-3 with previous test data. The data show the presence of a ground cushion in hover ($C_{Tc}=1.0$). The lift due to the ground cushion decreases with speed and vanishes when the downwash tucks under the aircraft. The difference between the ideal line and the data is a measure of the downwash-airframe interference lift.

Performance data was obtained in transition and cruise flight regimes (Figures 4-4 and 4-5) and will be used for correlation with theory in the final report. The data presented here, being greatly influenced by the model rotor dynamic characteristics, cannot be scaled up and be representative of the full scale Model 160 aircraft since the rotors are not dynamically scaled.

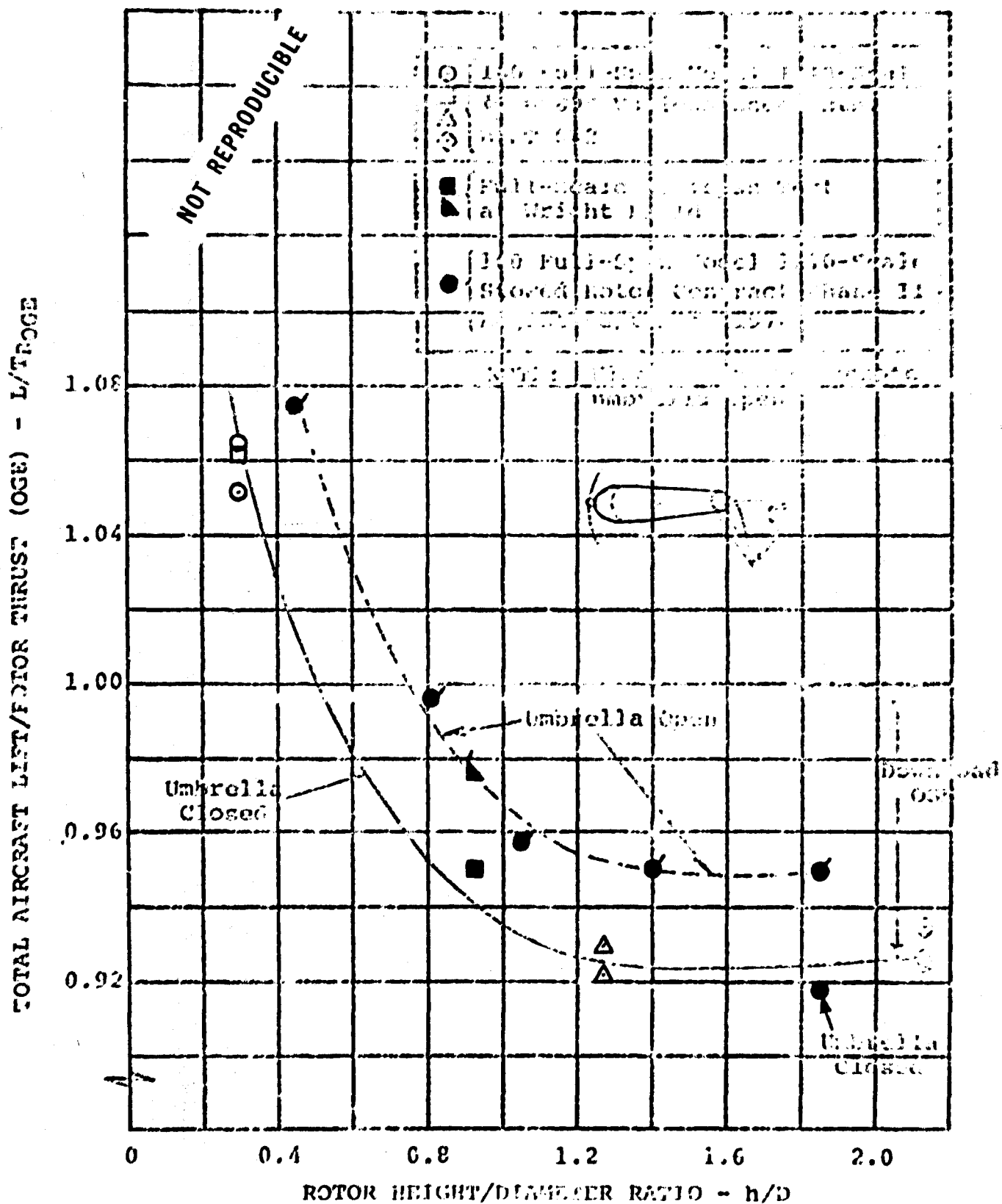


FIGURE 4-1

HOVER DOWNLOAD FROM FULL SCALE AND
MODEL TESTS

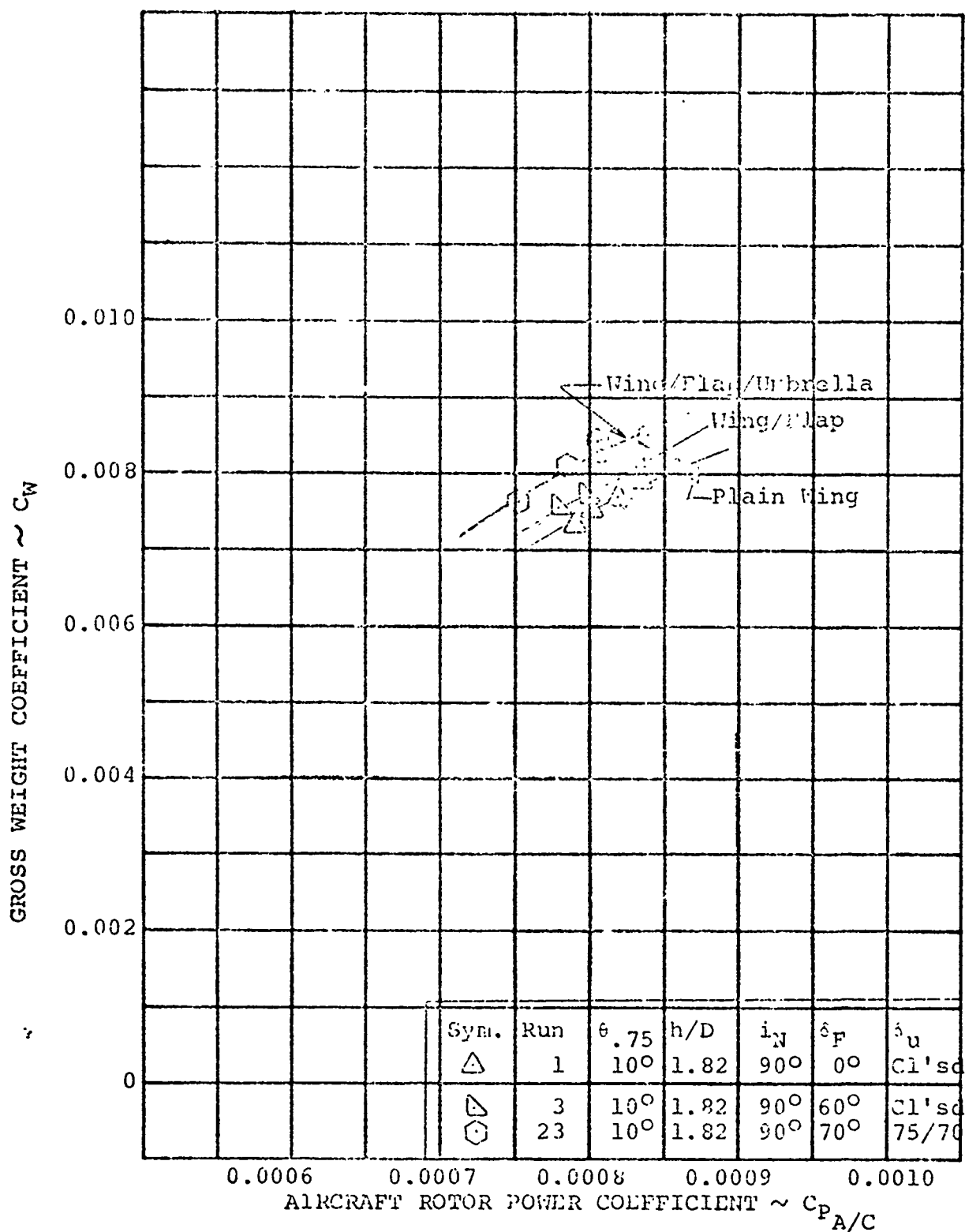


FIGURE 4-2 EFFECT OF UMBRELLA & FLAP ANGLE ON TOTAL AIRCRAFT HOVER PERFORMANCE

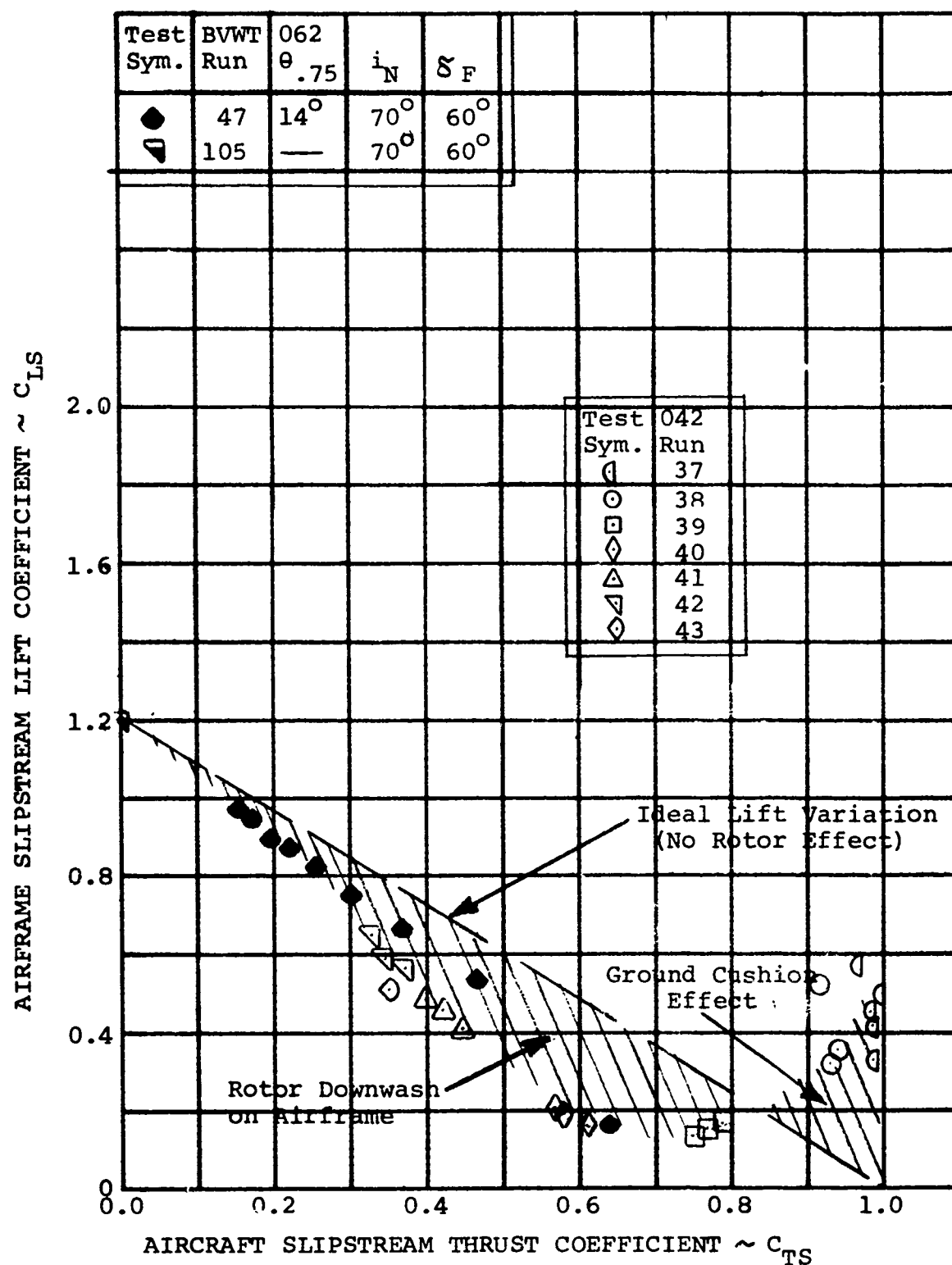


FIGURE 4-3

AIRFRAME LIFT VARIATION DURING IN
GROUND EFFECT TAKE OFF AT $h/D = 0.39$
(ZERO WHEEL HEIGHT)

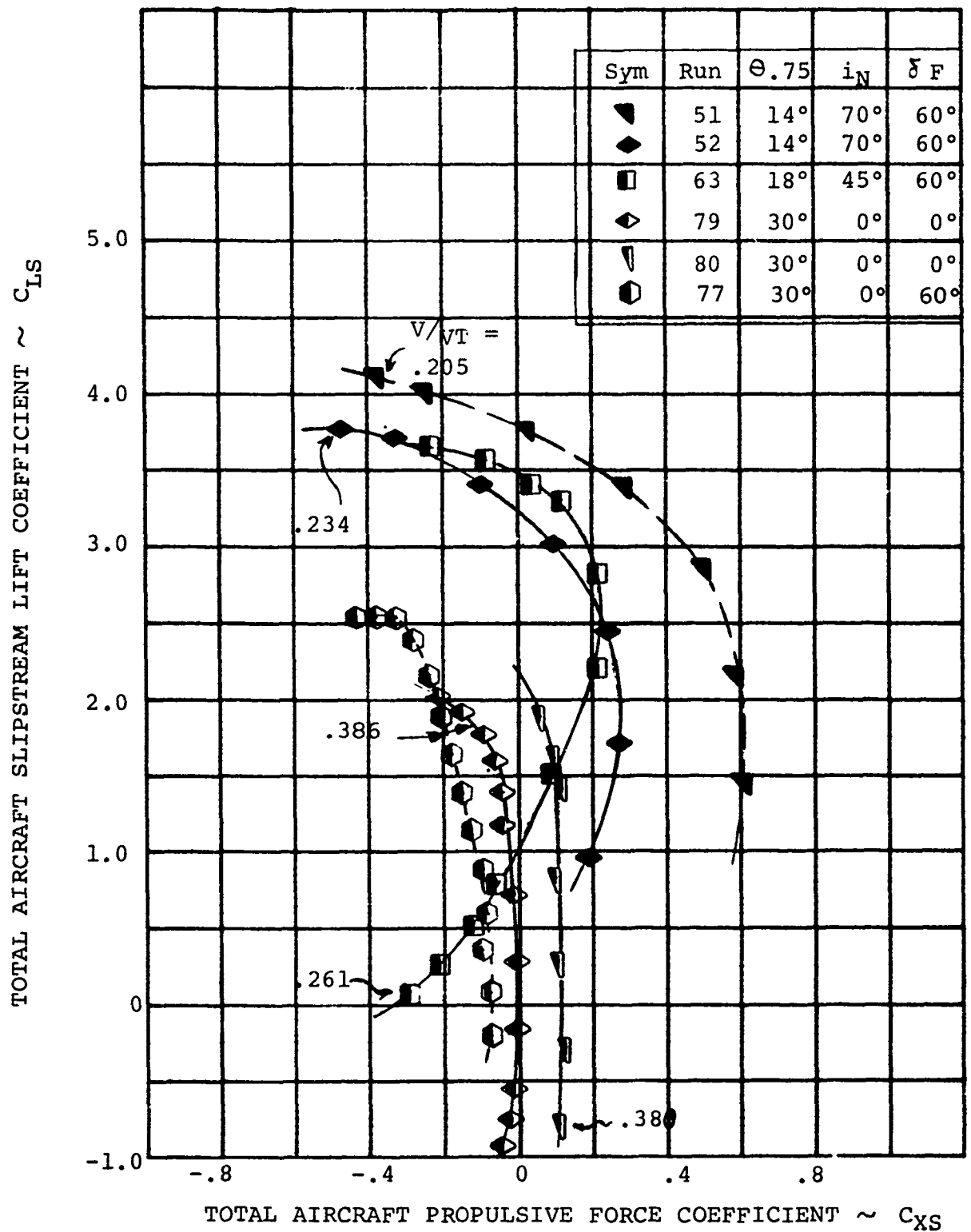


FIGURE 4-4 AIRCRAFT LIFT/PROPULSIVE FORCE VARIATION DURING TRANSITION AND CRUISE

TOTAL AIRCRAFT STREAMLIFT COEFFICIENT ~ C_{LS}

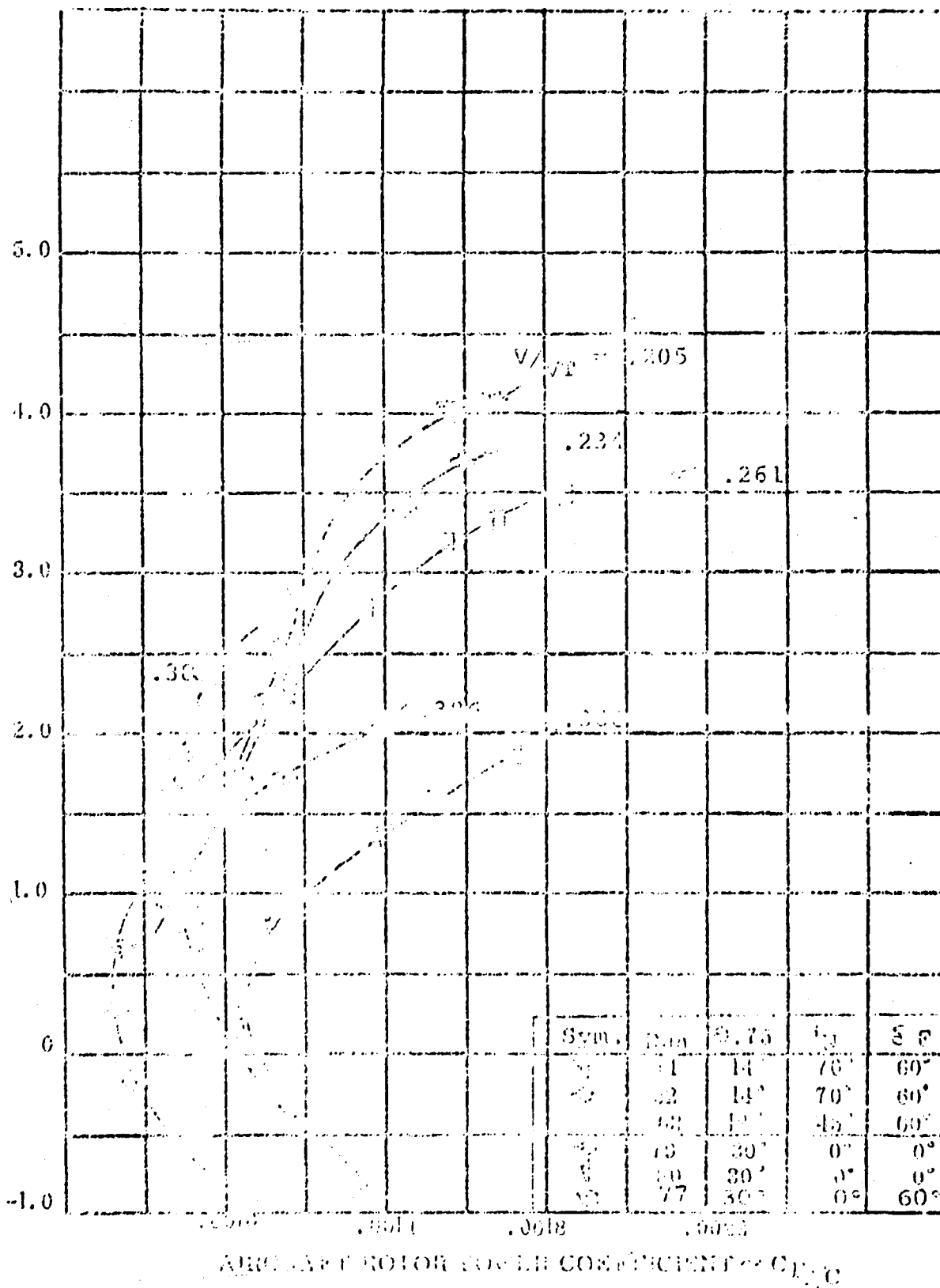


FIGURE 4-5 AIRCRAFT LIFT/ROTOR POWER VARIATION DURING TRANSITION AND CRUISE

4.1 HOVER PERFORMANCE

The hover mode refers to operation with the nacelle incidence at 90-degrees and with zero forward velocity. This discussion addresses download, flow recirculation, rotor performance, and the integration of these in total aircraft performance.

4.1.1 Download and Flow Recirculation

Download

The tilt rotor develops its lift in cruise from a wing and its propulsive force from rotors mounted at the wing tip. To hover the rotors are tilted up 90-degrees to provide vertical thrust, but the rotors are directly over the wing resulting in a download penalty. There are two download reduction devices; umbrella flaps on the leading edge of the wing, and the conventional trailing edge flap. Figure 4-6 illustrates the download of these configurations when hovering out of ground effect as a ratio of download-to-thrust. This ratio is used since the download is a vertical drag that is a function of a drag coefficient of the configuration, exposed area, and the slipstream dynamic pressure which is directly dependent on thrust. Therefore, dividing the vertical drag, or download, by thrust results in a ratio that is dependent only on the product of drag coefficient and the exposed area, which is a constant for a given configuration. The plain wing has a download/thrust ratio of 0.127 or 12.7% of the rotor thrust. Deflecting the 25 percent chord trailing edge flap 60-degrees reduced this to 0.087, a 32 percent reduction in download. Opening the 15 percent chord leading edge umbrellas produced a further reduction in download. This lower umbrella was set at 70-degree, and the upper umbrella was varied. A minimum value of download/thrust ratio of 0.050 was achieved at 75-degrees upper umbrella angle, 70-degrees for the lower umbrella, and the trailing edge flap deflection of 60-degrees, providing a net reduction of 61 percent. With the umbrella angles optimized at 75 and 70-degrees (upper and lower respectively) the flap deflection was varied to determine if any further reduction in download was attainable. This is presented in Figure 4-7 and indicates that a minimum download/thrust ratio of 0.048 was achieved with a 70 degree flap deflection. The download was minimized out of ground effect and the effect of ground height is presented in Figure 4-8. There is a slight decrease in download (0.048 to 0.040) as the height, represented by the ratio of height of the rotor disc above the ground to the rotor diameter, is decreased from 1.82 (out of ground effect) to 1.0. As the height is further reduced the download decreases rapidly to zero at the height/diameter ratio 0.66. At this point there is no download on the airframe and the lift is equal to the rotor thrust. The height is decrease further, to the point equivalent to the landing gear touching the ground, resulting in a negative download/thrust ratio of 0.072. This means that there is an upload equivalent to 7.2 percent of the rotor thrust. It appears to be a result of the rotor downwash creating a pressure pad under the fuselage.

A final area of investigation was the effect of the fuselage angle of attack on download. Figure 4-9 presents this effect and indicates that there is no change in download with angle of attack.

It is concluded from this analysis that the minimum download is achieved by deflecting the umbrella flap angles to 75 for the upper and 70 degrees for the lower flap, and the trailing edge flap to 70 degrees to achieve a download to thrust ratio of 0.048. The prediction technique utilized in Figures 4-7 and 4-8 will be presented in Volume VIII.

Hover Flow Recirculation

The trajectory of the rotor wake was visualized using tuft grids. The high-speed movie film data are summarized for a ground height of $h/D=.39$ in Figure 4-10. At this ground height, the vortices are seen to turn outward and create an upwash over the outer portion of the wing. The vortex trajectories seemed to oscillate over a wide band as indicated by the broken lines. The rotor downwash creates a pressure pad under and around the fuselage resulting in an upward flow around the fuselage. Another zero flow region or high static pressure zone appears under the outboard part of the wing and nacelle causing the rotor downwash to turn. It is thought that this pressure is maintained by the curtain effect of the rotor downwash outside the wing tip.

As the model ground height is increased to $h/D= 0.65$, Figure 4-11, a similar flow field is observed. The regions of zero flow still occur; however, since the turning effect on the rotor downwash is reduced, the static pressures under the model must be smaller as would be anticipated from increased fore and aft leakage.

The upward flow over a large part of the wing at the two ground heights precludes the formation of large wing Karman vortices; no evidence of wing Karman vortices was observed.

4.1.2 Rotor Performance

Rotor performance data was obtained in conjunction with the download testing. Data was obtained for both rotors operating and also with one rotor stopped. Figure 4-12 presents the variation of rotor thrust coefficient with rotor power coefficient for the right and left rotor when operating separately. The resulting trend indicates that the right rotor produces slightly more thrust for the same power. Also included on this figure is the prediction of the rotor performance. The relationship of the prediction and the test data indicates that the rotor blade may be "unwinding" or decreasing the twist as a result of the lift pitch coupling.

For all the configurations tested which have large variations in wing area exposed to the slipstream in hover and therefore various amounts of blockage, there is a potential influence on the rotor performance. The exposed area of the plain wing is 4.1 sq.ft. which is reduced to 3.70 sq.ft. by deflecting the flap 60 degrees and is further reduced by opening the umbrellas ($\delta_u=75^\circ/70^\circ$) to 3.3 sq.ft. However, Figure 4-13 presenting data at rotor tip speeds from 575 ft/sec to 750 ft/sec for the left rotor in the twin rotor configuration, shows essentially no effect from the change in blockage associated with deflecting the flap and then the umbrellas.

A comparison of rotor performance with both rotors operating and with one rotor alone is shown in Figure 4-14. The data indicate an increase in power required when both rotors are operating. This is contrary to tandem rotor helicopter test data which indicates a diminishing interference effect as the overlap approaches zero and suggests the possibility of a favorable effect for negative overlap as tested here. The alternating blade loads data, Section 6 increase with two rotor operating compared with one rotor alone. Model oscillations may be causing data system errors. Further tests are recommended to define the cause of this apparent performance loss.

4.1.3 Aircraft Performance

Total aircraft performance is an integration of the hover download and the rotor performance data discussed in the previous sections. This is presented in Figure 4-15 and shows the variation of the gross weight coefficient with power coefficient for various configurations tested. As indicated in Section 4.1.2, the changes in umbrella and flap setting do not affect the rotor performance. Therefore, the only difference will be a result of the download variation with the configuration changes. The level shifts in Figure 4-15 are commensurate with download variation in Section 4.1.1.

Reflected here is the increase in download/thrust ratio from 0.048 to 0.087 resulting from the umbrellas being closed. The lowest level of performance shown here represents the 0.127 download/thrust ratio associated with the plain wing with the flaps not deflected. This indicates that the best performance is obtained with the flap deflected 70 degrees and the umbrella flaps set at 75 and 70 degrees for the upper and lower flaps respectively.

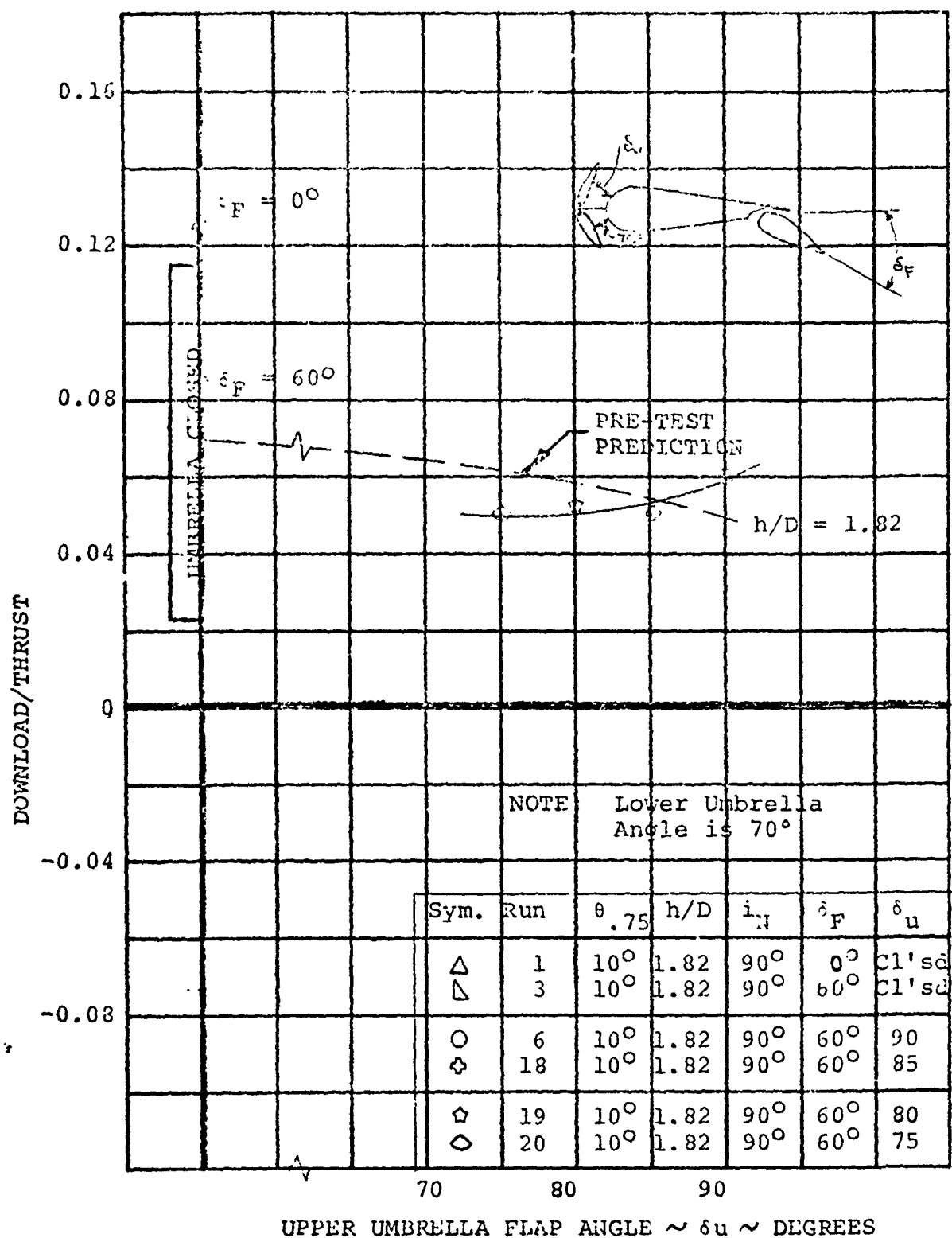


FIGURE 4-6 EFFECT OF UMBRELLA FLAP ANGLE ON AIRCRAFT HOVER DOWNLOAD/THRUST RATIO

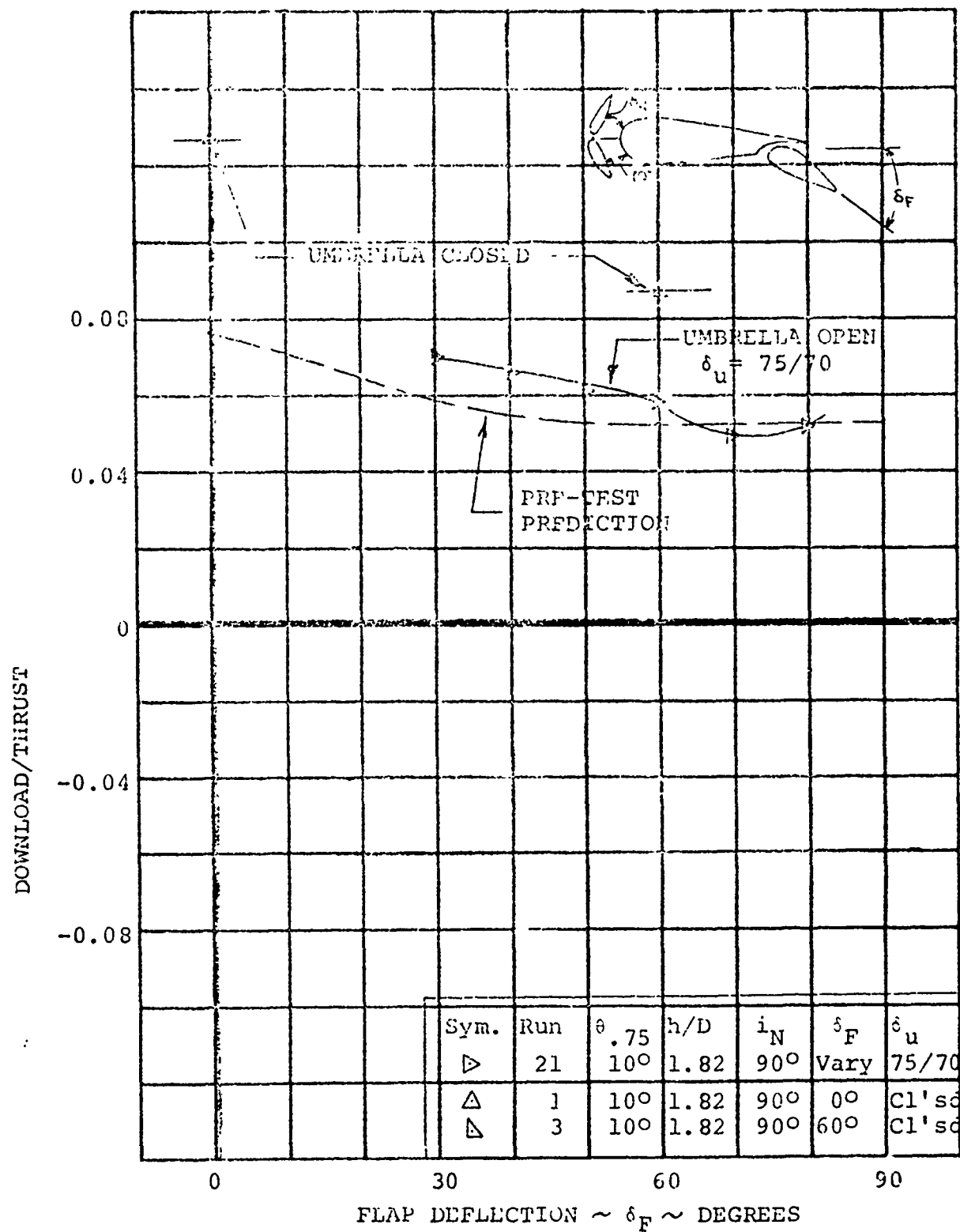


FIGURE 4-7 EFFECT OF FLAP DEFLECTION ON AIRCRAFT HOVER DOWNLOAD/THRUST RATIO

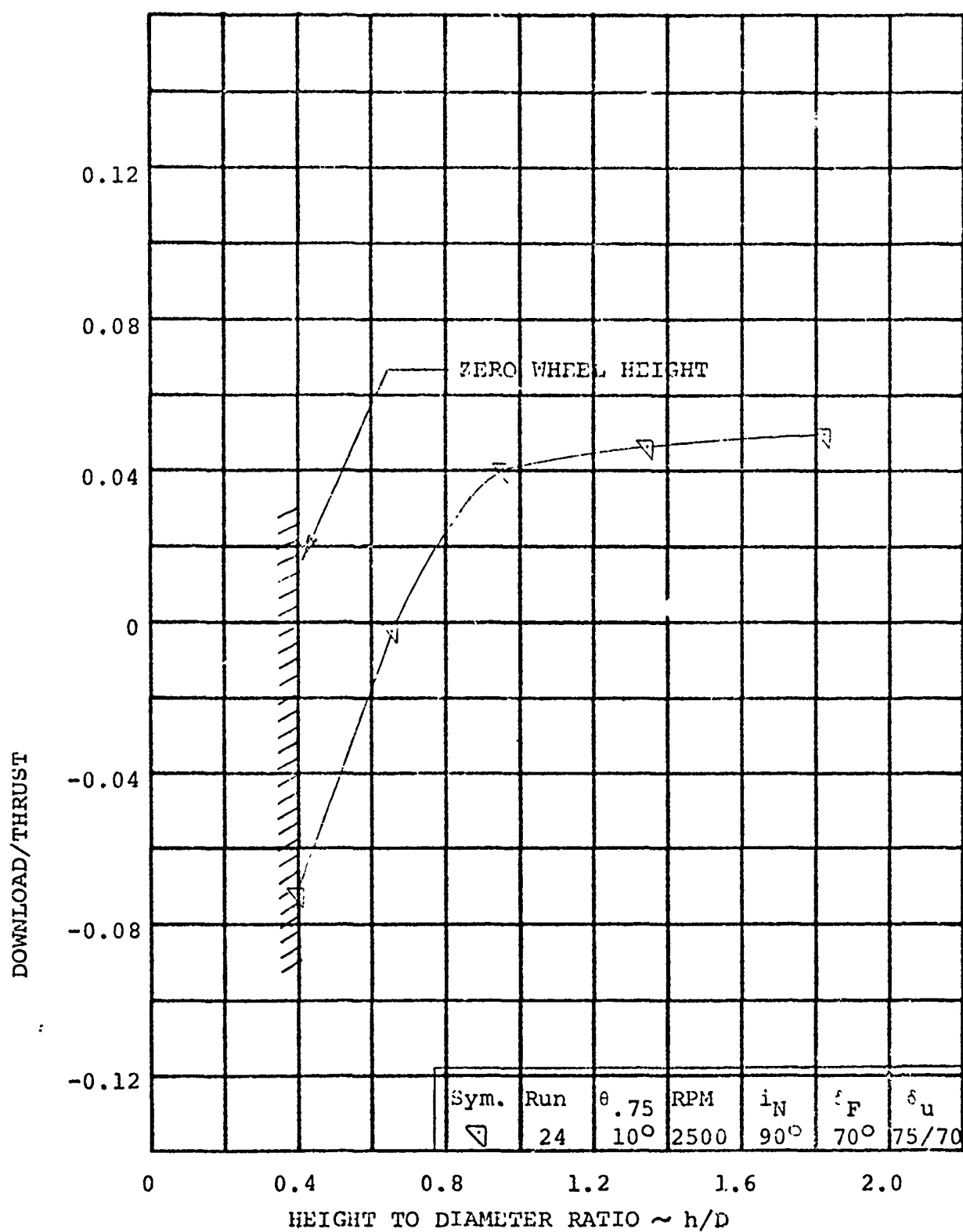


FIGURE 4-8 EFFECT OF GROUND HEIGHT ON AIRCRAFT HOVER
DOWNLOAD/THRUST RATIO

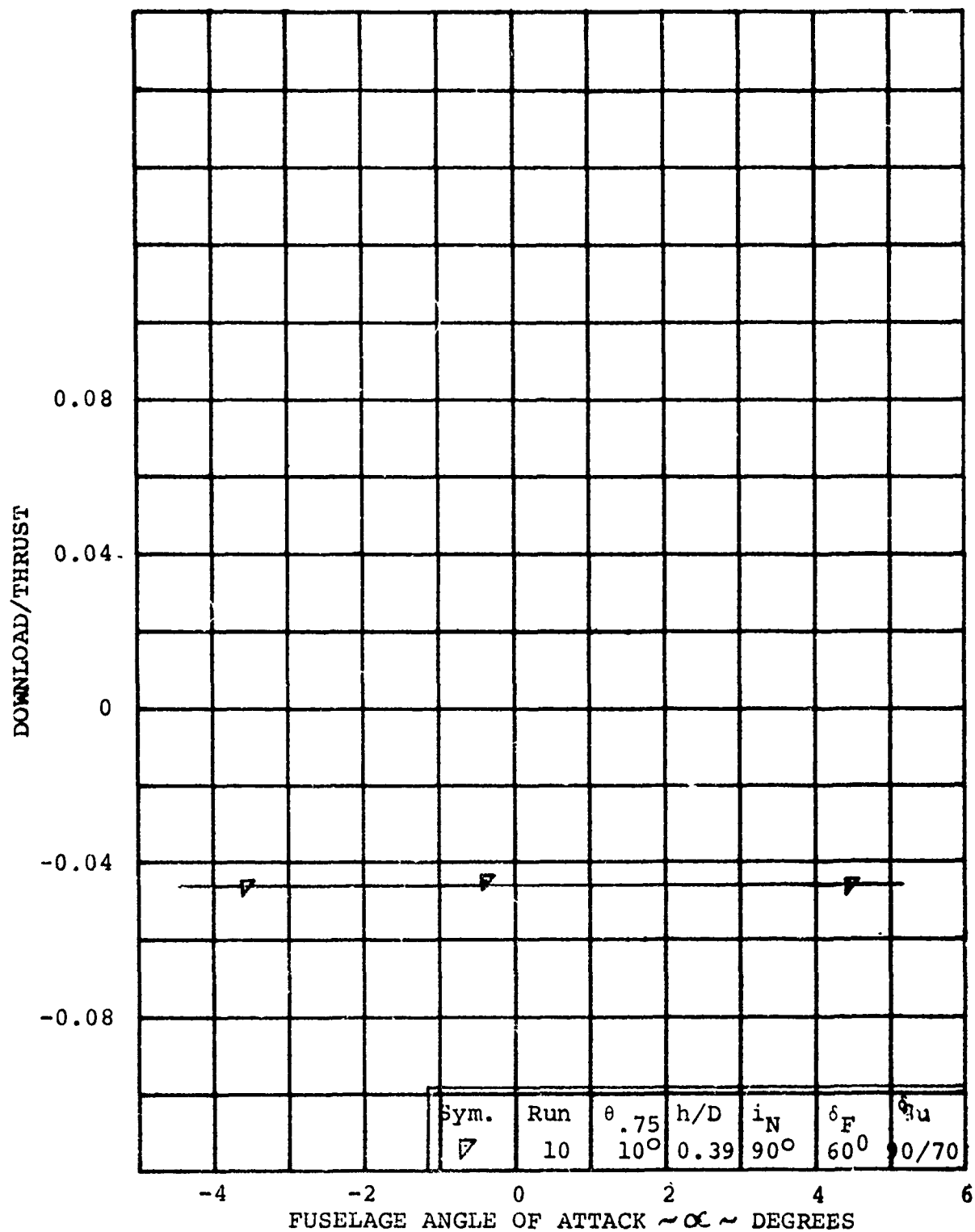


FIGURE 4-9

EFFECT OF FUSELAGE ANGLE OF ATTACK ON
AIRCRAFT HOVER DOWNLOAD/THRUST RATIO

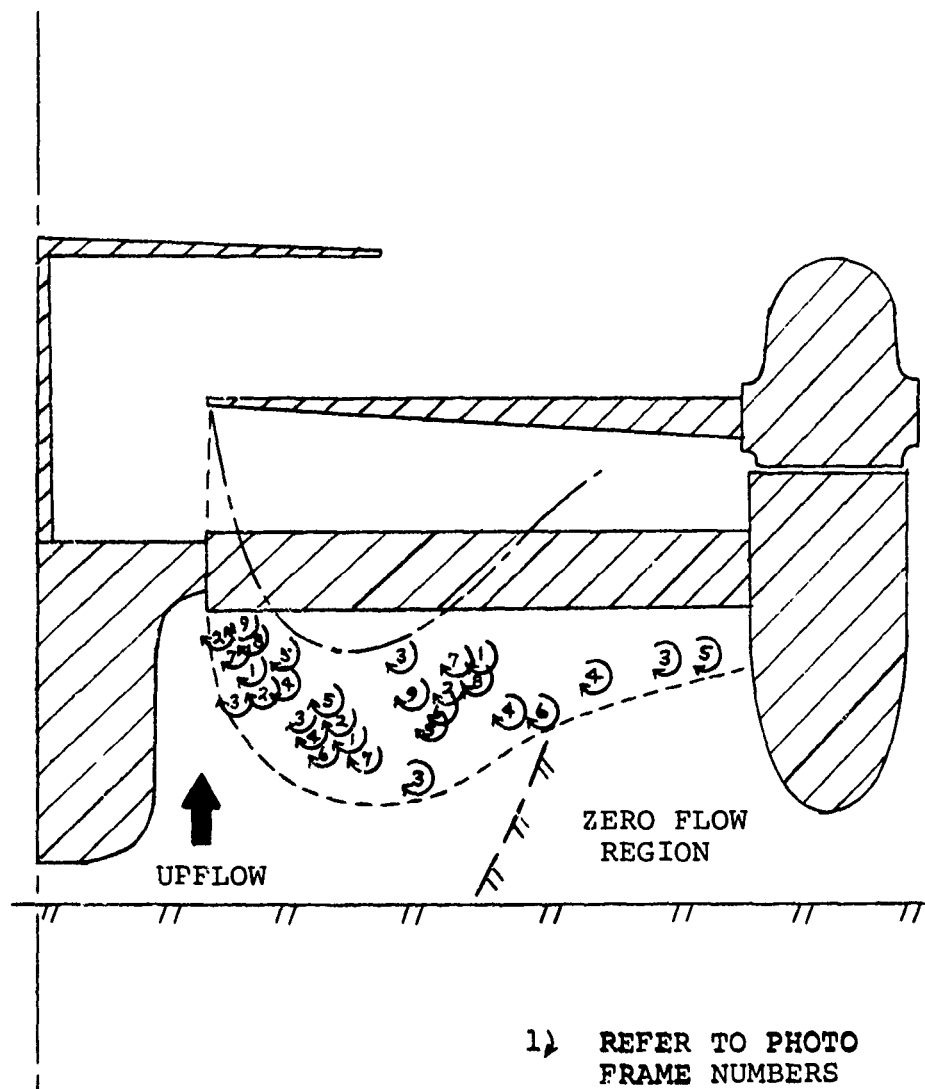


FIGURE 4-10

BLADE TIP VORTEX TRAJECTORIES AT
 $h/D = 0.39$

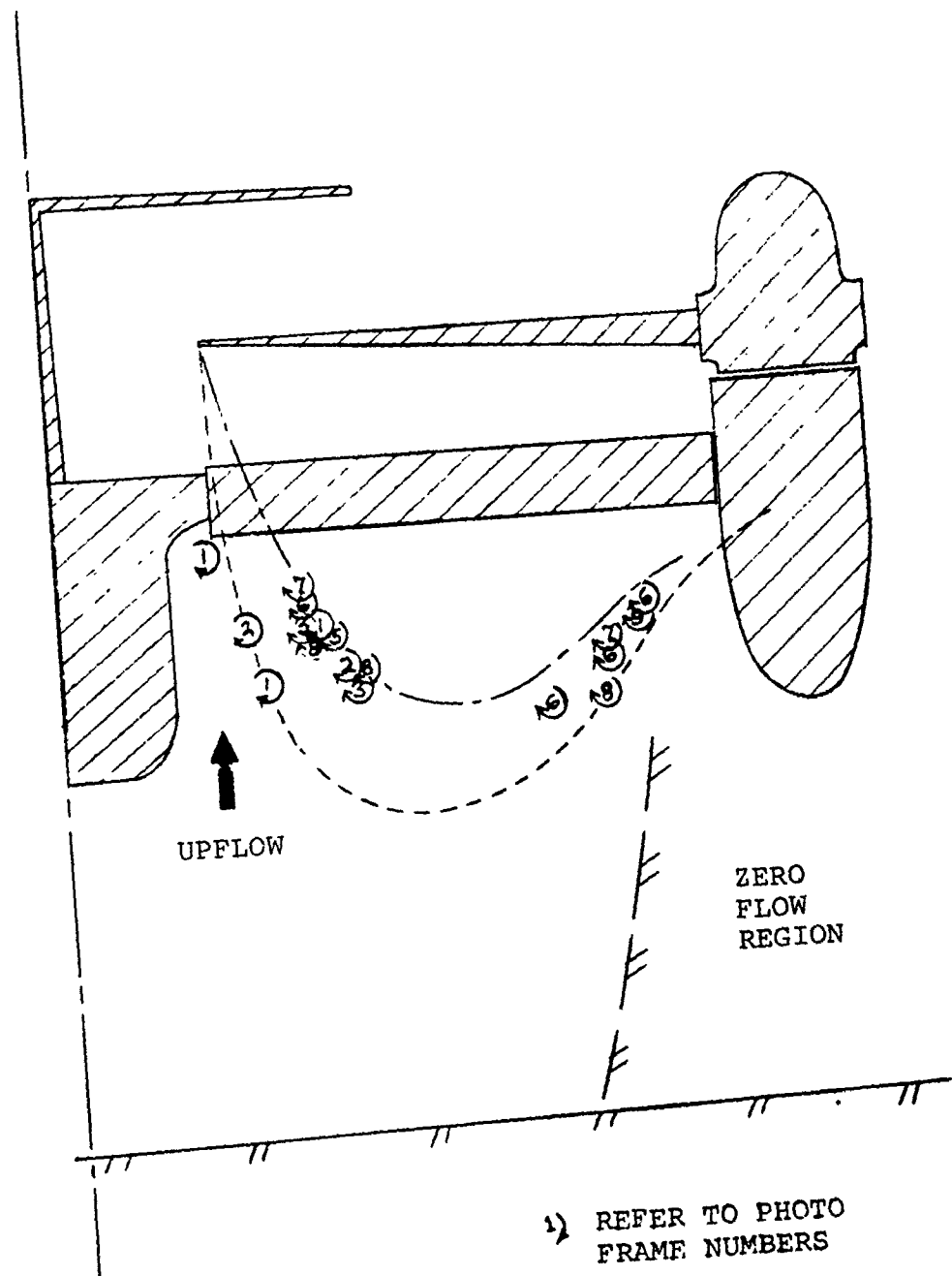


FIGURE 4-11

BLADE TIP VORTEX TRAJECTORIES AT
 $h/D = 0.65$

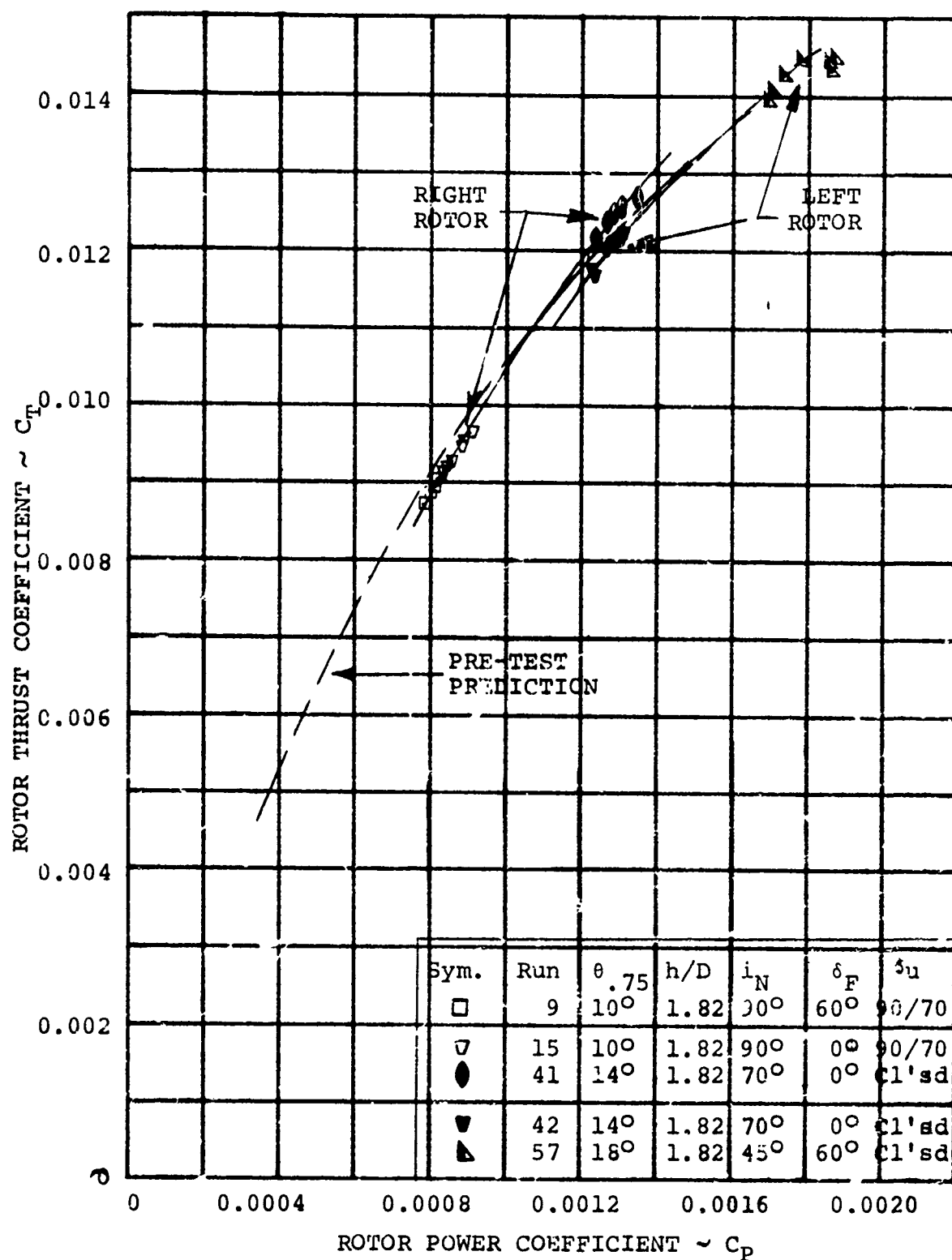


FIGURE 4-12 ISOLATED ROTOR HOVER PERFORMANCE (OUT OF GROUND EFFECT)

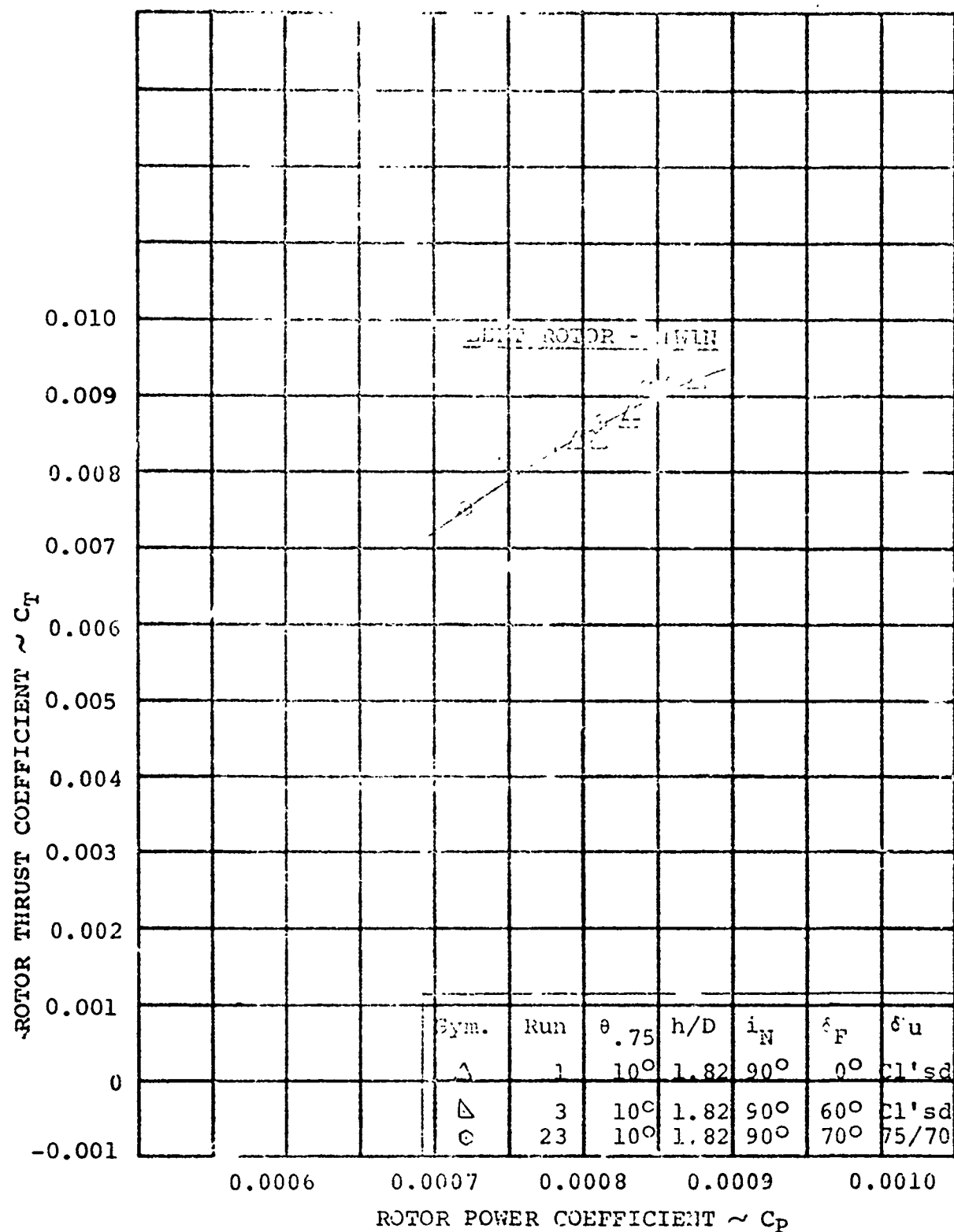


FIGURE 4-13 EFFECT OF UMBRELLA & FLAP ANGLE ON ROTOR HOVER PERFORMANCE

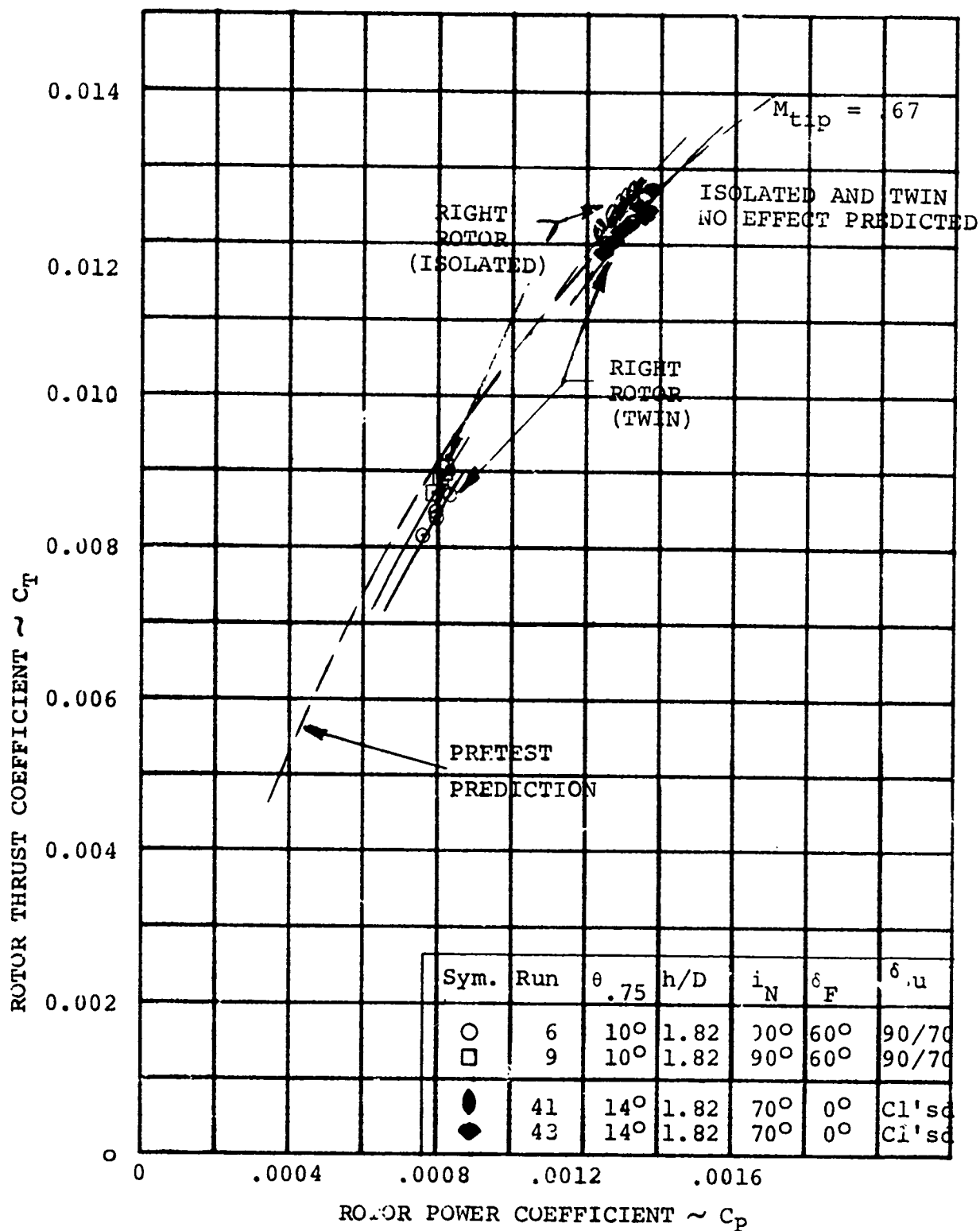


FIGURE 4-14 ROTOR/ROTOR INTERFERENCE EFFECTS ON HOVER PERFORMANCE

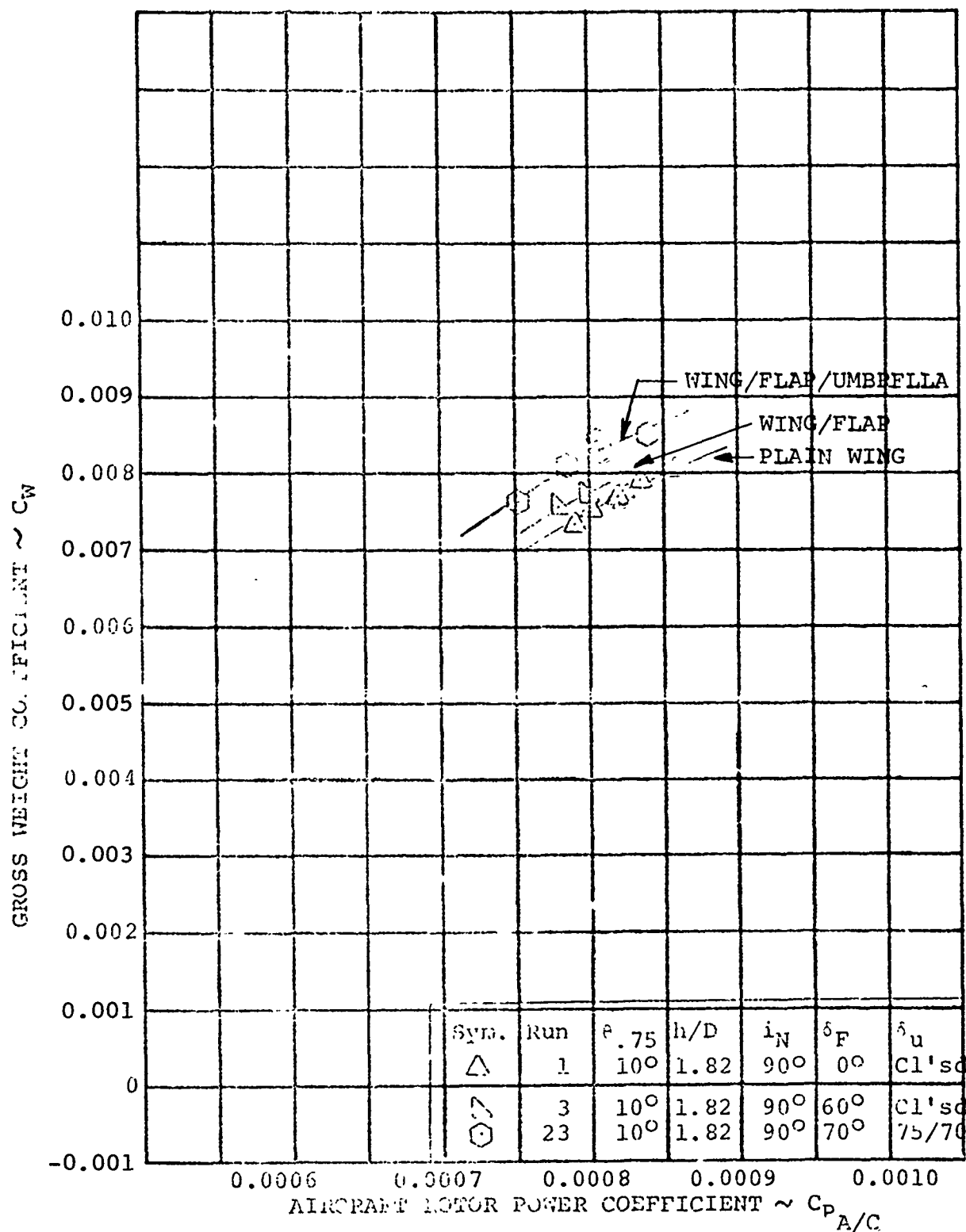


FIGURE 4-15 EFFECT OF UMBRELLA & FLAP ANGLE ON TOTAL AIRCRAFT HOVER PERFORMANCE

4.2 STOL PERFORMANCE

For the STOL flight regime, two primary performance areas investigated in this testing were the ground run and the climbout. The ground run was made with a nacelle incidence of 70-degrees and a rotor height-to-diameter (h/D) ratio of 0.39, equivalent to a wheel height of zero feet. A nacelle incidence of 70-degrees was utilized since it will provide the takeoff distance over a 50 foot obstacle of 500 feet as indicated in Reference 10. The climb-out was made at an acceleration of 0.1 "g's from a zero wheel height to the out of ground effect regime ($h/d=1.82$).

4.2.1 Rotor Airframe Interactions

In the STOL takeoff the rotor wake has a significant impact on the performance characteristics of the aircraft as a result of the interactions with the airframe. In hover and very low forward speeds the ground cushion produces an increment in lift. At higher speeds the rotor wake tucks under eliminating the ground cushion and the rotor downwash produces a download which decreases with increasing forward speed.

It was of major importance to establish that the ground cushion effect that existed in hover at this ground height had been eliminated before climb-out was initiated. If not the aircraft would settle after the climb-out had begun since the ground effect decreases very rapidly with increased height. Figure 4-16 presents the variation of airframe slipstream lift coefficient with aircraft slipstream thrust coefficient (C_{TS}) for the ground run. Slipstream thrust coefficient has a value of 1.0 at zero forward speed and approaches a value of zero at high forward speed. If the rotor produced no ground cushion or downwash on the airframe then the airframe lift variation would be a straight line; zero in hover ($C_{TS}=1.0$), and 1.2 in high speed flight ($C_{TS}=0$) as shown in Figure 4-16 by the ideal lift variation. The variation of the slipstream thrust coefficient with advance ratio in the ground run is presented in Figure 4-17. For the break-ground condition defined by the 0.1 "g" acceleration, the aircraft slipstream thrust coefficient is 0.36 which indicates in Figure 4-16 that the aircraft is beyond the point in transition where the ground cushion has been lost. The rotor downwash reduces the airframe slipstream lift coefficient by 0.1, approximately three percent of the total aircraft lift. Also shown on this figure is data obtained from the previous test of the 1/10 scale performance model, Reference 9, for a similar configuration. The ground cushion decreases to zero at C_{TS} of 0.83 as the rotor wake tucks under the aircraft and the rotor downwash effect becomes predominant.

4.2.2 Rotor Performance

For the STOL flight regime, testing was conducted for the ground run with a nacelle incidence of 70-degrees and at a rotor height-to-diameter ratio of 0.39 equivalent to a wheel height of zero feet. Figure 4-18 presents the rotor thrust variation during the ground run for the left and right rotors and indicates that rotor thrust gradually decreases with increasing advance ratio. The associated rotor power is presented in Figure 4-19.

Testing was performed in the climb-out at an advance ratio of 0.206 which was defined by a propulsive force to lift force ratio (X/L) of 0.1. Figures 4-20 and 4-21 present the rotor thrust and power variations for the left and right rotors from zero wheel height ($h/D=0.39$) to the out of ground effect condition ($h/D=1.82$). There was a slight decrease in thrust and power as the height/diameter ratio was increased to 0.8 and any further increase in height did not produce any change in thrust or power.

4.2.3 Aircraft Performance

The total aircraft performance for the ground run was obtained with a nacelle incidence of 70-degrees and an equivalent zero wheel height ($h/D=0.39$). Figures 4-22 and 4-23 present, for this condition, the variation of the aircraft slipstream lift and propulsive force coefficient with advance ratio. These data were combined in Figure 4-24 to show the acceleration capability during the ground run by presenting the propulsive force variation with lift. A 0.1 "g" acceleration, indicated on this figure by the dashed line, defined the breakground condition at which the climb-out was investigated. Figure 4-25 presents the variation of the rotor power coefficient with advance ratio for the ground run indicating a constant power takeoff.

Climb-out performance is presented in Figures 4-26 through 4-28 indicating the aircraft lift, propulsive force and rotor power variations with rotor height-to-diameter ratio. There is a slight decrease in the lift and power as the rotor height is increased. Associated with this is approximately a 15 percent decrease in propulsive force, but the net acceleration only decreases to 0.09 "g's".

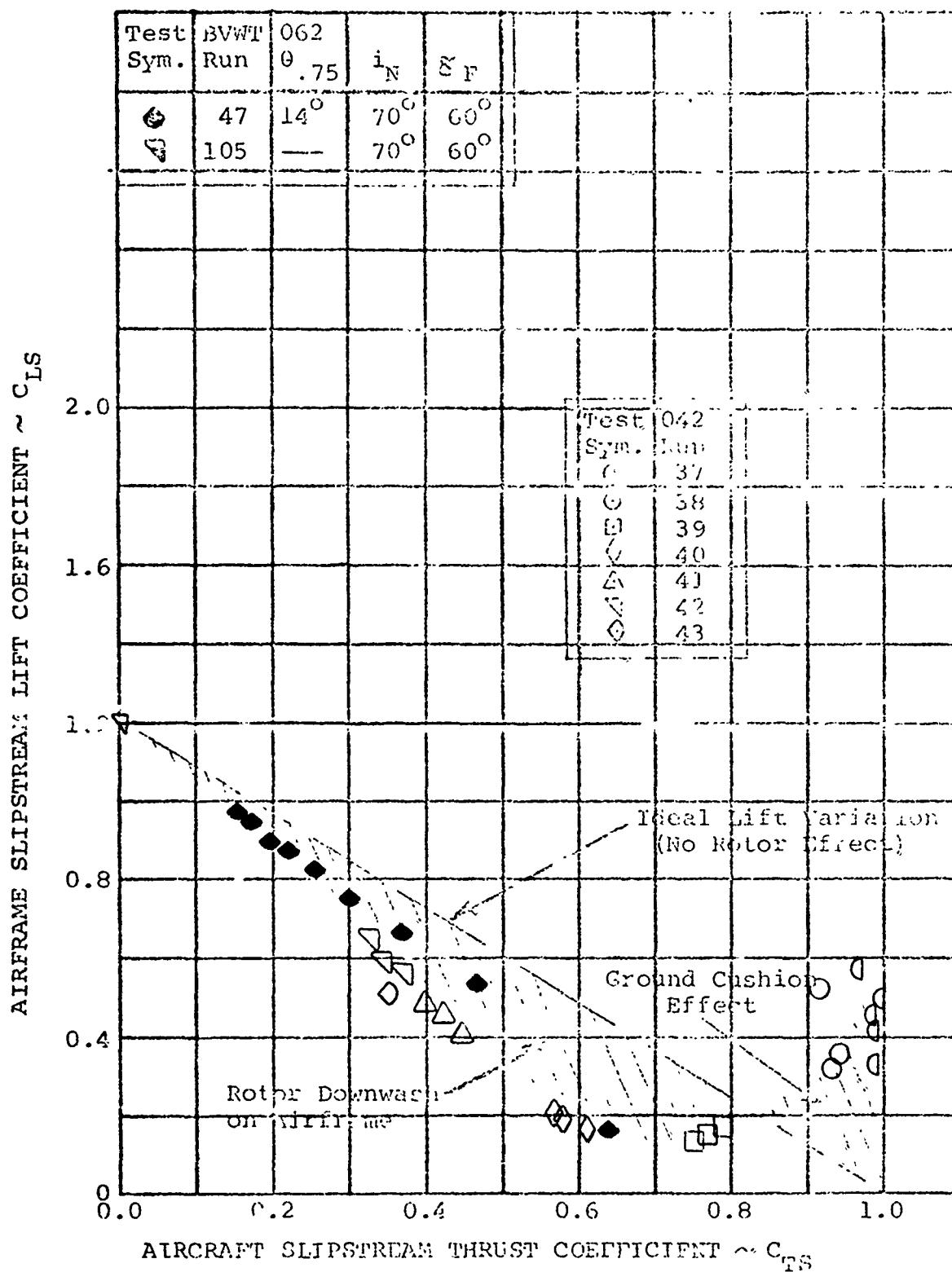


FIGURE 4-16

AIRFRAME LIFT VARIATION DURING IN
GROUND EFFECT TAKE OFF AT $h/D = 0.39$

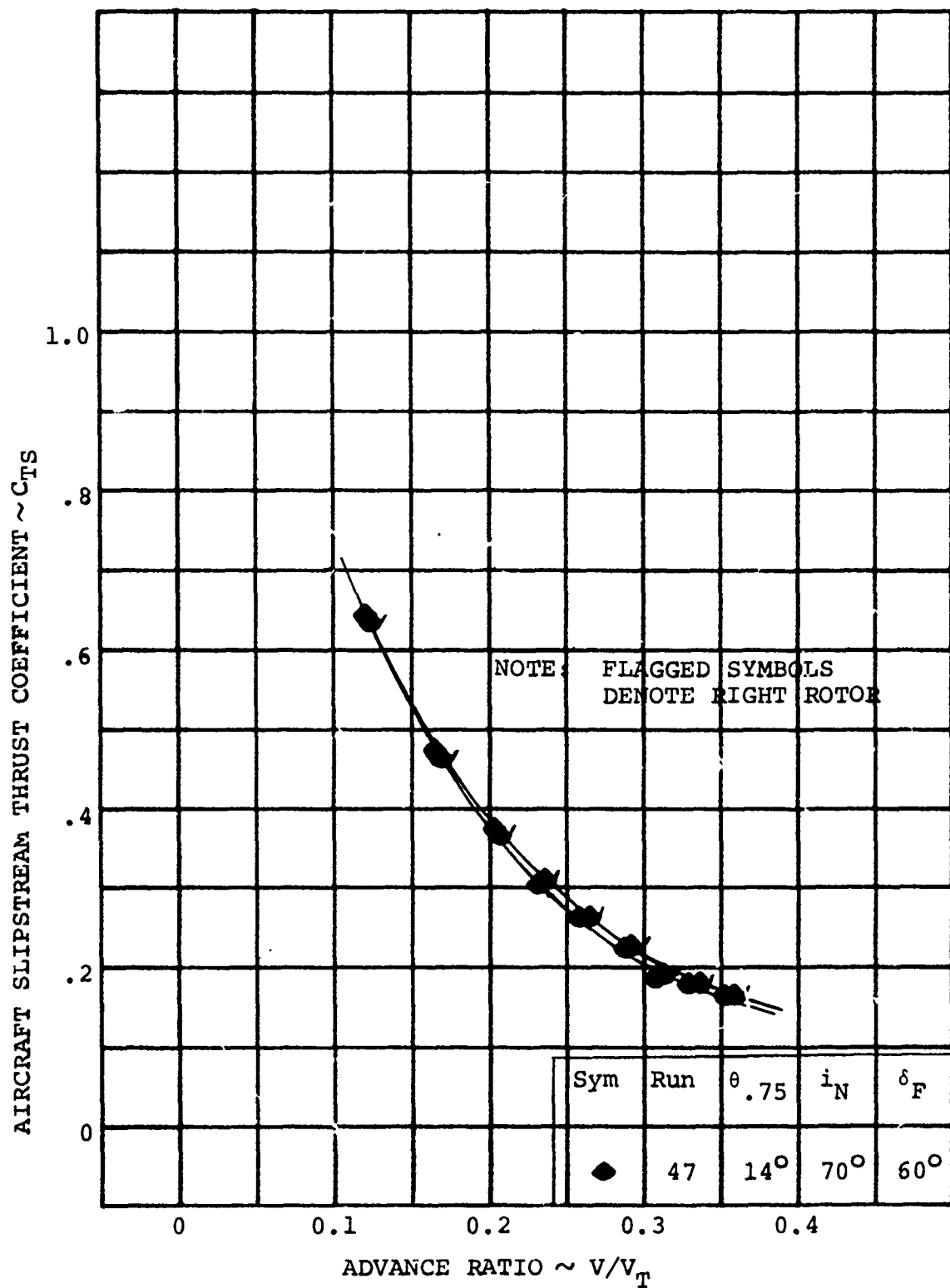


FIGURE 4-17

AIRCRAFT SLIPSTREAM THRUST COEFFICIENT
DURING IN GROUND EFFECT TAKEOFF AT
 $h/D = 0.39$

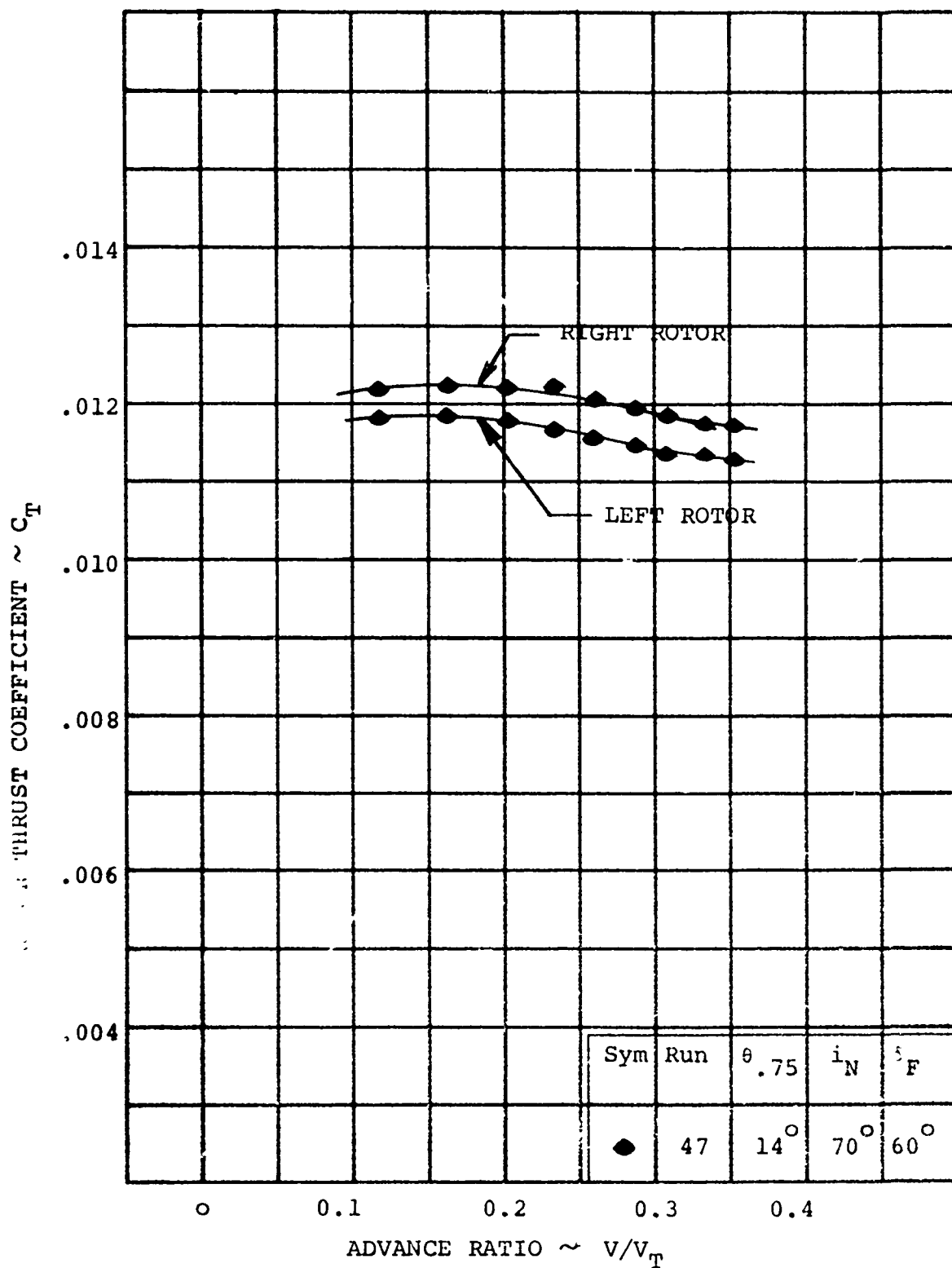


FIGURE 4-18

ROTOR THRUST VARIATION DURING IN GROUND EFFECT TAKEOFF AT $h/D = 0.39$

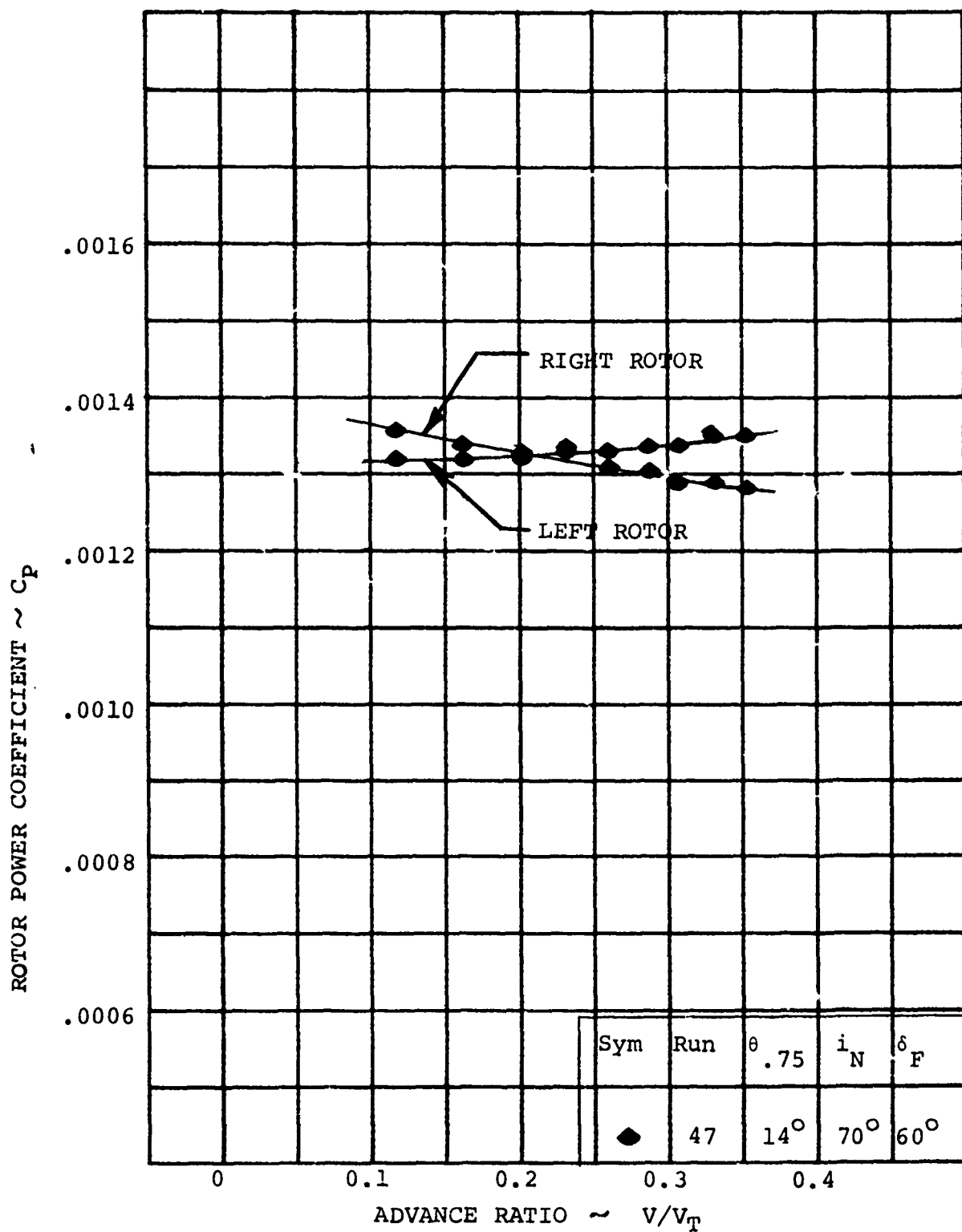


FIGURE 4-19

ROTOR POWER VARIATION DURING IN GROUND
EFFECT TAKEOFF AT $h/D = 0.39$

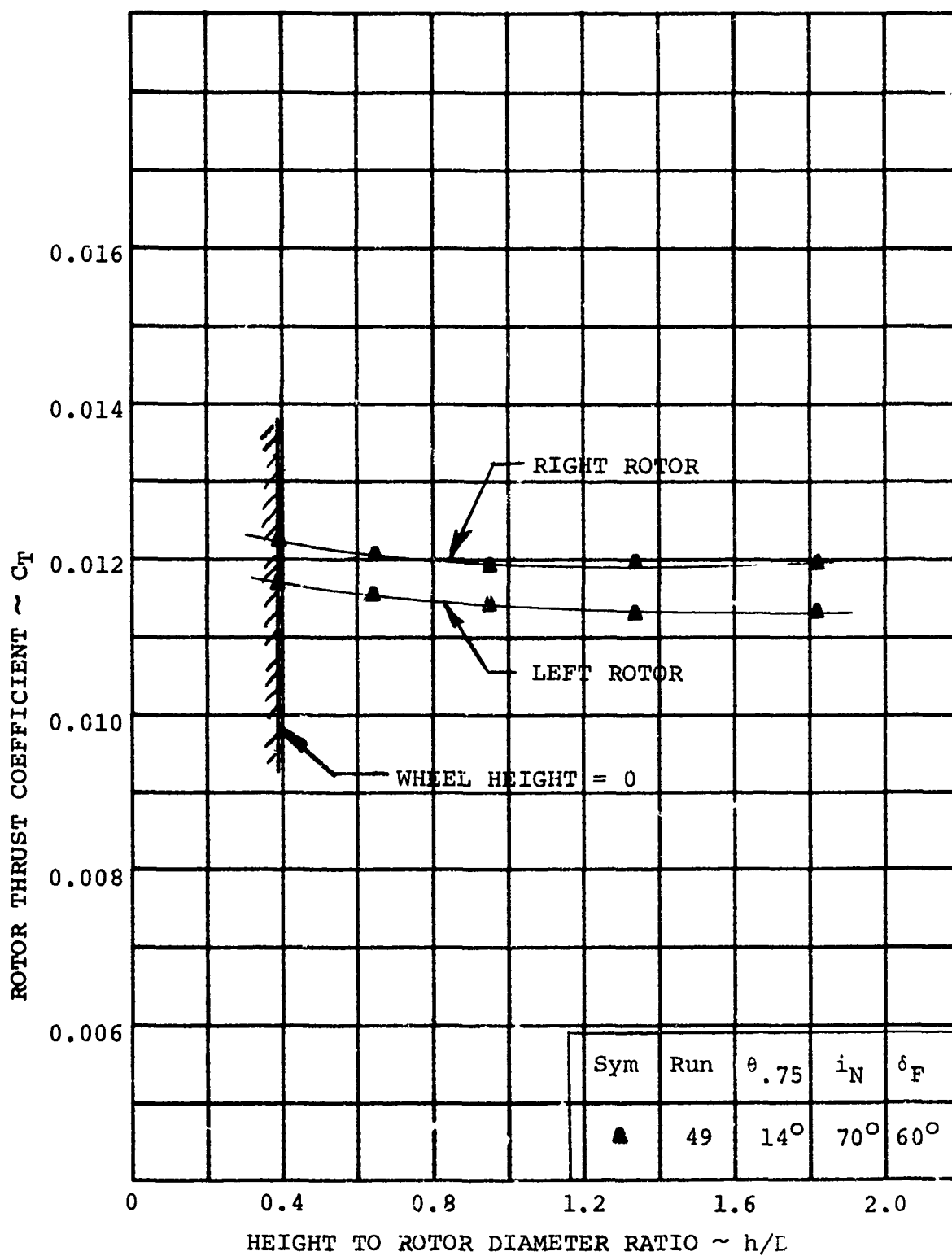


Figure 4-20 ROTOR THRUST VARIATION DURING
STOL CLIMB-OUT AT $V/V_T = 0.206$

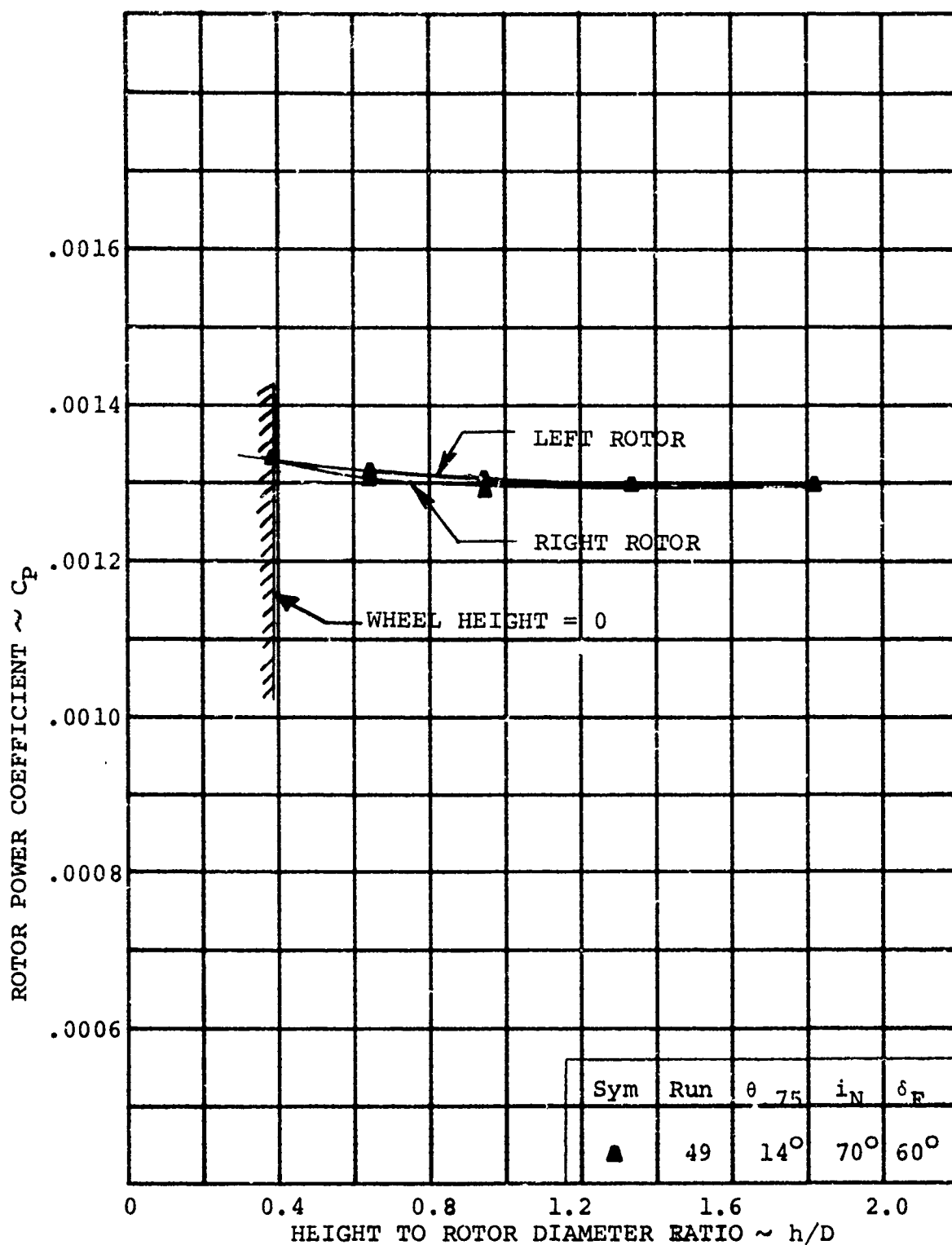


FIGURE 4- Δ 1 ROTOR POWER VARIATION DURING
STOL CLIMB-OUT AT $V/V_T = 0.206$

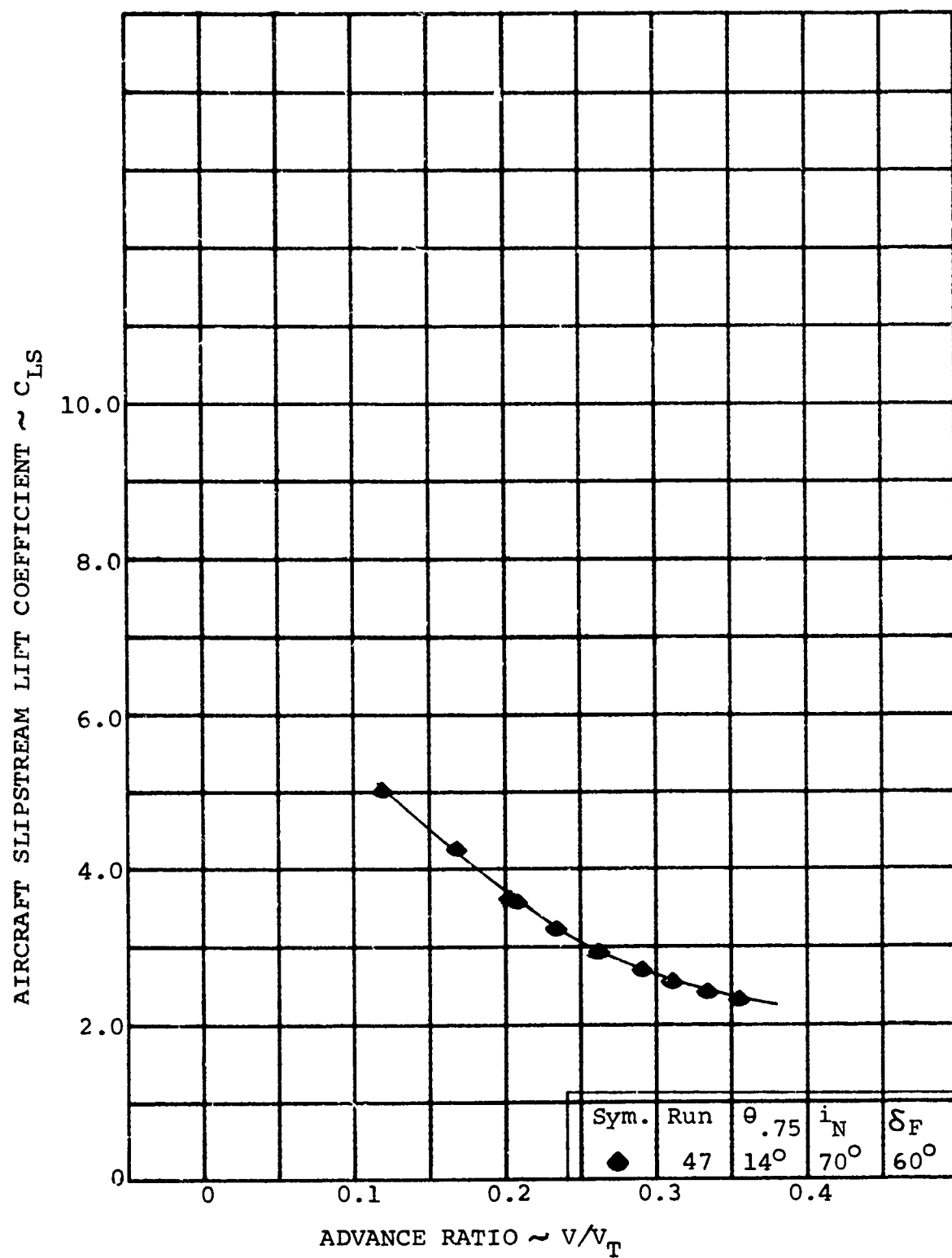


FIGURE 4-22

AIRCRAFT LIFT VARIATION DURING IN GROUND EFFECT TAKE OFF AT $h/i = 0.39$

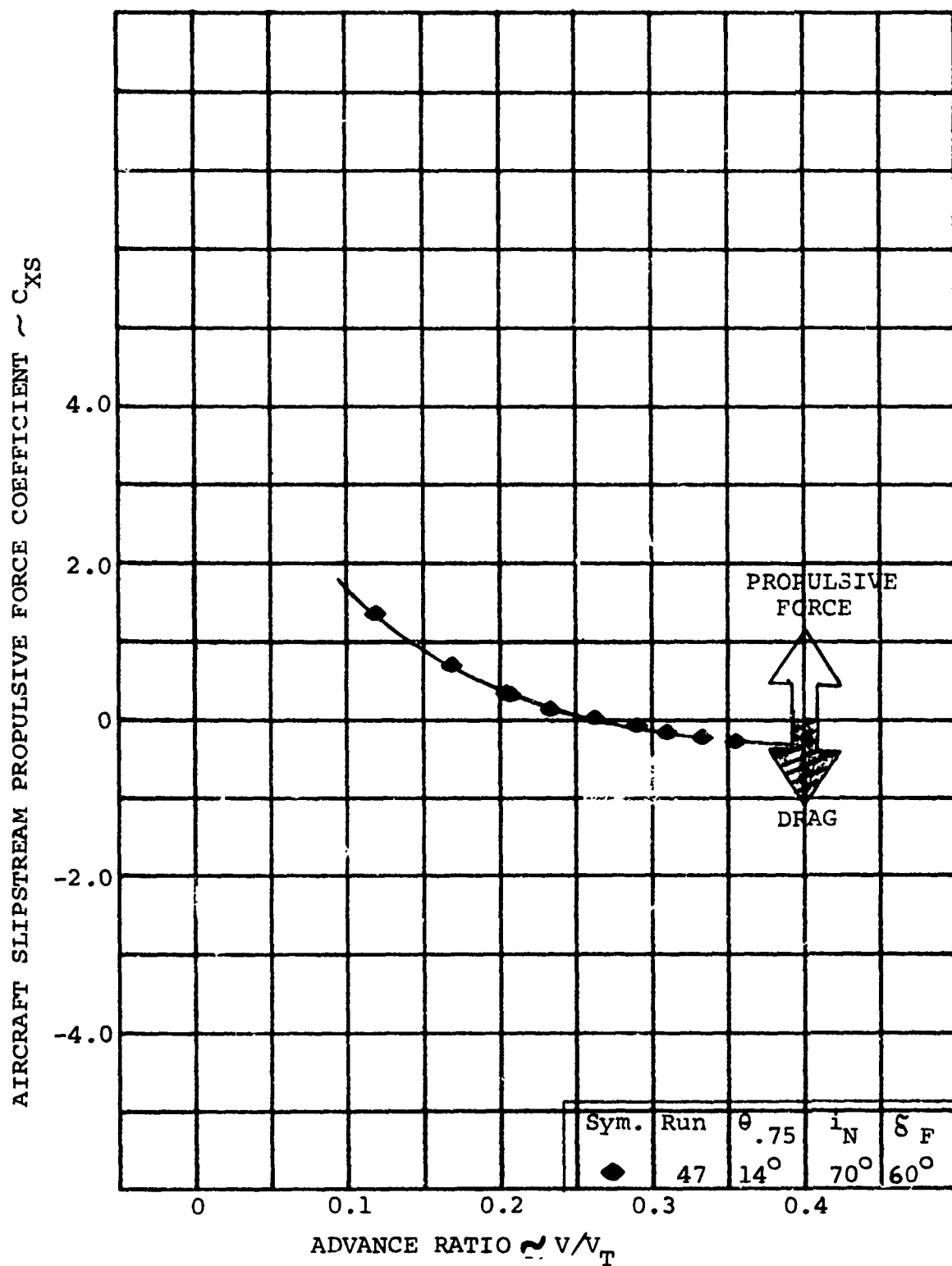


FIGURE 4-23 AIRCRAFT PROPULSIVE FORCE VARIATION
DURING IN GROUND EFFECT TAKE OFF AT
 $h/D = 0.39$

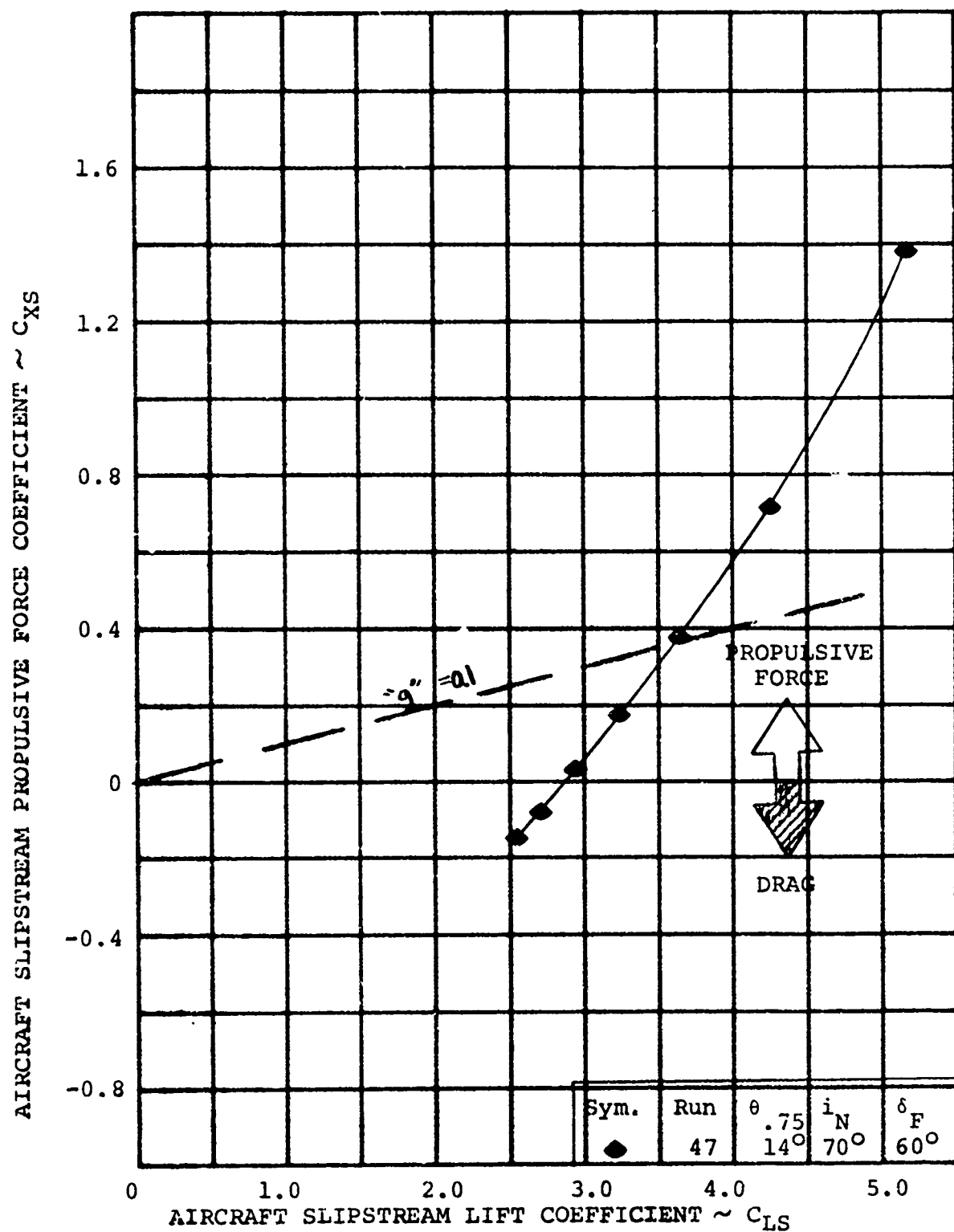


FIGURE 4-24 AIRCRAFT PROPULSIVE FORCES/LIFT VARIATION
FOR IN GROUND EFFECT TAKEOFF AT $h/D = 0.39$

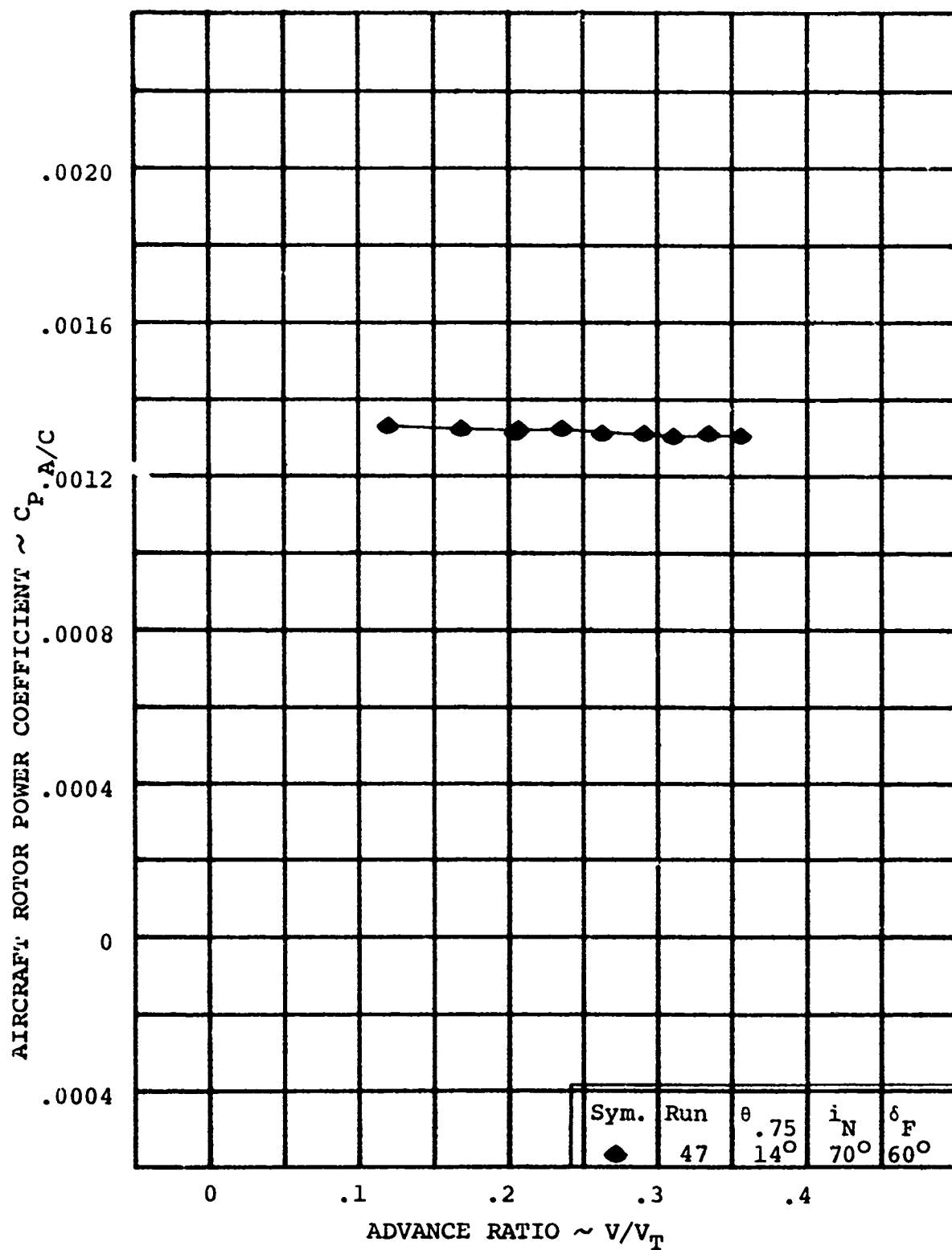


FIGURE 4-25 AIRCRAFT ROTOR POWER VARIATION DURING IN-GROUND EFFECT TAKEOFF AT $h/D = 0.39$

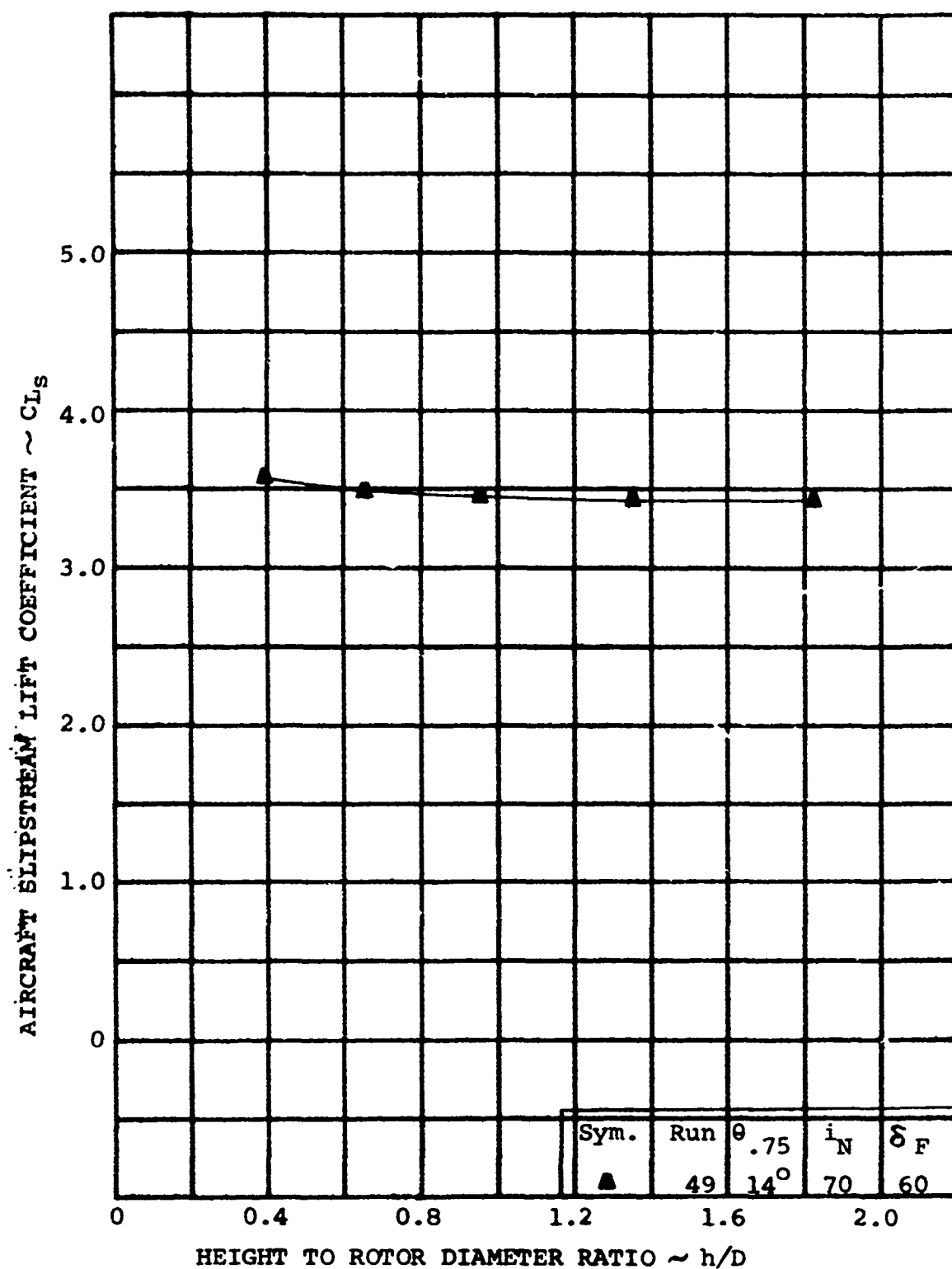


FIGURE 4-26

AIRCRAFT LIFT VARIATION DURING STOL
CLIMBOUT AT $V/V_T = 0.206$. $C_{TS} = 0.356$

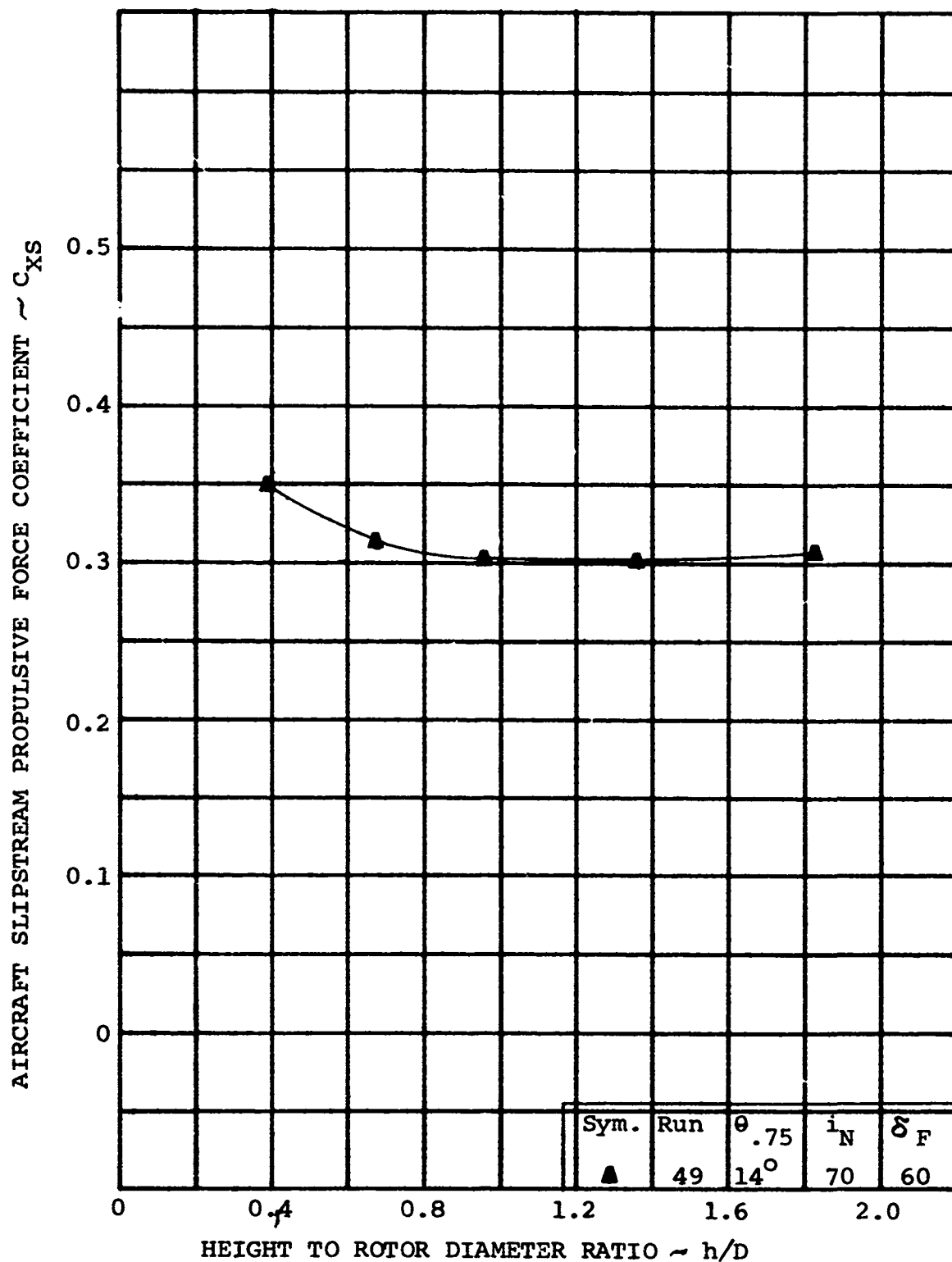


FIGURE 4-27

AIRCRAFT PROPULSIVE FORCE VARIATION
DURING STOL CLIMBOUT AT $V/V_T = 0.206$
 $C_{TS} = 0.356$

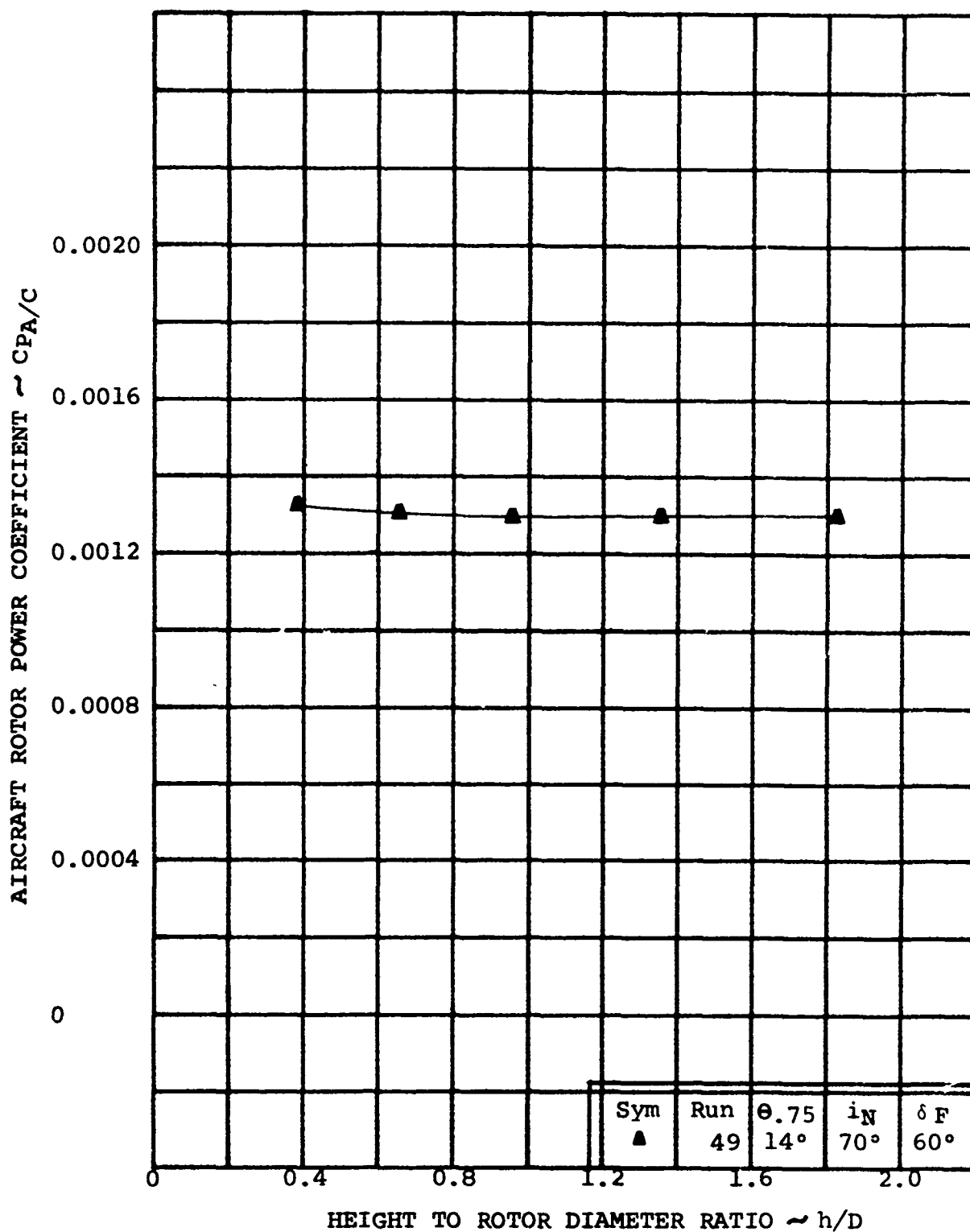


FIGURE 4-28

AIRCRAFT ROTOR POWER VARIATION DURING
STOL CLIMB OUT AT $V/V_T = 0.206$
 $C_{TS} = 0.356$

4.3 TRANSITION PERFORMANCE

The transition mode refers to operation out-of-ground effect from hover to the cruise regime. The nacelles rotate from 90-degree incidence (i_N) to zero-degree incidence. During this flight regime, the rotor has a significant influence on the aircraft performance since it provides the majority of the lift as well as all the propulsive force.

4.3.1 Rotor Airframe Interactions

In the transition regime, the high rotor induced velocity and rotor shaft angles have a significant impact on the local angle of attack of the wing and possibly have some impact on the tail and fuselage contribution to the airframe characteristics. This effect results in a shifting of the airframe lift by an incremental angle equal to the average downwash over the wing.

The aircraft lift data are presented in Figures 4-29 and 4-30 for the 70 and 45-degree nacelle incidences. At 70 degrees, the airframe minus tail lift curve slope (C_L/α) of 0.065 per degree is increased to 0.083 per degree by the addition of the horizontal tail. Adding the rotors increase the lift curve slope to 0.217 per degree. Maximum wing lift coefficient (C_{LMAX}) of 1.64 occurs at 8 degrees angle of attack with the tail and rotors removed. The horizontal tail increases the wing C_{LMAX} by 0.06 but does not change the angle of attack at which it occurs. Testing was terminated at 13 degrees with the rotors on as a result of model operational limitations. Total aircraft lift does not appear to have reached stall but included in Figure 4-29 is the lift of the airframe obtained by subtracting the rotor lift contribution from the total aircraft. This airframe lift curve is displaced approximately 6 degrees as a result of the rotor downwash and stall occurs at 13 degrees with a maximum lift coefficient of 1.45.

When changing the nacelle incidence to 45 degrees, the lift curve slope with tail on increases from 0.083 to 0.089 per degree and increases to 0.175 per degree with the addition of the rotors.

The maximum airframe lift coefficient obtained with the nacelle incidence of 45 degrees is 1.83 as compared to 1.70 when the nacelles were at 70 degrees. This again indicates an increased lift effectiveness of the wing and nacelle. A maximum lift coefficient of 5.1 is obtained at 21 degrees angle of attack for the total aircraft and 4.65 for the aircraft minus tail. Included in Figure 4-30 is the lift of the airframe obtained by subtracting the rotor lift contribution from the total aircraft. This airframe lift curve is displaced by approximately 3 degrees at zero lift but decreases as the angle of attack is

increased. The increase in lift curve slope appears to be the result of the increase in local dynamic pressure over the wing produced by the rotor. This also accounts for the increase in maximum lift coefficient to 2.0. Stall for the aircraft with the rotor on is very gentle with the maximum lift occurring at 16 degrees angle of attack.

The displacement of the lift curve at 70 and 45 degrees nacelle incidence is approximately the same as the downwash angle defined by the induced velocity through the rotor disc and freestream velocity.

Figures 4-31 and 4-32 present the influence of the rotors on the airframe characteristics in yawed flight. Airframe data obtained with the rotors off is compared to the total aircraft data and the aircraft minus the rotor contributions. The shaded area indicates that the rotor downwash on the airframe produced a change in the side force/yaw angle slope. This is a result of the rotor induced velocity producing a local angle of attack change on the fuselage and the nacelles. For the nacelle incidence (i_N) of 70 degrees, Figure 4-31, the rotor downwash appears to have delayed a possible separation of flow on the fuselage or nacelles occurring at -12 degrees of yaw. At a nacelle incidence of 45 degrees, Figure 4-32, the rapid change in side force at -12 degrees yaw is not evident in the airframe data. This indicates that the flow separation in $i_N=70$ was occurring on the nacelle and was eliminated by the rotor downwash.

4.3.2 Rotor Performance

Rotor performance data was obtained in the transition regime at nacelle incidence values of 70 and 45 degrees to provide data that would adequately describe the performance capabilities between hover and cruise. Data obtained with the nacelle incidence of zero and the flaps deflected 60 and 0 degrees is also presented to represent the end of transition and the beginning of cruise.

The rotor thrust variation with angle of attack is presented in Figures 4-33 and 4-34. For the shaft incidence of 70 degrees ($V/V_T=0.206$ and 0.234) there is a definite reduction in slope at approximately minus two degrees angle of attack. A similar but less severe change in slope occurs at an angle of attack of 12 degrees for the nacelle incidence of 45 degrees ($V/V_T=0.260$). This is indicative of stall and to confirm it, the associated thrust/power variation is presented in Figures 4-35 and 4-36 for nacelle incidence values of 70 and 45 degrees respectively. Rotor stall is evident by the sharp decrease in slope resulting from the reduced thrust-angle of attack slope and the associated

increase in rotor power. The rotor loads discussed in Section 6 show that the rotor is at the stall flutter inception point. First harmonic flap bending is reduced as shown in Figure 6-74 and thus explains the marked reduction in pitching moment derivative observed in Figures 5-46 and 5-47.

Indicated also in Figures 4-33 and 4-34 is the influence of flap deflection on the rotor thrust at the end of transition at a nacelle incidence of zero degrees. Deflecting the flap from 60 to 0 degrees decreased the wing circulation which affects the flow through the rotor disc and results in a decrease in the thrust.

The power variation with angle of attack for the transition regime associated with the thrust data of Figures 4-33 and 4-34 is presented in Figures 4-37 and 4-38.

4.3.3 Aircraft Performance

The testing performed in the transition regime was accomplished at nacelle incidence values of 70 and 45 degrees. The performance data obtained with the nacelle incidence of zero and the flaps deflected 0 and 60 degrees is also presented to represent the end of transition and the beginning of cruise. Shown in Figure 4-39 is the variation of slipstream lift coefficient with angle of attack. This indicates that the flap increases the lift coefficient by 1.05 and any additional lift is provided by the rotors as they are tilted up from the horizontal position. When the rotors are tilted up to 45 degrees additional increment in lift coefficient produced by the rotors is 0.8 and approximately 1.6 to 2.0 for 70 degree nacelle incidence.

Figure 4-40 presents the variation of aircraft propulsive force with lift for the angle of attack sweeps shown on the previous figure. For the 70 degree nacelle incidence there is a decrease of 0.35 in propulsive force coefficient associated with the change in advance ratio of 0.206 to 0.234. Only one advance ratio is presented for the 45 degree incidence because of model motor operational problems. Two advance ratios are presented for zero nacelle incidence indicating a 0.11 propulsive force decrease when the advance ratio is increased only 0.06. These variations illustrate the sensitivity of the rotor propulsive capability with small changes in advance ratio. It also indicates that the rotor is most sensitive to forward speed or rotor speed in the end of transition since the blade section angle of attack is very low.

The associated aircraft rotor power required characteristics are presented in Figure 4-41. This data in conjunction with Figures 4-39 and 4-40 provide a summary of the aircraft performance data of the transition regime and will also form the basis for comparison of the existing prediction techniques and development of new methodology where none exists currently.

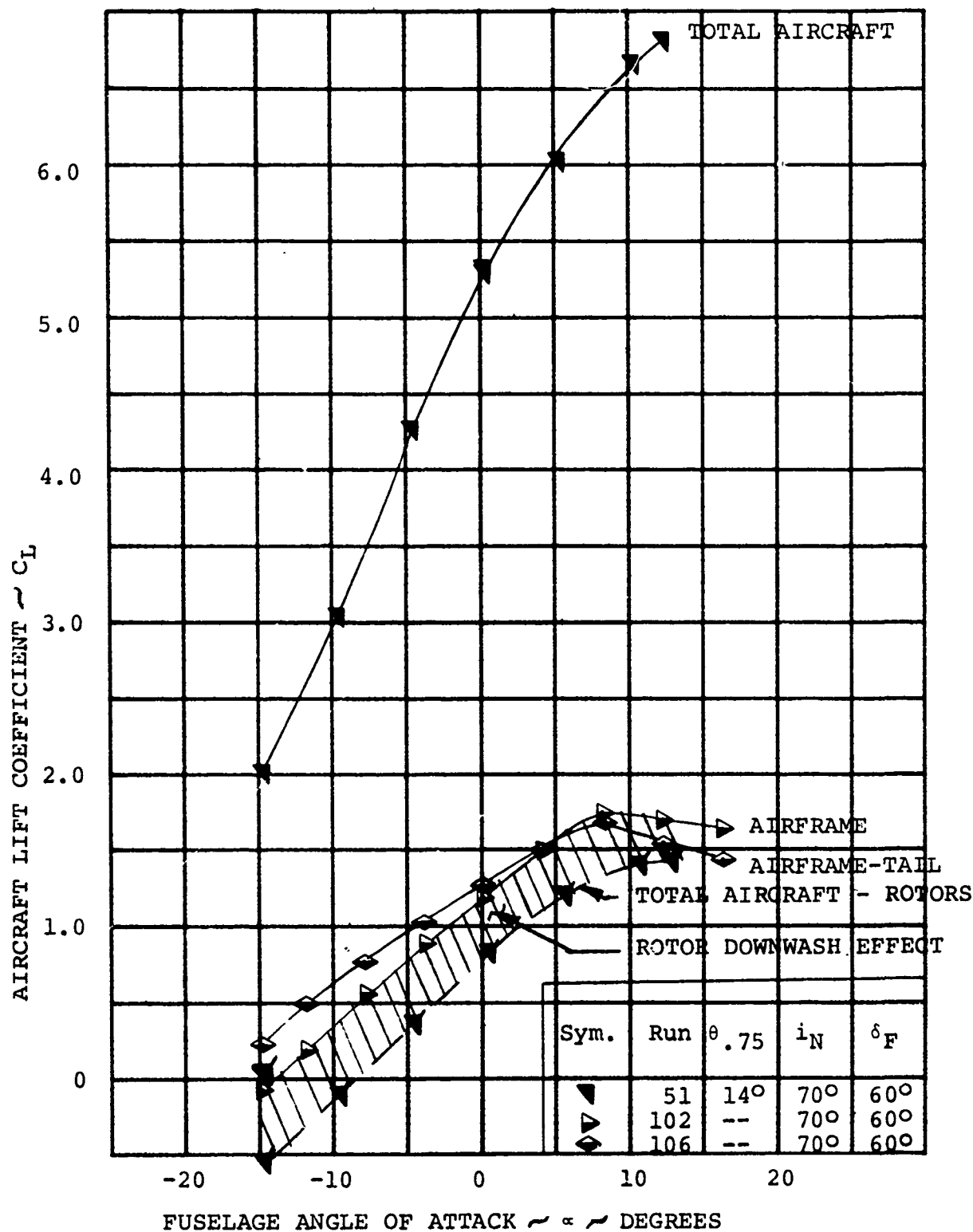


FIGURE 4-29 CONTRIBUTION OF PROP/ROTOR AND HORIZONTAL TAIL TO AIRCRAFT LIFT AT $V/V_T = 0.206$ WITH $i_N = 70^\circ$

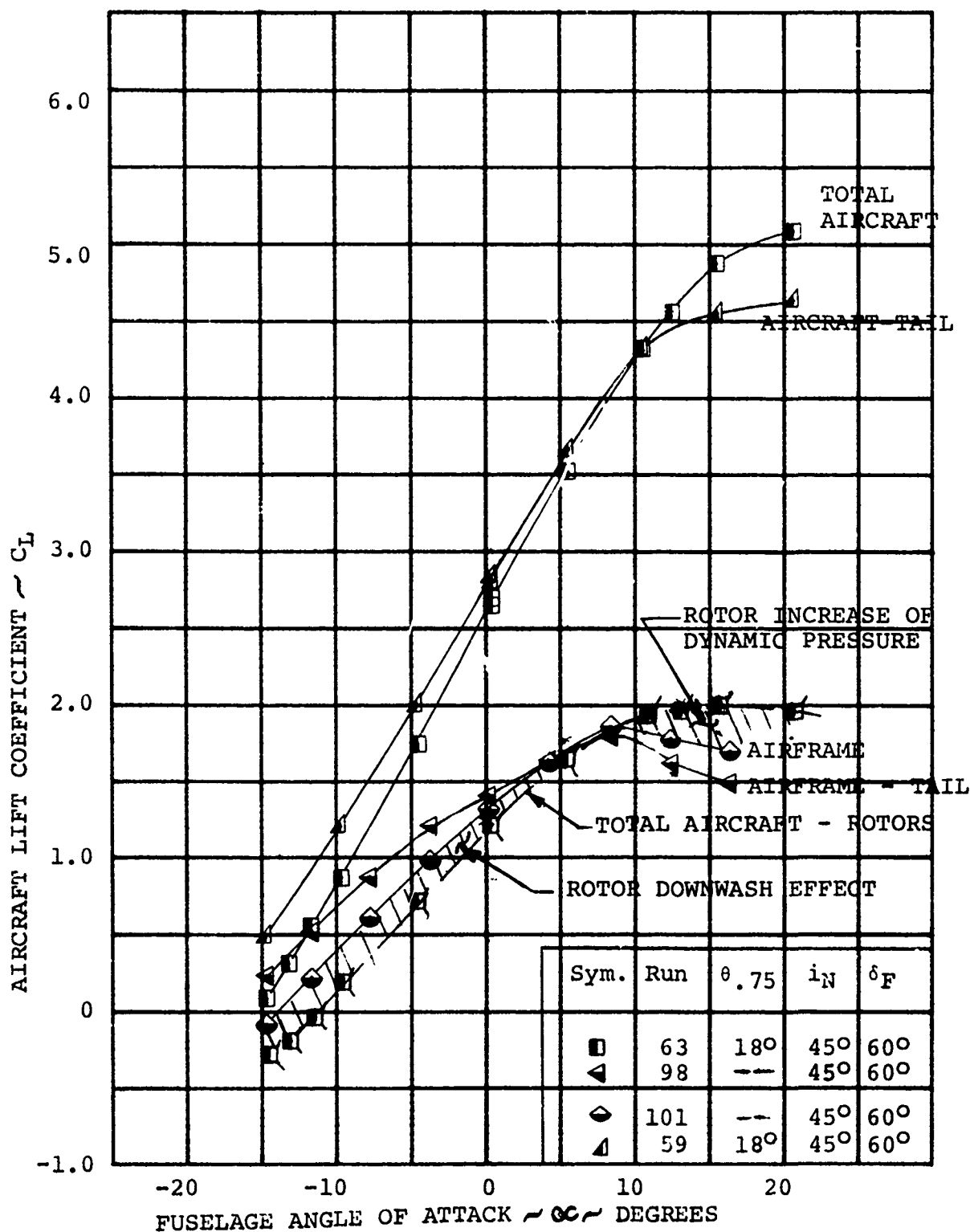


FIGURE 4-39 CONTRIBUTION OF PROP/ROTOR AND HORIZONTAL TAIL TO AIRCRAFT LIFT AT $V/V_T = 0.260$ WITH $i_N = 45^\circ$

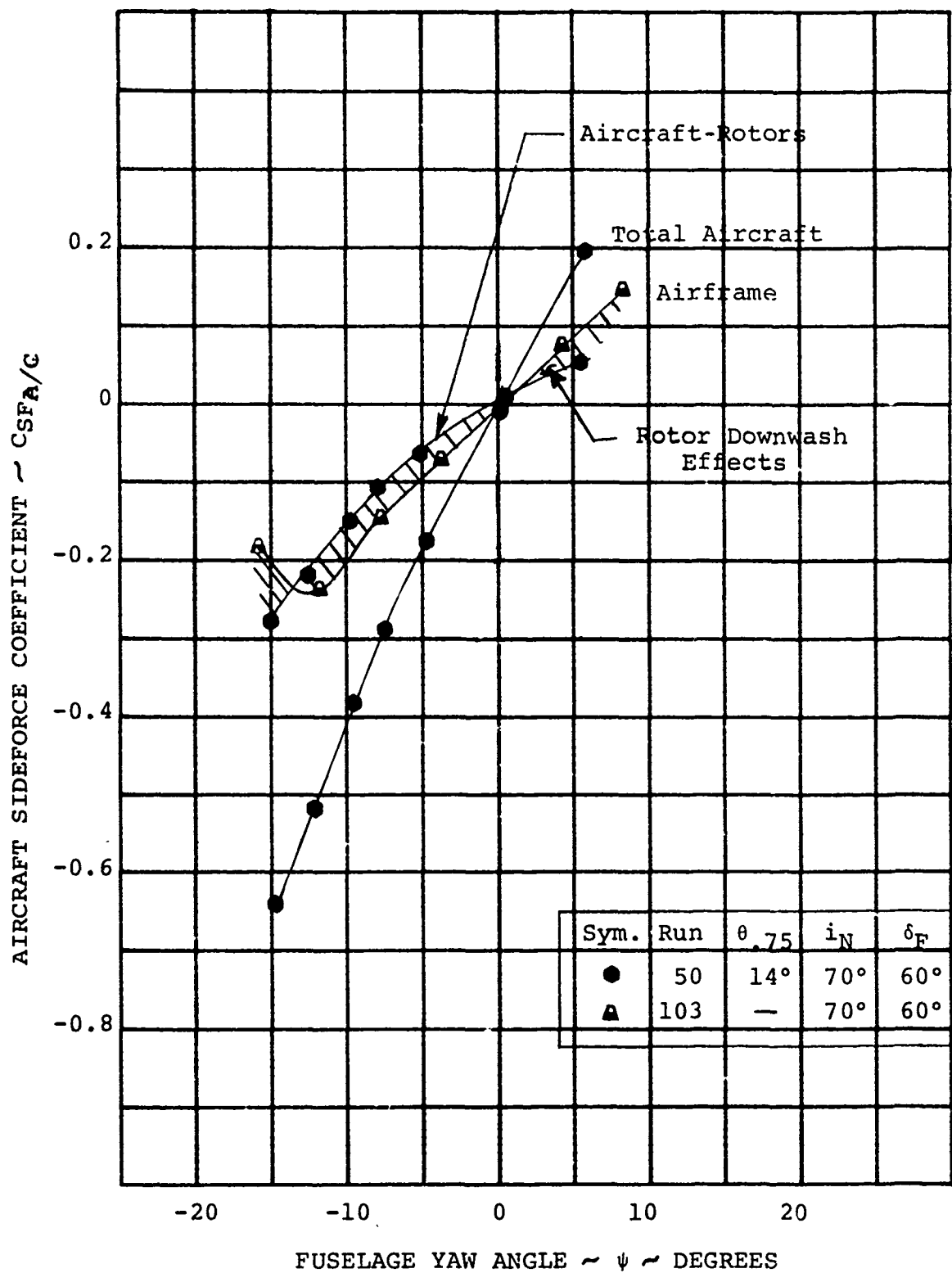


FIGURE 4-31

ROTOR-AIRFRAME INTERACTION ON AIRCRAFT
SIDEFORCE AT $V/V_T = 0.206$ WITH $i_N = 70^\circ$

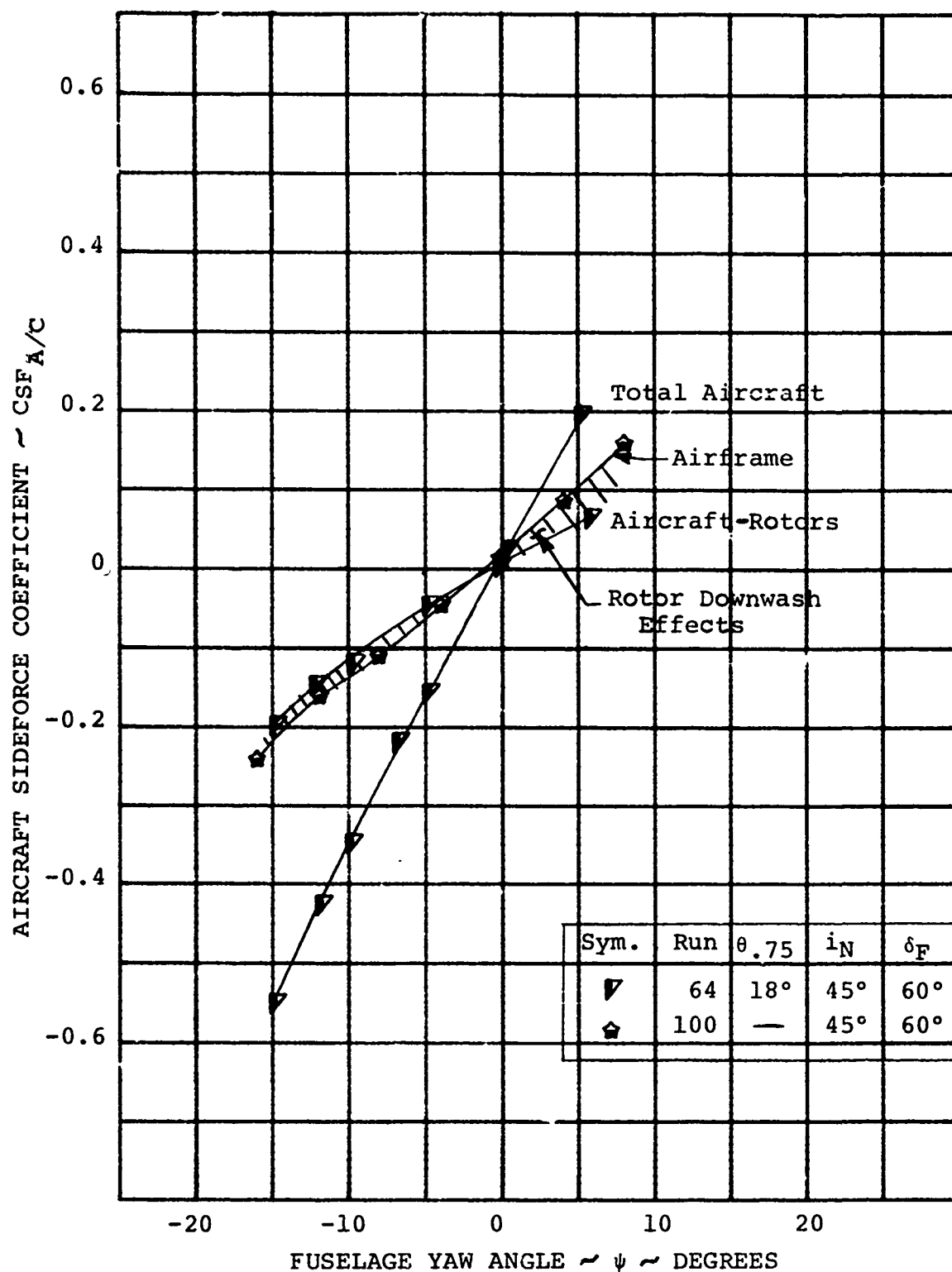


FIGURE 4-32

ROTOR-AIRFRAME INTERACTION ON AIRCRAFT
SIDEFORCE AT $V/V_T = .260$ WITH $i_N = 45^\circ$

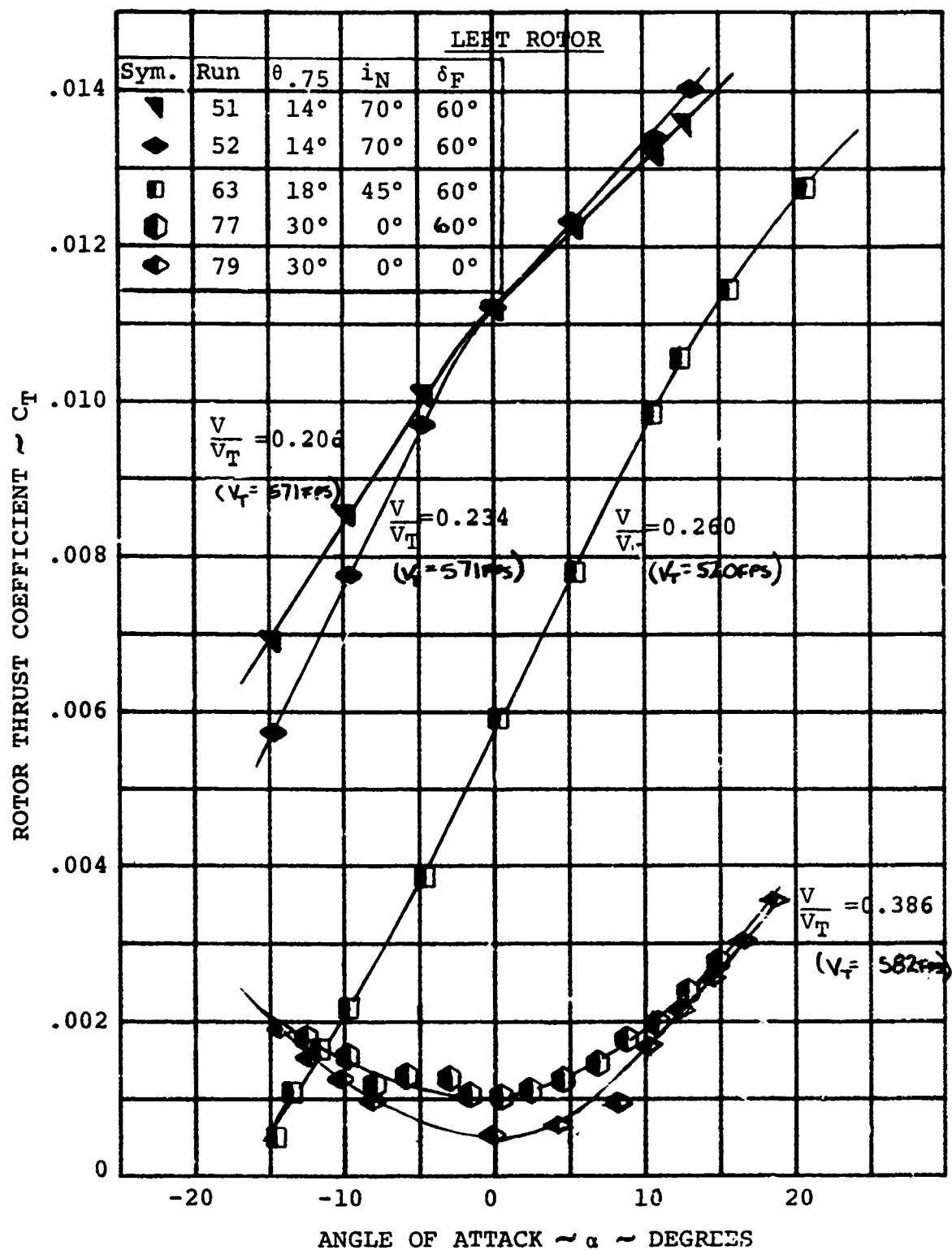


FIGURE 4-33

ROTOR THRUST/ANGLE OF ATTACK VARIATION DURING TRANSITION

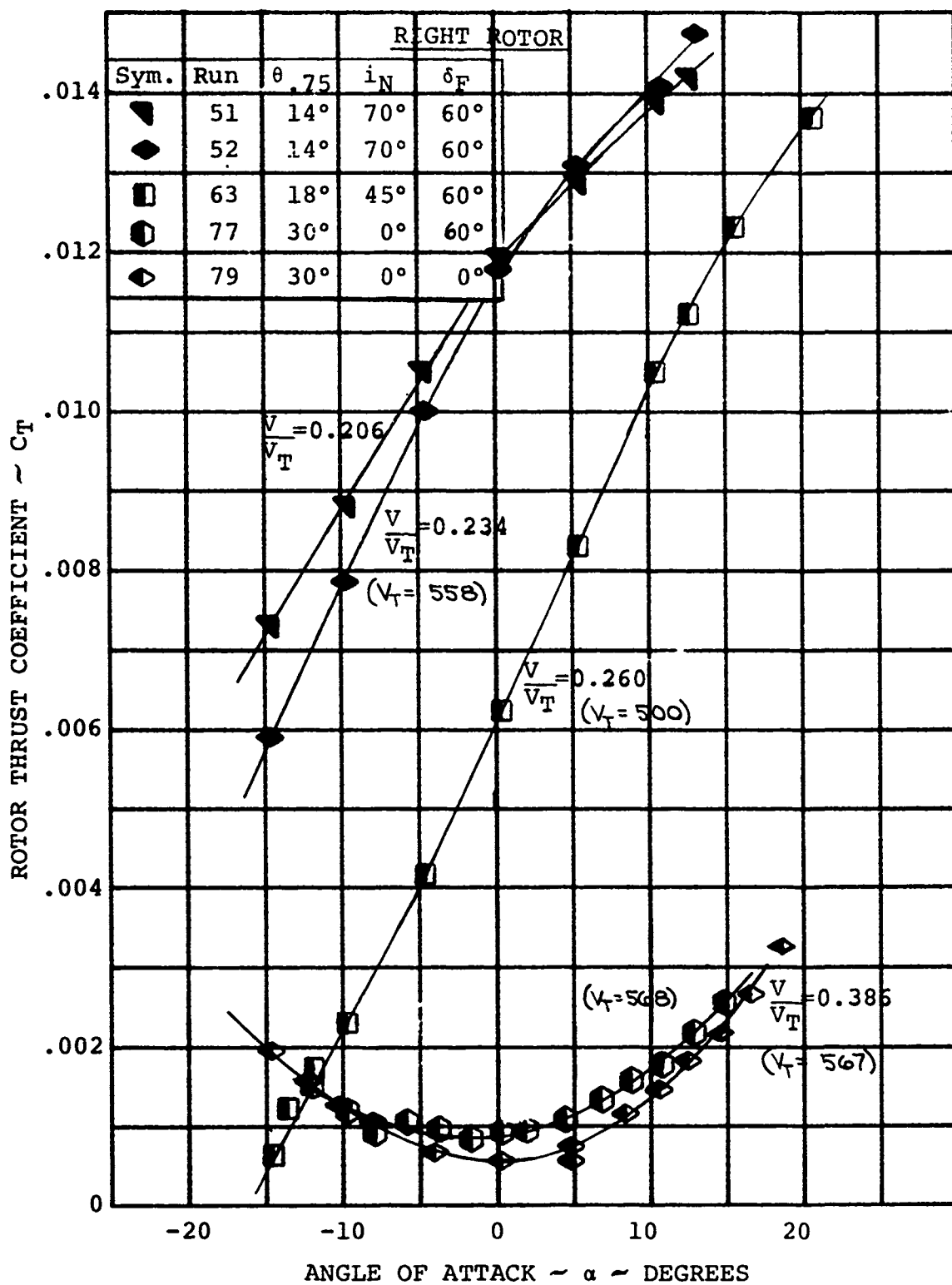


FIGURE 4-34

ROTOR THRUST/ANGLE OF ATTACK
VARIATION DURING TRANSITION

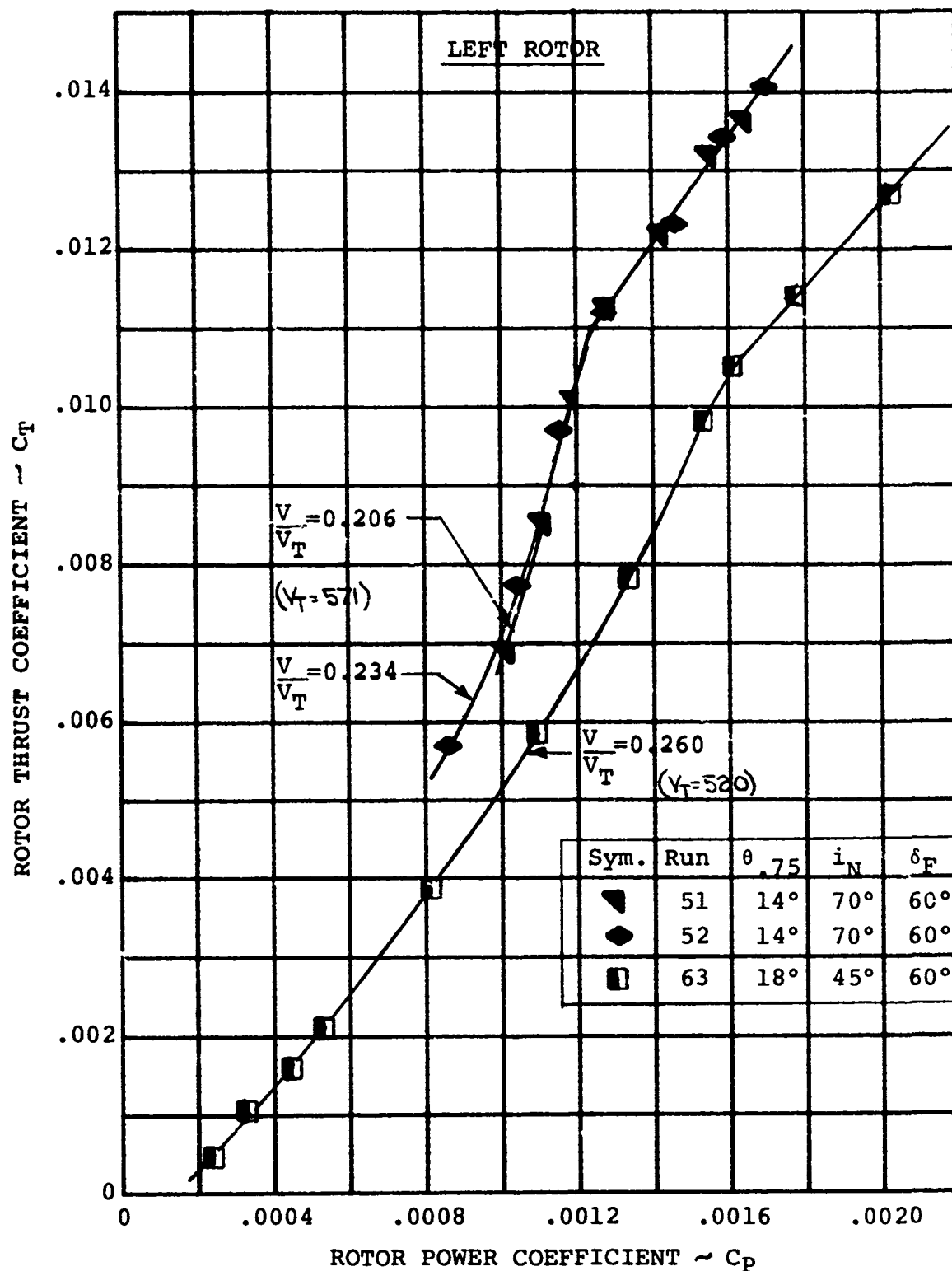


FIGURE 4-35 ROTOR THRUST/POWER VARIATION
DURING TRANSITION

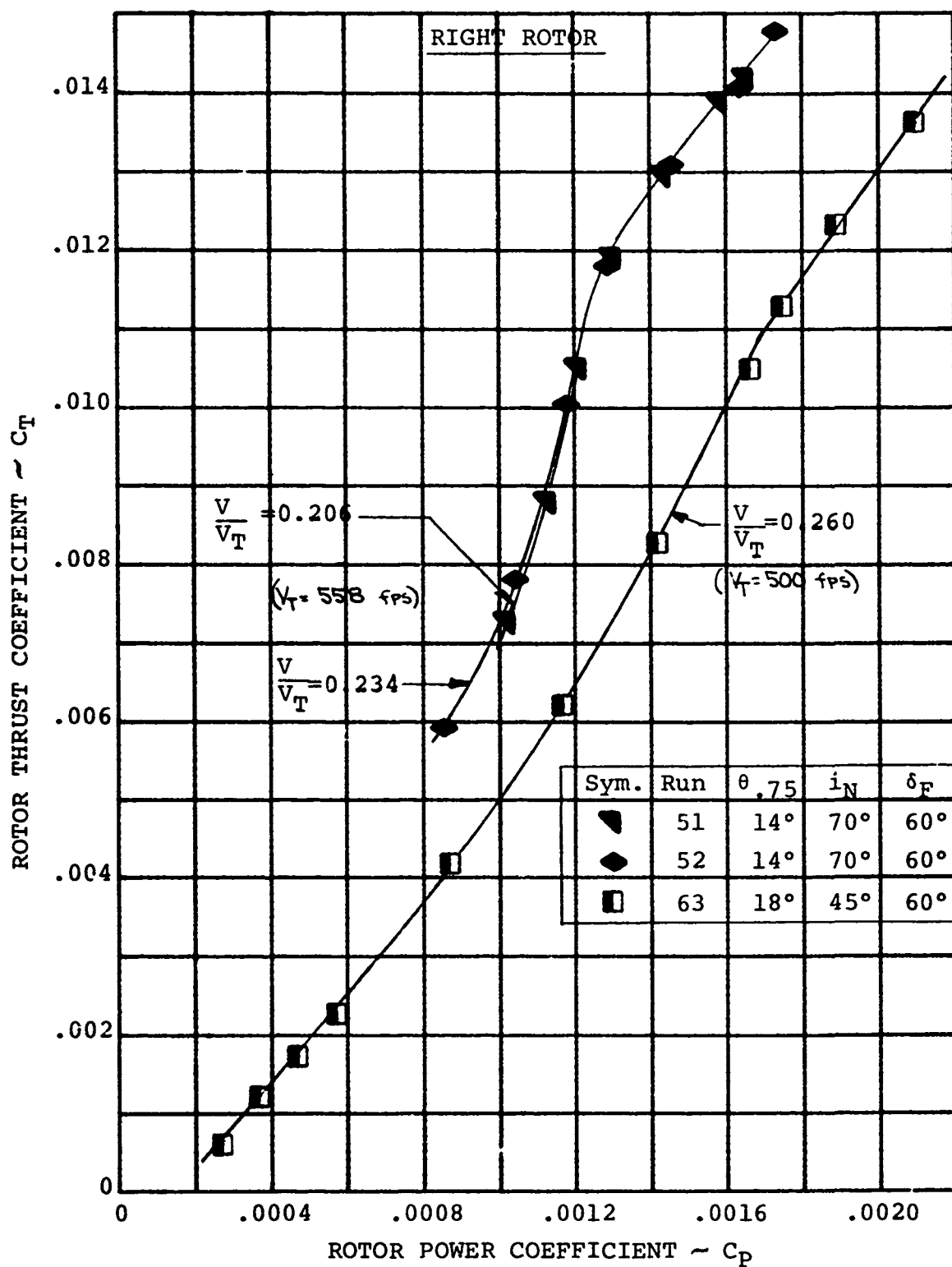


FIGURE 4-36 ROTOR THRUST/POWER VARIATION DURING TRANSITION

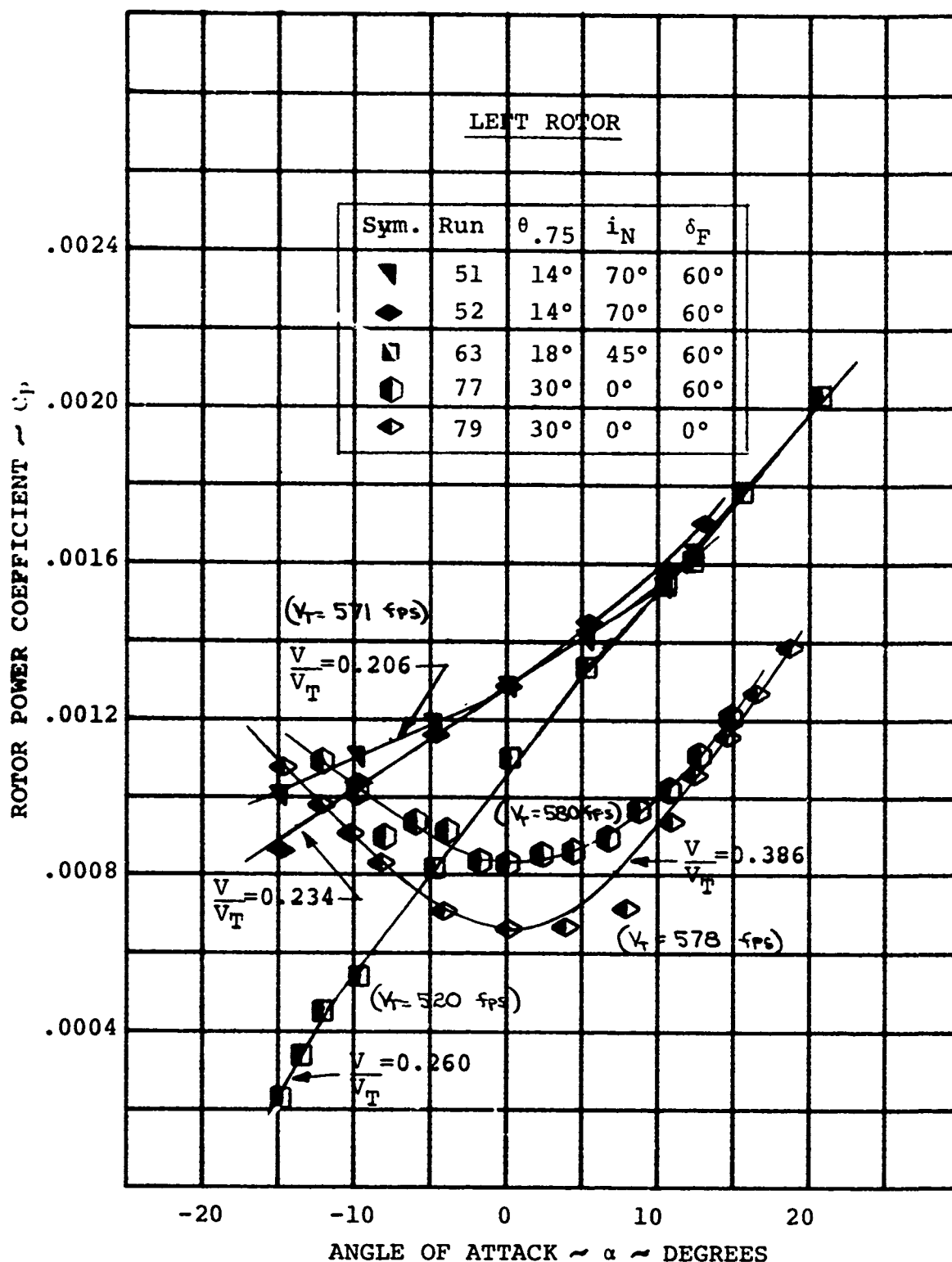


FIGURE 4-37 ROTOR POWER/ANGLE OF ATTACK VARIATION DURING TRANSITION

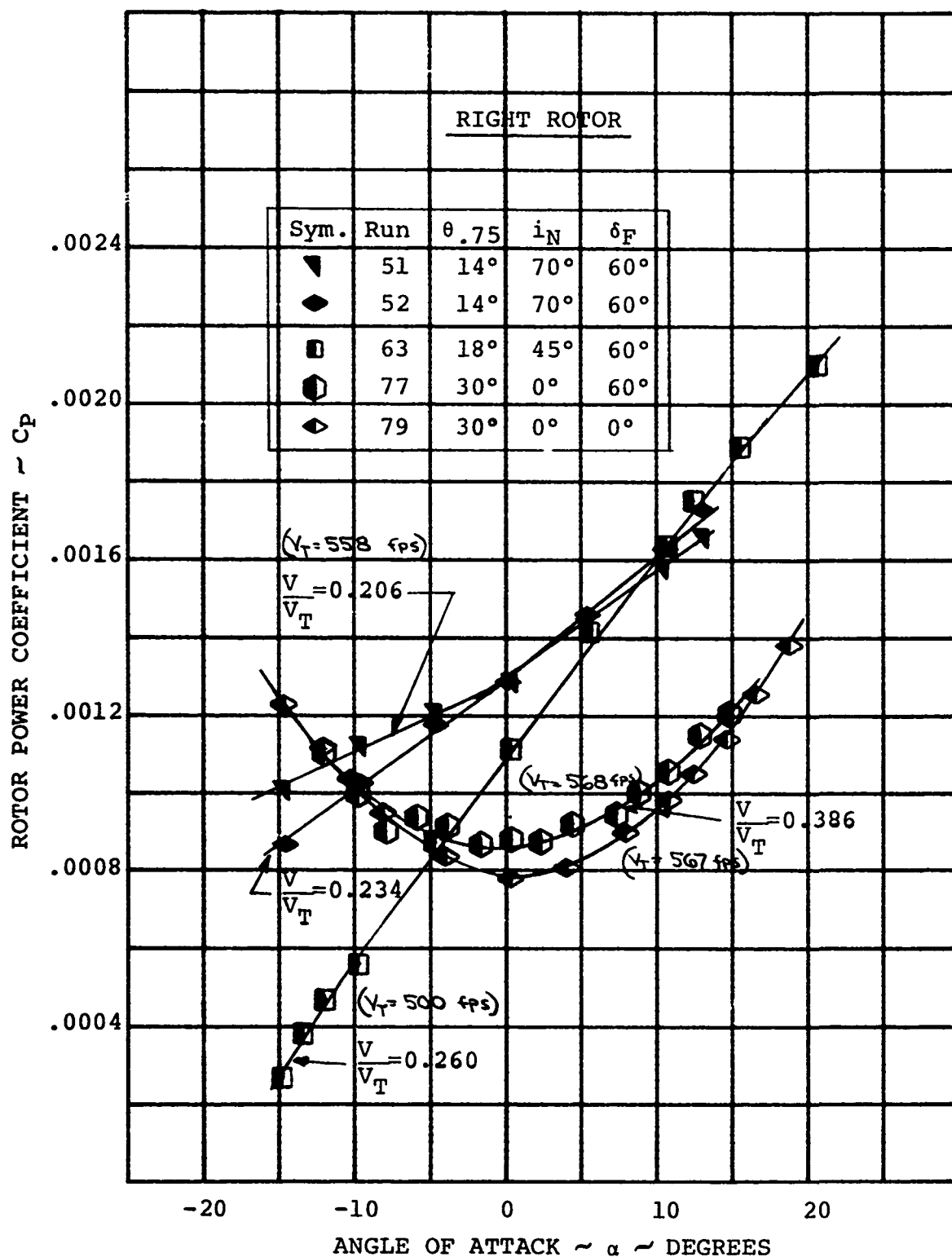


FIGURE 4-38 ROTOR POWER/ANGLE OF ATTACK VARIATION DURING TRANSITION

TOTAL AIRCRAFT SLIPSTREAM LIFT COEFFICIENT $\sim C_{LS}$

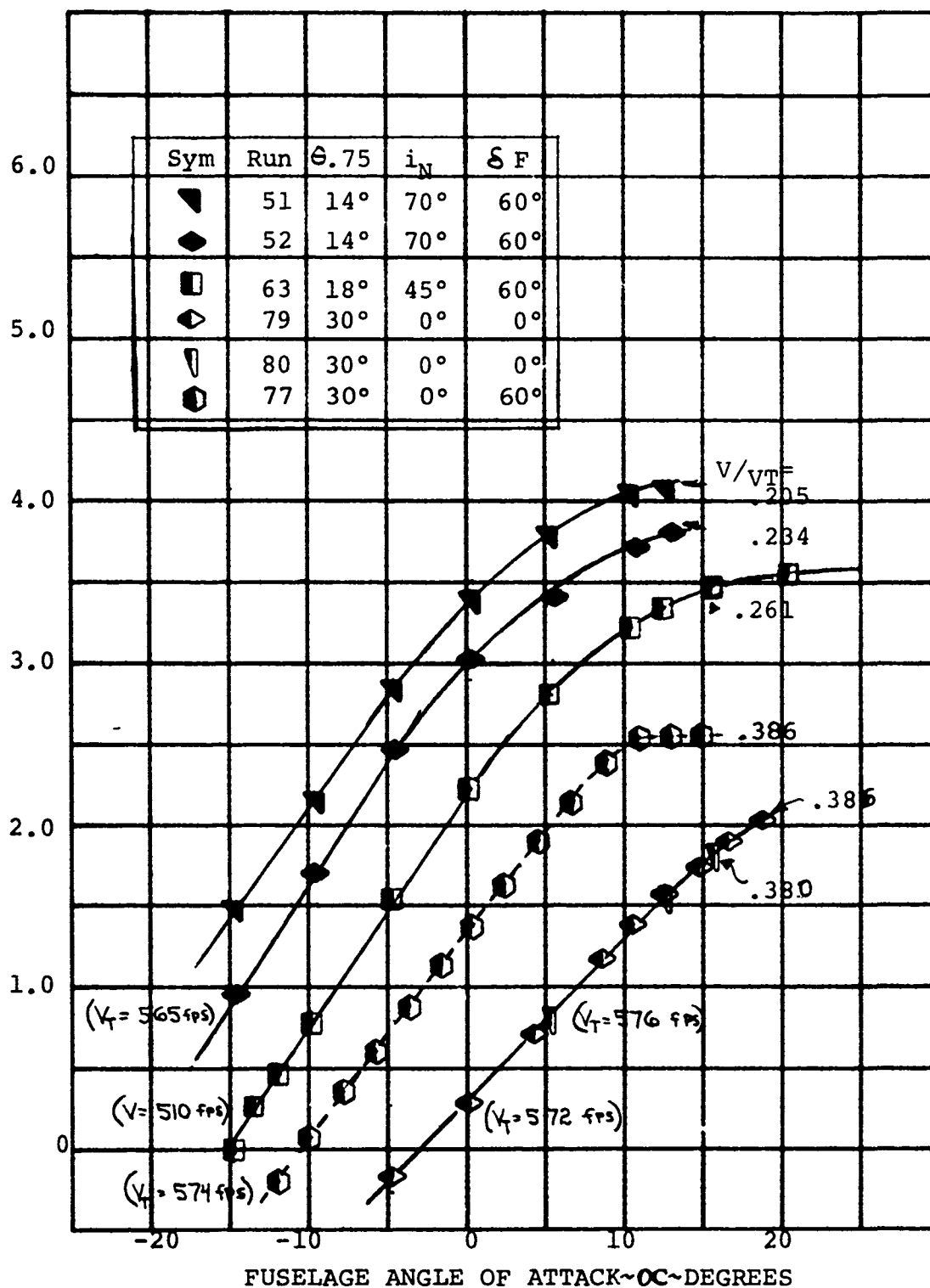


FIGURE 4-39 AIRCRAFT LIFT/ANGLE OF ATTACK VARIATION DURING TRANSITION

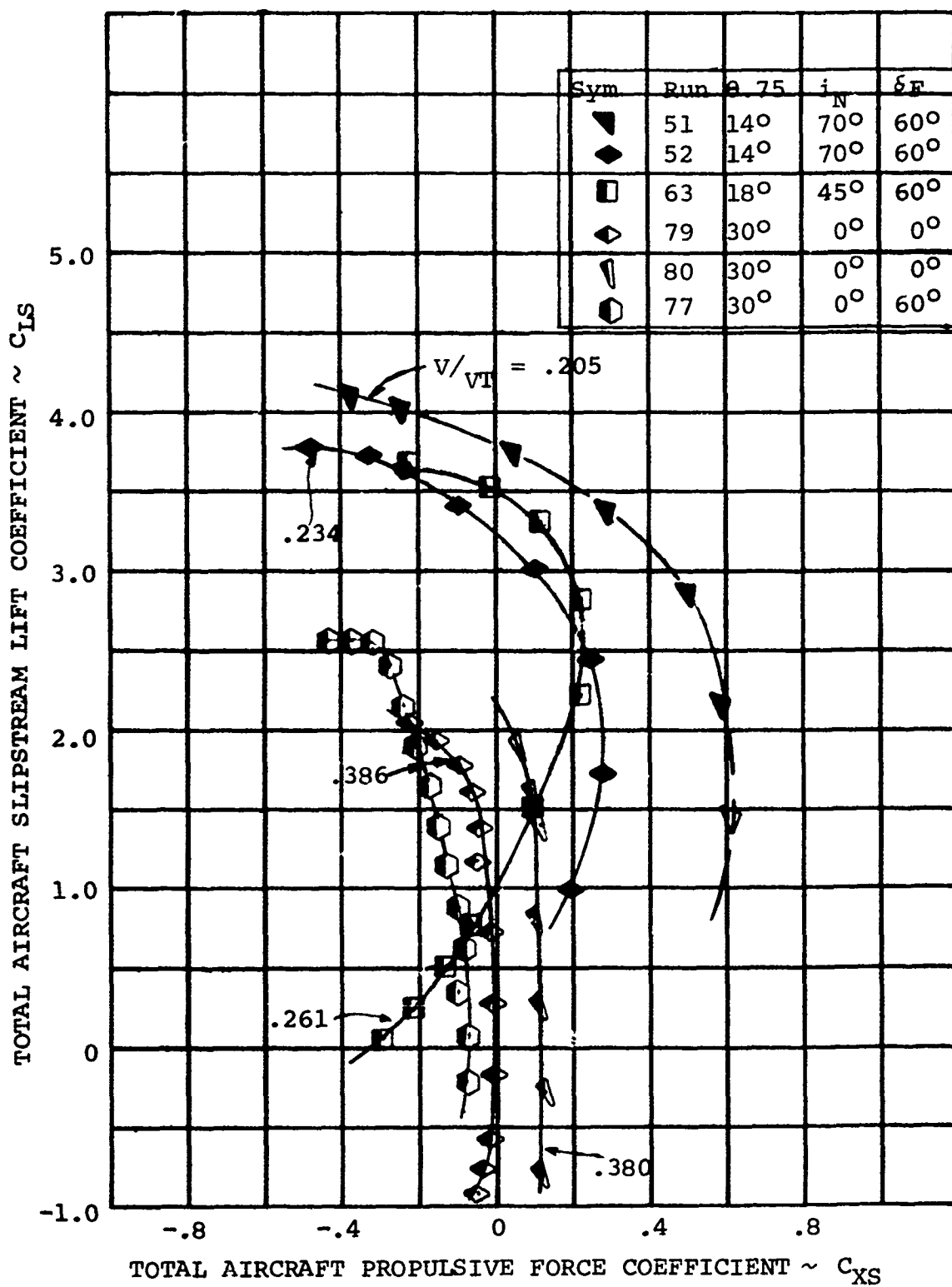


FIGURE 4-40. AIRCRAFT LIFT/PROPULSIVE FORCE VARIATION DURING TRANSITION

TOTAL AIRCRAFT SLIPSTREAM LIFT COEFFICIENT $\sim C_{LS}$

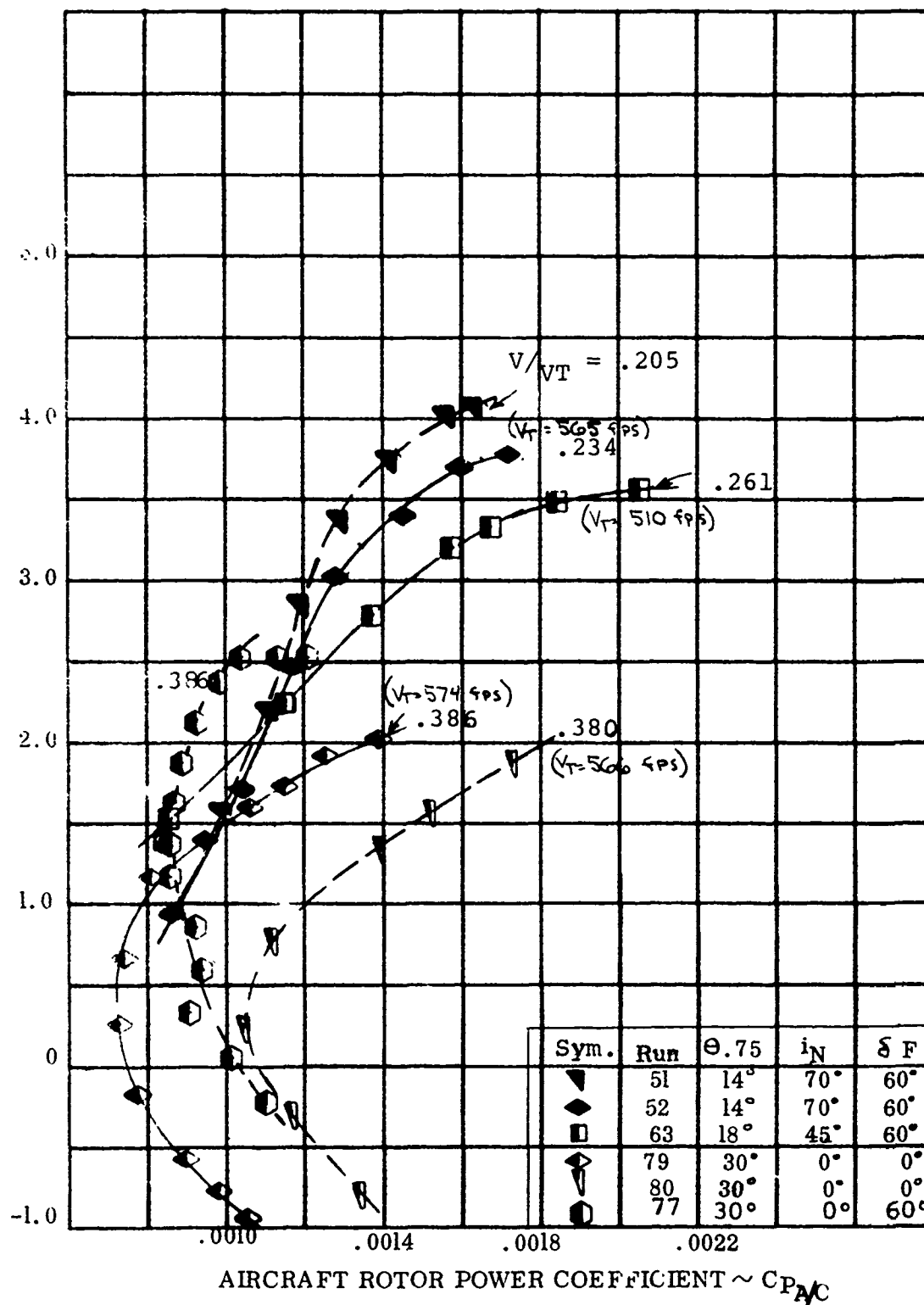


FIGURE 4-41

AIRCRAFT LIFT/POWER REQUIRED VARIATION DURING TRANSITION

4.4 CRUISE

The cruise mode, as discussed here, will refer to operation as a conventional aircraft with the nacelle in the full-down position ($i_N=0^\circ$) and the rotor is in axial flight. In this flight regime, the rotors have a major impact on the aircraft stability and performance in that they are larger and more flexible than conventional propellers. Both these factors can greatly affect the rotor performance and gust sensitivity.

4.4.1 Rotor Performance

Rotor performance data was obtained at a nacelle incidence of zero degrees for a range of flap deflection ($0^\circ, 45^\circ$ and 60°) at a speed representative of the end of transition and the beginning of cruise. Figures 4-42 and 4-43 present the rotor thrust variation with angle of attack. This indicates that deflecting the flap increases the wing circulation and produces an increase in rotor thrust at angles below stall. The thrust variation with angle of attack for 45 and 60 degrees is approximately the same; this is due to the small increase in lift and a slight variation in advance ratio offsetting the increased circulation sensitivity of thrust to advance ratio. The rotor thrust coefficient decreases from 0.0015 to 0.0005 as a result of increasing the advance ratio from 0.380 to 0.386. The rotor characteristics are significantly affected by changes in the local flow field and hence the local blade angle of attack. Since there is a difference in the dynamic characteristics between the model rotor and the full scale rotor and result in different blade response, the performance data presented here cannot be scaled up and be representative of the full scale aircraft.

Figures 4-44 and 4-45 present the model rotor power variation with angle of attack associated with the thrust data of Figures 4-42 and 4-43.

4.4.2 Aircraft Performance

From the testing accomplished in cruise, the basic model performance characteristics will be presented here for an advance ratio of 0.386. This is representative of the end of the transition regime before the blade folding conversion is initiated. The variation of the aircraft lift with angle of attack is presented in Figure 4-46 for flap deflections of 0, 45 and 60 degrees. It indicates that there is an increase in lift coefficient of 0.9 for 45 degrees and 1.05 for 60 degrees at zero angle of attack.

Figure 4-47 presents the variation of aircraft propulsive force with lift for the angle of attack sweeps presented in the previous figure. There is a decrease in propulsive force coefficient of .02 for 45-degree flap deflection and 0.06 for the 60-degree flap deflection. From Figure 5-129, the drag coefficient increase associated with the 60-degree flap deflection is 0.19 at zero degree angle of attack but the change in propulsive force is only 0.13. This indicates that the deflecting of the flap increases the rotor propulsive capability by 0.06. Also shown in this figure is the large variation in rotor thrust that results from very small changes in rotor tip speed or forward speed. This increment in rotor propulsive force obtained from a 1.5-percent increase in tip speed is almost the same magnitude as that associated with a 60-degree flap deflection. The associated rotor power required characteristics are presented in Figure 4-48. Deflecting the flap 60 degrees has increased the rotor power from 0.00072 to 0.00085 at zero angle of attack but the variation of advance ratio from 0.386 to 0.380 increases the power coefficient ($C_{P_{A/C}}$) from 0.00072 to 0.00105.

In obtaining the performance characteristics of the aircraft, it is necessary to determine the effects of yawed flight. Aircraft lift variation with yaw angle is very slight as illustrated in Figure 4-49. The propulsive force increase with yaw angle presented in Figure 4-50 is typical of the thrust increase resulting from a rotor angle-of-attack change. Figure 4-51 shows the power increase with yaw angle is directly proportional to the increase in rotor thrust and indicates no influence in rotor cruise efficiency.

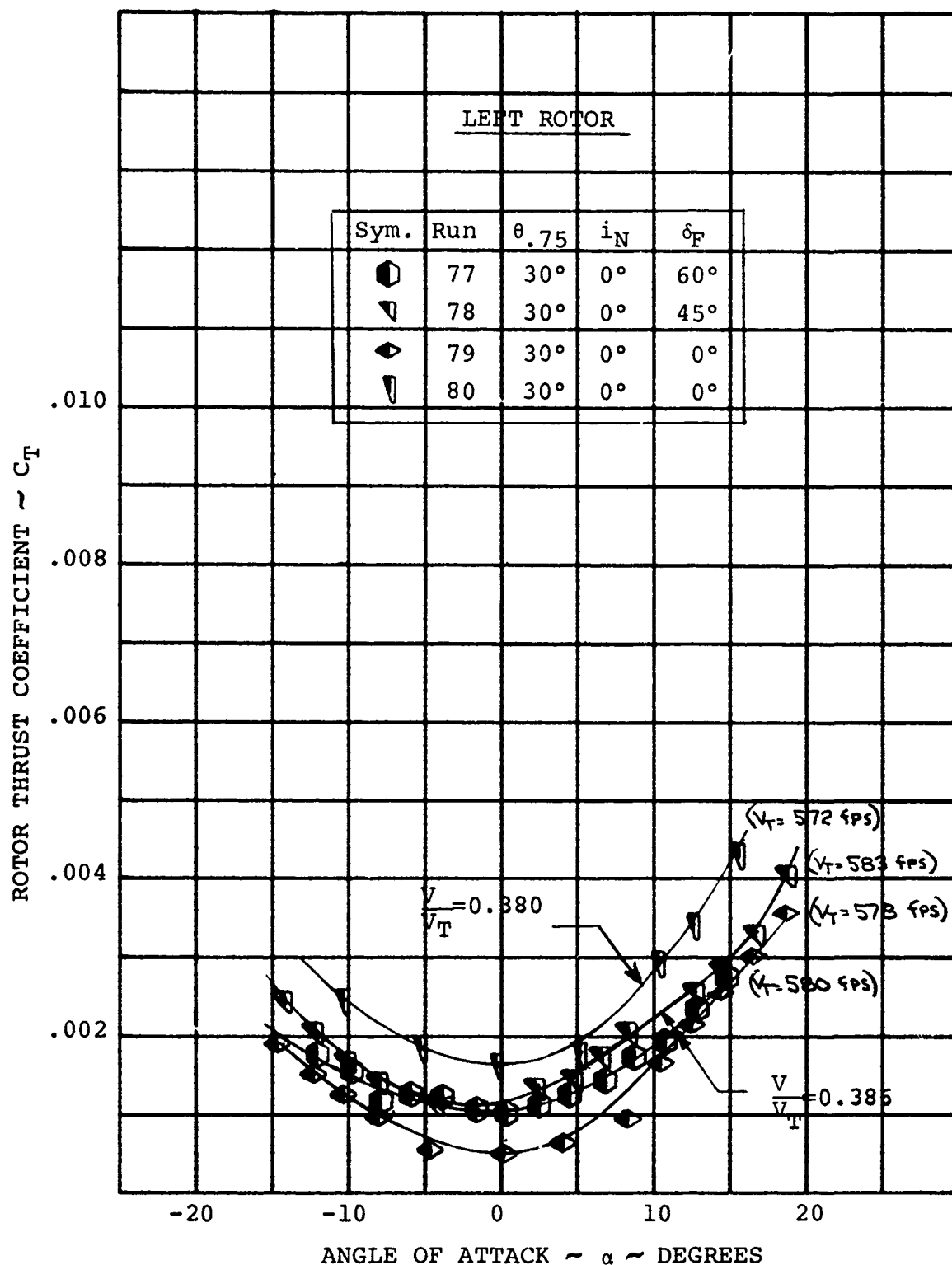


FIGURE 4-42 ROTOR THRUST/ANGLE OF ATTACK
VARIATION IN CRUISE

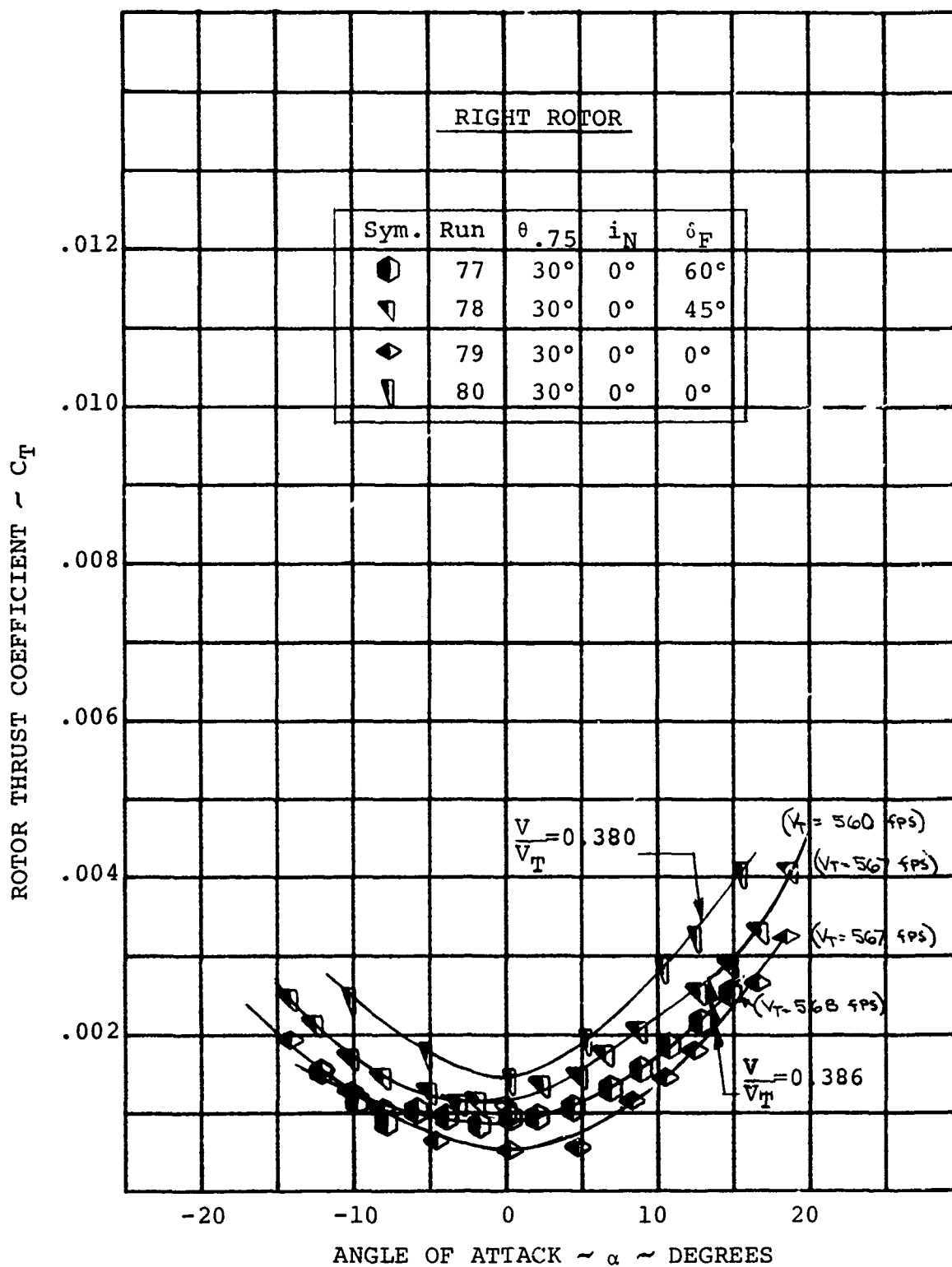


FIGURE 4-43 ROTOR THRUST/ANGLE OF ATTACK
VARIATION IN CRUISE

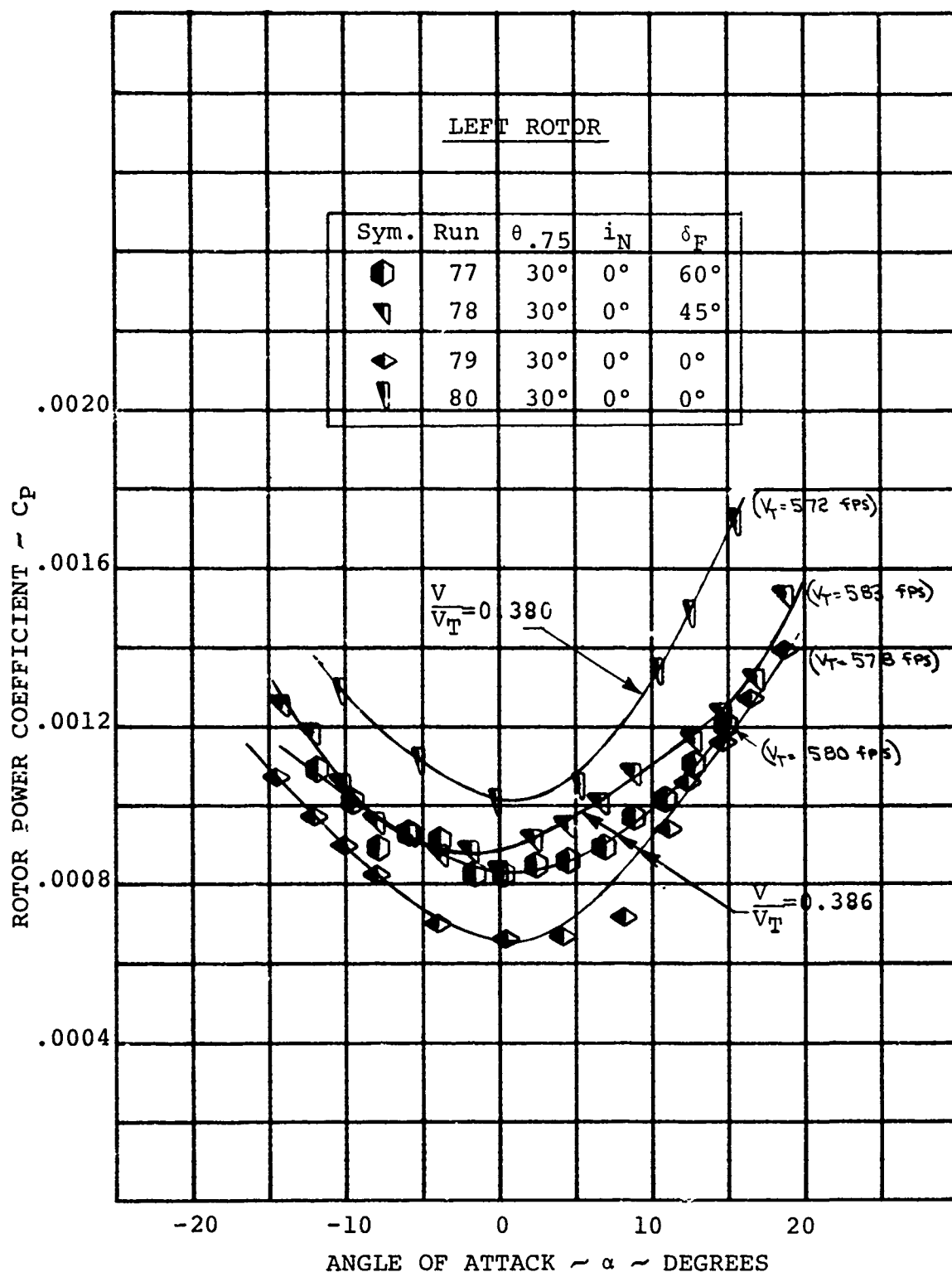


FIGURE 4-44 ROTOR POWER/ANGLE OF ATTACK
VARIATION IN CRUISE

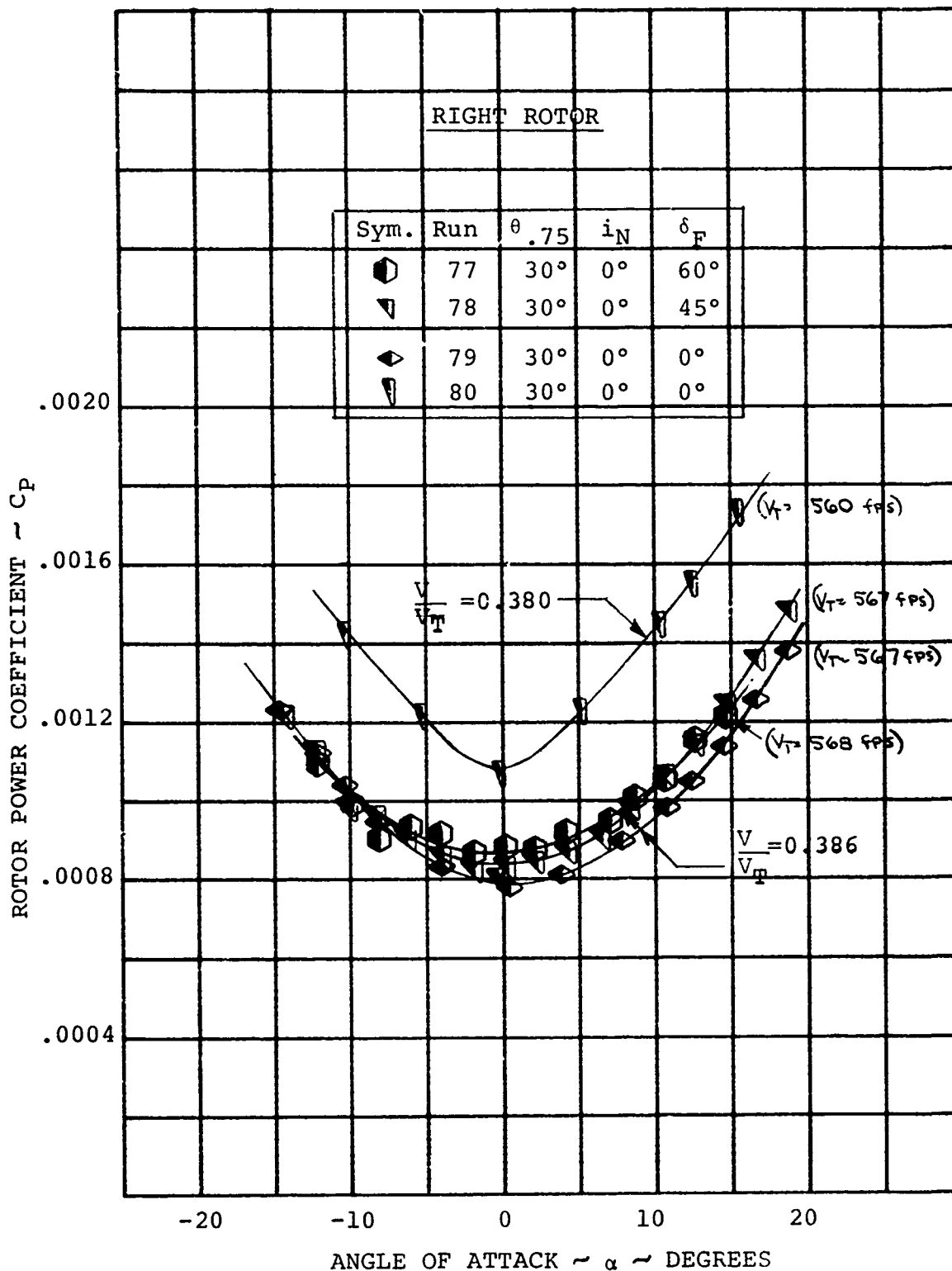


FIGURE 4-45 ROTOR POWER/ANGLE OF ATTACK
VARIATION IN CRUISE

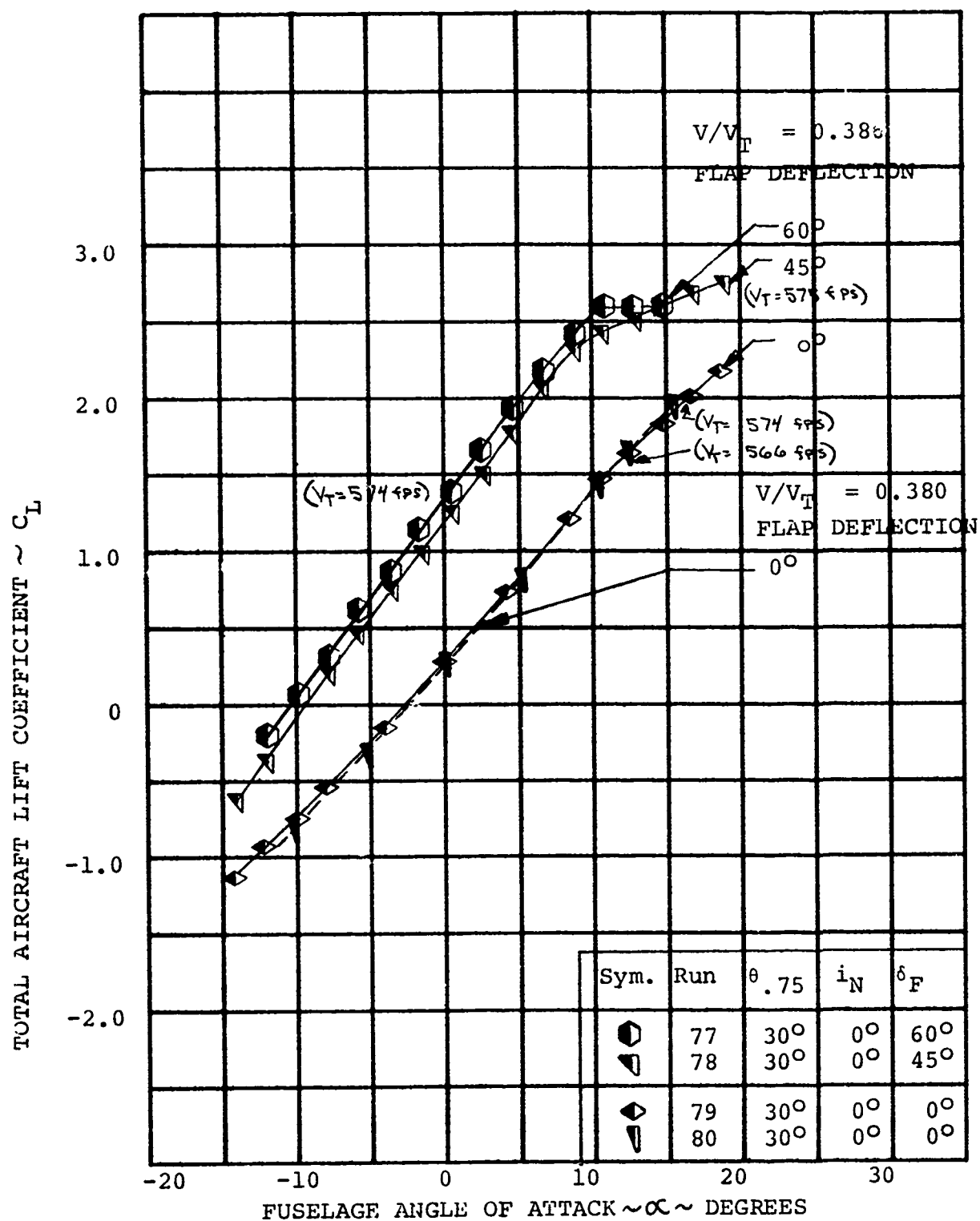


FIGURE 4-46 TOTAL AIRCRAFT LIFT/ANGLE OF ATTACK
 VARIATION IN CRUISE $i_N = 0$

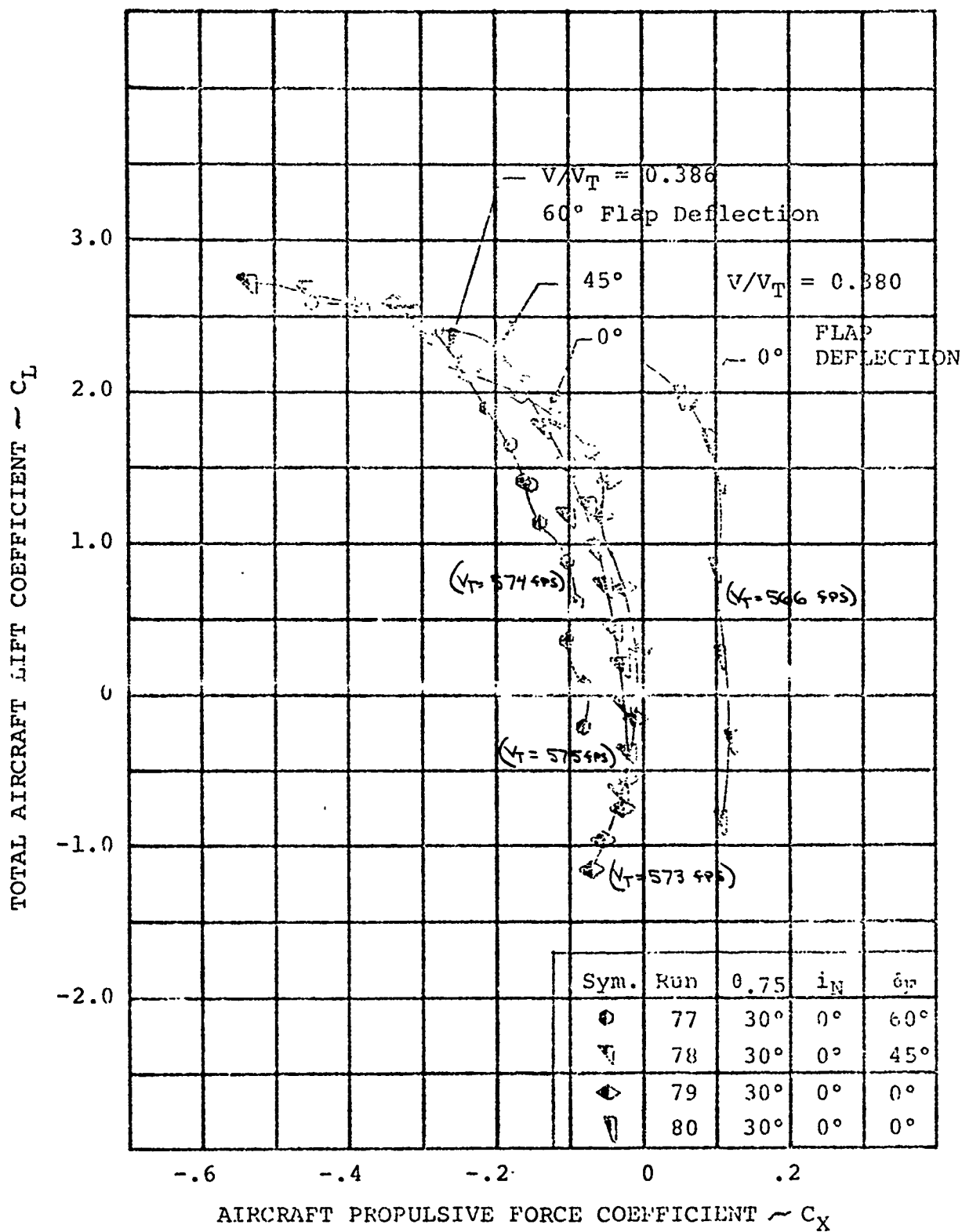


FIGURE 4-47 TOTAL AIRCRAFT LIFT/PROPULSIVE FORCE VARIATION IN CRUISE $i_N = 0$

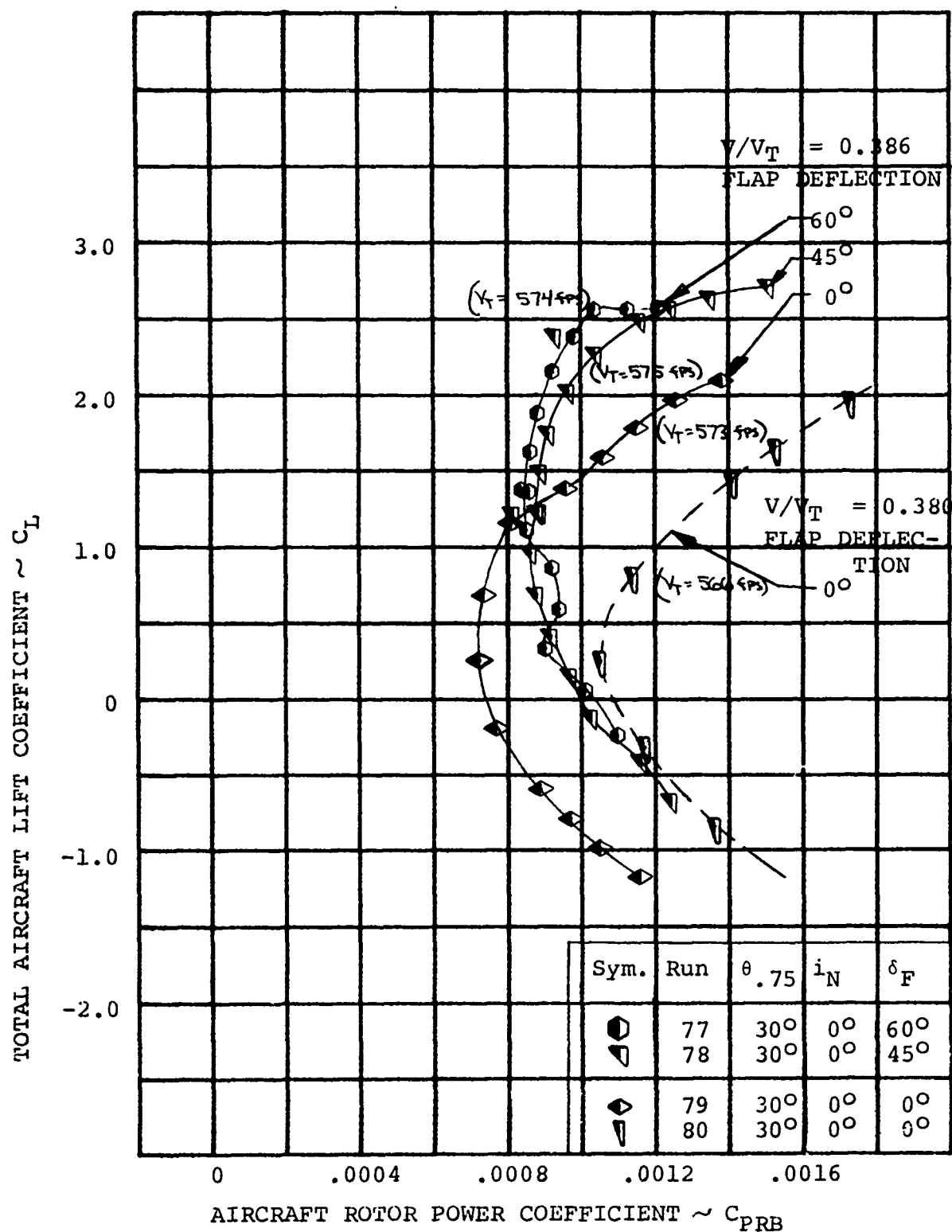


FIGURE 4-48 TOTAL AIRCRAFT LIFT/ROTOR POWER VARIATION IN CRUISE $i_N = 0^\circ$

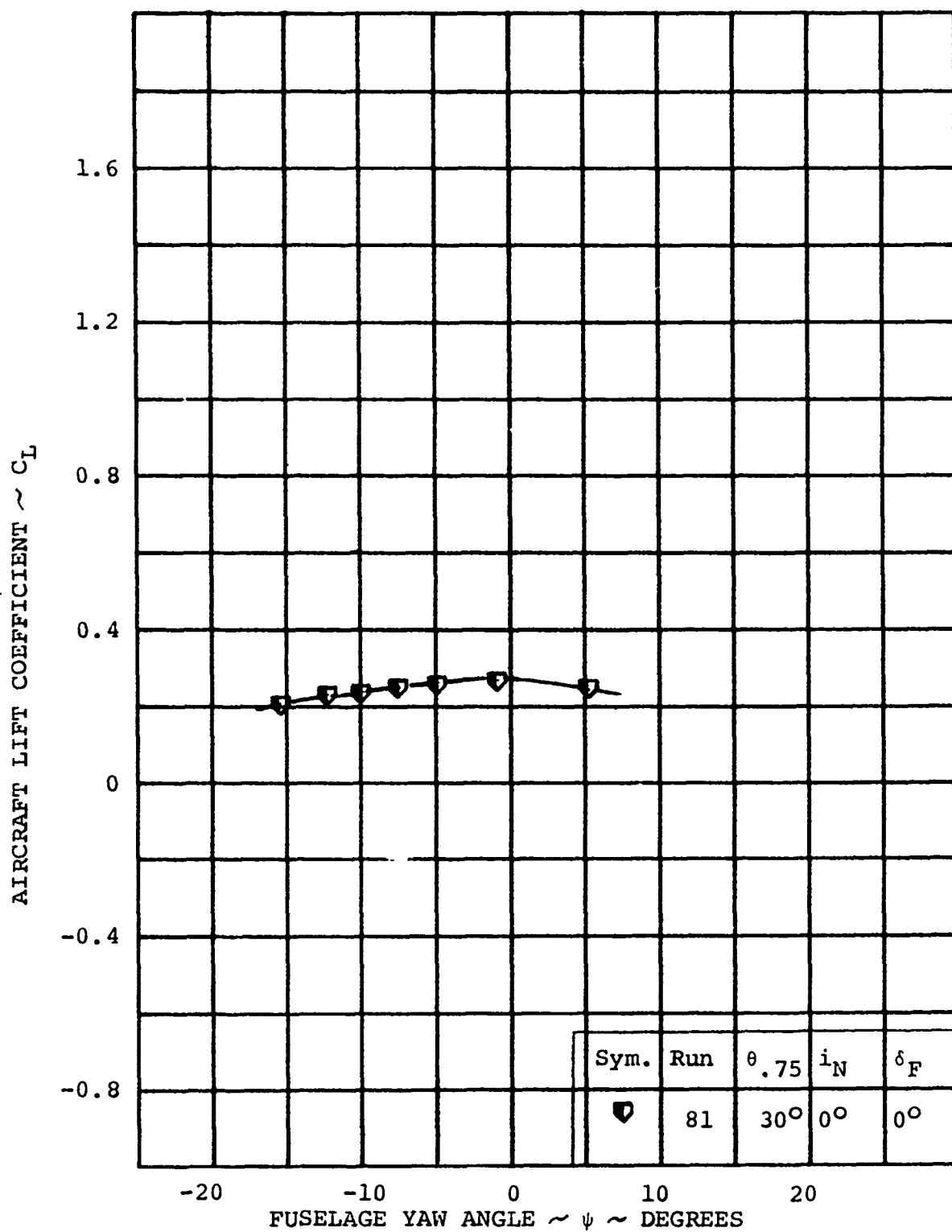


FIGURE 4-49 AIRCRAFT LIFT/YAW ANGLE VARIATION AT $V/V_T = 0.382$

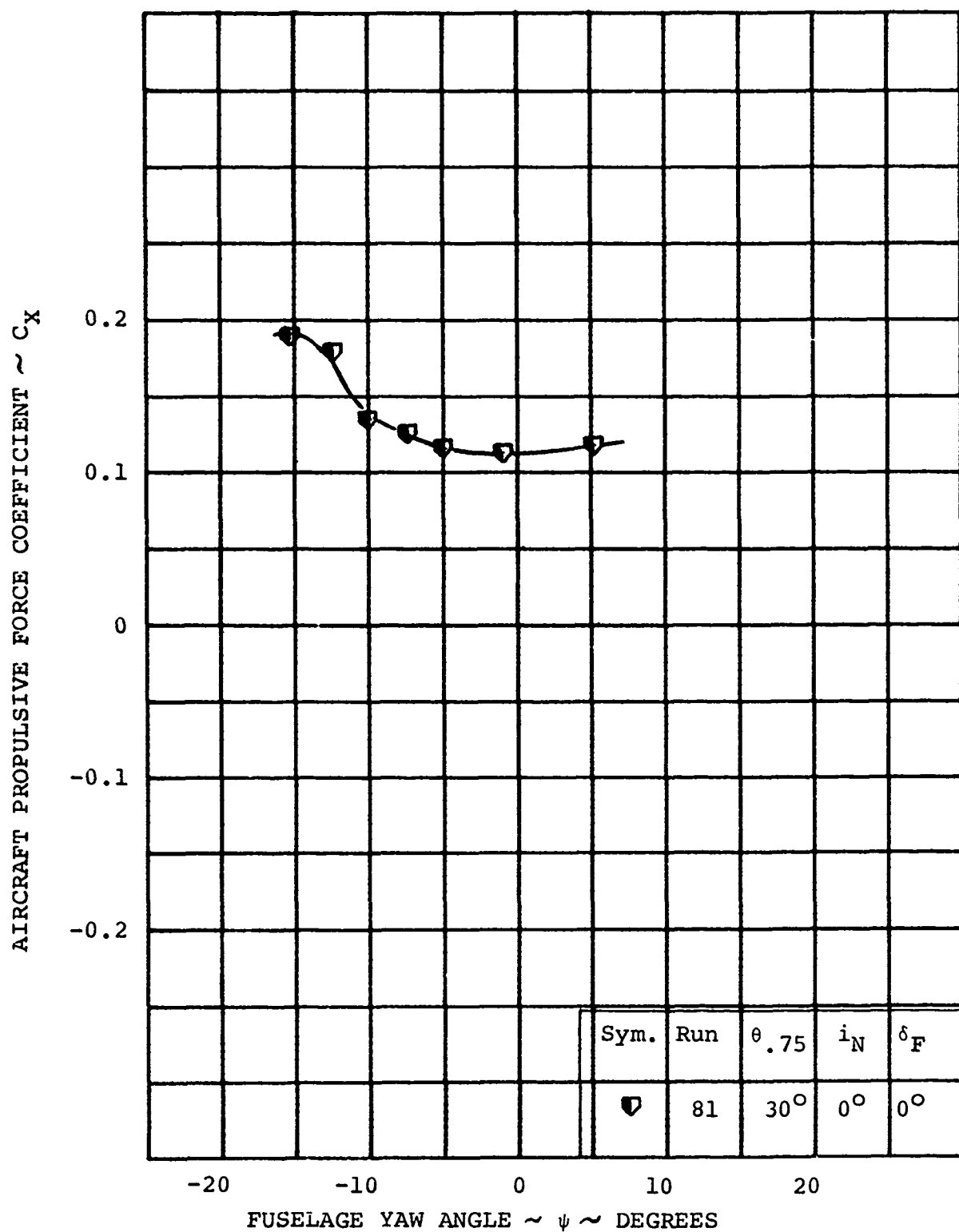


FIGURE 4-50 AIRCRAFT PROPULSIVE FORCE/YAW ANGLE
VARIATION AT $V/V_T = 0.382$ $i_N = 0^\circ$

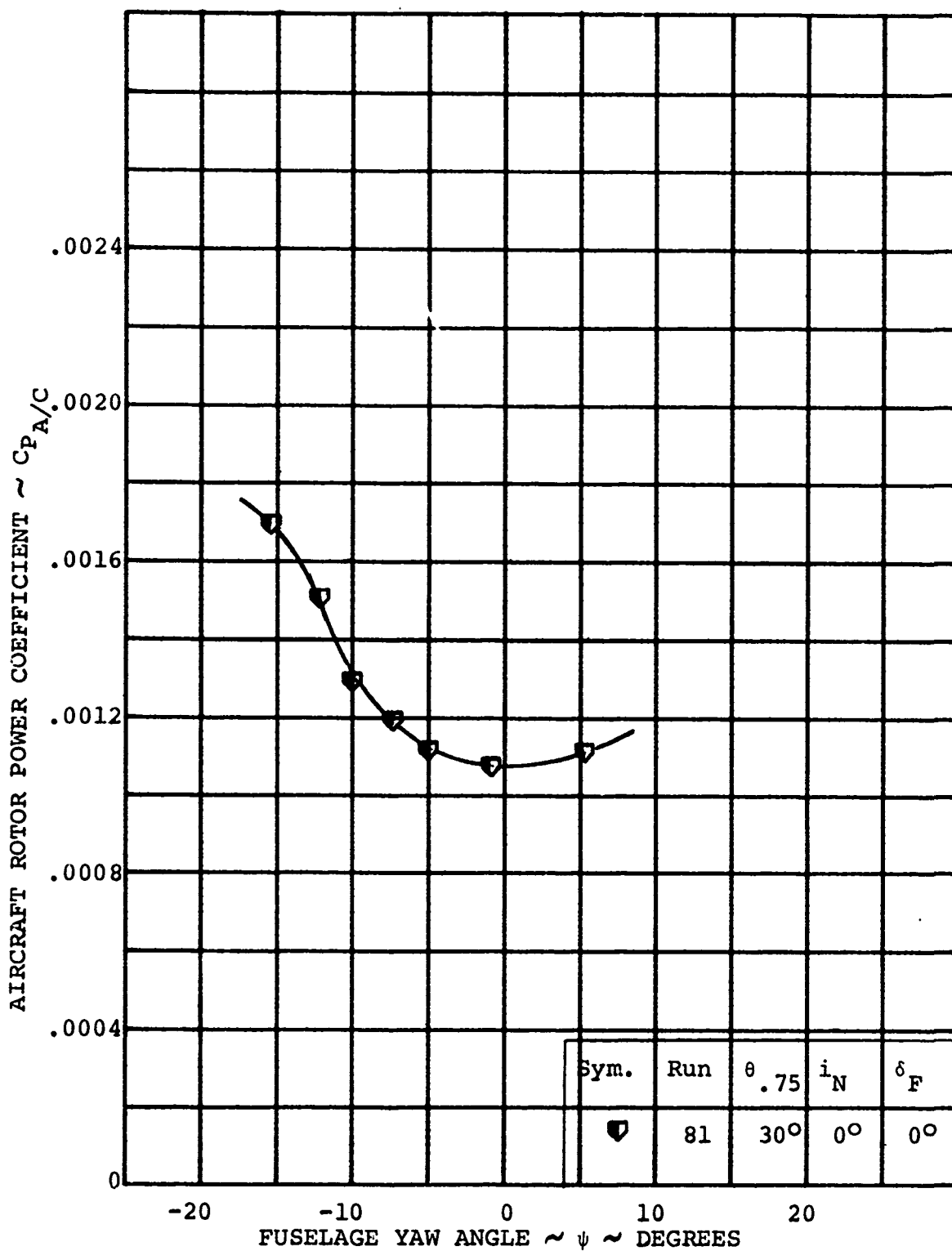


FIGURE 4-51 AIRCRAFT ROTOR POWER/YAW ANGLE VARIATION
AT $V/V_T = 0.382$ $i_N = 30^\circ$

4.5 CONCLUSIONS - PERFORMANCE

Analysis of the performance test data presented here allows the following conclusions to be made:

1. Minimum download was achieved in hover with a flap setting of 70 degrees and umbrella flaps set at 75°/70°. The download out of ground effect is less than 5 percent of the aircraft thrust.
2. Flap setting and umbrella angle has no effect on rotor performance.
3. The minimum download configuration produces the best total aircraft performance.
4. The maximum lift loss due to rotor airframe interference is 3 percent of the total lift available in STOL operation.
5. The total aircraft maximum lift occurs at an angle of attack of 20 degrees in mid-transition.
6. The rotor performance data cannot be scaled up and be representative of the full scale aircraft but is adequate for the correlation with theory for the contract final report.

5.0 STABILITY AND CONTROL

A brief summary of the stability and control data obtained in the hover, transition and cruise flight regime follows.

Control moment data in hover show that adequate pitch and yaw control can be obtained with cyclic pitch control (Figure 5-1). The effects of ground proximity on control moments were found to be small for tests with one rotor. Tests with both rotors were prevented by motor failure. Twin rotors could give different results.

Rotor stability derivatives measured in transition are shown in Figure 5-2. At 12 degrees angle of attack, the rotor stalls and accounts for the derivative becoming stable. The total aircraft stability derivative data for the same condition (Figure 5-3) show that the rotor contribution is large and destabilizing. The change in slope between 5 and 10 degrees reflects wing stall followed a few degrees later by rotor stall. Wing and rotor stall now define the limits of the transition envelope. The model rotors, not being dynamically scaled, produce more destabilizing moment than the full scale aircraft would as a result of the significant difference in flapwise frequency ratio and blade Lock Number.

At the test conditions the model has a flapwise frequency ratio ($\frac{\omega_b}{\Omega}$) 1.66 and a blade Lock Number (γ) of 17.28 while the full scale Model 213 rotor has a flapwise frequency ratio of 1.22 and a Lock Number of 11.81. This is a substantial difference.

Roll and yaw control in transition is provided by the use of differential thrust and differential cyclic pitch. Figure 5-4 shows the required mixing for pure control based on test data and cross-plots from test data.

A comparison of the predicted isolated rotor pitching moment derivative and test data crossplotted to zero wing lift in cruise show good agreement (Figure 5-5) and indicates a 50-percent increase in hub moment due to wing-rotor interference. The total model pitching moment derivative (Figure 5-6) is seen to be unstable and this is predicted by the isolated rotor theory corrected for wing interference. The same methodology was used to compute the full-scale aircraft derivative and is shown to be stable.

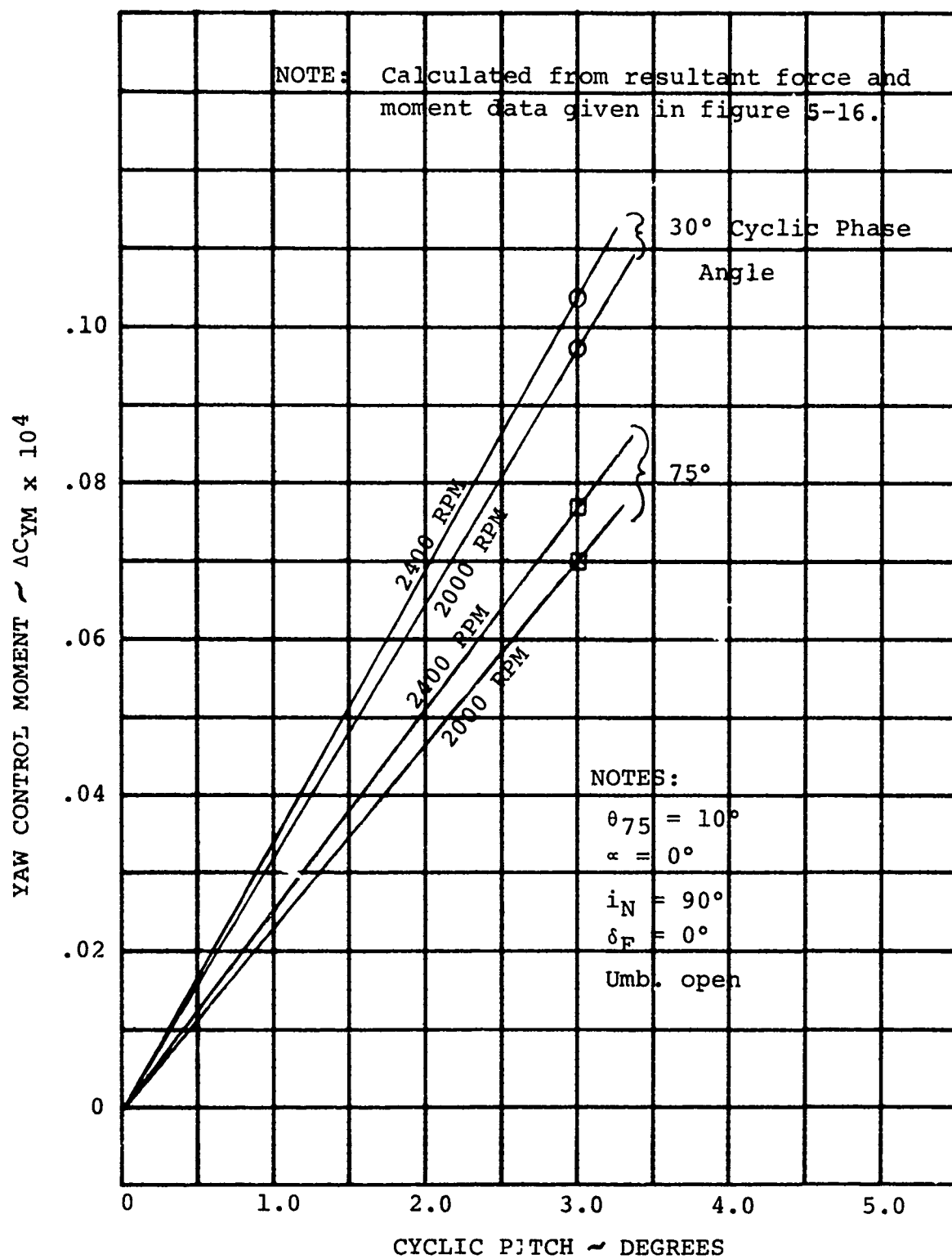


FIGURE 5-1

YAW CONTROL HOVER, OGE

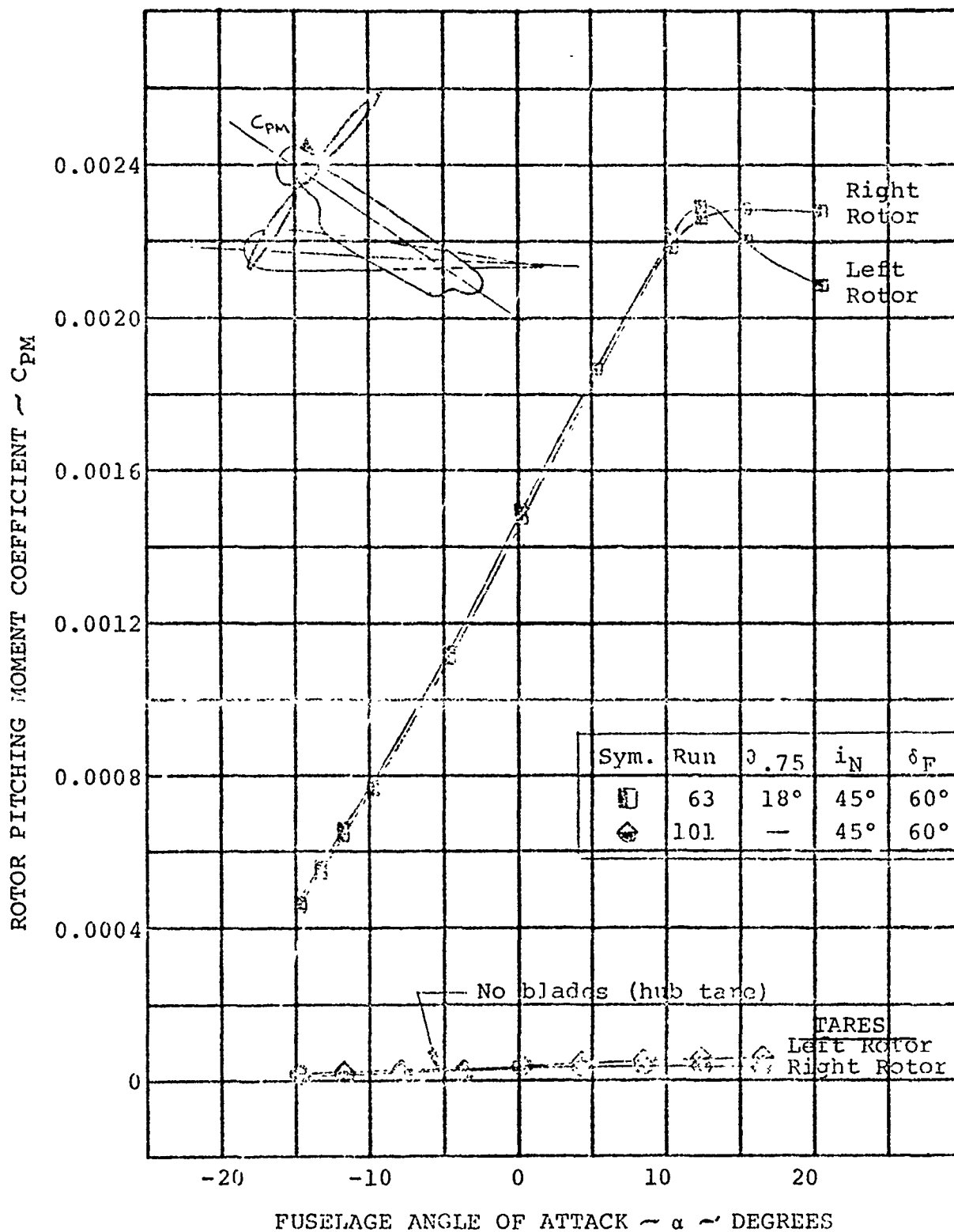


FIGURE 5-2 ROTOR PITCHING MOMENT/ANGLE OF ATTACK VARIATION AT $V/V_T = 0.260$ WITH $i_N = 45^\circ$

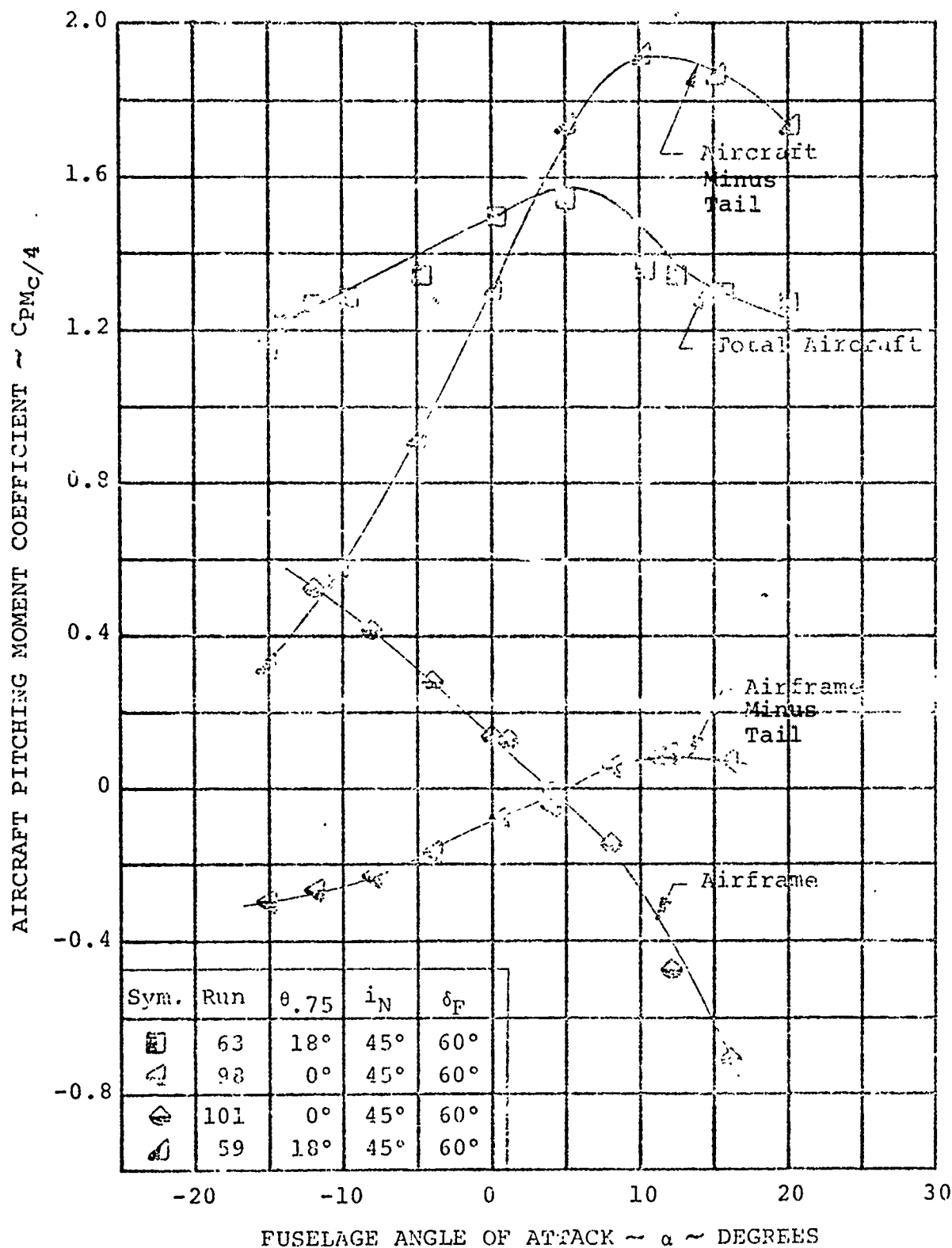


FIGURE 5-3

CONTRIBUTION OF PROP/ROTORS AND HORIZONTAL TAIL TO AIRCRAFT PITCHING MOMENT AT $V/V_T = 0.26$ WITH $i_N = 45^\circ$

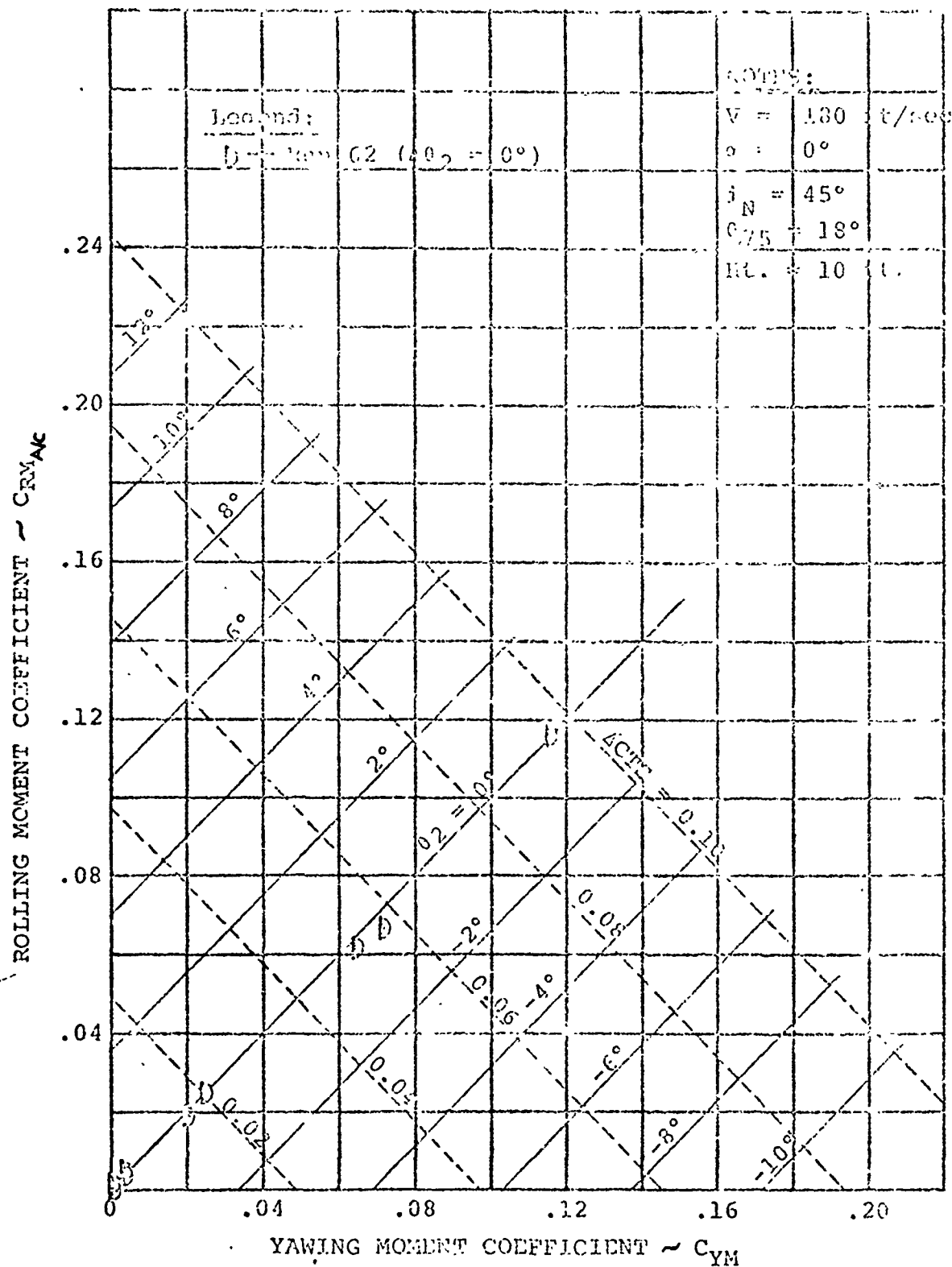


FIGURE 5-4

CONTROL MIXING DURING TRANSITION

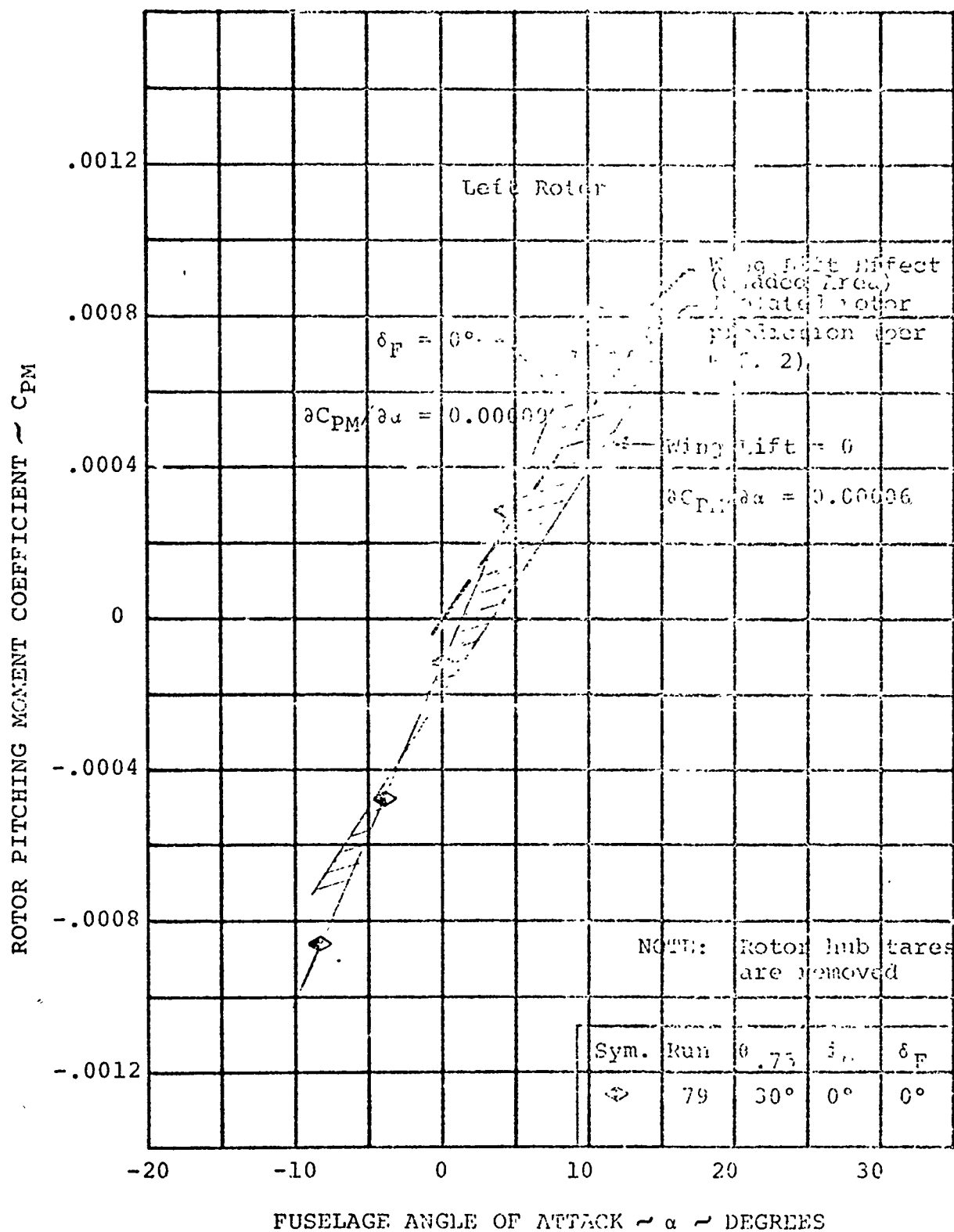


FIGURE 5-5

INFLUENCE OF WING LIFT ON ROTOR
PITCHING MOMENT AT $V/V_T = 0.386$

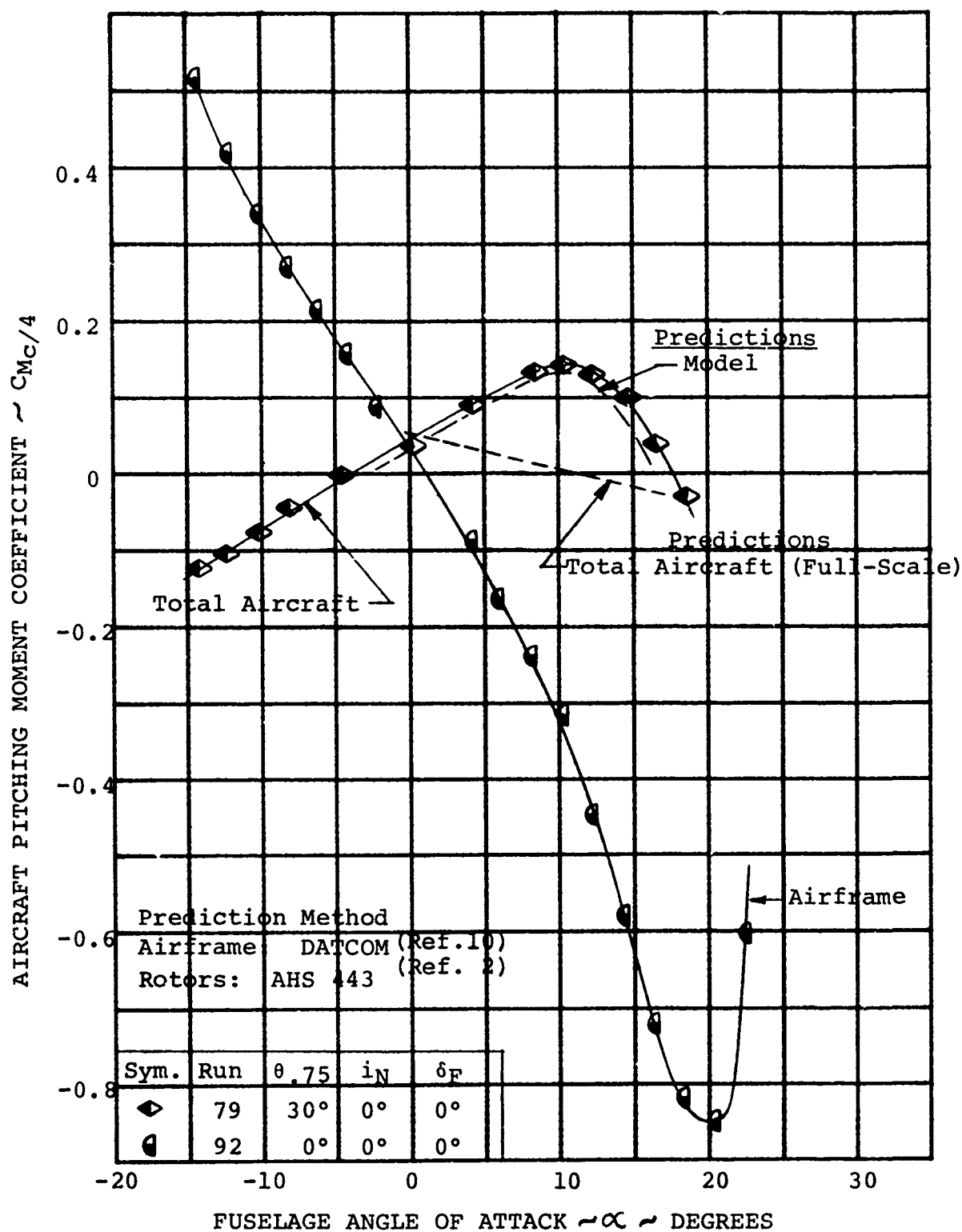


FIGURE 5-6

CONTRIBUTION OF PROP/ROTORS AND HORIZONTAL TAIL TO AIRCRAFT PITCHING MOMENT AT $V/V_T = 0.386$

5.1 HOVER STABILITY AND CONTROL

The hover mode refers to operation with the nacelle incidence at 90 degrees and with zero forward velocity. This discussion addresses rotor and aircraft stability, cyclic pitch control, control phasing and ground effect and skittishness.

5.1.1 Rotor Stability Derivatives

As can be seen from Figure 5-7, angle of attack changes produce no variation of rotor pitching moment during hovering in ground effect, i.e., $\frac{\partial C_{pm}}{\partial \alpha} = 0$. The data shown is for both left and

right rotors. Similarly, rotor normal force is insensitive to angle of attack, $\frac{\partial C_N}{\partial \alpha} = 0$, for the hovering case, as can be seen

in Figure 5-8. Similarly, $\frac{\partial C_{pm}}{\partial \alpha}$ and $\frac{\partial C_N}{\partial \alpha}$ are zero for out of ground effect operation as seen from Figure 5-9. It is to be noted that although this flight condition was performed at a freestream dynamic pressure (q) of 4 psf the rotor pitching moment and normal force are insensitive to angle of attack changes.

5.1.2 Aircraft Stability Derivatives

The aircraft lift coefficient based on slipstream dynamic pressure, q_s , from Figure 5-10 varies linearly with fuselage angle of attack for the range of angles from -5° to $+5^\circ$, thus giving the stability derivative, $\frac{\partial C_{Ls}}{\partial \alpha} = 0.033/\text{degree}$. The pitching

moment derivative with α for the linear range from -5° to approximately 2.6° is, $\frac{\partial C_{pm}}{\partial \alpha} = .0245/\text{degree}$ from Figure 5-11.

5.1.3 Cyclic Pitch Control

Two runs were obtained in the hover tests with cyclic pitch on the right-hand rotor only. For these runs, the rotor swashplate was set to give 3 degrees nose-up cyclic. The control phase angle was set at 65 degrees; that is, the swashplate was set so that the zero longitudinal cyclic pitch position was at 65 degrees azimuth (Figure 5-12) rather than 0 degrees as for pure helicopter phasing. The model rotor heights used were 2.15 feet and 10 feet.

The rotor forces and moments generated by cyclic pitch are shown in Figures 5-13 through 5-16. The rotor normal force generated by 3 degrees cyclic pitch is about 4 percent of the thrust. The corresponding thrust vector tilt is about .8 degrees per degree of cyclic pitch. The rotors are also strong hub moment producers because of the stiffness of the blades.

The data indicate an increase in power coefficient of 8 percent with a 3 degree increase in cyclic as indicated in Figure 5-15. A large part of this may be due to increased friction in the swashplate bearing with cyclic on, however. The magnitudes of the resultant in-plane force and moment vectors due to cyclic are given as a function of rotor speed in Figure 5-16. These data show little or no variation with RPM. This is typical of the rest of the rotor data in coefficient form.

5.1.4 Control Phasing

The effect of blade stiffness is seen in the cyclic phase angles required for pure longitudinal or lateral control. The control phase angle is the angle through which the zero cyclic pitch axis must be shifted in order to align the moment vector due to cyclic with the aircraft axis about which control is desired. This angle is the complement of the angle between the axis for maximum cyclic excitation and that for maximum control output. Thus, for a hinged rotor, the phase angle is 0 degrees (90 degrees between maximum cyclic and maximum disc plane tilt). For a completely rigid propeller, the phase angle is 90 degrees (0 degrees between cyclic input and hub moment output).

The control phase angles obtained in the tests are shown in Figure 5-17. Included for comparison are results from the first test series with this model (Reference 9). Two angles are shown: one based on hub moment and other based on in-plane force. The moment phase angles are close to 90 degrees as might be expected for very stiff blades. The in-plane force phase angles are small indicating that some flapping freedom remains; however, since the in-plane forces are very small, the magnitude of the flapping is very small.

The moment phase angles obtained in this test agree very well with those obtained in the Reference 9 tests. The phase angles obtained from in-plane forces are independent of RPM for this test series; however, the Reference 9 tests indicate variations of phase angle with RPM. The cause of this has not yet been determined.

The influence of cyclic phase angle on control power is illustrated in Figures 5-18 and 5-19. These data have been calculated from the resultant in-plane forces and moments shown in Figure 5-16. For yaw control in hover, a small phase angle will be required for longitudinal cyclic due to the small in-plane forces. It is noted that the yaw control shown for 30 degrees phase angle in Figure 5-19 is larger than with 75 degrees phase angle. The 30-degree phase angle, however, reduces the pitch control power somewhat as indicated in Figure 5-18. In actual operation, wing torsional bending will act to give additional effective yaw control due to rotor disc plane tilt (on the order of 1.5 degrees which is equivalent to almost 2 degrees of cyclic). During these tests, the stiff wing did not contribute this to yaw control.

5.1.5 Ground Effect and Skittishness

Ground Effect

No large effects of ground proximity can be detected in the data shown in Figures 5-13 through 5-16. It cannot be concluded that ground effects are small however, since only one rotor was operating in the hover cyclic tests. This removed the image effect of the other rotor and changed the character of the rotor downwash field obtained in ground effect. Further tests are required with both rotors operating to determine the effect of ground proximity on control effectiveness.

Skittishness

Skittishness is the name given to unexpected movements of VTOL aircraft in hover or near-hover flight. Past experience in this area is summarized by References 3 to 8. The causes of these motions on previous VTOL aircraft have been ascribed to various phenomena, control slop, harmony, force feedback, gusts, pilot technique, downwash, upwash, Karman vortices and so on. Almost no measured data exist and most of the data are in the form of pilot opinion. The "skittishness" experienced on VTOL aircraft has been experienced only in-ground-effect operation in hover and low forward speed. The only reported data on a tilt-rotor vehicle is the XV-3 which exhibited an erratic tendency to dart laterally and oscillated in roll when hovering within 5 feet of the ground. The tests described in this section were performed to determine if this model showed evidence of skittishness and if its causes could be isolated.

Tests were performed in hover both in and out-of-ground effect at various rotor RPM's and also RPM splits. Further, the effect of tilting the wing and rolling the model were also investigated. The model balance in the fuselage recorded oscillatory moments in one or more directions at nearly all of the

hover test conditions both in and out of ground effect. These oscillations were approximately at the natural frequency of the model on its balance-sting mounting as determined from static disturbance tests reported in Appendix B. Vibratory moments were also noted in roll in the cruise flight mode with rotors off. No long-period oscillations in model forces were observed in any flight condition; however the model natural frequencies in the force directions are high (of the order of two per rev; see Appendix B). Model oscillations occur whenever the model damping is low. In hover, the roll model damping ratio is $L\dot{\phi}/I_{YY} = -0.6$ and for the full-scale, $L\dot{\phi}/I_{YY} = -2.0$. The yaw damping of the model is also very low. ($N\dot{\psi}/I_{ZZ\text{model}} = -.00292$, $N\dot{\psi}/I_{ZZ} = -0.08$ full scale.)

The oscillatory model moments measured are shown in Figures 5-20 to 5-25.

The response of the model at its natural frequencies is indicative of an impulsive or random disturbance. Several potential excitation forces exist. The prebend in the sting mount causes an inertial torque or roll moment on the model balance which could cause the model to oscillate in roll when ground height was changed. The rates of change of RPM with time are not equal for the two rotors, and hence, can provide roll and yaw disturbances due to the manner in which the test point conditions are set up.

The absence of the cross-shaft allows a further possible excitation from the rotor out-of-balance forces. When the rotors are at slightly different RPM's, an out-of-balance beat phenomenon exists. The potential aerodynamic excitations are thought to be 1) the effects of rotor downwash and induced flows on the fuselage and wings, and 2) wing Karman vortices causing the rotor downwash to oscillate backward and forward, and 3) the rotor tip vortices could also produce beating phenomena at slightly different RPM's.

Figure 5-26 shows a comparison of alternating roll moments measured on the model for various tests plotted against test point number (as an approximate time indicator) from the last change in RPM. For most of the tests, the RPM was a variable but for Run No.33, where the RPM was a constant, the data indicate reduced amplitude with time. On this run, the incidence in-ground effect was varied for -4 to +4 degrees. The initial point at zero incidence gave an alternating roll moment equivalent to a 29.5 percent lift offset. The zero incidence point at the end of the run showed no alternating roll moment. The data obtained at various ground heights, Run 24, were also at constant RPM and do not seem to be time dependent, but the data trend could be the

result of inertial disturbances due to the model movement. Time dependence of the amplitude of the vibratory moments measured would indicate the vibratory moments are not present for the model in quiescent air but are the result of an extraneous disturbance (for example, tunnel operator induced).

The yaw data shown in Figure 5-27 show a much smaller reduction with time. The steady model yaw moments are shown for a small angle of attack range and two roll angles in-ground effect in Figure 5-28. There are no substantial changes in the steady moments. A low confidence level must be ascribed to the data because of the presence of unrepresentative excitations and the low damping of the model.

It is recommended that this model be retested with additional damping provided up to expected full scale damping ratios. Tests should be run allowing time for model motions due to test condition set up to damp out before data are taken. Deliberate and measured control inputs (i.e., differential thrust) can be made to determine their effects on model behavior. Trace records over at least one minute should be taken in order to provide adequate visibility in the data.

Steady forces and moments in ground effect should be measured over a wide range of incidence, roll and control input to determine if any large non-linearities in aircraft stability or control derivatives exist.

Tests of the dynamic model should be performed in and out of ground effect using accelerometers to measure model response.

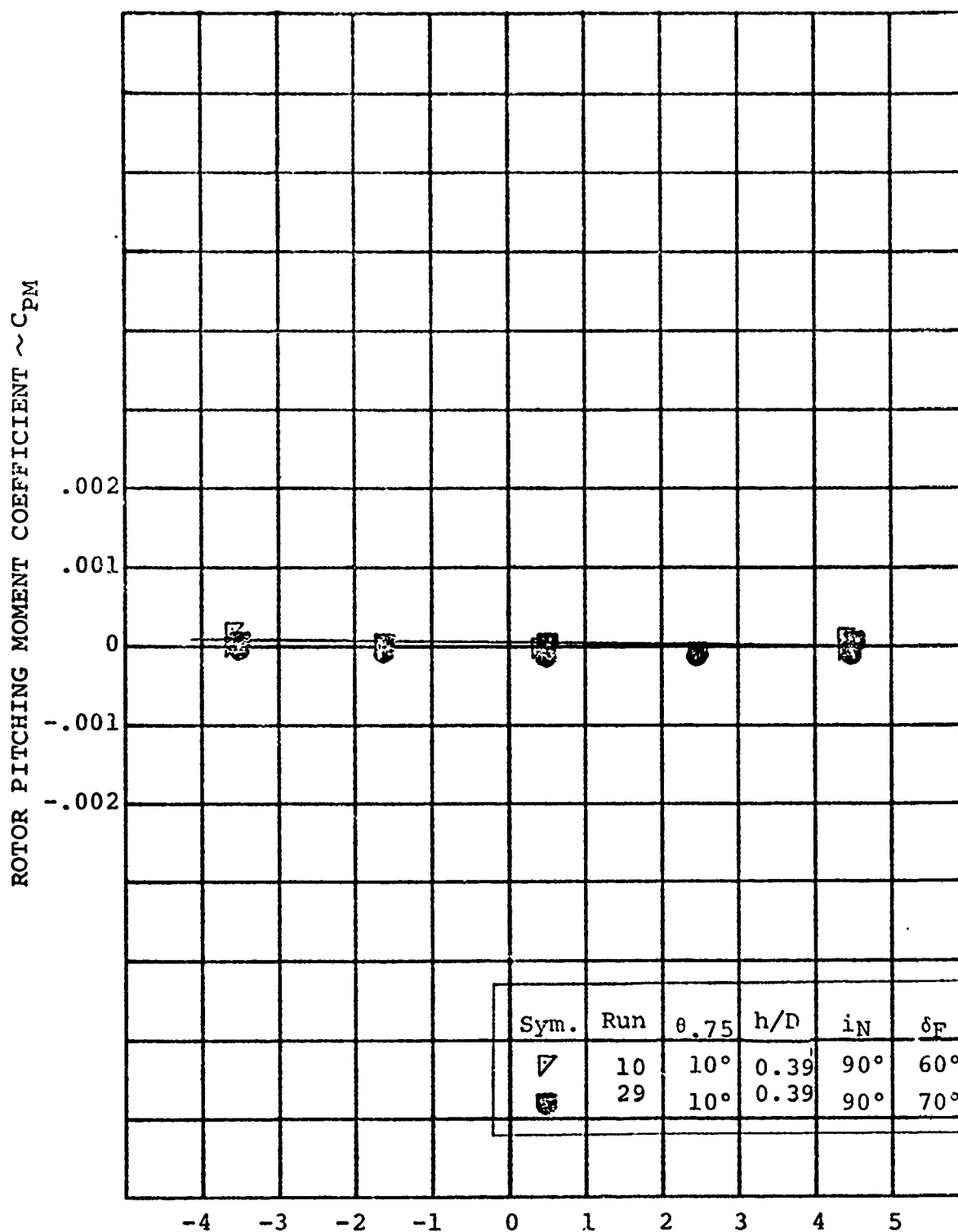
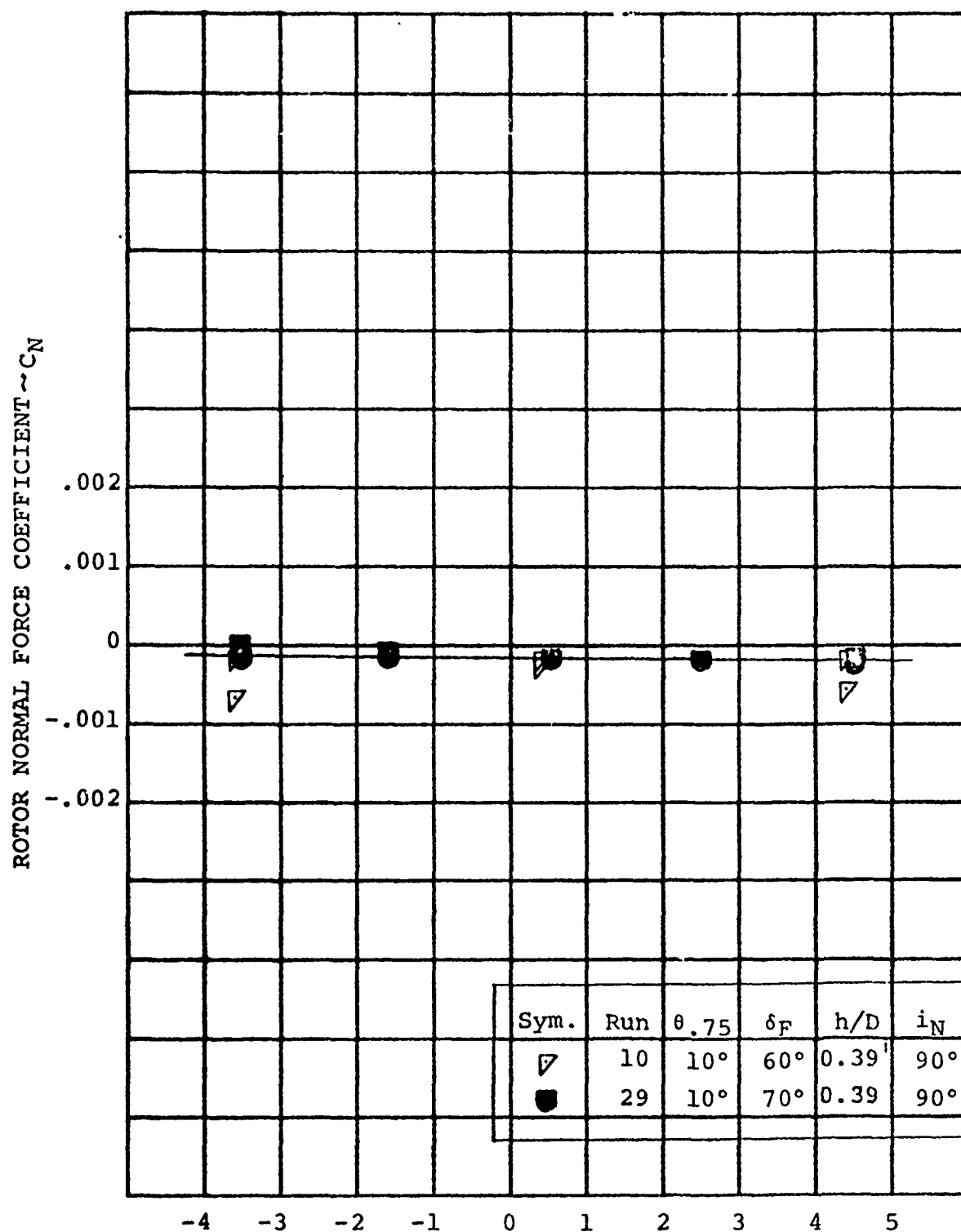


FIGURE 5-7 EFFECT OF ANGLE OF ATTACK ON ROTOR PITCHING MOMENT IN HOVER



EFFECT OF ANGLE OF ATTACK ON ROTOR
FIGURE 5-8 NORMAL FORCE IN HOVER

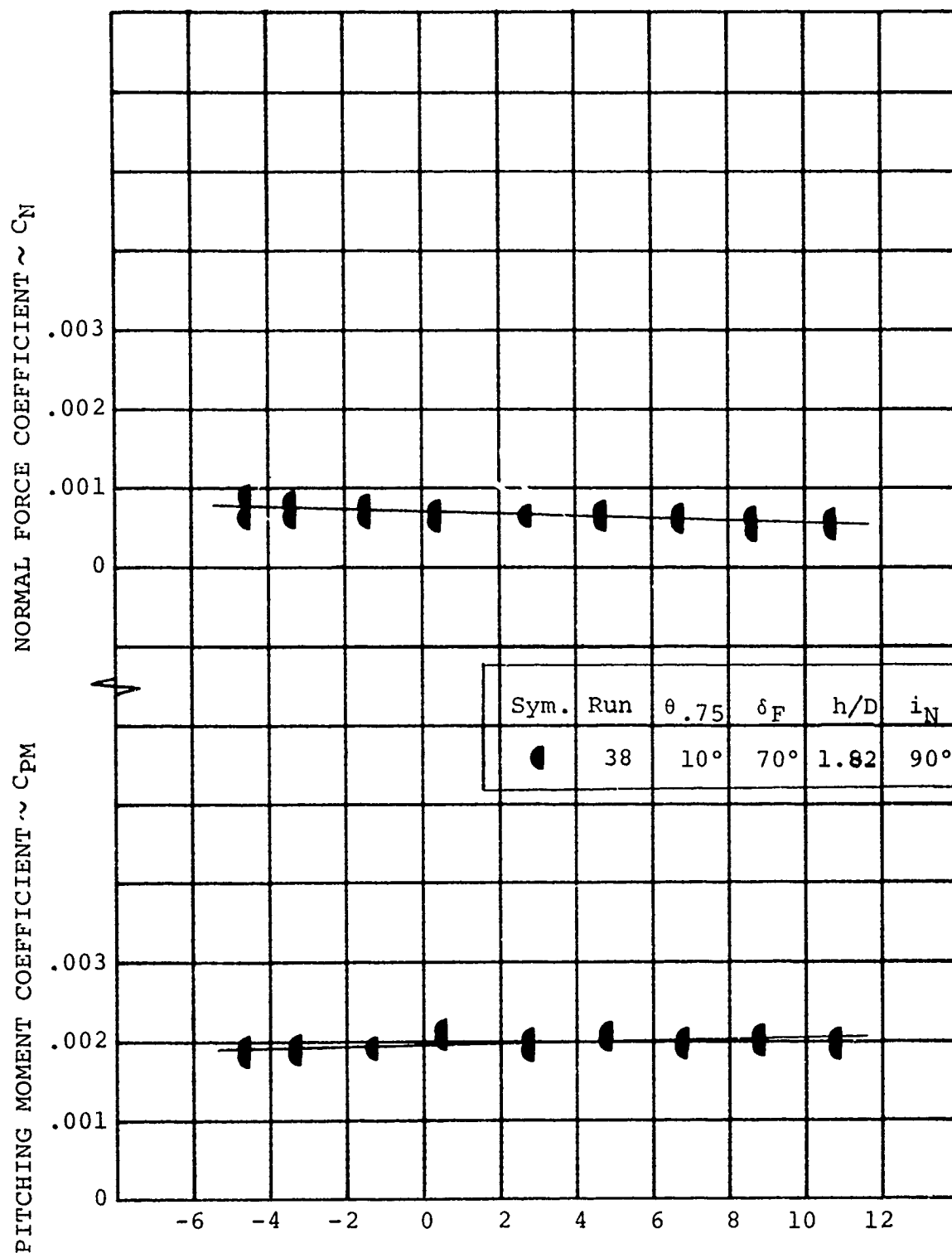


FIGURE 5-9 EFFECT OF ANGLE OF ATTACK ON ROTOR NORMAL FORCE AND PITCHING MOMENT IN THE NEAR HOVER MODE AT $q=4$ psf.

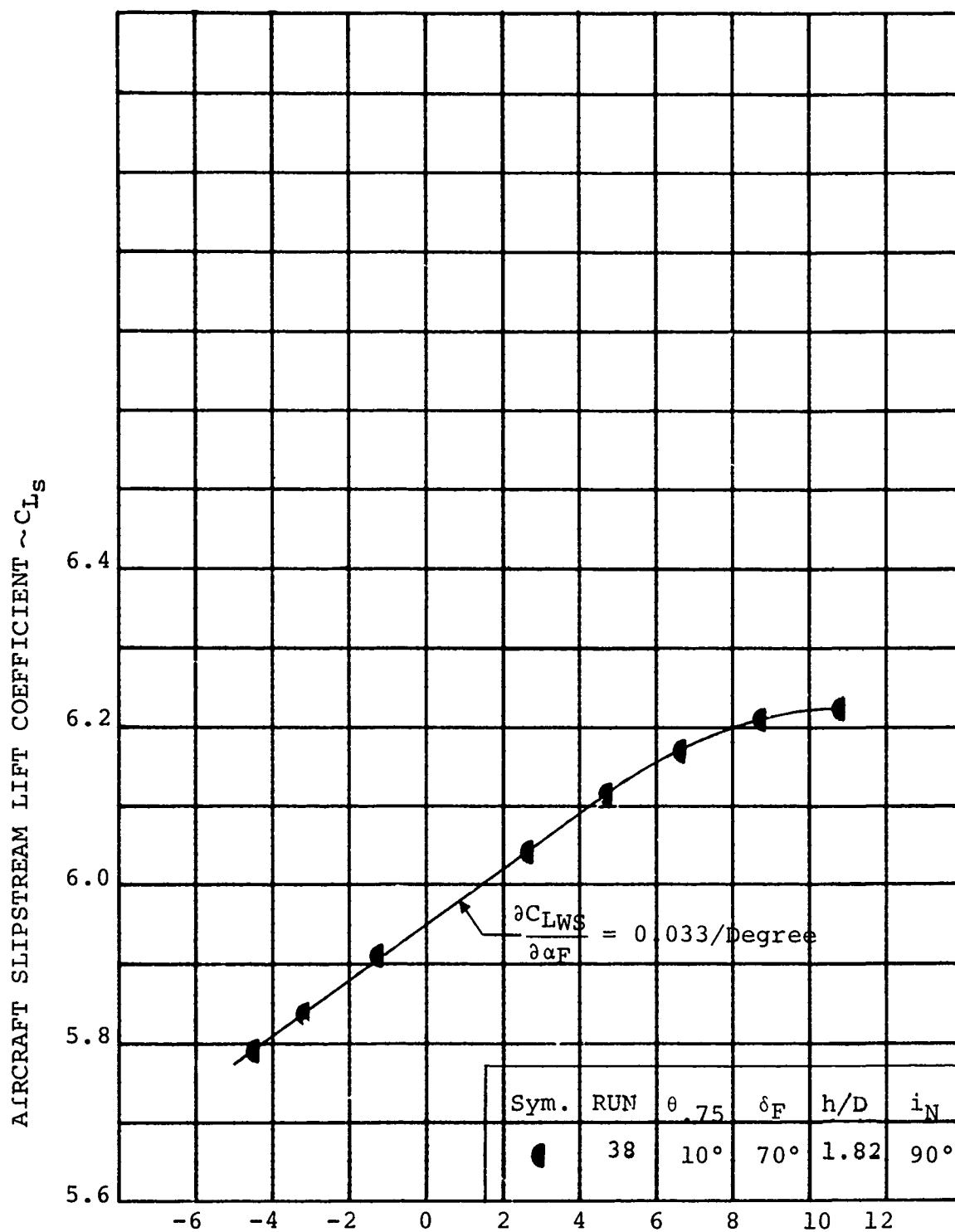


FIGURE 5-10 EFFECT OF ANGLE OF ATTACK ON AIRCRAFT LIFT
IN THE NEAR HOVER MODE AT $q=4$ psf.

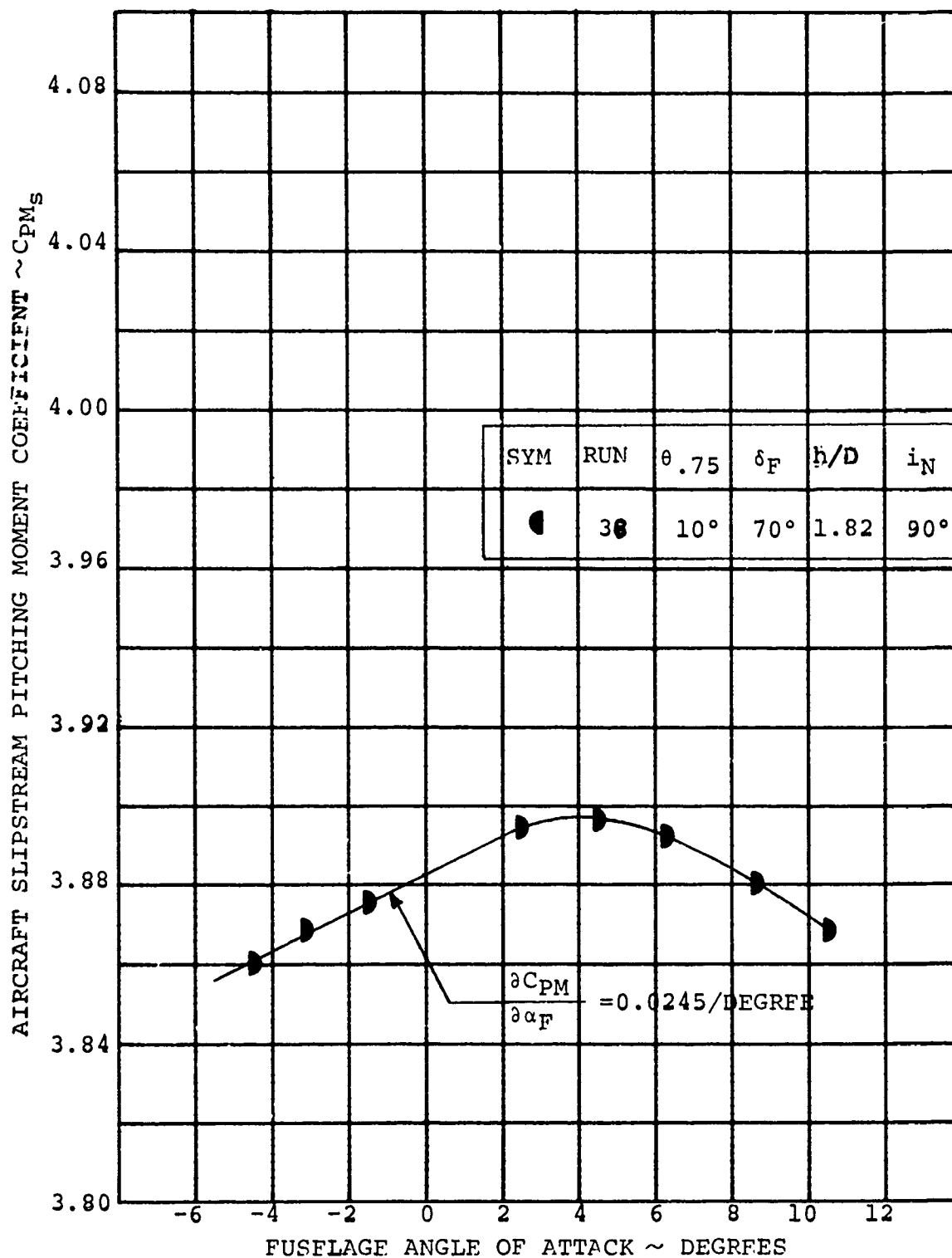


FIGURE 5-11 EFFECT OF ANGLE OF ATTACK ON AIRCRAFT PITCHING MOMENT IN THE NEAR HOVER MODE AT $q=4\text{psf}$.

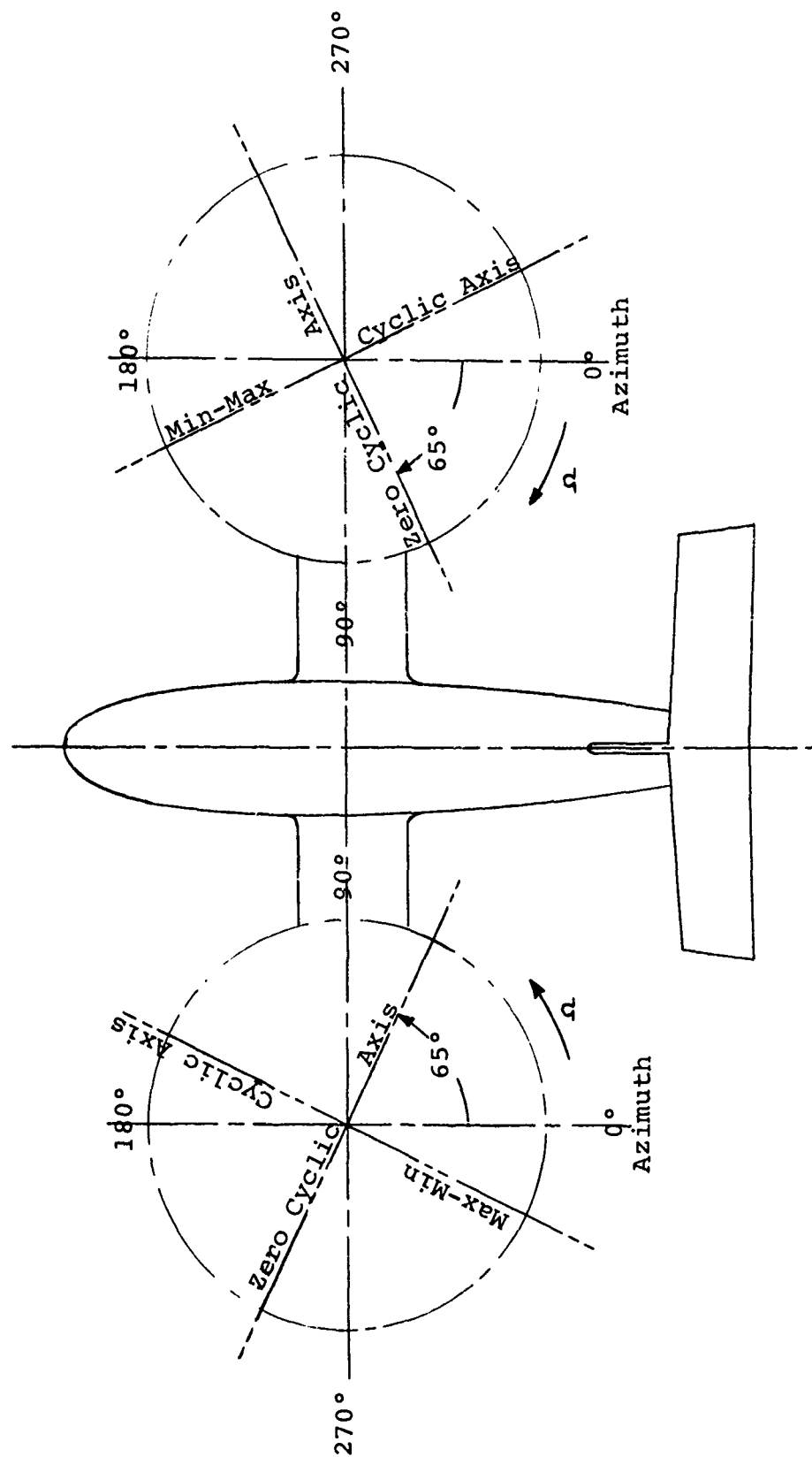


FIGURE 5-12 INPUT CYCLIC PITCH PHASE ANGLE GEOMETRY

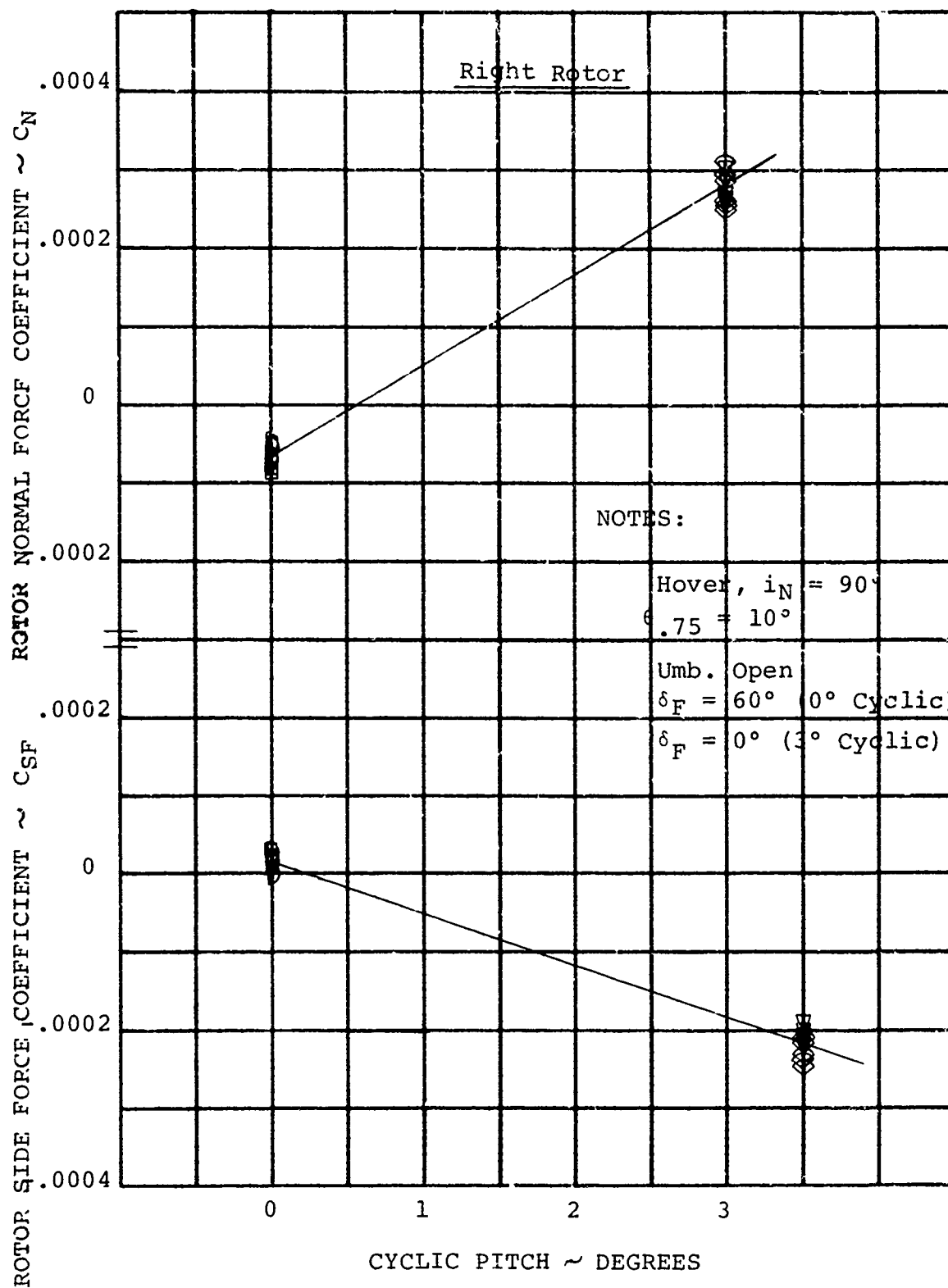


FIGURE 5-13

EFFECT OF CYCLIC PITCH ON ROTOR FORCES

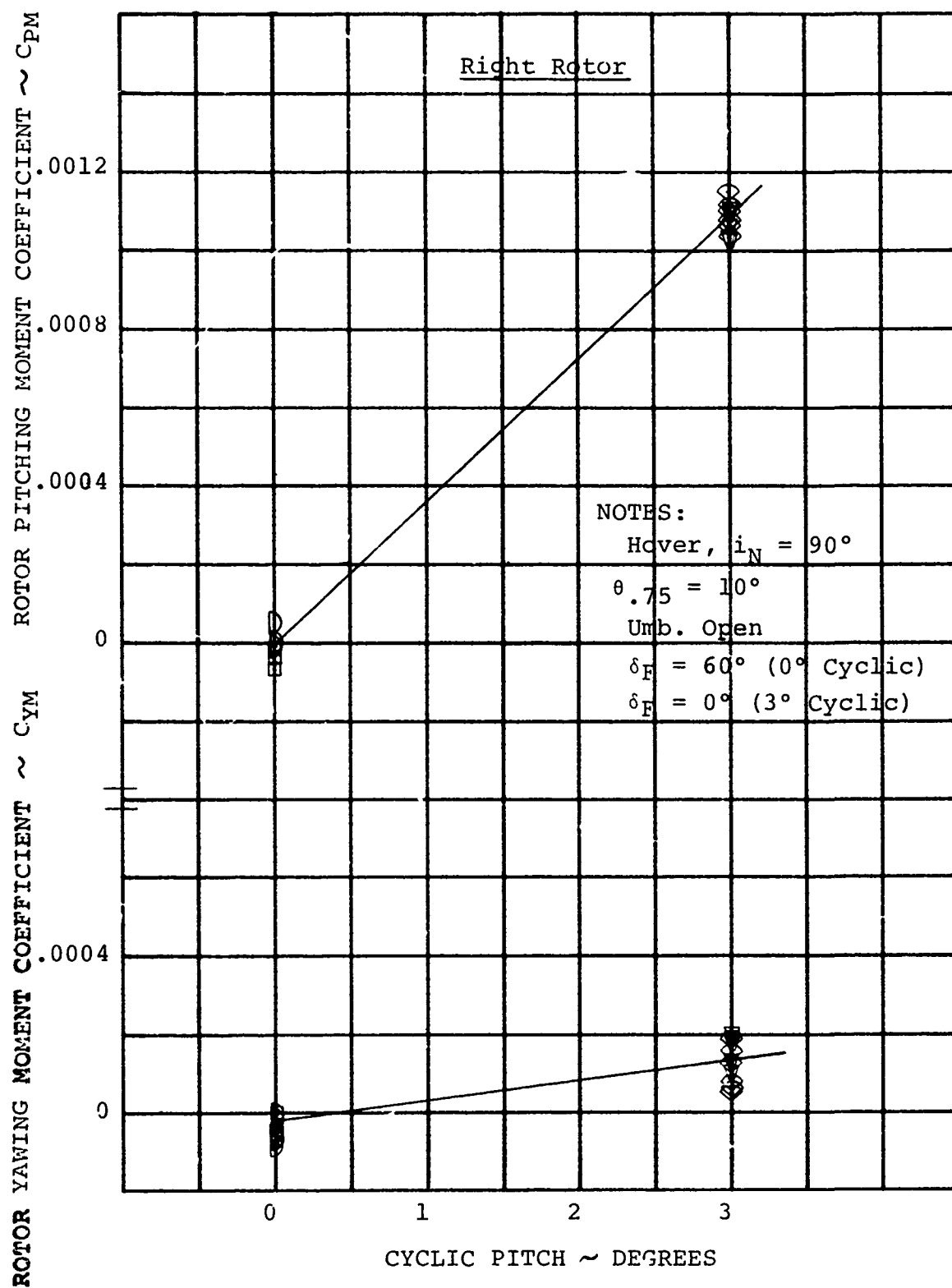


FIGURE 5-14

EFFECT OF CYCLIC PITCH ON ROTOR MOMENTS

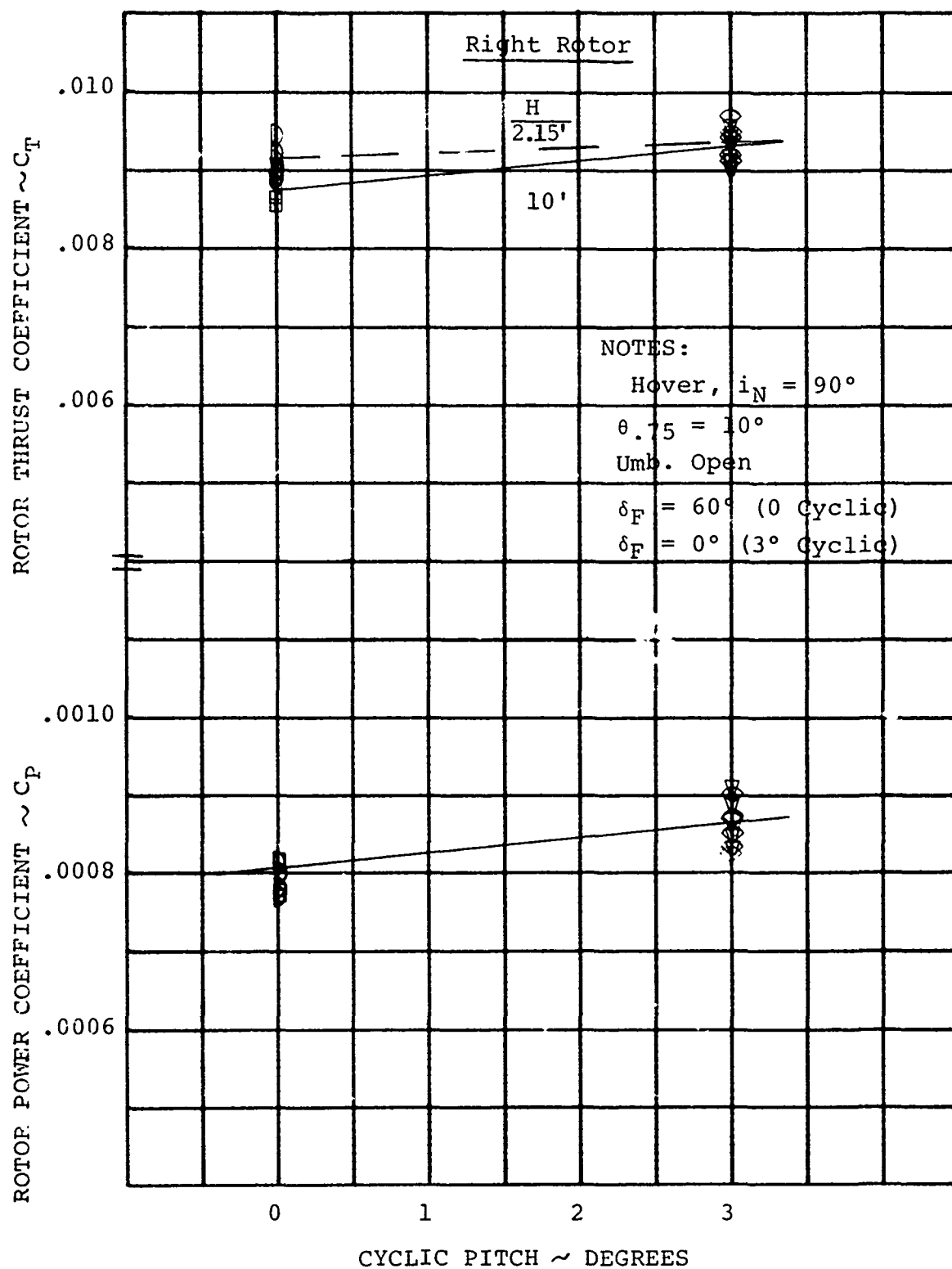


FIGURE 5-15

EFFECT OF CYCLIC PITCH ON THRUST AND POWER

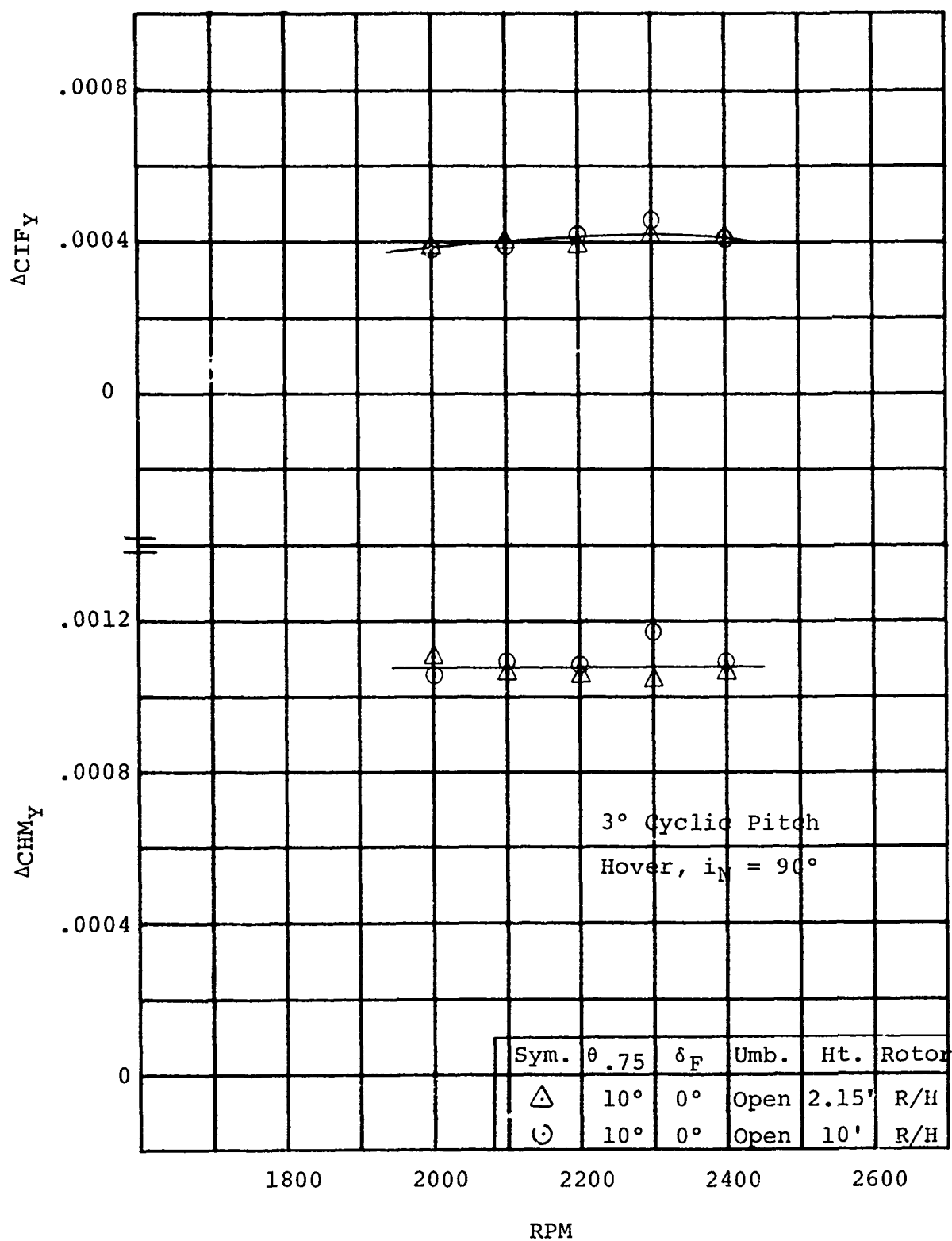


FIGURE 5-16

RESULTANT IN-PLANE FORCE AND HUB MOMENT
DUE TO CYCLIC PITCH

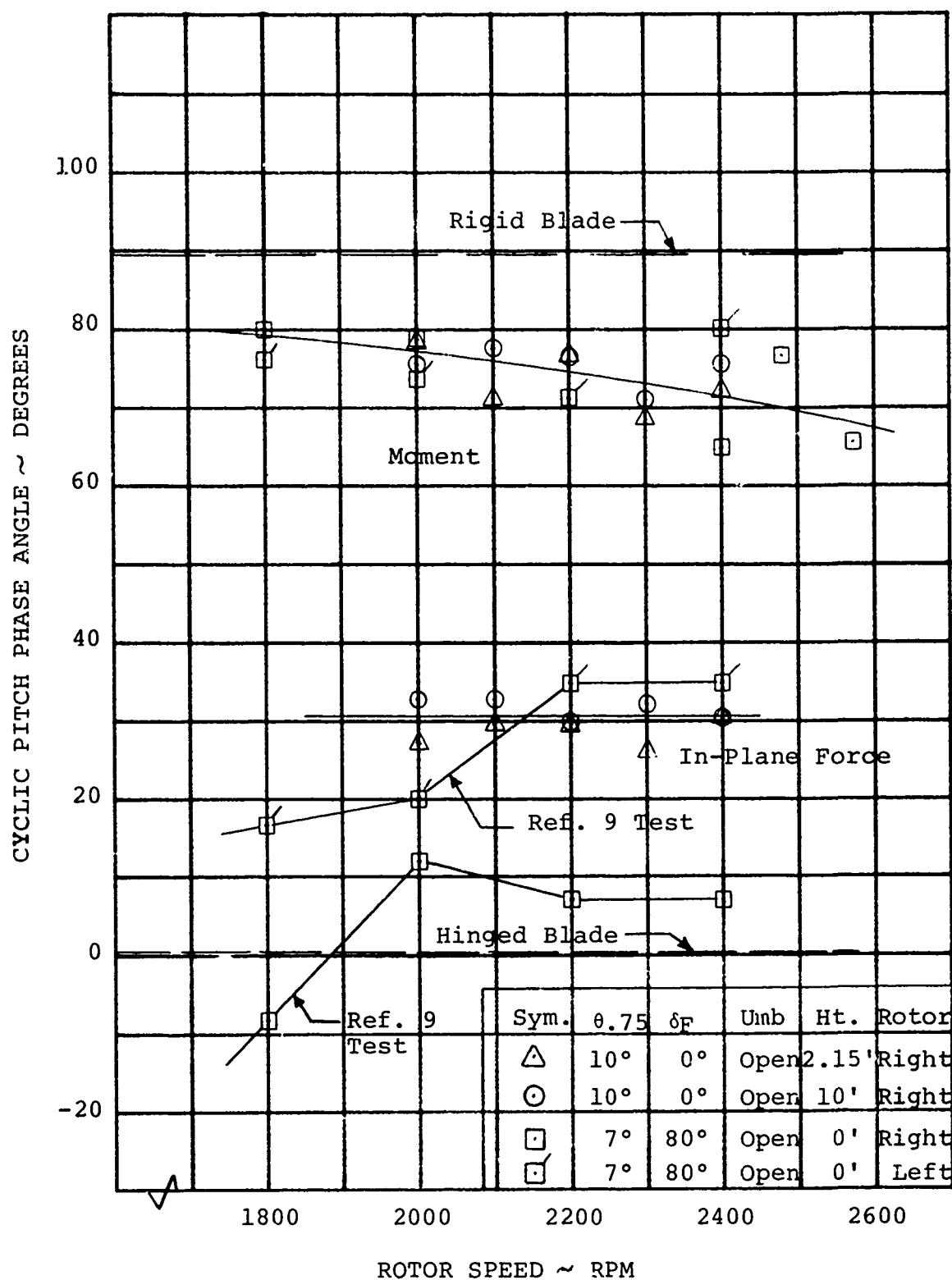


FIGURE 5-17

HOVER CYCLIC PITCH PHASE ANGLE

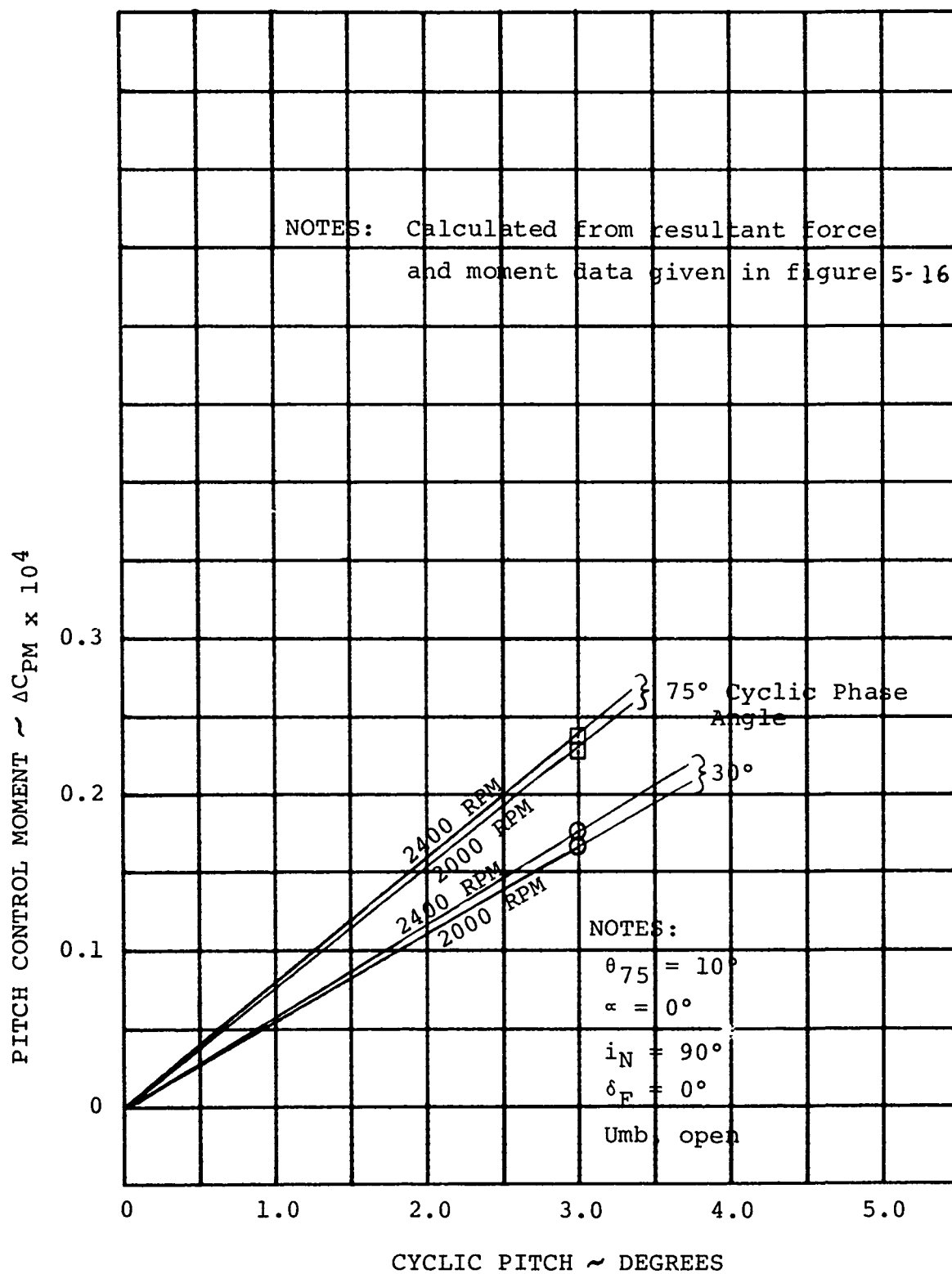


FIGURE 5-18

PITCH CONTROL HOVER, OGE

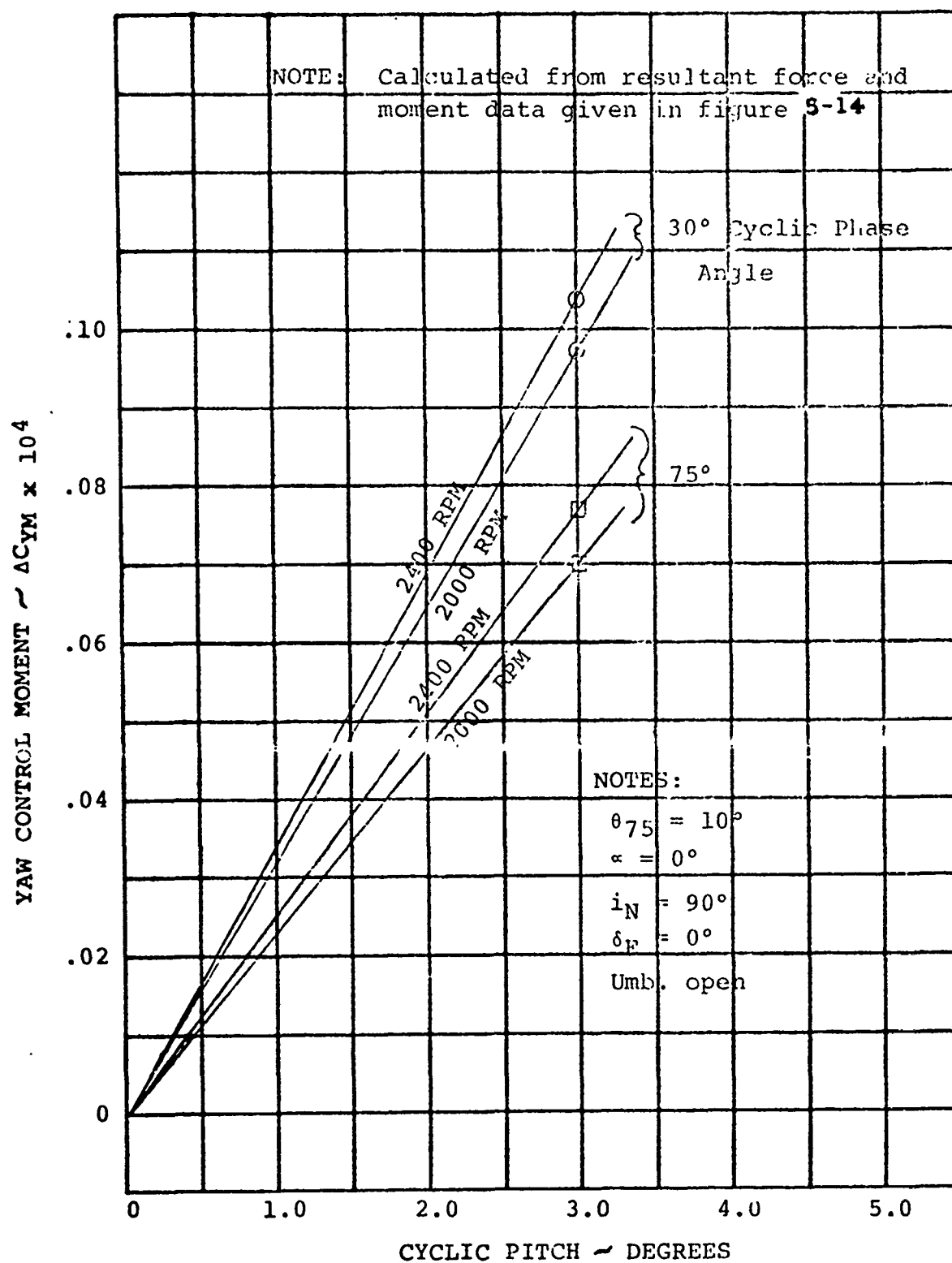


FIGURE 5-19

YAW CONTROL HOVER, OGE

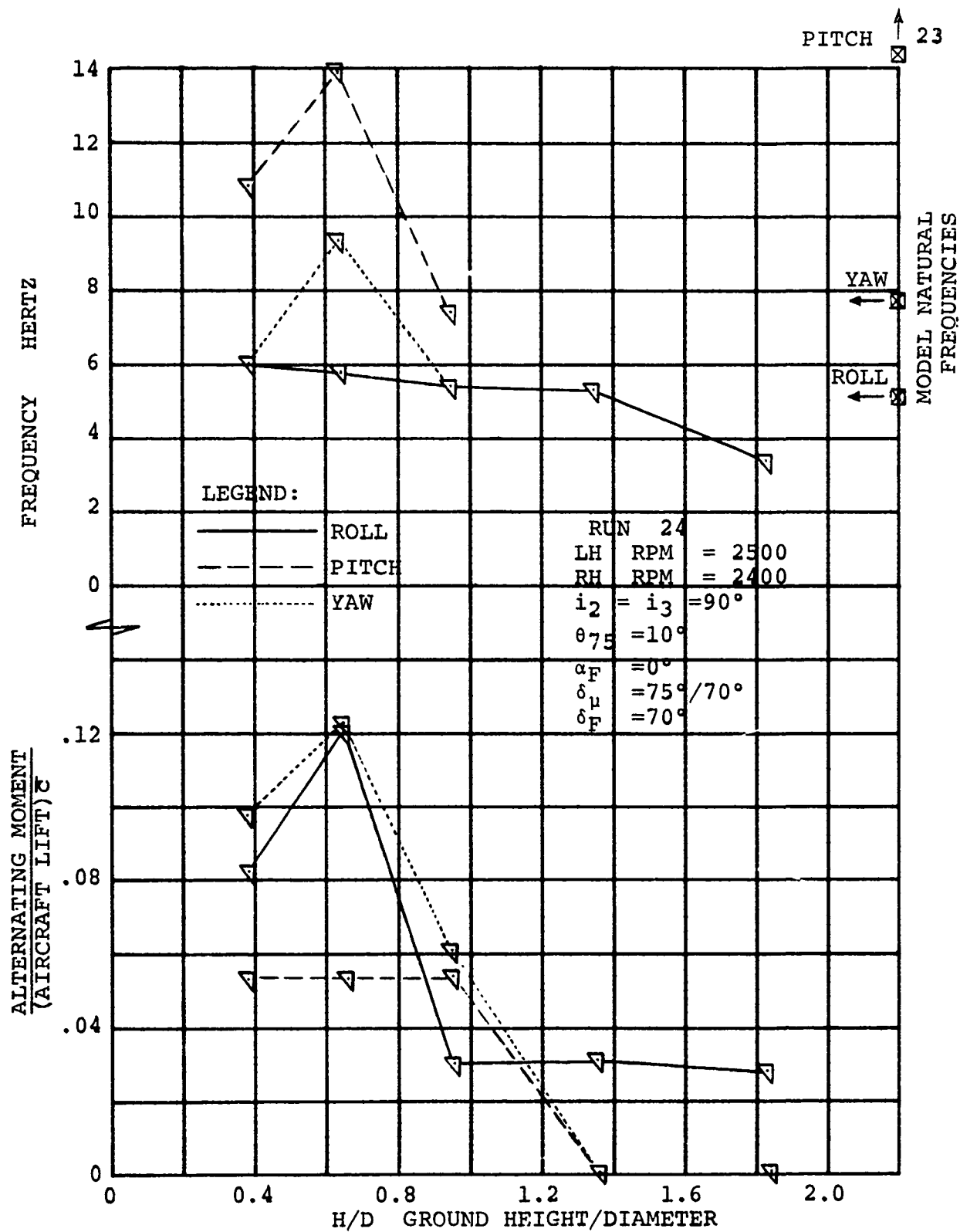


FIGURE 5-20 EFFECT OF GROUND HEIGHT ON ALTERNATING AIRCRAFT MOMENTS IN HOVER

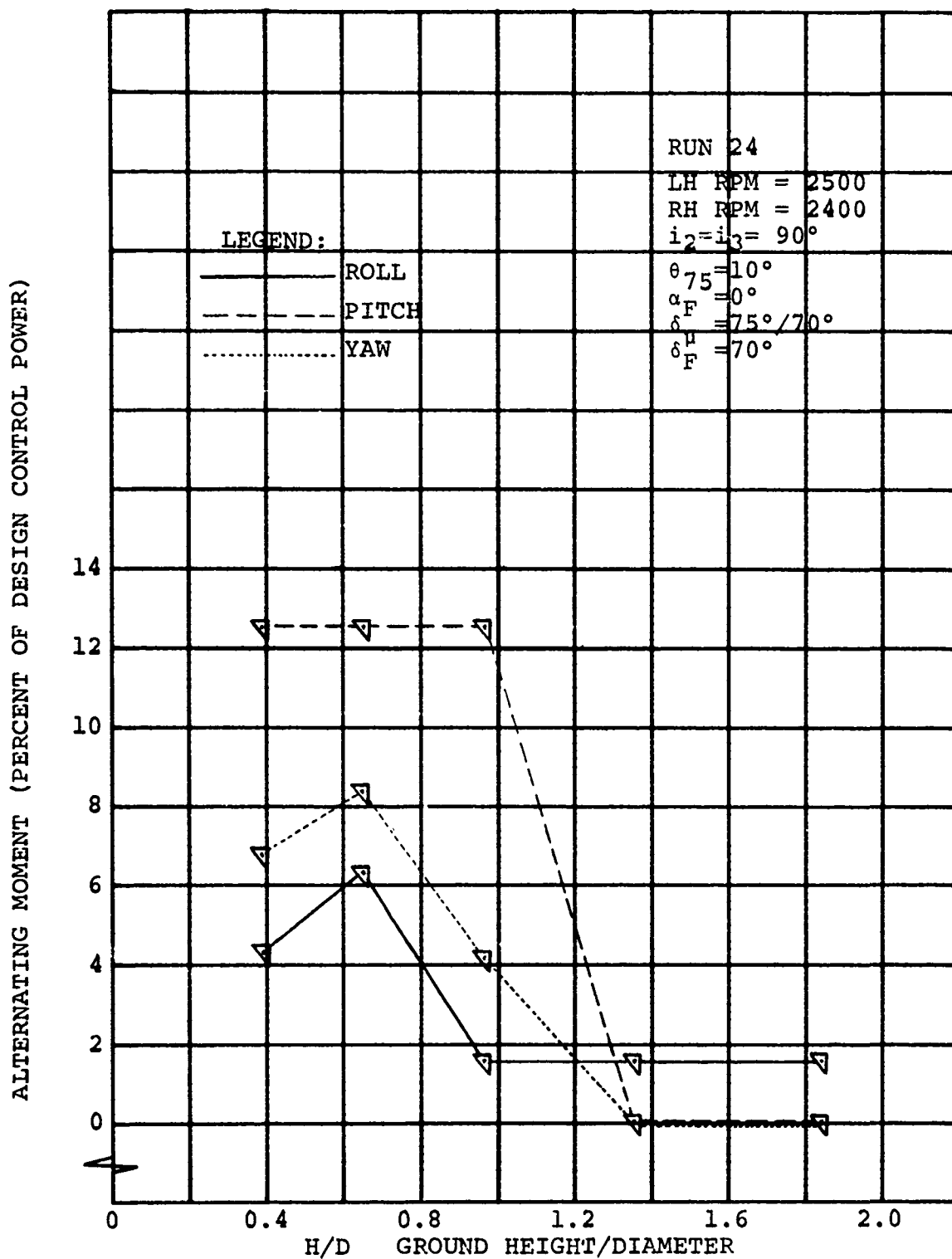


FIGURE 5-21 MODEL ALTERNATING MOMENTS IN TERMS OF DESIGN CONTROL POWER

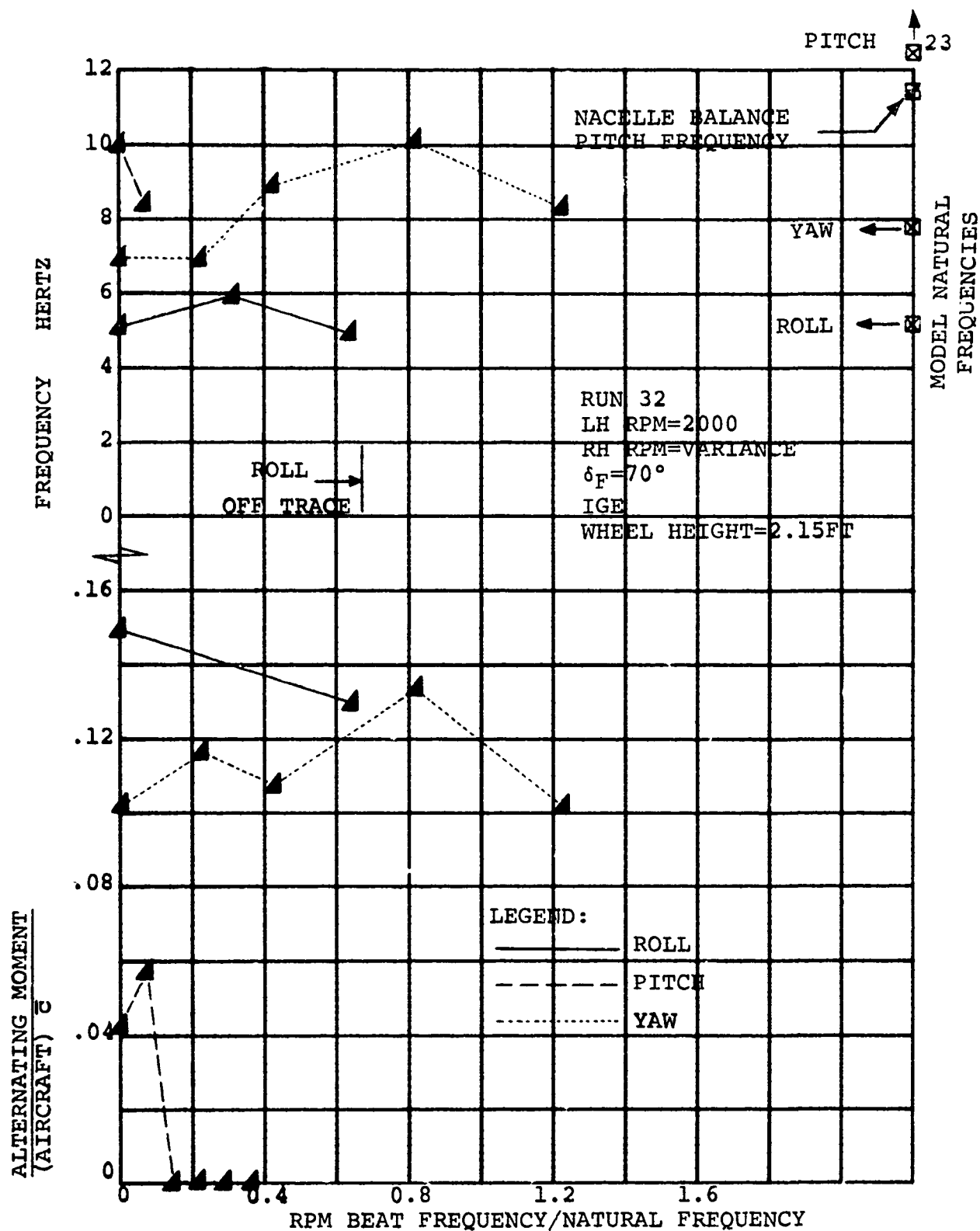


FIGURE 5-22 EFFECT OF RPM DIFFERENCE (BEATING) ON AIRCRAFT LONG PERIOD FORCES AND MOMENTS

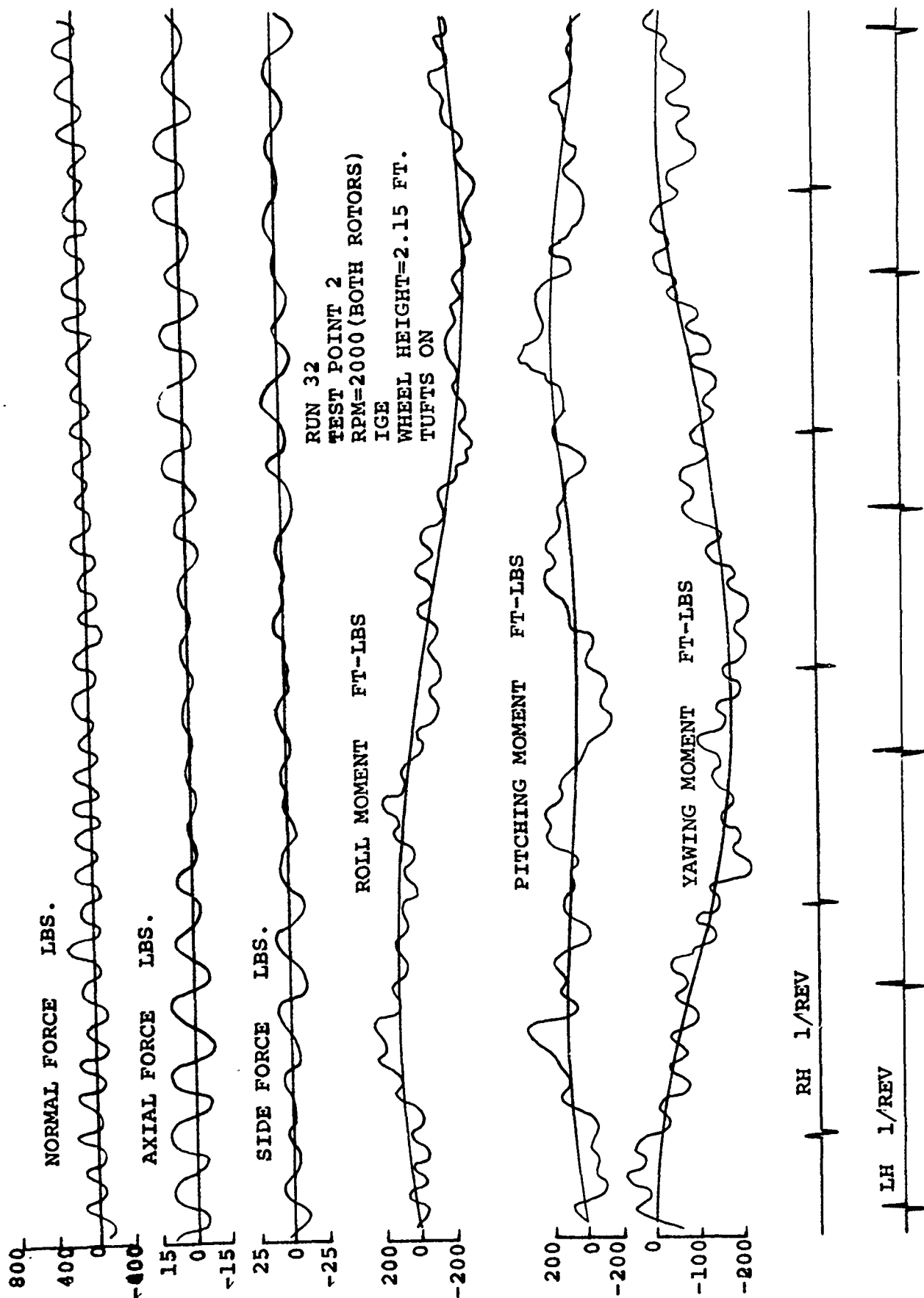


FIGURE 5-23 EXAMPLE OF FUSELAGE BALANCE OSCILLOGRAPH TRACES

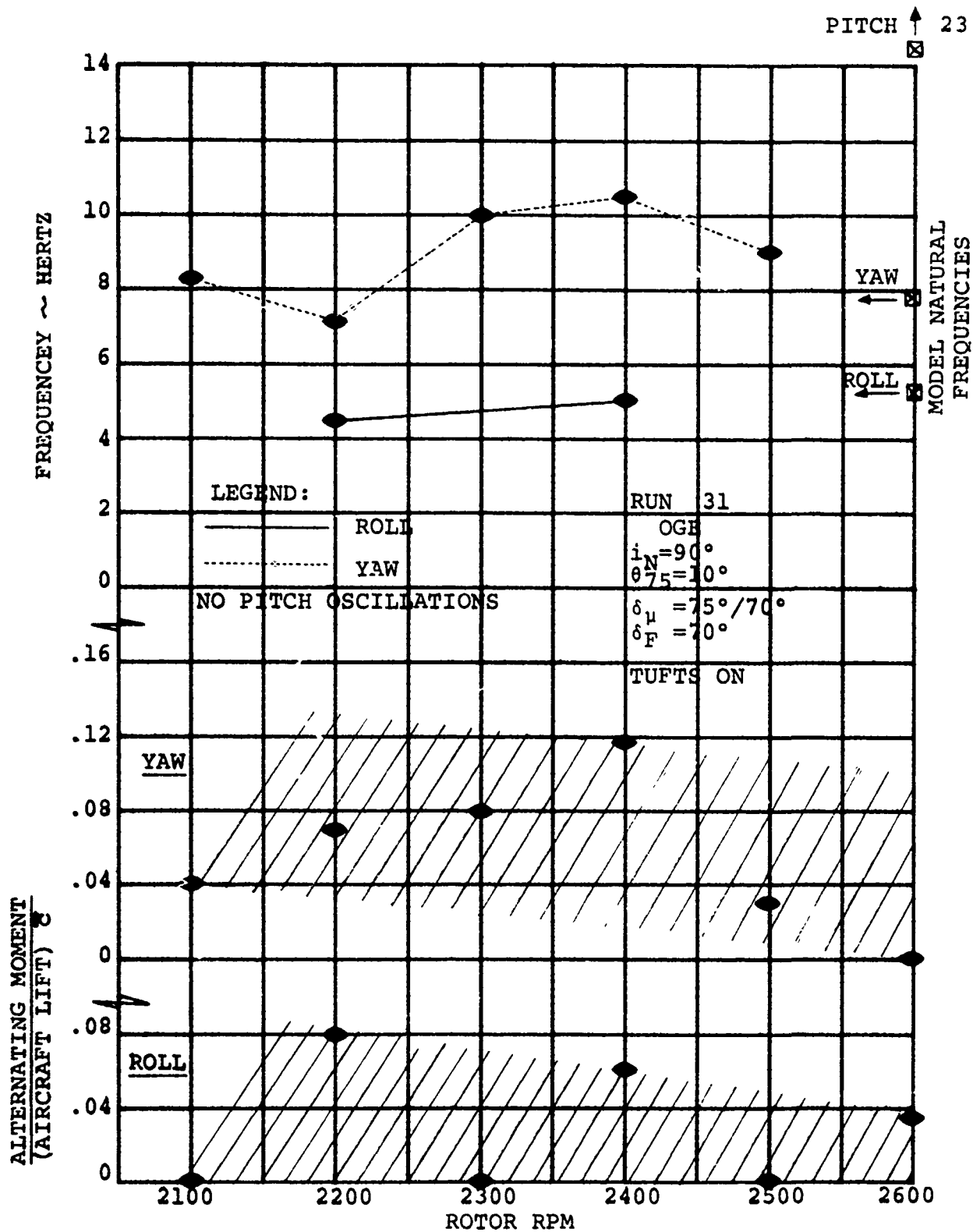


FIGURE 5-24 EFFECT OF ROTOR RPM ON ALTERNATING MODEL MOMENTS IN HOVER

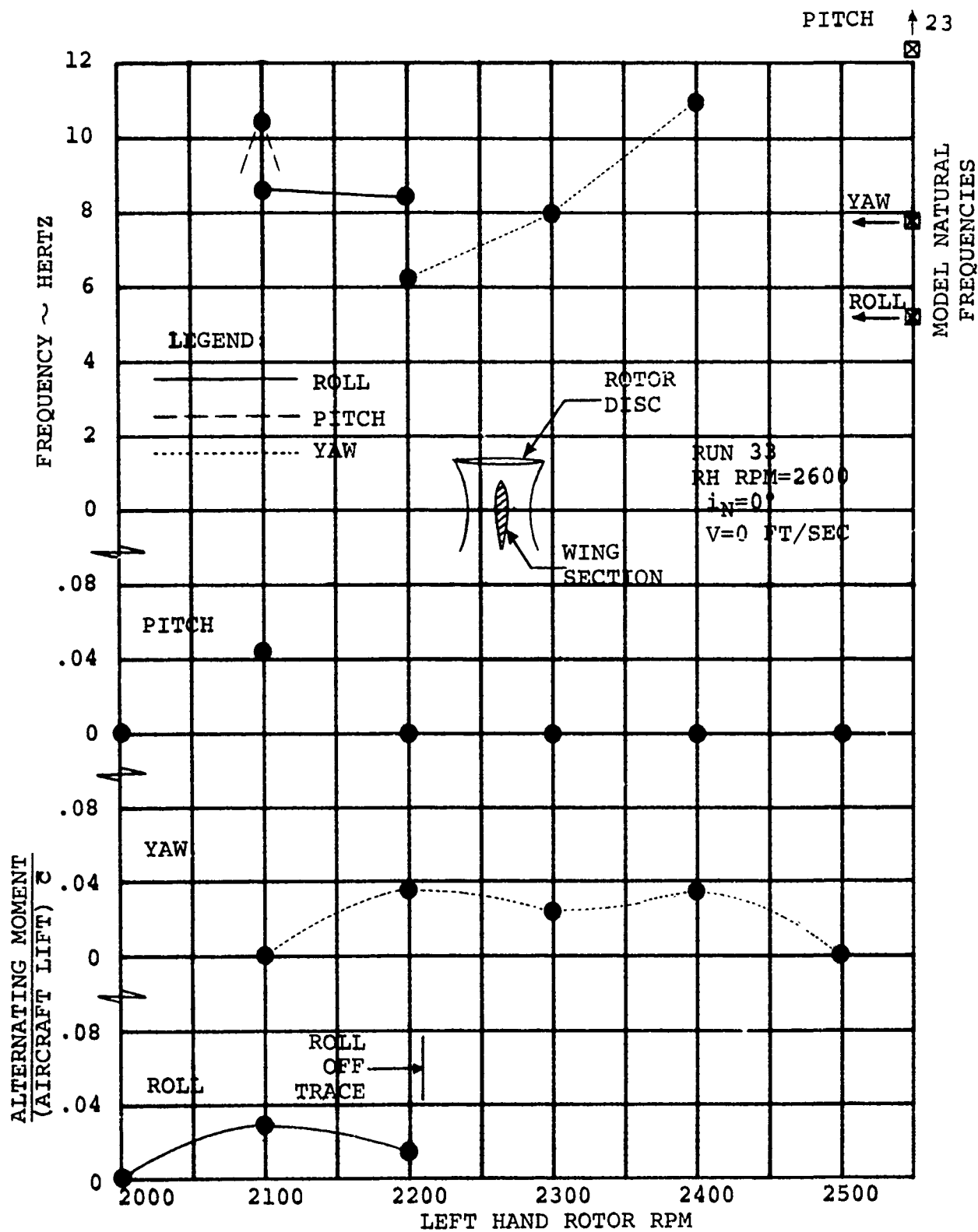


FIGURE 5-25 ALTERNATING MODEL MOMENTS OBTAINED WITH ROTOR SHAFT IN LINE WITH CHORD

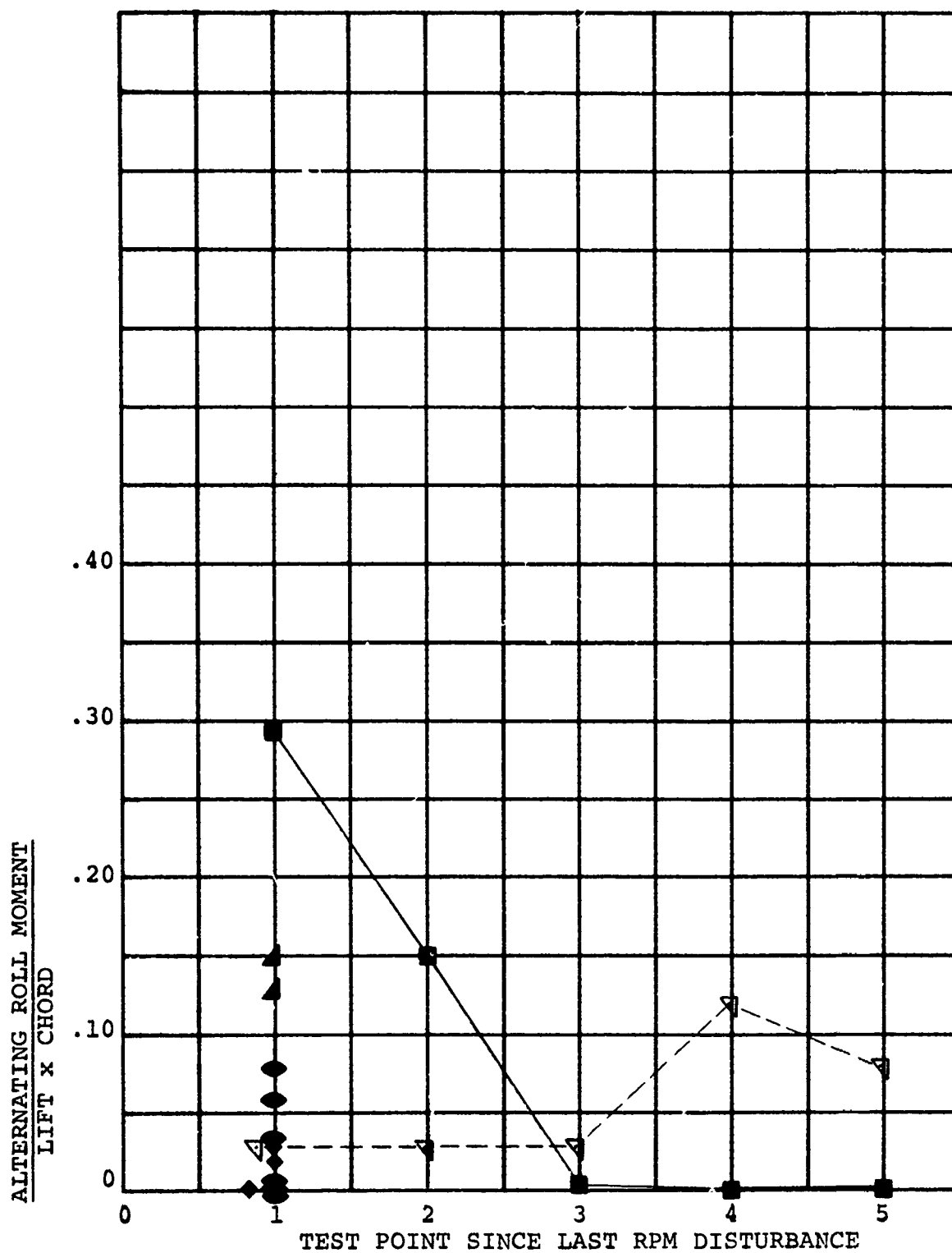


FIGURE 5-26 EFFECT OF TIME ON ALTERNATING ROLL MOMENT

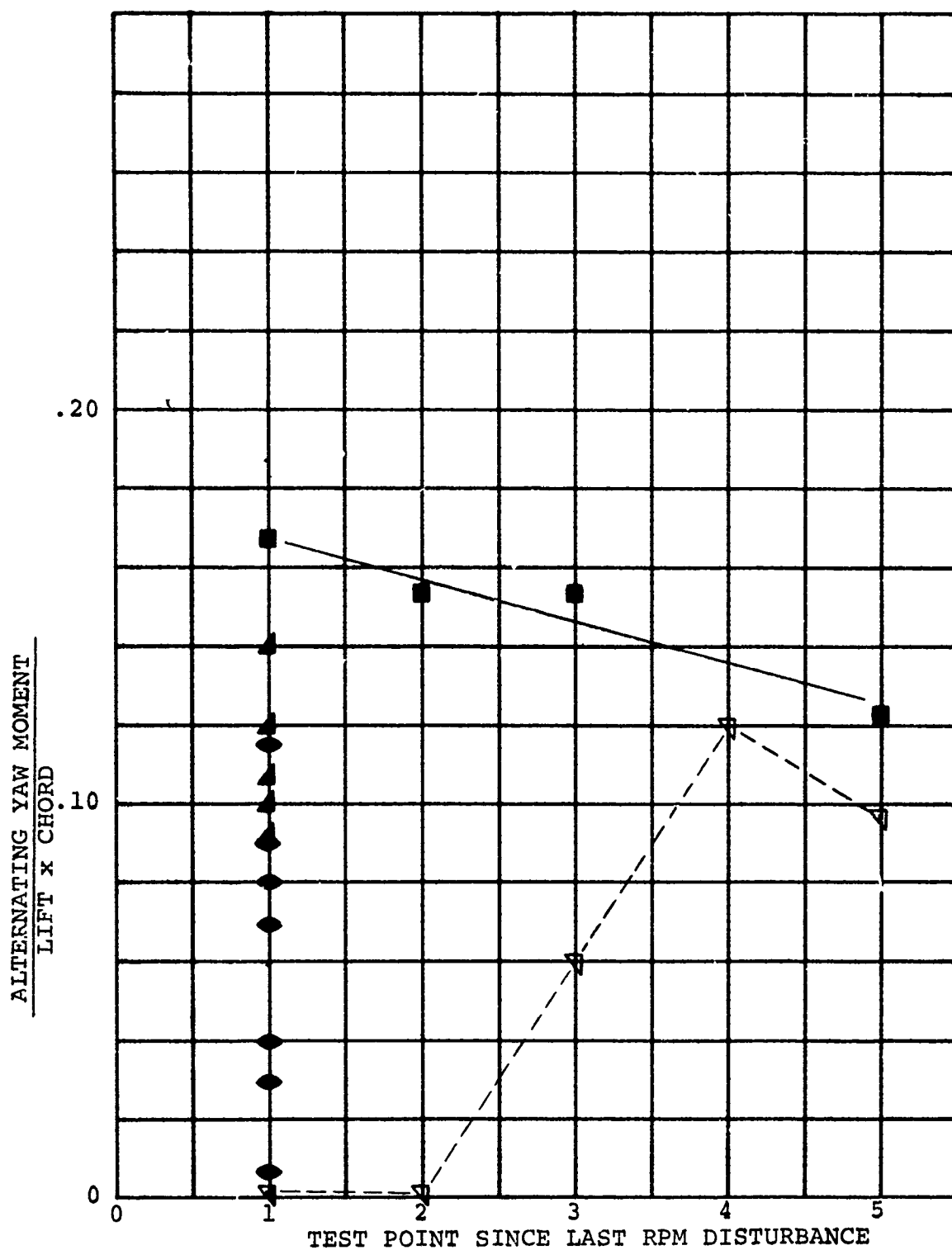


FIGURE 5-27 EFFECT OF TIME ON ALTERNATING YAW MOMENT

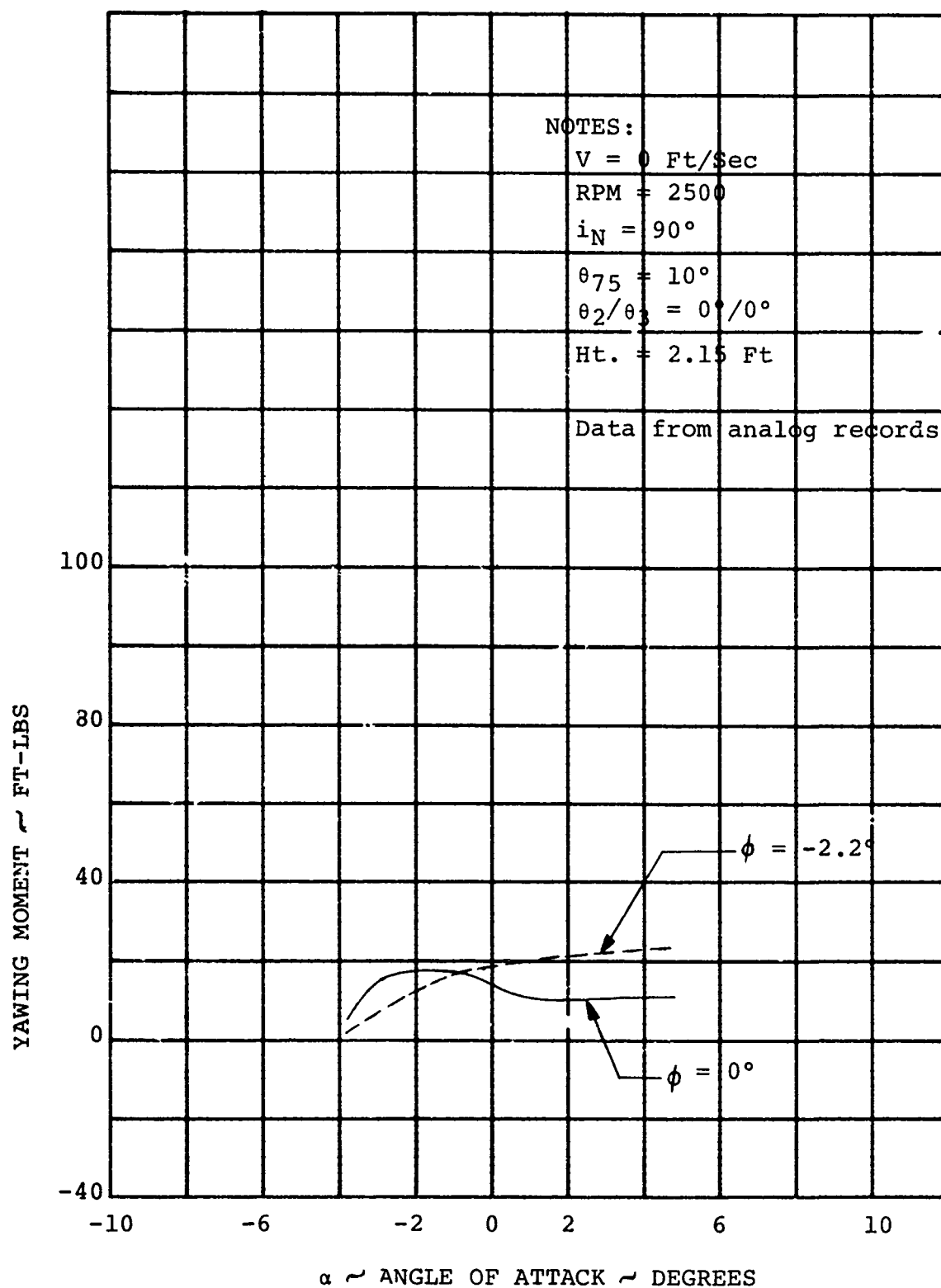


FIGURE 5-28

HOVER TRIM MOMENTS PRODUCED BY ANGLE
OF ATTACK WITH ROLL ANGLE VARIATION
IN GROUND EFFECT

5.2 STOL STABILITY

STOL refers to the in-ground effect rolling takeoff associated with the overload gross weight condition. Testing was performed to examine the in-ground effect takeoff and climb-out. This discussion includes the aircraft stability characteristics of this flight regime.

5.2.1 Rotor Stability Derivatives

Testing accomplished in the STOL flight regime investigated the rotor stability characteristics in three individual areas: the ground run, break ground and climb-out. The ground run is representative of a rolling takeoff with a rotor height/diameter ratio of 0.39 and a nacelle incidence of 70 degrees. Figures 5-29 through 5-32 present the rotor pitching moment, normal force, yawing moment, and side force, variation with advance ratio for this condition. There is a significant increase in the rotor normal force and pitching moment, and accounts for the total aircraft pitching moment doubling as discussed in Section 5.2.2. The rotor yawing moment variation with advance ratio is approximately the same as the pitching moment indicating the flapping is increasing but the phase angle is not changing significantly.

A second phase of the STOL takeoff is breakground. Testing of this regime was performed at a 0.1 g aircraft acceleration at a rotor height/diameter ratio of 0.39. The rotor yawing moment, side force, pitching moment and normal force variation with yaw angle are presented in Figures 5-33 through 5-37. There is some evidence of stall appearing in the right rotor normal force at yaw angles less than negative 5 degrees; therefore, the derivatives tabulated below are obtained from the left rotor.

i_N	V/V_T	$\partial C_{YM}/\partial \psi$	$\partial C_{SF}/\partial \psi$	$\partial C_{PM}/\partial \psi$	$\partial C_N/\partial \psi$
70°	0.206	0.000028	0.00002	0.000042	0.000008

Climb-out testing was performed at an advance ratio of 0.206 which was defined by the 0.1g acceleration in the ground run. Figures 5-38 through 5-41 present the pitching moment, normal force, yawing moment and side force variation with rotor height/diameter ratio. There is a very slight variation in these characteristics up to a h/D of 0.8 but no change beyond this which indicates there is only a minor ground effect on the rotor stability.

5.2.2 Aircraft Stability Derivatives

To define the aircraft stability characteristics for the STOL flight regime, the following three areas were investigated: ground run, break ground and climb-out. Figure 5-42 presents the variation of aircraft pitching moment during the ground run at a height-to-diameter of 0.39. As the advance ratio is increased, the pitching moment coefficient decreases but the pitching moment is increasing. To illustrate this point a line of constant pitching moment was added to Figure 5-42 and indicates that as the advance ratio increases from 0.11 to 0.35 the pitching moment doubles.

The breakground condition was defined as the speed at which the propulsive force-to-lift force ratio was 0.1. Directional stability characteristics of side force and yawing moment are presented for this condition in Figures 5-43 and 5-44 respectively. For the rotors off case the side force has a slope of 0.017 per degree and reaches a minimum value at approximately 14 degrees. Addition of the rotors increases this slope to 0.038 per degree. The yawing moment variation presented in 5-44 indicates a stable yawing moment derivative of -0.0018 per degree. The addition of the rotors results in an unstable derivative of 0.0007 per degree. At approximately 7 degrees negative yaw there is a reversal in the yawing moment which is due to blade stall effect on rotor normal force (Figure 5-37).

Figure 5-45 presents the variation in the aircraft pitching moment during the climb-out phase. There is a slight increase in moment up to a height-to-diameter ratio of 1.0, but it is effectively constant, at a value of 2.70, for any further increase in height.

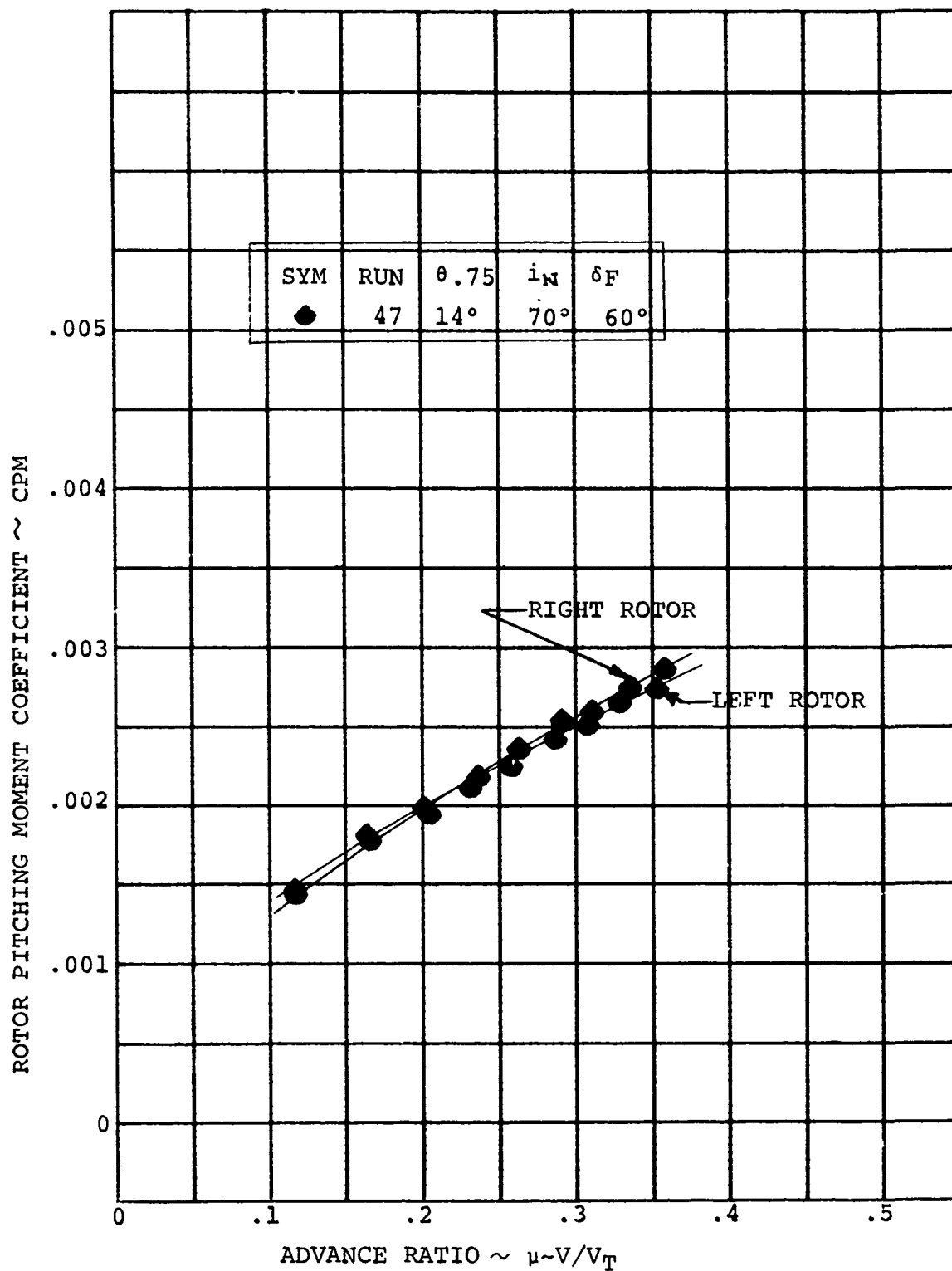


FIGURE 5-29 ROTOR PITCHING MOMENT VARIATION FOR IN GROUND EFFECT TAKEOFF AT $h/D=0.39$, $i_N=70^\circ$

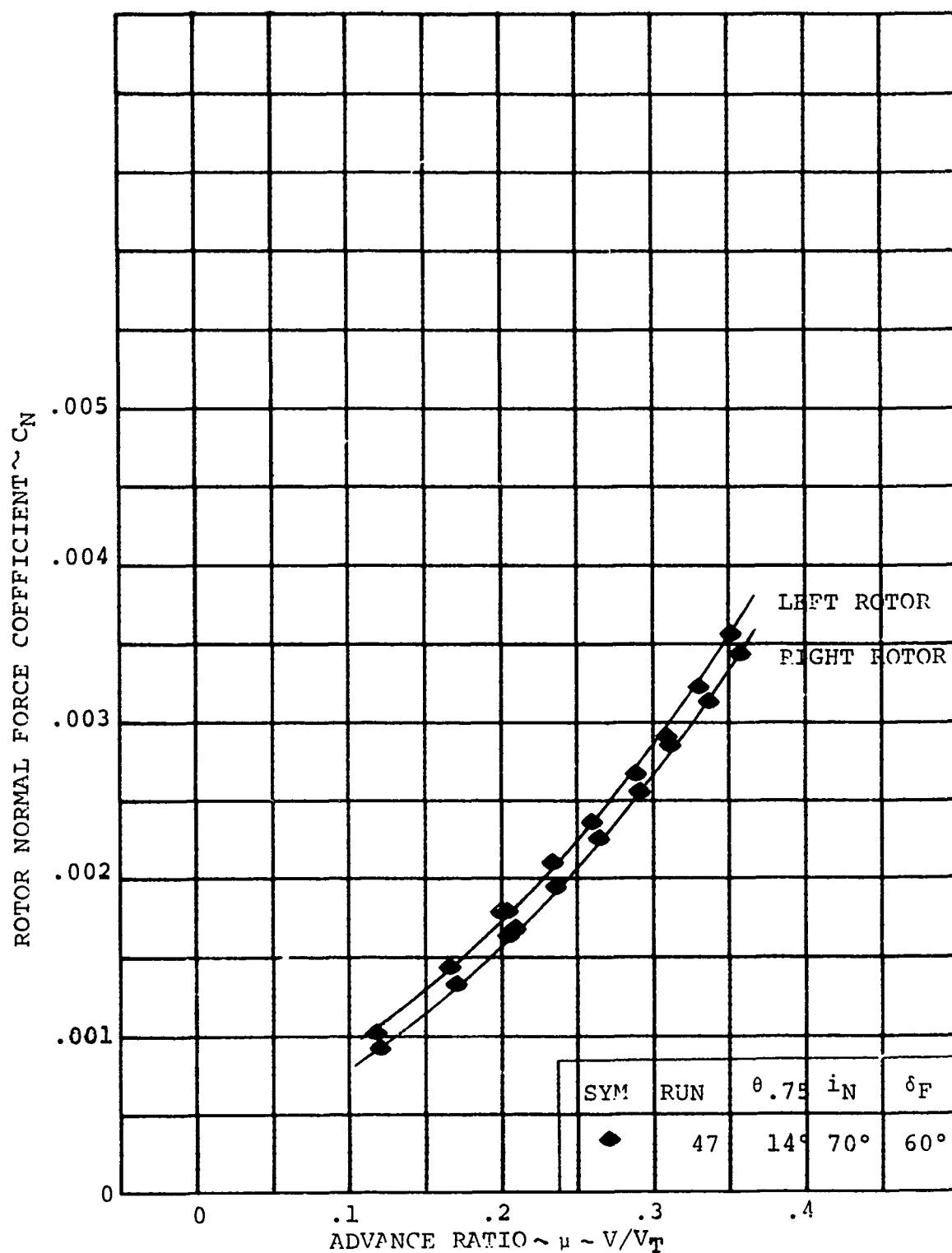
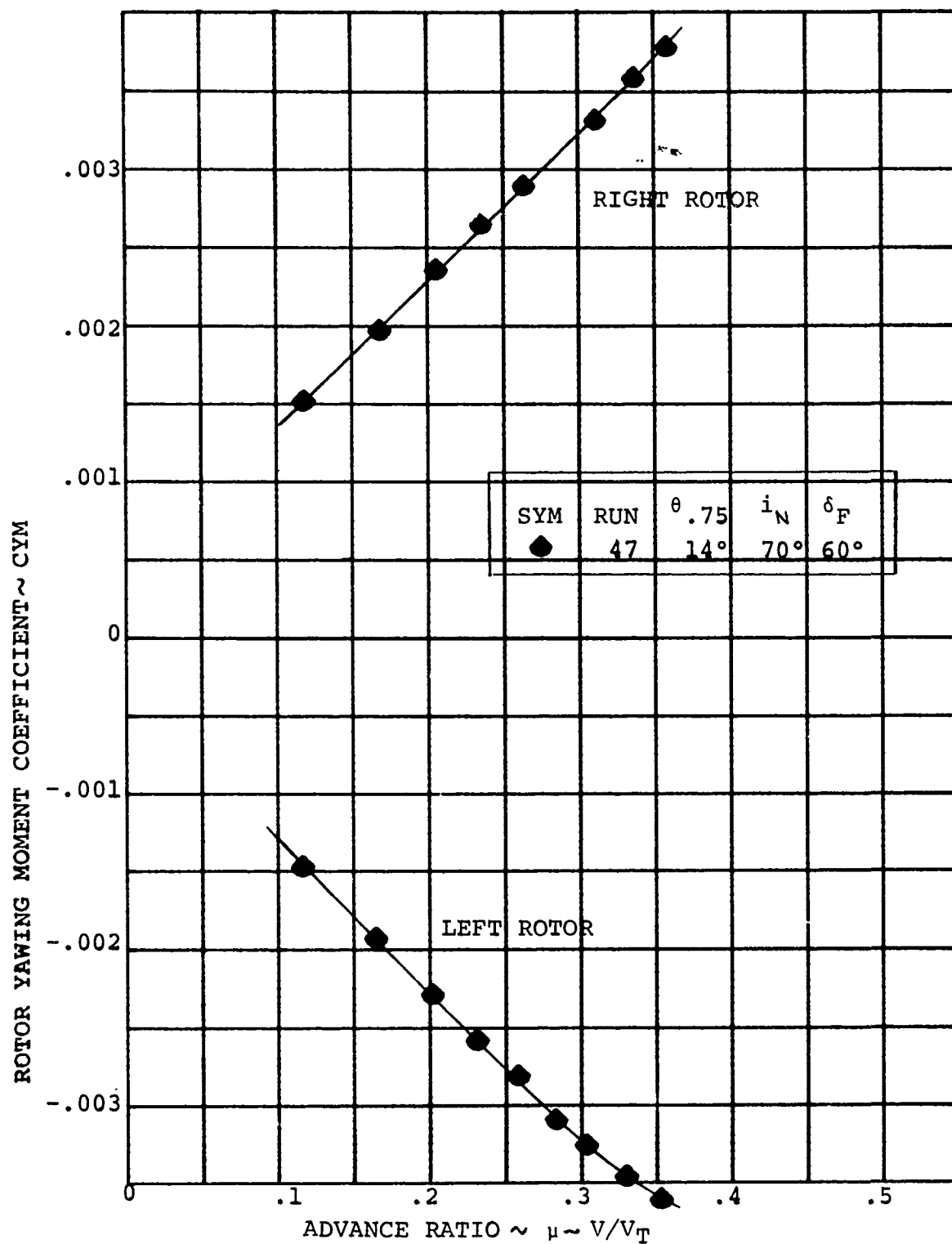


FIGURE 5-30 ROTOR NORMAL FORCE VARIATION FOR IN GROUND EFFECT TAKEOFF AT $h/D=0.39$, $i_N=70^\circ$



ROTOR YAWING MOMENT VARIATION FOR IN GROUND
 FIGURE 5-31 EFFECT TAKEOFF AT $h/D=0.39$ $i_N=70^\circ$

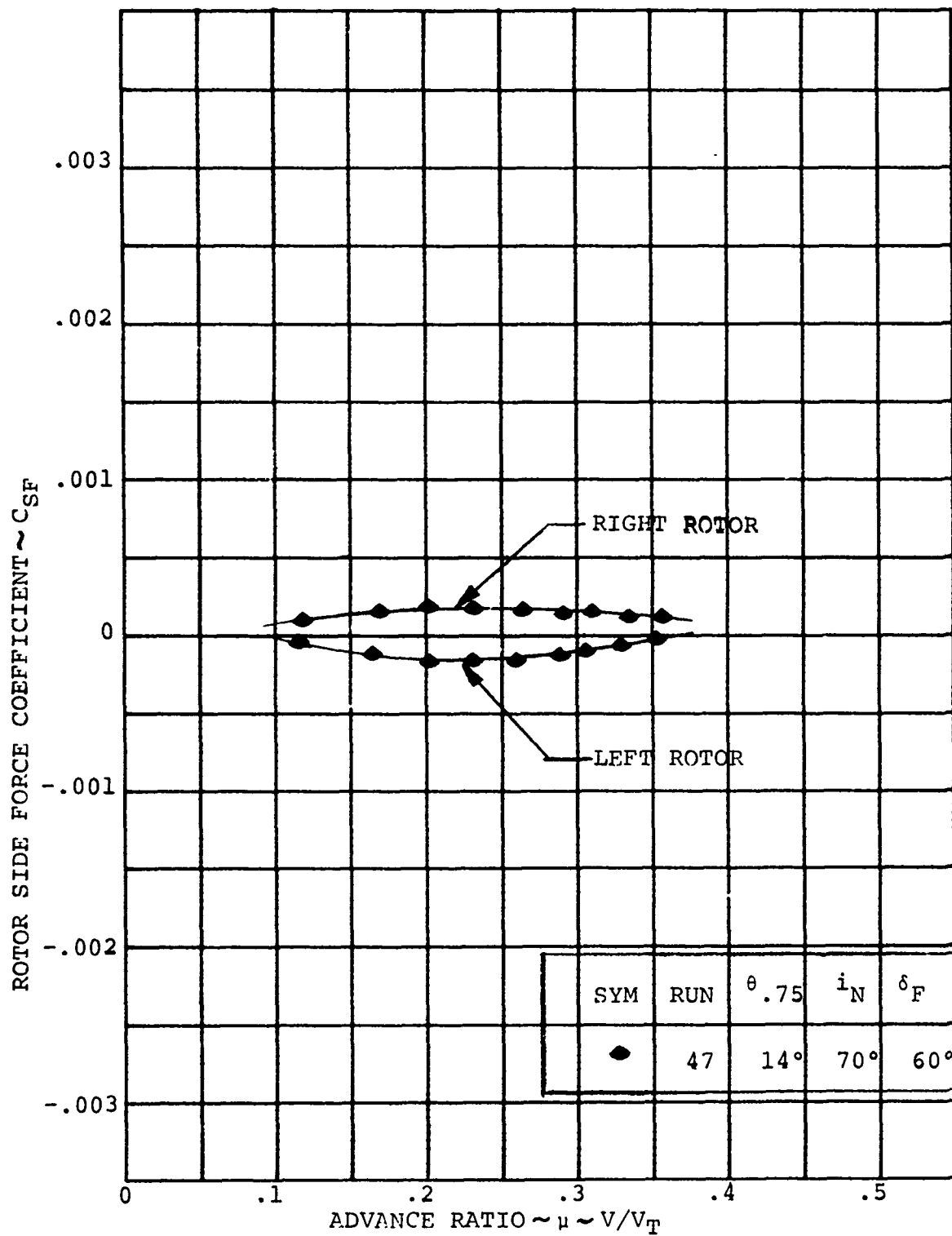


FIGURE 5-32 ROTOR SIDE FORCE VARIATION FOR IN GROUND EFFECT TAKEOFF AT $h/D=0.39, i_N=70^\circ$

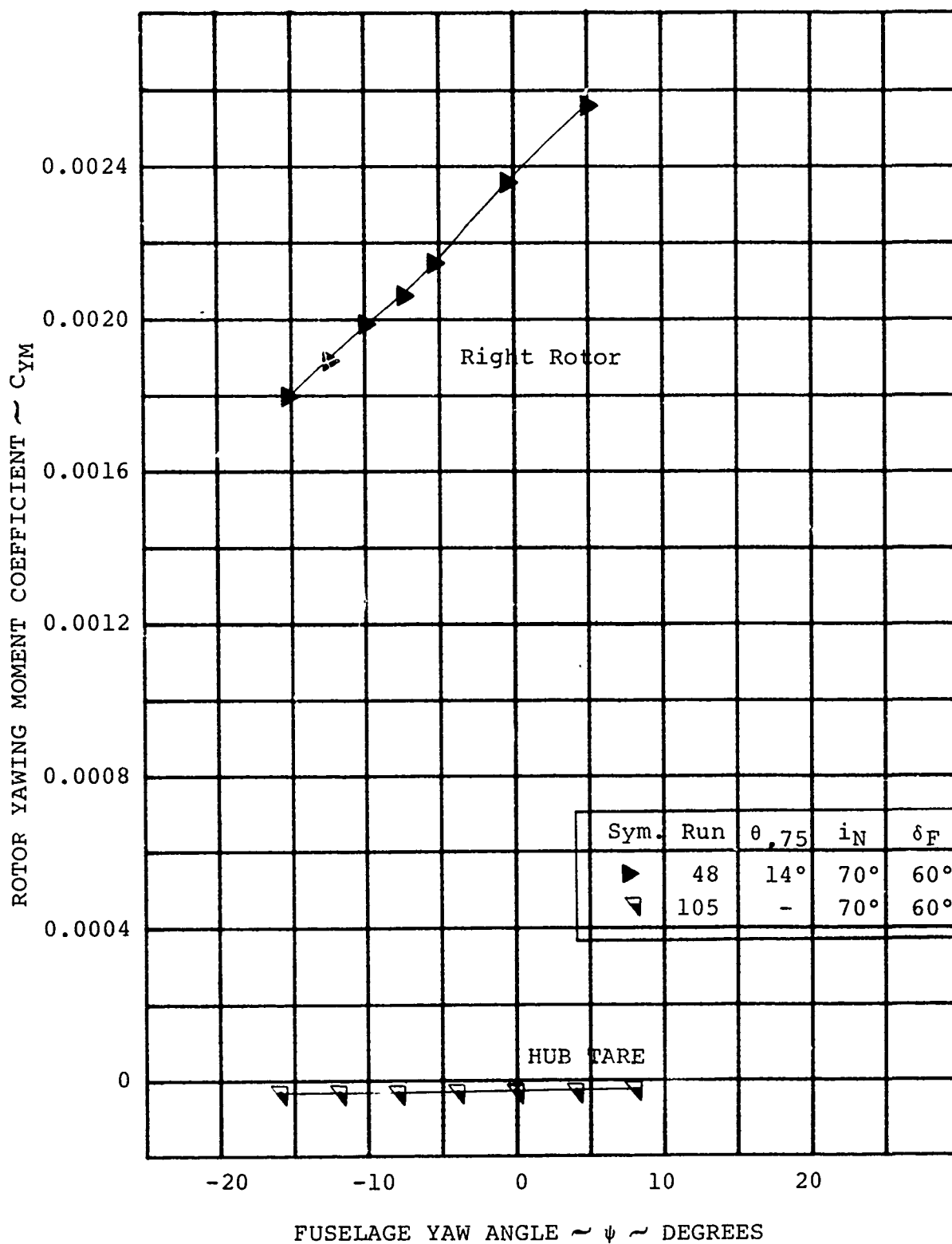


FIGURE 5-33

ROTOR YAWING MOMENT/YAW ANGLE VARIATION
IN GROUND EFFECT AT $h/D = 0.39$ AND $V/V_T = 0.206$ (RIGHT ROTOR)

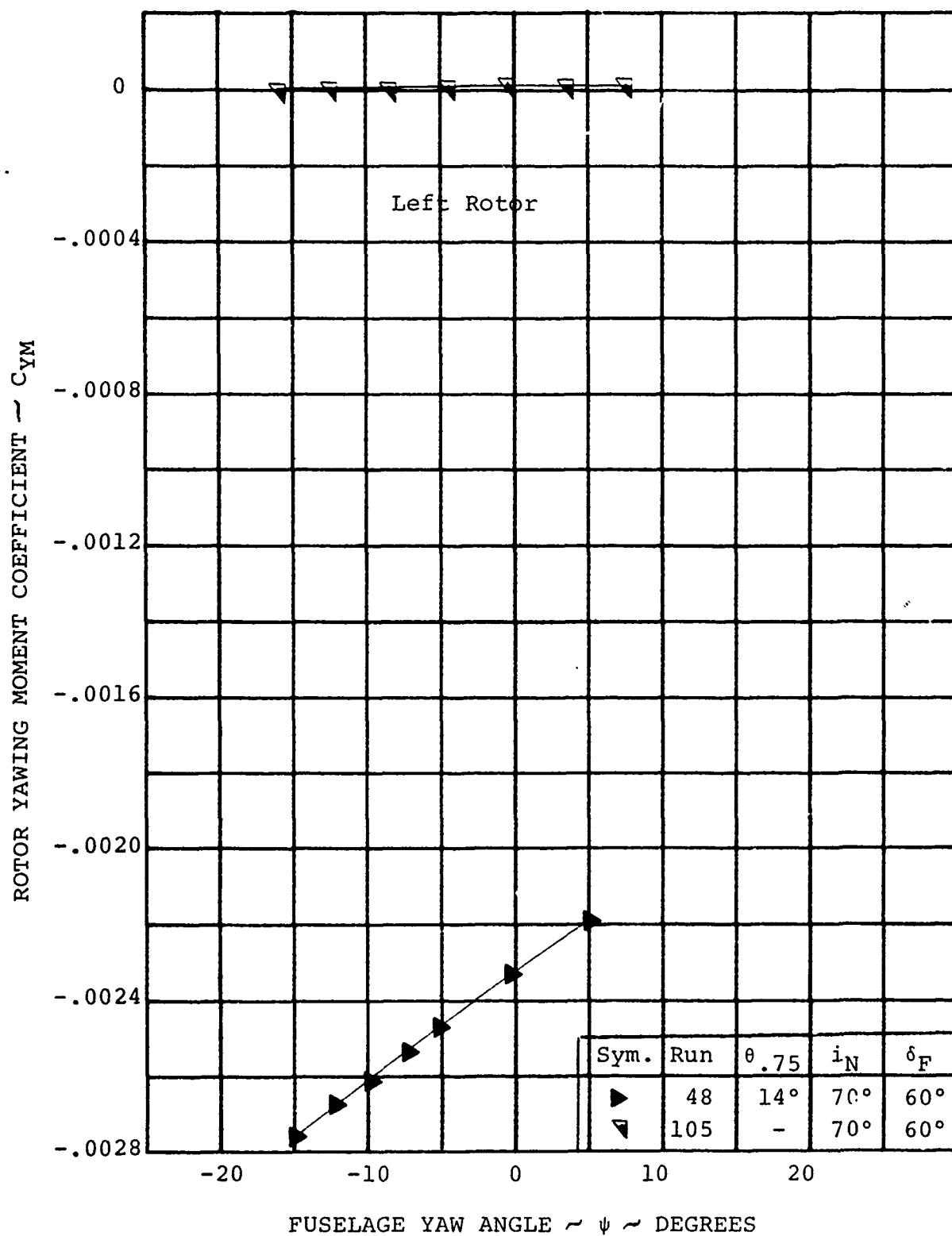


FIGURE 5-34

ROTOR YAWING MOMENT/YAW ANGLE VARIATION
IN GROUND EFFECT AT $h/D = 0.39$ AND $V/V_T = 0.206$
(LEFT ROTOR)

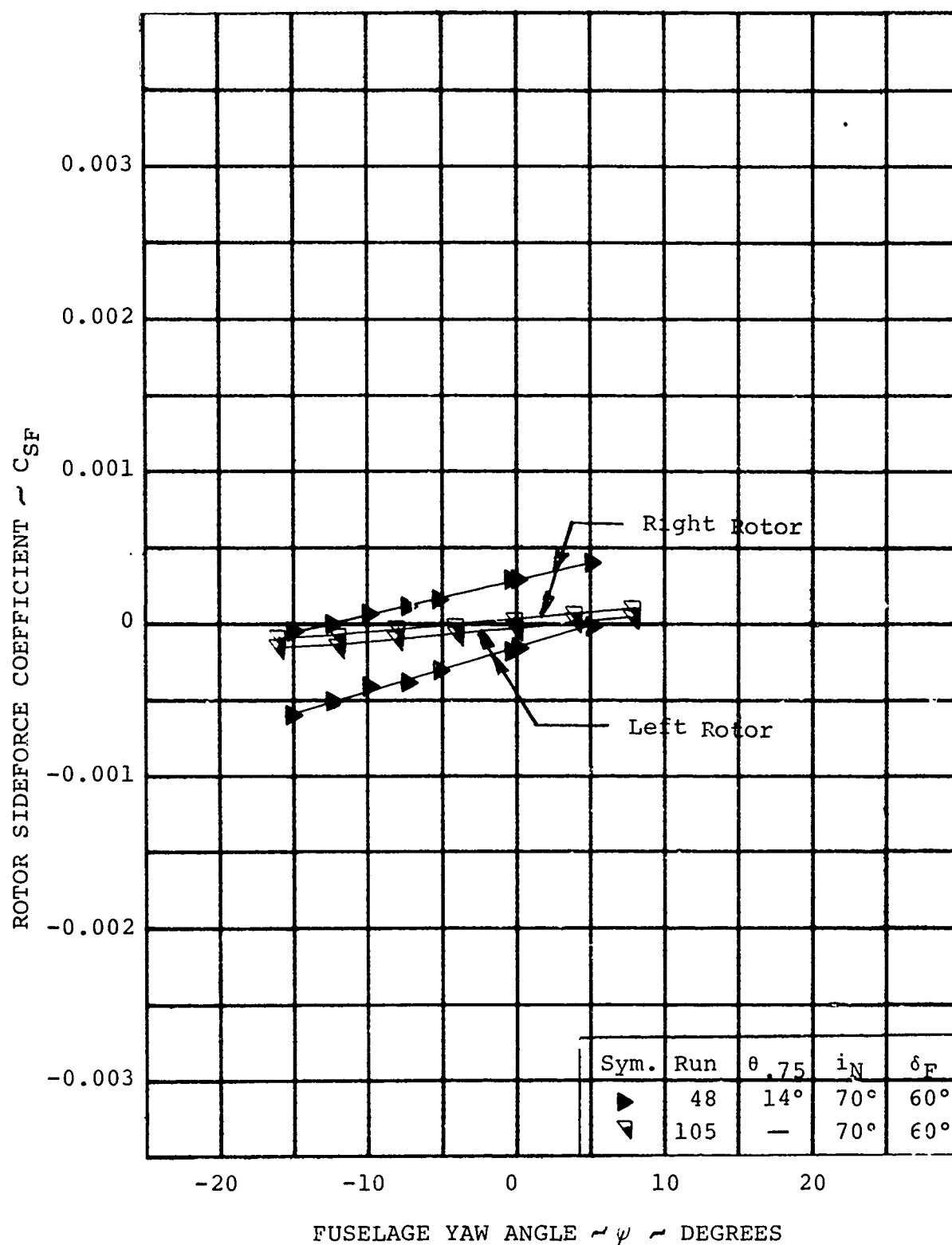


FIGURE 5-35

ROTOR SIDEFORCE/YAW ANGLE VARIATION IN-GROUND EFFECT AT $h/D = 0.39$ AND $V/V_T = 0.206$

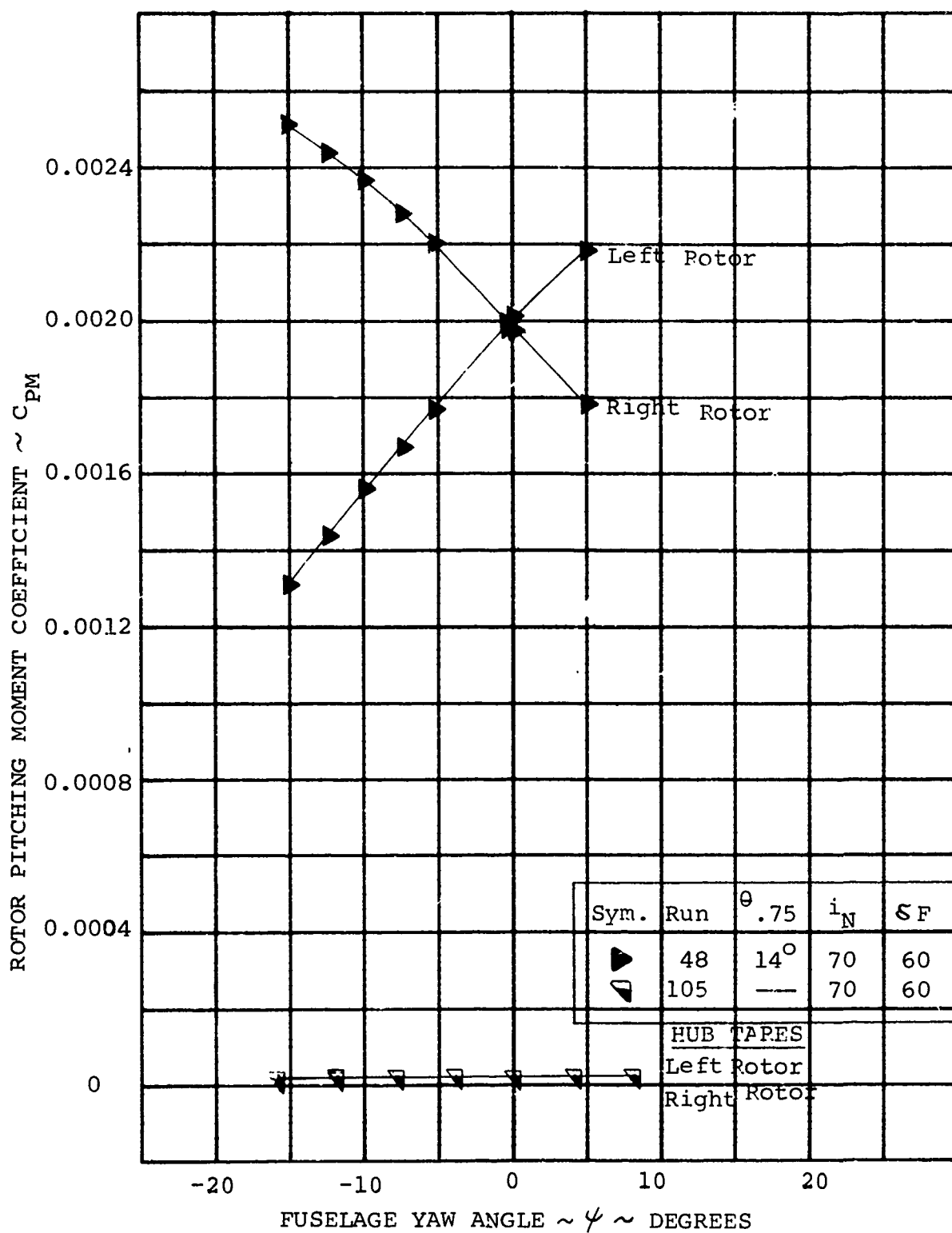


FIGURE 5-36

ROTOR PITCHING MOMENT/YAW ANGLE
VARIATION IN GROUND EFFECT AT $h/D = 0.39$
AND $V/V_T = 0.206$

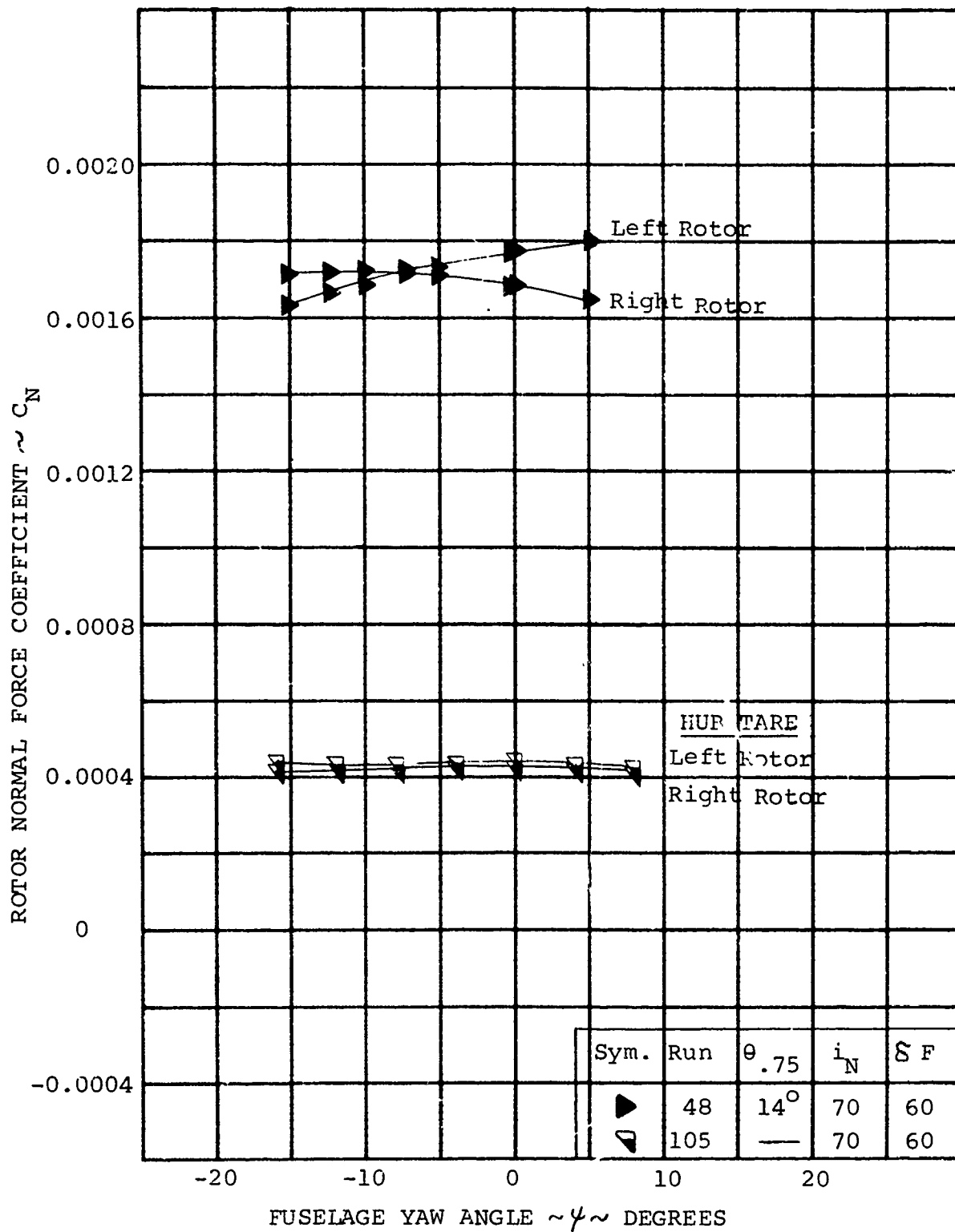
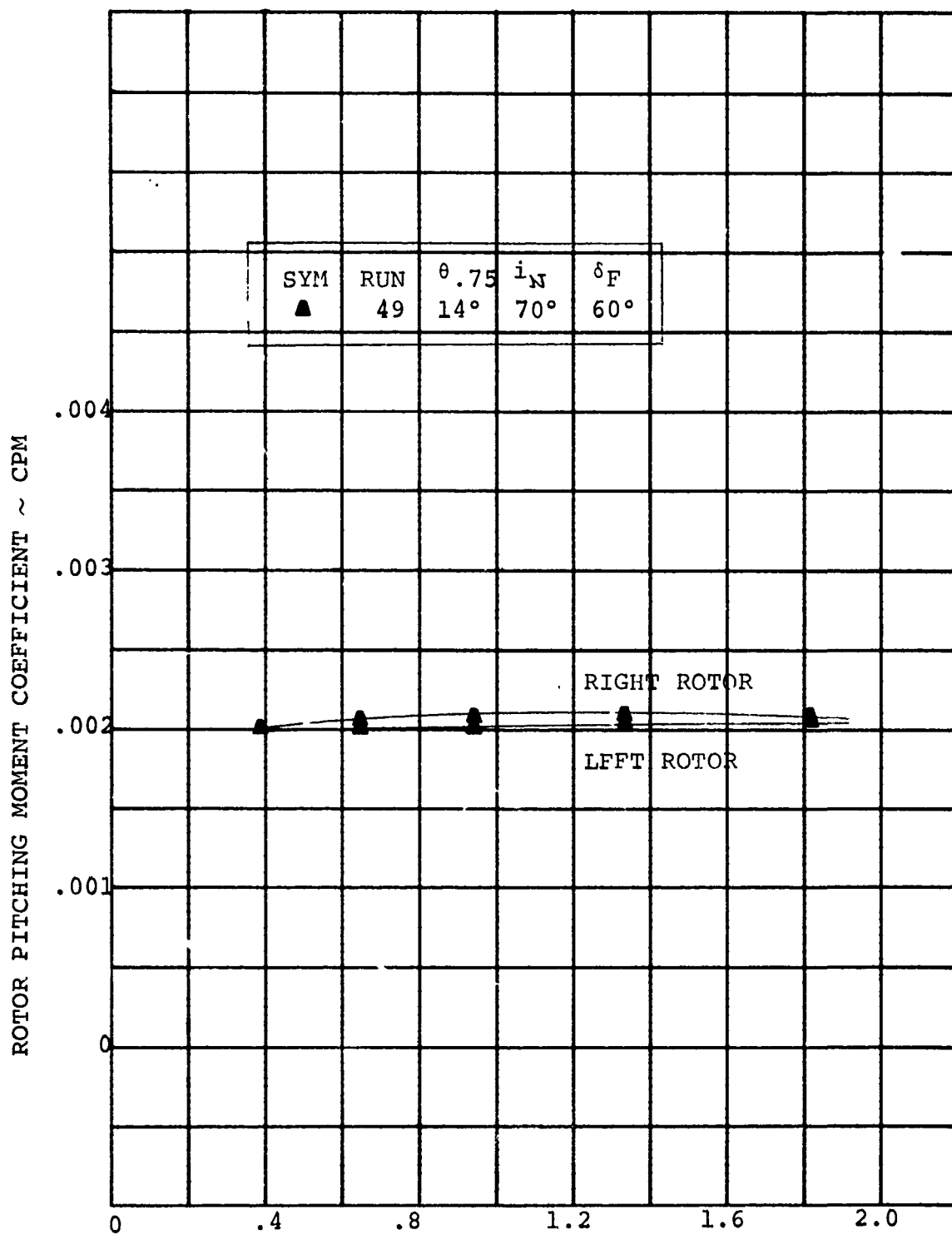
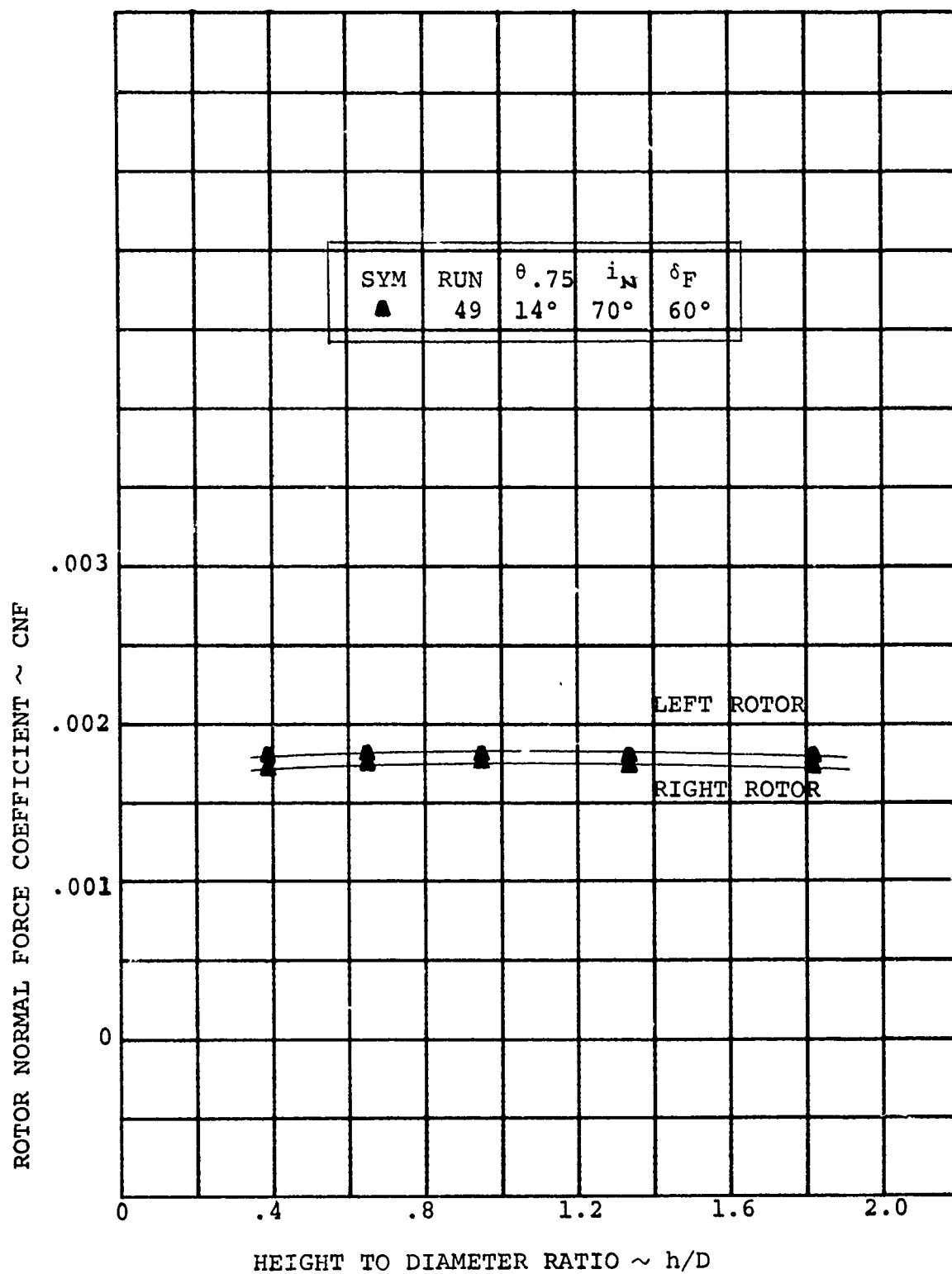


FIGURE 5-37

ROTOR NORMAL FORCE/YAW ANGLE VARIATION
IN GROUND EFFECT AT $h/D = 0.39$ AND
 $V/V_T = 0.206$



HEIGHT TO DIAMETER RATIO $\sim h/D$
 ROTOR PITCHING MOMENT VARIATION DURING
 FIGURE 5-38 STOL CLIMB OUT $V/V_T = 0.206$



ROTOR NORMAL FORCE VARIATION DURING STOL
 FIGURE 5-39 CLIMB OUT $V/V_T = 0.206$

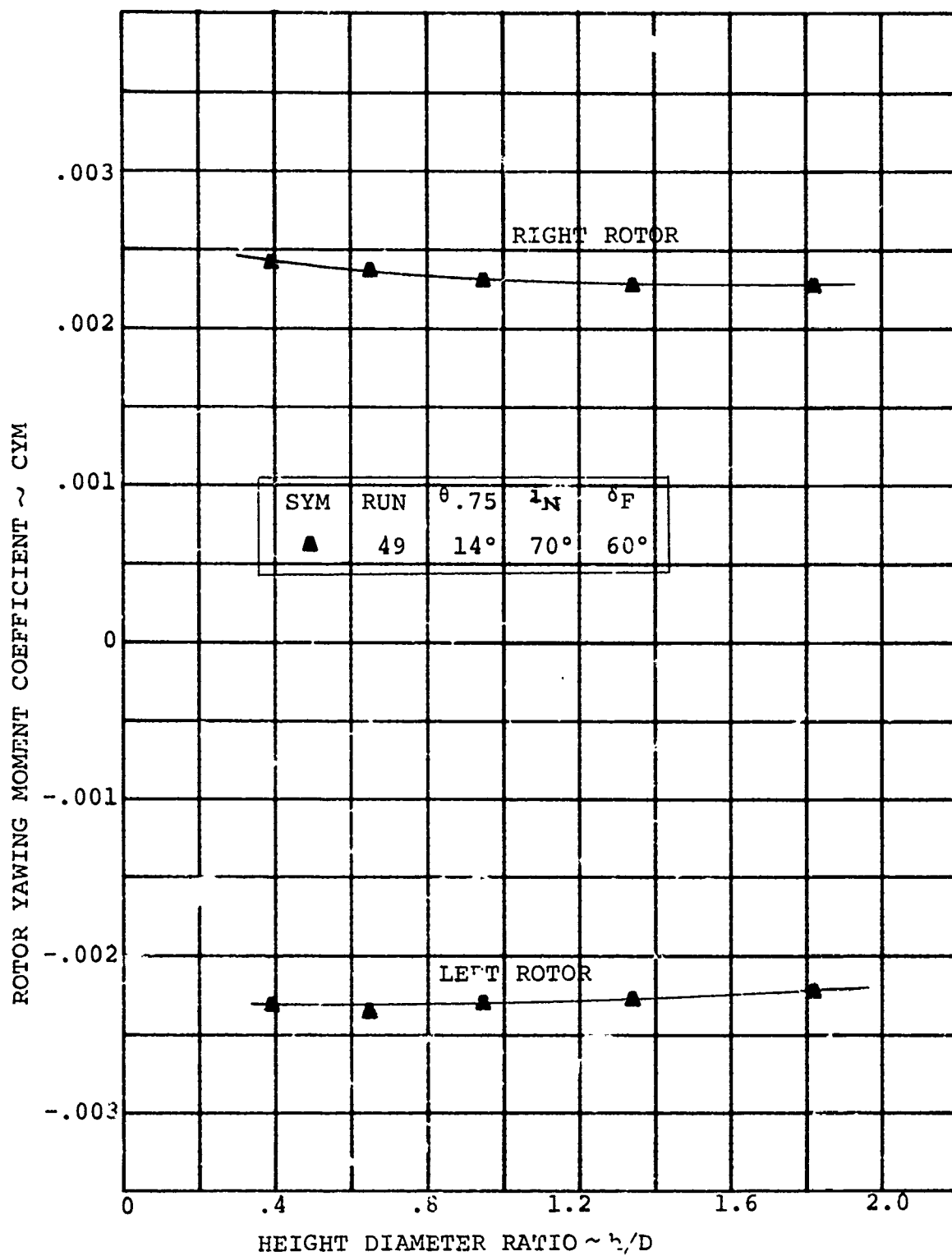


FIGURE 5-40 ROTOR YAWING MOMENT VARIATION DURING STOL CLIMB OUT AT $V/V_T = 0.206$

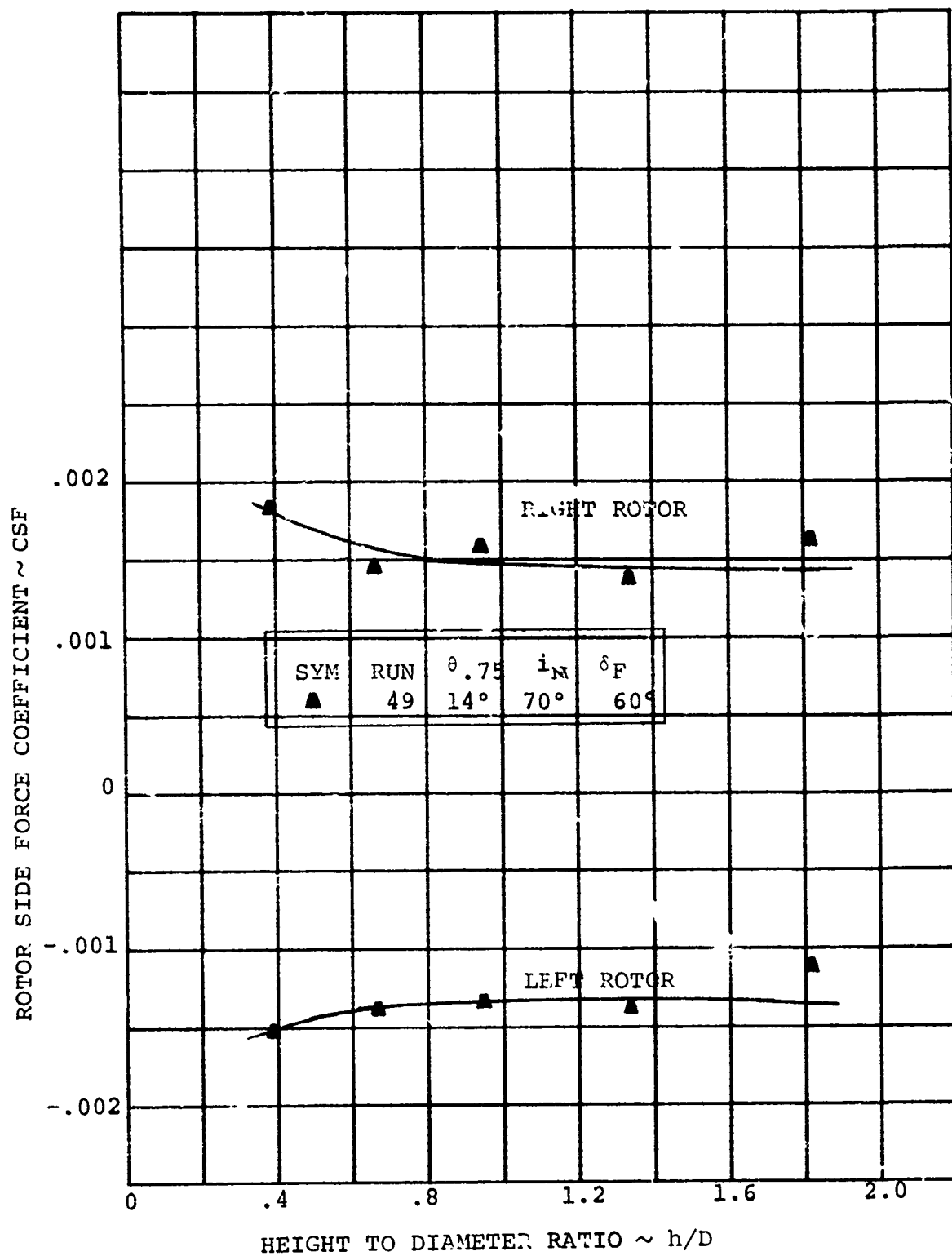


FIGURE 5-41 ROTOR SIDE FORCE VARIATION DURING STOL
CLIMB OUT $V/V_T = 0.206$

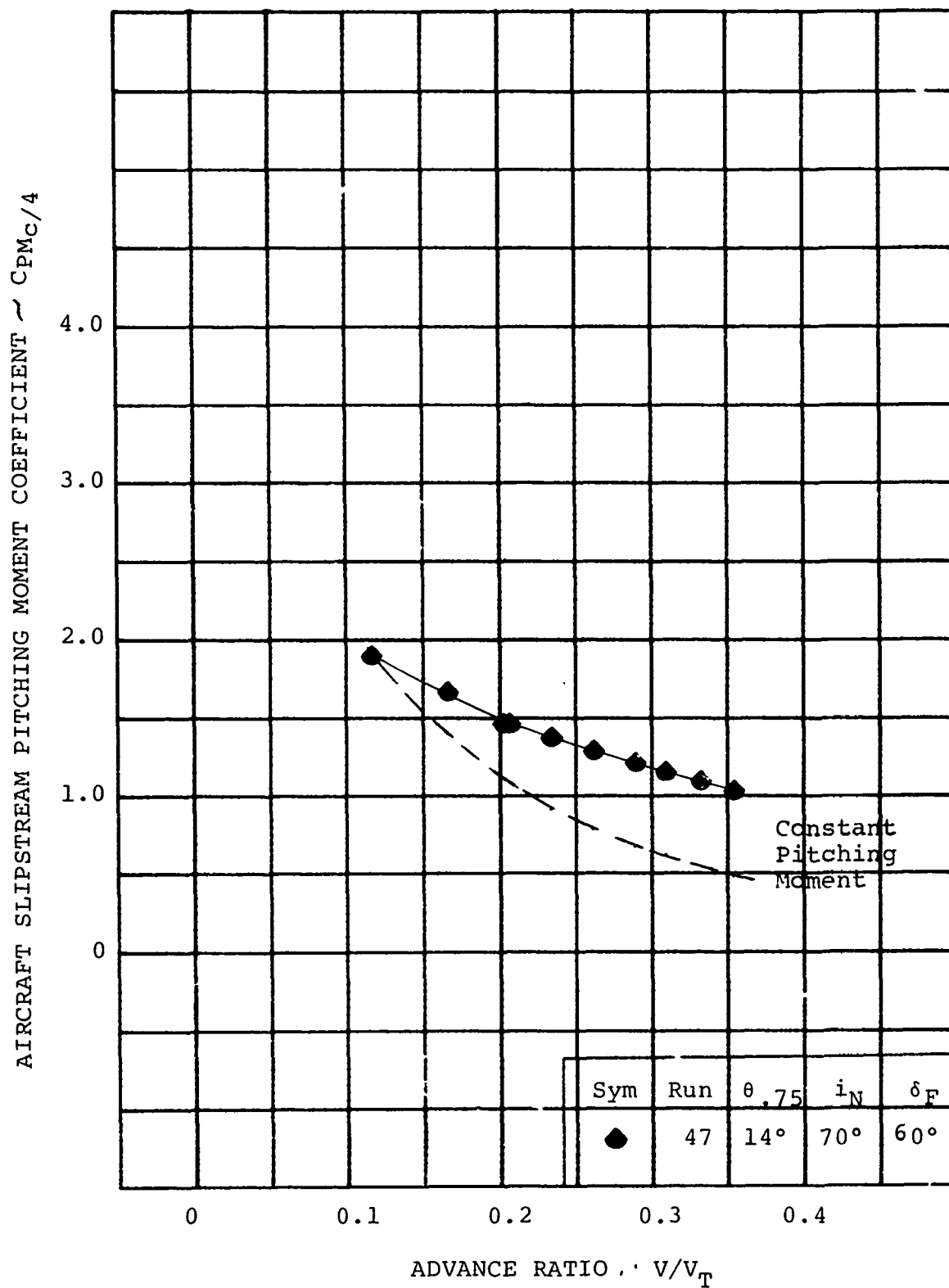


FIGURE 5-42

AIRCRAFT PITCHING MOMENT VARIATION FOR
IN GROUND EFFECT TAKEOFF AT $h/D = 0.39$

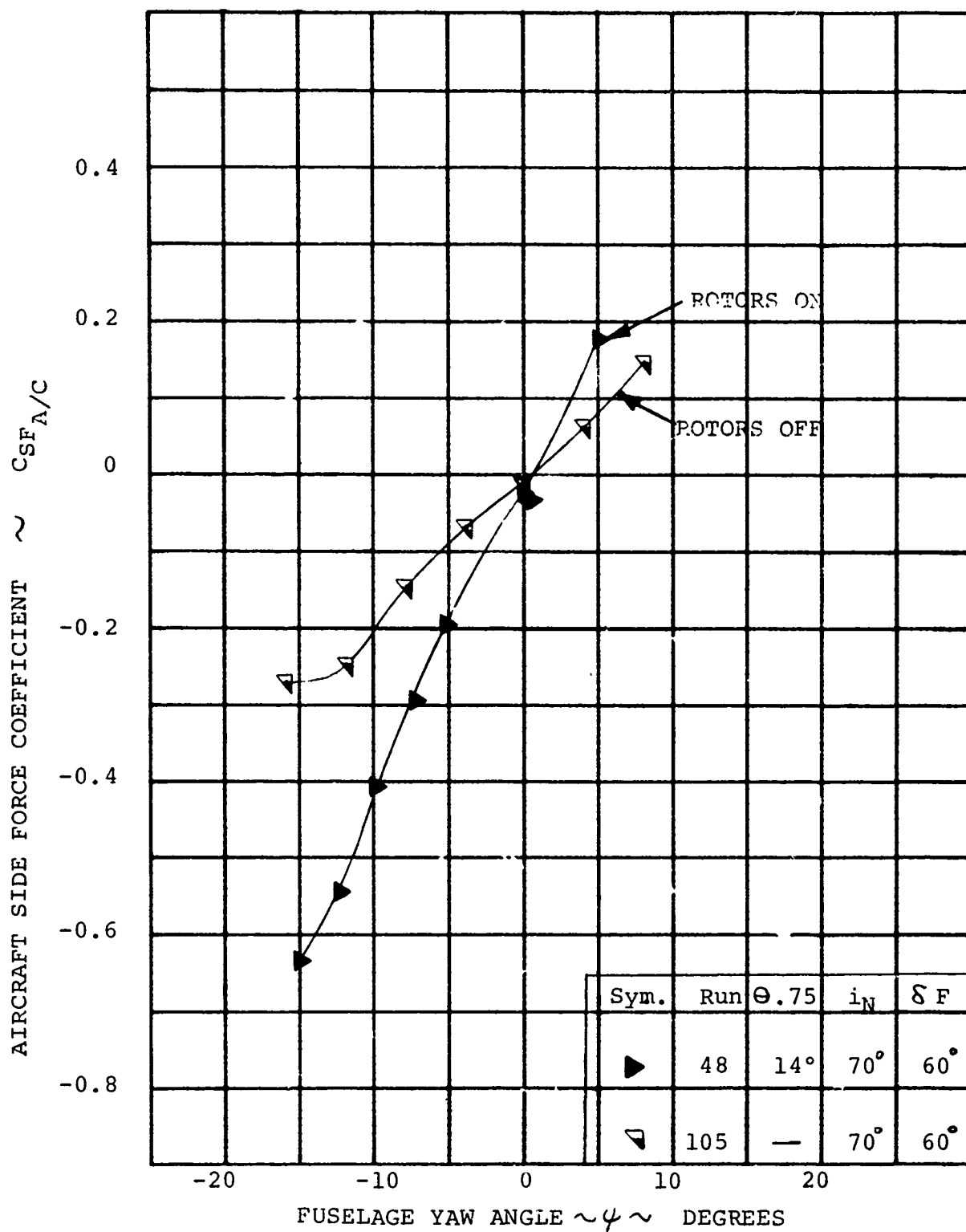


FIGURE 5-43 AIRCRAFT SIDE FORCE/YAW ANGLE VARIATION IN GROUND EFFECT AT $h/D=0.39$ AND $V/V_T=0.206$

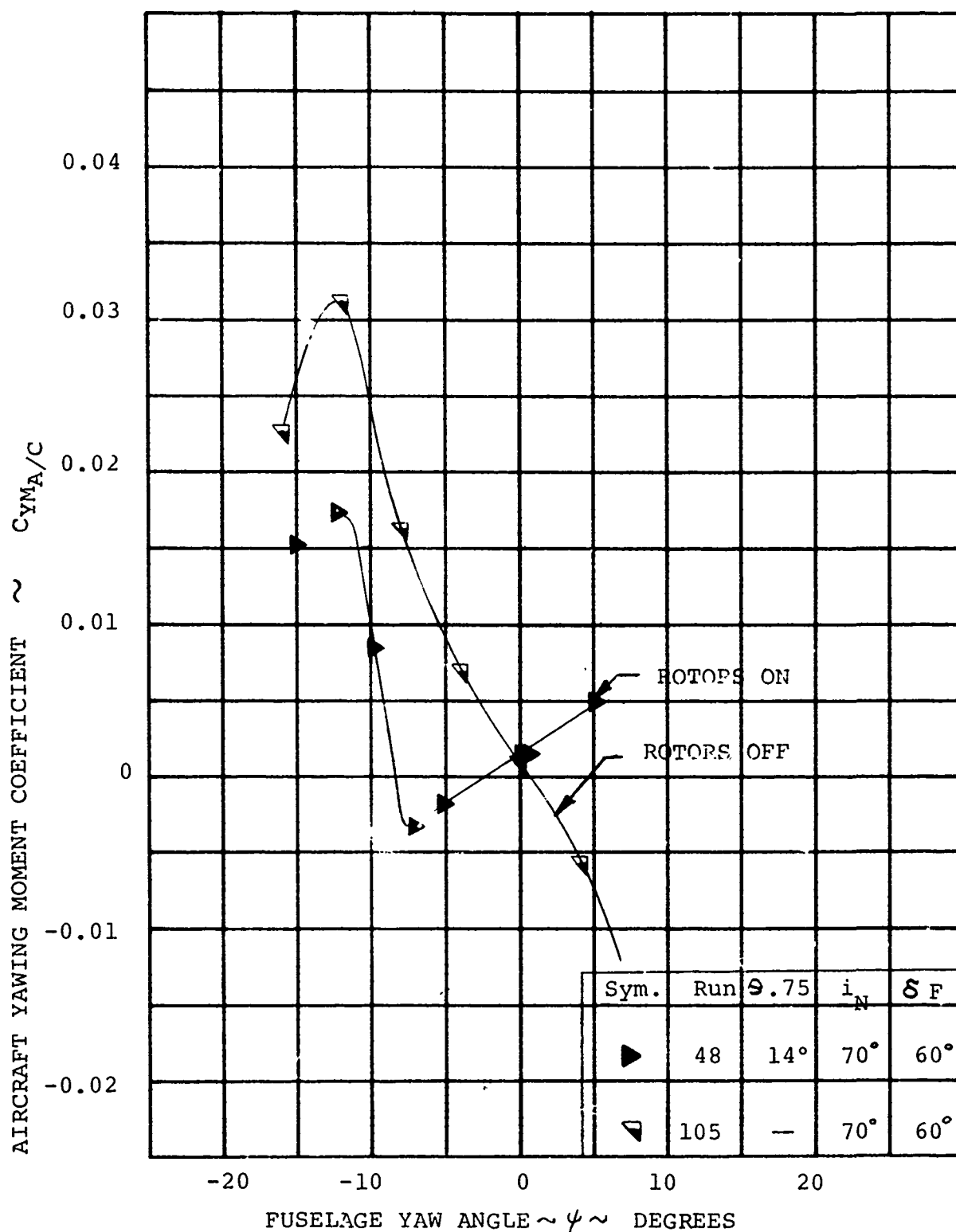


FIGURE 5-44

AIRCRAFT YAWING MOMENT/YAW ANGLE VARIATION IN GROUND EFFECT AT $h/D=0.39$ AND $V/V_T = 0.206$

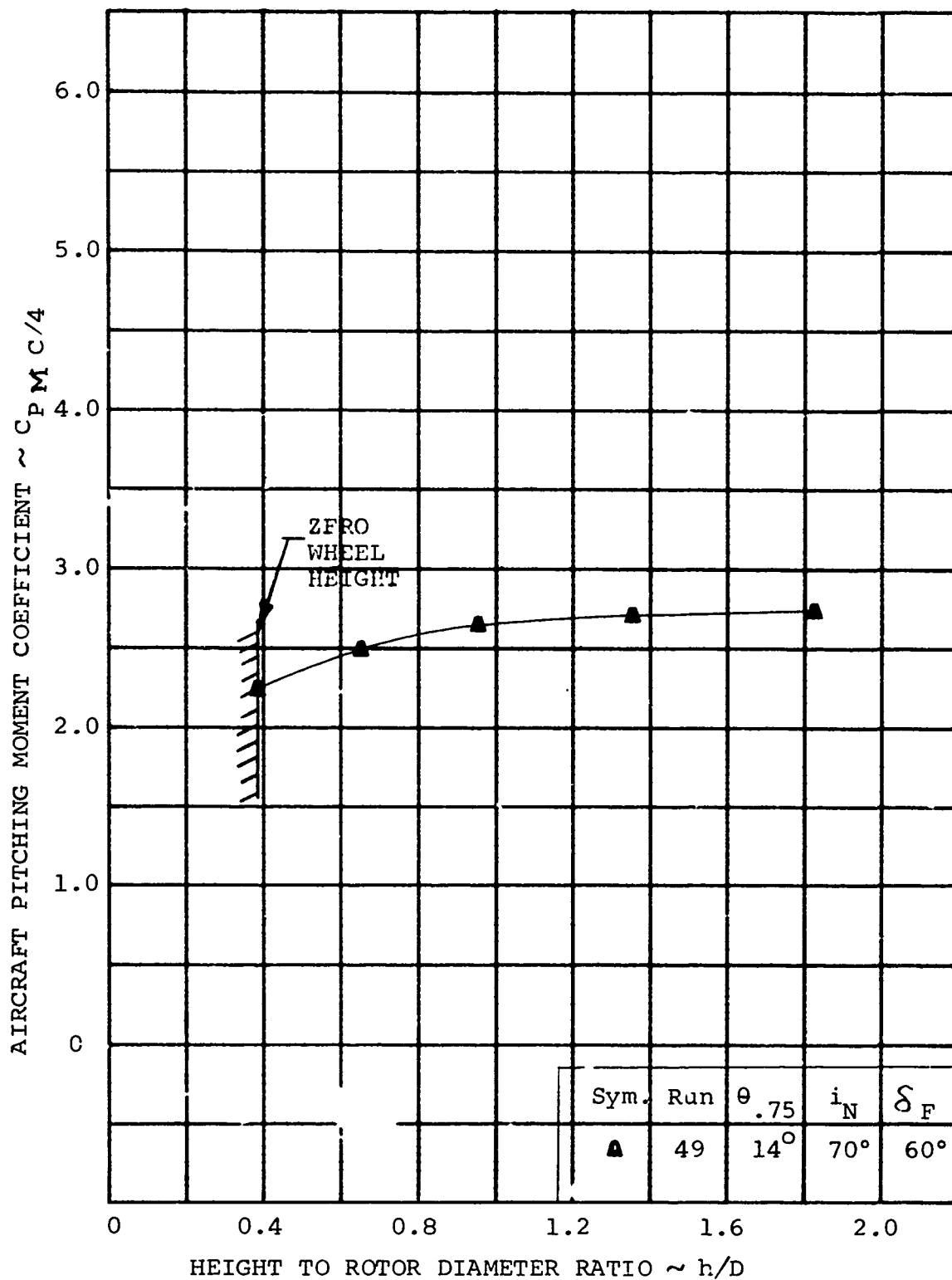


FIGURE 5-45 AIRCRAFT PITCHING MOMENT VARIATION DURING STOL CLIMBOUT $V/V_T = 0.206$

5.3 TRANSITION STABILITY AND CONTROL

The transition mode refers to operation out-of-ground effect from hover to the cruise regime. The nacelles rotate from 90-degree incidence (i_N) to zero-degree incidence. During this flight regime, the rotor has a significant influence on the aircraft stability and control since it provides the majority of the lift as well as all the propulsive force. Included in this section is the discussion of the rotor stability, the total aircraft stability, control mixing and attitude effects on control.

5.3.1 Rotor Stability Derivatives

Testing was performed to obtain data that would define rotor force and moment variation with angle of attack for nacelle incidence (i_N) angles between hover ($i_N=90^\circ$) and cruise ($i_N=0^\circ$). Two incidence values were selected that would provide a wide coverage of the transition regime. These angles were 70 and 45 degrees.

A summary of the longitudinal and directional rotor stability derivatives is presented in Table 5-1 for transition as well as the derivatives obtained in cruise ($i_N=0^\circ$). The data are presented for the left rotor and indicates the derivatives for flight in the unstalled region of the rotor operation.

Figures 5-46 through 5-53 present the rotor characteristics for a nacelle incidence of 70 degrees at an advance ratio of 0.206 and 0.234 as the angle of attack is varied. The test data presented in transition include the aerodynamic interference effects of the wing. Figures 5-46 and 5-47 present the rotor pitching moment variation with angle of attack and indicates a decrease in slope as the angle of attack becomes more positive than minus 2 degrees. This is due to rotor stall as discussed in Section 4.3.2. For operation below stall, the derivatives are 0.000064 and 0.000072 per degree for advance ratios of 0.206 and 0.234, respectively. The reduction in flapping is thought to be the result of a reduction in first harmonic blade torsion due to stall, Figure 6-84. The rotor elastic axis is aft of the aerodynamic center of the blades (See Appendix 1). This implies that a part of the destabilizing rotor moment in transition is due to lift pitch coupling prior to stall as evidenced by the increasing first harmonic torsion loads shown in Figure 6-83.

The normal force data are plotted in Figures 5-48 and 5-49, indicate a derivative of $\partial C_N / \partial \alpha = 0.00002$, and also show a reduction in derivative consistent with stall.

TABLE 5-1

TRANSITION ROTOR STABILITY DERIVATIVES

LEFT ROTOR

LONGITUDINAL MODE

i_N	V/V_T (RPM)	$\theta, 75$	$\partial C_M / \partial \alpha$	$\partial C_N / \partial \alpha$	$\partial C_{YM} / \partial \alpha$	$\partial C_{SF} / \partial \alpha$
70	0.206 (1980)	14°	0.000064	0.000020	-0.000033	-0.000010
70	0.234 (1980)	14°	0.000072	0.000022	-0.000038	-0.000010
45	0.260 (1800)	18°	0.000074	0.000035	-0.000067	0.000002
0	0.386 (2000)	30°	0.000090	0.000068	-0.000118	0.000058

DIRECTIONAL

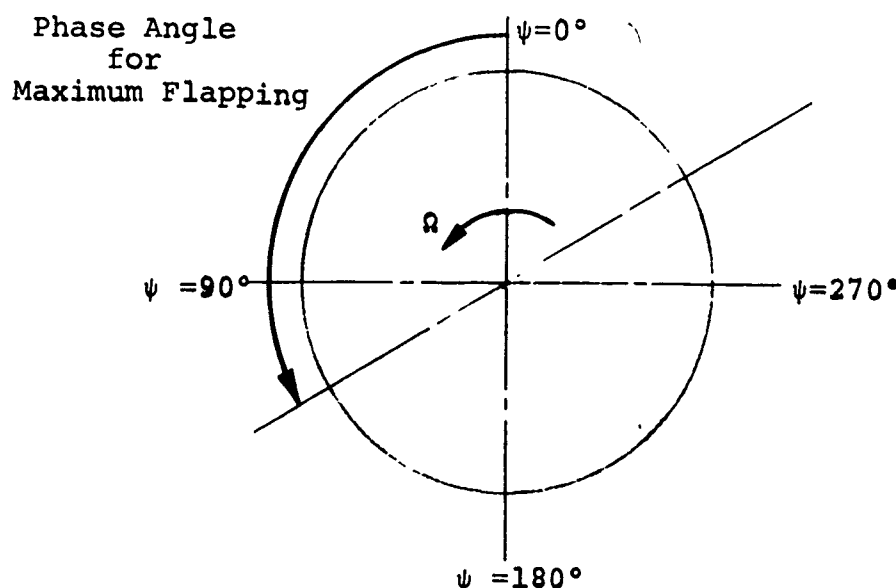
i_N	V/V_T (RPM)	$\theta, 75$	$\partial C_{YM} / \partial \psi$	$\partial C_{SF} / \partial \psi$	$\partial C_{PM} / \partial \psi$	$\partial C_N / \partial \psi$
70	0.206 (1980)	14°	0.000026	0.000025	0.000043	0.000011
45	0.260 (1800)	18°	0.000027	0.000035	0.000051	-0.000004
0	0.386 (2000)	30°	0.000060	0.000137	0.000107	-0.000031

The rotor yawing moments (Figures 5-50 and 5-51) have a slope of $\partial C_{YM}/\partial \alpha$ of -0.000033 and -0.000038 for advance ratios of 0.206 and 0.234. An inflection is shown in the data at about -2 degrees and finally, the derivative is reduced to zero between 5 and 10 degrees. The torsional blade loads show a marked increase in this range, mostly due to the seventh and eighth harmonics. The rotor torsional natural frequency at this RPM is 7.5 per rev. The change in hub moments at this point is probably due to the first harmonic torsion phasing changing. Further investigation is required to define these phenomena.

The rotor side force data, Figures 5-52 and 5-53, show only a small change due to stall consistent with the normal force. The conditions under which stall occurred on this model are not necessarily flight limits on the full-scale aircraft since they depend upon the rotor dynamics which are not scaled. Further, although the C_L , C_x trim point for the model lies in the stall region, the aircraft pitching moment is not trimmed and the cyclic required to trim will change the blade section angles of attack.

The same rotor trends are presented for a nacelle incidence of 45 degrees in Figures 5-54 through 5-58 for an advance ratio of 0.260 and the associated blade load trends shown in Figures 6-76, Section 6.4. As discussed in Section 4.3.2 there is a definite indication of rotor stall at fuselage angles of attack greater than 12 degrees for a nacelle incidence of 45 degrees. The derivatives that are defined for this nacelle incidence are therefore obtained for the fuselage angle of attack range below 10 degrees. Pitching moment data presented in Figure 5-54 indicate a slope of 0.000074 that becomes zero or negative beyond 12 degrees angle of attack. The first harmonic of the flap bending, Figure 6-76, shows a smaller change in slope than did the data for a nacelle incidence of 70 degrees. Further investigation of the change in moment derivatives is required. This same effect is present in the normal force trends presented in Figure 5-55 and for the yawing moment, in Figures 5-56 and 5-57. The associated derivatives are: $\partial C_N/\partial \alpha = 0.000035$ and $\partial C_{YM}/\partial \alpha = -0.000067$. Stall produces an unusual effect on the trend of sideforce with angle of attack shown in Figure 5-58. For the left rotor, there is a positive slope at low angles of attack, an almost neutral slope in the mid-angle of attack range and a negative slope at high angles. Although these data cannot be directly interpreted as flight envelope limits for the full-scale aircraft, they provide a means of verifying the methodology for the prediction of rotor stall which was an objective of this test.

It should be pointed out that the rotor was run at approximately 1800 RPM because of motor power limitations for this collective and nacelle incidence, whereas the other configurations were tested at approximately 2000 RPM. This reduced RPM increases the flapwise frequency ratio, reduces the flapping derivative and results in a lower pitching moment and higher normal force derivatives than would be obtained from operation at approximately 2000 RPM. The flapwise frequency increase also decreases the phase angle at which maximum flapping occurs.



Since the phase angle decreases, it decreases the side force derivative and increases the yawing moment derivative.

Looking at the trend of the longitudinal derivatives with advance ratio in Table 5-1 indicates that the data presented for an advance ratio of 0.26 (operating at 1800 RPM) do not conform with the data for advance ratios of 0.206, 0.234 and 0.386 obtained with a rotor speed of 2000 RPM. The derivatives for pitching moment and side force are lower than the trend and normal force yawing moment are higher than that trend that is evident from the data for operation at 2000 RPM.

Testing was also done to obtain the directional stability characteristics for the configurations with the nacelle incidence of 70 and 45 degrees. Figures 5-59 through 5-63 present the rotor yawing moment (right rotor), yawing moment (left rotor), side force, pitching moment, and normal force respectively for a nacelle incidence of 70 degrees at an advance ratio of 0.206.

Tabulated below are derivatives obtained from the left rotor at yaw angles more negative than -5 degrees.

i_N	V/V_T	$\partial C_{YM}/\partial \psi$	$\partial C_{SF}/\partial \psi$	$\partial C_{PM}/\partial \psi$	$\partial C_N/\partial \psi$
70	.206	0.000026	0.000025	0.000043	0.000011

For the configuration with the nacelle at 70 degrees, the left rotor is operating in stall at zero degrees yaw and angle of attack. It appears from the data that at yaw angles more negative than -5 degrees this stall condition is alleviated and results in large force and moment derivatives.

When yaw sweeps were made for the configuration with the nacelle incidence of 45 degrees as stated before there appears to be no stall for zero yaw and angle of attack. This is shown by no significant change in slope in the rotor yawing moment, side force, pitching moment and normal force presented in Figures 5-64 through 5-68 respectively. The derivatives obtained from this data are presented in the following tabulation:

i_N	V/V_T	$\partial C_{YM}/\partial \psi$	$\partial C_{SF}/\partial \psi$	$\partial C_{PM}/\partial \psi$	$\partial C_N/\partial \psi$
45	0.260	0.000027	0.000035	0.000051	-0.000004

Since this testing was performed at a rotor speed of 1800 RPM it will result in the yawing moment and normal force derivatives being lower than those that would be obtained at 2000 RPM. Also the side force and pitching moment derivatives will be higher for 1800 RPM than for 2000 RPM. As discussed in the previous paragraphs on the longitudinal derivative this is a result of the first mode flapping frequency ratio increasing as RPM is decreased. It is of major importance to repeat this fact, to make clear that the data obtained at 45 nacelle incidence must not be used in conjunction with the 70 and zero degree nacelle incidence to define a consistent trend with advance ratio.

These derivatives have been defined for transition, out of ground effect, from hover to cruise. In ground effect testing with a nacelle incidence of 70 degrees has been performed in conjunction with STOL takeoff to define the directional stability characteristics. A comparison is included here to determine if there are

any differences in the rotor stability derivatives when operating in or out of ground effect. Presented in Figures 5-69 through 5-73 are the yawing moment, side force, pitching moment and normal force variations with yaw angle in ground effect, at a rotor height to diameter ratio of 0.39, and out of ground effect. The conclusion drawn from this data is that there is no change in rotor stability derivatives induced by flying in ground effect. The difference in level of the two sets of data can be attributed to a slight difference in angle of attack.

5.3.2 Aircraft Stability Derivatives

Testing performed to define the rotor stability in transition was supplemented with tail-off runs to define the total aircraft stability in transition. From these data, an assessment can be made of the contribution of the prop/rotor and the tail to stability. This section presents the analysis of longitudinal stability for nacelle incidences of 70 and 45 degrees and a discussion of directional stability including the impact of ground effect.

Figure 5-74 shows the total aircraft stability and the contribution of the horizontal tail and the prop/rotor with a nacelle incidence of 70 degrees. The airframe minus tail is unstable having a stability derivative ($\partial C_{PM}/\partial \alpha$) of 0.015 per degree. This decreases to approximately zero beyond 8 degrees angle of attack, reflecting stall. Adding the tail decreases the derivative to -0.040 per degree providing a very stable aircraft. Adding the rotor results in an unstable aircraft at angles of attack more negative than -5 degrees. As the angle of attack is increased, the aircraft becomes neutrally stable and then as stable as the rotors-off aircraft up to 10 degrees angle of attack. This is a result of the stall effect of the rotor contribution to the total aircraft stability. As discussed in the previous section, stall reduces the rotor stability derivatives contribution to the total aircraft and therefore explains why the aircraft has neutral to positive stability at angles of attack greater than -5 degrees.

For the nacelle angle of 45 degrees, the airframe-minus-tail stability derivative is 0.018 per degree as presented in Figure 5-75. This is a slight decrease in stability resulting from the change in the nacelle incidence. The slope of the moment reduces to zero at eight degrees indicating wing stall. This matches the maximum lift shown in Figure 4-30. This stall effect is very pronounced in the airframe characteristics in that the tail effectiveness increases because of the reduced downwash.

For this configuration, data were obtained for tail on and off with the rotors on. The aircraft minus tail reflects the destabilizing contribution of the rotor and shows the impact of rotor and power on wing stall at approximately 10 degrees. Adding the tail improves the total aircraft stability resulting in a derivative that

is approximately the same as the airframe minus tail for angles of attack more nose-down than 5 degrees. Since the rotor and wing stall result in a stable derivative at angles of attack above 5 degrees, the addition of the tail just increases the level of the pitching moment derivative. As discussed in the cruise section, the rotor contribution of the model is significantly higher than that anticipated for the full-scale aircraft. This would reduce the unstable contribution of the rotor to a level that would have neutral to positive stability.

An examination of the directional stability characteristics is presented in Figures 5-76 and 5-77 for 70 degrees nacelle incidence. The variation of side force with yaw angle presented in Figure 5-76 becomes a minimum at -12 degrees yaw, indicating that there is possibly a flow separation occurring. The vertical tail increases the slope of the side force variation with yaw angle from 0.0077 to 0.018 and the rotor further increases the slope to 0.031. The addition of the rotors extends the linear side force beyond 12 degrees. This is representative of flow re-attachment increasing the effectiveness of the fuselage, wing and nacelle to produce side force. The yawing moment variation with yaw angle is presented in Figure 5-77. Stability derivatives shown in this figure indicate that the airframe minus tail is unstable ($\partial C_{YM}/\partial \psi = 0.00183$) and when 12 degrees of yaw is reached, the aircraft is very unstable. The tail having an incremental yawing moment slope of 0.0036 per degree, improves the stability up to 12 degrees but at greater angles, the tail is inadequate to stabilize the airframe which is separated. Adding the rotors with an unstable contribution to total aircraft stability results in the total aircraft characteristics, as demonstrated by the model, being as unstable as the model minus the tail. At approximately 8 degrees negative angle of yaw, the aircraft derivative is neutral and then becomes positive as the yaw angle is decreased. This appears to be the impact of flow re-attachment improving the tail effectiveness at a greater rate than the rotor contribution as evidenced by the side force variation.

For the nacelle incidence of 45 degrees, the side force variation with yaw angle is presented in Figure 5-78. The contribution of the vertical tail is the same as that presented in Figure 5-76 but the influence of the rotor tends to reduce the tail contribution. The associated variation in yawing moment is presented in Figure 5-79. Airframe-minus-tail indicates an unstable configuration with a yawing moment derivative ($\partial C_{YM}/\partial \psi$) of 0.0023 per degree and the addition of the tail provides a stable aircraft with a $\partial C_{YM}/\partial \psi$ of -0.0007 per degree. Addition of the rotors produces an increase in the unstable moment by 0.003 per degree resulting in a model with a directional stability derivative of -0.0023 per degree which is the same as the airframe minus tail.

The characteristics of the model rotor are such that they produce a larger destabilizing moment than would be expected from the full aircraft. Also the model nacelles are oversized to provide clearance for the electric motors and balance support which contributes a large amount to the unstable characteristics of the airframe. Both these items result in longitudinal and directional stability characteristics for the model that are more unstable than the full scale aircraft would be.

An assessment has been made for cruise in Section 5.4.2 indicating that the full scale rotor is significantly less unstable resulting in a stable aircraft.

5.3.3 Control Mixing

A series of runs was made during the transition tests for the purpose of measuring control power in transition. The model was set up for a typical mid-transition condition; i.e., 45° nacelle incidence 60° flaperon and leading edge umbrellas closed. The swashplates were set to give differential cyclic: 3° nose-down on the left-hand rotor and 3° nose-up on the right-hand rotor. The control phase angle was set at 65°, similar to the hover runs.

The data obtained show the effects of angle of attack, yaw and advance ratio on the rotor control forces and moments and the cyclic pitch phase angles. In addition, data were obtained with differential thrust and cyclic for the purpose of investigating roll and yaw control mixing in transition.

The results of the control mixing tests are shown in Figure 5-80. The data show large changes in rolling and yawing moment due to differential thrust and little or no effect due to differential cyclic pitch. The latter is caused by the input cyclic phase angle being close to that required for maximum hub moment as shown in Figure 5-81. Estimated rolling and yawing moment trends for differential thrust and cyclic are presented in Figure 5-80 for the phase angle for maximum in plane force. Thus, for example, a differential thrust coefficient of $\Delta C_{T_S} = 0.02$ (model scale) and differential cyclic of 4 degrees (that is, 4 degrees nose-up on the left-hand rotor and 4 degrees nose-down on the right-hand rotor) results in roll control ($C_{R_M} = 0.049$) with no yaw coupling. The complementary condition (4 degrees nose-down cyclic on the left-hand rotor and 4 degrees nose-up on the right-hand rotor) produces yaw control ($C_{Y_M} = 0.049$) with no roll coupling.

5.3.4 Attitude Effects on Control

Angle of Attack

The variations of the roll control forces, moments and phase angles with angle of attack are shown in Figures 5-82 through 5-84. The force and moment data shown are the increments in rotor normal force, side force, pitching moment and yawing moment coefficient due to 3° cyclic. In general, these parameters are insensitive to angle of attack except for a loss in pitching moment at high angles where rotor stall occurs as discussed in Section 4.3.2.

The effect of angle of attack on cyclic phase angle is shown in Figure 5-84. Both the moment and the force phase angle show an increase with increasing angle of attack, up to $\alpha \approx 6^\circ$.

Yaw

The effects of yaw on the transition control parameters is shown in Figures 5-85 to 5-87. As can be seen from these figures, pitching and yawing moment are unaffected by yaw angle variation.

Advance Ratio

The changes in transition control parameters with advance ratio are shown in Figures 5-81, 5-88 and 5-89. Also shown for comparison are the hover points for the right-hand rotor. The hover and transition results show consistent effects of advance ratio on the control parameters.

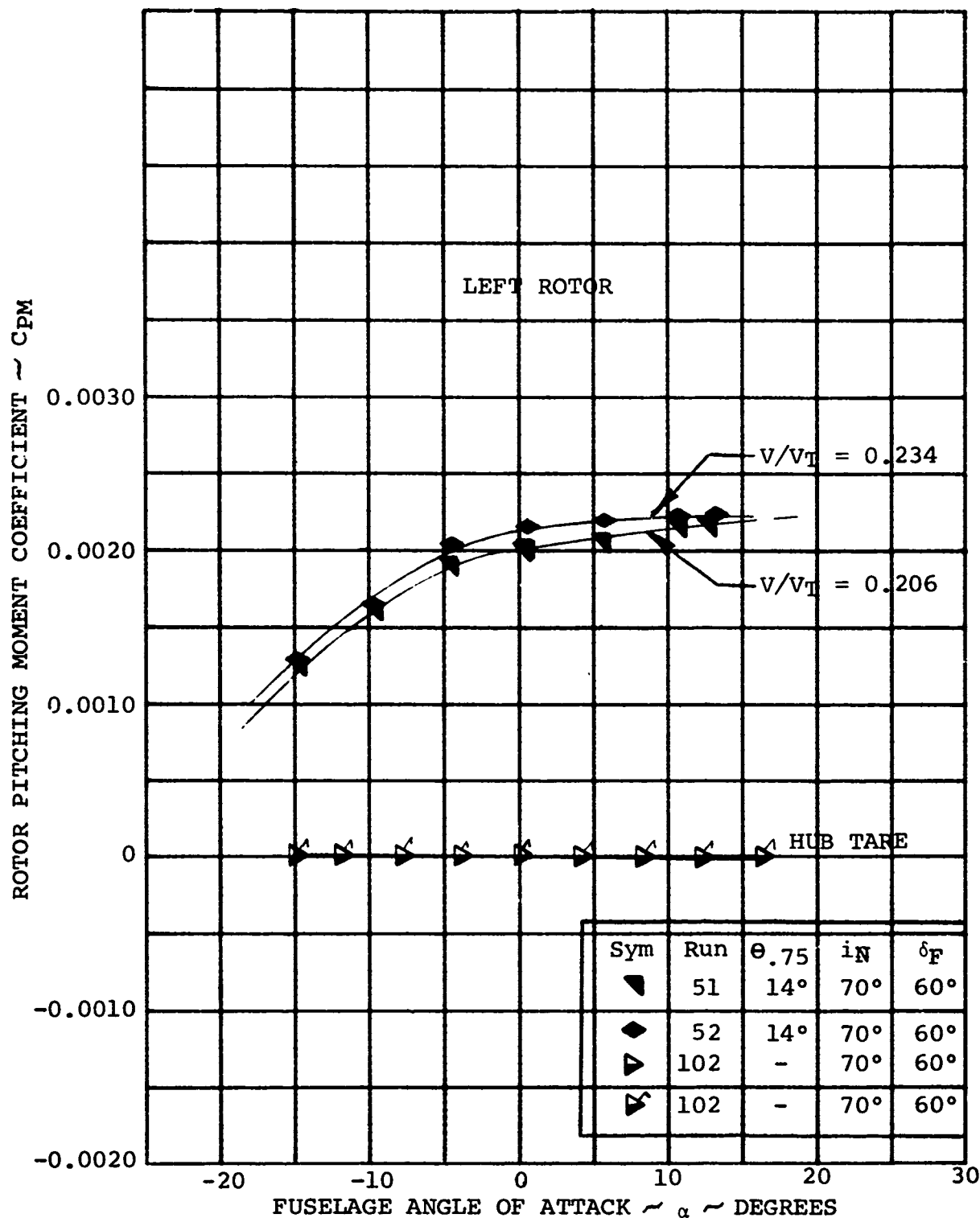


FIGURE 5-46. ROTOR PITCHING MOMENT/ANGLE OF ATTACK VARIATION AT $V/V_T = 0.206$ & 0.234 with $i_N = 70^\circ$

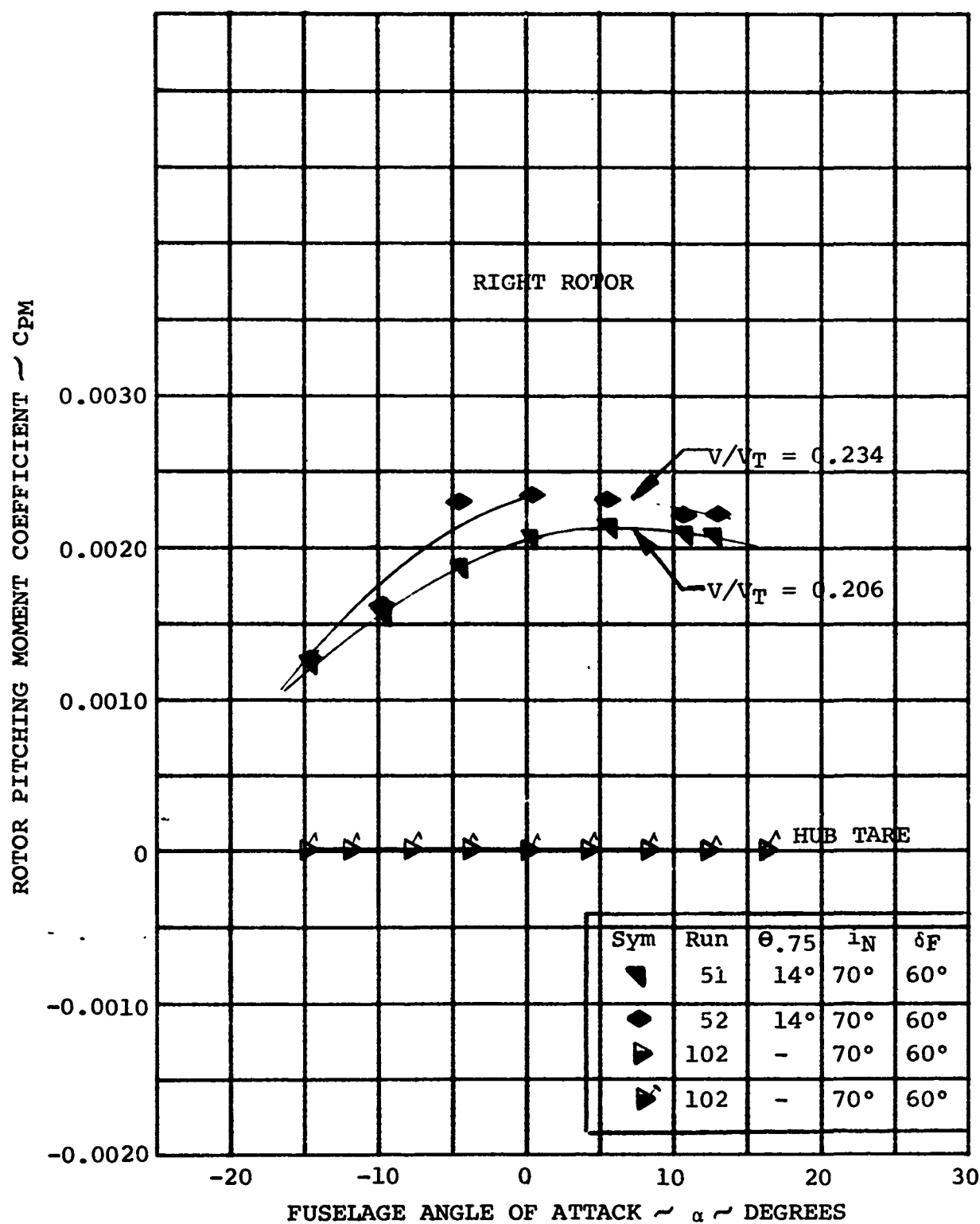


FIGURE 5-47. ROTOR PITCHING MOMENT/ANGLE OF ATTACK VARIATION AT $V/V_T = 0.206$ and 0.236 WITH $i_N = 70^\circ$

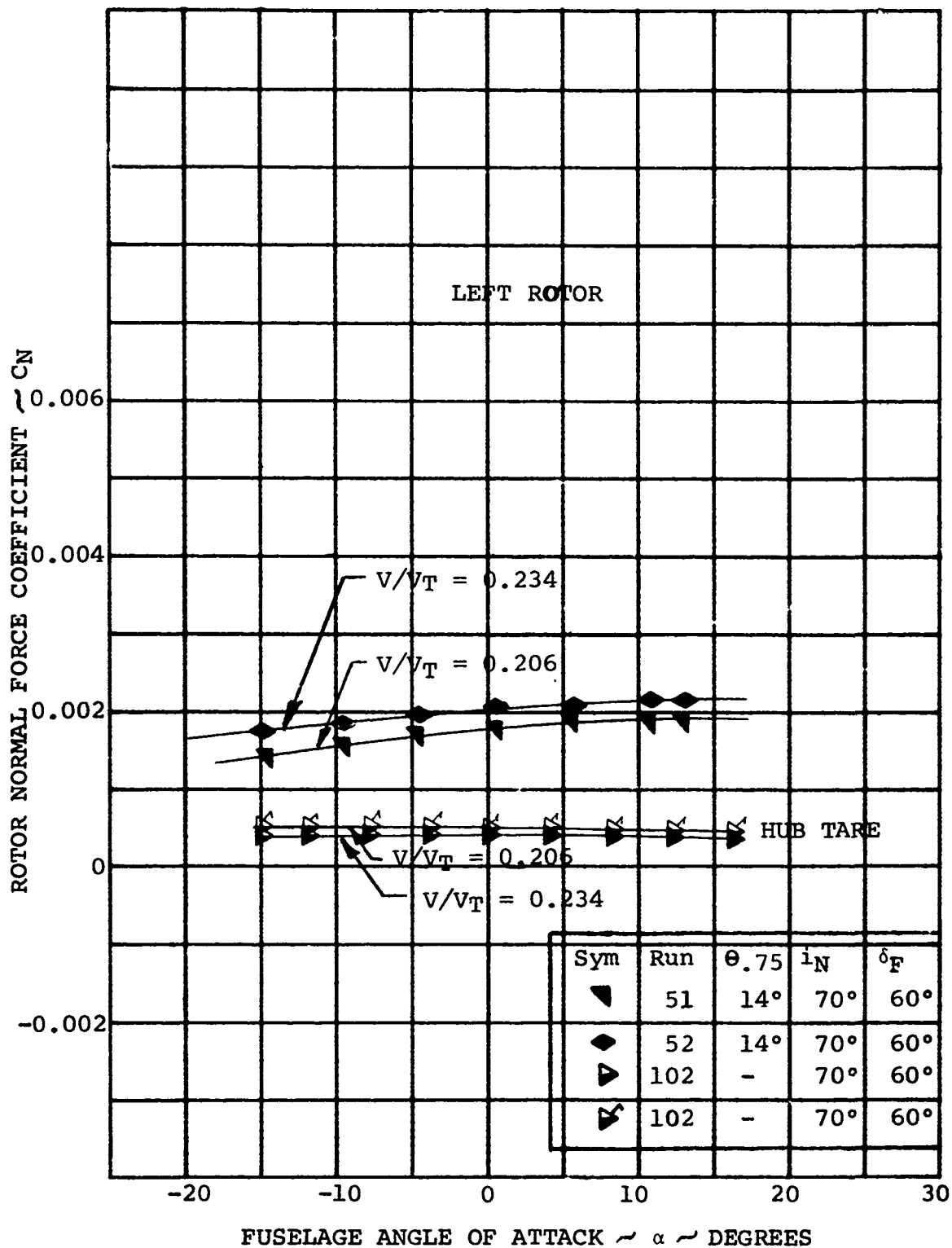


FIGURE 5-48. ROTOR NORMAL FORCE/ANGLE OF ATTACK
VARIATION AT $V/V_T = 0.206$ and 0.234
WITH $i_N = 70^\circ$

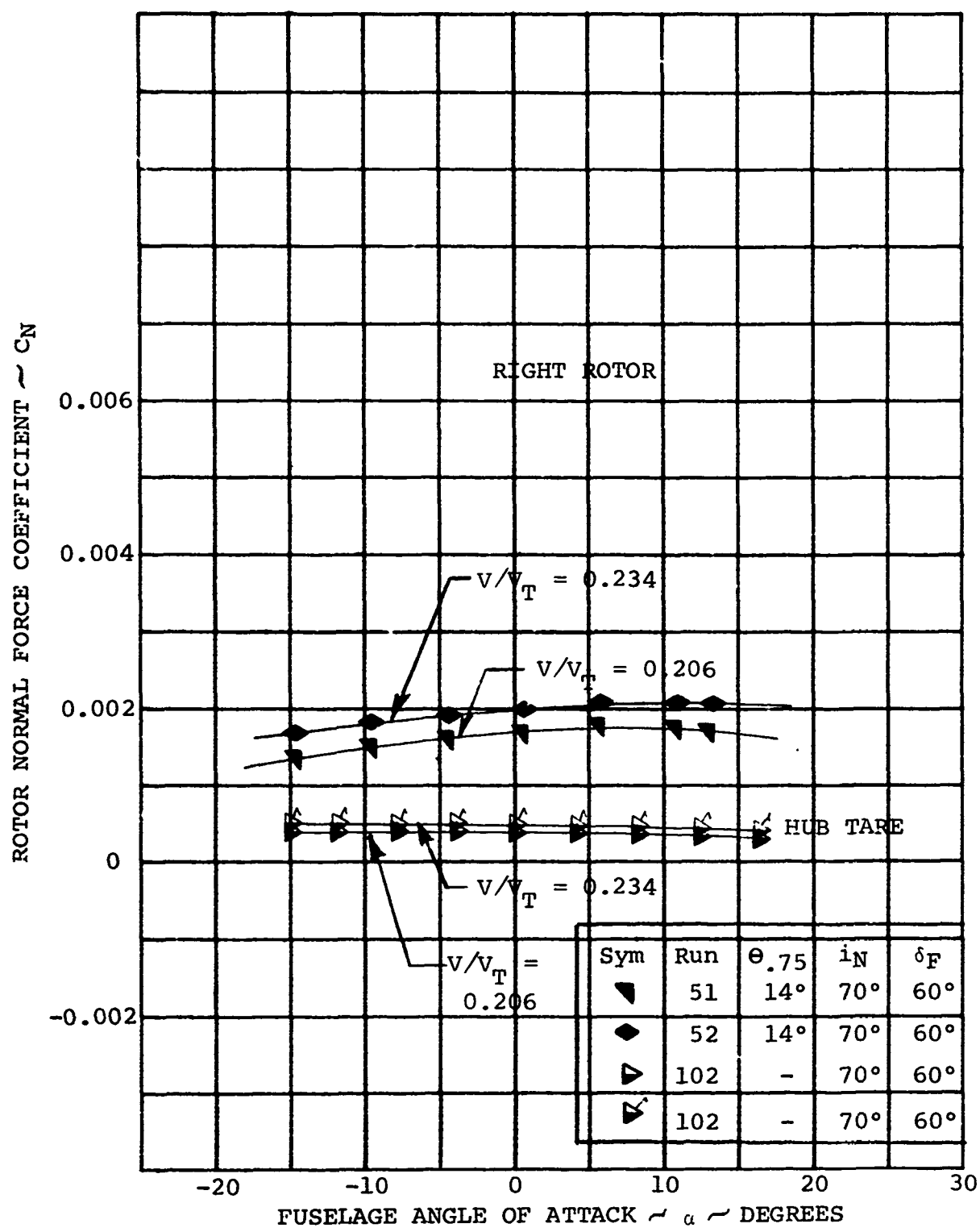


FIGURE 5-49. ROTOR NORMAL FORCE/ANGLE OF ATTACK
VARIATION AT $V/V_T = 0.206$ and 0.234
WITH $i_N = 70^\circ$

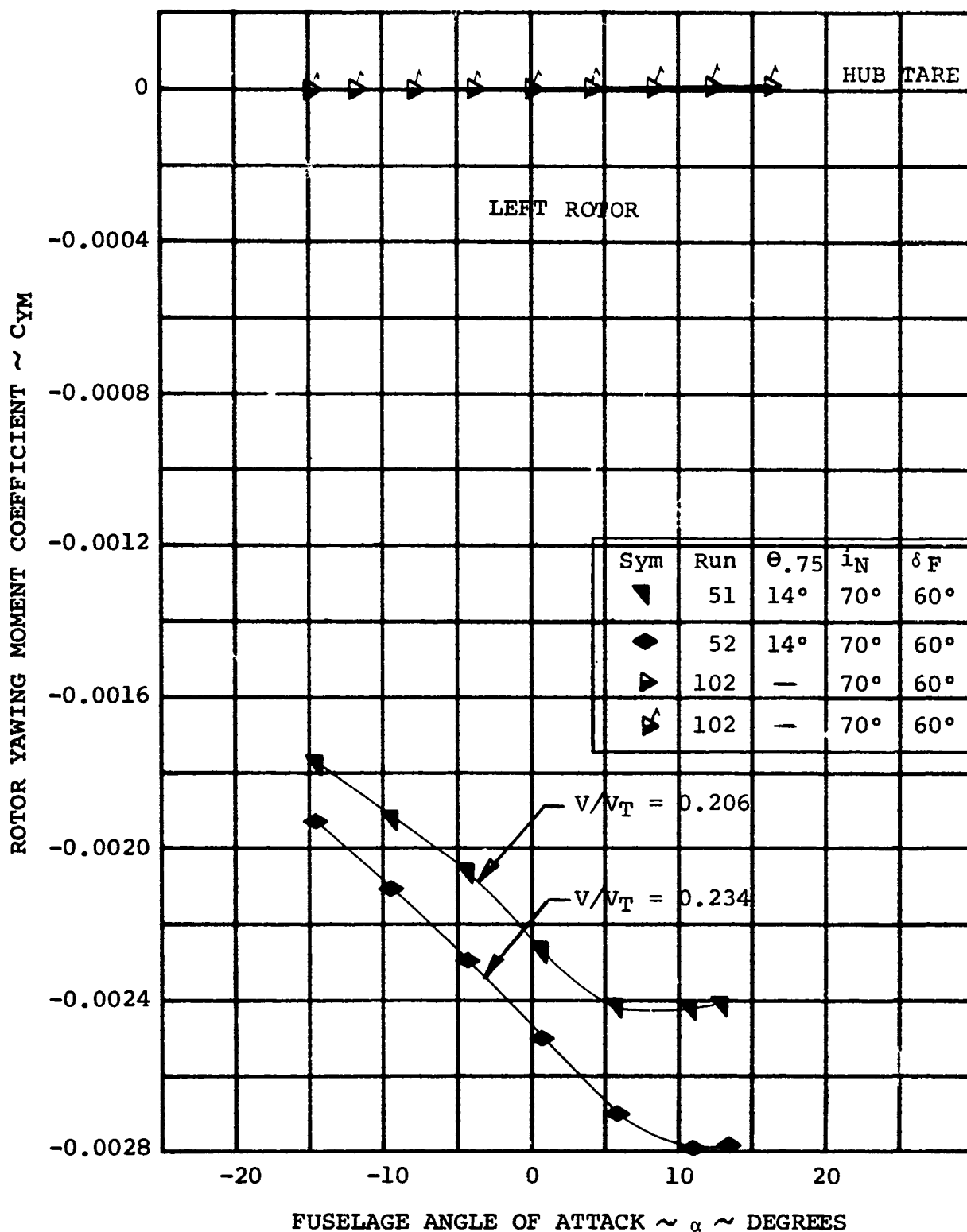


FIGURE 5-50. ROTOR YAWING MOMENT/ANGLE OF ATTACK
VARIATION AT $V/V_T = 0.206$ and 0.234
WITH $i_N = 70^\circ$

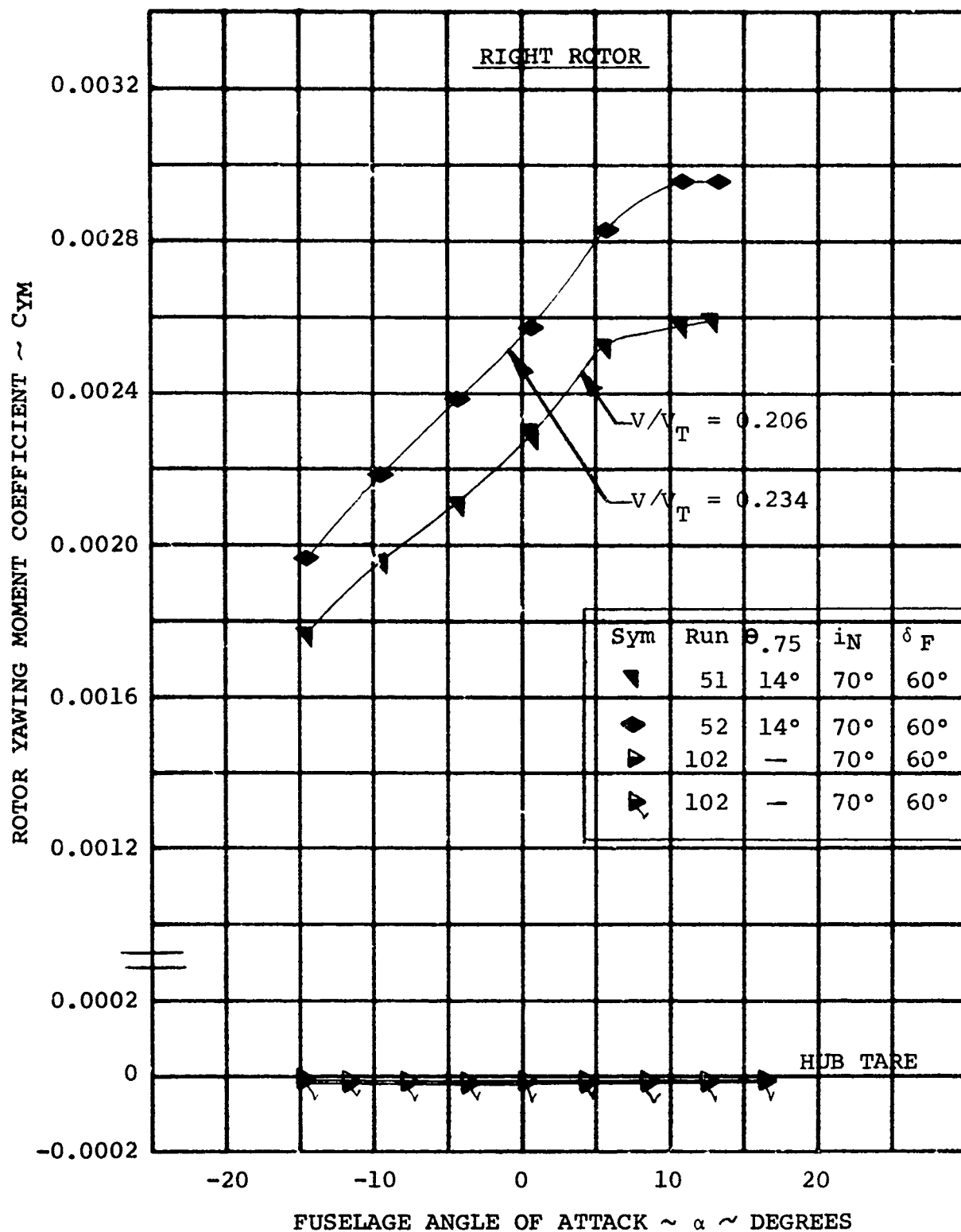


FIGURE 5-51. ROTOR YAWING MOMENT/ANGLE OF ATTACK
VARIATION AT $V/V_T = 0.206$ and 0.234
WITH $i_N = 70^\circ$

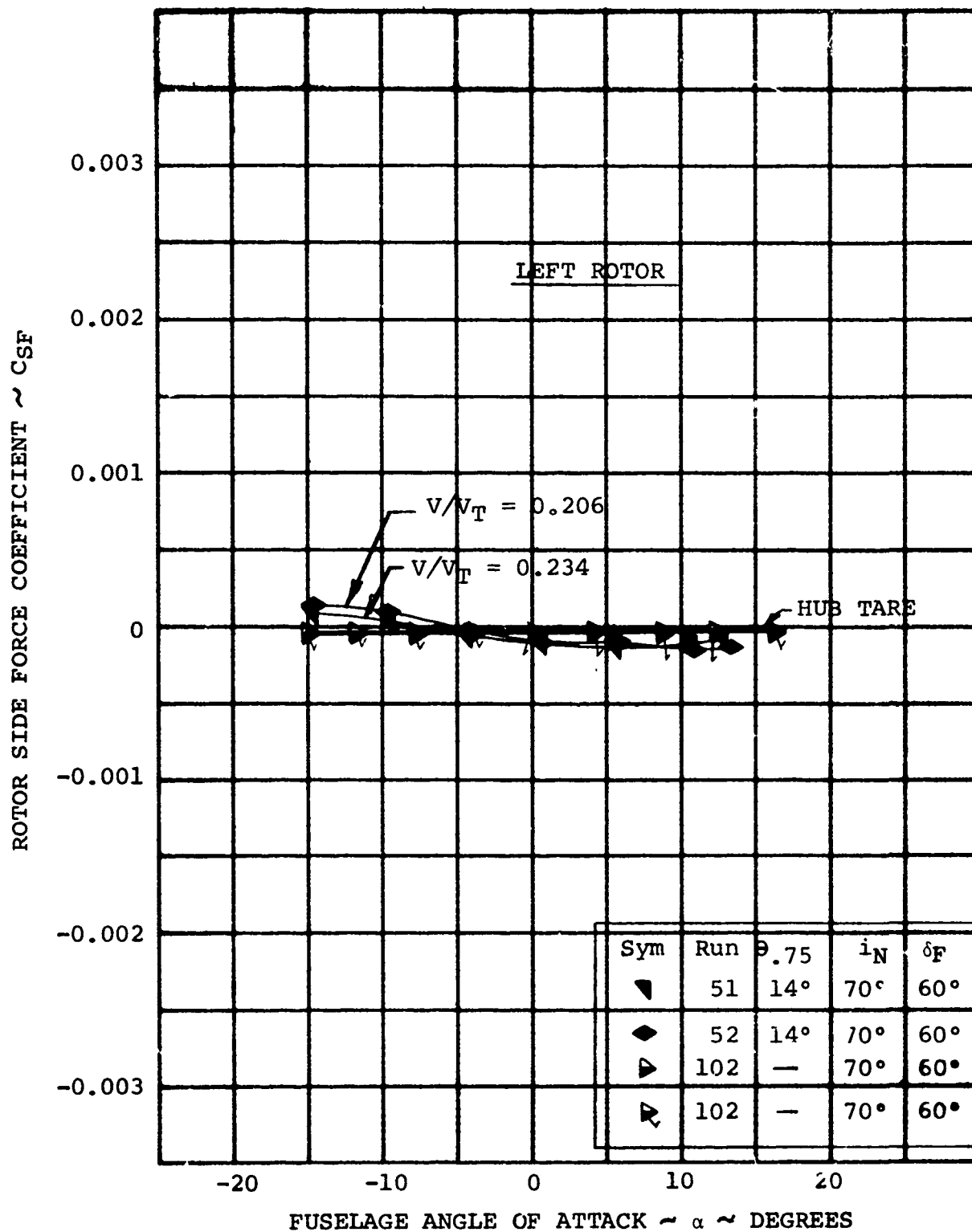


FIGURE 5-52. ROTOR SIDE FORCE/ANGLE OF ATTACK VARIATION
AT $V/V_T = 0.206$ and 0.234 WITH $i_N = 70^\circ$

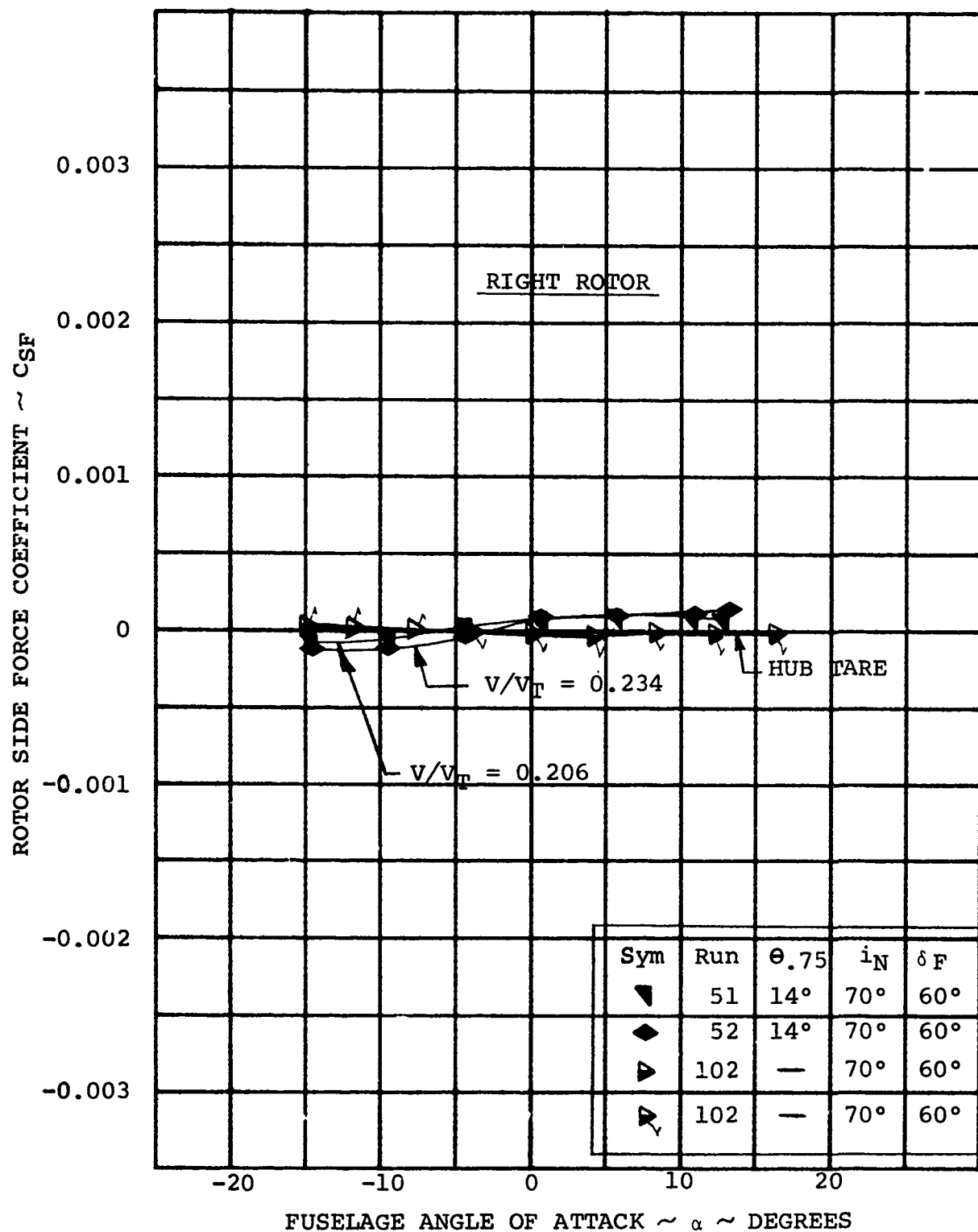


FIGURE 5-53. ROTOR SIDE FORCE/ANGLE OF ATTACK VARIATION
AT $V/V_T = 0.206$ and 0.234 with $i_N = 70^\circ$

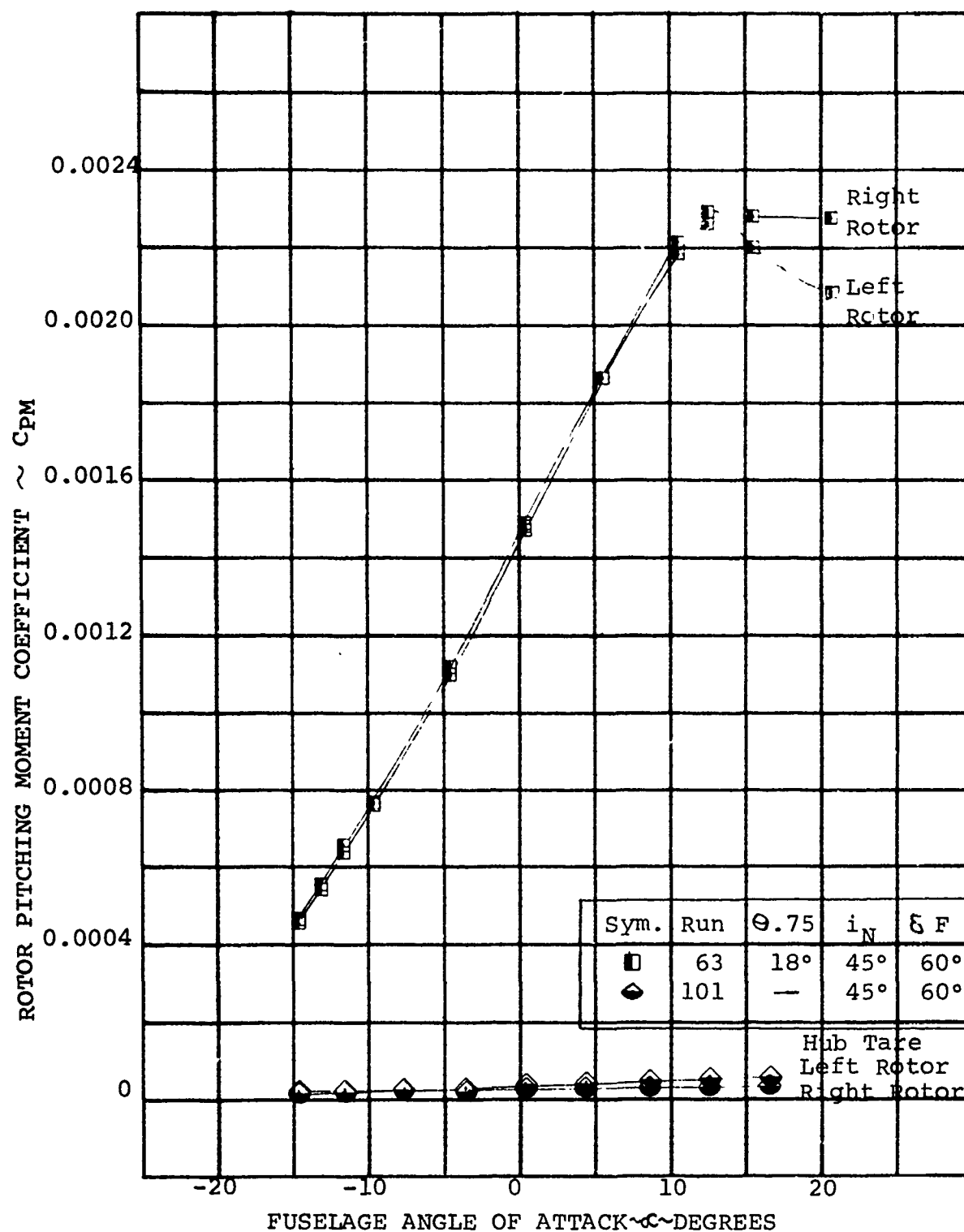


FIGURE 5-54. ROTOR PITCHING MOMENT/ANGLE OF ATTACK VARIATION AT $V/V_T=0.260$ WITH $i_N=45^\circ$

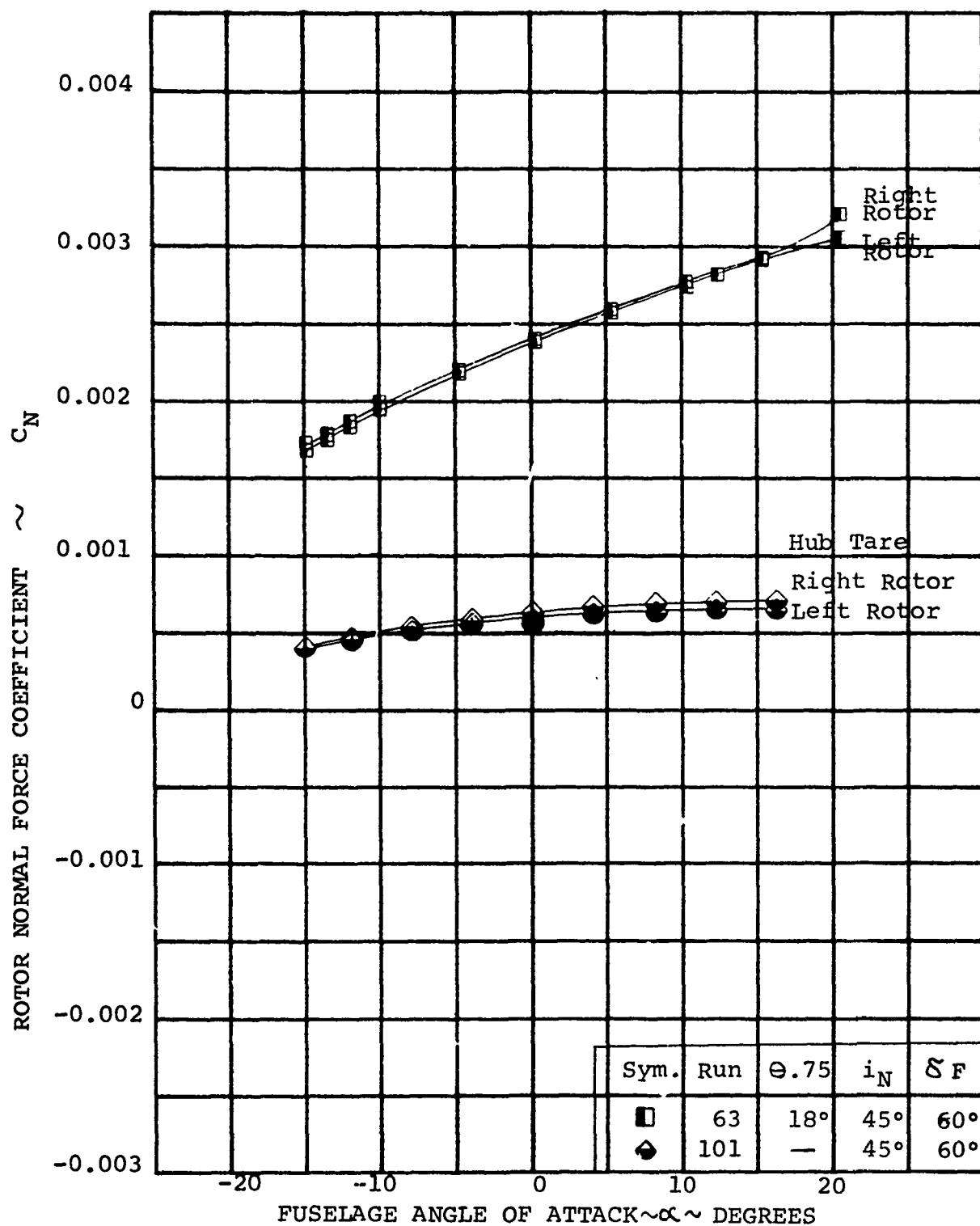


FIGURE 5-55. ROTOR NORMAL FORCE/ANGLE OF ATTACK VARIATION AT $V/V_T = 0.260$ WITH $i_N = 45^\circ$

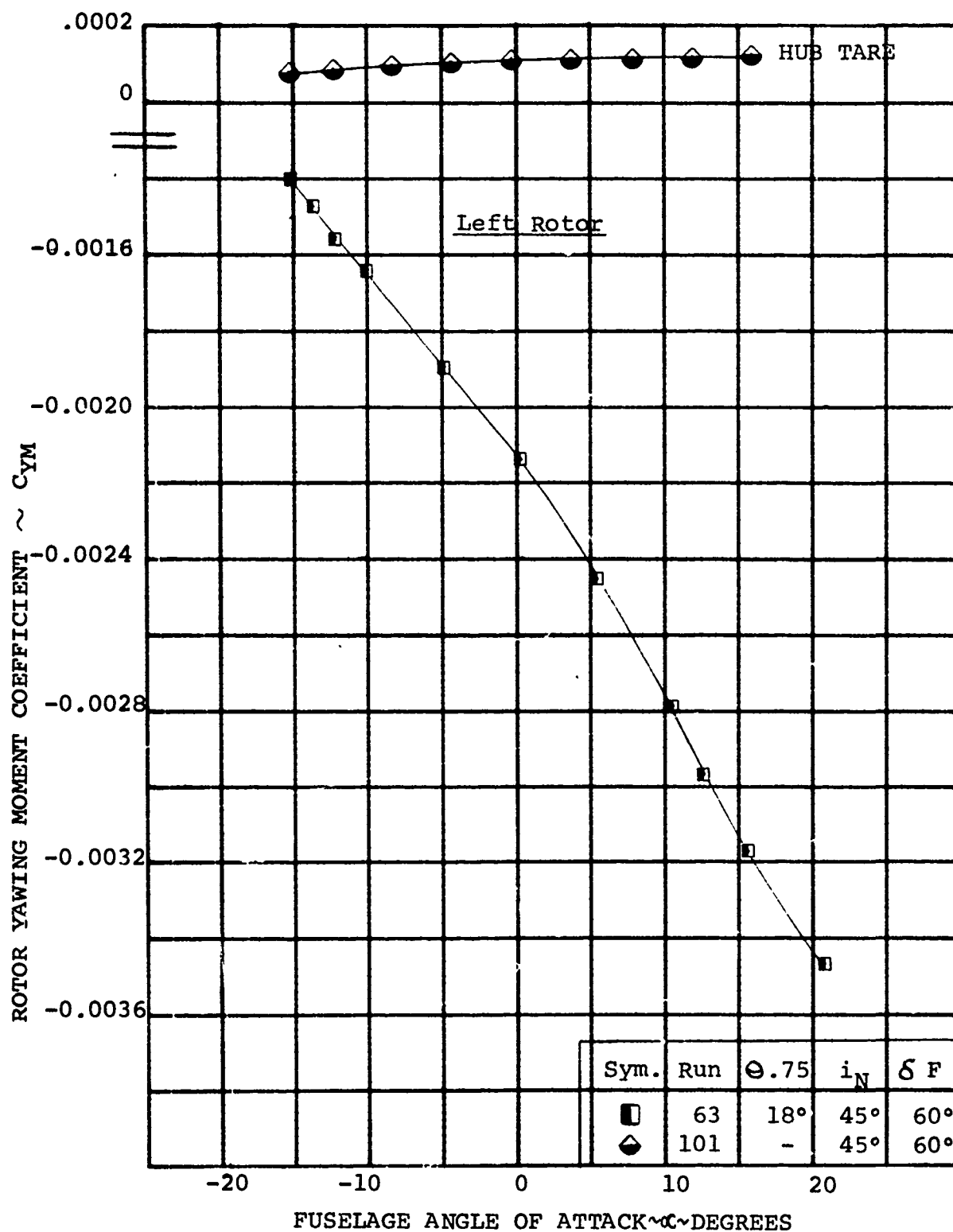


FIGURE 5-56. ROTOR YAWING MOMENT/ANGLE OF ATTACK VARIATION AT $V/V_T=0.260$ WITH $i_N=45^\circ$

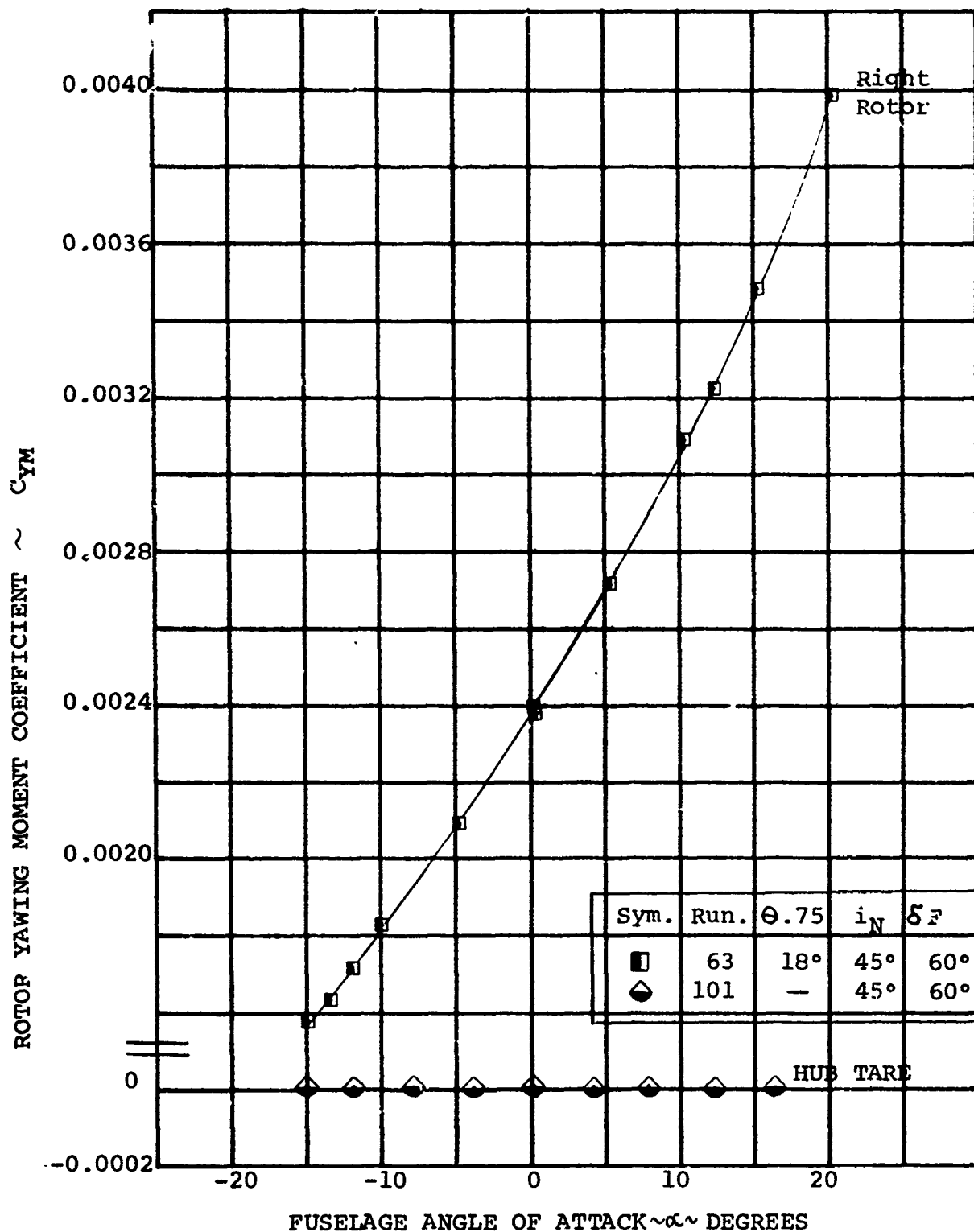


FIGURE 5-57.

ROTOR YAWING MOMENT/ANGLE OF ATTACK
VARIATION AT $V/V_T=0.260$ WITH $i_N=45^\circ$

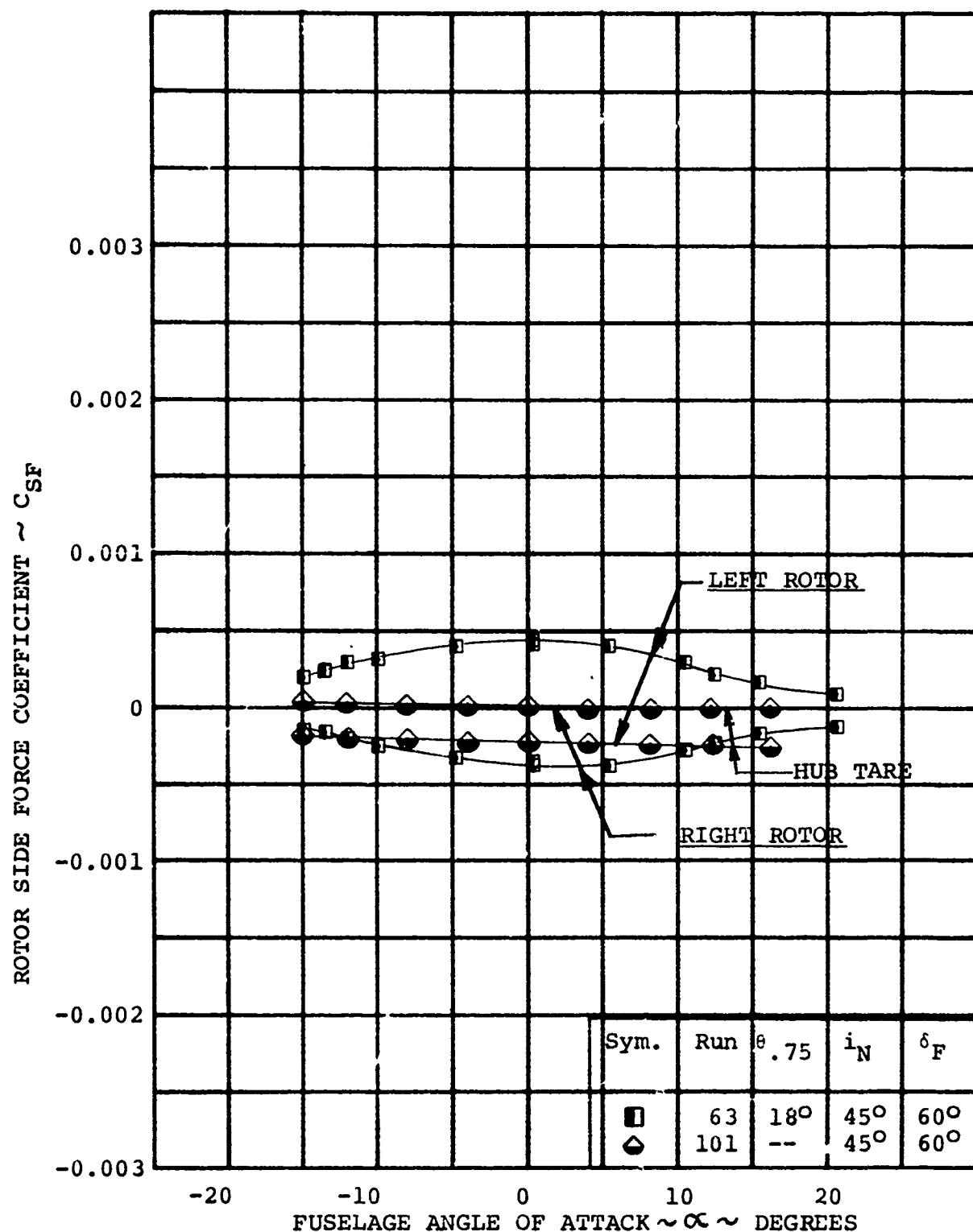


FIGURE 5-58. ROTOR SIDE FORCE/ANGLE OF ATTACK VARIATION
AT $V/V_T = 0.260$ WITH $i_N = 45^\circ$

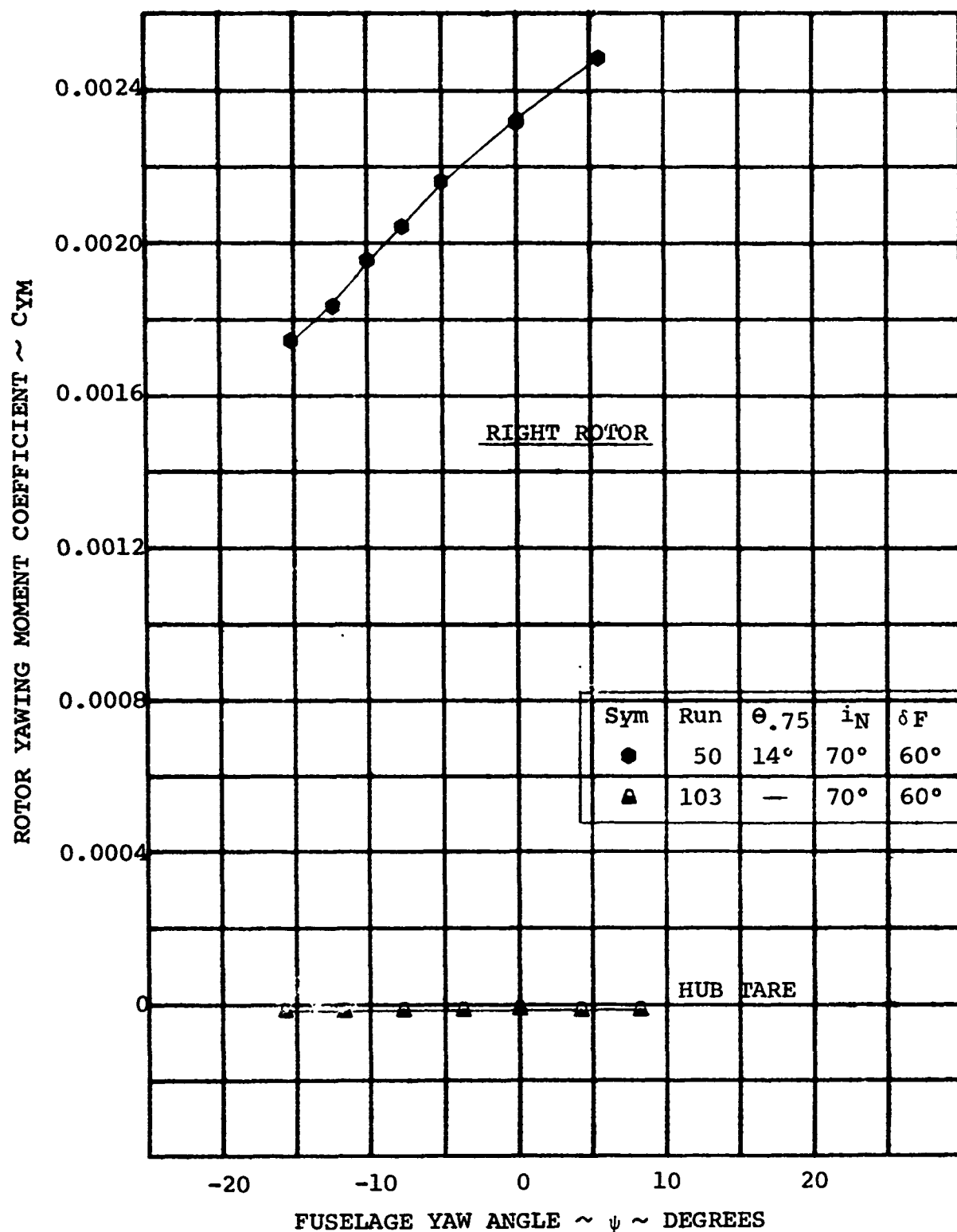


FIGURE 5-59. ROTOR YAWING MOMENT/YAW ANGLE VARIATION
AT $V/V_T = 0.206$ WITH $i_N = 70^\circ$

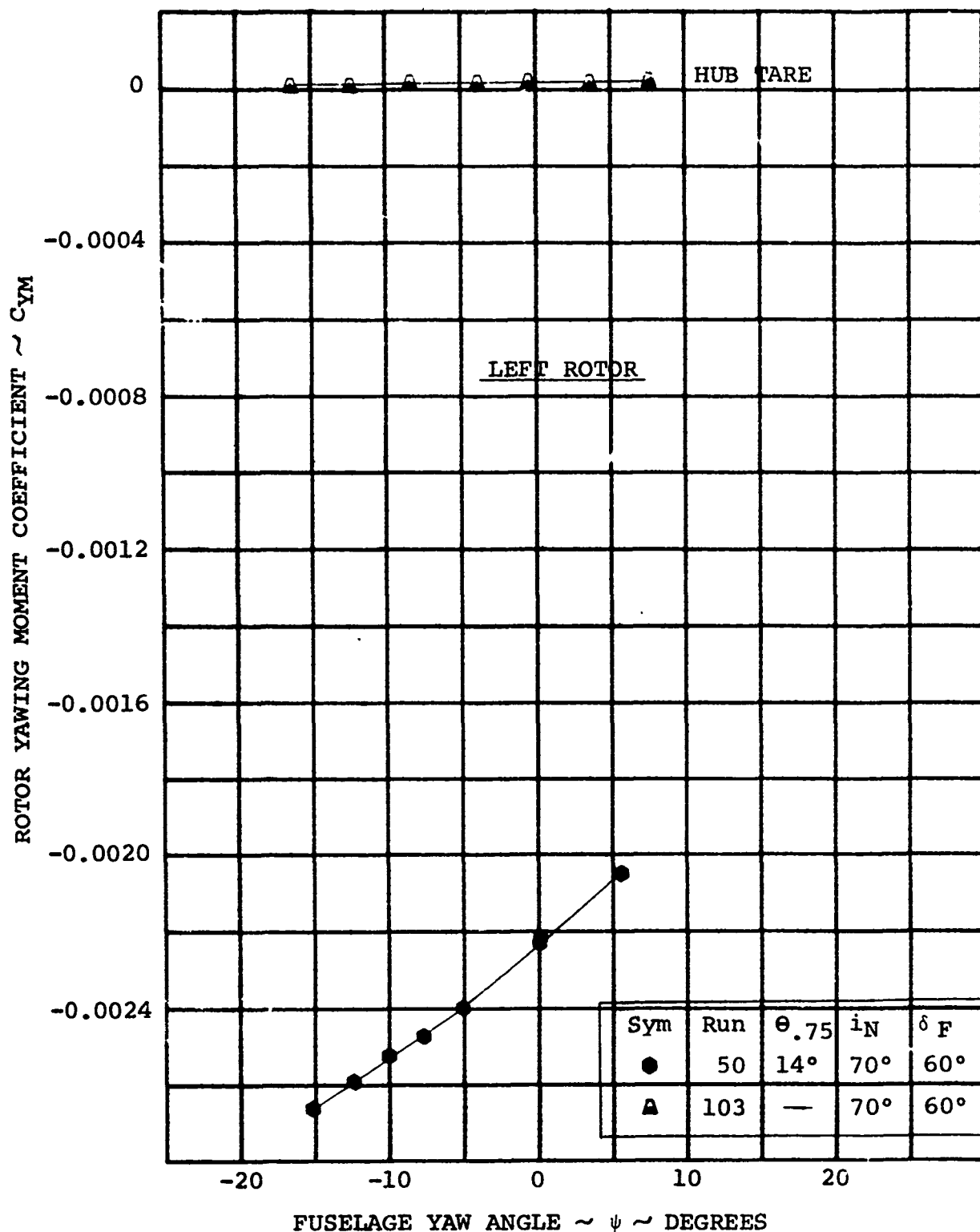


FIGURE 5-60. ROTOR YAWING MOMENT/YAW ANGLE VARIATION
AT $V/V_T = 0.206$ with $i_N = 70^\circ$

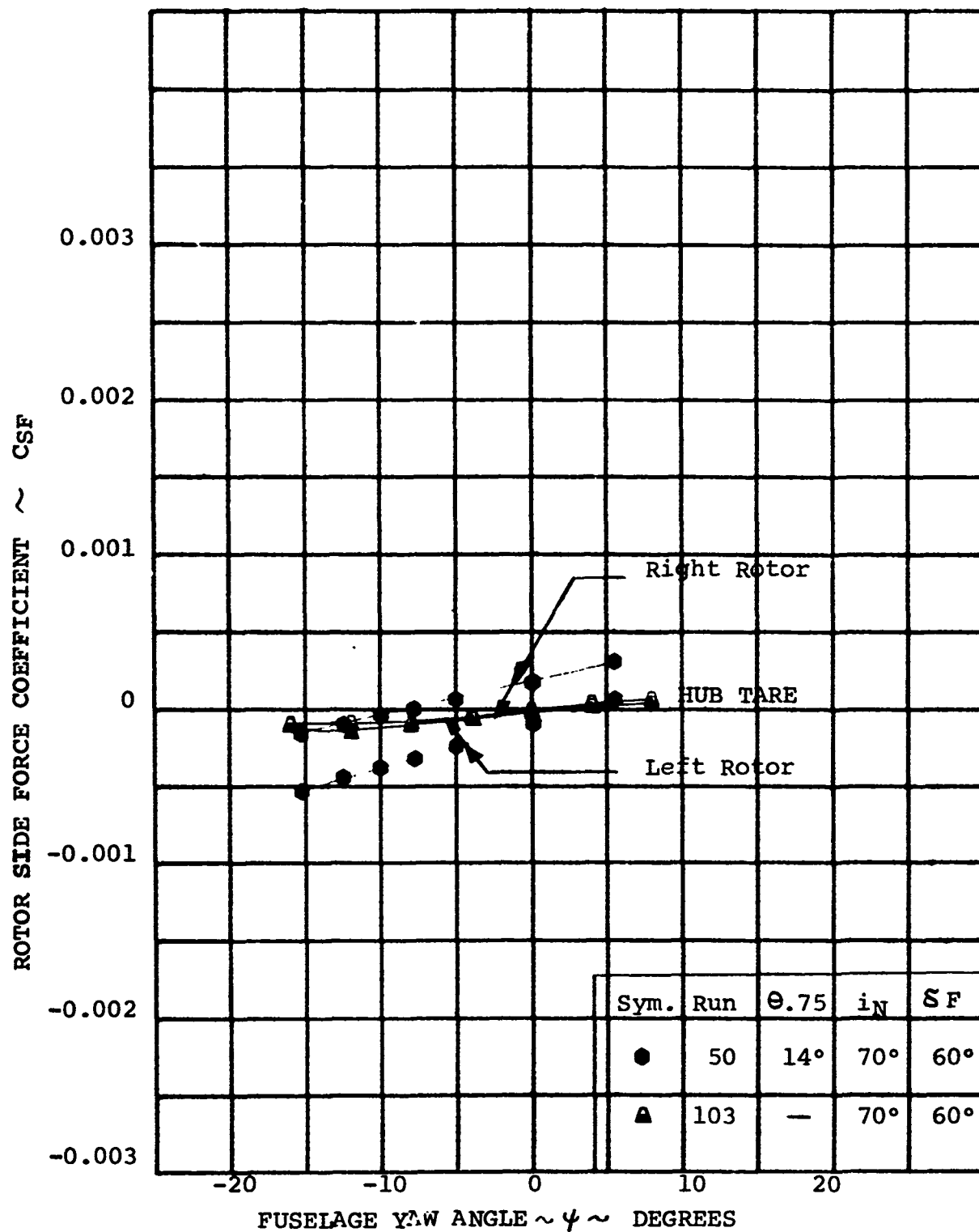


FIGURE 5-61.

ROTOR SIDE FORCE/YAW ANGLE VARIATION
AT $V/V_T = 0.206$ WITH $i_N = 70^\circ$

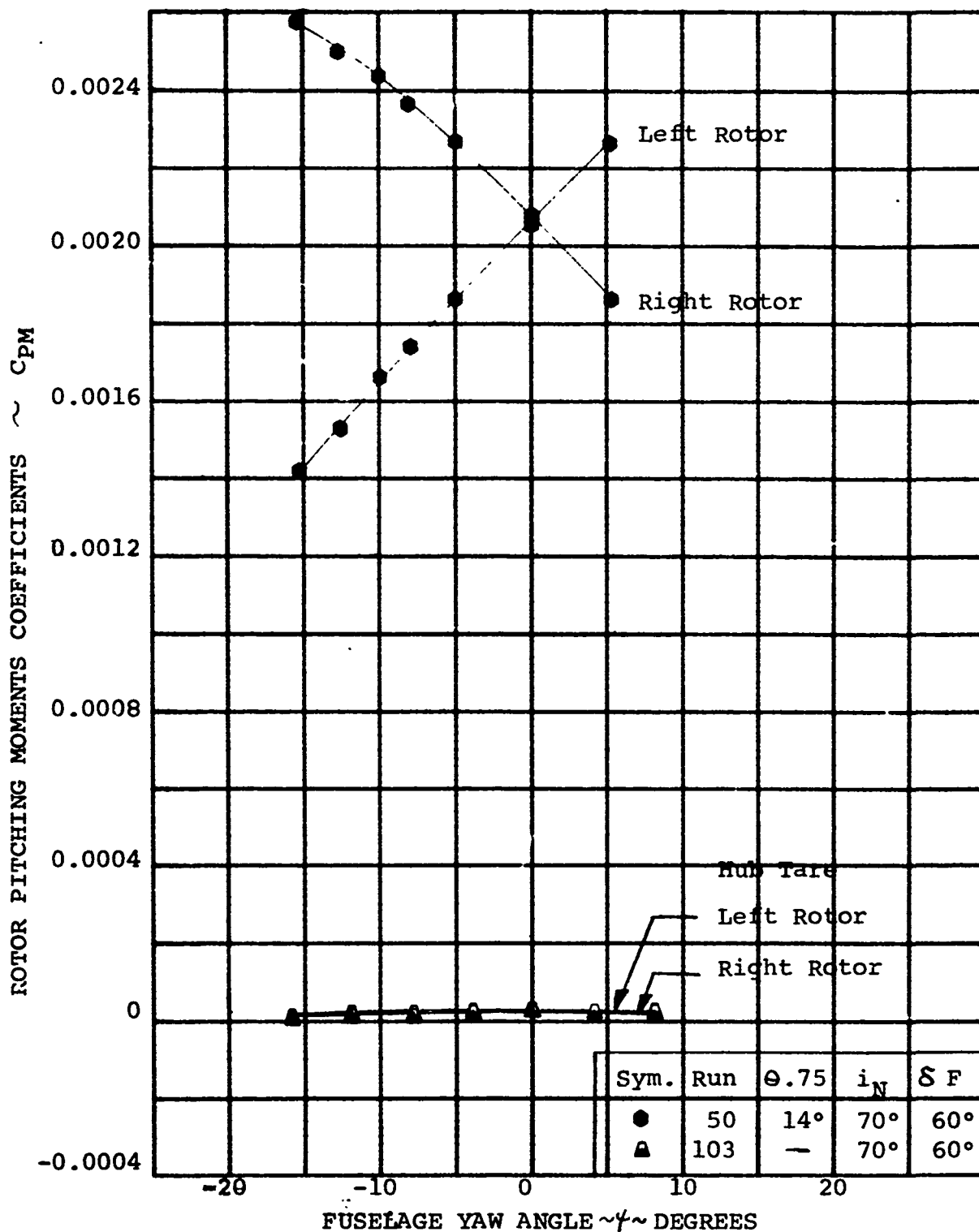


FIGURE 5-62.

ROTOR PITCHING MOMENT/YAW ANGLE VARIATION
AT $V/V_T=0.206$ WITH $i_N=70^\circ$

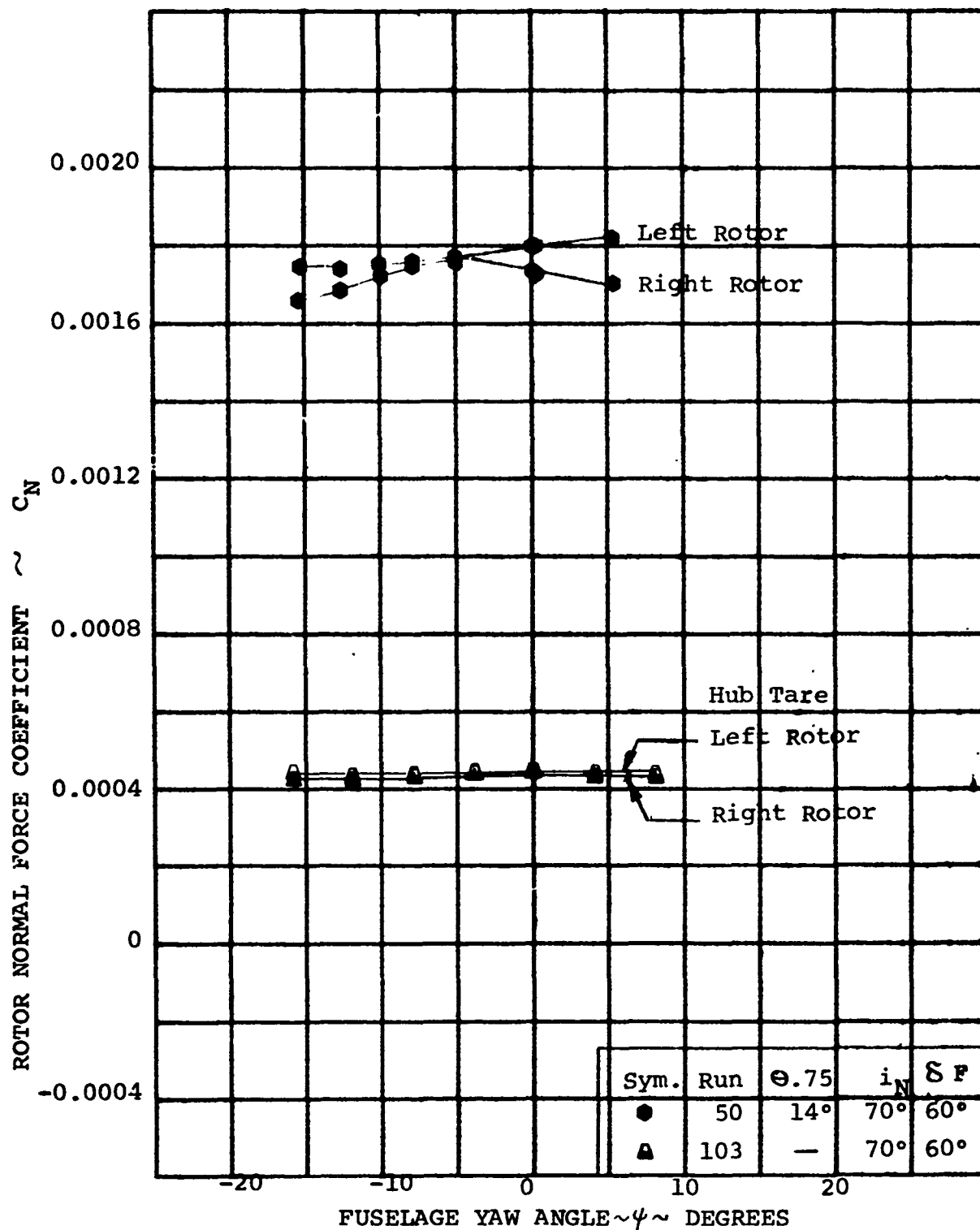


FIGURE 5-63.

ROTOR NORMAL FORCE/YAW ANGLE VARIATION
AT $V/V_T = 0.206$ WITH $i_N = 70^\circ$

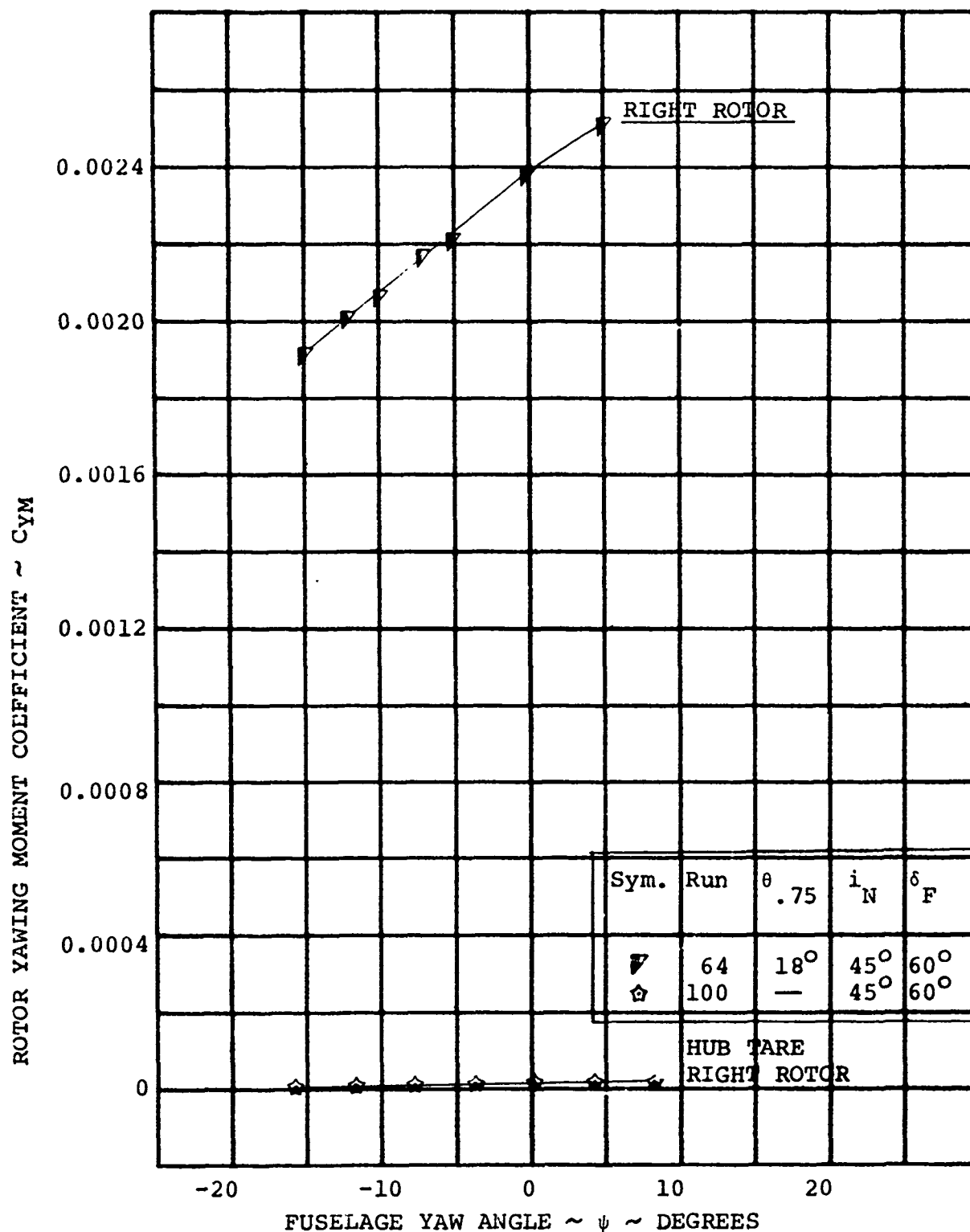


FIGURE 5-64. ROTOR YAWING MOMENT/YAW ANGLE VARIATION
AT $V/V_T = 0.260$ WITH $i_N = 45^\circ$

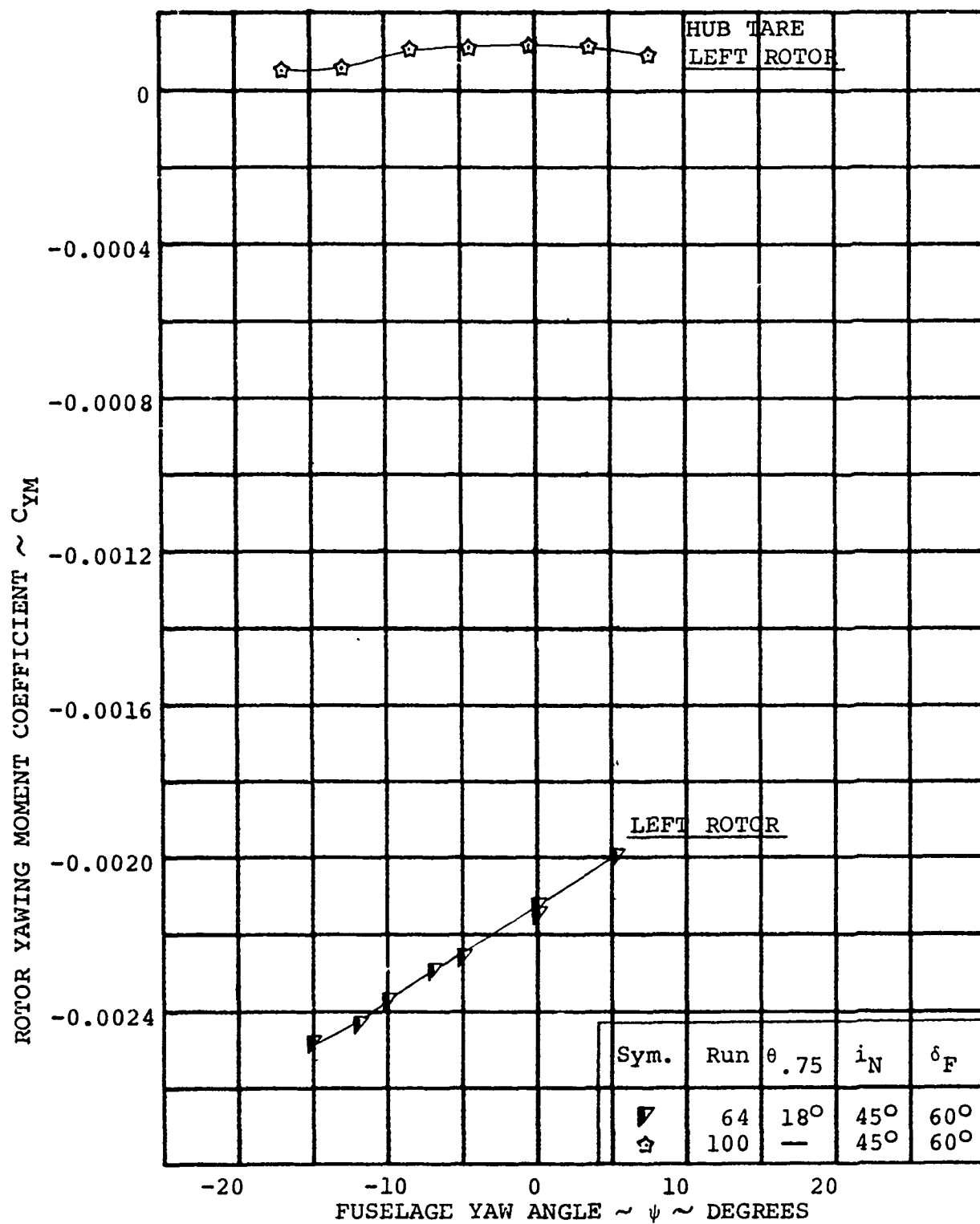


FIGURE 5-65. ROTOR YAWING MOMENT/YAW ANGLE VARIATION
AT $V/V_T = 0.260$ WITH $i_N = 45^\circ$

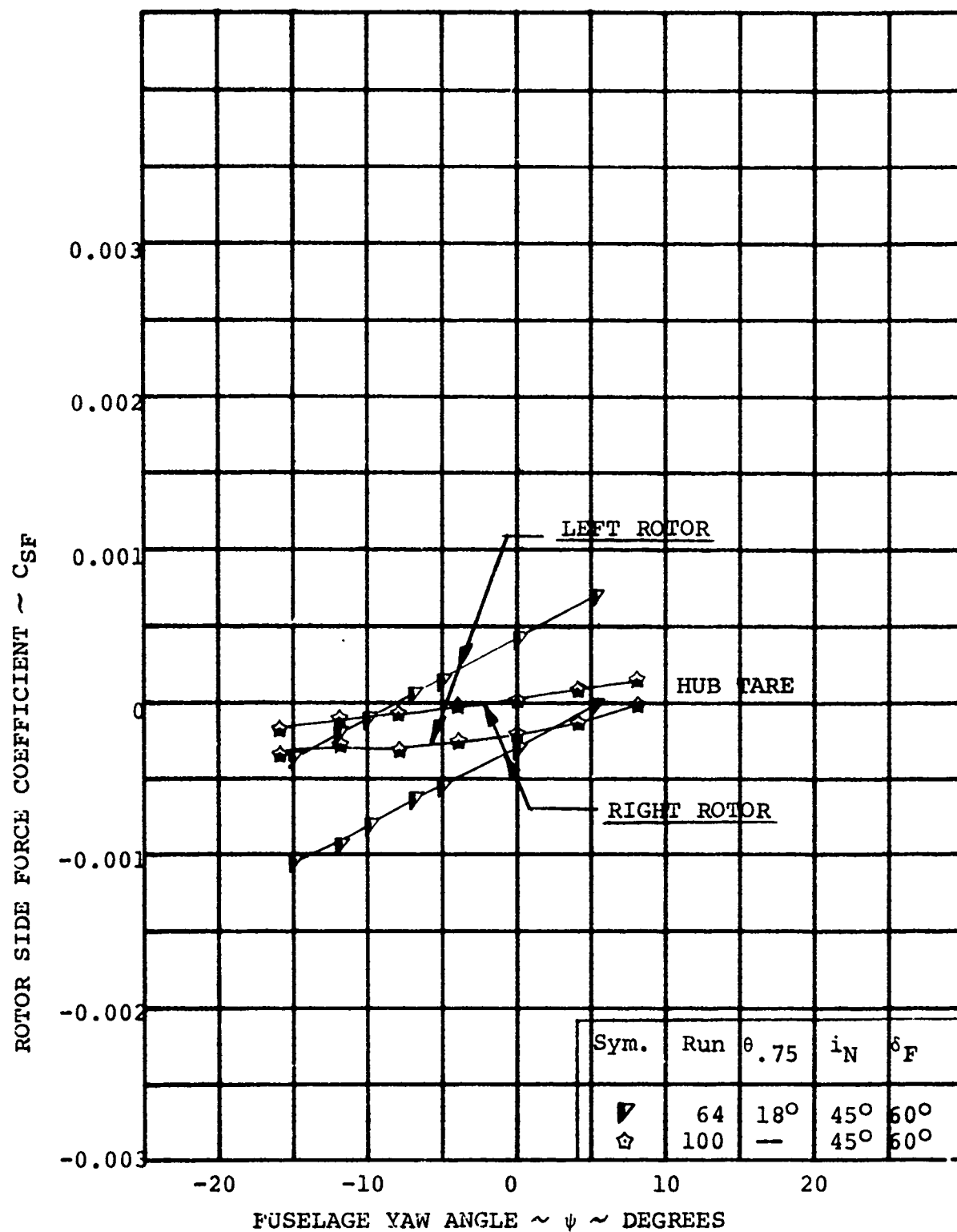


FIGURE 5-66. ROTOR SIDE FORCE/YAW ANGLE VARIATION
AT $V/V_T = 0.260$ WITH $i_N = 45^\circ$

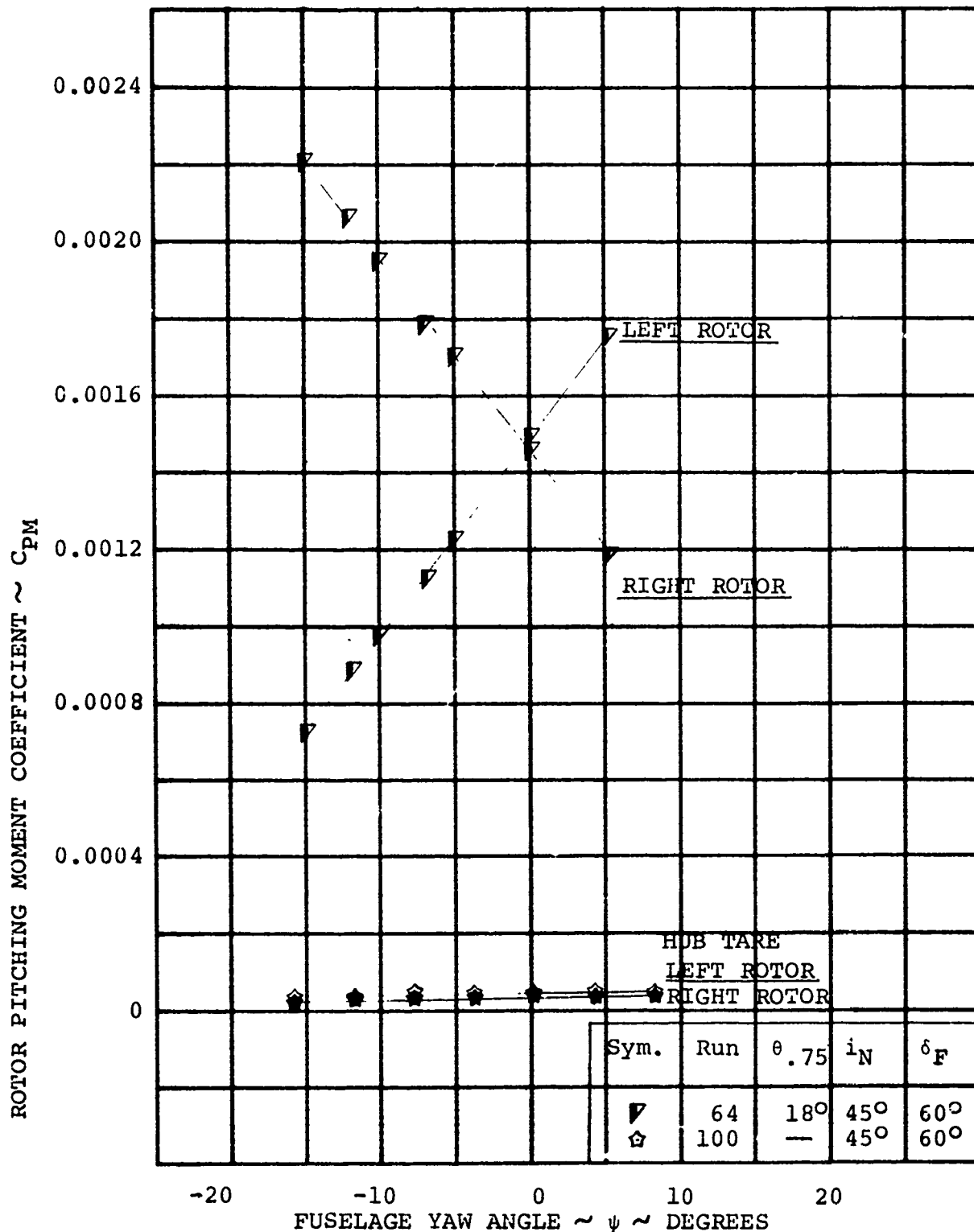


FIGURE 5-67. ROTOR PITCHING MOMENT/YAW ANGLE VARIATION
AT $V/V_T = 0.260$ WITH $i_N = 45^\circ$

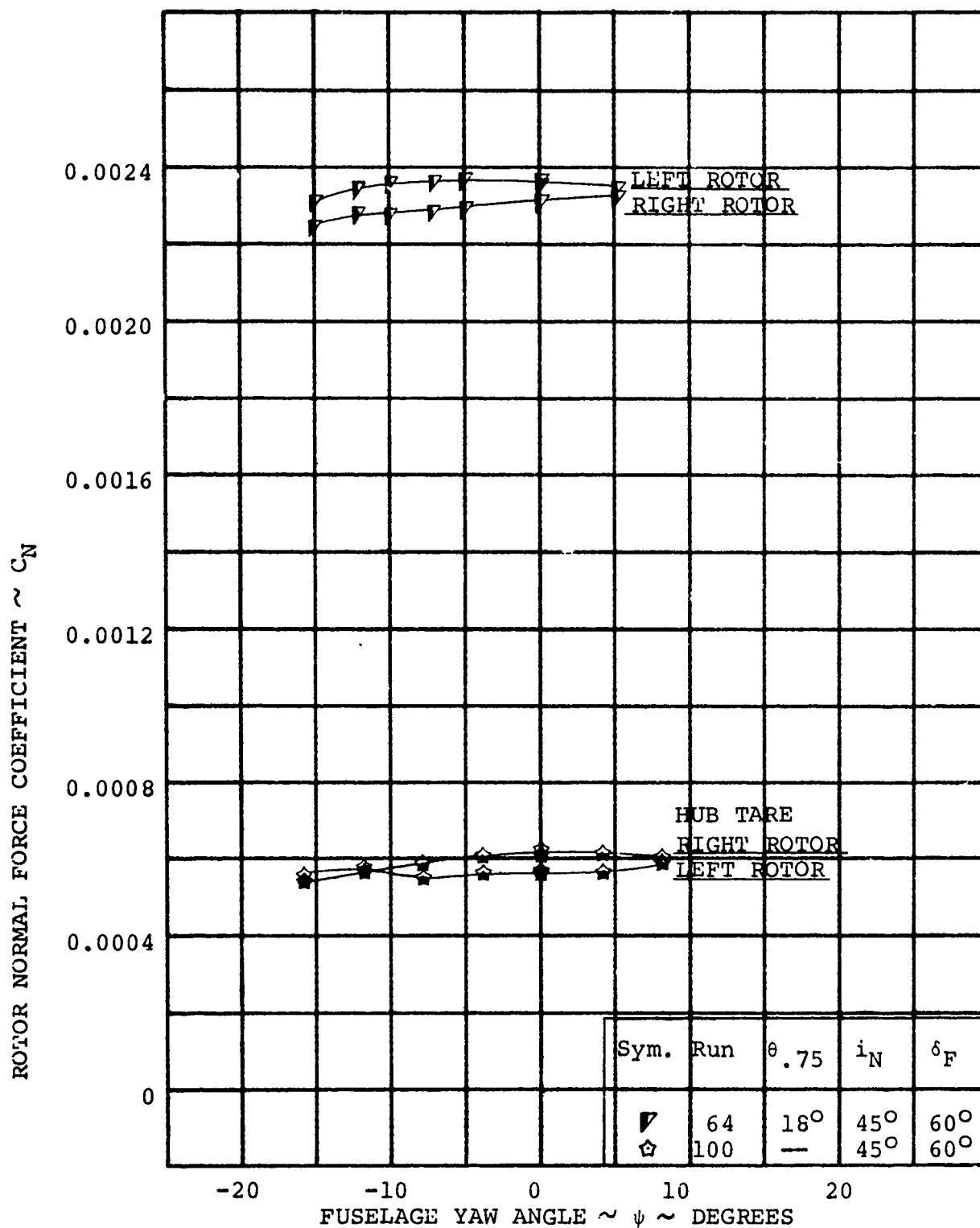


FIGURE 5-68. ROTOR NORMAL FORCE/YAW ANGLE VARIATION
AT $V/V_T = 0.260$ WITH $i_N = 45^\circ$

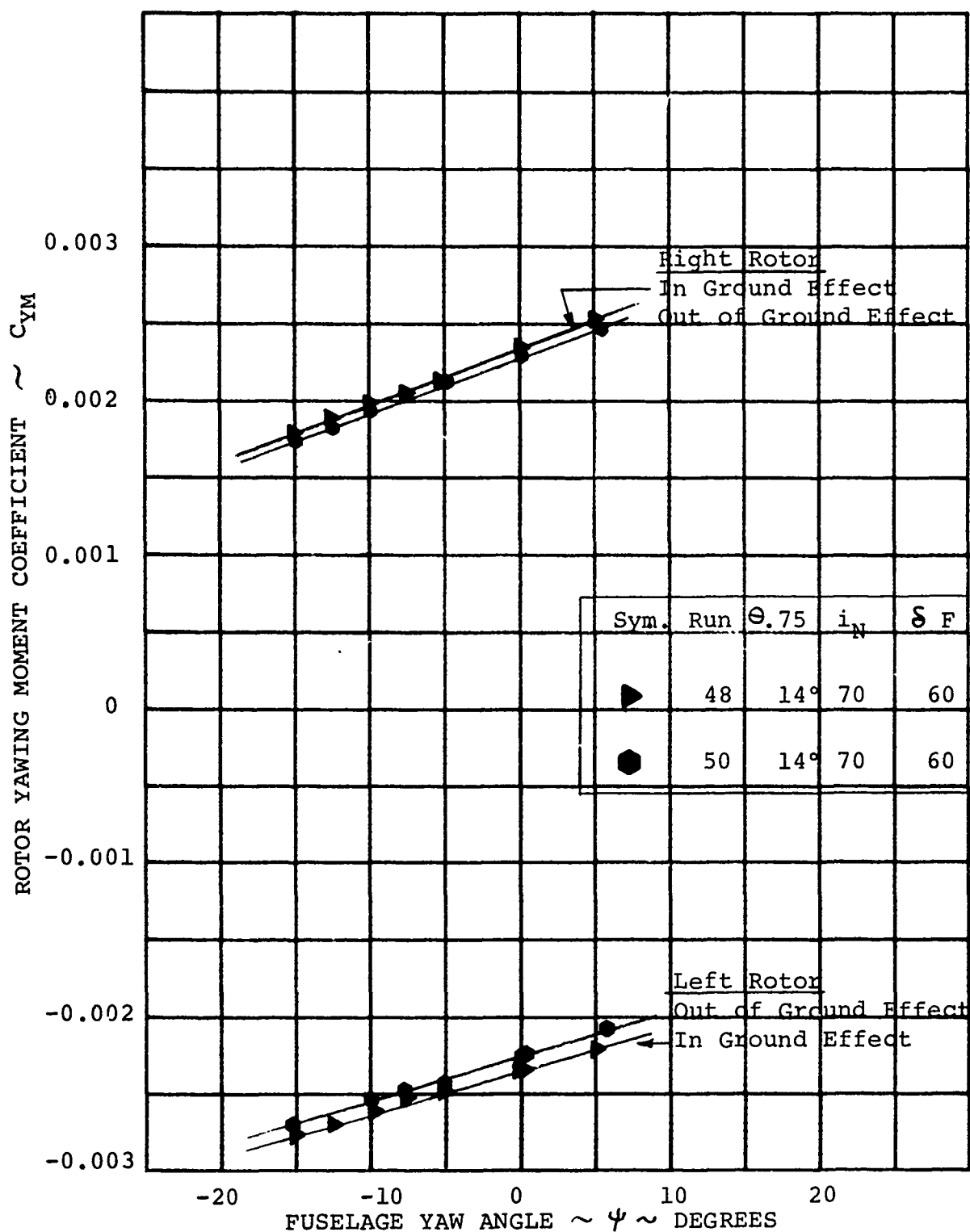


FIGURE 5-69. IMPACT OR GROUND EFFECT ON ROTOR
YAWING MOMENT AT $V/V_T = 0.206$ WITH $i_N = 70^\circ$

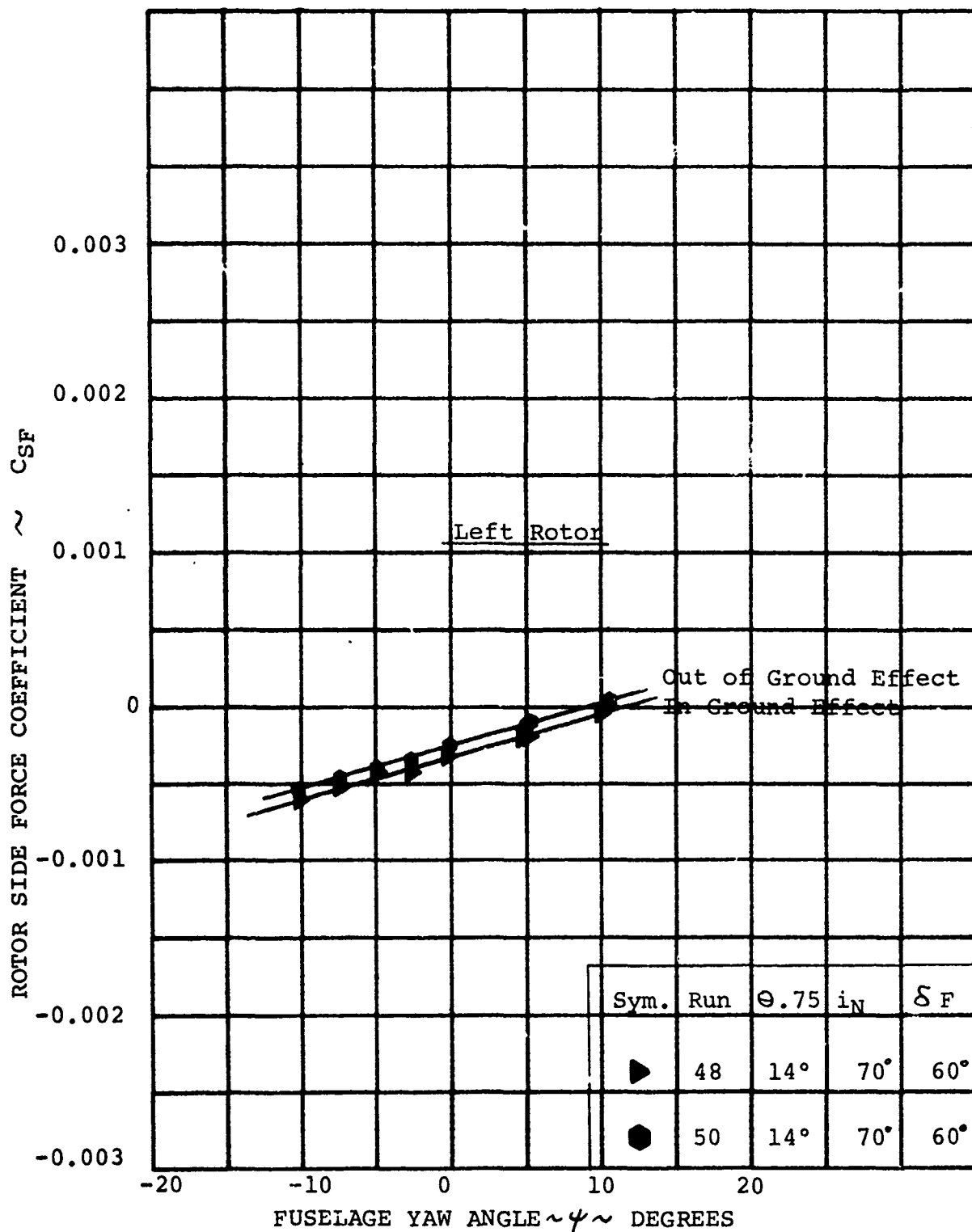


FIGURE 5-70. IMPACT OF GROUND EFFECT ON ROTOR SIDE FORCE AT $V/V_T = 0.206$ WITH $i_N = 70^\circ$

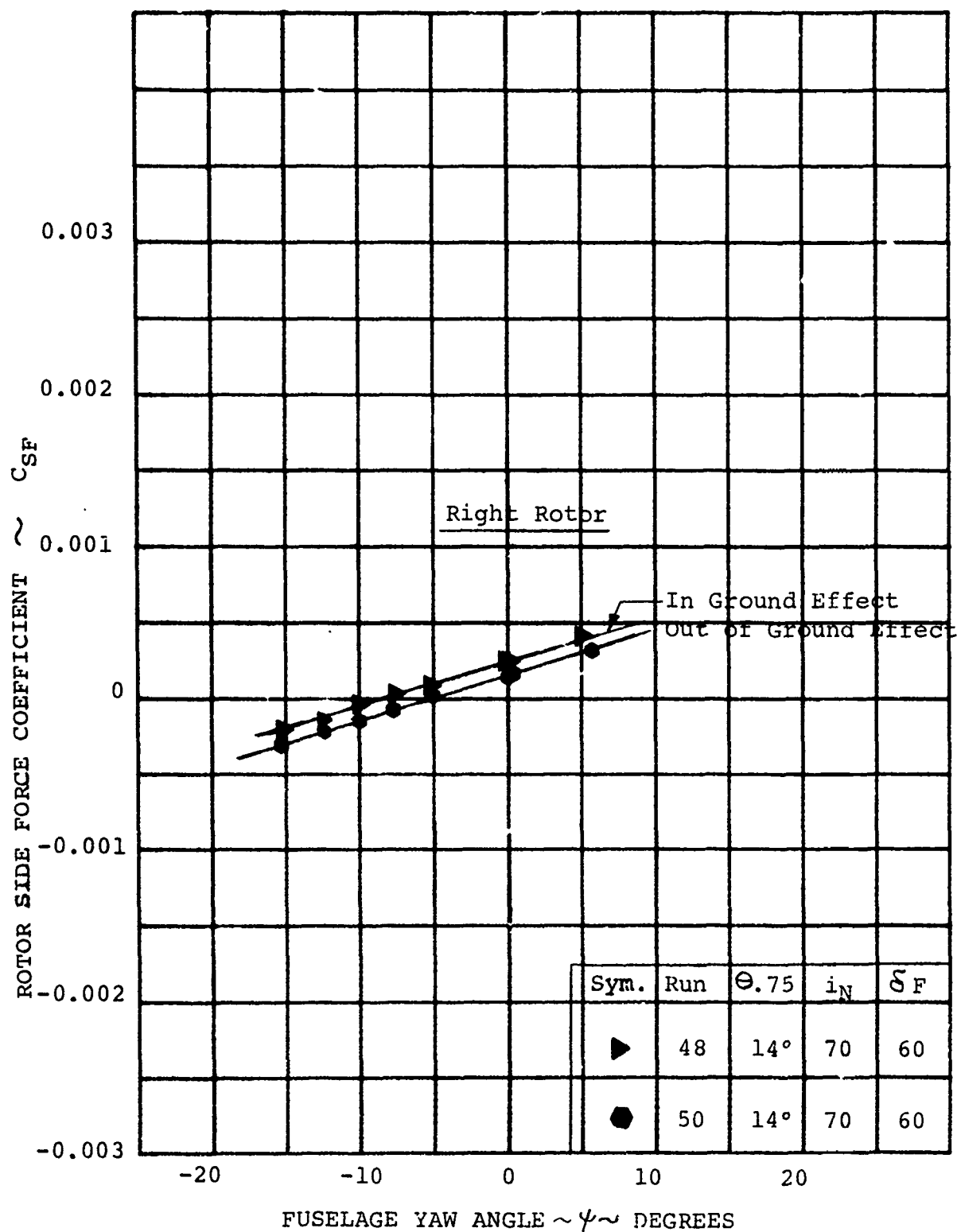


FIGURE 5-71. IMPACT OF GROUND EFFECT ON ROTOR SIDE FORCES AT $V/V_T=0.206$ WITH $i_N = 70^\circ$

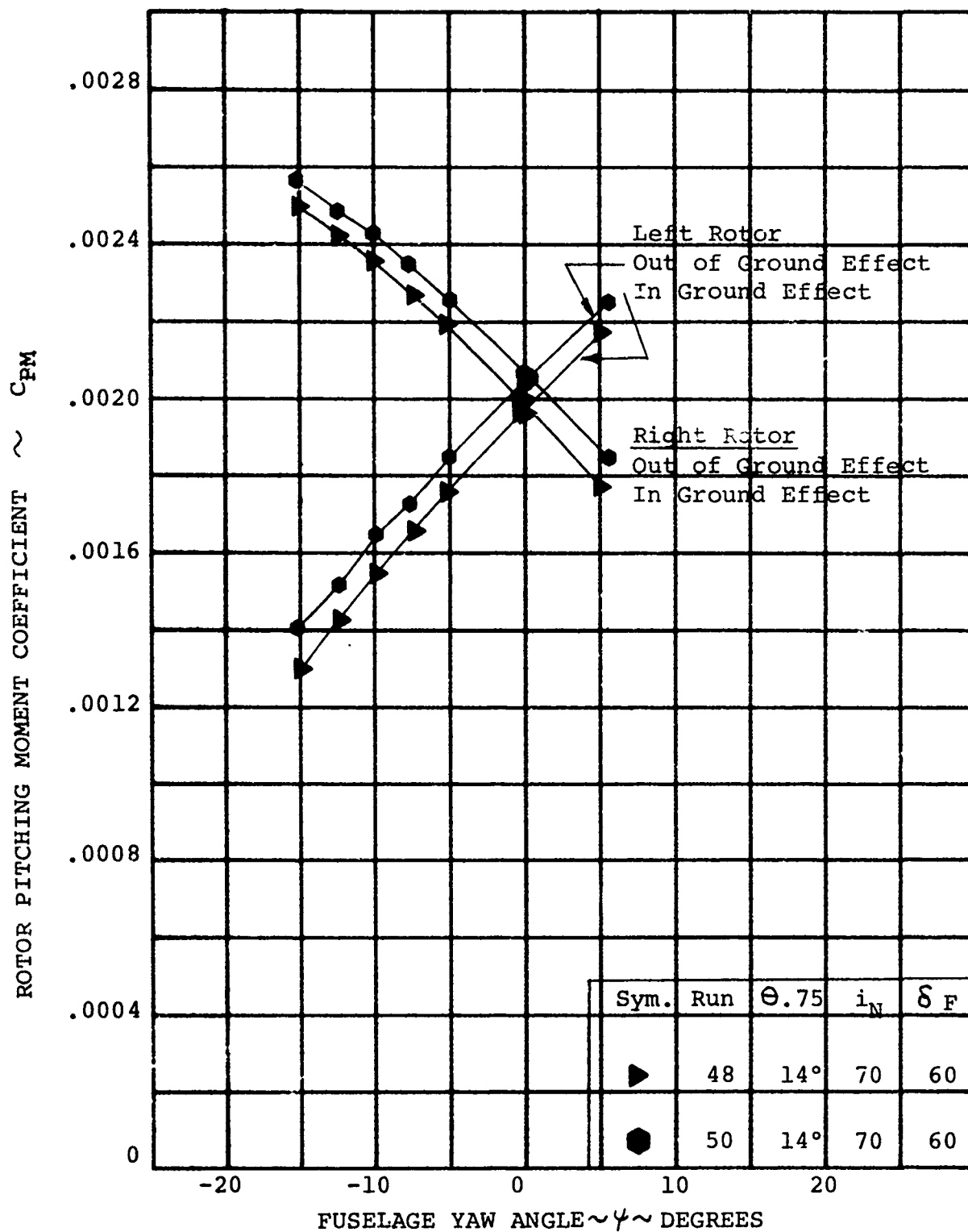


FIGURE 5-72. IMPACT OF GROUND EFFECT ON ROTOR PITCHING MOMENT AT $V/V_T = 0.206$ $i_N = 70^\circ$

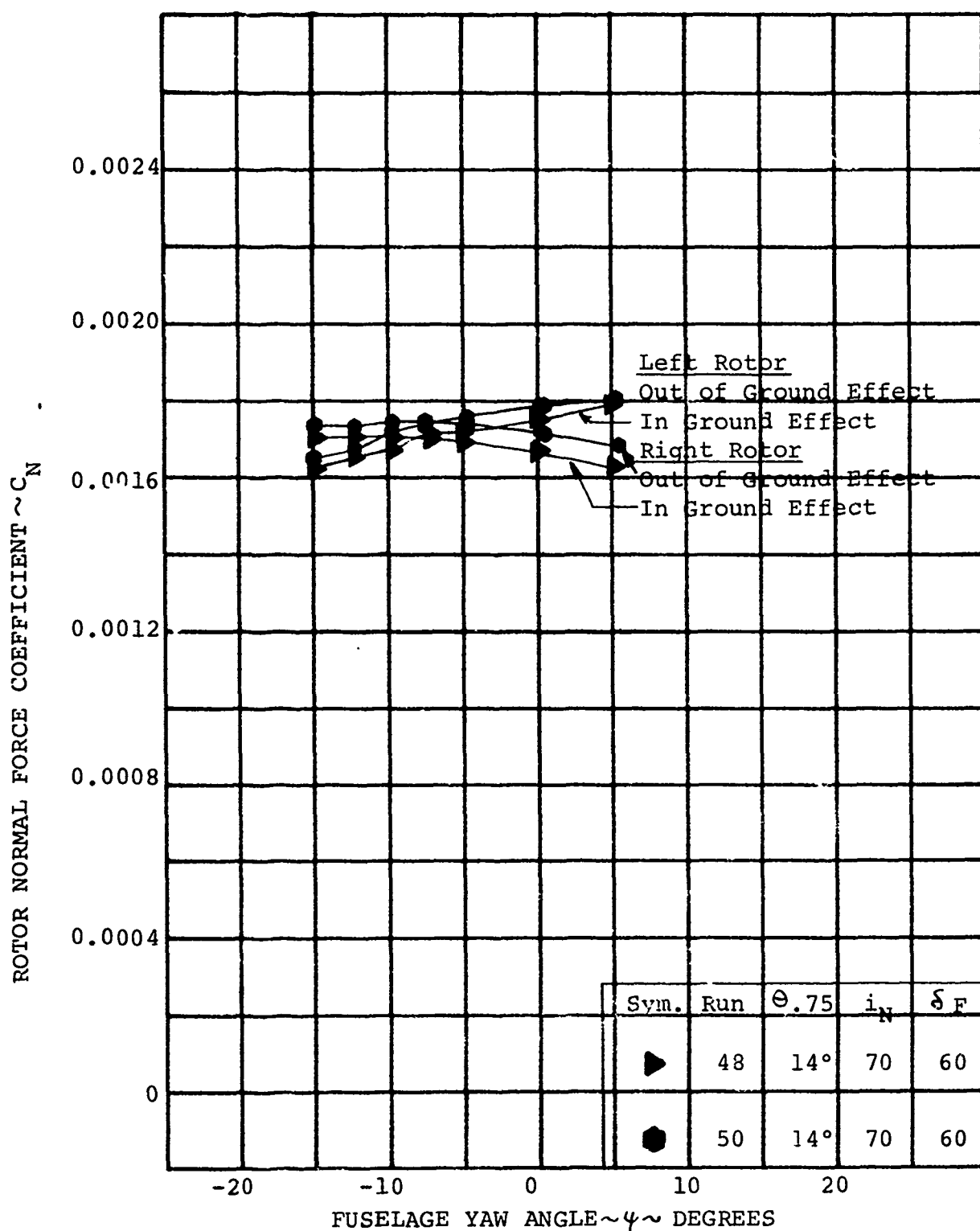


FIGURE 5-73. IMPACT OR GROUND EFFECT ON ROTOR
NORMAL FORCE AT $V/V_T = 0.206$ WITH $i_N = 70^\circ$

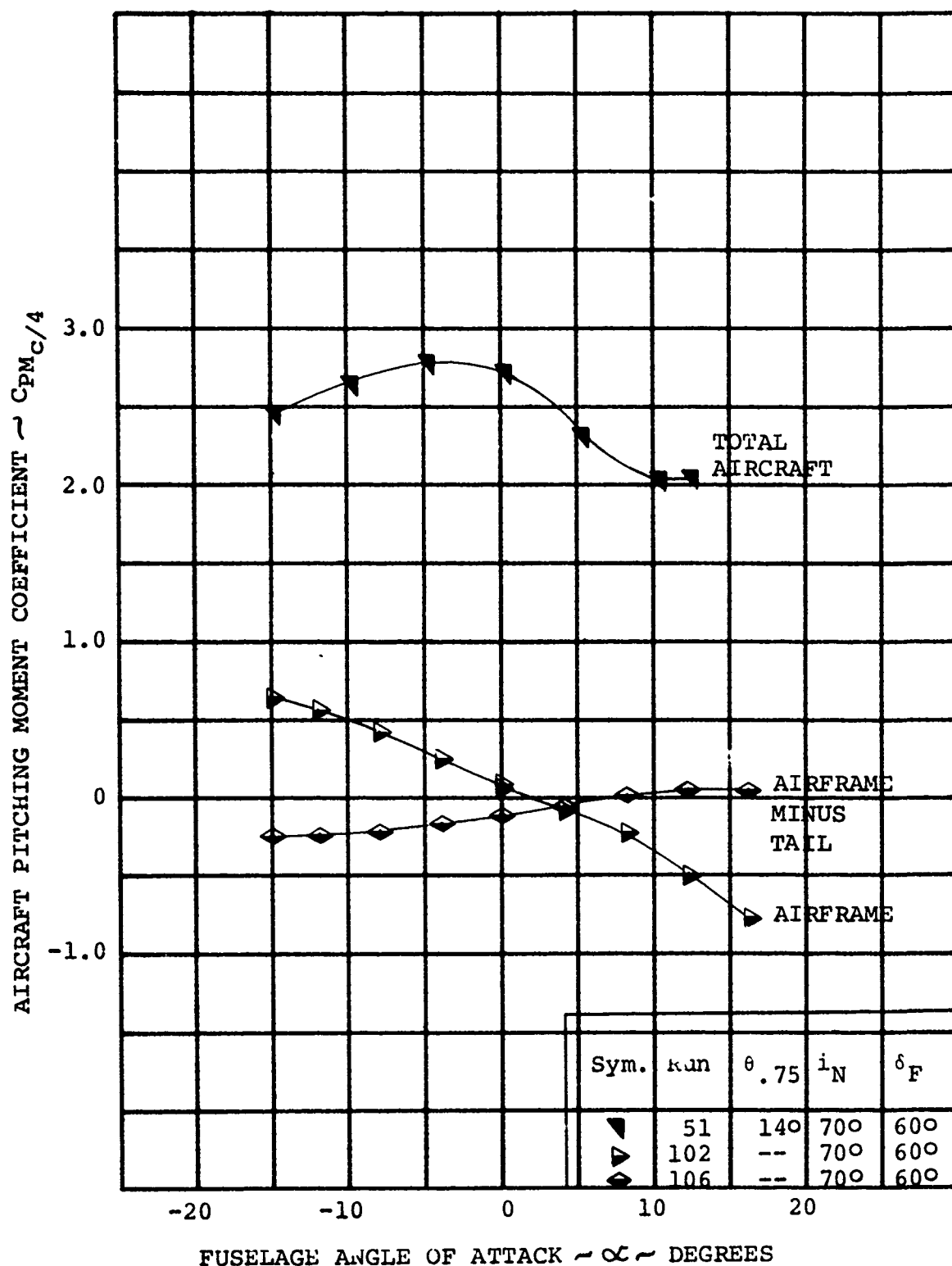


FIGURE 5-74. CONTRIBUTION OF PROP/ROTOR AND HORIZONTAL TAIL TO AIRCRAFT PITCHING MOMENT AT $V/V_T = 0.206$ WITH $i_N = 70^\circ$

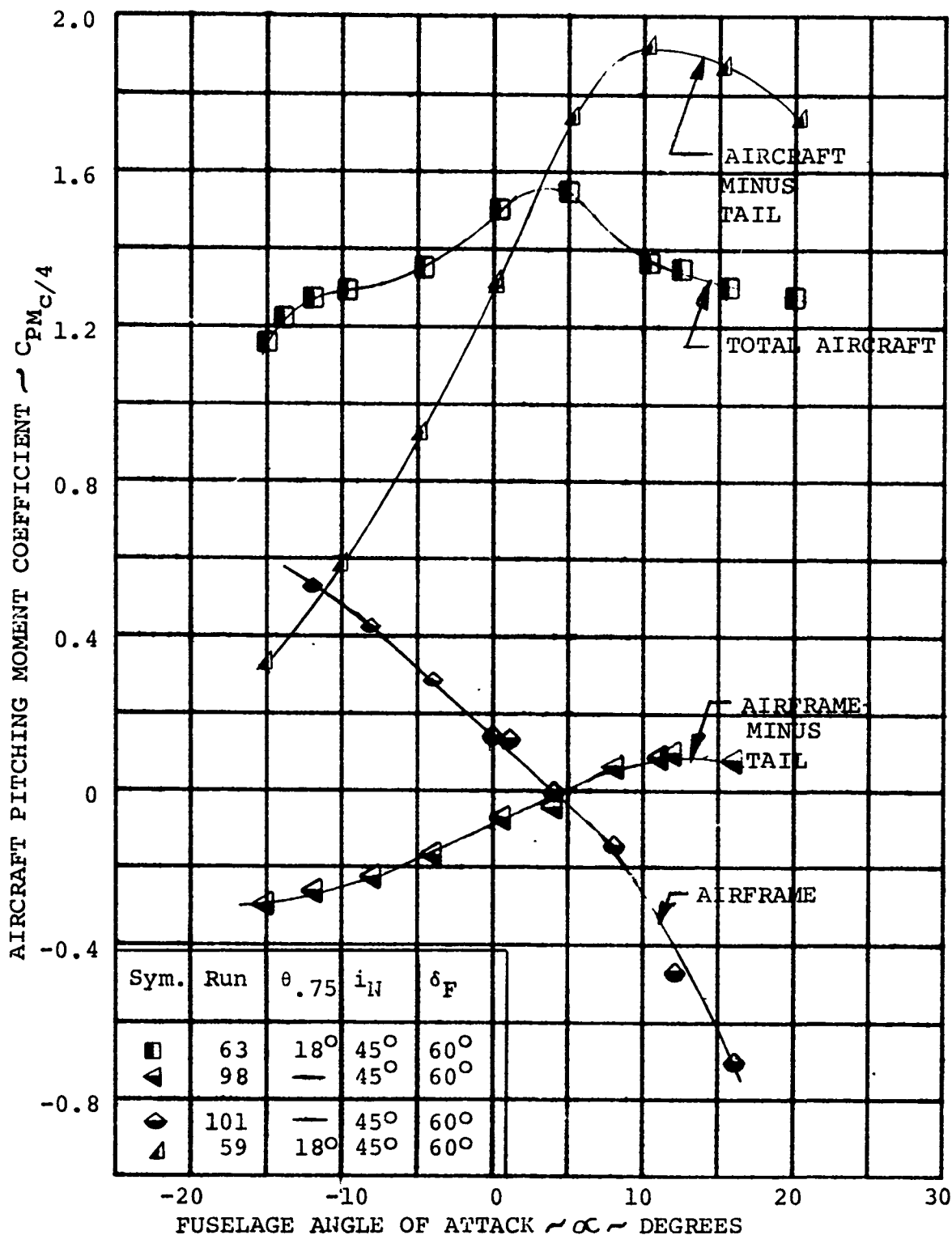


FIGURE 5-75. CONTRIBUTION OF PROP/ROTORS AND HORIZONTAL TAIL TO AIRCRAFT PITCHING MOMENT AT $V/V_T = 0.26$ WITH $i_N = 45^\circ$

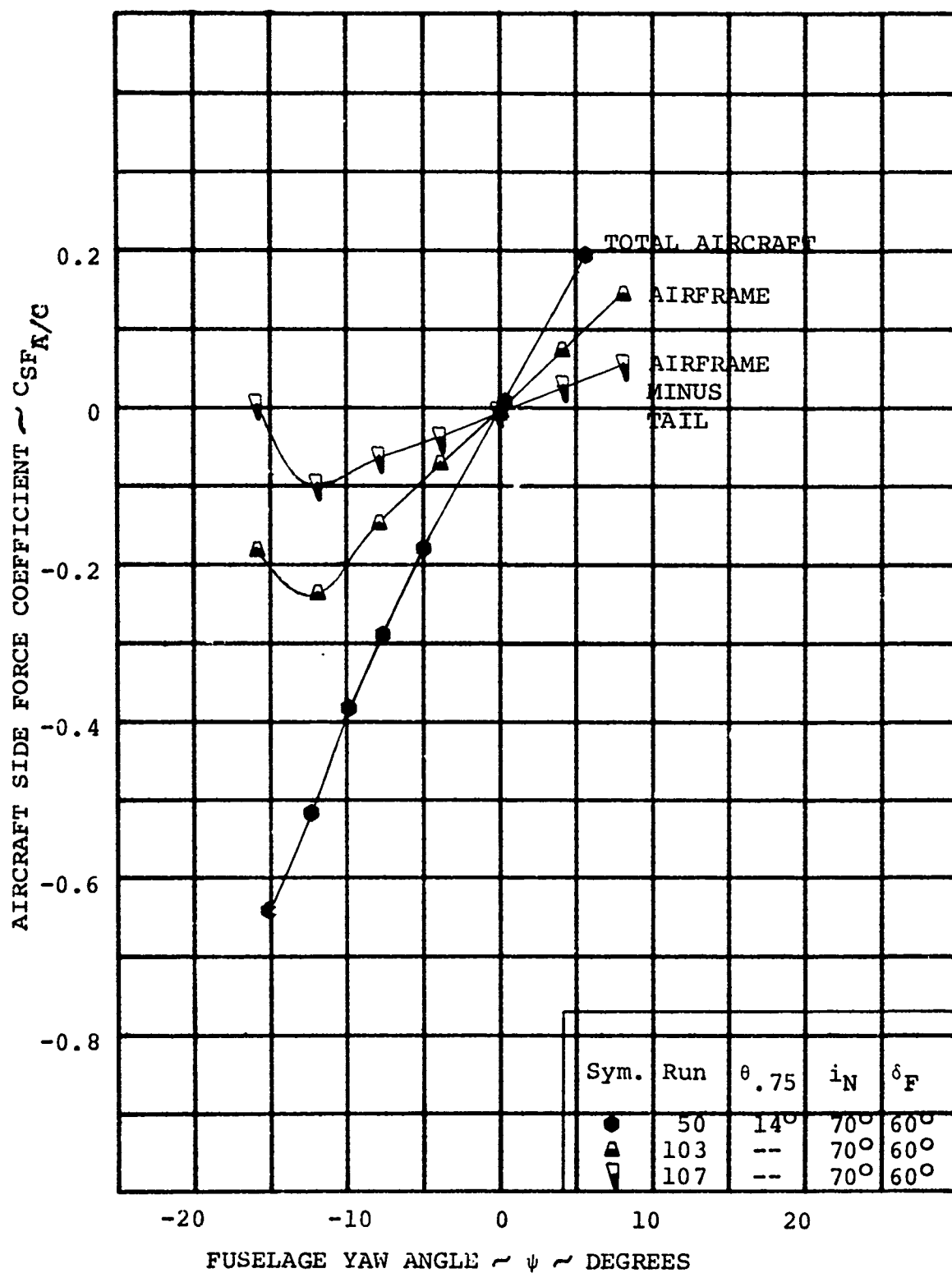


FIGURE 5-76. CONTRIBUTION OF PROP/ROTOR AND VERTICAL TAIL TO AIRCRAFT SIDE FORCE AT $V/V_T = 0.206$ WITH $i_N = 70^\circ$

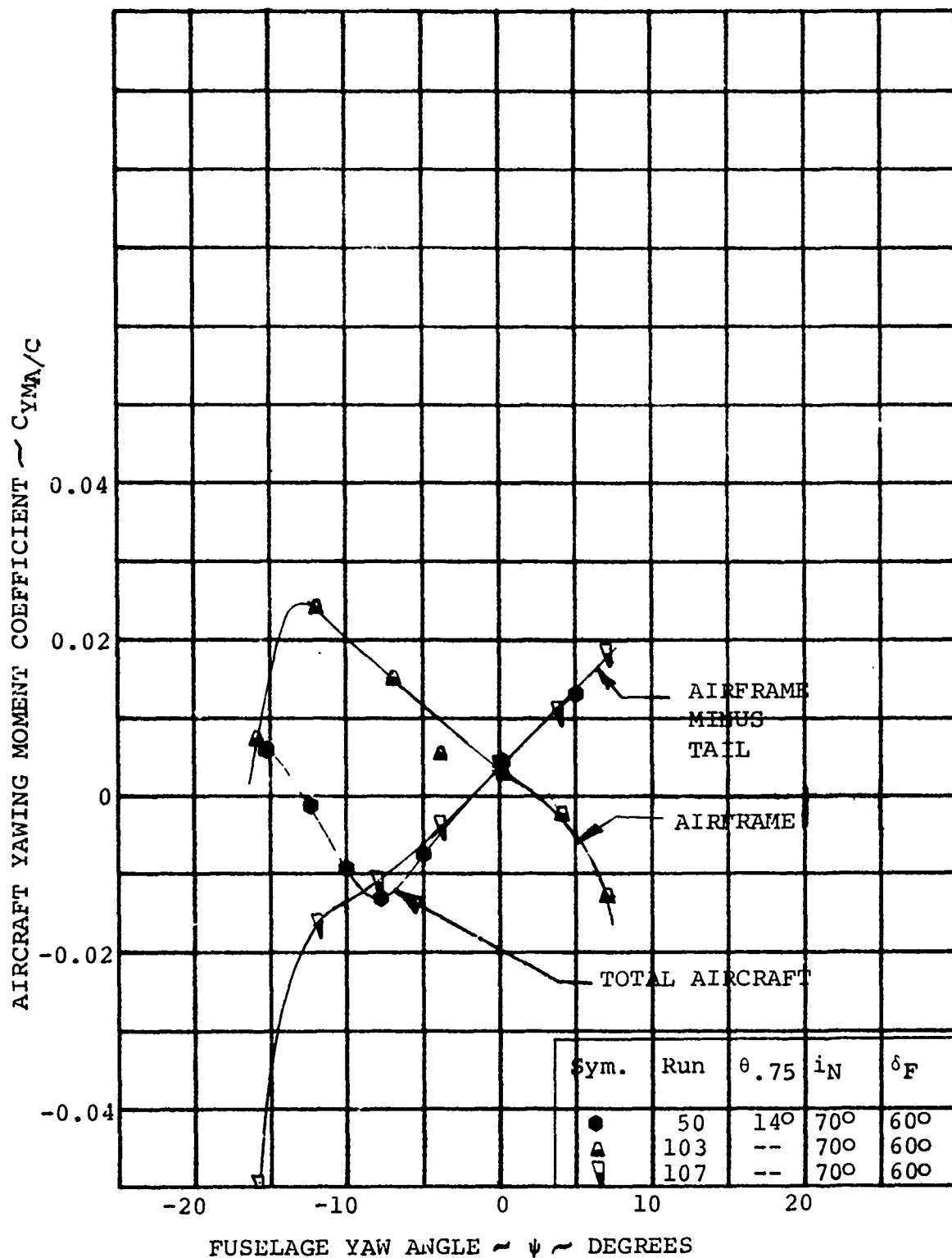


FIGURE 5-77. CONTRIBUTION OF PROP/ROTORS AND VERTICAL TAIL TO AIRCRAFT YAWING & MOMENT AT $V/V_T = 0.206$ WITH $i_N = 70^\circ$

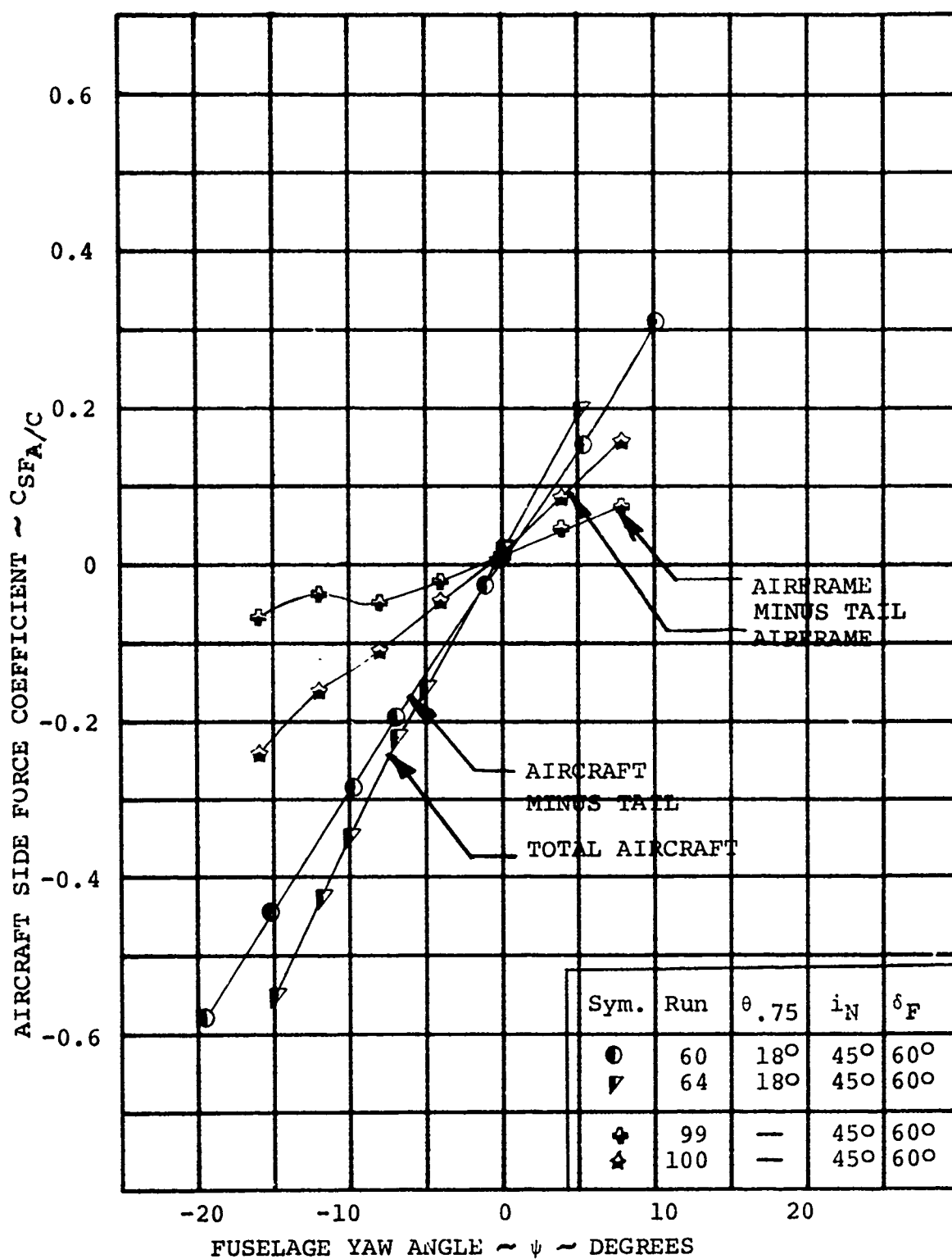


FIGURE 5-78. CONTRIBUTION OF PROP/ROTOR AND VERTICAL TAIL TO AIRCRAFT SIDE FORCE AT $V/V_T = 0.260$ WITH $i_N = 45^\circ$

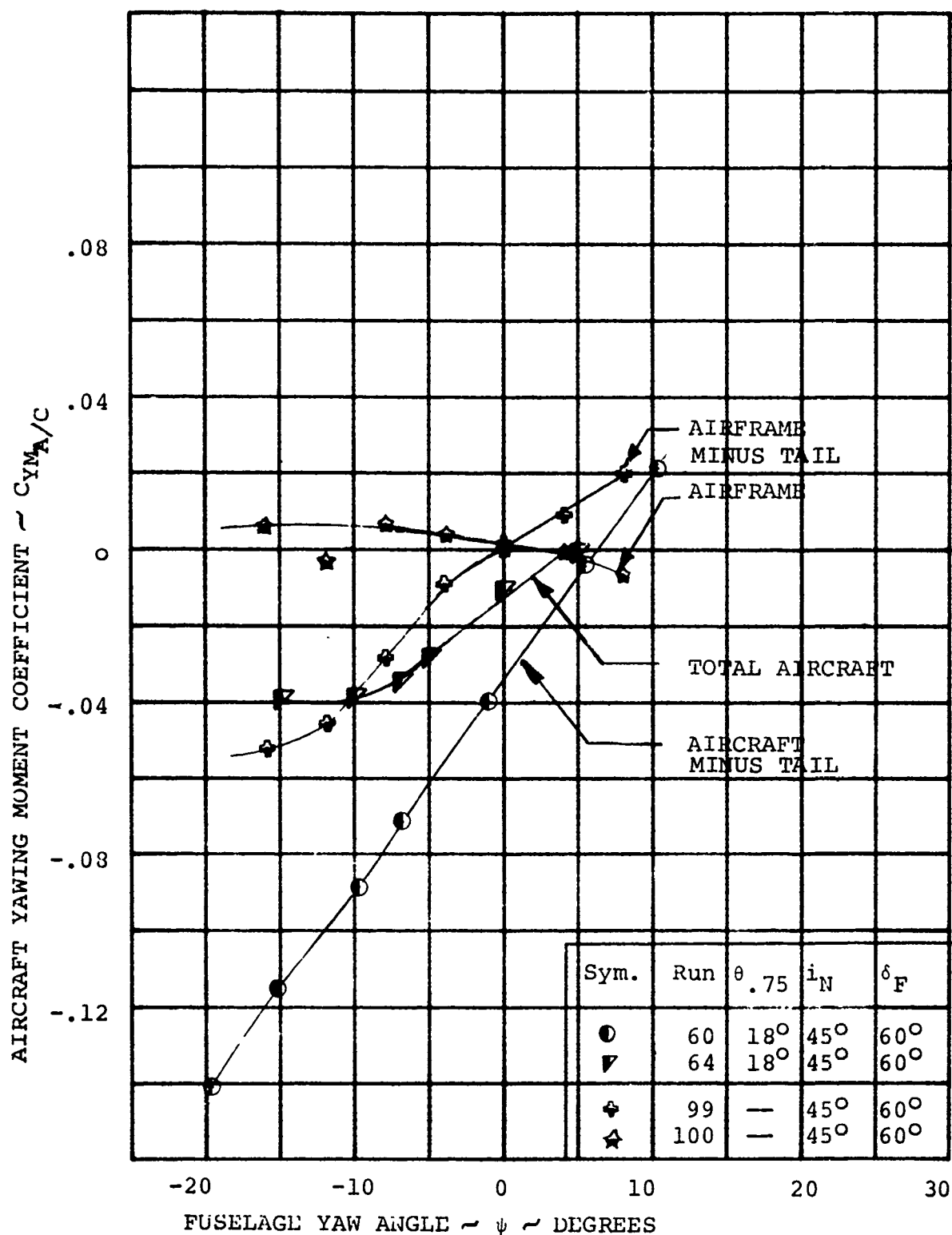


FIGURE 5-79. CONTRIBUTION OF PROP/ROTORS AND VERTICAL TAIL TO AIRCRAFT YAWING MOMENT AT $V/V_T = 0.26$ WITH $i_N = 45^\circ$

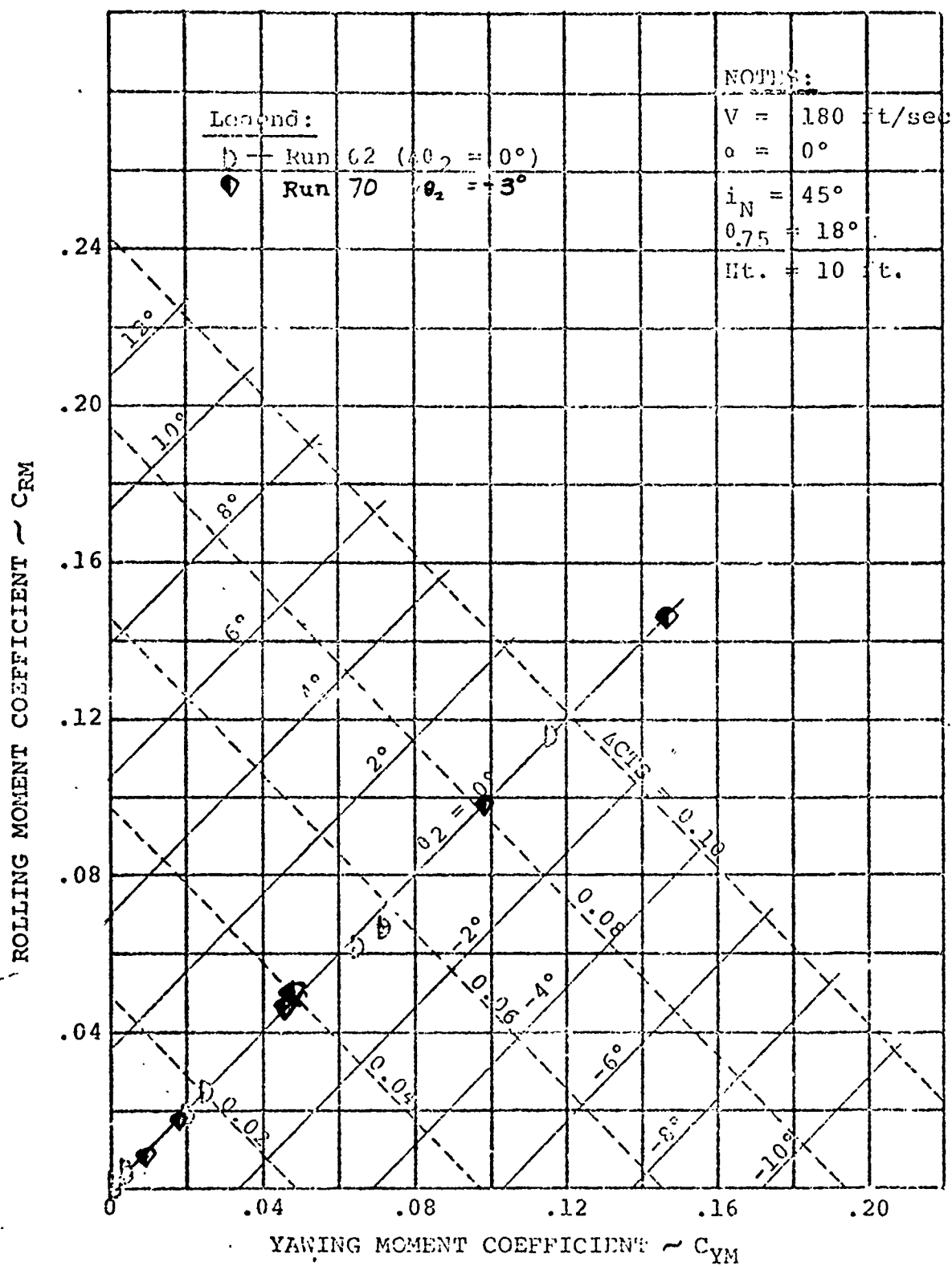


FIGURE 5-80. CONTROL MIXING DURING TRANSITION

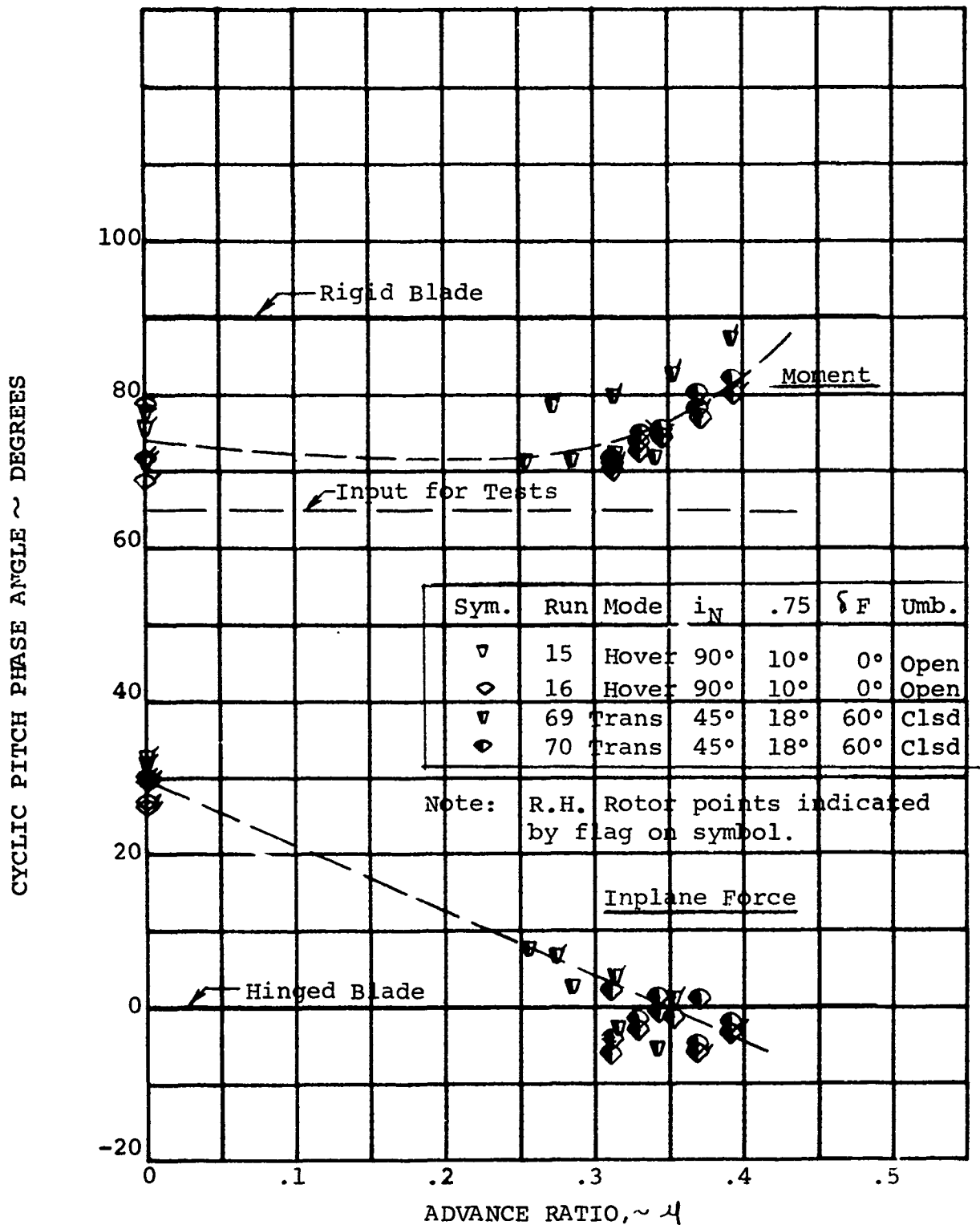


FIGURE 5-81. VARIATION OF CYCLIC PHASE ANGLE WITH ADVANCE RATIO

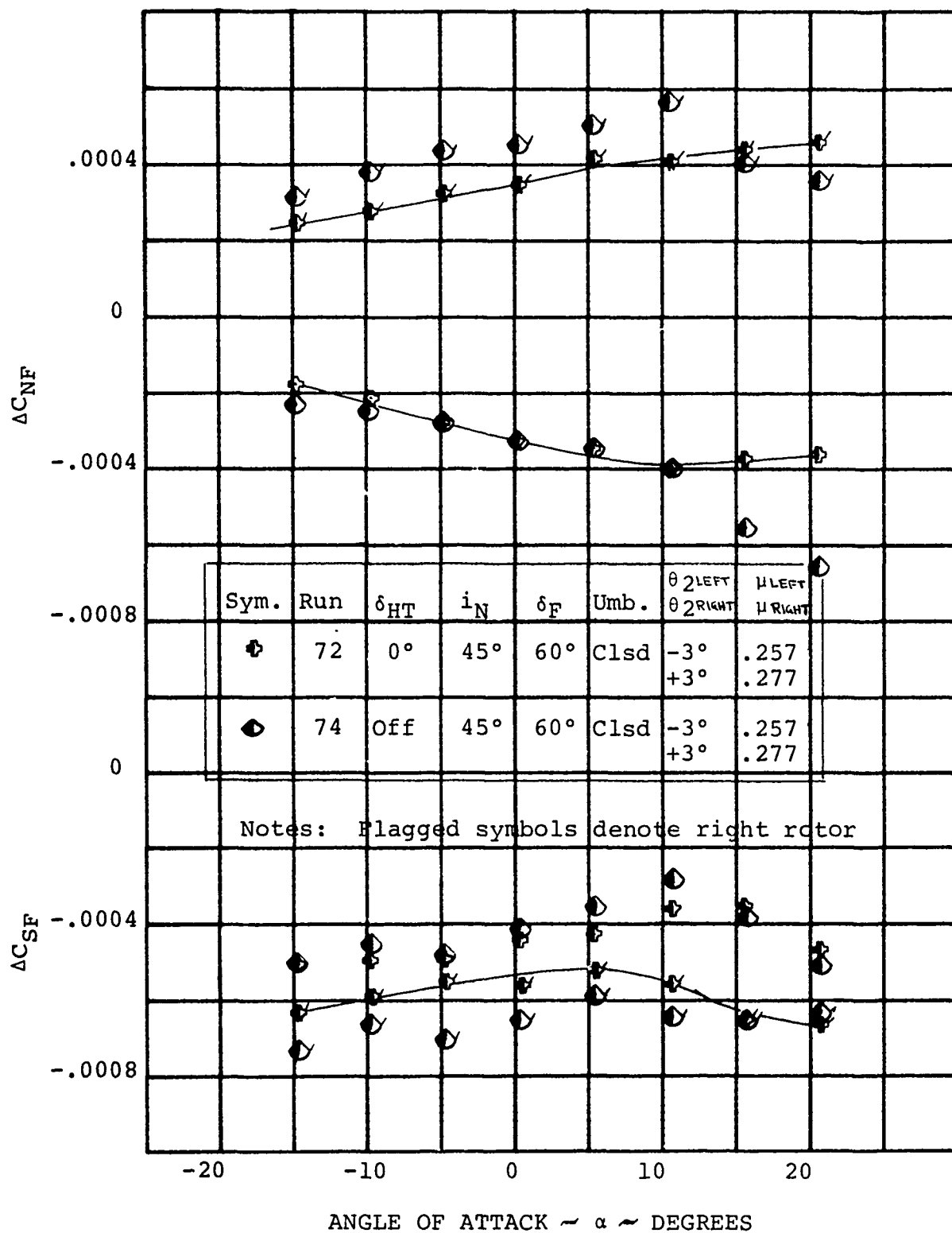


FIGURE 5-82. VARIATION OF ROTOR CONTROL FORCES WITH ANGLE OF ATTACK IN TRANSITION

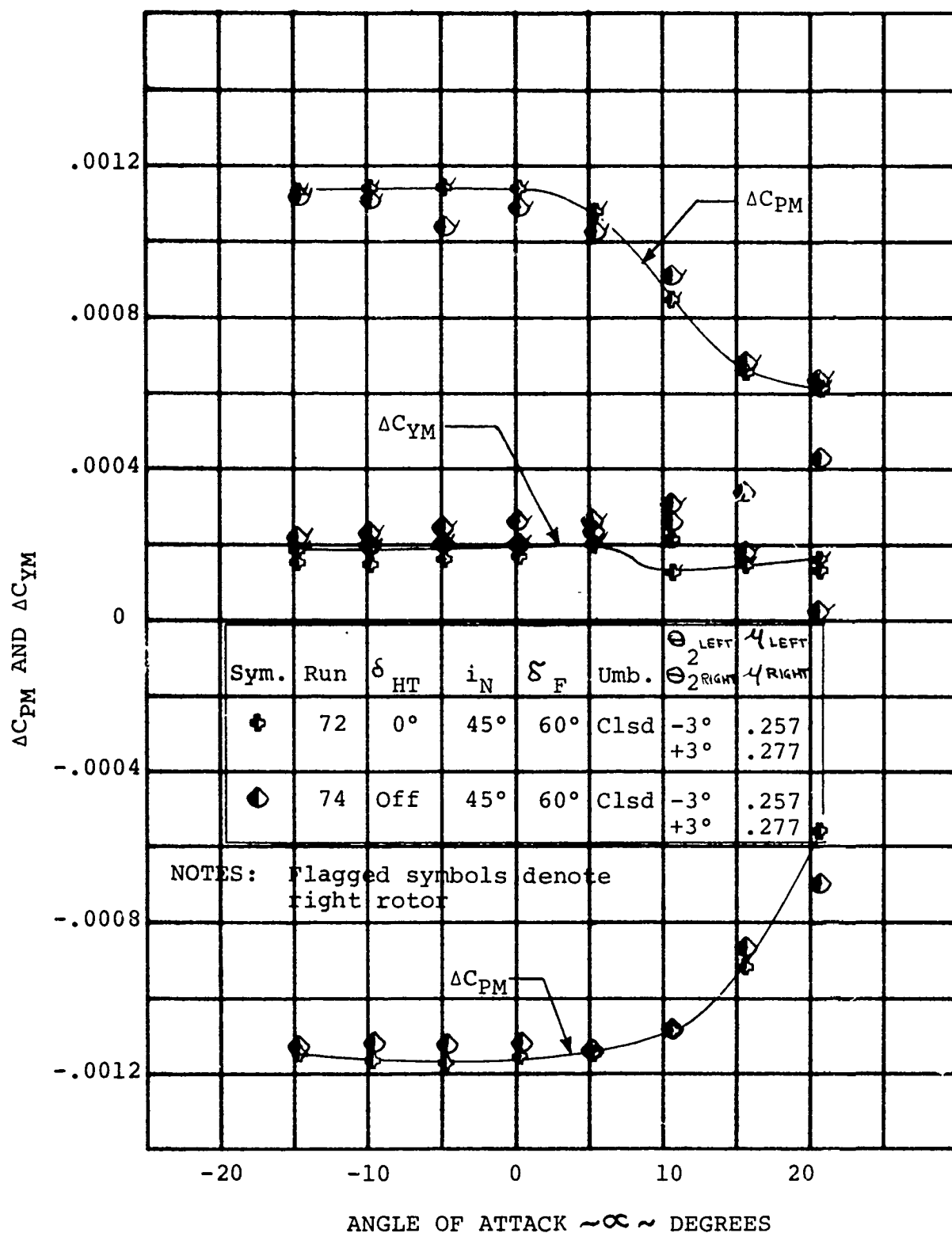


FIGURE 5-83. VARIATION OF ROTOR CONTROL MOMENTS WITH ANGLE OF ATTACK IN TRANSITION

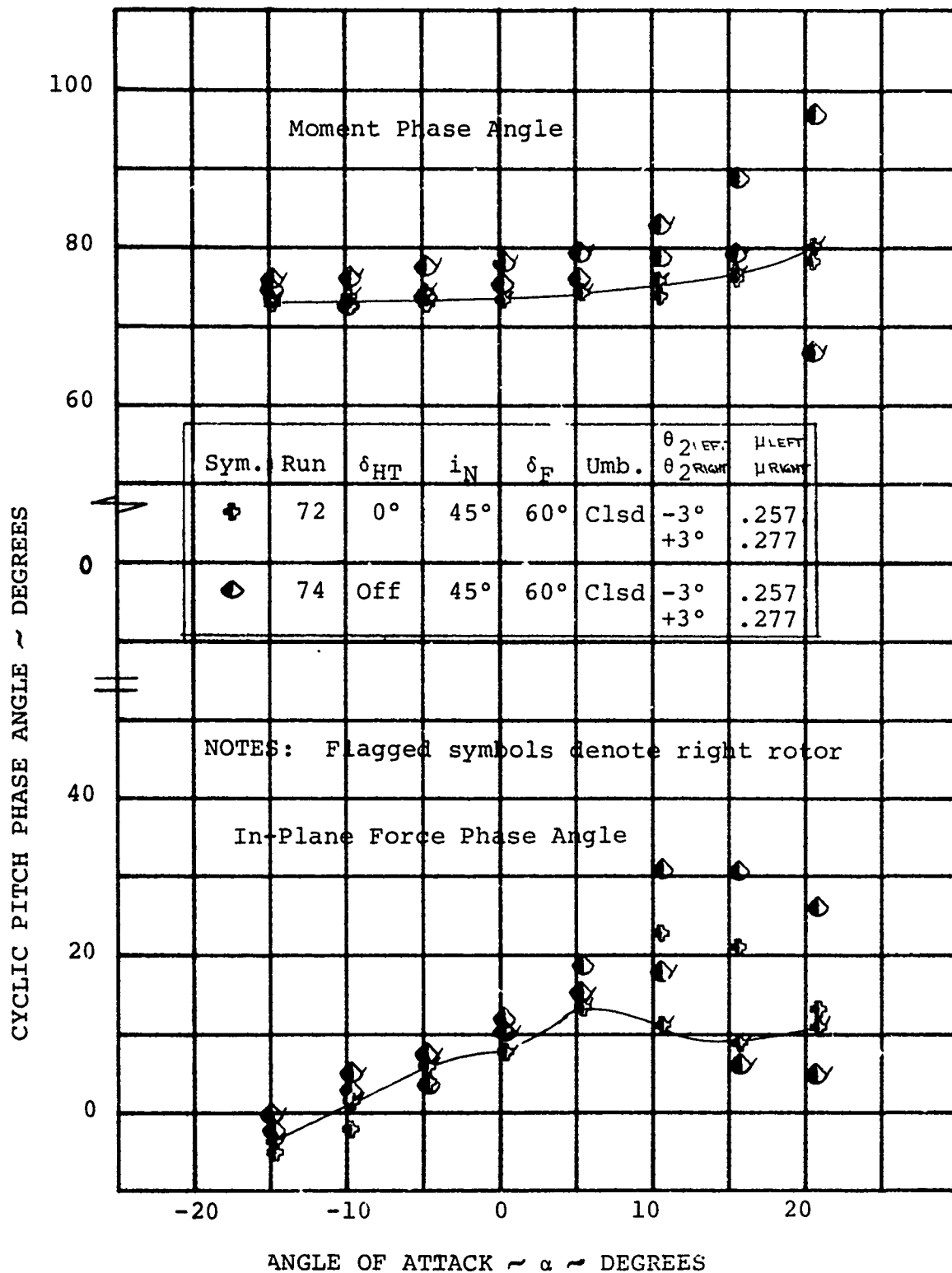


FIGURE 5-84. VARIATION OF CYCLIC PHASE ANGLE WITH ANGLE OF ATTACK IN TRANSITION

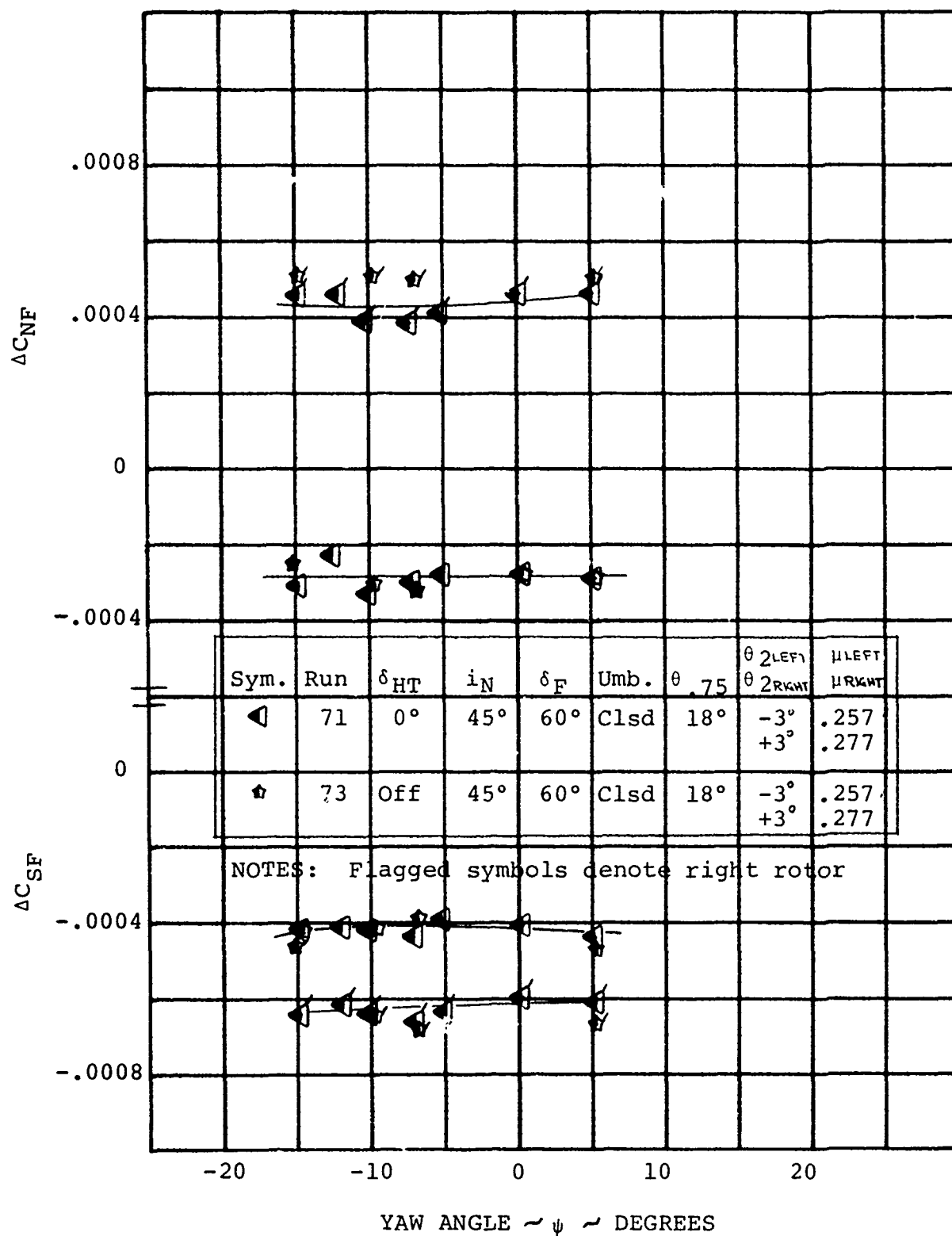


FIGURE 5-85. VARIATION OF ROTOR CONTROL FORCES WITH YAW ANGLE IN TRANSITION

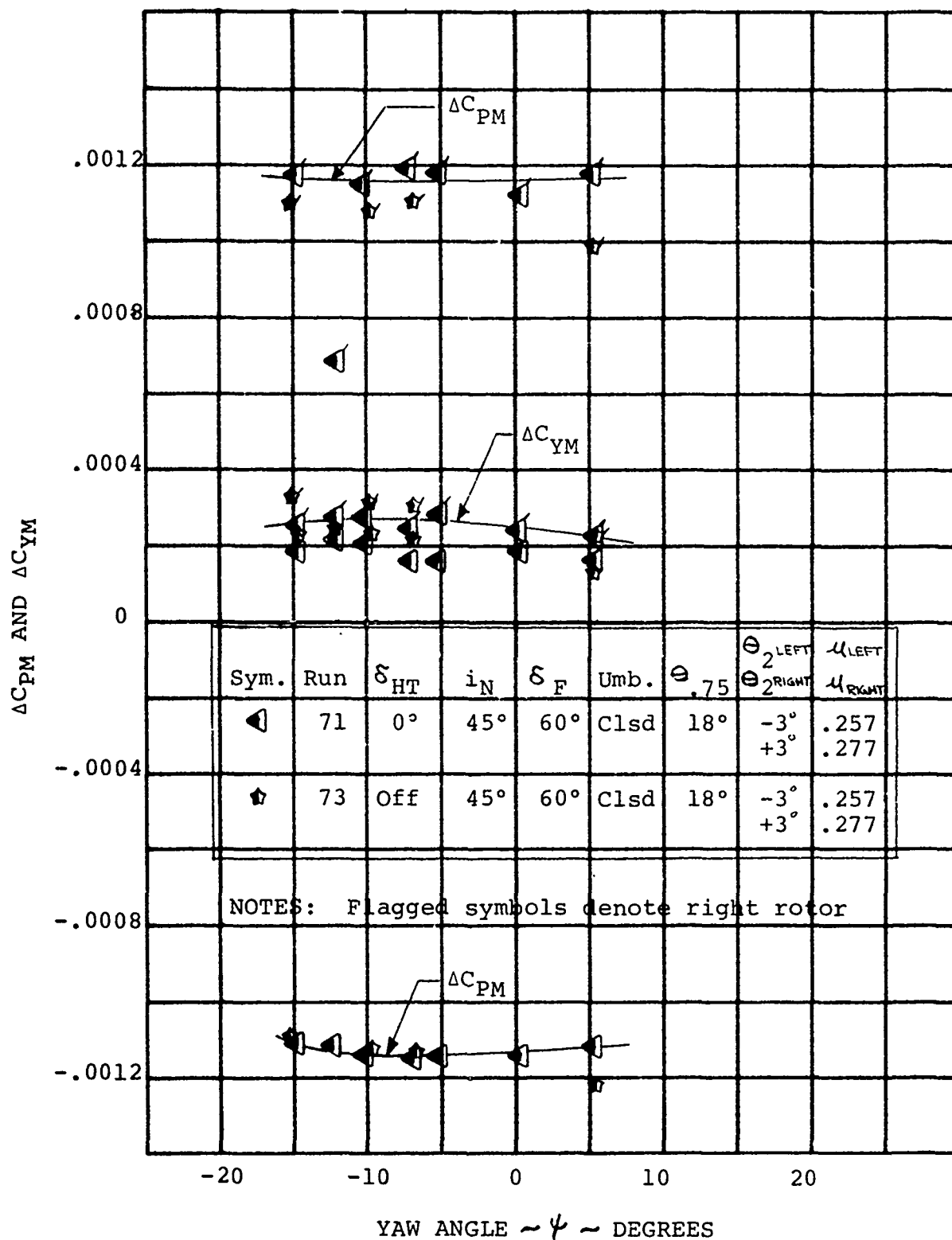


FIGURE 5-86.

VARIATION OF ROTOR CONTROL MOMENTS
WITH YAW ANGLE IN TRANSITION

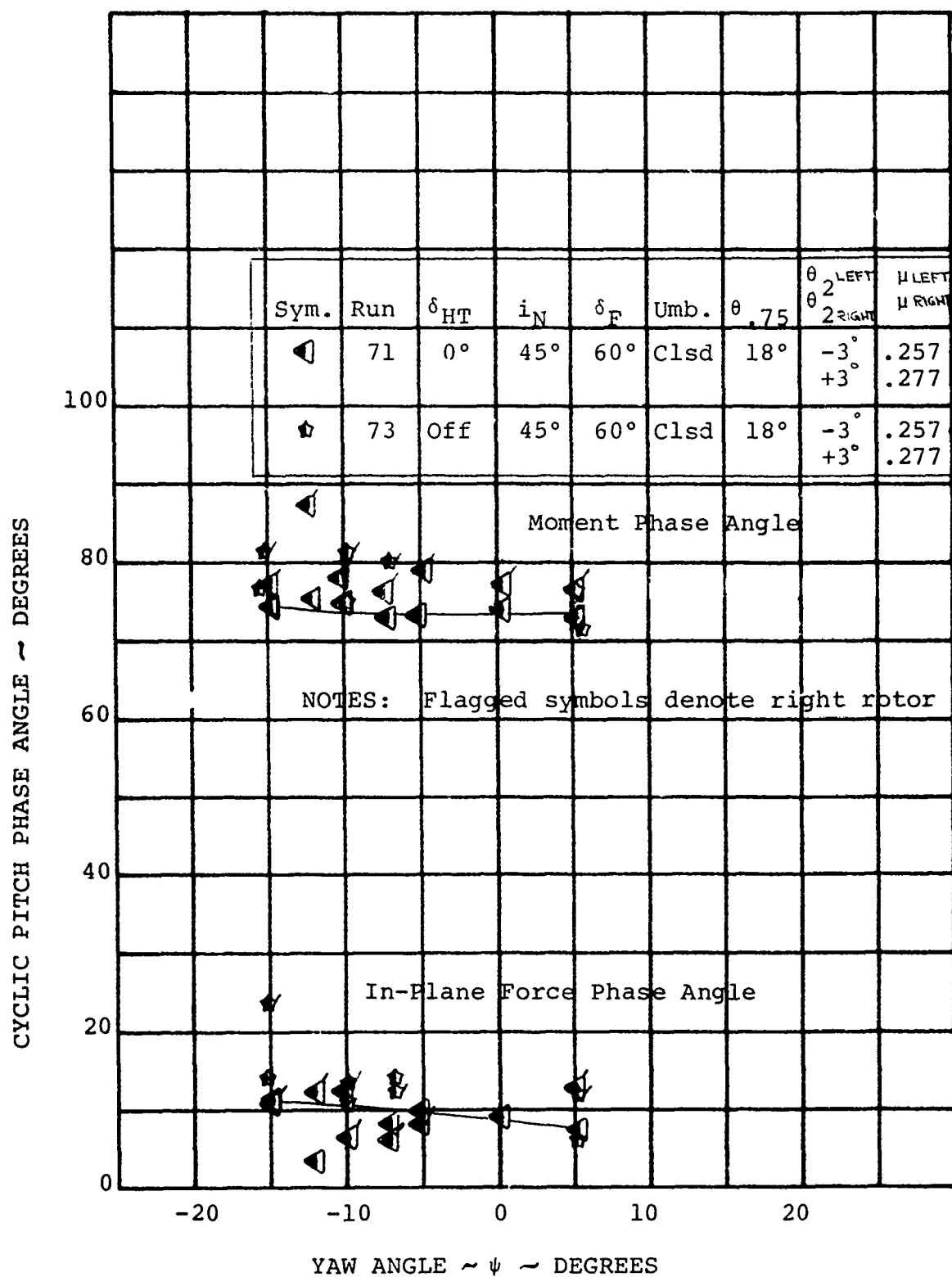


FIGURE 5-87. VARIATION OF CYCLIC PHASE ANGLE WITH YAW ANGLE IN TRANSITION

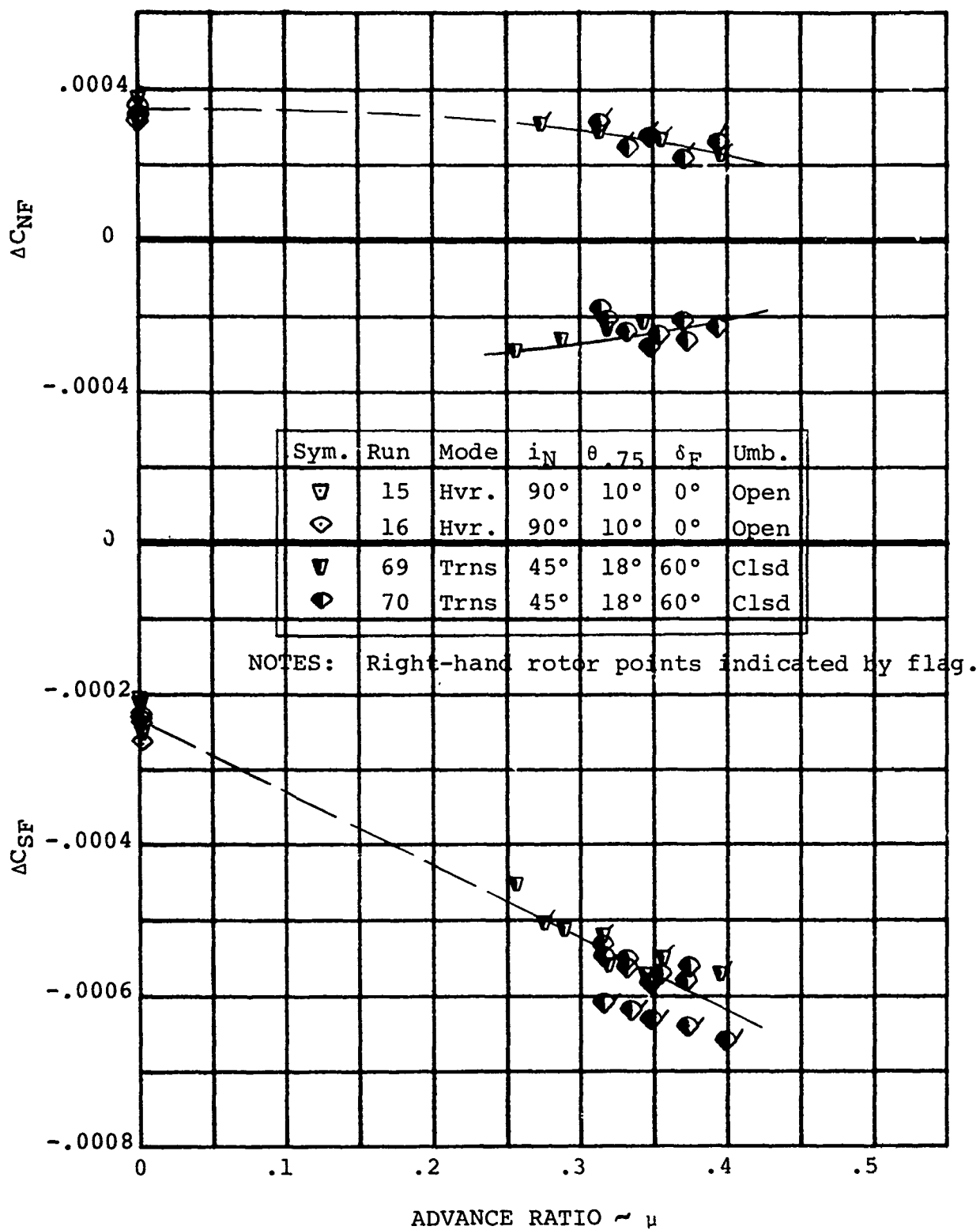


FIGURE 5-88. VARIATION OF ROTOR CONTROL FORCES WITH ADVANCE RATIO

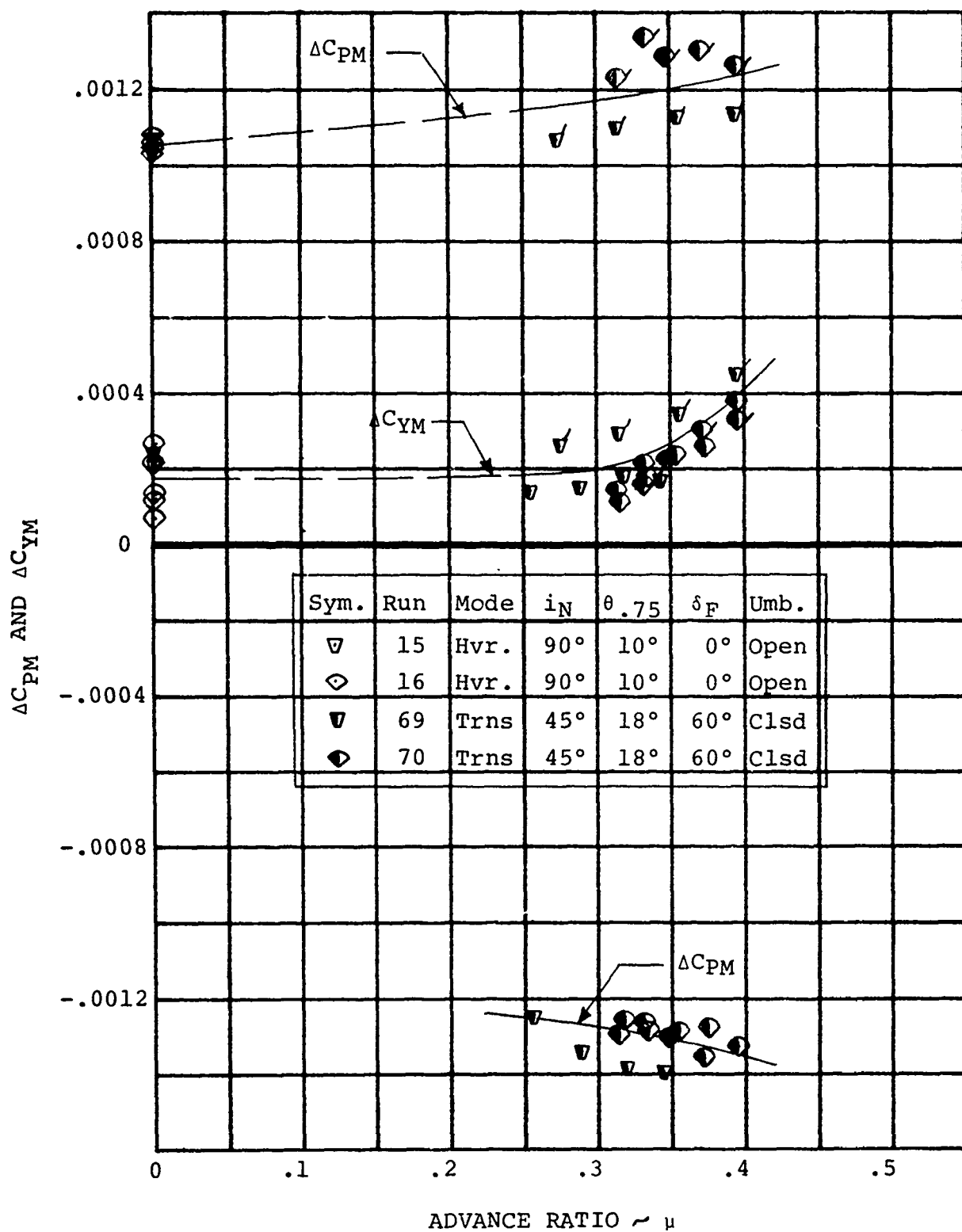


FIGURE 5-89. VARIATION OF ROTOR CONTROL MOMENTS WITH ADVANCE RATIO

5.4 CRUISE STABILITY

The cruise mode, as discussed here, will refer to operation as a conventional aircraft with the nacelle in the full-down position ($i_N = 0^\circ$) and the rotor is in axial flight. In this flight regime, the rotors have a major impact on the aircraft stability in that they are larger and more flexible than conventional propellers. These rotor properties decrease its static stability and increase the gust sensitivity of the aircraft. The following section discusses the analysis of the rotor stability and then the impact on total aircraft stability.

5.4.1 Rotor Stability Derivatives

Rotor Static Stability

Testing was performed to establish the variation of the rotor forces and moments with angle of attack and yaw in "axial" flight. Since the rotors are large, flexible and lightly loaded, changes in blade section angle of attack resulting from any disturbance in the flow through the rotor or blade flapping response will have a large impact on the rotor stability derivatives. The model rotors are not dynamically scaled and have a Lock Number of 17.28 and a flapwise frequency of 1.66 in the cruise condition. Both these parameters are significantly higher than the properties of the full scale rotor with a Lock Number of 11.81 and a flapwise frequency ratio of 1.22. This results in model rotor derivatives being higher than that of the full scale rotor. The wing circulation can significantly affect the rotor forces and moments also.

A summary of the rotor stability derivatives is presented in Table 5-2 in both longitudinal and directional modes. It indicates the magnitude of the derivative as obtained directly from the test data and also what they would be with the wing lift equal to zero, equivalent to an isolated rotor, obtained by cross plotting test data. As can be seen in this table, the wing lift significantly affects rotor pitching moment and sideforce, increasing the pitching moment derivative by approximately 50 percent and the side-force by approximately 90 percent. There is also a 10 to 15-percent increase in the normal force and yawing moment derivatives.

TABLE 5-2
CRUISE ROTOR STABILITY DERIVATIVES
LEFT ROTOR
LONGITUDINAL MODE

WING LIFT	$\partial C_{PM} / \partial \alpha$	$\partial C_N / \partial \alpha$	$\partial C_{YM} / \partial \alpha$	$\partial C_{SF} / \partial \alpha$
VARIABLE	0.00009	0.000168	-0.000118	0.000058
ZERO	0.00006	0.000143	-0.000106	0.000030

DIRECTIONAL MODE

WING LIFT	$\partial C_{YM} / \partial \psi$	$\partial C_{SF} / \partial \psi$	$\partial C_{PM} / \partial \psi$	$\partial C_N / \partial \psi$
CONSTANT	0.00006	0.000137	0.000107	-0.000031

As substantiation for the derivatives in pitch with the wing lift removed, the comparable derivatives in yaw are shown directly below the pitch derivatives. The variation in lift with yaw angle is negligible and therefore will not affect the derivative. The agreement in magnitude is very good and indicates that the wing lift effects as obtained from analyses of these test data are correct. The reversal in signs on the directional pitching moment and sideforce derivatives is a result of sign convention. A detailed discussion of the analysis is contained in the following paragraphs.

To define the rotor longitudinal stability derivatives requires making pitch angle sweeps. Since lift also varies as angle of attack, it is necessary to first determine if wing lift has any effect on the rotor forces and moments. This can be done by changing lift for fixed angles of attack by deflecting the flaps. Figure 5-90 indicates the influence of flap deflection and angle of attack on airframe lift. Figures 5-91 and 5-92 present the variation of rotor pitching moment coefficient and hub tares with angle of attack for flap deflections (δ_F) of 0 and 45 degrees.

Figures 5-93 and 5-94 present rotor normal force coefficient; Figures 5-95 and 5-96 show rotor yawing moment coefficient; and Figures 5-97 and 5-98 illustrate rotor sideforce coefficient variations with angle of attack for flap deflections of 0° and 45°. Testing was also performed to obtain the variation of the rotor characteristics for yaw angle sweeps. Figures 5-99 to 5-102 present the yawing moment, sideforce, pitching moment and normal force coefficients for yaw angle sweeps with the flap deflection of 0 degrees. In the presentation of these test data, hub tares are represented by Runs 90, 91, 92 and 93.

As shown in Figure 5-90, there is an increment in lift coefficient of approximately 0.9 for a flap deflection of 45 degrees. Associated with this increased lift at a fixed angle of attack is a change in rotor pitching moment coefficient (C_{PM}) of 0.0003 as shown in Figure 5-103. This is equivalent to changing the rotor angle of attack by four degrees. To better understand the wing lift influence, Figures 5-90 and 5-103 have been combined in Figure

5-104 to show the rotor pitching moment variation with lift at fixed angles of attack for the two flap deflections. Extrapolating the fixed angle of attack lines back to zero lift will define the variation of the rotor pitching moment coefficient without the effects of wing circulation. This is presented in Figure 5-105 as the zero wing lift line which has a pitching moment derivative ($\partial C_{PM}/\partial \alpha$) of 0.00006 per degree which agrees with the prediction. As indicated in this figure, the rotor derivative in the presence of the wing is 0.00009 per degree, a 50-percent increase over that of an isolated rotor.

To provide further substantiation that the pitching moment derivative obtained with the wing lift effects extracted, a comparison of this data was made with the variation of rotor yawing moment in a yaw angle (ψ) sweep. During the yaw sweep, the wing lift remains constant which will affect the level of the yawing moment but not the slope with yaw angle. This comparison is made on Figure 5-106 showing the pitching moment variation with angle of attack with and without the wing lift effect (previously shown in Figure 5-105) and the yawing moment variation with yaw angle with and without wing lift. Of major significance is that the yawing moment derivative $\partial C_{YM}/\partial \psi$ is 0.00006 which is exactly the same as the pitching moment derivative $\partial C_{PM}/\partial \alpha$ with wing lift effects removed. Also shown in Figure 5-106 is that the wing lift effects on the yaw sweep are low at zero fuselage angle of attack and results in a small level shift.

The other major rotor characteristic affecting total aircraft longitudinal stability is normal force. Figure 5-107 shows that the 0.9 increase in lift coefficient due to a $\delta_F = 45^\circ$ causes a 0.00020 increase in normal force which is equivalent to changing the rotor angle of only one degree. To define the impact of wing lift and establish the normal force derivative ($\partial C_N/\partial \alpha$) without the wing circulation effect, the variation of normal force with lift for fixed angles of attack is developed in Figure 5-108. Extrapolating the lines of constant angle of attack back to zero lift will define the normal force variation without any wing circulation. This is presented in Figure 5-109 and indicates that the wing increases the normal force derivative of 0.000143 by approximately 17 percent. To confirm the zero lift normal force derivative, a comparison was made with the

variation of sideforce with yaw angle. This is shown in Figure 5-110 and indicates relatively good agreement: $\partial C_N / \partial \alpha = 0.000143$ and $\partial C_{SF} / \partial \psi = 0.000137$.

Analyses of the wing lift effects on yawing moment and sideforce variations with angle of attack are done in the same manner as described above for pitching moment and normal force. Increasing the lift with a 45-degree flap deflection, as shown in Figure 5-111, decreases the yawing moment coefficient by 0.00008 which is equivalent to decreasing the angle of attack by approximately one degree. Figure 5-112 presents the variation of yawing moment with airframe lift for 0 and 45-degree flap deflections. This provides the basis for extracting the wing lift effects that account for approximately a 12-percent increase in the isolated rotor derivative shown in Figure 5-113. To confirm this trend of yawing moment with angle of attack, the variation of pitching moment with yaw angle must be explained. For the rotor being used in this discussion, it is important to understand its response to pitch and yaw angle disturbances and the impact on the forces and moments. When increasing the rotor angle of attack, the blade section angle of attack is increased on the advancing side (right, looking from behind the rotor) and decreased on the retreating (left) side. This produces an increase in lift on the advancing side and a decrease in lift on the retreating side. The net effect is that the rotor normal force increases with increasing rotor angle of attack as shown in Figure 5-107. Blade flexibility allows the rotor to flap aft on the top and retreating side of the disc with increasing rotor angle of attack. This produces a positive pitching moment, sideforce and a negative yawing moment as shown in Figures 5-103, 5-97 and 5-111, respectively.

Correspondingly, in a yaw sweep, the advancing blade is now at the top of the rotor and the retreating blade is on the bottom of the rotor. When increasing the yaw angle (right side moving back), the blade section angle is decreased on the advancing and increased on the retreating side. This results in an increase in sideforce to the right, as shown in Figure 5-100. Blade flexibility will cause the rotor to flap aft on the top and right sides causing a positive pitching moment, yawing moment and negative normal force, as shown in Figures 5-101, 5-99 and 5-102, respectively. Therefore, the yawing moment

derivative with angle of attack ($\partial C_{YM}/\partial \alpha$) will be negative and the pitching moment derivative with yaw angle ($\partial C_{PM}/\partial \psi$) will be positive but both will have the same magnitude if there is no wing circulation effect. This is indeed the case as presented in Figure 5-114: $\partial C_{YM}/\partial \alpha$ is -0.000106 and $\partial C_{PM}/\partial \psi$ is +0.000107.

The analysis for the wing lift effects on the side force are similar to that presented for the normal force. Deflecting the flap 45° decreases the side force by approximately 0.0003 or an equivalent four-degree decrease in angle of attack as shown in Figure 5-115. These data are then combined with the data of Figure 5-90 as the variation of side force airframe lift in Figure 5-116. The variation of side force with angle of attack for zero wing lift is then defined. Figure 5-117 presents this side force derivative ($\partial C_{SF}/\partial \alpha$) and indicates that the wing lift increases the isolated rotor (wing lift=0) by approximately 93 percent. To verify the zero wing lift line, a comparison is made with the variation of rotor normal force with yaw angle ($\partial C_N/\partial \psi$) in Figure 5-118. This comparison indicates that the side force and normal force derivatives are of the same magnitude but opposite in sign: $\partial C_{SF}/\partial \alpha = 0.00003$, $\partial C_N/\partial \psi = -0.00003$). This is consistent with the discussion of the variation of forces and moments in pitch and yaw sweeps presented earlier.

The influence of the wing on the rotor stability derivatives has the largest effect on pitching moment and side force. With counter rotating rotors, the effect of the wing on side force is equal and opposite; therefore, it has no impact on the total aircraft stability.

A single test run was made at an advance ratio of 0.57 to provide data that would assist in the definition of rotor stability derivative variation with advance ratio. The power requirements and model blade loads associated with this cruise condition were high and resulted in an aborted run with two data points. These data are presented in Figures 5-119 through 5-122 showing the variation of rotor pitching moment, normal force, yawing moment and side force variation with angle of attack. The derivatives obtained from these data are presented in the table below.

MODE	WING LIFT	$\partial C_{PM}/\partial \alpha$	$\partial C_N/\partial \alpha$	$\partial C_{YM}/\partial \alpha$	$\partial C_{SF}/\partial \alpha$
Longitudinal	Variable	0.000187	0.000414	-0.000225	0.000151

These derivatives, although based on only two data points, result in approximately 150-percent increase in the force derivatives and 100 percent in the moment derivatives compared with Table 5-2. This indicates that the phase angles at which the blade angle reaches a maximum and where the moments are a maximum for an advance ratio of 0.57 are approximately the same as those at an advance ratio of 0.386. Therefore, the rotor response has not

changed and the first harmonic thrust and the flapping magnitudes have increased with speed as would be expected.

Correlation of Theory with Test Data

A simplified method of predicting rotor stability derivative is presented in Reference 2 . Utilizing this prediction technique for the model rotor, with a Lock number (γ) of 17.28 and a flap-wise frequency ratio (ω/Ω) of 1.66, a pitching moment derivative ($\partial C_{PM}/\partial \alpha$) of 0.0000538 per degree is obtained and presented on Figure 5-105. The theory and the test data have approximately the same slope ($\frac{\partial C_{PM}}{\partial \alpha}$) but there is a difference in level. The

primary reason for this is that the model was yawed approximately 0.8 degrees during this test run and the cross coupling between the rotor pitching and yawing moment in yaw reduces the pitching moment approximately 0.0001. Accounting for this yaw angle reduces the increment between the theory and test to half that shown in Figure 5-105. The same prediction technique was utilized to define the normal force derivative in pitch ($\partial C_N/\partial \alpha$) and is shown in Figure 5-109. The predicted value of $\partial C_N/\partial \alpha$ is 0.000164; this is slightly higher than the test data with the wing lift removed. Accounting for the 0.8 degree of yaw will lower the zero lift line very slightly (0.000025).

The simplified theory provides a rapid and relatively accurate method of defining the rotor stability derivatives and their contributions to total aircraft stability. It is significant to note that the prediction of the normal force is high and the pitching moment is low. This would indicate that the contribution made by the longitudinal and lateral flapping is underestimated since this contribution tends to reduce the normal force and increase the pitching moment.

Rotor/Rotor Interference on Cruise Rotor Characteristics

Another potential source of disturbance to the rotor flow field and hence, an additional influence on the rotor stability derivatives is the effect of one rotor on the other when in the cruise mode. If there is a rotor-to-rotor interference in cruise, it can be determined by first testing with both rotors operating and then with only one operating for the same test conditions. This testing was performed and the data are presented in Figures 5-123 to 5-126 showing pitching moment, normal force, yawing moment and side force, respectively. Runs 79 and 80 are the twin rotor cases at tunnel dynamic pressures (q) of 55 lb/ft² and 50 lb/ft², respectively. The associated advance ratios (V/V_T) are 0.386 and 0.380. The small difference in advance ratio should have negligible

effect on the forces and moments presented here and is demonstrated in the above figures with the exception of side force. There are small deviations in advance ratio within these two runs which possibly accounts for the scatter. When comparing the isolated rotor (Run 85) to the twin rotor cases, there is a level shift in each of the rotor parameters presented. As indicated by the previous discussion on the rotor derivatives, a level shift can be the result of having a difference in yaw angle between the two pitch sweeps. Close scrutiny of the test data indicated that Runs 79 and 80 were tested at a negative yaw angle of approximately 0.8 degree which accounts for the level shifts presented here. This, therefore, indicates that there is no rotor-to-rotor interference when operating in the cruise mode.

Rotor Dynamic Stability

The rotor derivatives of pitching moment and normal force with $\dot{\alpha}$ were obtained from the initial input data of Runs 83 and 84. These are as follows:

$$\frac{\partial C_N}{\partial \dot{\alpha}} = .00189$$

and

$$\frac{\partial C_{PM}}{\partial \dot{\alpha}} = .0008$$

It is to be noted, however, that the rotor and balance inertia effects are included in the determination of these derivatives since response data were used. Since rotor inertia was not scaled from the full scale, the magnitudes are presented to show relative magnitudes.

The effects of velocity on pitching moment and normal force for low-speed flight (helicopter mode) may be seen in Figures 5-127 and 5-128. The stability derivative of normal force is seen to be $\partial C_N / \partial V = .0000124$. Since pitching moment is a function of V^2 , then $\partial C_M / \partial V$ must be calculated at each trim speed.

5.4.2 Aircraft Stability Derivatives

Aircraft Static Stability

Testing was performed in cruise to define the total stability characteristics of the wind tunnel model as well as the contributions of the prop/rotors, and the horizontal and vertical tail. As indicated in Section 5.4.1, the model rotor derivatives are significantly larger than those of the full scale rotor because the model rotor is not dynamically scaled. Since the rotor contribution to the total aircraft is destabilizing, the total model

stability derivatives obtained from the test data cannot be scaled up and be representative of the full scale aircraft. The estimated full-scale stability will be discussed later in this section presenting the correlation of prediction techniques and test data.

When determining the stability, it is of primary importance to obtain the airframe characteristics, establish the wing and tail stall and define any associated moment nonlinearities. In addition, data were obtained for the total aircraft and its components to provide a basis for a correlation effort of existing prediction techniques to be conducted in the next phase of the current contract. In conjunction with this later requirement, airframe lift and drag characteristics were obtained with rotors removed and are presented in Figure 5-129. Illustrated in this figure is the prediction of the airframe lift variation with angle of attack, obtained using the methods described in DATCOM. The prediction shows good correlation.

As indicated in Figure 5-129, there is a break in the lift curve at approximately 8° angle of attack with a reduction in slope from 0.092 to 0.052 per degree out to 16° for zero-degree flap deflection. This is typical for the NACA 63₄421 airfoil wing section of this model. The data presented for 60° flap deflection indicate that there is an increase in aircraft drag coefficient of 0.19 and maximum lift occurs at 7.5 degrees angle of attack. It is important to define effect of the rotors on these characteristics and determine the tail contribution. Figures 5-130 through 5-132 present the prop/rotor and horizontal tail contributions to the aircraft lift variation with angle of attack for flap deflections of 0, 45 and 60 degrees. The increase in lift curve slope (ΔC_{L_α}) associated with the tail is 0.018 per degree for the three flap deflections. Since there is not a significant increase in the airframe-minus-tail lift curve slope, there should be no increase in the rate of change of downwash at the tail with angle of attack and hence, no change in the incremental lift curve slope from the tail. The maximum airframe lift coefficient (C_L) of 1.57 is obtained at 19 degrees angle of attack for the fuselage when the flaps are not deflected ($\delta_F=0$). Deflecting the flap 45 degrees provides an increase in lift coefficient of 0.9 at zero angle of attack and a maximum C_L of 1.90 at 7.5 degrees angle of attack. Increasing the flap to 60 degrees gives an additional 0.15 increment in C_L and maximum C_L but does not change the stall angle. The variation of lift beyond stall shows a gentle stall characteristic at positive angles. Testing was performed at negative angles of attack up to -15 degrees which appears to be the angle of negative stall for zero flap deflection. The rotor contribution to the lift characteristics indicates an increase in lift curve slope (C_{L_α}) of 0.015 and reduces the impact of stall. It provides an extension in the maximum lift angle of at least 12 degrees for a flap deflection of 45 degrees and 7 degrees for a

flap deflection of 60 degrees due to reduction in wing angles of attack by the rotor slipstream. In Figure 5-132, a maximum lift coefficient of 2.6 is achieved from 11 to 15 degrees angle of attack. This is constant since the decrease in airframe lift is approximately equal to the increase associated with the rotor.

Longitudinal stability characteristics, pitching moment variation with angle of attack, associated with the lift characteristics discussed above, are presented in Figures 5-133 through 5-135. These figures present the total aircraft and the contribution of the rotors and also the horizontal tail to the pitching moment. The longitudinal stability derivative ($\partial C_M / \partial \alpha$) for the airframe minus the tail indicates an unstable slope of 0.019 per degree up to an angle of attack of 8 degrees. There is a sharp decrease in slope beyond this angle indicating the same trends as the lift coefficient.

Deflecting the flap to 45 and 60 degrees decreases the magnitude of the airframe-minus-tail pitching moment by 0.19 and 0.22, respectively, but not the slope. These increments directly reflect the increase in lift coefficient for a fixed center of pressure. Adding the horizontal tail to make the aircraft stable decreases the stability derivative to -0.0315 per degree to 8 degrees angle of attack. Beyond this angle, there is a further decrease in slope which is indicative of the decrease for the airframe minus tail. Stall is directly reflected in pitching moment by the sharp reversal from very stable to unstable beyond 20 degrees angle of attack. A significant item to point out is that the magnitude and slope of the airframe pitching moment does not vary with flap deflection. This results from the increase in downwash increasing the tail contribution by the same magnitude that the wing pitching moment decreases.

The rotor contribution to total aircraft stability is destabilizing. For zero flap deflection, the rotor has an incremental stability derivative of 80 percent of the tail contribution which is 0.05 per degree. When deflecting the flap 45 and 60 degrees, the rotor derivatives increase, as discussed in Section 5.4.1, and its destabilizing increment is approximately equal to the stabilizing contribution of the tail; therefore, the total aircraft has low angle of attack stability characteristics similar to the airframe minus tail. The rapid change in the airframe slope beyond 8 degrees is large enough to overcome the rotor contribution and is the reason that the total aircraft becomes stable beyond 8 degrees angle of attack for each of the flap deflections. The basic trend exhibited by these three configurations in the cruise mode is that the longitudinal stability of the airframe itself is very stable but the addition of the model rotors with its large destabilizing contribution results in an unstable aircraft.

Examining the directional stability characteristics in cruise indicates that the variation of side force with yaw ($\partial C_{SF}/\partial \psi$) is increased from 0.0096 to 0.02 as shown in Figure 5-136 by the addition of the tail. There is an increase in slope at approximately positive four degrees and negative seven degrees in the airframe minus tail. This could be a result of flow reattachment on the aft end of the fuselage. When the vertical tail is added, the change in slope increases in the high yaw angle region indicating that the base of the tail is less separated and therefore produces increased side force. The rotors provide an additional increase in slope of 0.0135 resulting from the variation of side force with yaw angle. This is approximately the same increase in slope as obtained in lift.

The associated yawing moment characteristics are presented in Figure 5-137. For the airframe minus tail, there is a decrease in the slope of yawing moment at approximately minus 7 and plus 4 degrees that would be representative of an aft shift in center of pressure in conjunction with the increased side force slope. Incorporating the tail makes the aircraft stable and also makes the decreased slopes very pronounced beyond minus 7 and plus 4 degrees yaw. This significant change in the stability increment of the tail confirms the flow reattachment and increased tail effectiveness suggested above. When the model rotors are added, the destabilizing contribution more than offsets the vertical tail. The addition of the rotors, as represented by the total aircraft line in Figure 5-137, appears to cause tail stall as represented by the reversal in the yawing moment at approximately 12 degrees. This is not the case, for the increase in effectiveness of the tail in providing the stabilizing moment is greater than the destabilizing contribution of the rotor. While analyzing the directional stability, a check was made to determine if any cross coupling effects existed between roll and yaw. No unusual trends were exhibited in the rolling moment variation with yaw angle for the airframe with or without the tail in Figure 5-138; but the total aircraft rolling moment maximized at -14 degrees yaw and then indicated a slope reversal. This was inconsistent with the trends of side force and yawing moment. A close study of the variation of the rotor characteristics indicate that the rotor normal force maximizes at approximately -12 degrees yaw, as shown in Figure 5-102, for the left rotor. This does not occur in the right rotor normal force indicating the possible influence of the fuselage on left rotor normal force in yawing to the left.

Basic directional stability trends presented here indicate that the airframe is very stable but the addition of the model rotors introduces a large unstable contribution resulting in an unstable aircraft directionally as well as longitudinally. These characteristics are not representative of the full-scale aircraft in that the model rotor has different flapping and damping characteristics. The estimated full-scale stability will be discussed later in this section presenting the correlation of prediction techniques and test data.

The evaluation of the aircraft stability characteristics is significantly affected by the rotor forces and moments. Any influence of the rotor slipstream on the airframe is not immediately obvious. To examine this effect, the rotor contributions were subtracted from the total aircraft and compared with the airframe characteristics for pitching moment in Figure 5-139 and yawing moment in Figure 5-141. The solid lines, noted as rotors on, indicate the aircraft minus rotors or airframe characteristics including slipstream effects. The dashed lines are the data obtained with rotors off. The difference between the lines defines the horizontal tail contribution shown in Figure 5-140 and the vertical contribution in Figure 5-142. There is a negligible slipstream effect exhibited in both of these figures.

Pretest predictions of the airframe, the prop/rotor and tail contributions to total aircraft pitching moment characteristics were made and are compared to the test data in Figure 5-143. The airframe components were predicted by the methods defined in Reference 1 DATCOM. Airframe-minus-tail pitching moment prediction of $\partial C_{PM}/\partial \alpha = 0.011$ is lower than that obtained from test, $\partial C_{PM}/\partial \alpha = 0.018$. Further analysis to be accomplished in the next phase of the stowed rotor effort must be performed to understand this difference. The contribution of the horizontal tail to total aircraft stability ($\Delta \partial C_{PM}/\partial \alpha$) is 0.052 per degree as predicted by the methods defined by DATCOM. Adding this increment to the airframe-minus-tail test data results in excellent agreement with the airframe test data. This indicates that the tail characteristics as well as the wing downwash are correctly accounted for. The rotor contribution was defined by the isolated rotor characteristics as discussed in Reference 2 increased by the empirical lift effects induced by the wing. This results in a rotor contribution of 0.043 per degree and when adding this to the airframe test data indicates good agreement with the total model aircraft data.

The model nacelles are oversized to house the electric motors. Rotor characteristics for the model are such that they produce a larger destabilizing moment than would be expected from the full-scale rotor. A preliminary estimate of the increments in pitch stability associated with these two items is -0.003 per degree for the nacelles and -0.013 for the rotors. This indicates that the full-scale aircraft would have a total aircraft longitudinal stability derivative -0.016 per degree more stable than the test data. This is represented by the dotted line on Figure 5-143, showing that the full scale aircraft is stable.

Aircraft Dynamic Stability

As discussed in Section 7.2, a model step input in angle of attack was used to examine the whirl flutter phenomenon. Alternately,

the dynamic response of the model system to a 4-degree step input is shown in Figure 5-44. As can be seen from the pitching moment response, the resulting damped oscillation has a frequency of 9 CPS with damping of 2.55 percent. The sting natural frequency as obtained from disturbance tests (Table B-5) is 4 CPS with 4-percent damping. The corresponding sting plus model and balance frequency in the static position was 24 CPS with damping of 0.9% (Table B-3). Thus, rotor damping, as a result of the step input, shows a value almost equal to the basic sting system, with the corresponding frequency. Similarly, the normal force responding frequency is seen to be 5 CPS as compared to a balance natural frequency of 4 CPS. Based on these data, it appears that rotor derivatives are not able to be separated from the system dynamics.

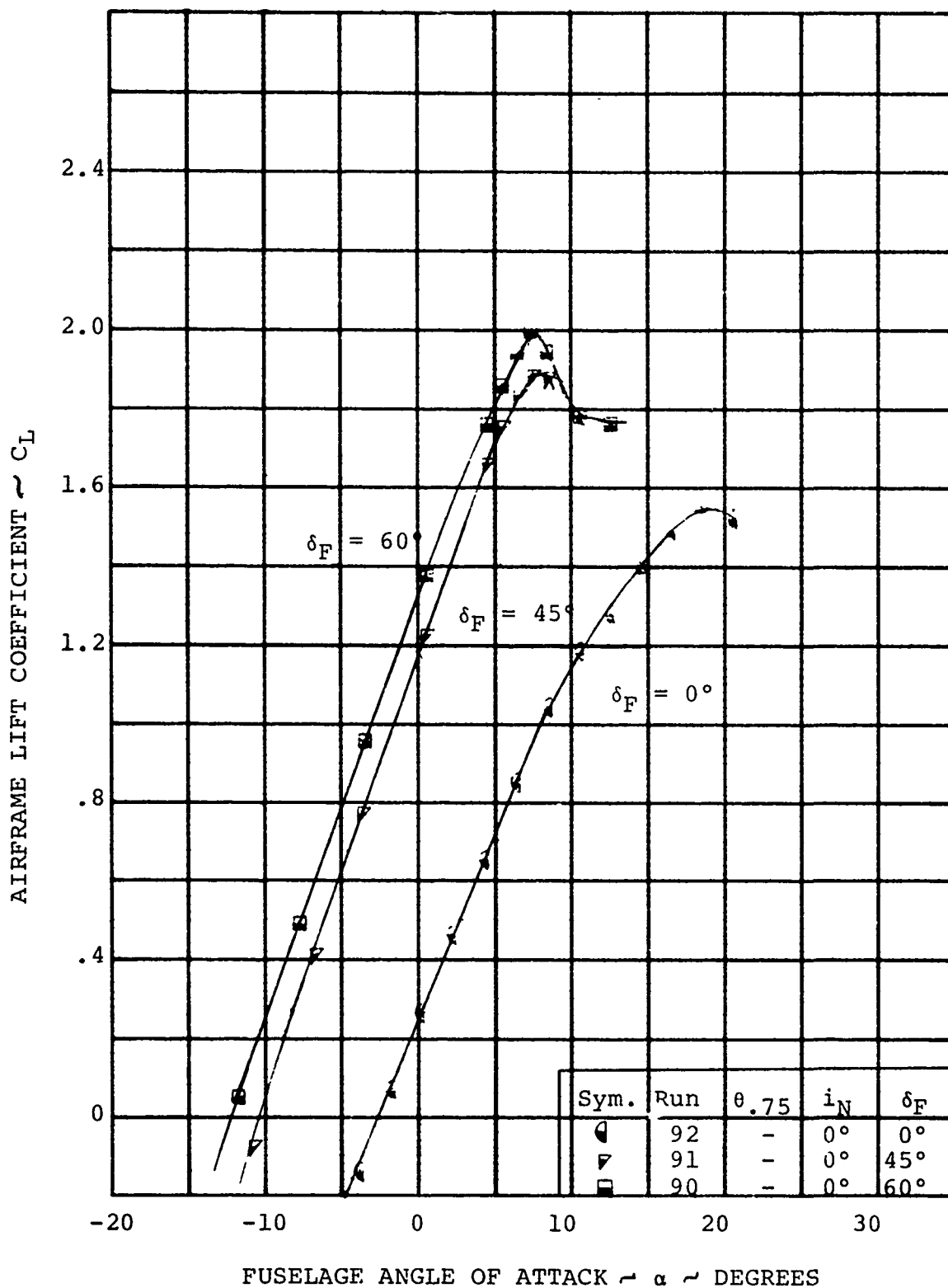


FIGURE 5-90

INFLUENCE OF FLAP DEFLECTION ON
AIRFRAME LIFT

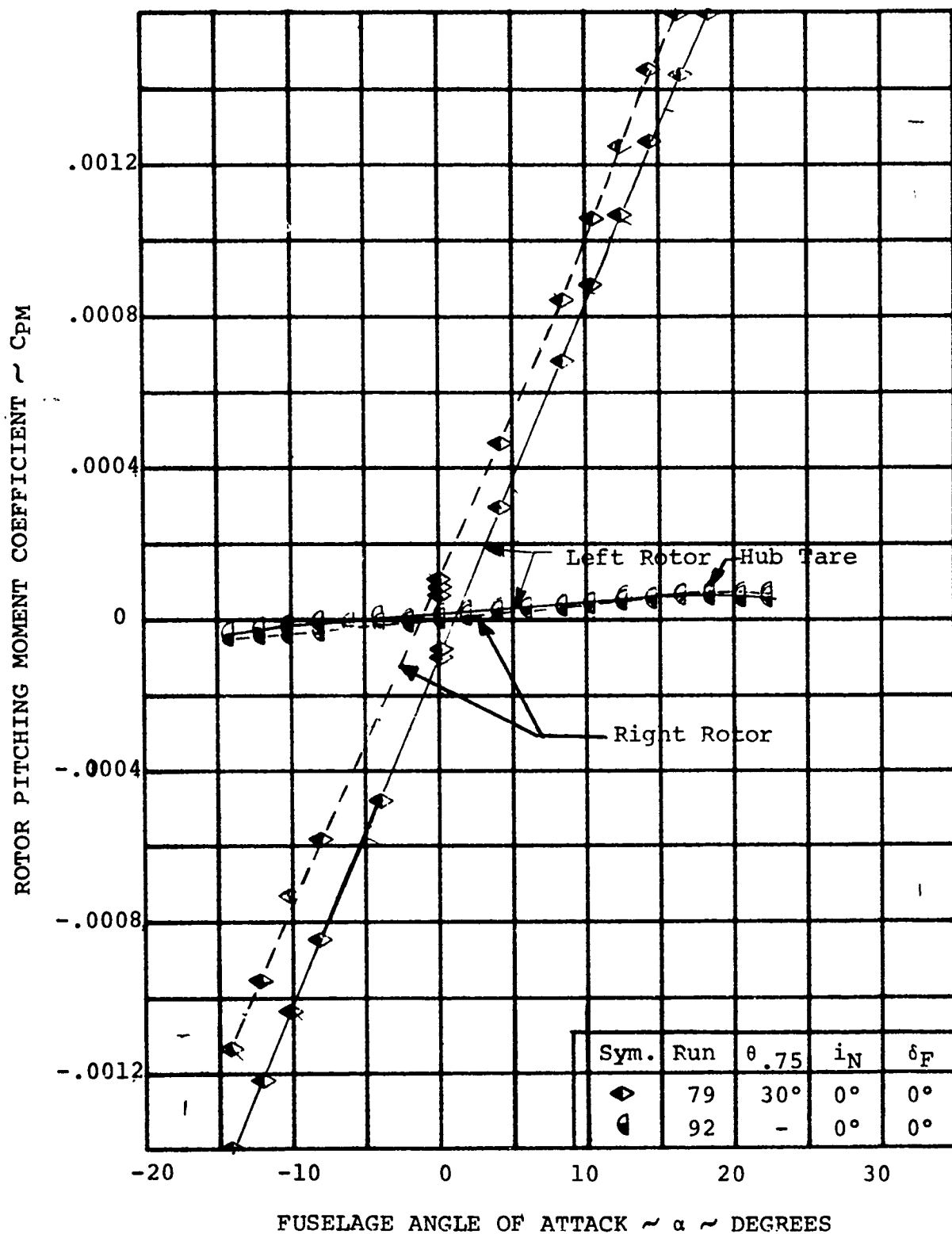


FIGURE 5-91

ROTOR PITCHING MOMENT/ANGLE OF ATTACK
VARIATION AT $V/V_T = 0.386$ AND $\delta_F = 0^\circ$

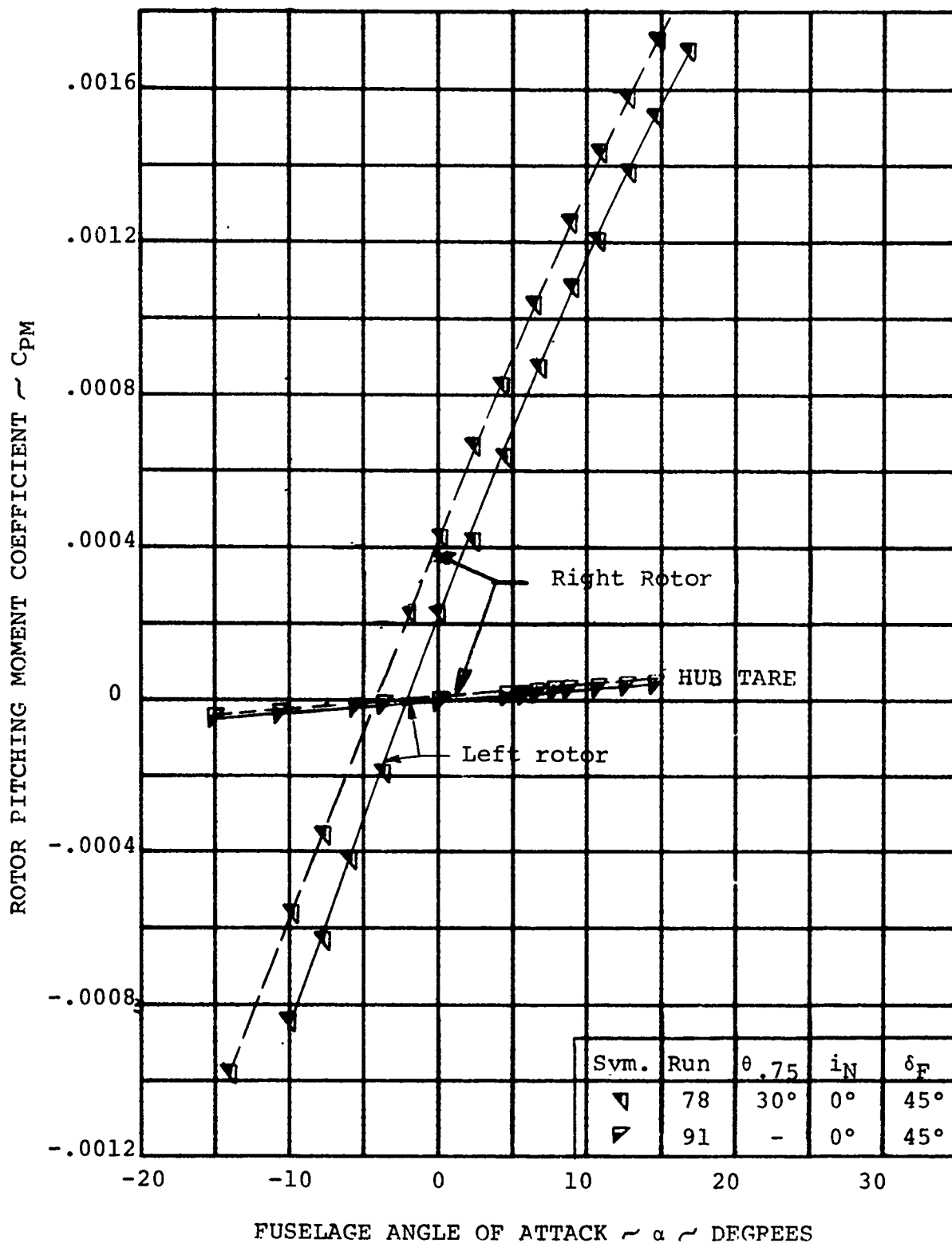


FIGURE 5-92

ROTOR PITCHING MOMENT/ANGLE OF ATTACK
VARIATION AT $V/V_T = 0.386$, $\delta_F = 45^\circ$

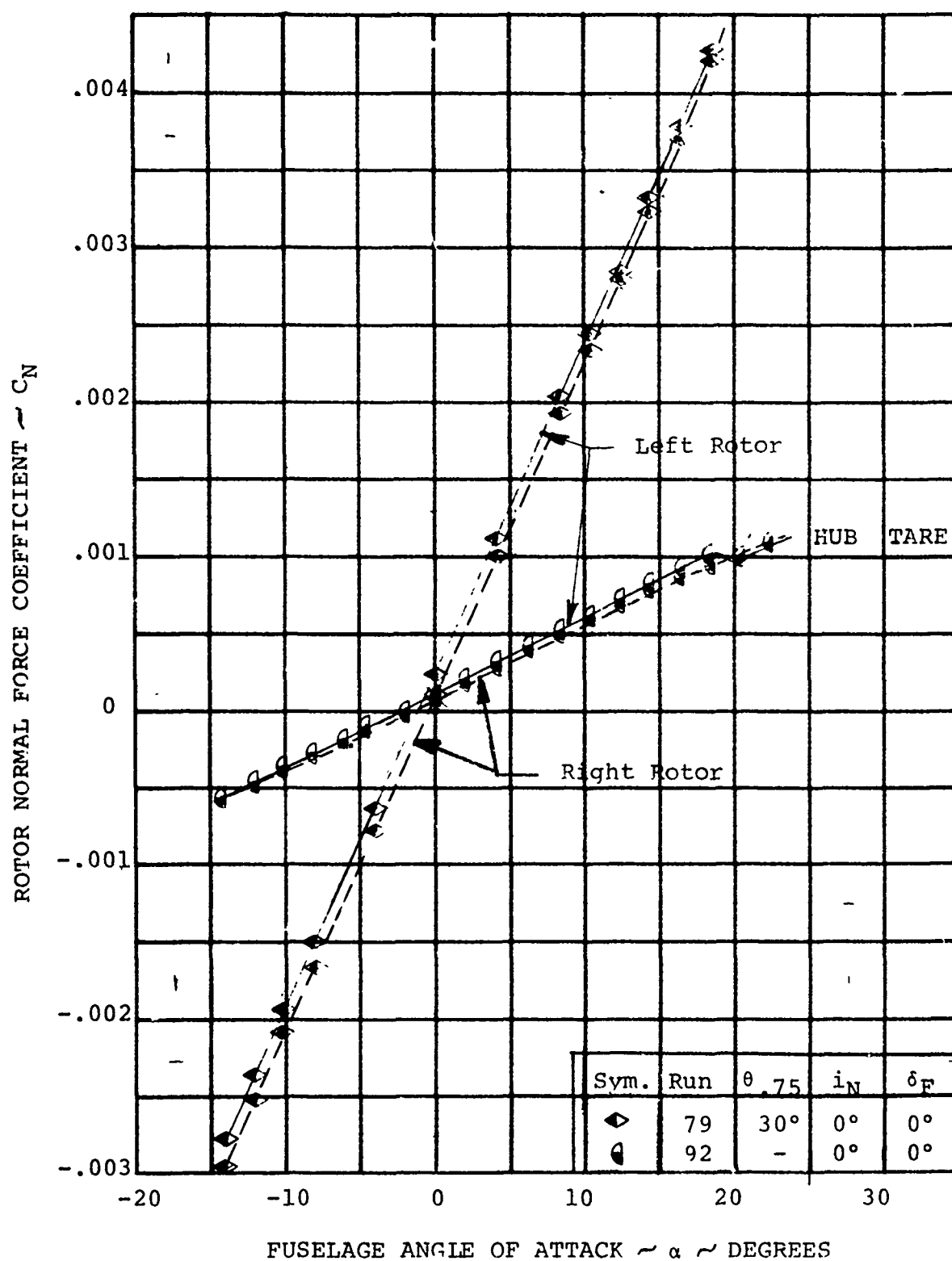


FIGURE 5-93

ROTOR NORMAL FORCE/ANGLE OF ATTACK
VARIATION AT $V/V_T = 0.386$, $\delta_F = 0^\circ$

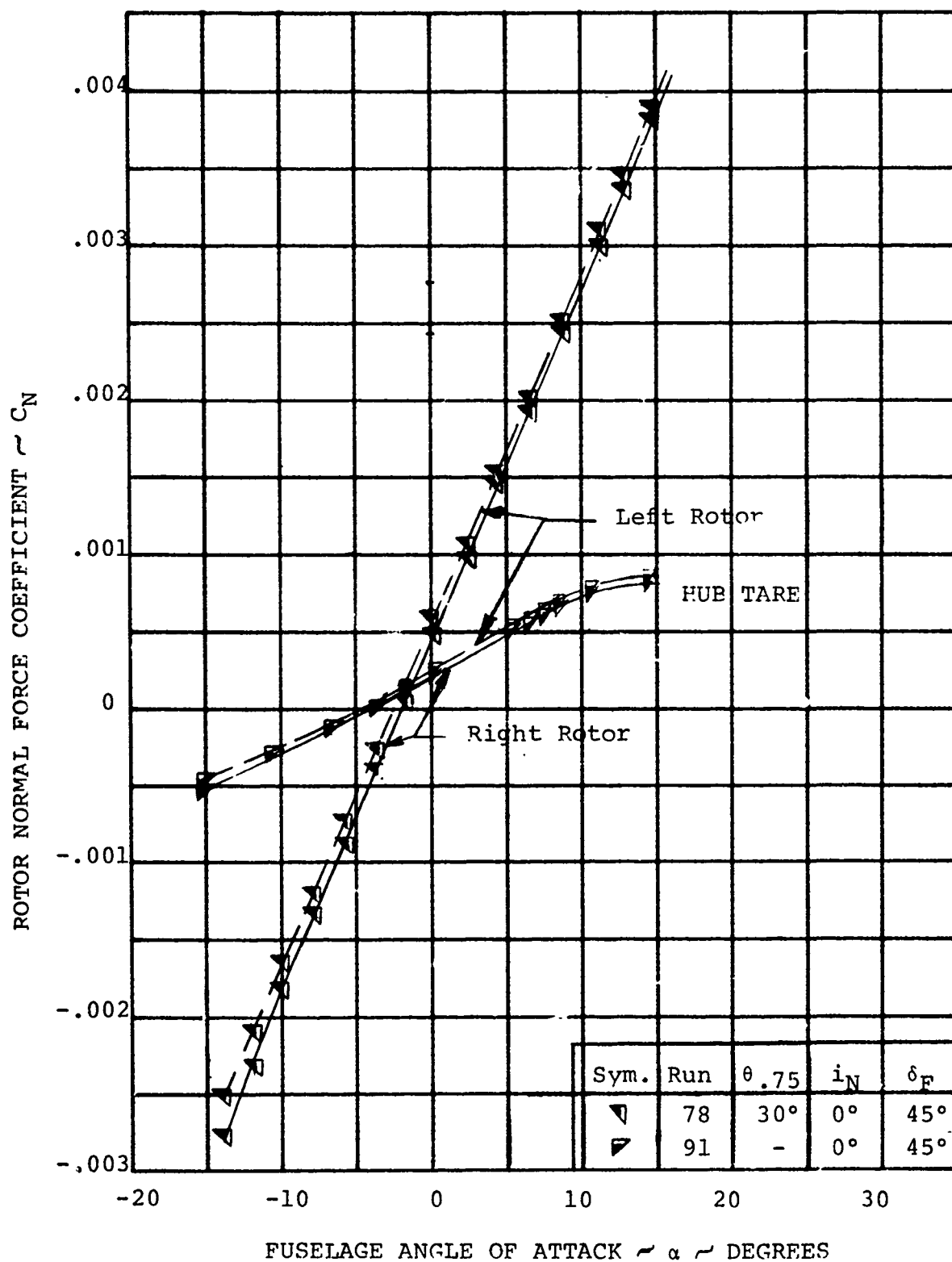


FIGURE 5-94

ROTOR NORMAL FORCE/ANGLE OF ATTACK
VARIATION AT $V/V_T = 0.386$, $\delta_F = 45^\circ$

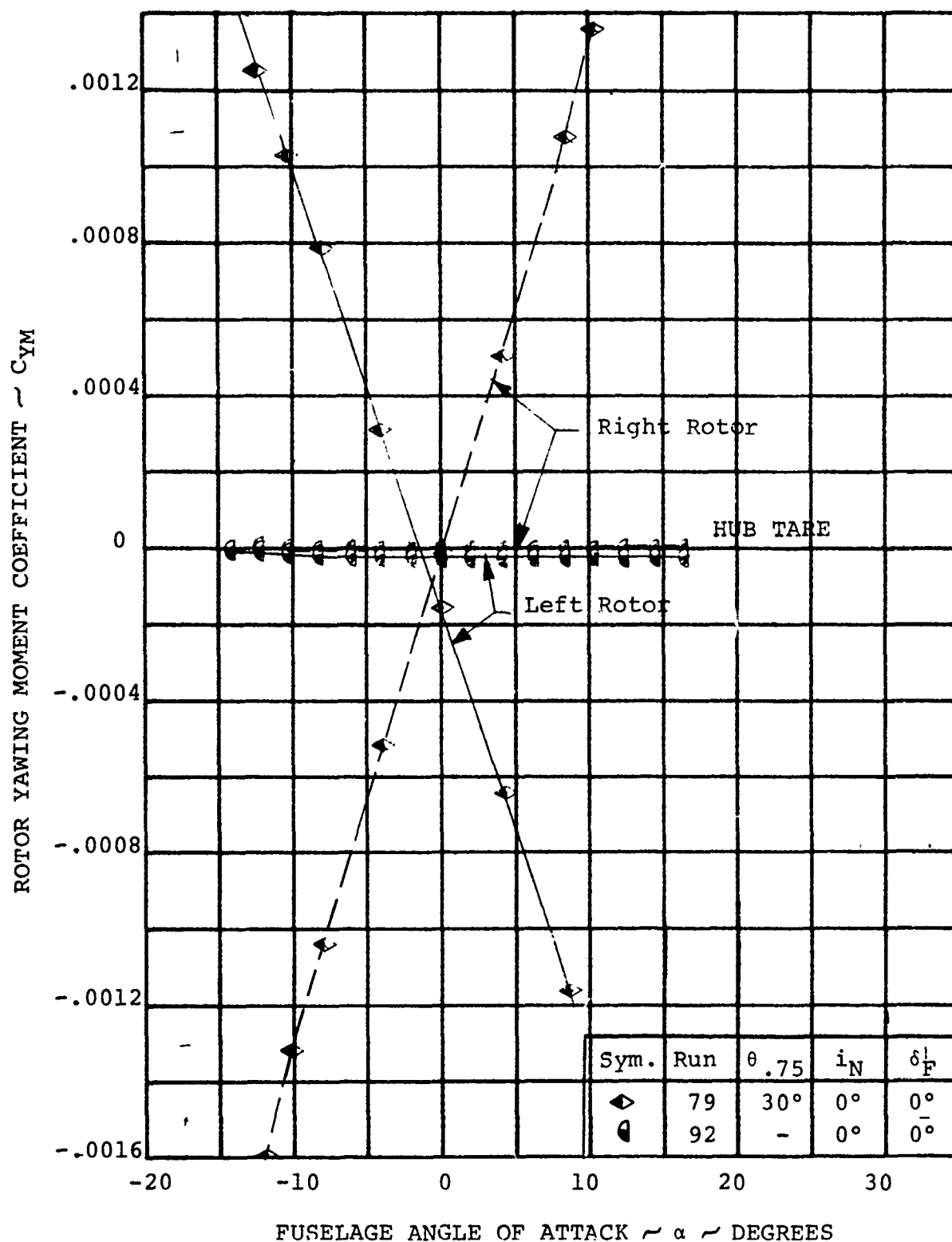


FIGURE 5-95

ROTOR YAWING MOMENT/ANGLE OF ATTACK
VARIATION AT $V/V_T = 0.386$, $\delta_F = 0^\circ$

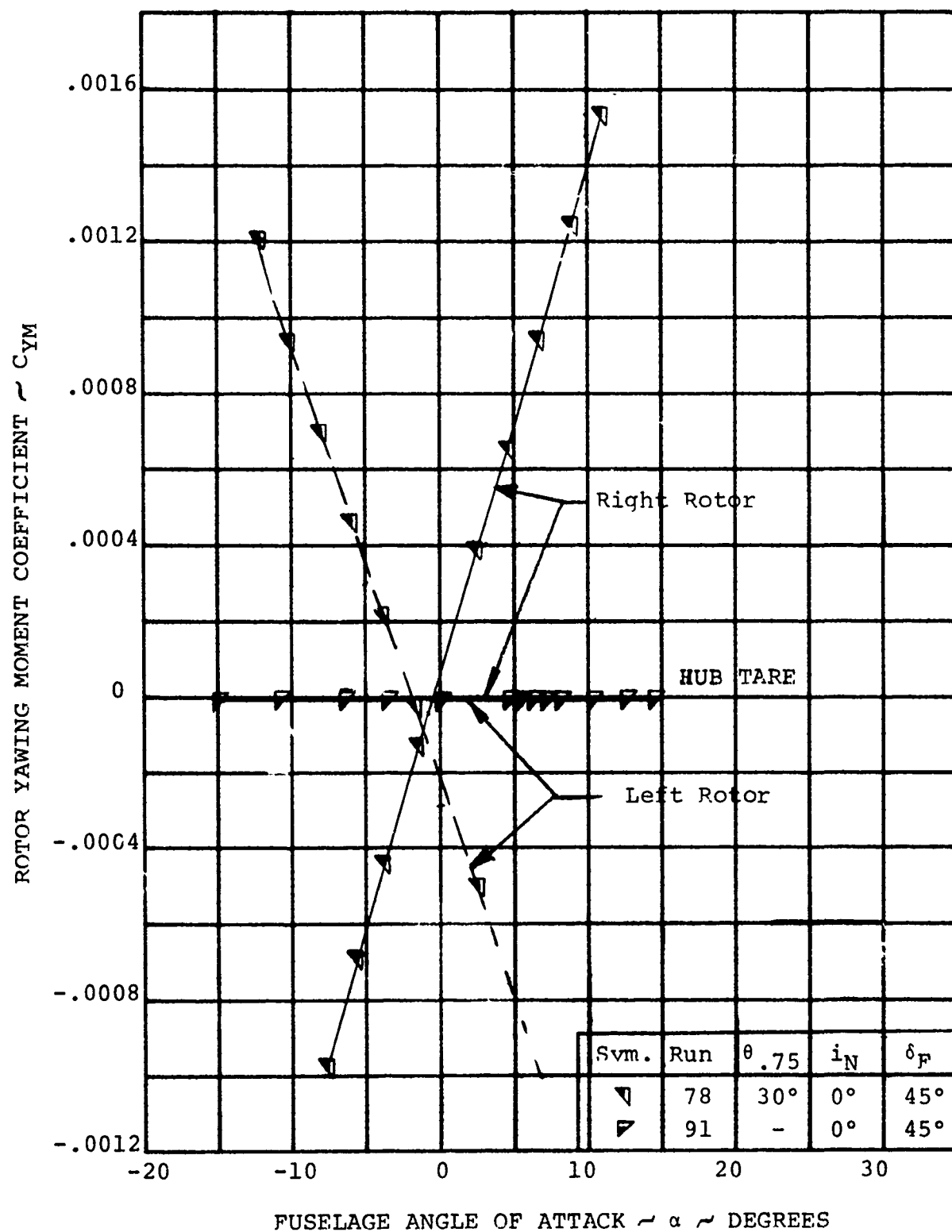


FIGURE 5-96

ROTOR YAWING MOMENT/ANGLE OF ATTACK
VARIATION AT $V/V_T = 0.386$, $\delta_F = 45^\circ$

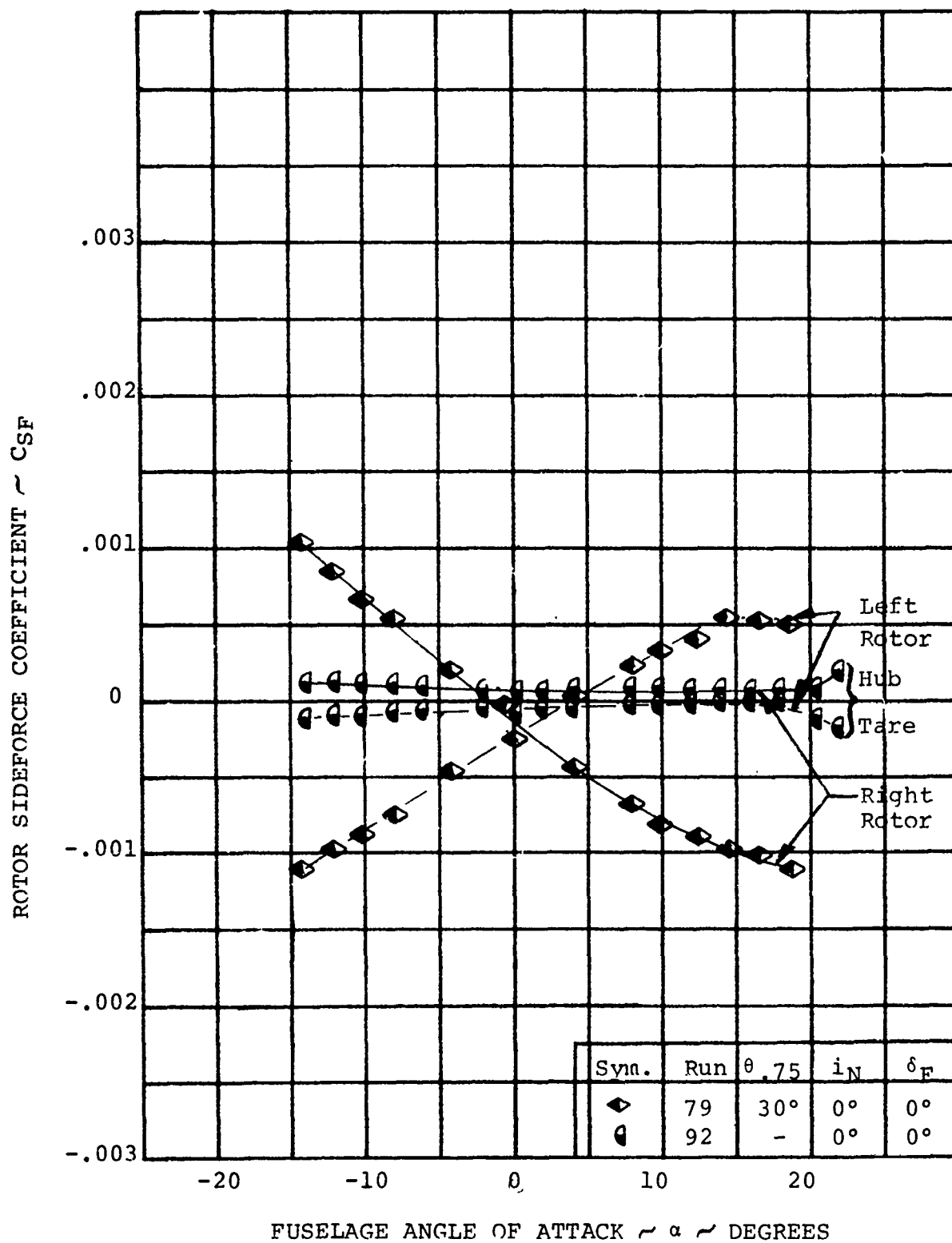


FIGURE 5-97

ROTOR SIDEFORCE/ANGLE OF ATTACK
VARIATION AT $V/V_T = 0.386$, $\delta_F = 0^\circ$

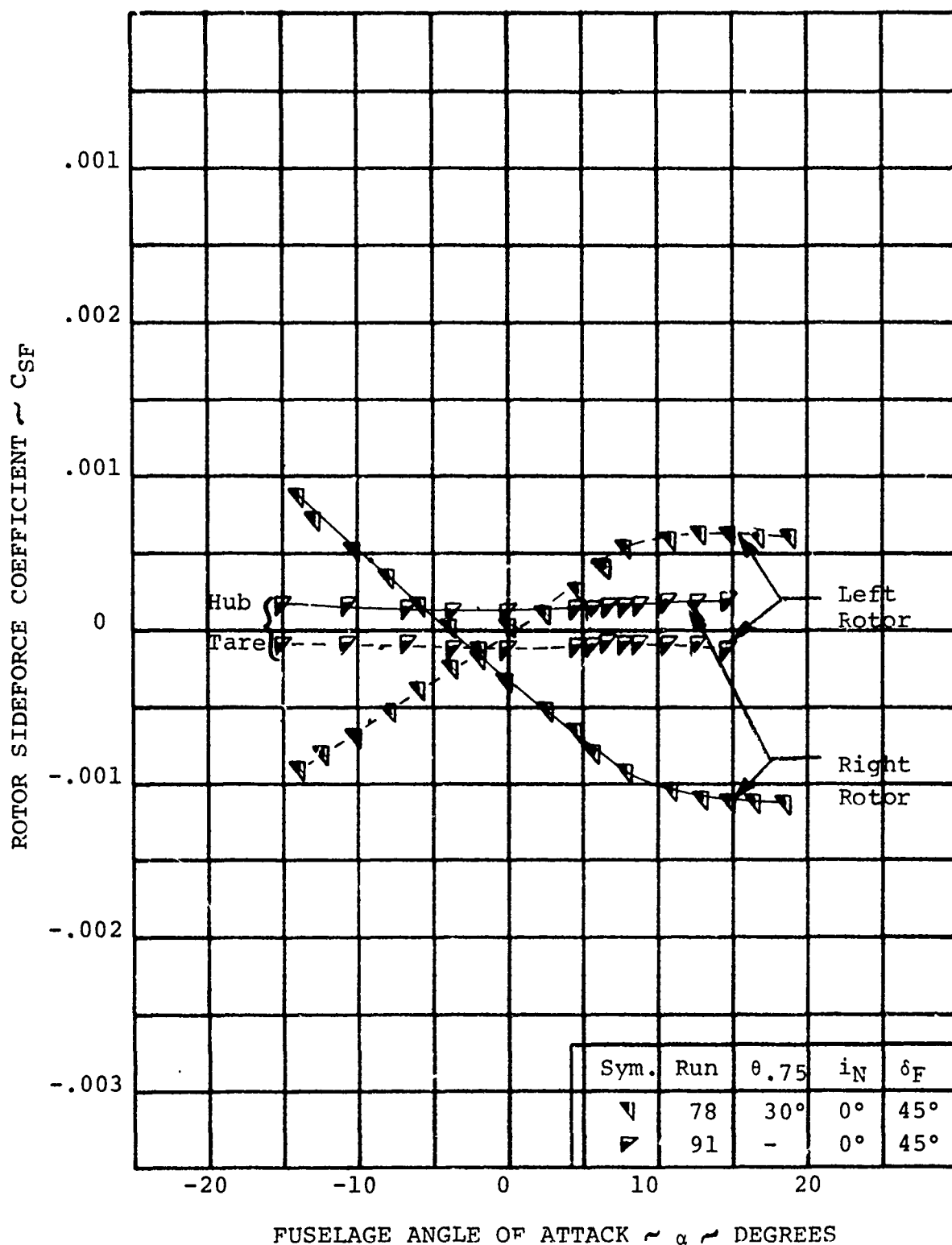


FIGURE 5-98

ROTOR SIDEFORCE/ANGLE OF ATTACK
VARIATION AT $V/V_T = 0.386$, $\delta_F = 45^\circ$

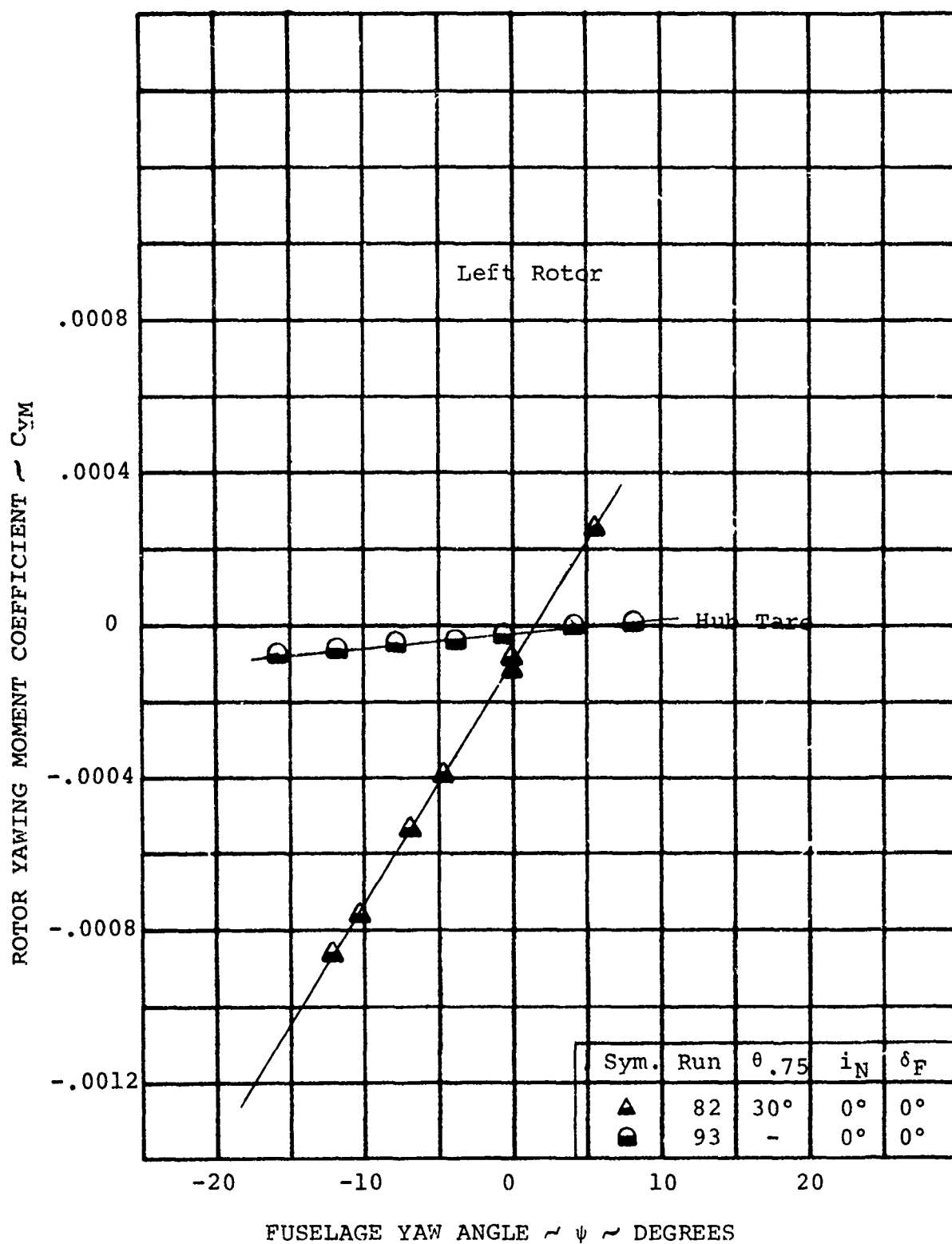


FIGURE 5-99

ROTOR YAWING MOMENT/YAW ANGLE
VARIATION AT $V/V_T = 0.386$, $\delta_F = 0^\circ$

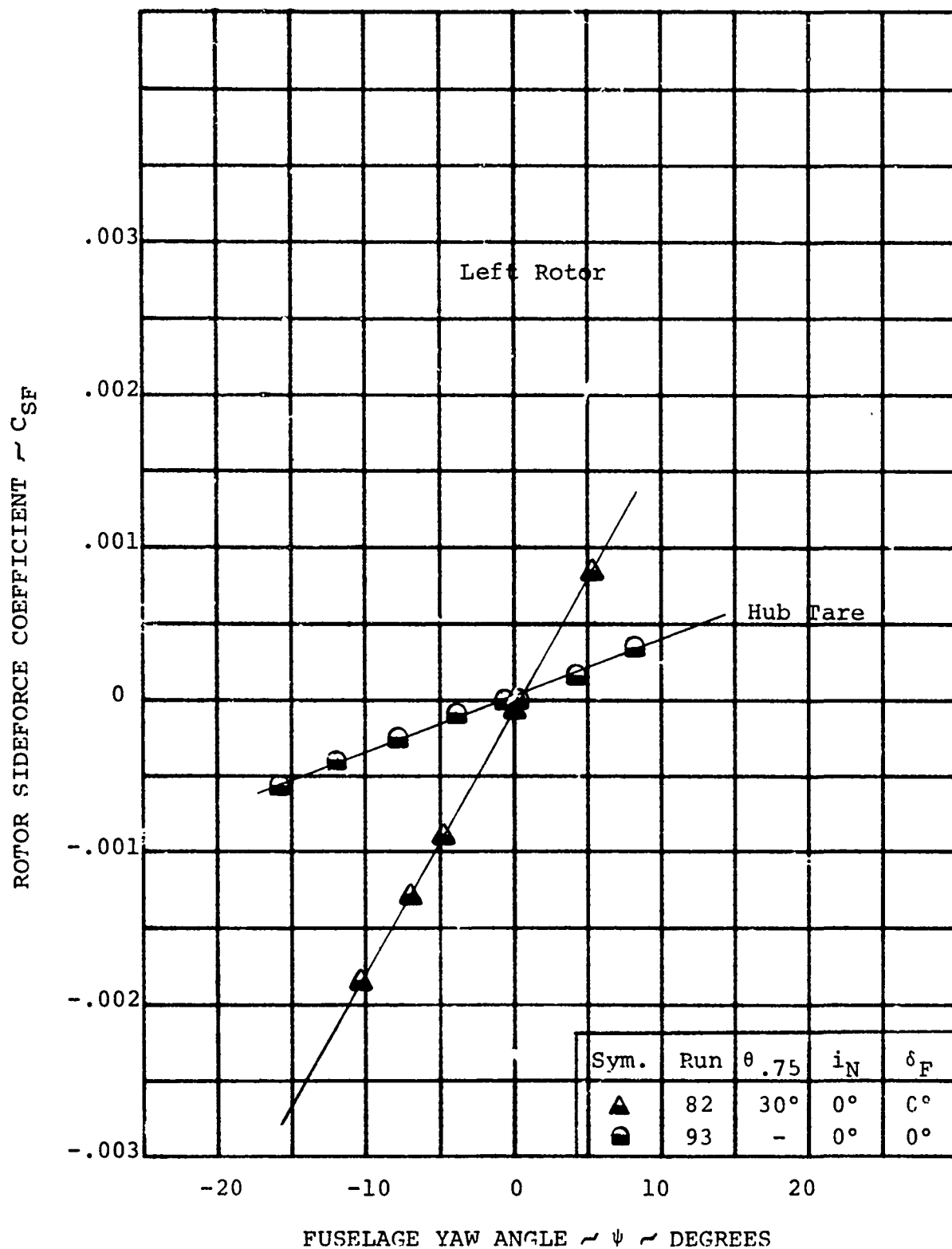


FIGURE 5-100

ROTOR SIDEFORCE/YAW ANGLE VARI-
ATION AT $V/V_T = 0.386$, $\delta_F = 0^\circ$

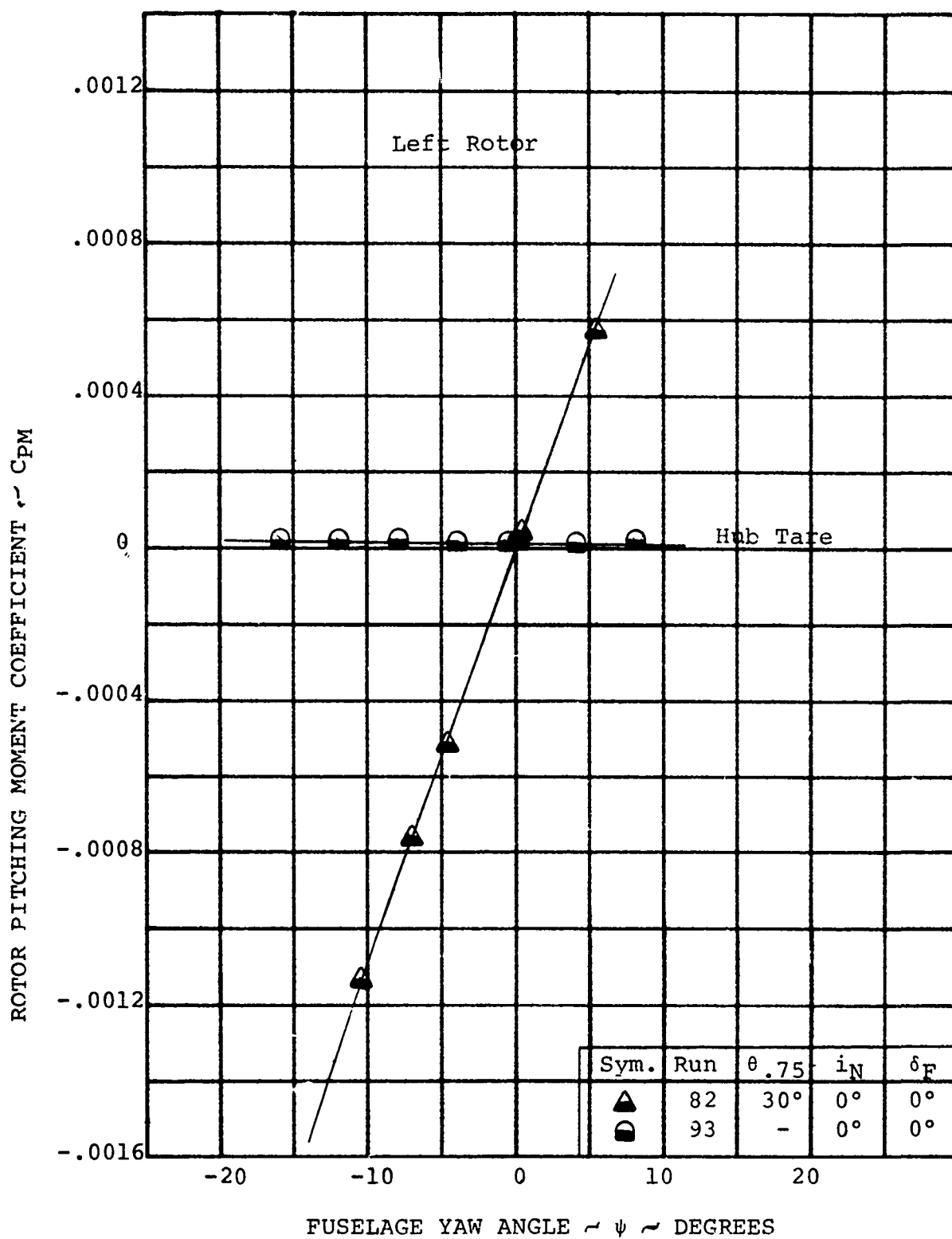


FIGURE 5-101

ROTOR PITCHING MOMENT/YAW ANGLE
VARIATION AT $V/V_T = 0.386$, $\delta_F = 0^\circ$

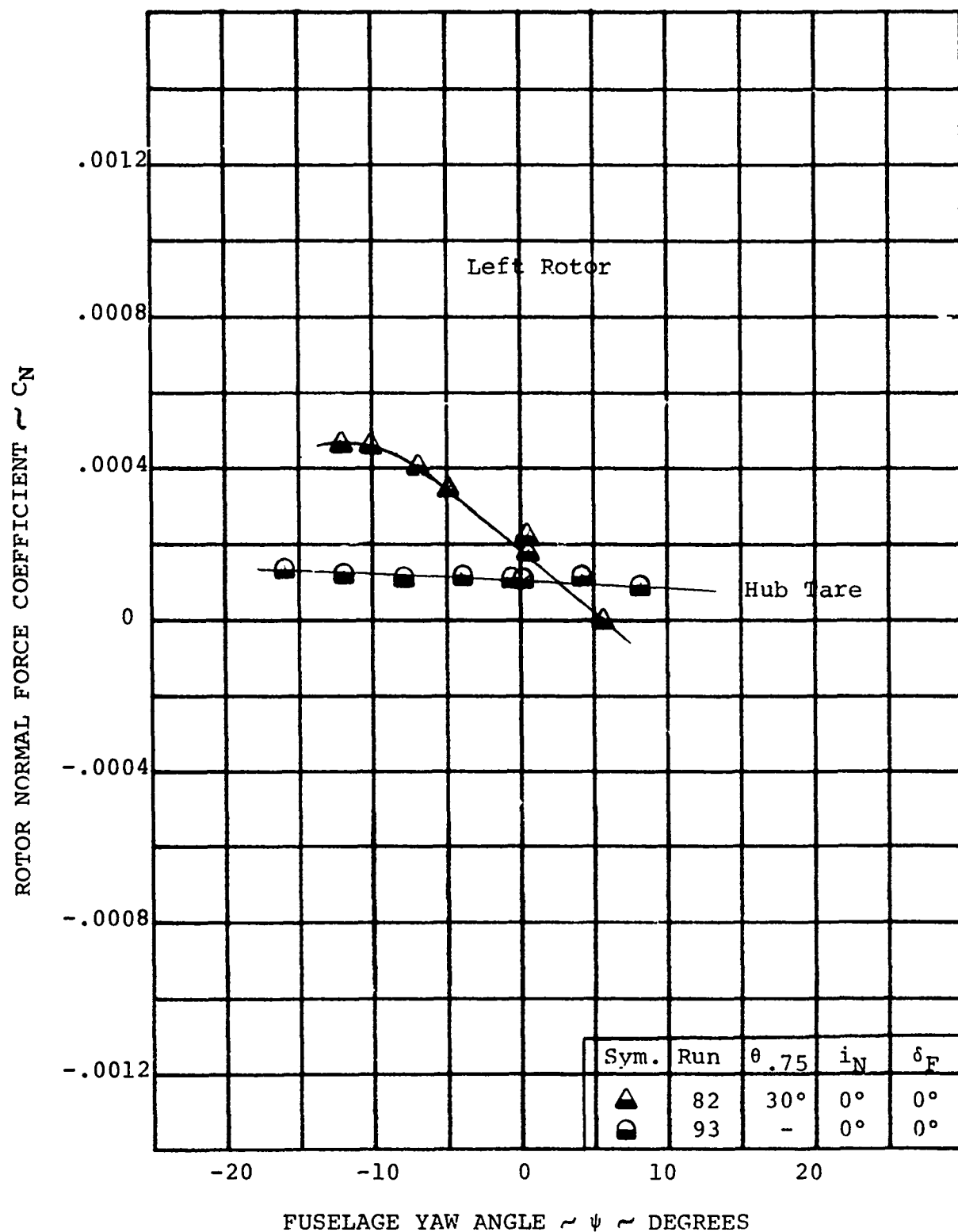


FIGURE 5-102

ROTOR NORMAL FORCE/YAW ANGLE VARIATION AT $V/V_T = 0.386$, $\delta_F = 0^\circ$

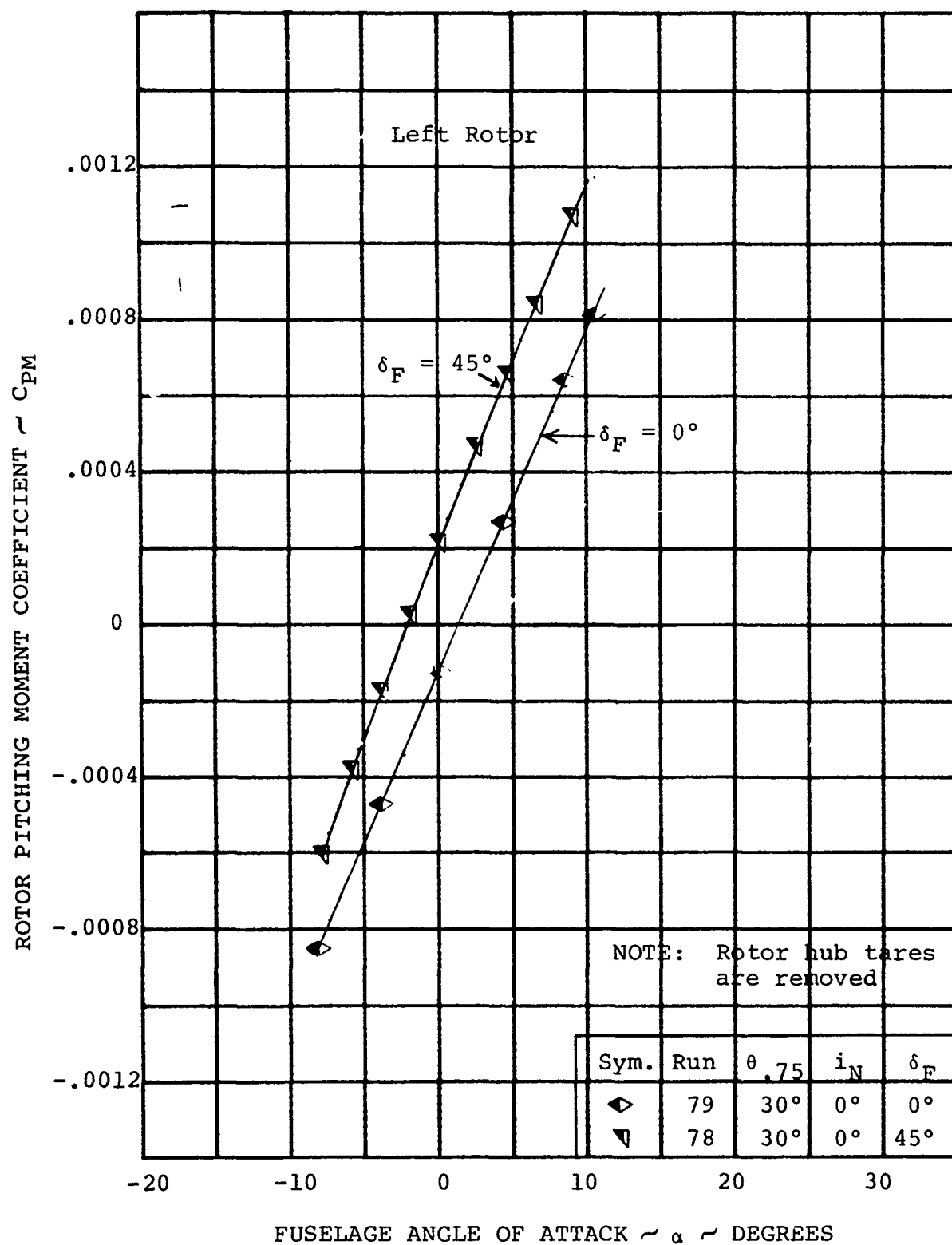


FIGURE 5-103

INFLUENCE OF FLAP DEFLECTION ON
ROTOR PITCHING MOMENT AT $V/V_T = 0.386$

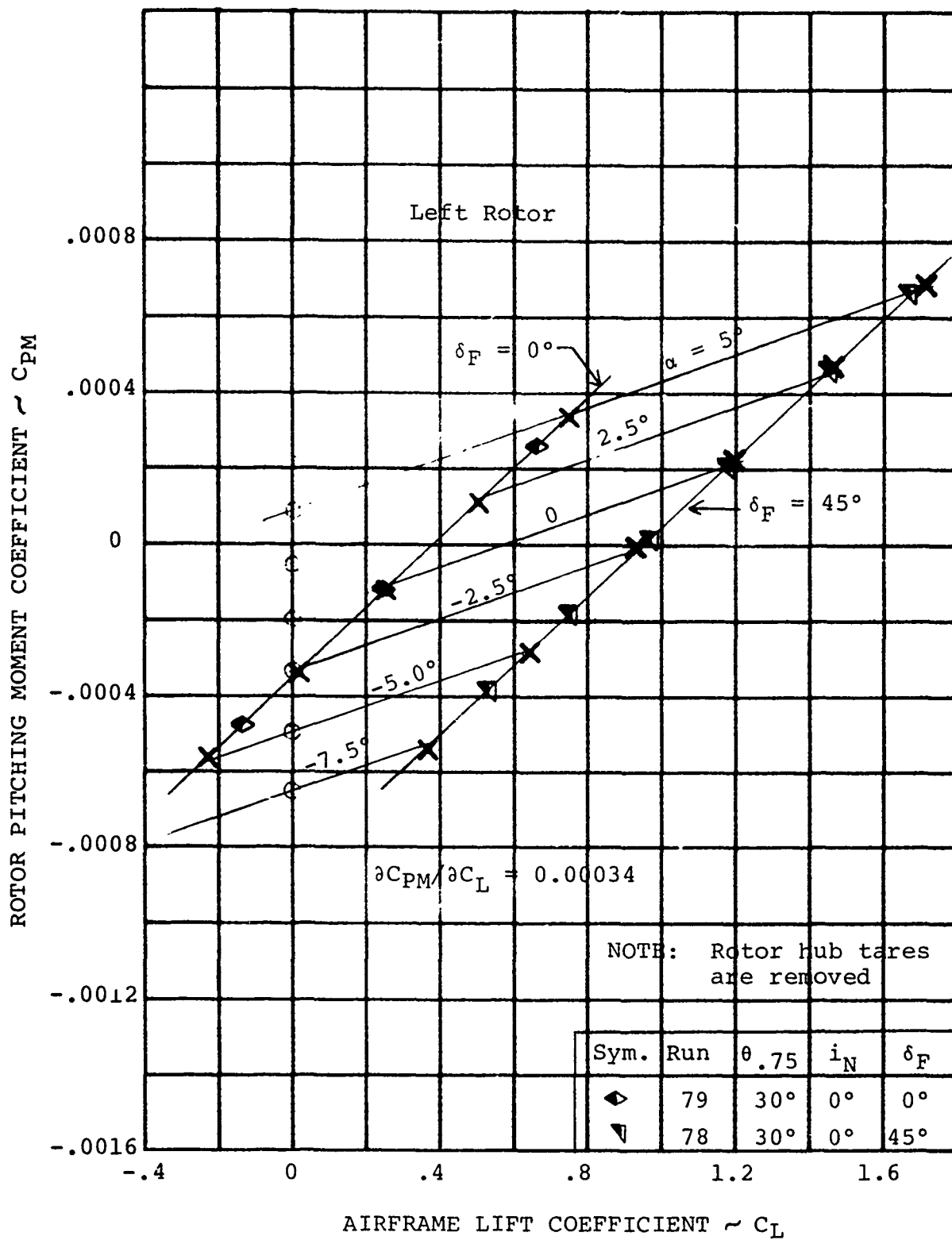


FIGURE 5-104

INFLUENCE OF WING LIFT ON ROTOR
PITCHING MOMENT AT $V/V_T = 0.386$

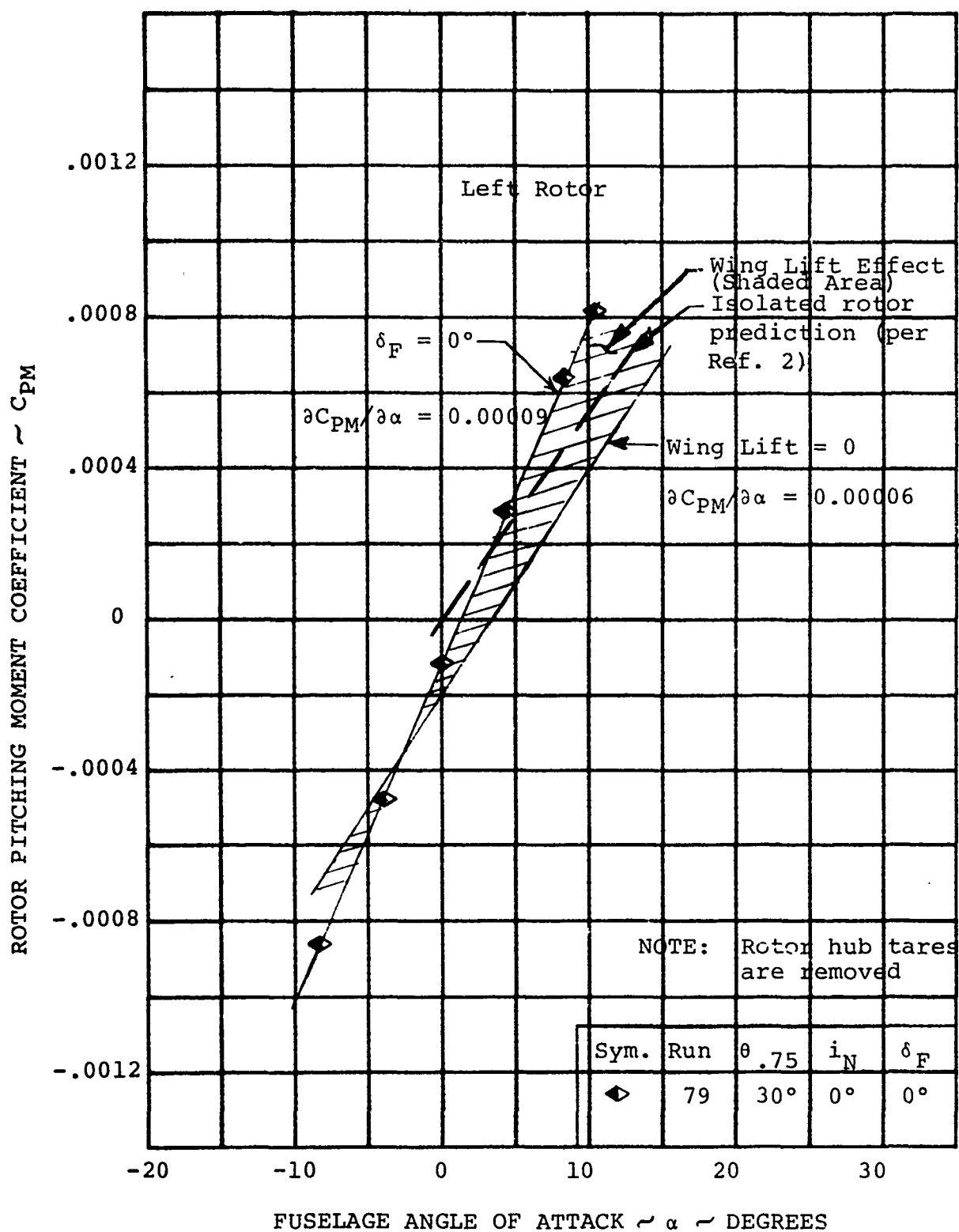


FIGURE 5-105

INFLUENCE OF WING LIFT ON ROTOR
PITCHING MOMENT AT $V/V_T = 0.386$

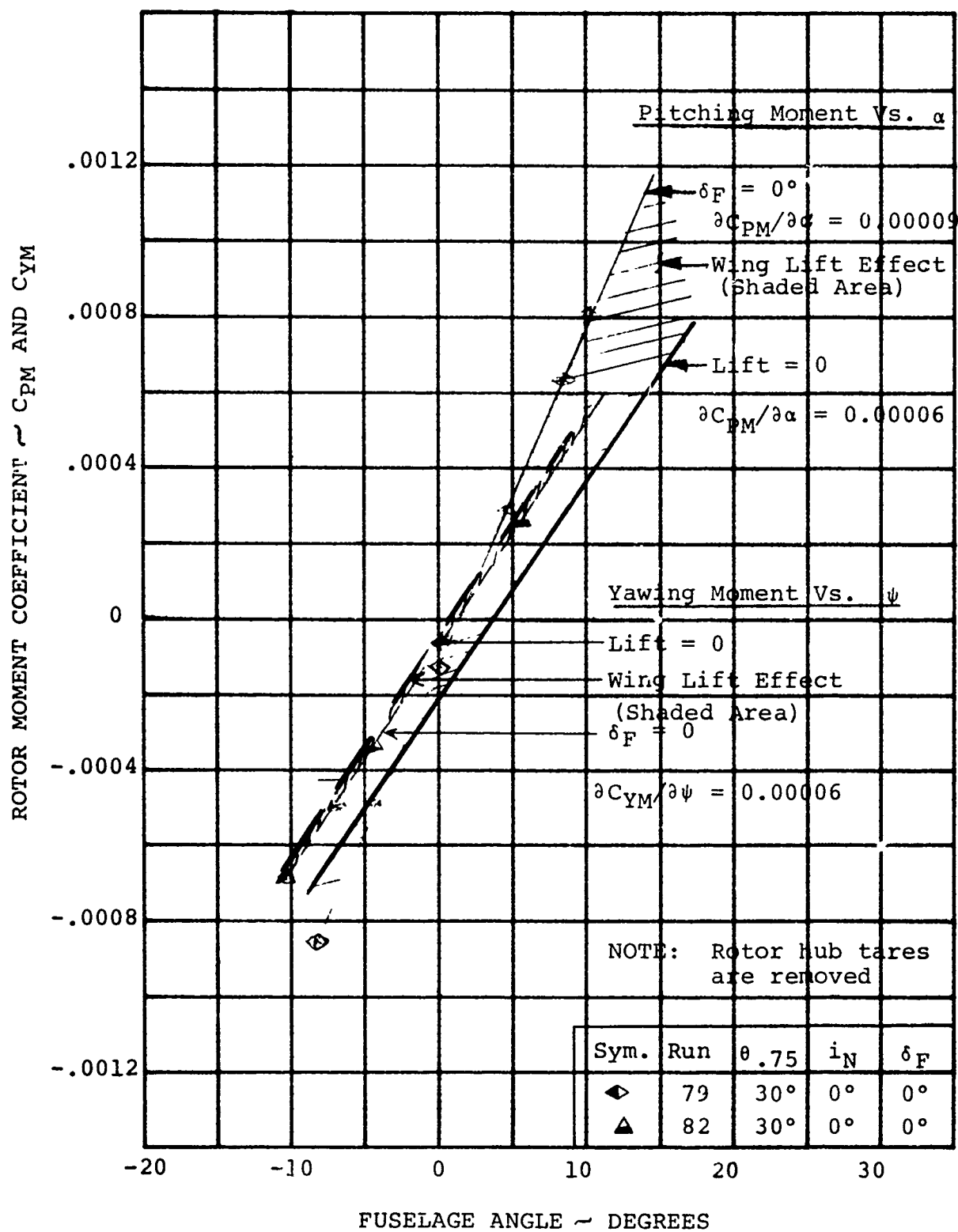


FIGURE 5-106

COMPARISON OF ROTOR MOMENT DERIVATIVES AT $V/V_T = 0.386$

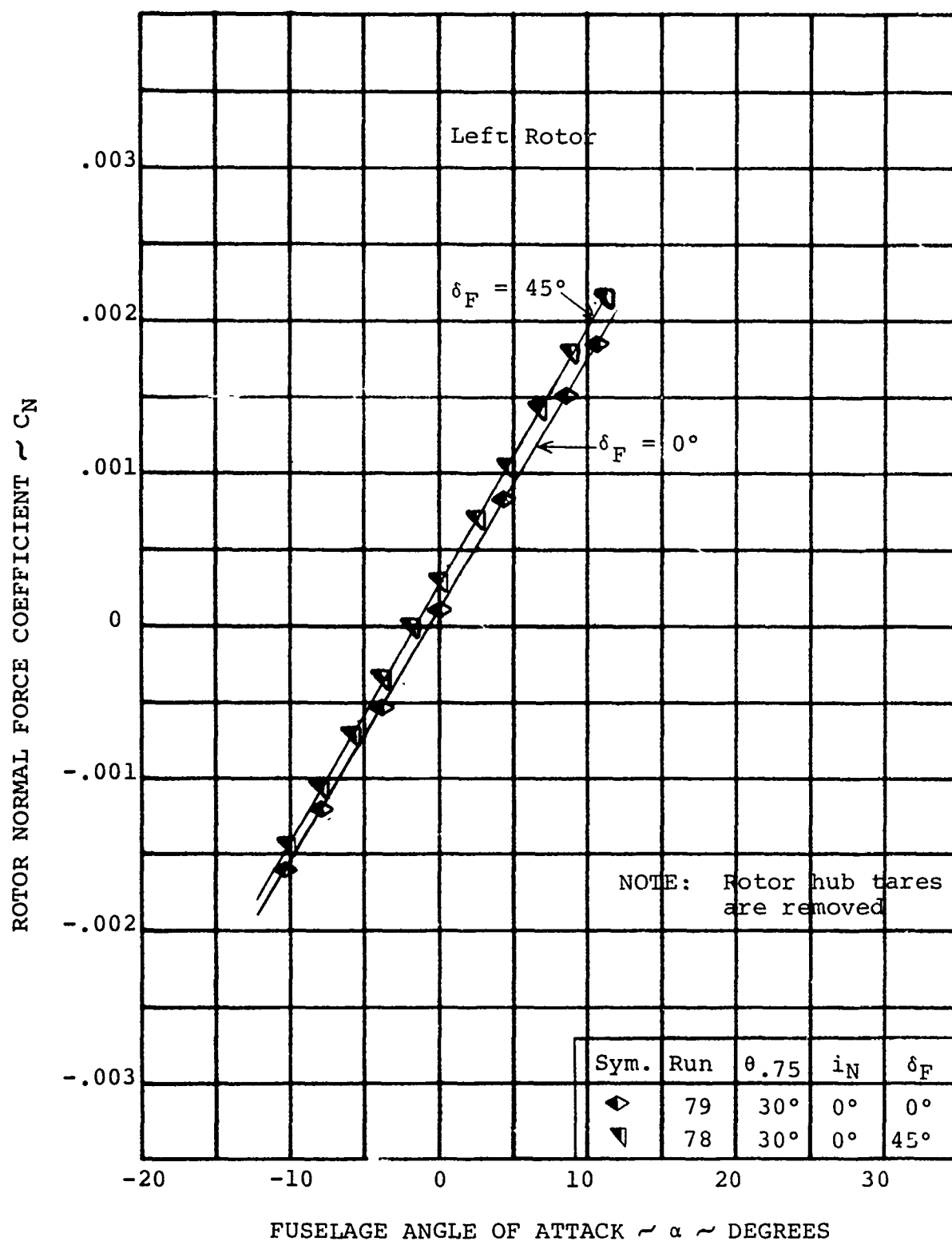


FIGURE 5-107

INFLUENCE OF FLAP DEFLECTION ON
ROTOR NORMAL FORCE AT $V/V_T = 0.386$

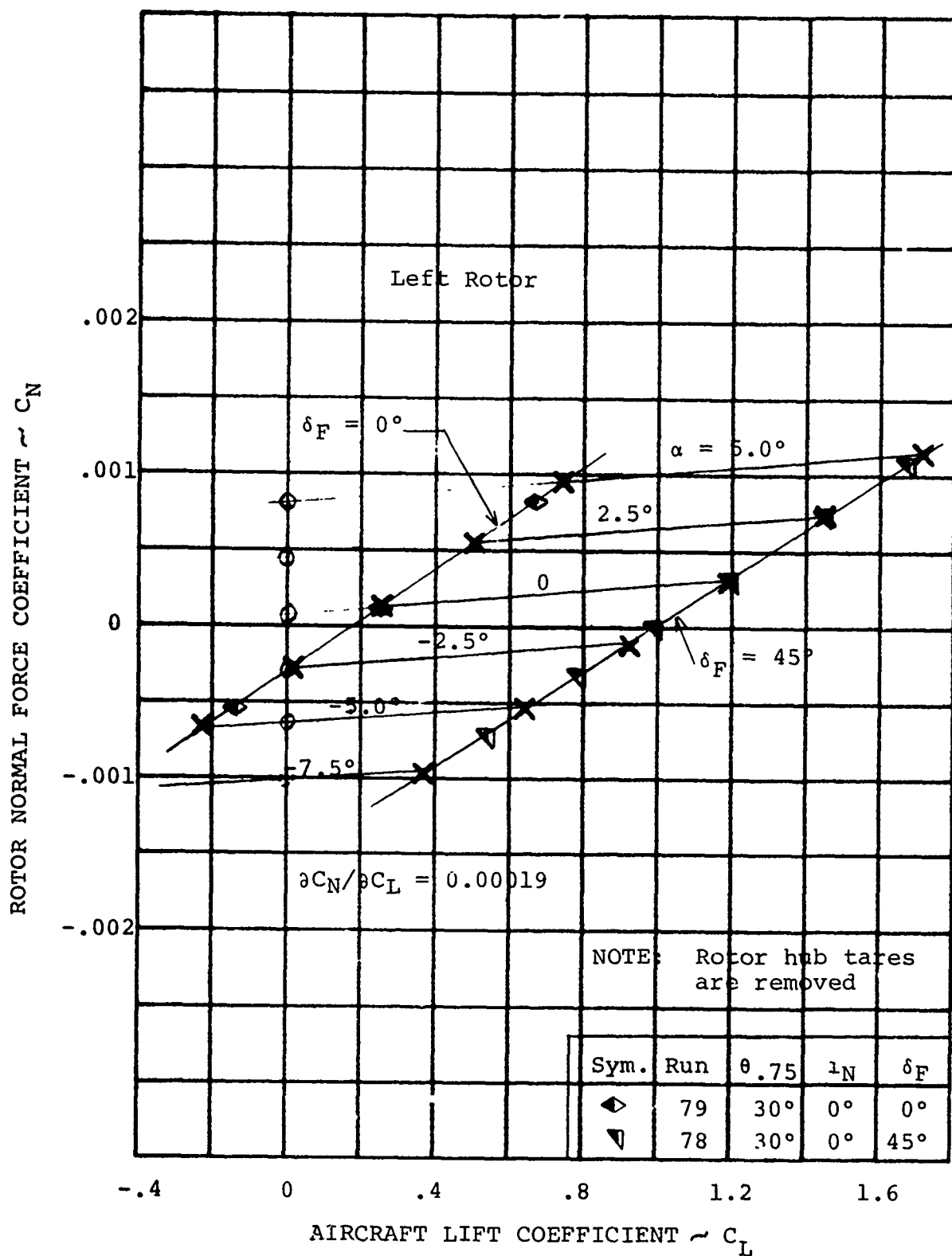


FIGURE 5-108

INFLUENCE OF WING ON ROTOR NORMAL
FORCE AT $V/V_T = 0.386$

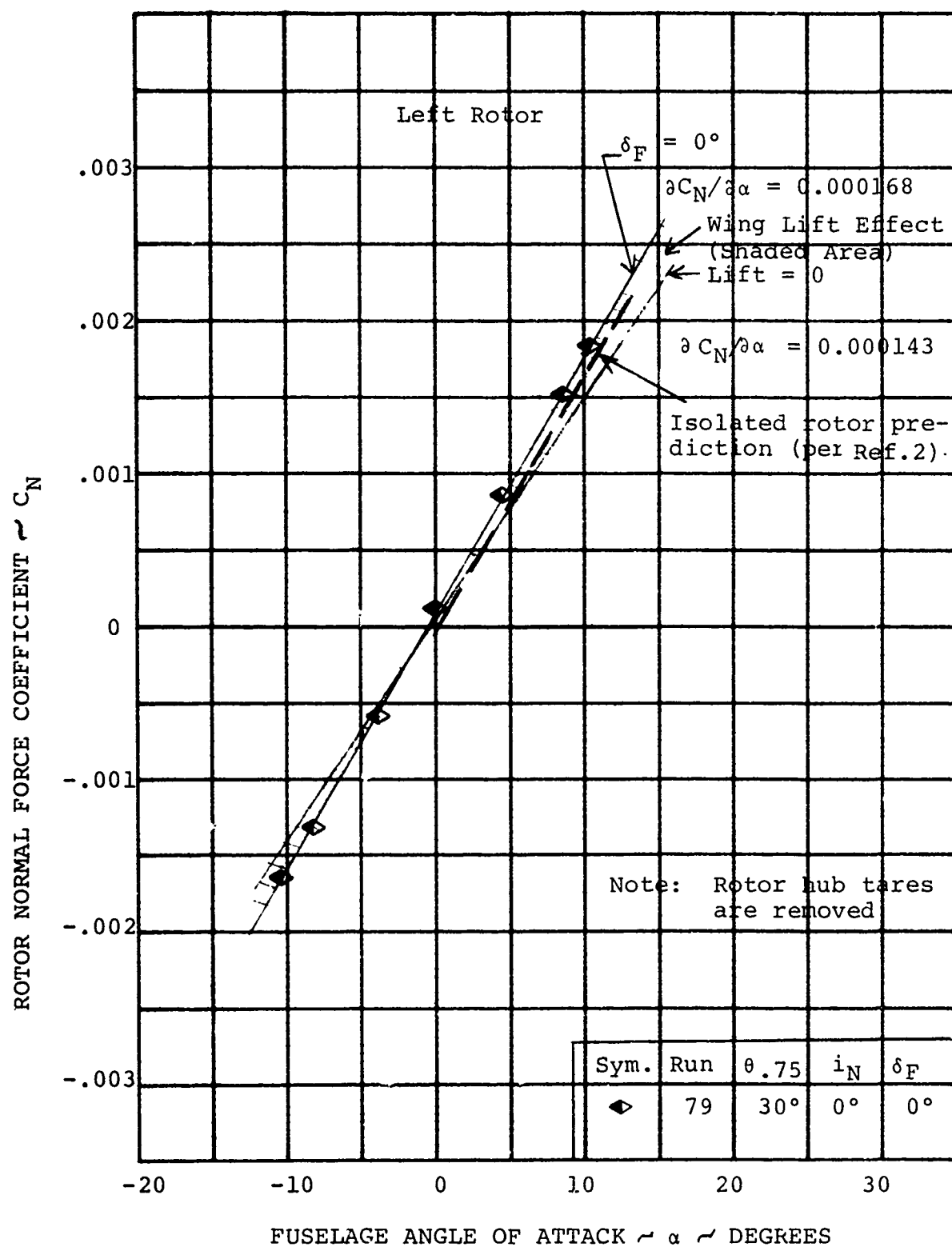


FIGURE 5-109

INFLUENCE OF WING LIFT ON ROTOR NORMAL FORCE AT $V/V_T = 0.386$

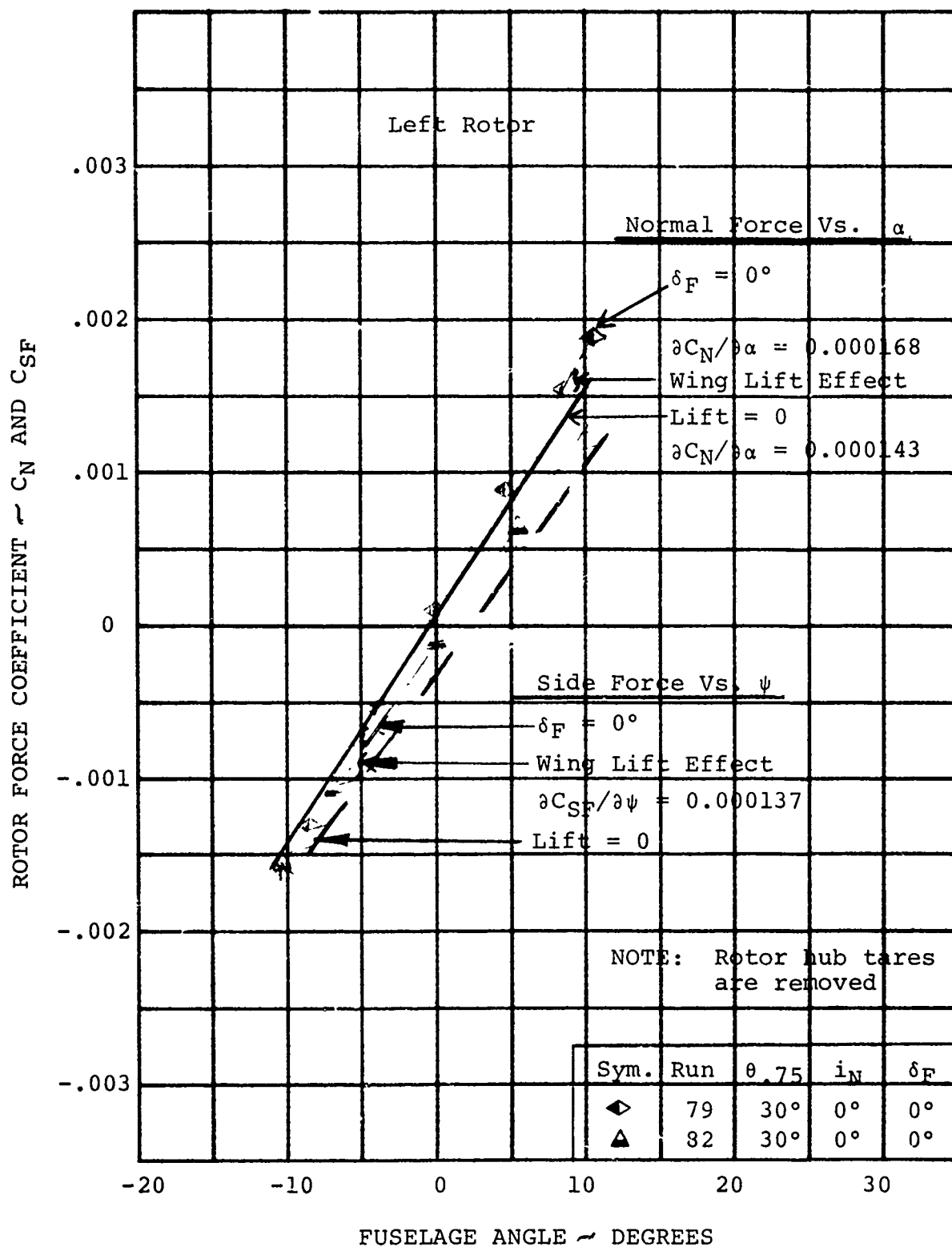


FIGURE 5-110

COMPARISON OF ROTOR FORCE DERIVATIVES
 $\partial C_N / \partial \alpha$ AND $\partial C_{SF} / \partial \psi$ AT $V/V_T = 0.386$

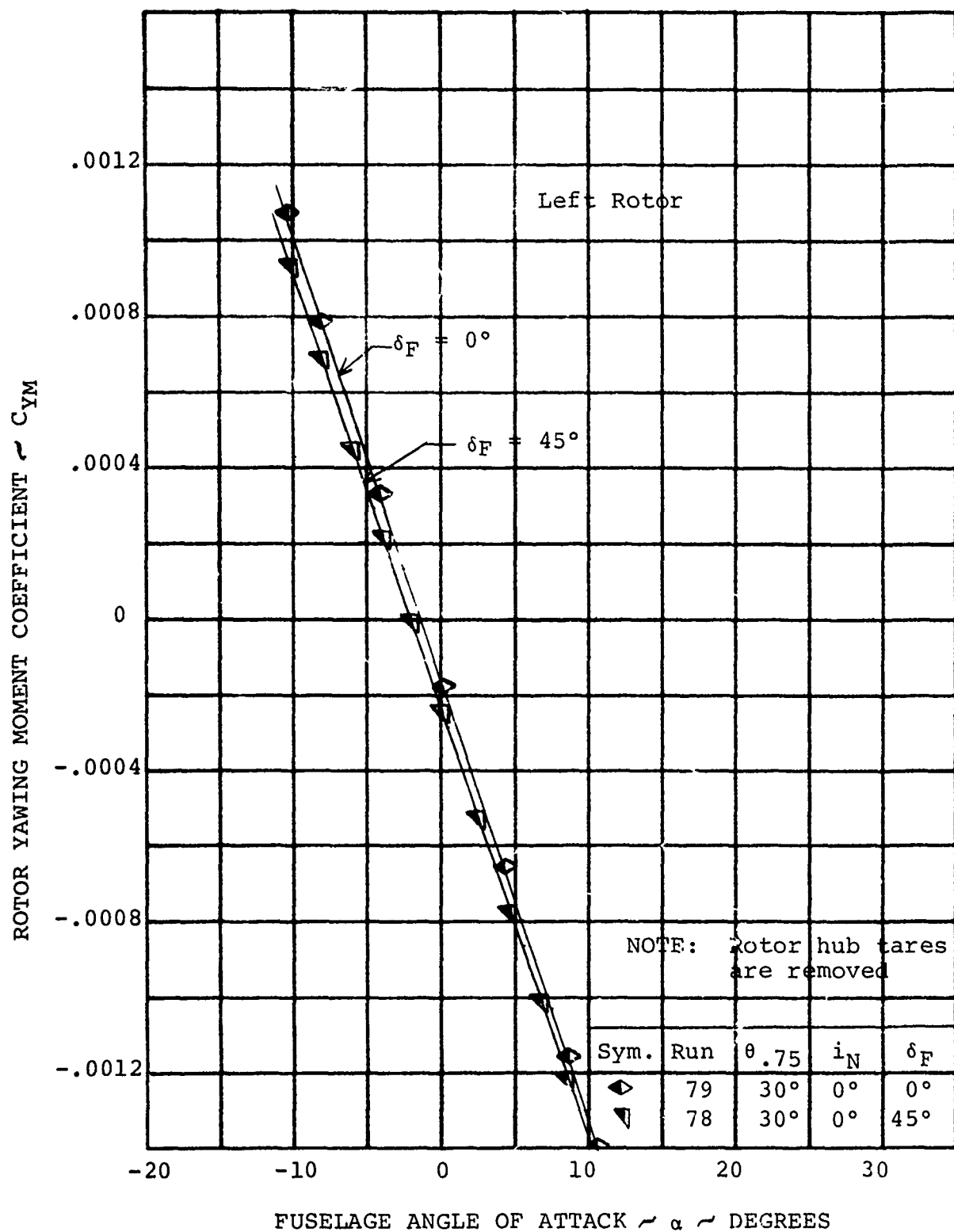


FIGURE 5-111

INFLUENCE OF FLAP DEFLECTION ON ROTOR
YAWING MOMENT AT $V/V_T = 0.386$

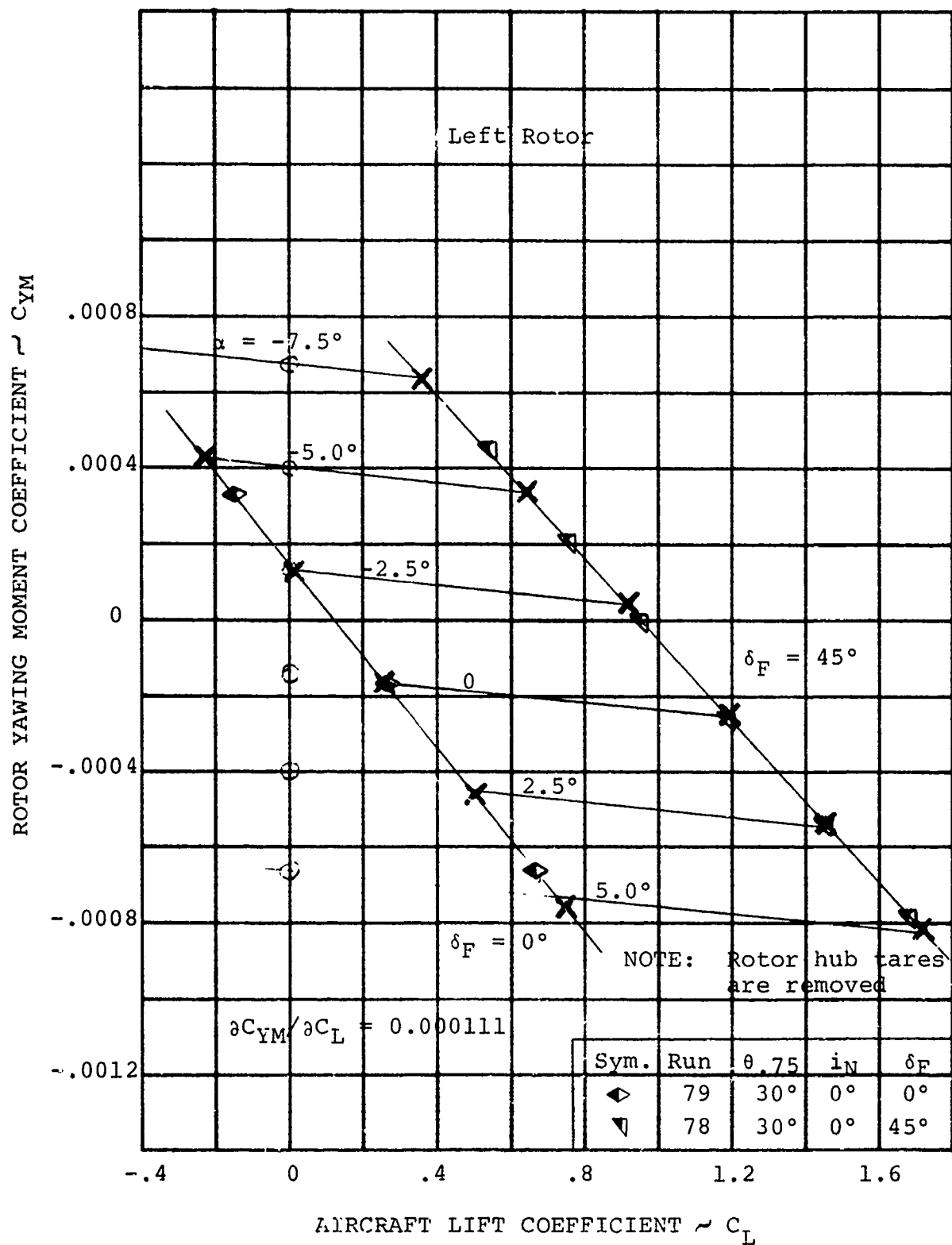


FIGURE 5-112 INFLUENCE OF WING LIFT ON ROTOR YAWING MOMENT AT $V/V_T = 0.386$

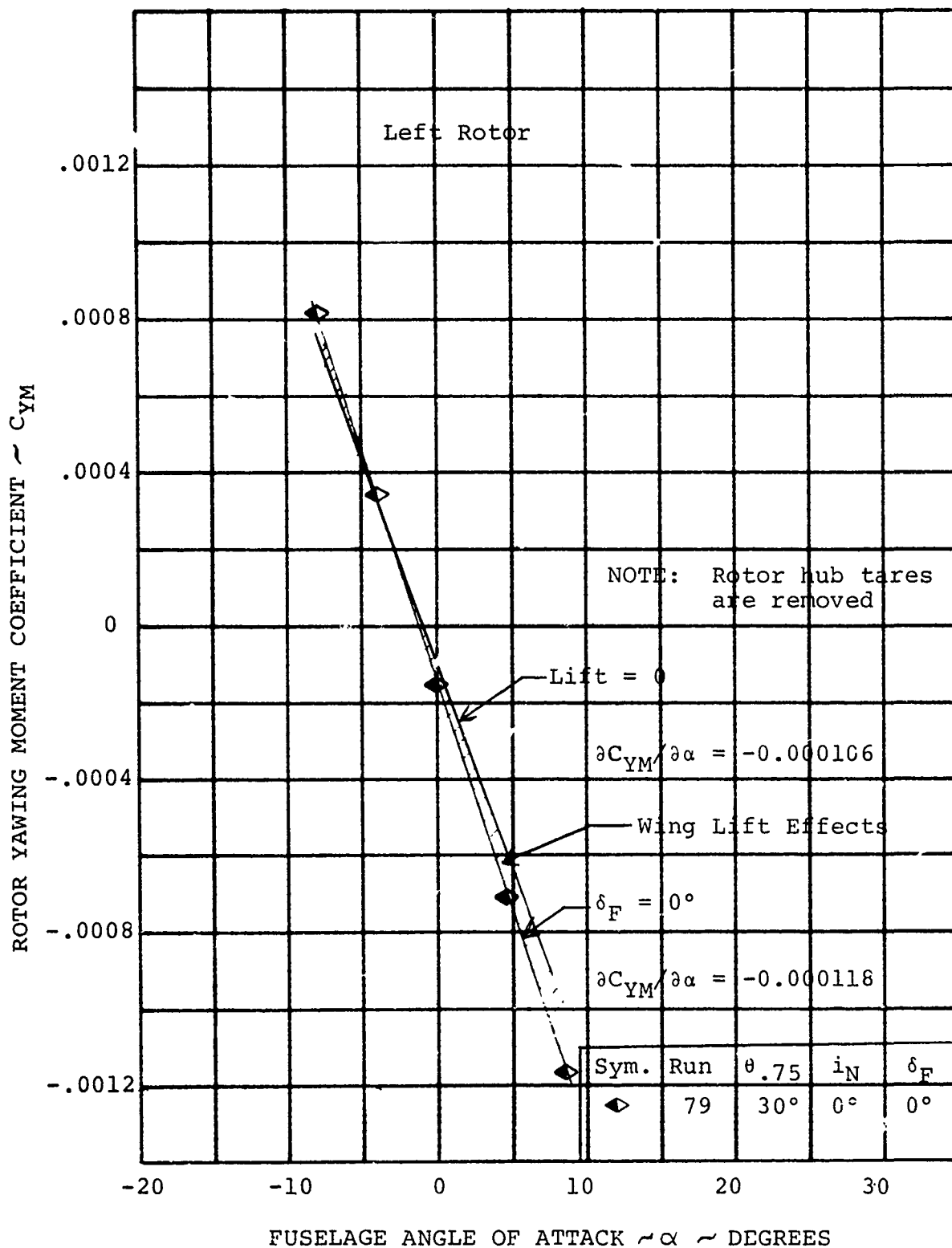


FIGURE 5-113

INFLUENCE OF WING LIFT ON ROTOR
YAWING MOMENT AT $V/V_T = 0.386$

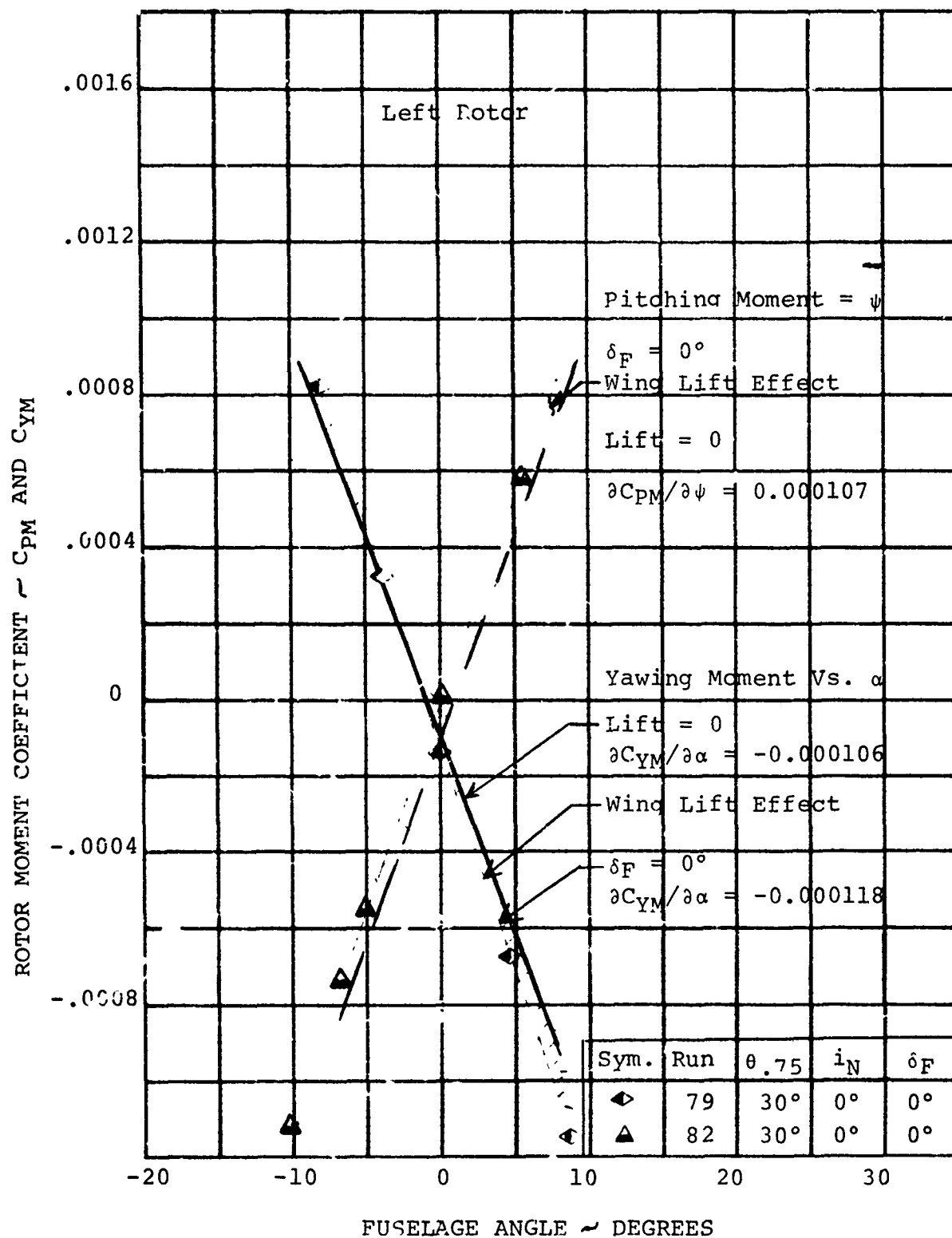


FIGURE 5-114

COMPARISON OF ROTOR MOMENT DERIVATIVES
 $\partial C_{YM} / \partial \alpha$ AND $\partial C_{PM} / \partial \psi$ AT $V/V_T = 0.386$

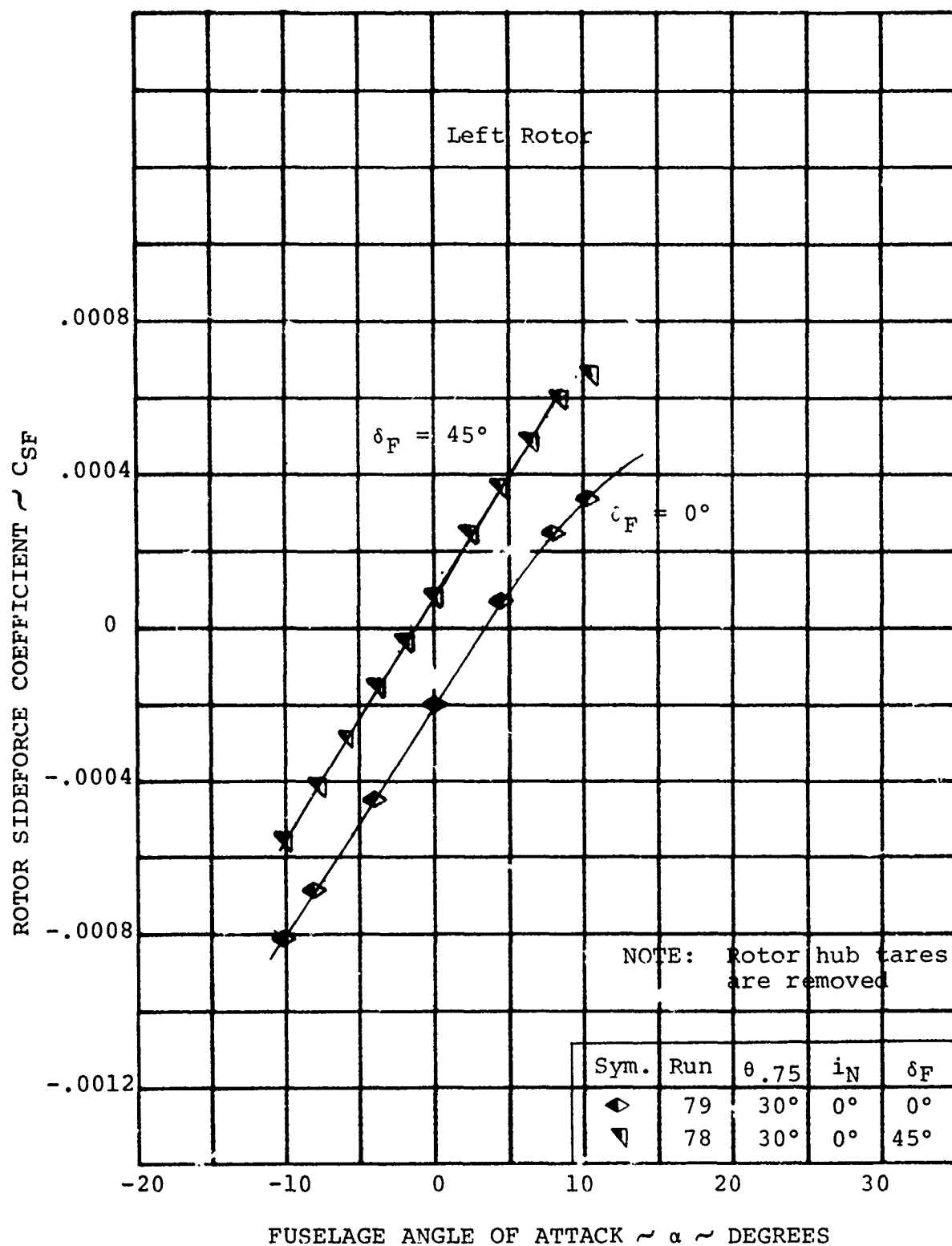


FIGURE 5-115

INFLUENCE OF FLAP DEFLECTION ON ROTOR
SIDEFORCE AT $V/V_T = 0.386$

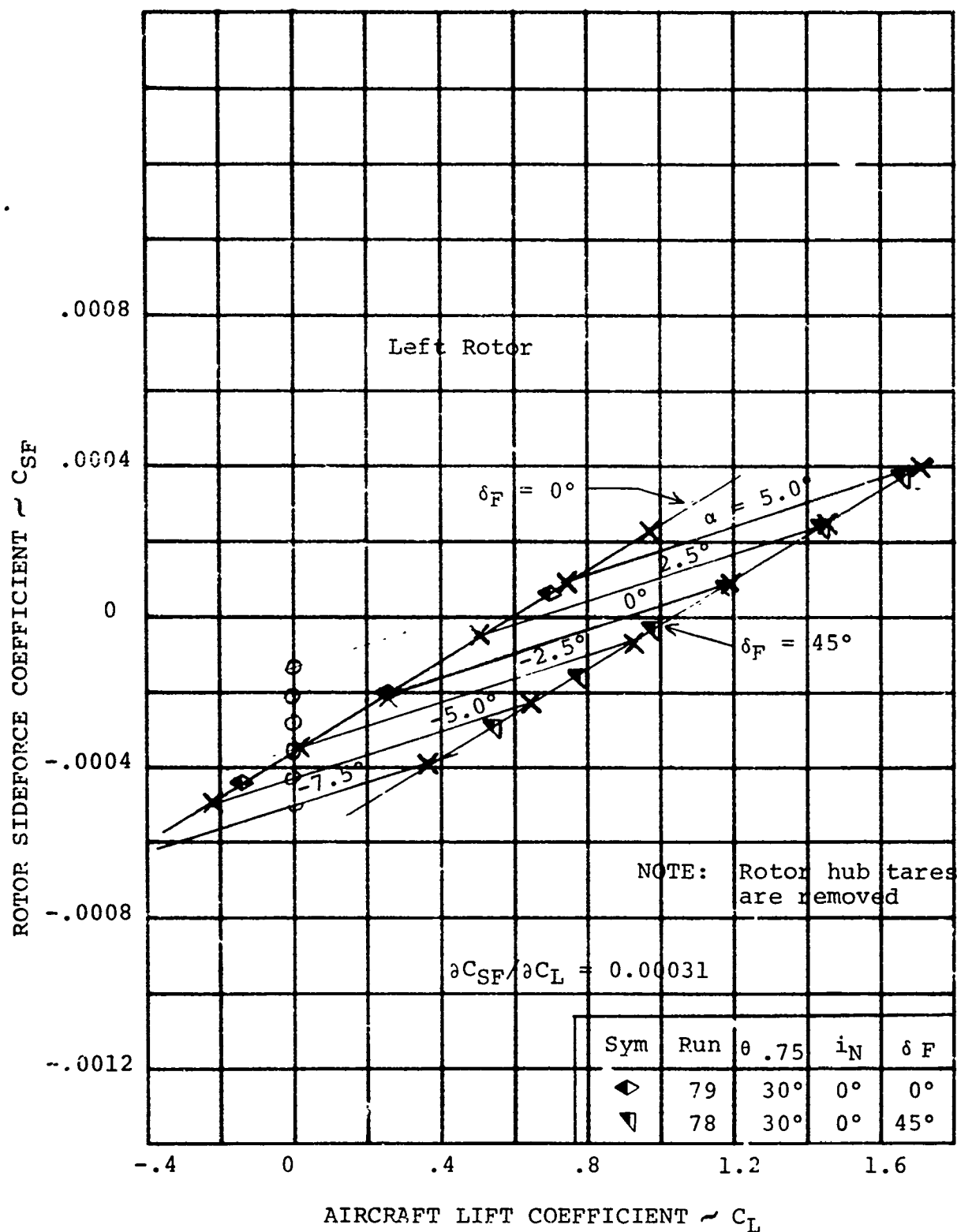


FIGURE 5-116

INFLUENCE OF WING LIFT ON ROTOR SIDE-
FORCE AT $V/V_T = 0.386$

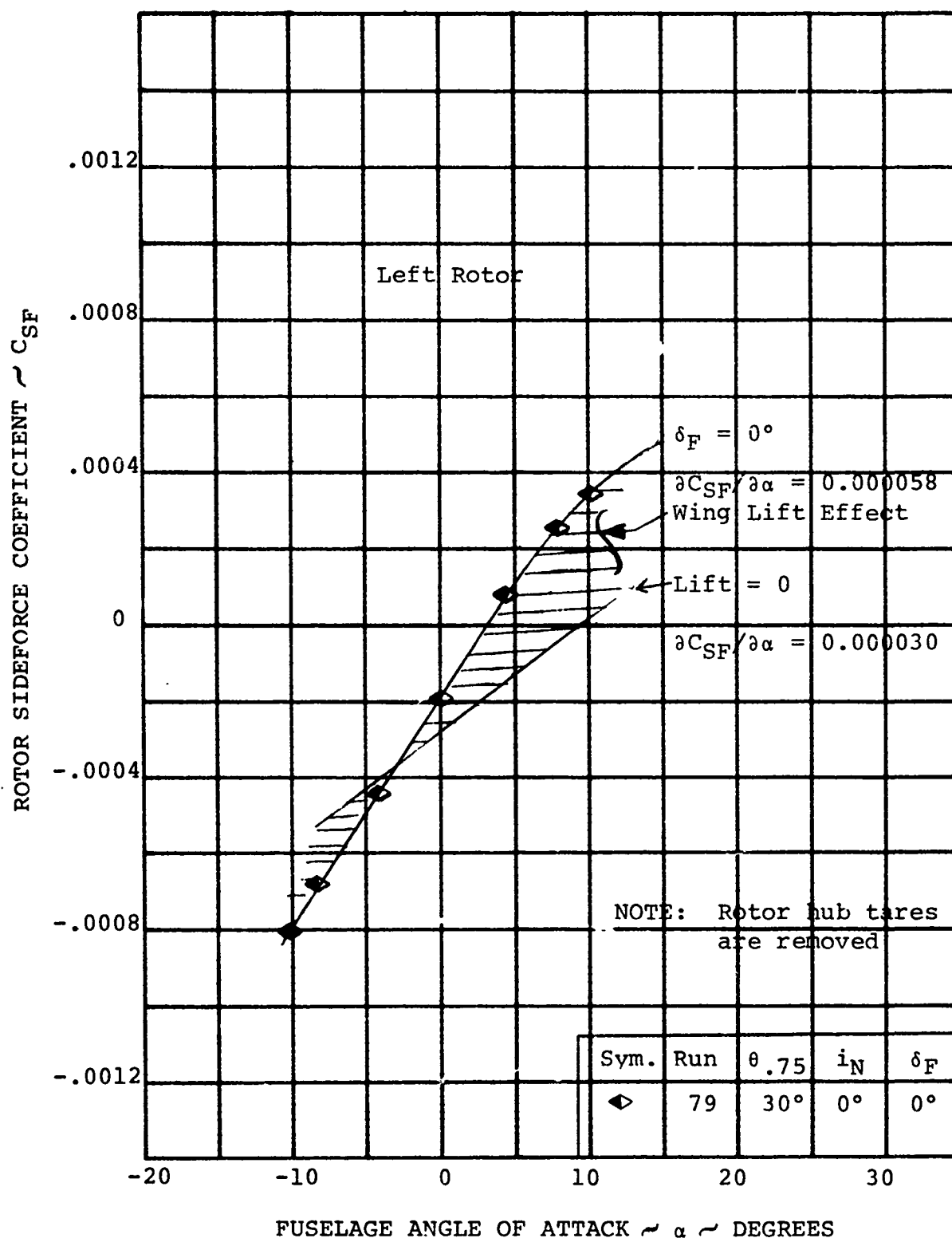


FIGURE 5-117

INFLUENCE OF WING LIFT ON ROTOR SIDE-
FORCE AT $V/V_T = 0.386$

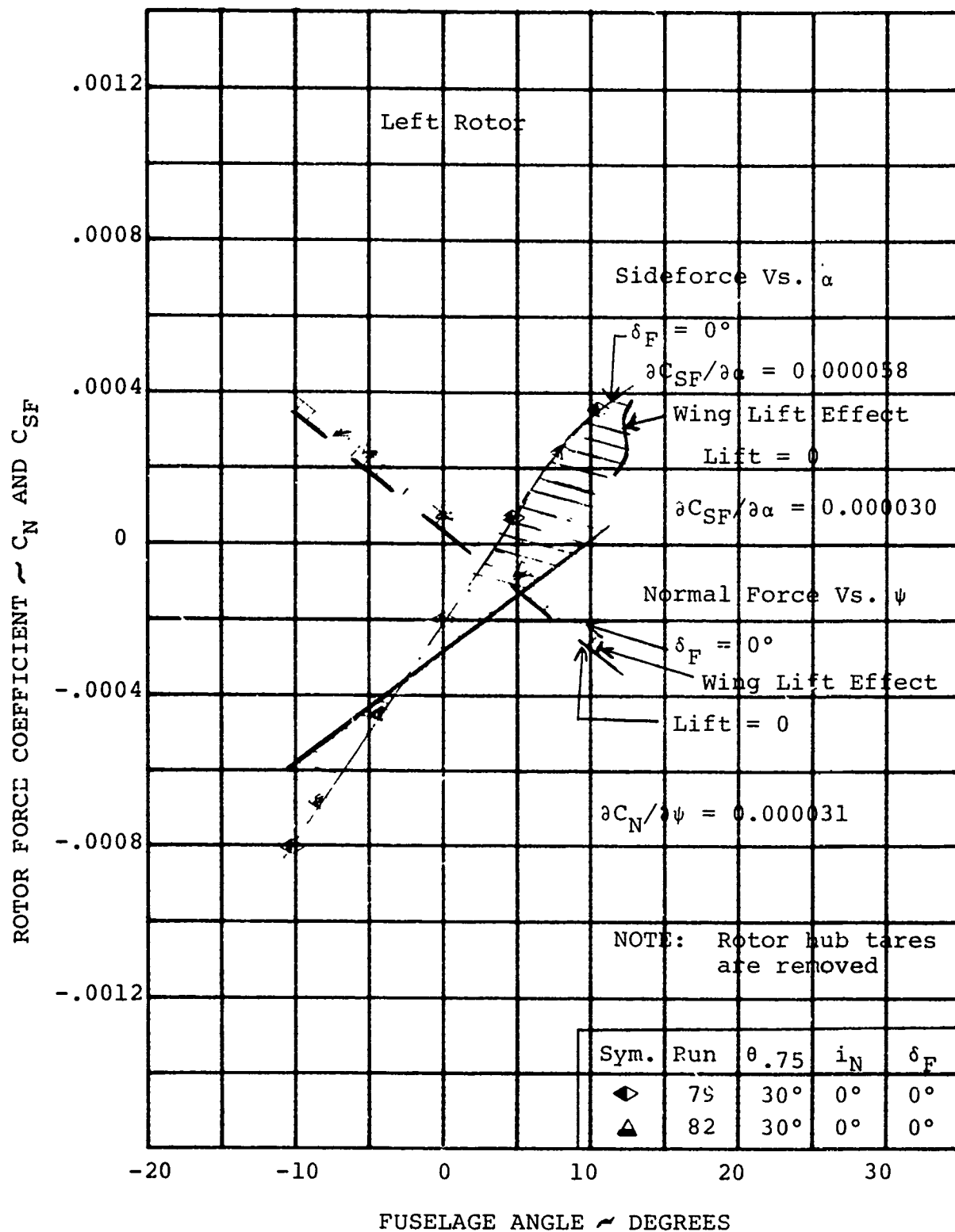


FIGURE 5-118

COMPARISON OF ROTOR FORCE DERIVATIVES
 $\partial C_{SF} / \partial \alpha$ AND $\partial C_N / \partial \psi$ AT $V/V_T = 0.386$

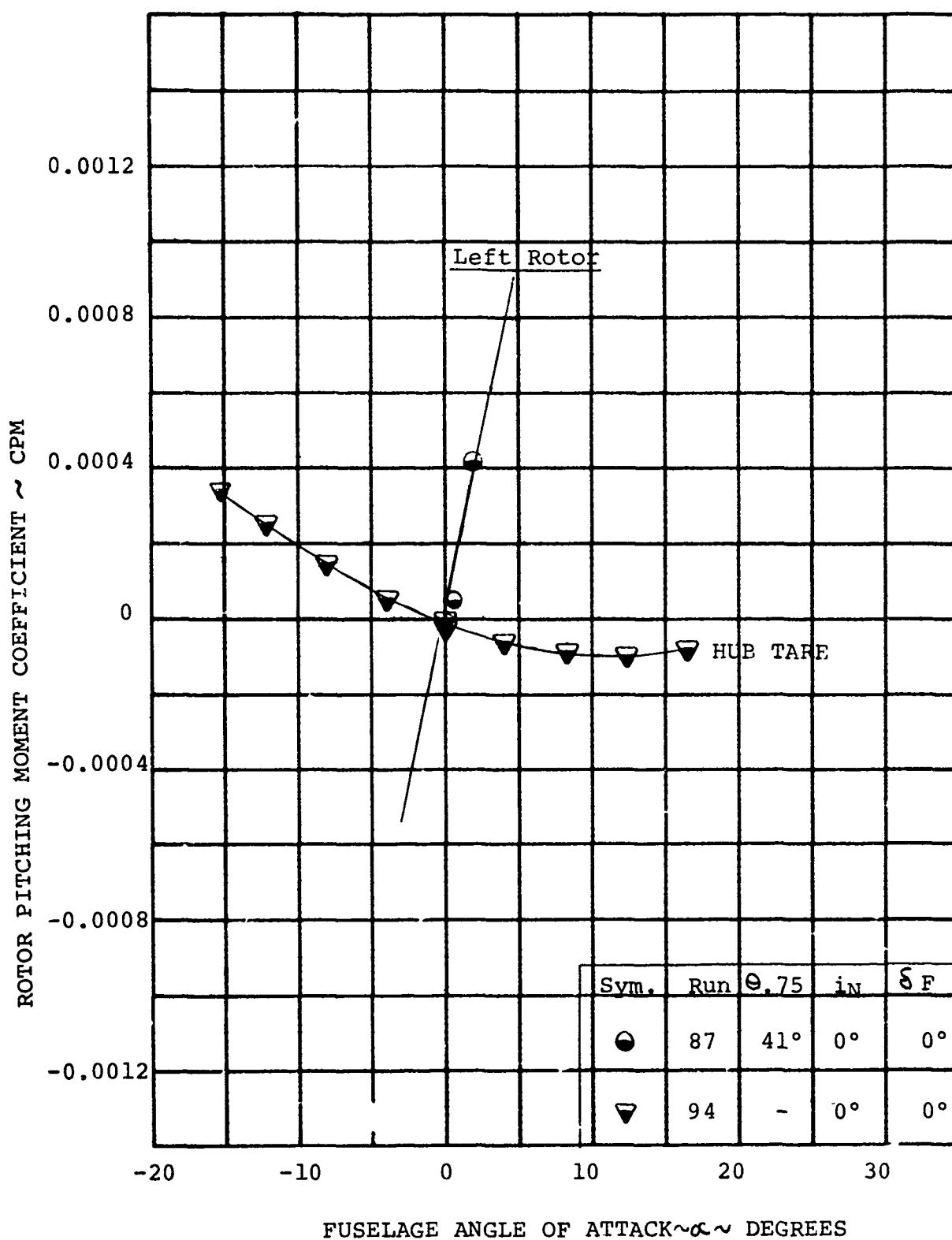


FIGURE 5-119 ROTOR PITCHING MOMENT/ANGLE OF ATTACK VARIATION AT $V/V_T = 0.57$, $\delta_F = 0^\circ$

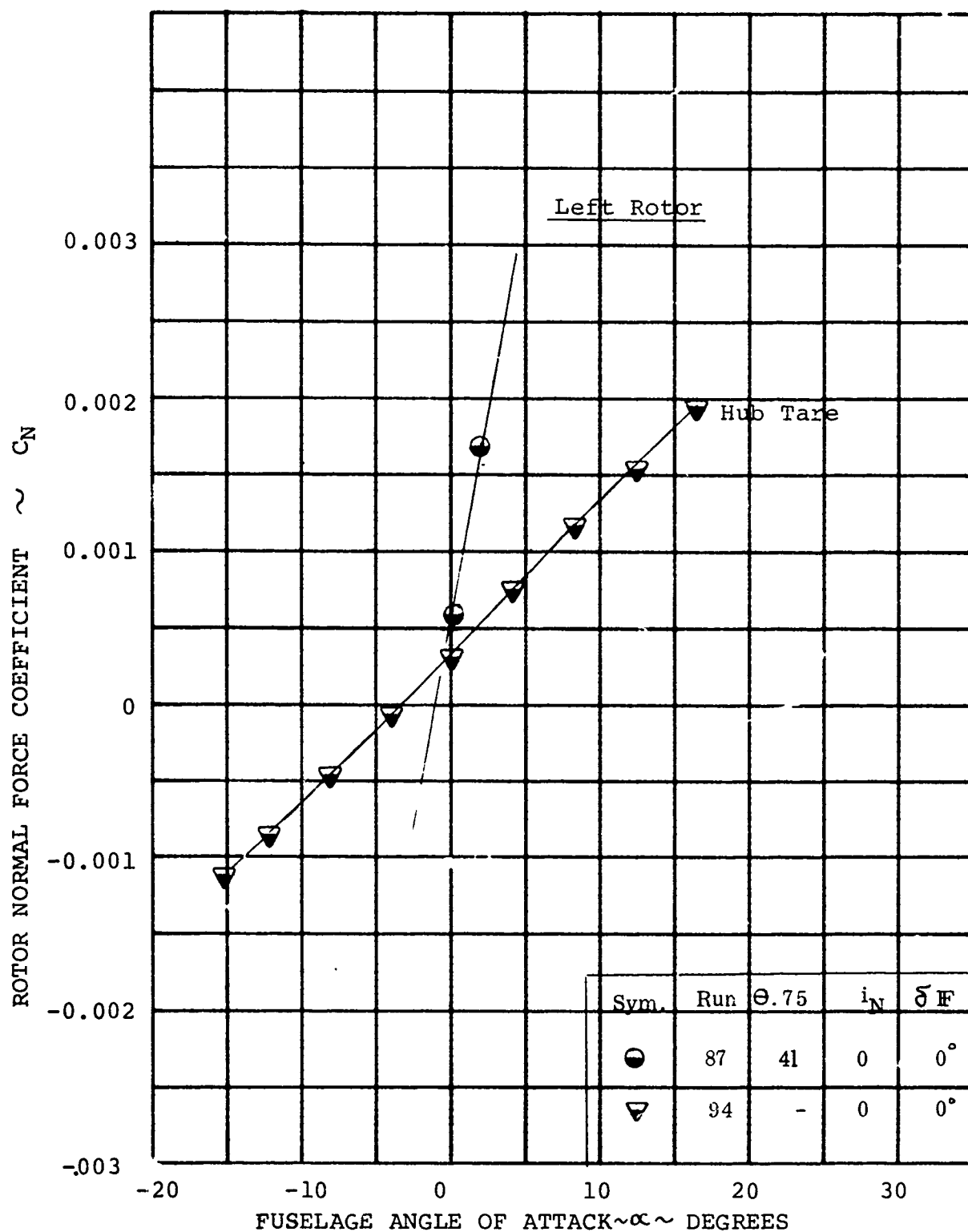


FIGURE 5-120 ROTOR NORMAL FORCE/ANGLE OF ATTACK VARIATION AT $V/V_T = 0.57$, $\delta_F = 0^\circ$

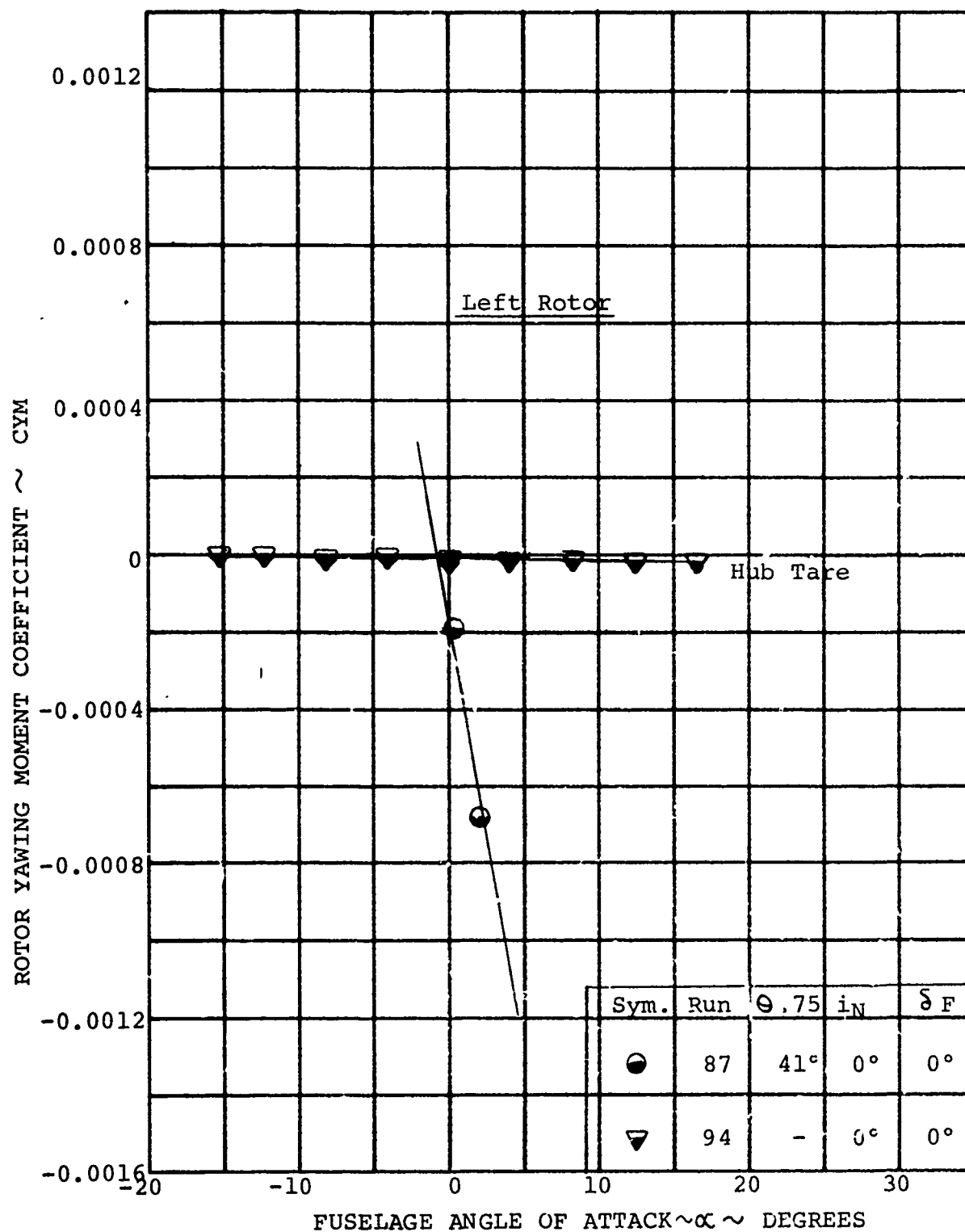


FIGURE 5-121 ROTOR YAWING MOMENT/ANGLE OF ATTACK
VARIATION $V/V_T = 0.57$ $\delta_F = 0^\circ$

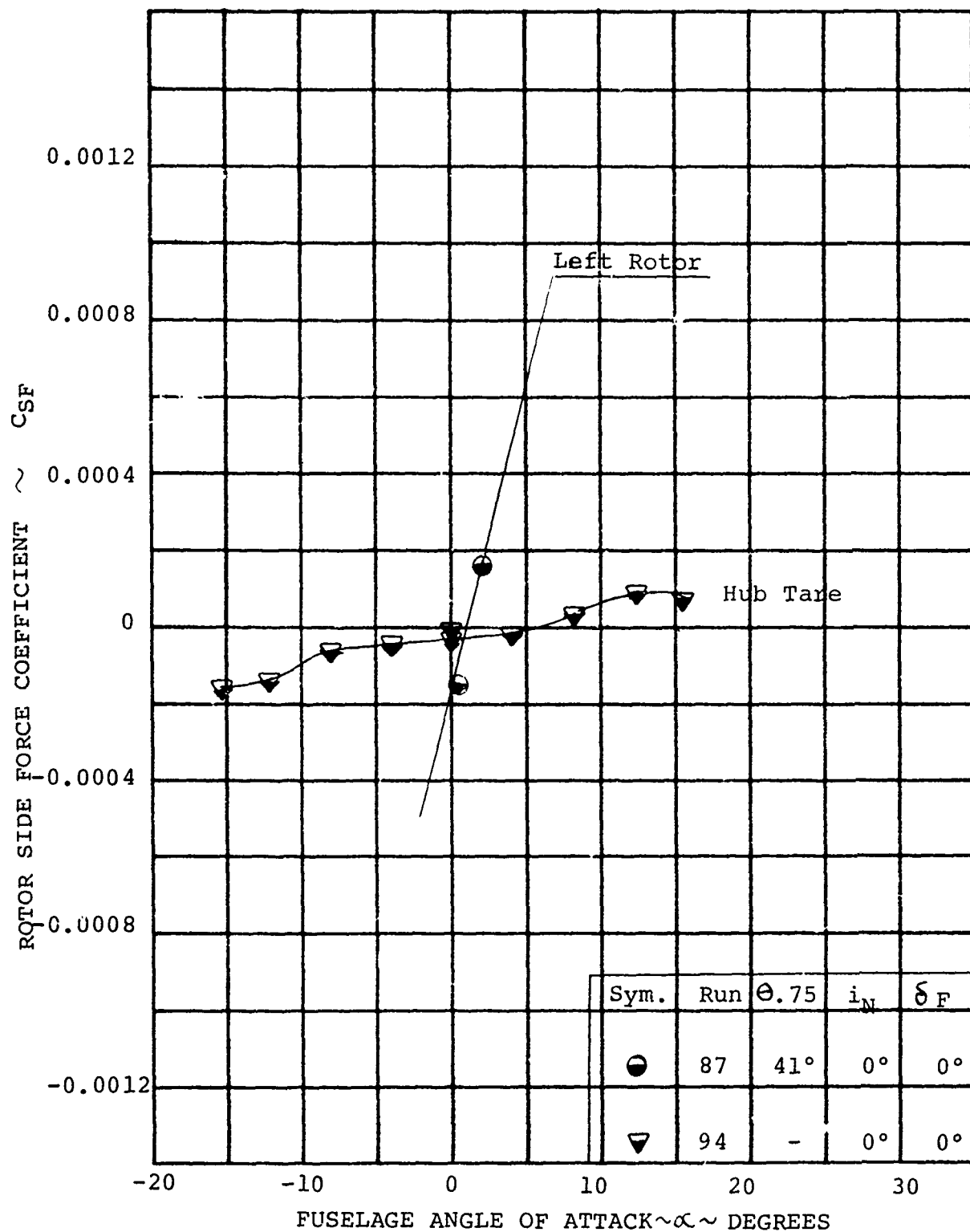


FIGURE 5-122 ROTOR SIDE FORCE/ANGLE OF ATTACK VARIATION AT $V/V_T = 0.57$ $\delta_F = 0^\circ$

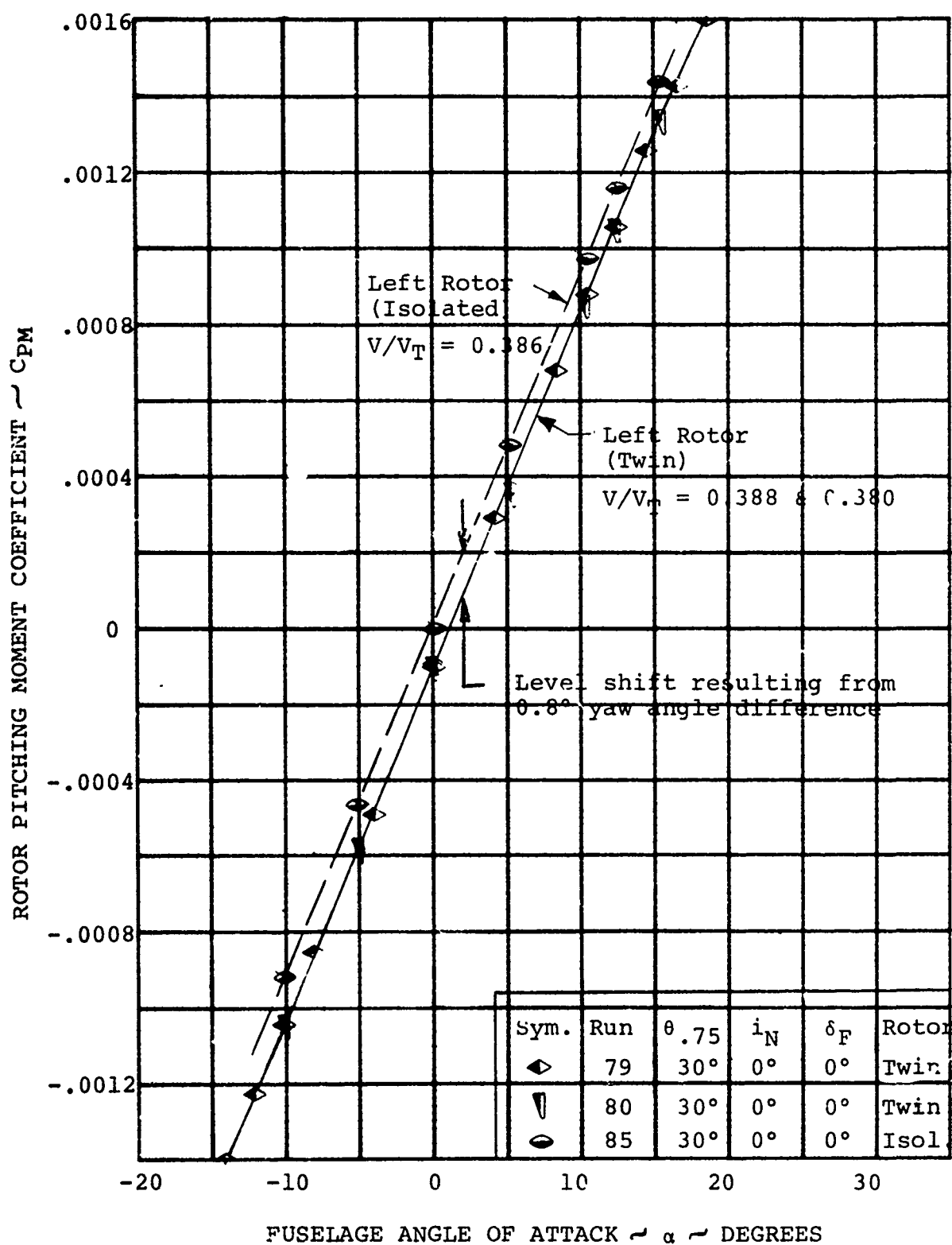


FIGURE 5-123 ROTOR/ROTOR INTERFERENCE EFFECTS ON CRUISE ROTOR CHARACTERISTICS, $V/V_T = 0.386$

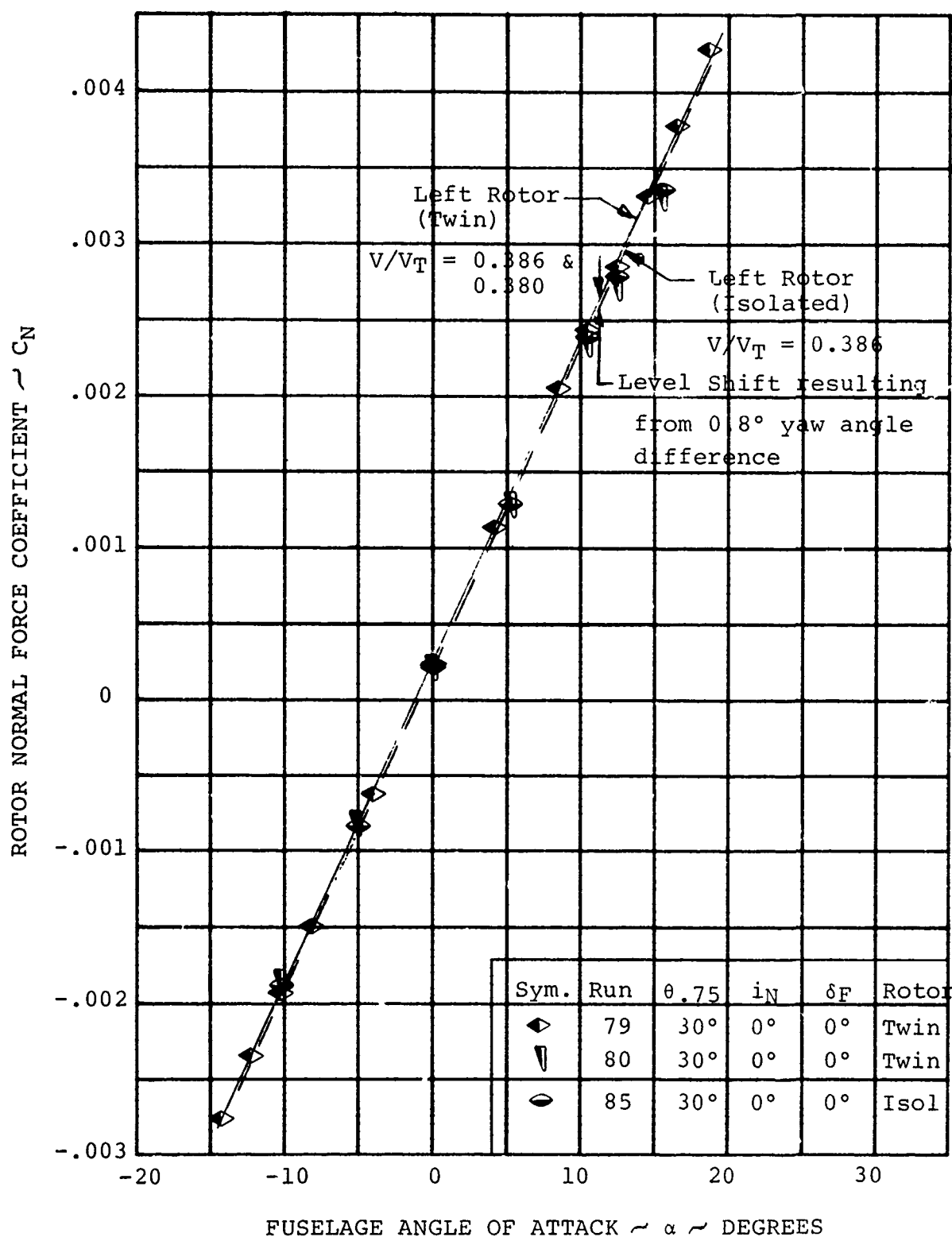


FIGURE 5-124 ROTOR/ROTOR INTERFERENCE EFFECTS ON CRUISE ROTOR CHARACTERISTICS, $V/V_T = 0.386$

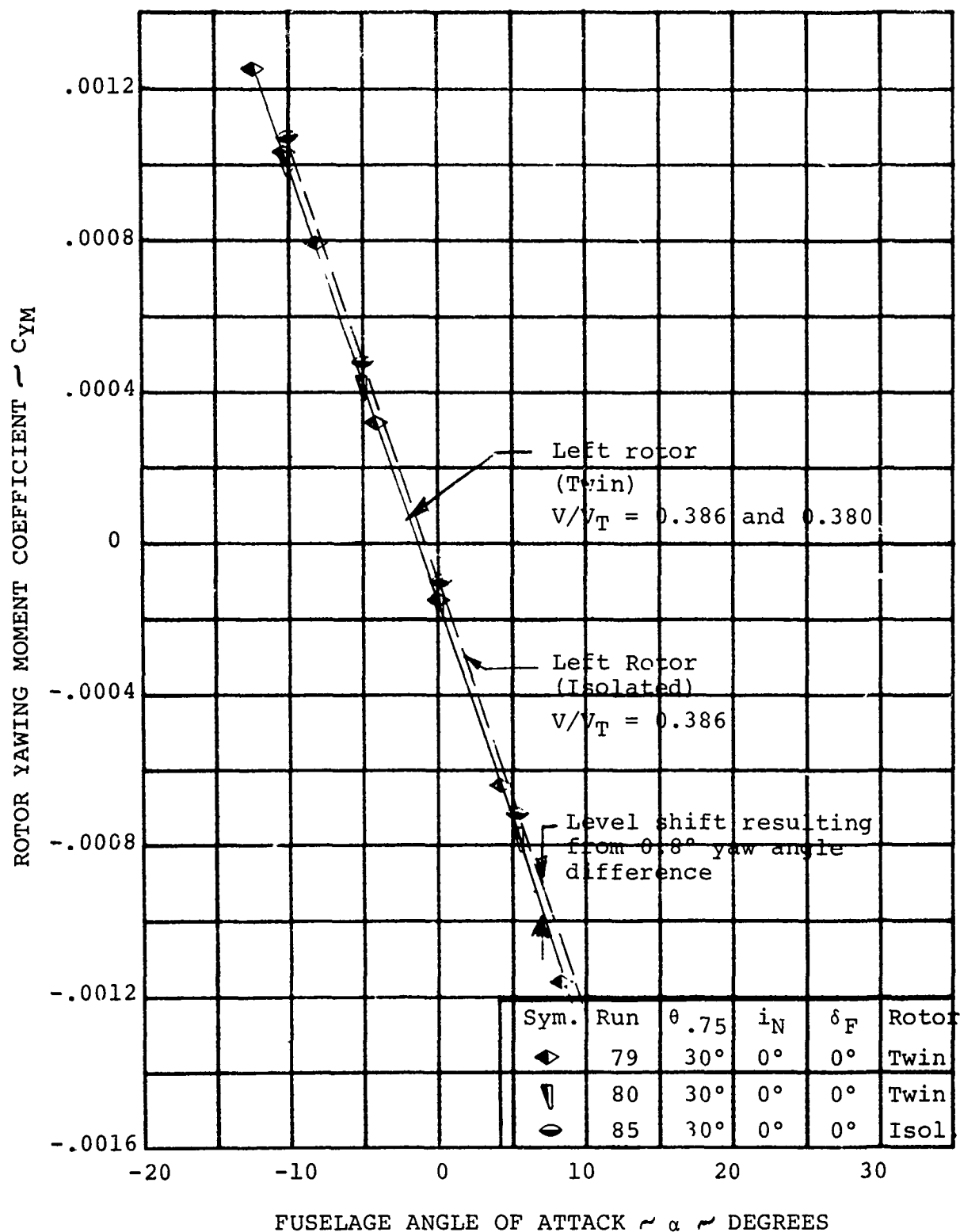


FIGURE 5-125

ROTOR/ROTOR INTERFERENCE EFFECTS ON
CRUISE ROTOR CHARACTERISTICS, $V/V_T = 0.386$

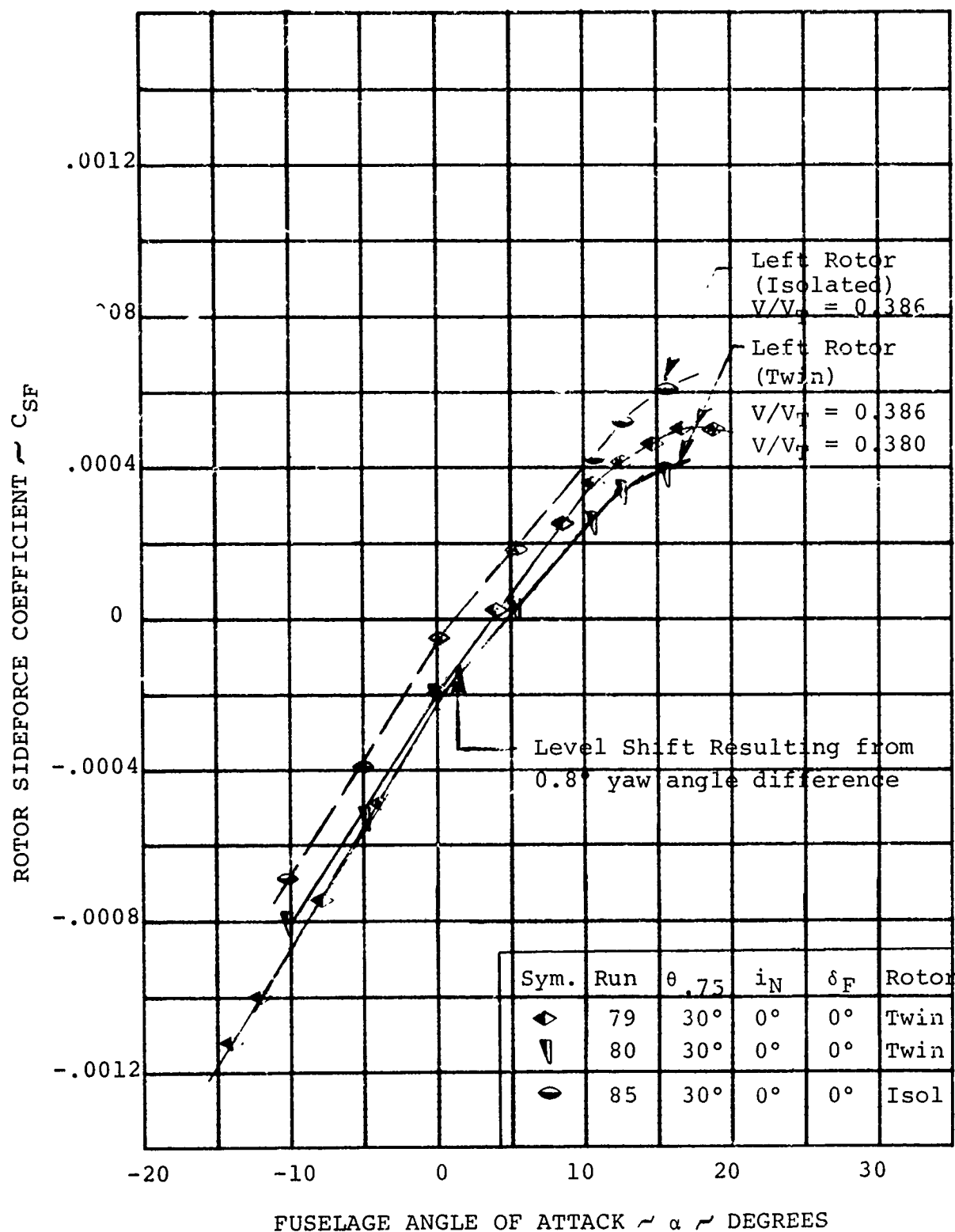


FIGURE 5-126

ROTOR/ROTOR INTERFERENCE EFFECTS ON
CRUISE ROTOR CHARACTERISTICS, $V/V_T = 0.386$

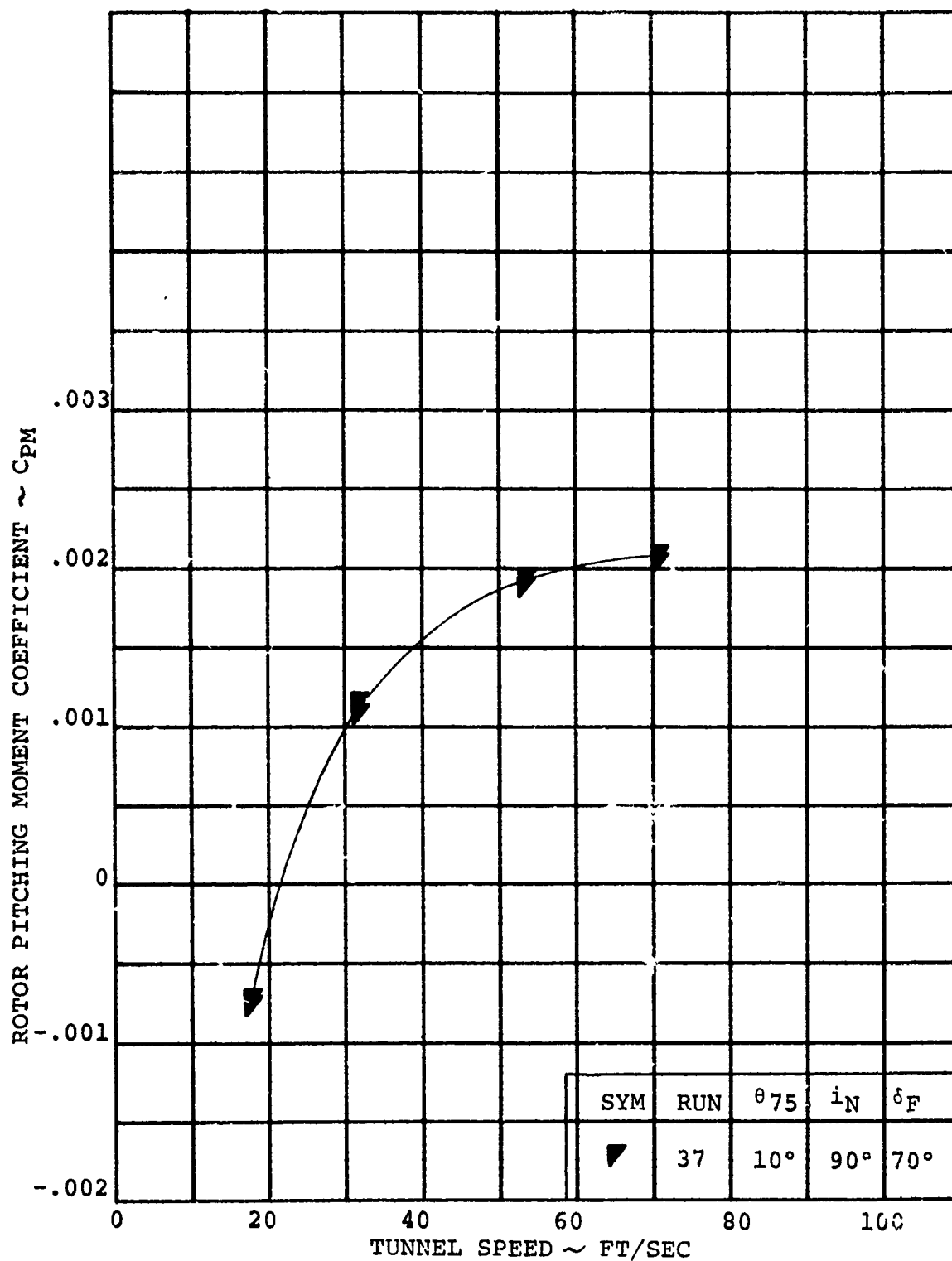


FIGURE 5-127 EFFECT OF SPEED ON ROTOR PITCHING MOMENT
IN THE HELICOPTER MODE

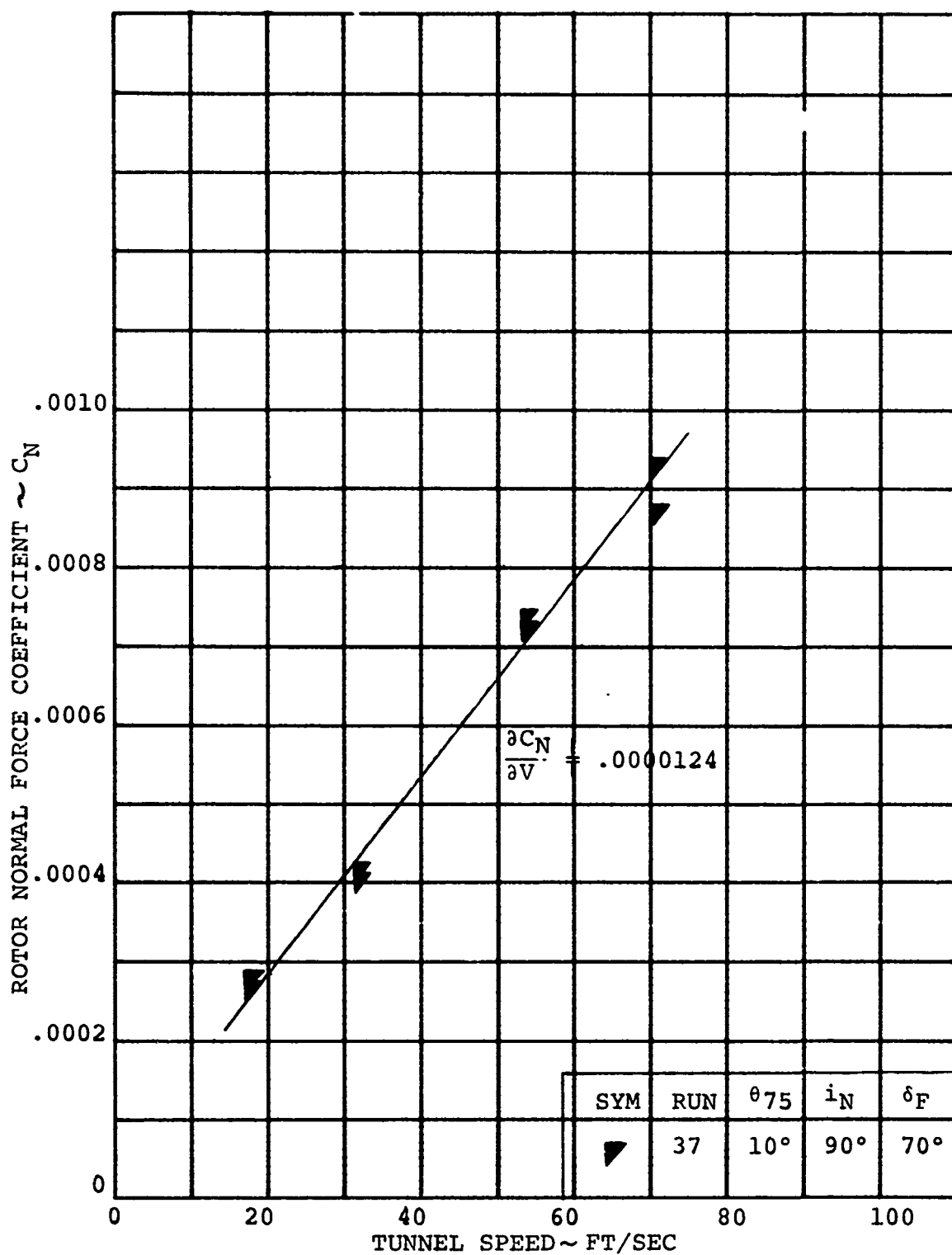


FIGURE 5-128 EFFECT OF SPEED ON ROTOR NORMAL FORCE
IN THE HELICOPTER MODE

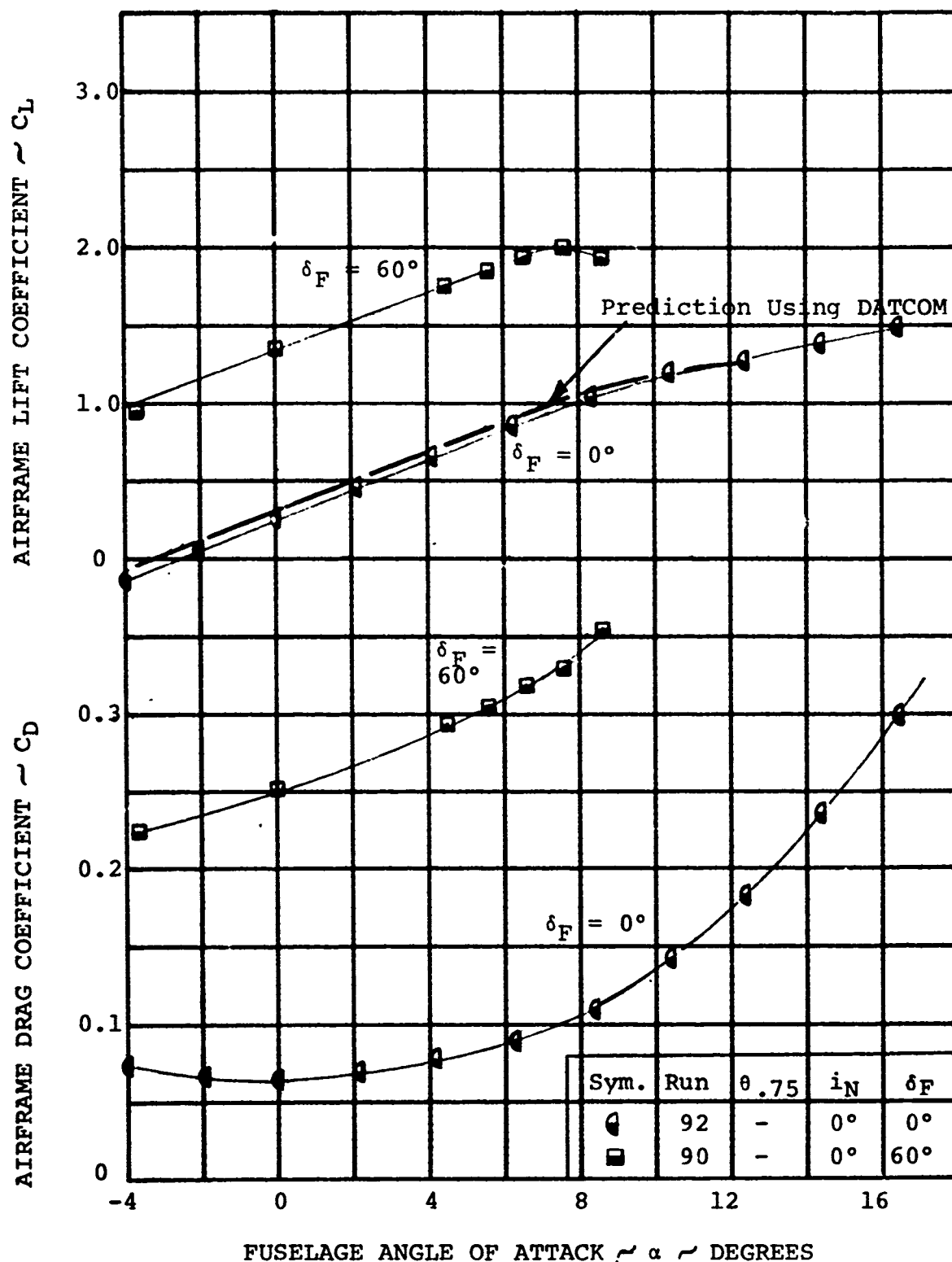


FIGURE 5-129

AIRFRAME LIFT AND DRAG CHARACTERISTICS IN CRUISE WITH ROTORS REMOVED AND $i_t = 0^\circ$

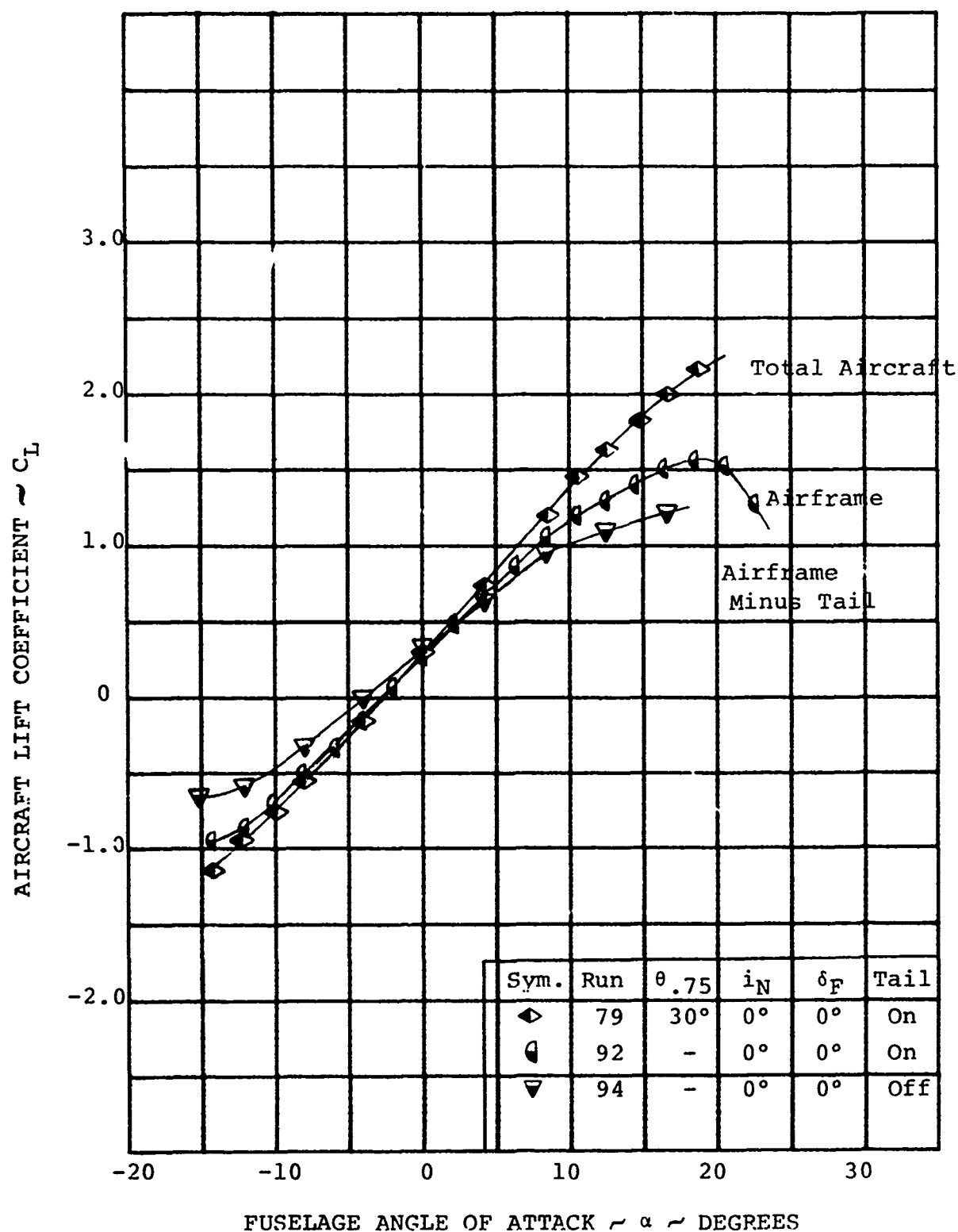


FIGURE 5-130

CONTRIBUTION OF PROP/ROTORS AND HORIZONTAL TAIL TO AIRCRAFT LIFT WITH $\delta_F = 0^\circ$ AND $V/V_T = 0.386$

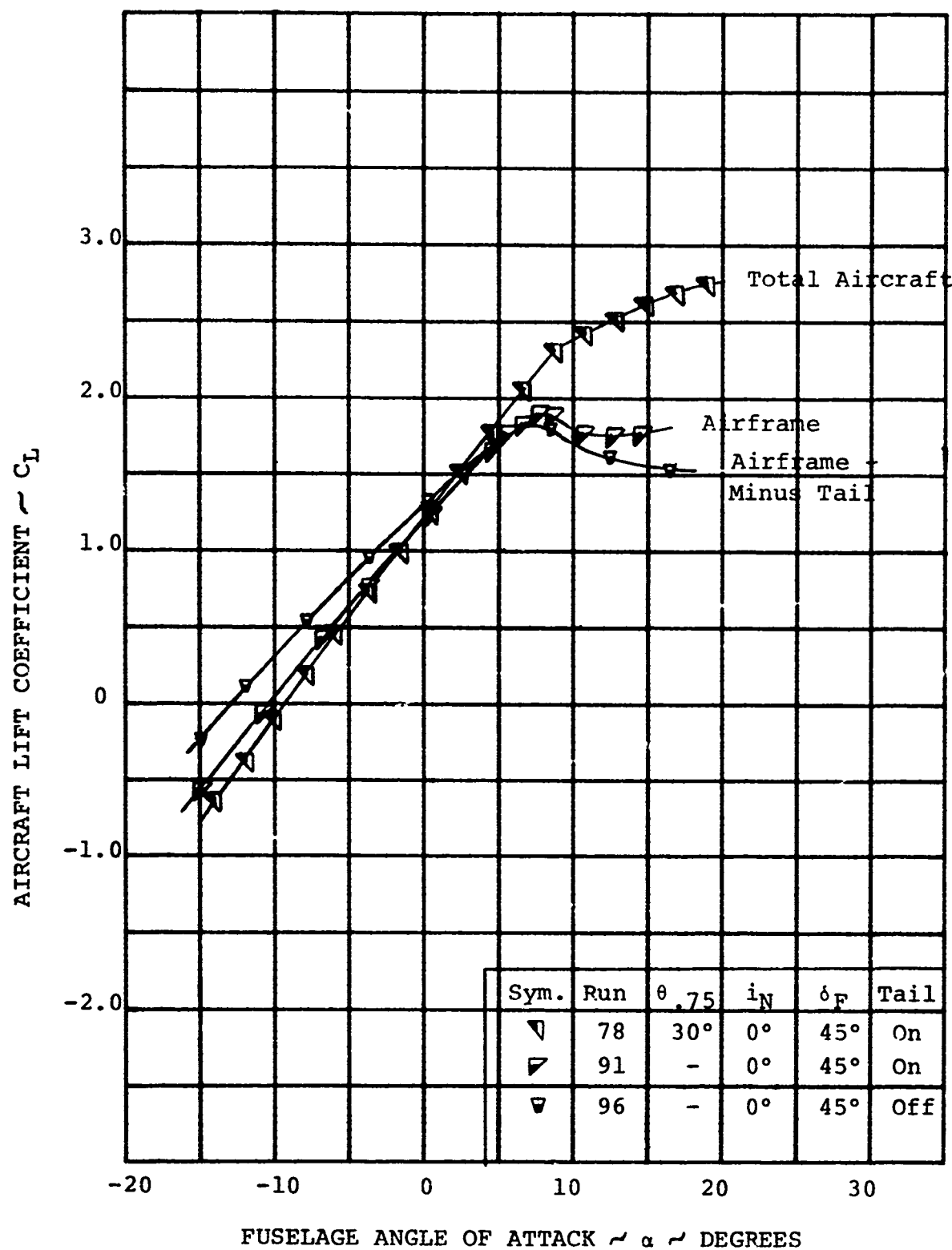


FIGURE 5-131

CONTRIBUTION OF PROP/ROTORS AND HORIZONTAL TAIL TO AIRCRAFT LIFT WITH
 $\delta_F = 45^\circ$ AND $V/V_T = 0.386$

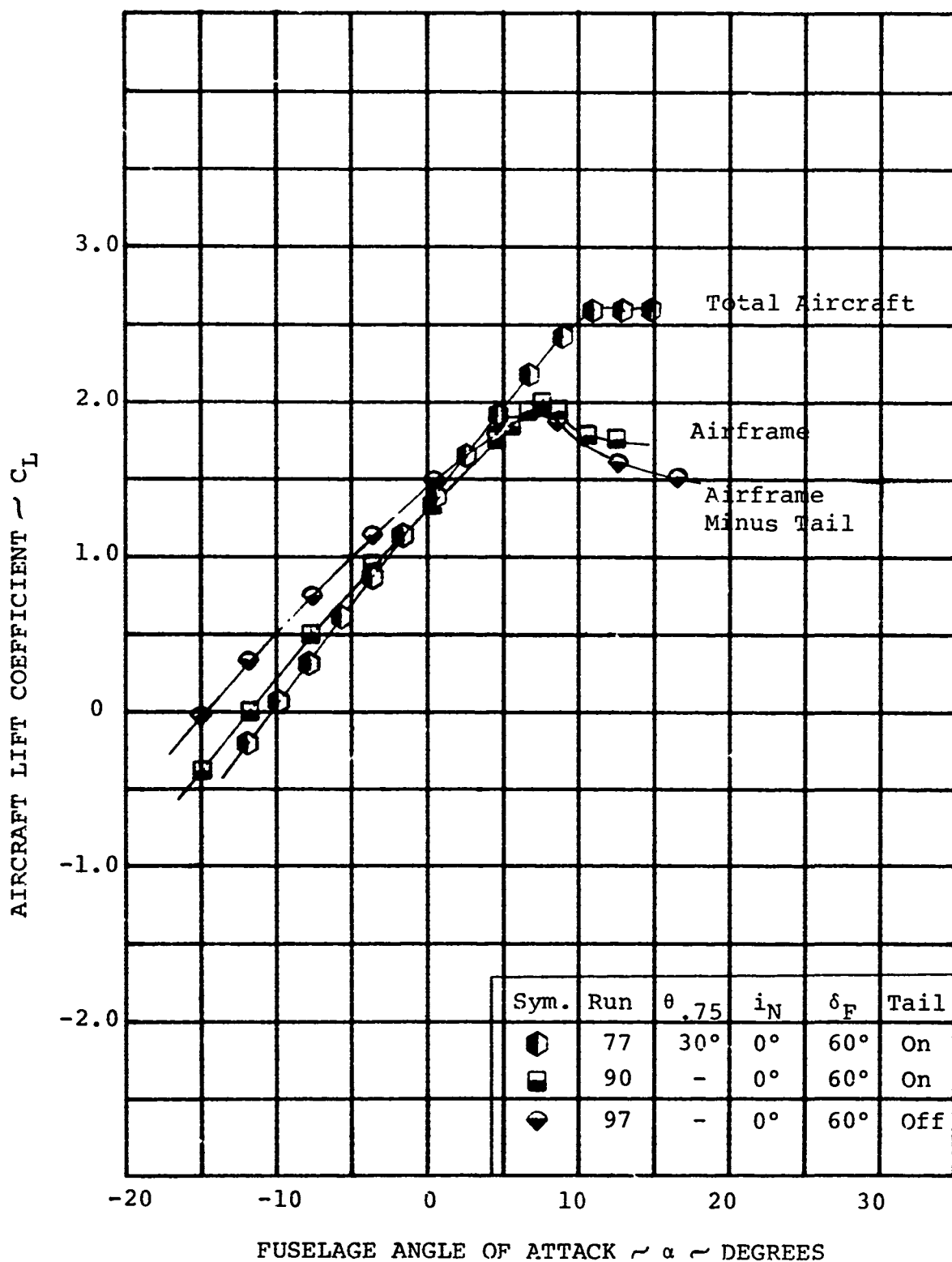


FIGURE 5-132

CONTRIBUTION OF PROP/ROTORS AND HORIZONTAL TAIL TO AIRCRAFT LIFT WITH $\delta_F = 60^\circ$ AND $V/V_T = 0.386$

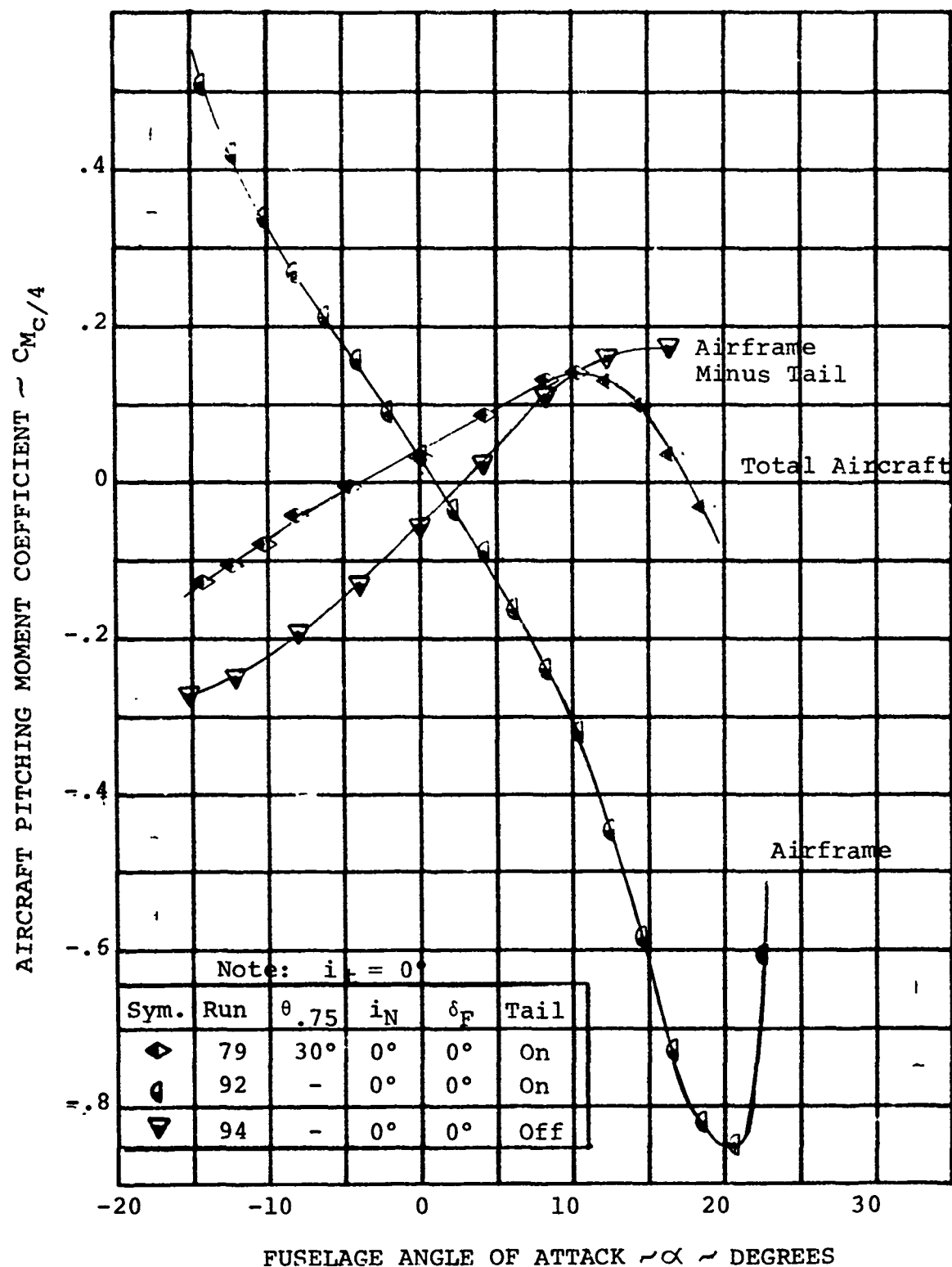


FIGURE 5-133

CONTRIBUTION OF PROP/ROTORS AND HORIZONTAL TAIL TO AIRCRAFT PITCHING MOMENT, $\delta_F = 0^\circ$, $V/V_T = 0.386$

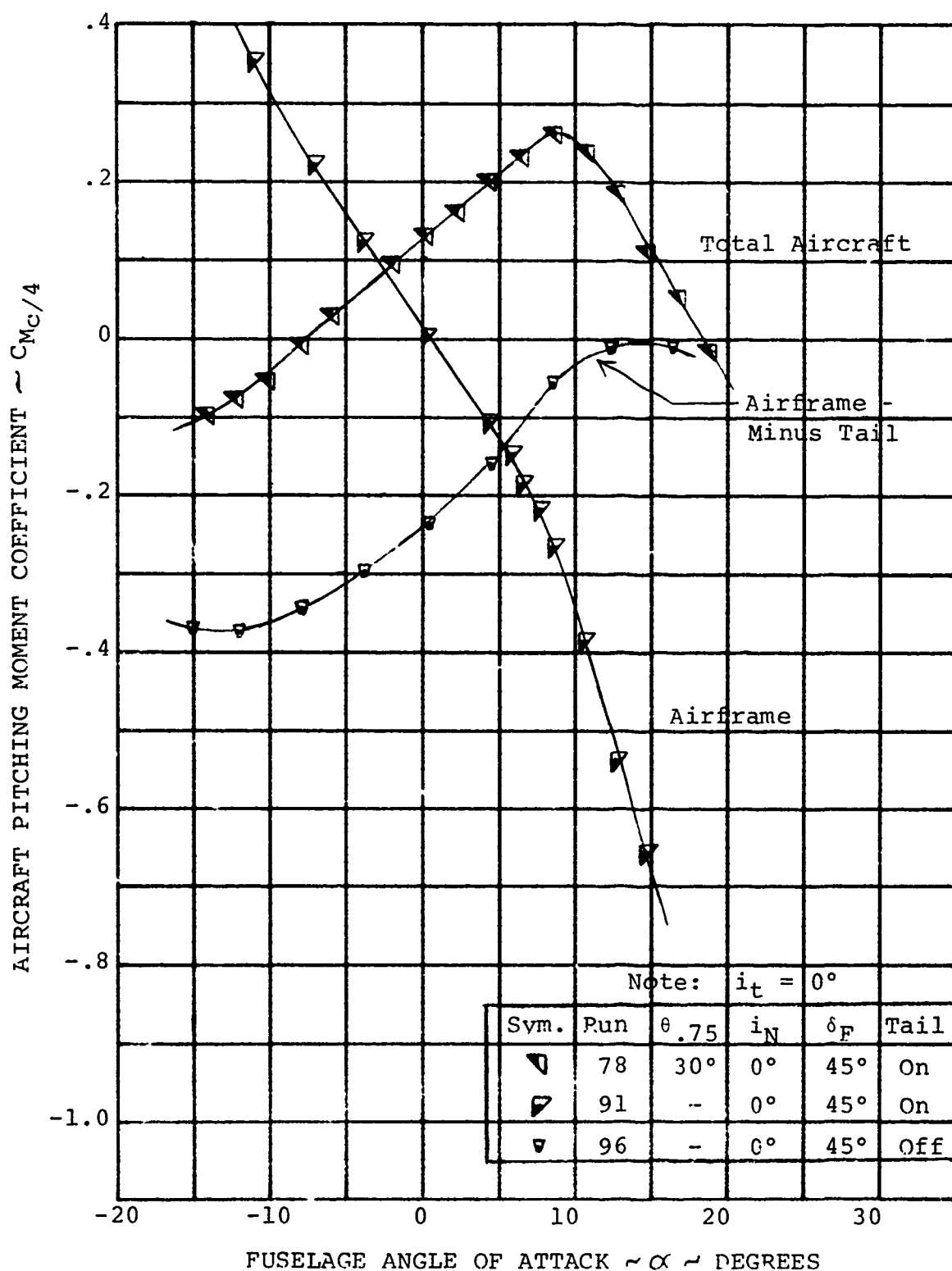


FIGURE 5-134

CONTRIBUTION OF PROP/ROTORS AND HORIZONTAL TAIL TO AIRCRAFT PITCHING MOMENT, $\delta_F = 45^\circ$, $V/V_T = 0.386$

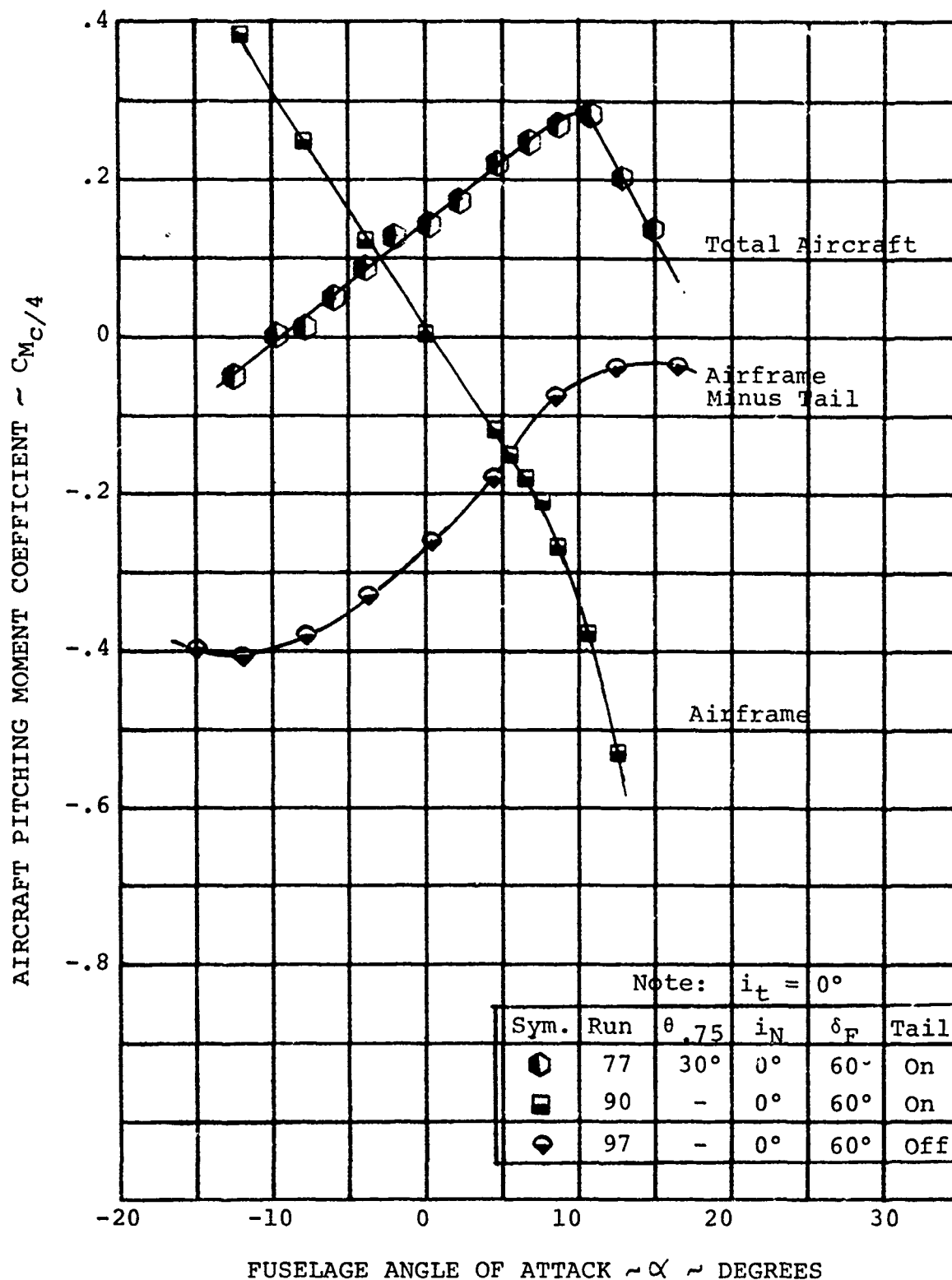


FIGURE 5-135

CONTRIBUTION OF PROP/ROTORS AND HORIZONTAL TAIL TO AIRCRAFT PITCHING MOMENT, $\delta_F = 60^\circ$, $V/V_T = 0.386$

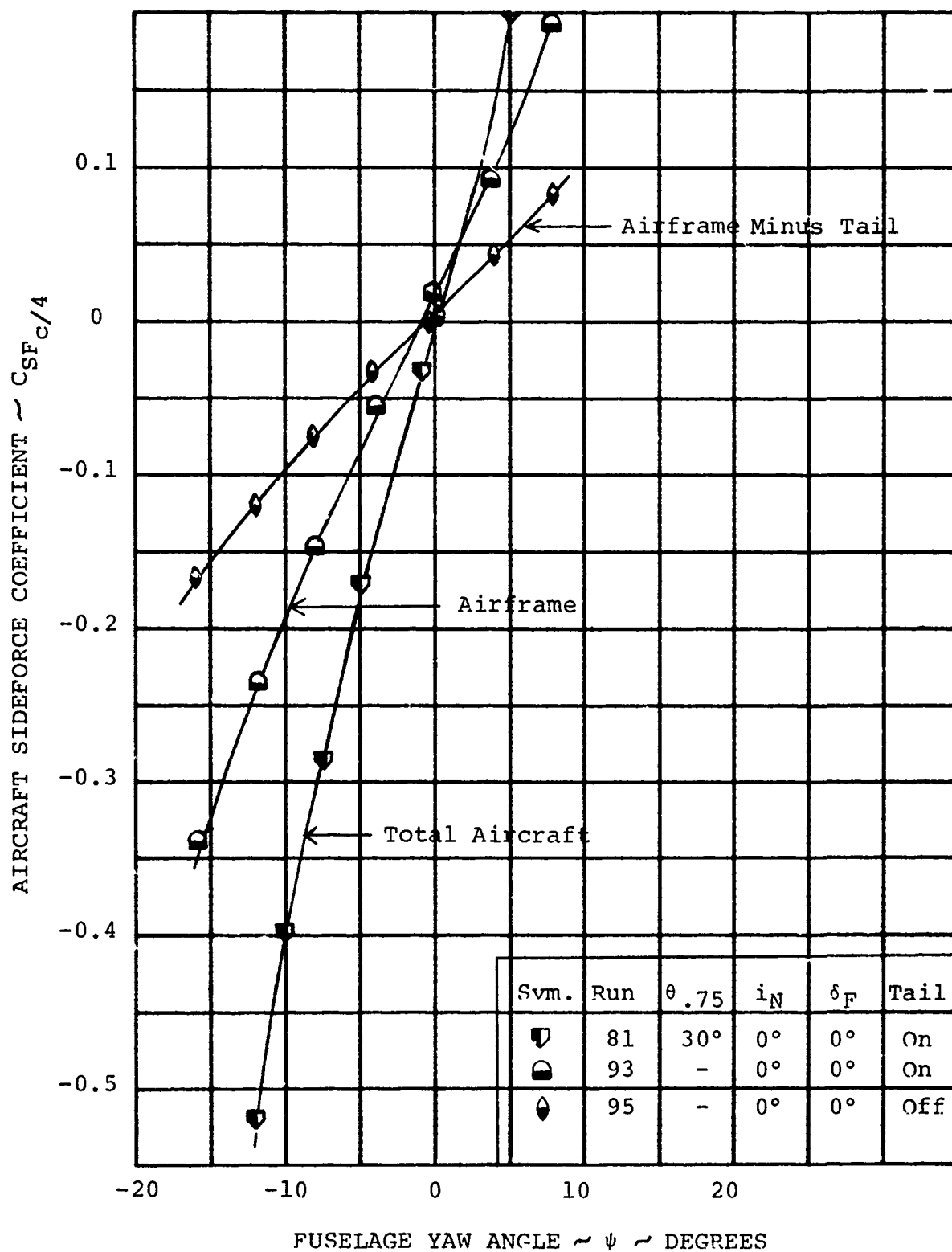


FIGURE 5-136

CONTRIBUTION OF PROP/ROTOR AND VERTICAL
TAIL TO AIRCRAFT SIDE FORCE, $\delta_F = 0^\circ$,
 $V/V_T = 0.382$

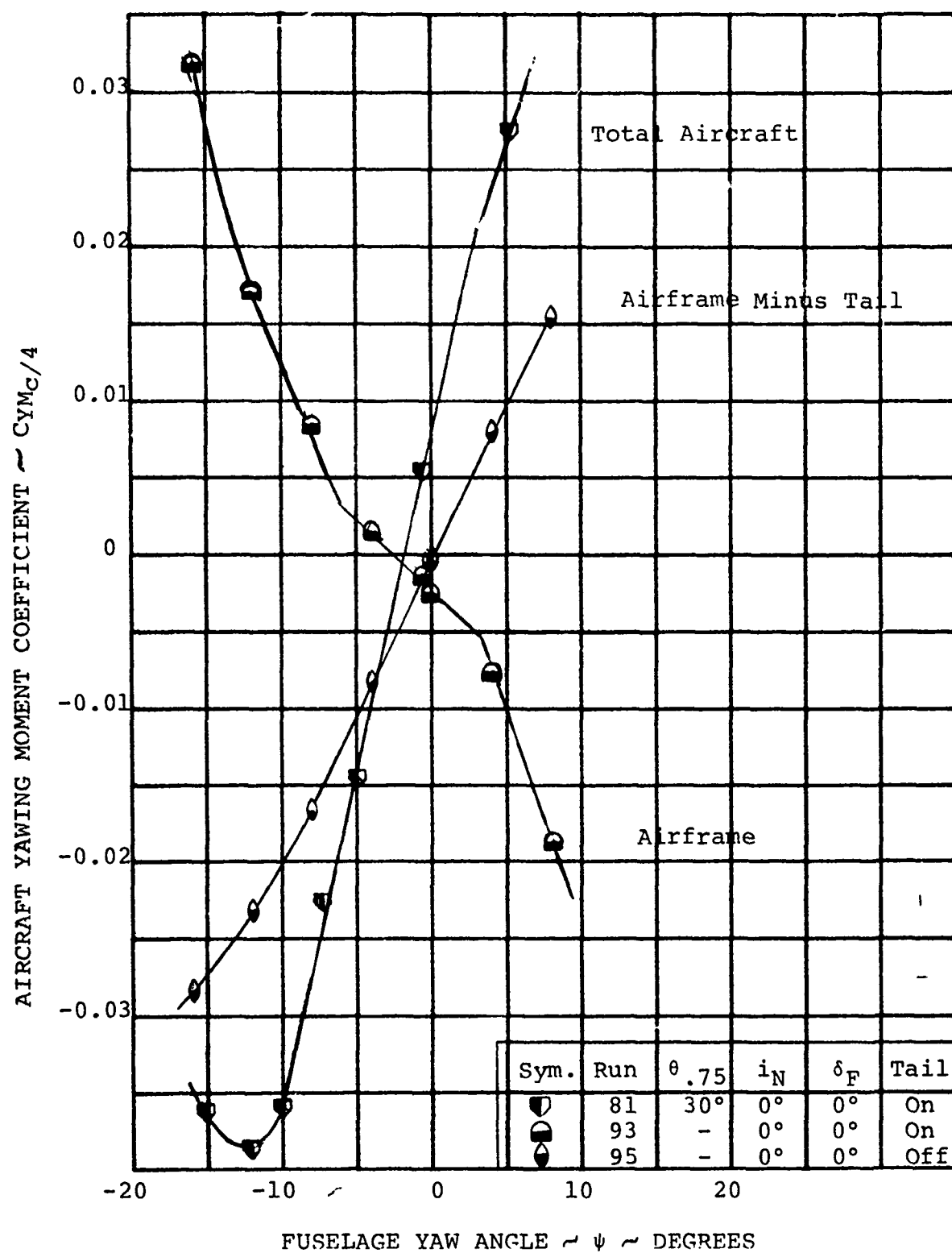


FIGURE 5-137

CONTRIBUTION OF PROP/ROTOR AND VERTICAL
TAIL TO AIRCRAFT YAWING MOMENT, $\delta_F = 0$,
 $V/V_T = 0.382$

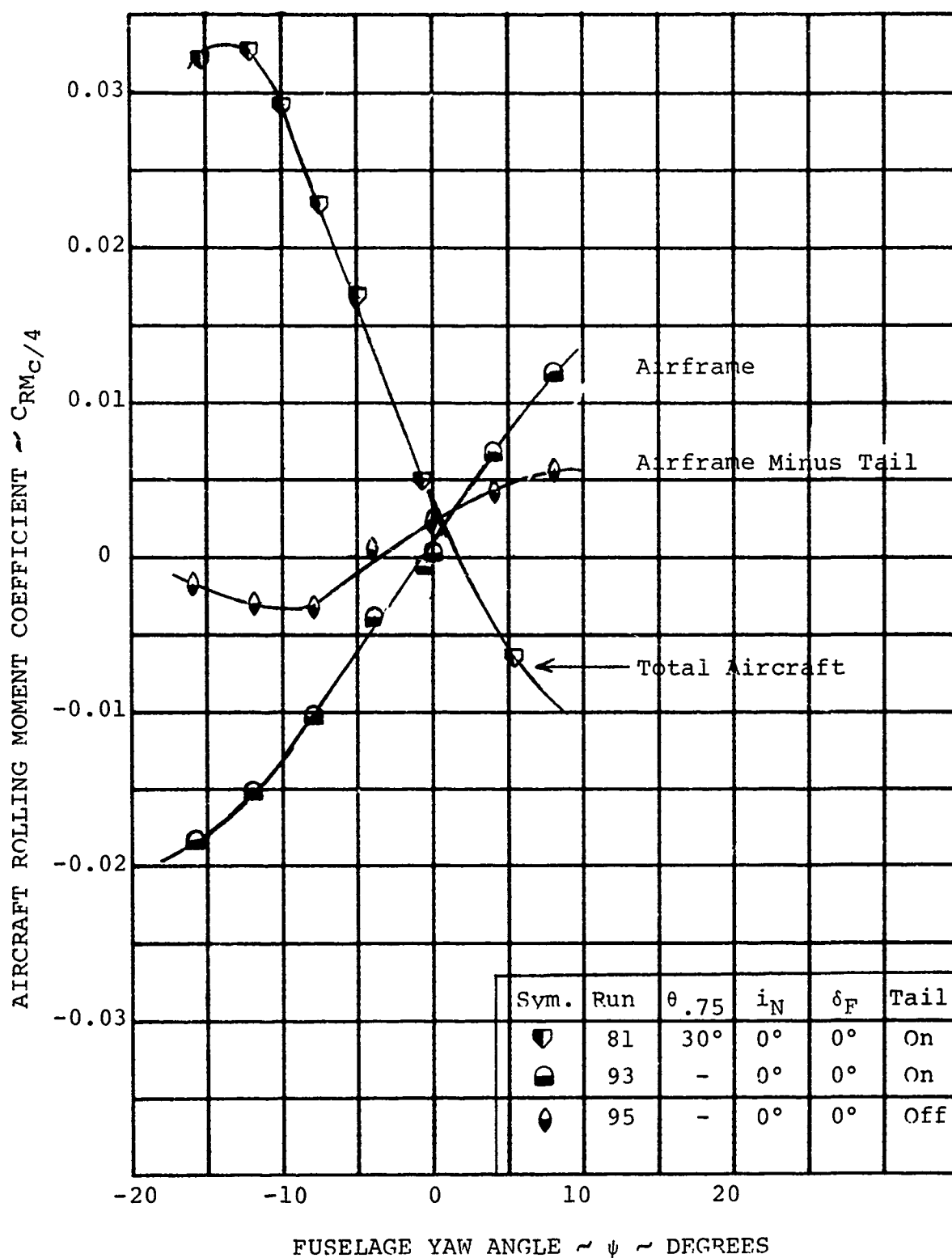


FIGURE 5-138

CONTRIBUTION OF PROP/ROTOR AND VERTICAL
TAIL TO AIRCRAFT ROLLING MOMENT, $\delta_F = 0$,
 $V/V_T = 0.382$

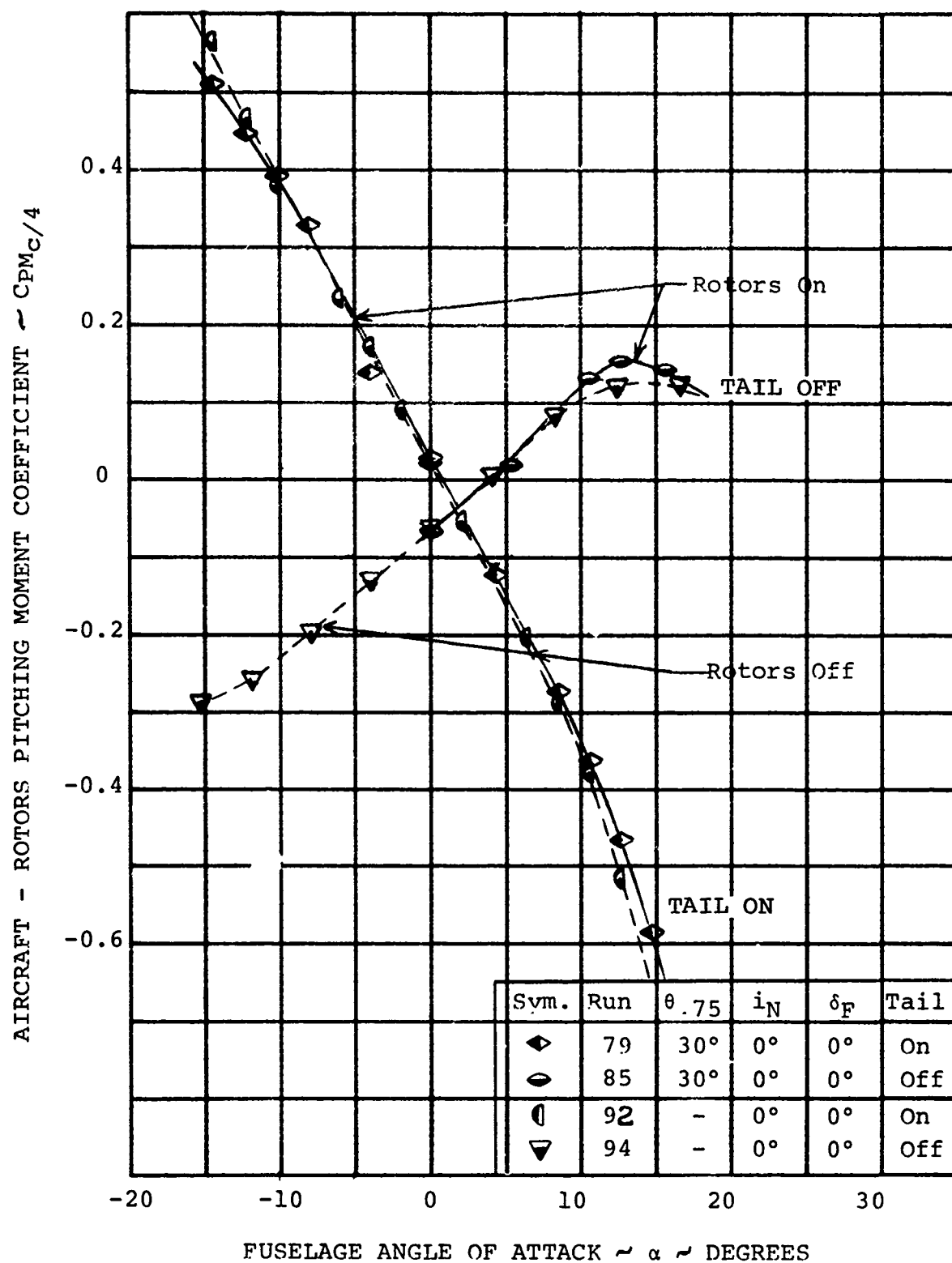


FIGURE 5-139

COMPARISON OF ROTORS ON/ROTORS OFF
PITCHING MOMENT WITH AND WITHOUT TAIL

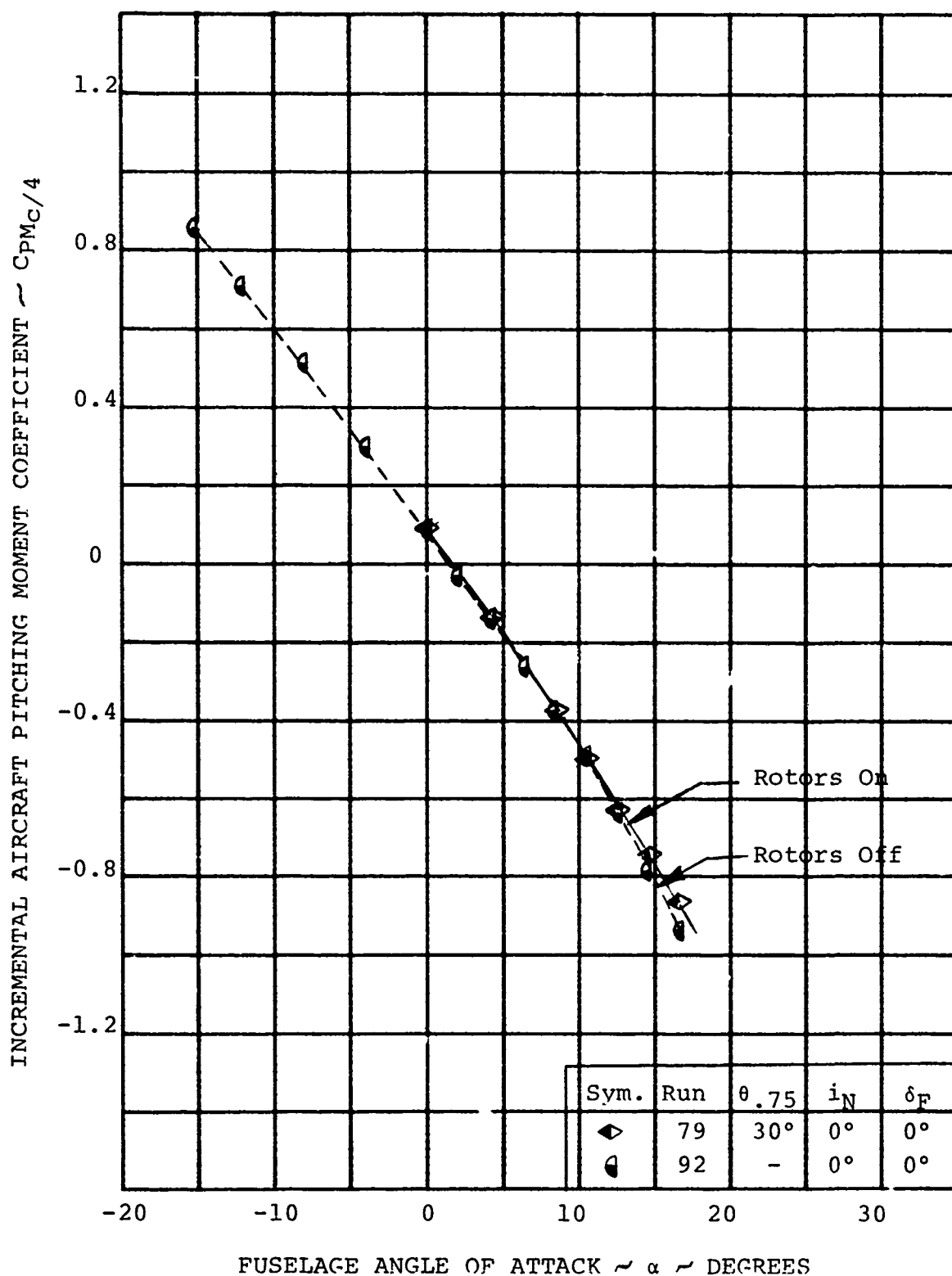


FIGURE 5-140

EFFECT OF ROTORS ON HORIZONTAL TAIL
CONTRIBUTION TO AIRCRAFT PITCHING MOMENT

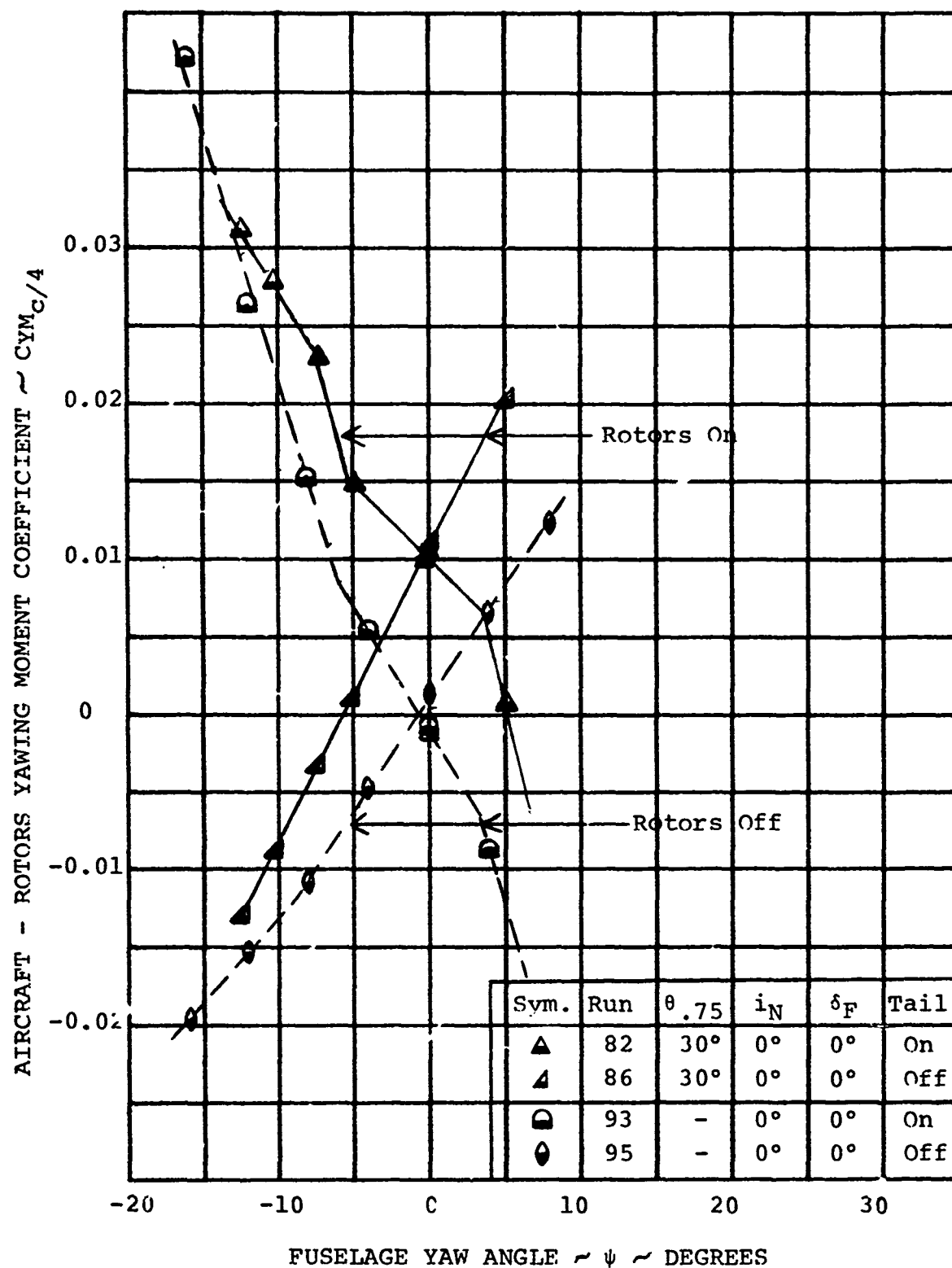


FIGURE 5-141

COMPARISON OF ROTORS ON/ROTORS OFF
YAWING MOMENT WITH AND WITHOUT TAIL

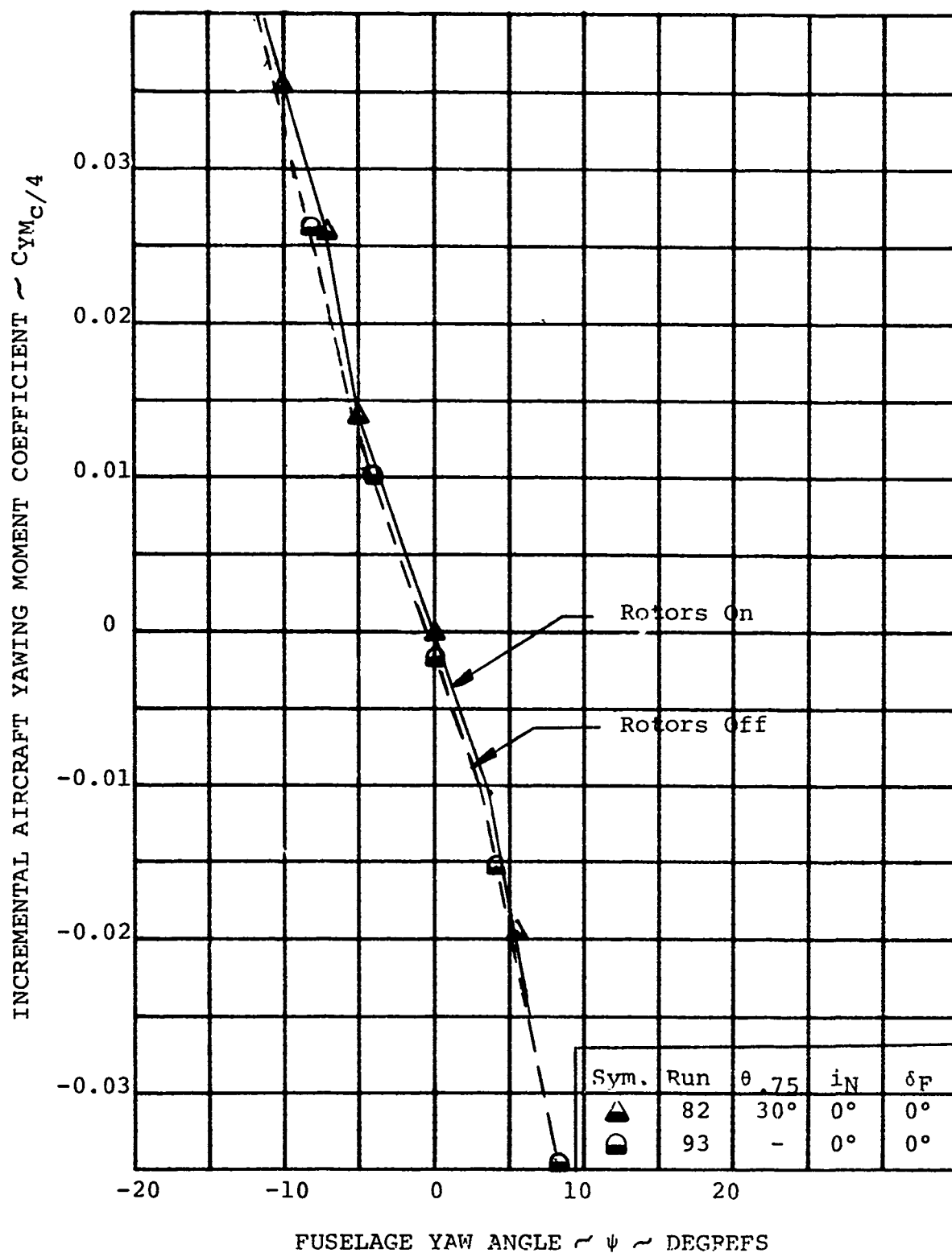


FIGURE 5-142

EFFECT OF ROTORS ON VERTICAL TAIL
CONTRIBUTION TO AIRCRAFT YAWING MOMENT

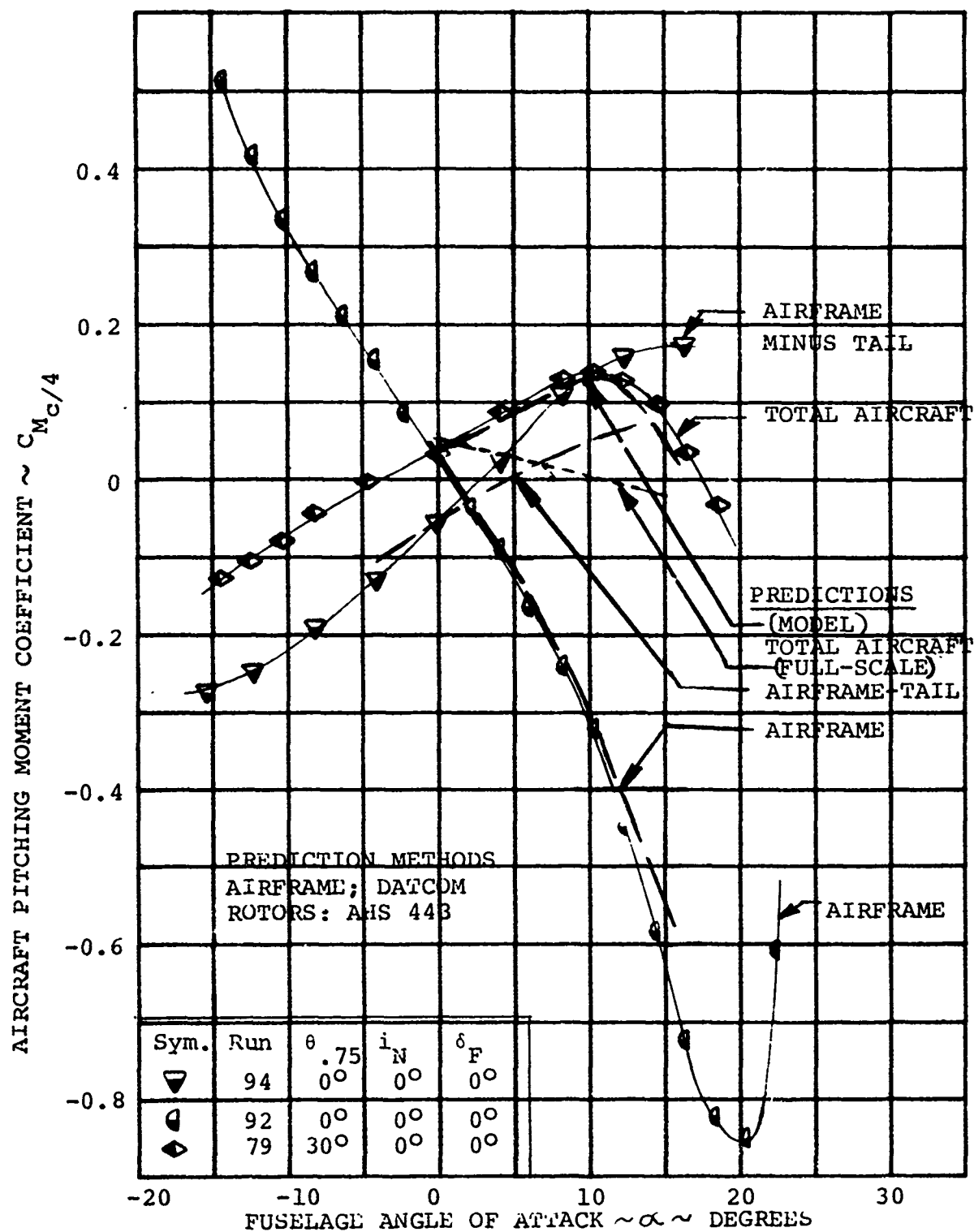
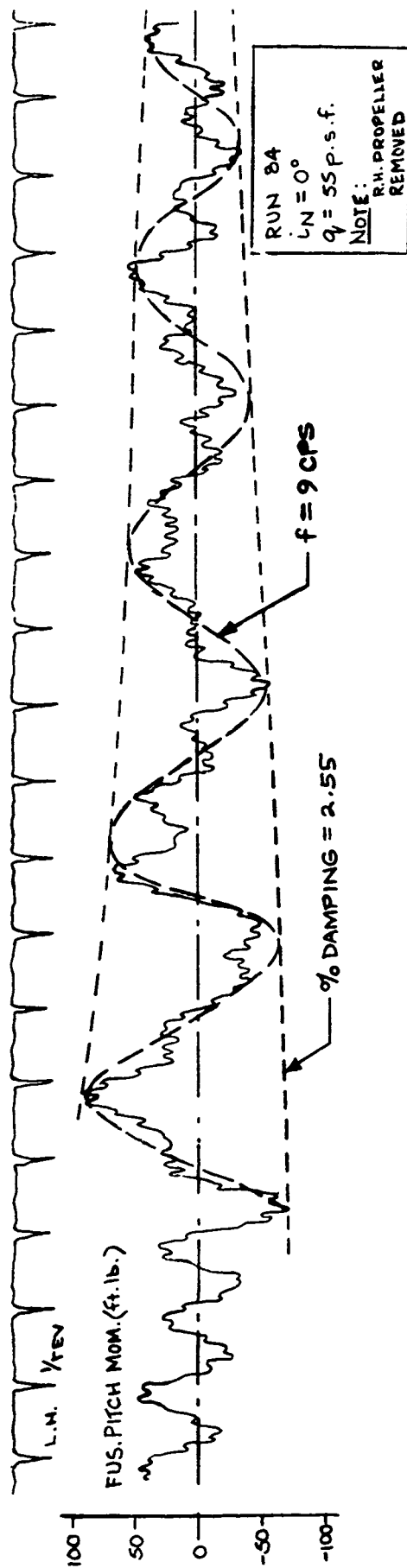
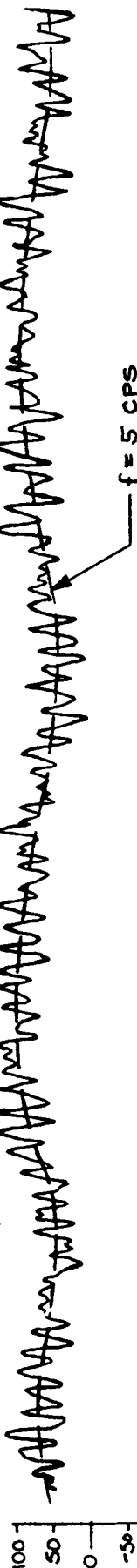


FIGURE 5-143 CONTRIBUTION OF PROP/ROTORS AND HORIZONTAL TAIL TO AIRCRAFT PITCHING MOMENT AT $V/V_T = 0.386$



L.H. NAC. NORM. FORCE (lb.)



L.H. NAC. PITCH MOM. (ft. lb.)



TIME ~ SECS. (FOLLOWING COMPLETION OF STEP INPUT)

Figure 5-144 - RESPONSE RESULTING FROM 4° PITCH STEP INPUT IN THE CRUISE MODE

5.5 CONCLUSIONS - STABILITY AND CONTROL

Analysis of the stability and control test data presented here allows the following conclusions to be made:

1. Hover, pitch, roll and yaw control powers measured are sufficient to meet the specifications of Level 1 flying qualities of Reference 8.
2. The rotor has a large destabilizing effect on the aircraft in transition and cruise.
3. Rotor stall limits the destabilizing effects of the model rotor in transition.
4. Roll and yaw control moments can be obtained in transition using differential thrust with differential cyclic used as a decoupler.
5. The wing lift interference effect increases the rotor pitching moment derivative by 50 percent in cruise.
6. Predictions of isolated rotor derivatives agree well with data at zero wing lift.
7. Correlation of theory and test rotor stability derivatives provides confidence that the full-scale design aircraft will be stable as predicted.

6.0 ROTOR LOADS

Rotor loads data were obtained in the hover, transition and cruise modes to accomplish rotor loads objectives. The test objectives included the determination of rotating blade frequencies in the hover mode and the effect of various tilt-rotor flight conditions on blade bending moments and rotor loads.

A coupled flap-lag frequency analysis was used to predict the rotating blade frequencies for the first flap and first lag bending modes and an uncoupled flap-lag-torsion frequency analysis was used to predict the first torsional frequency. Baffle test data were used to substantiate the analysis and a comparison of test data and prediction are shown in Figure 6-1.

A semi-empirical approach was used to predict blade loads in hover due to cyclic pitch. Blade loads due to ground proximity effects were predicted from past test data and blade loads due to cyclic were predicted by a coupled flap-pitch uncoupled lag rotor loads analysis. Correlation of the test data with prediction is shown in Figure 6-2. Correlation of the hub moment test data with prediction is shown in Figure 6-3.

Past prop-rotor and helicopter blade stall flutter inception data was used to predict the inception of stall flutter in hover. Stall flutter was predicted to occur at hover at a collective pitch of 14 degrees. Stall flutter did not occur in hover.

The effect of angle of attack on blade flap bending in cruise was predicted by the coupled flap-pitch uncoupled lag analysis and correlation of the test data with prediction is shown in Figures 6-4 and 6-5. Hub moment due to angle of attack in cruise was also predicted and the results are shown in Figure 6-6. The effect of wing flap deflection on blade flap bending in cruise was also predicted and the results are shown in Figure 6-7.

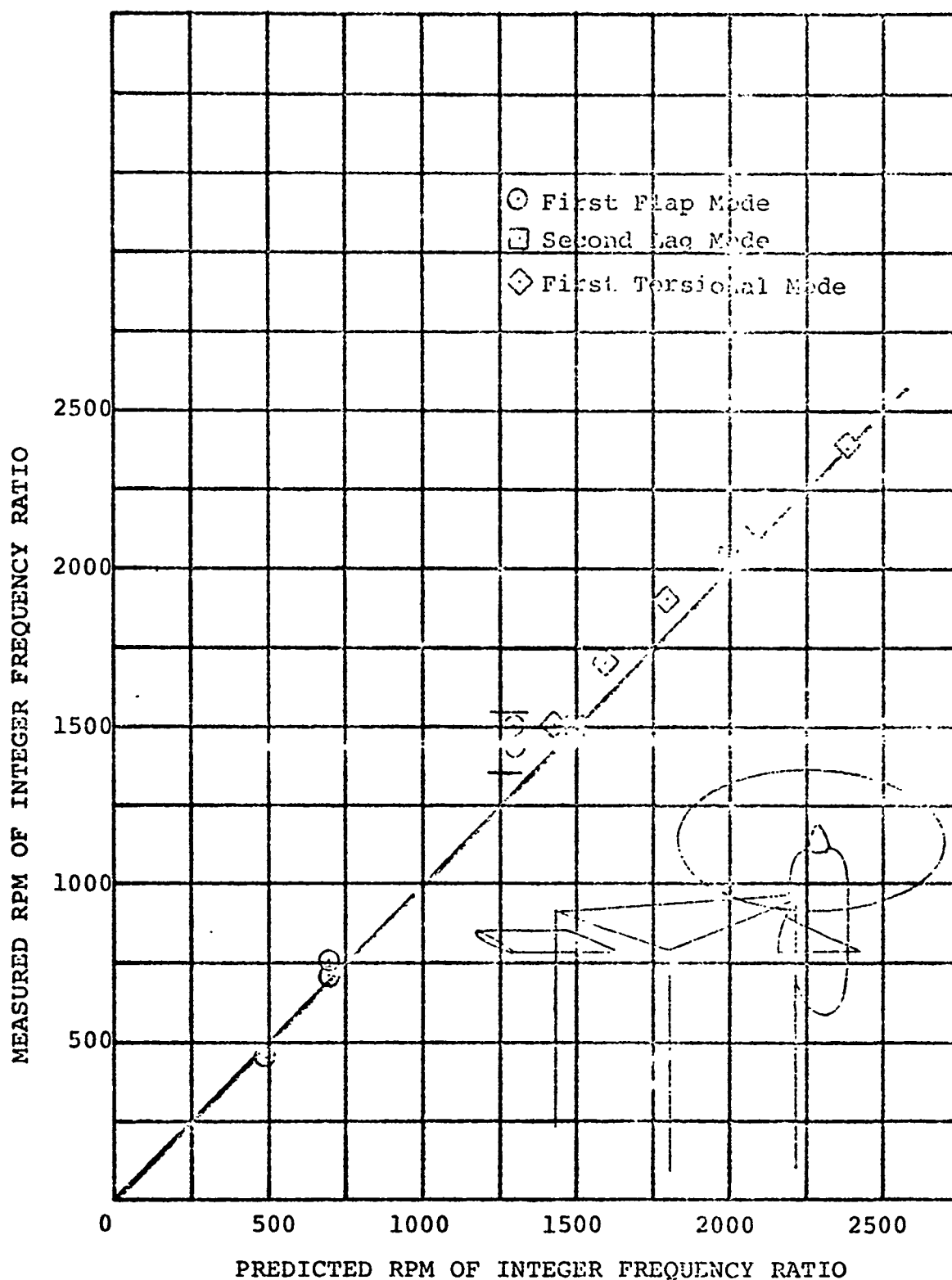


FIGURE 6-1

CORRELATION OF MEASURED AND PREDICTED
BLADE FREQUENCIES

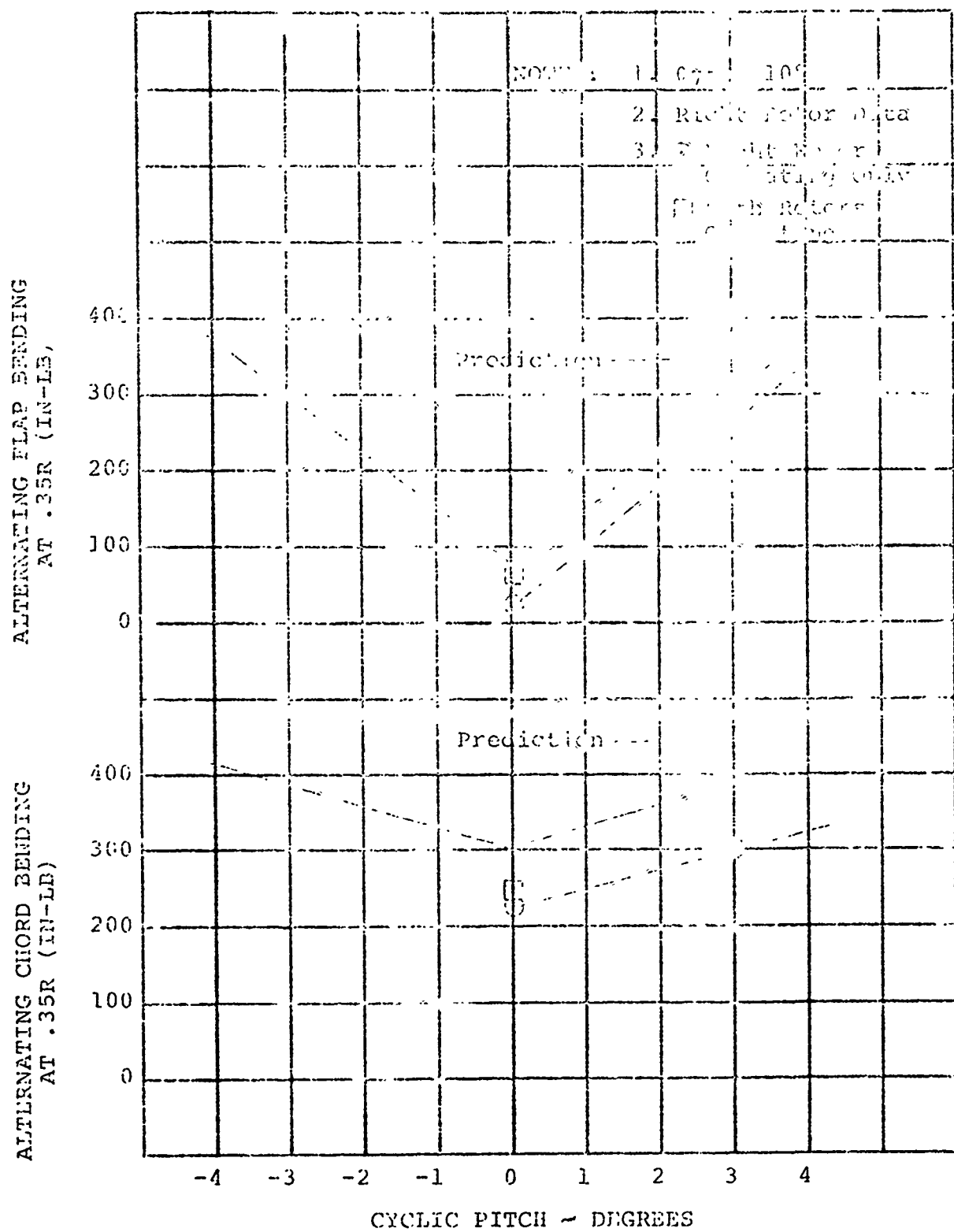


FIGURE 6-2

MEASURED AND PREDICTION BLADE LOADS PRODUCED BY CYCLIC PITCH IN HOVER AT $V_{TIP} = 750$ FPS AND $h/D = .39$

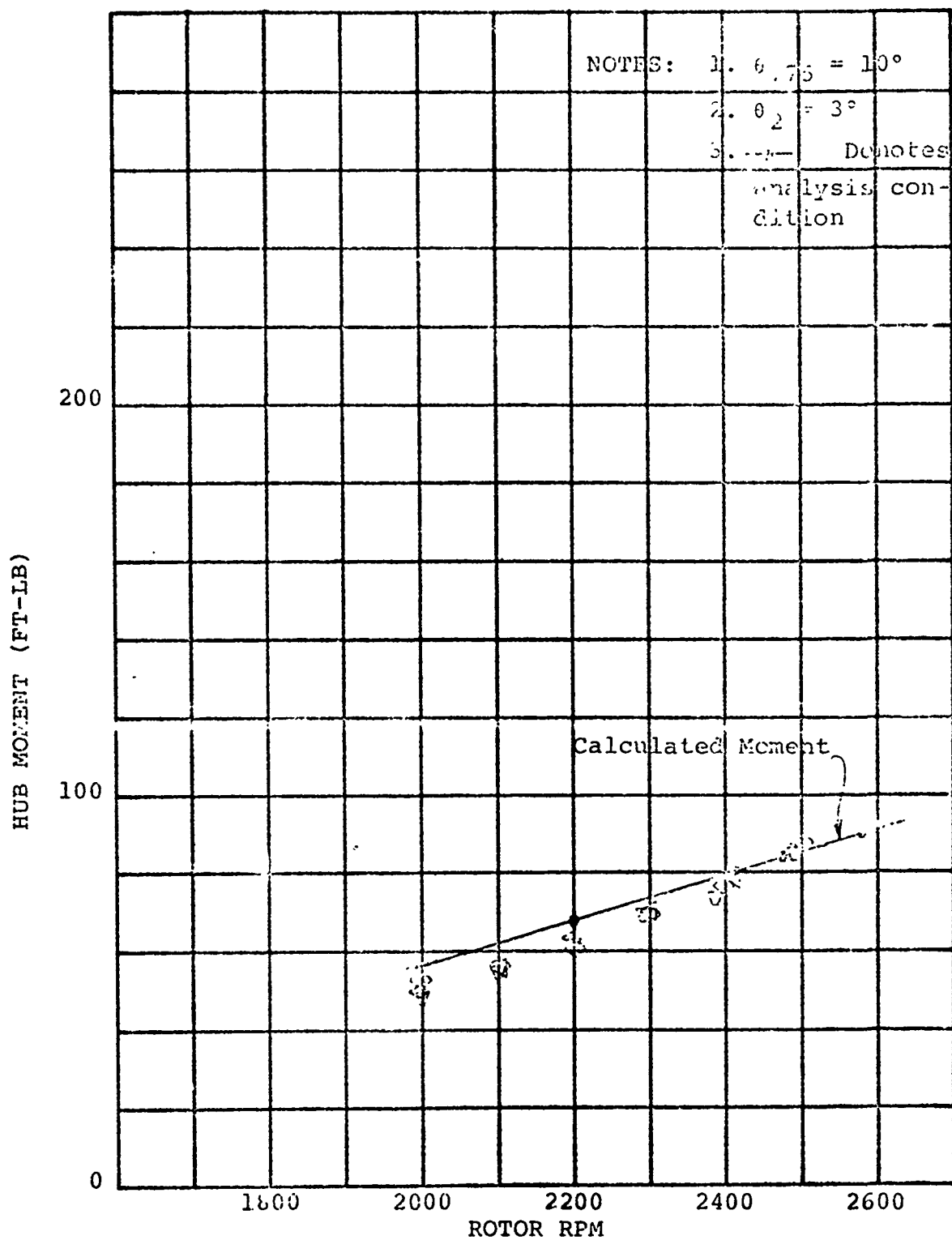


FIGURE 6-3
 COMPARISON BETWEEN MEASURED AND CALCULATED STEADY HUB
 MOMENT VS. RPM FOR 3° CYCLIC AND $V = 0$

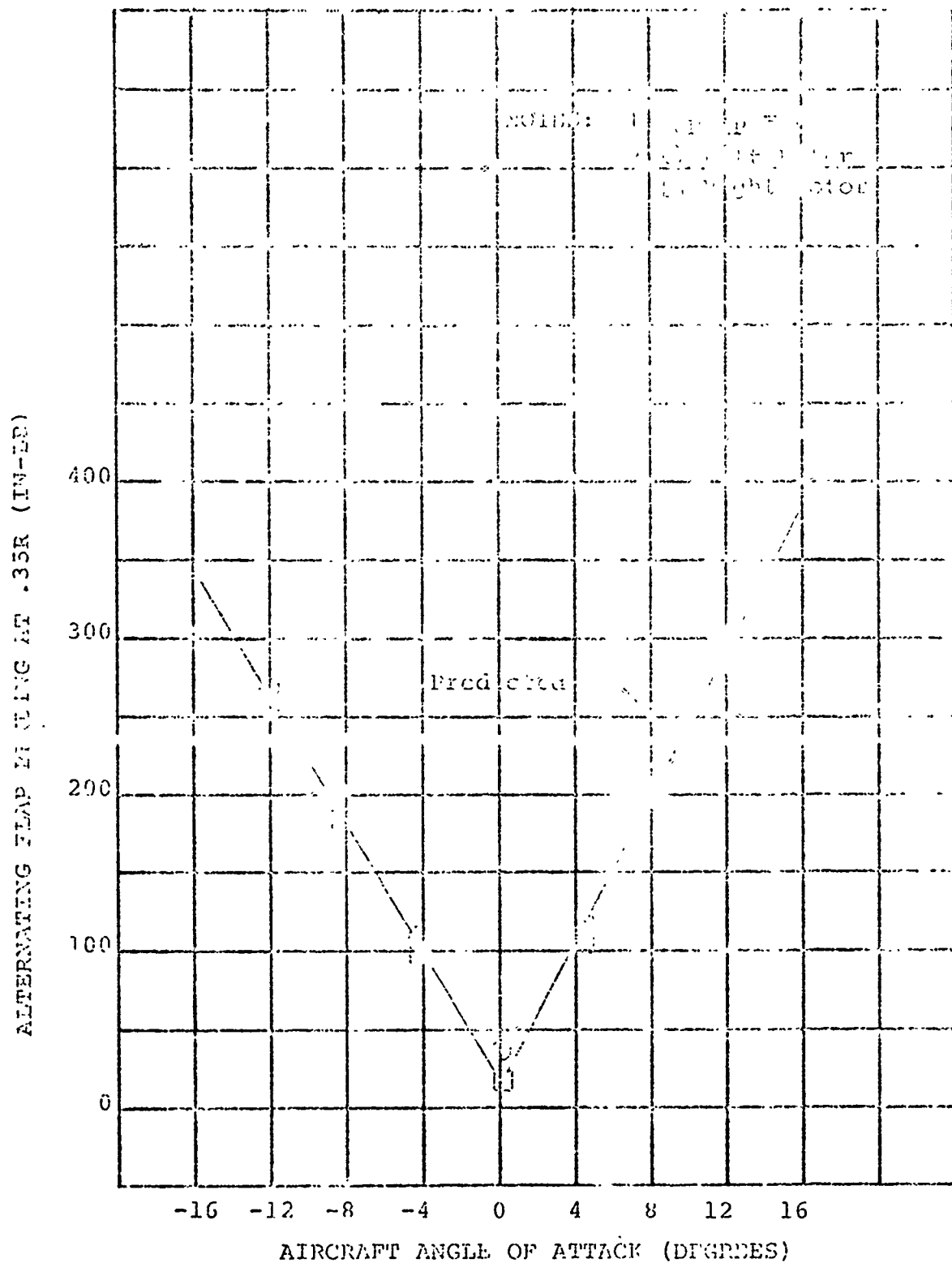


FIGURE 6-4

MEASURED AND PREDICTED ALTERNATING FLAP BENDING PRODUCED BY AIRCRAFT ANGLE OF ATTACK IN CRUISE AT $\alpha = 30^\circ$, $V_{TIP} = 570$ FPS AND $V_{TUNNEL} = 220$ FPS

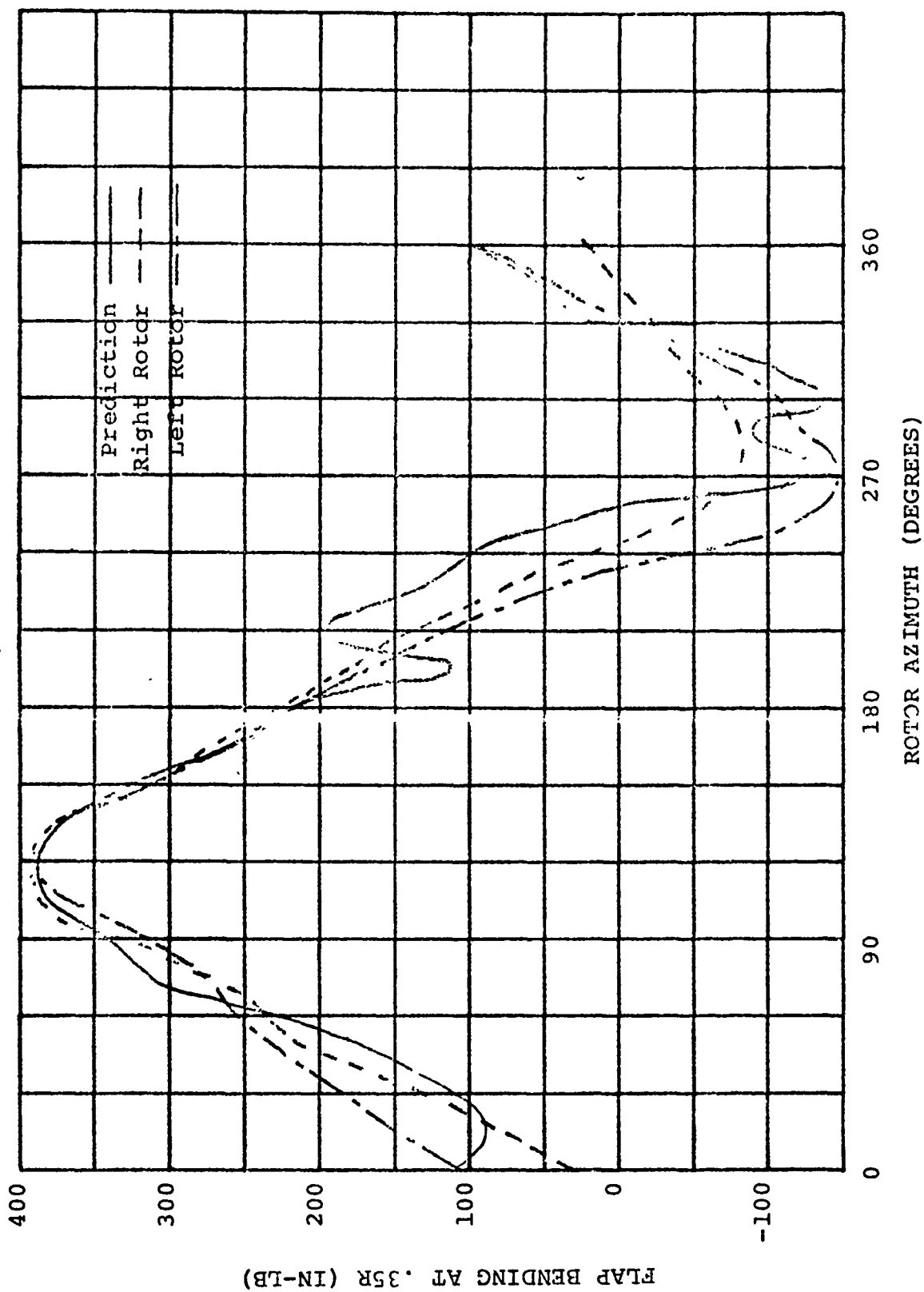


FIGURE 6-5
 MEASURED AND PREDICTED BLADE FLAP BENDING IN CRUISE
 FOR $\alpha = 10^\circ$, $75 = 30^\circ$, $V_{TIP} = 570$ FPS AND V_{TUNNEL}
 220 FPS

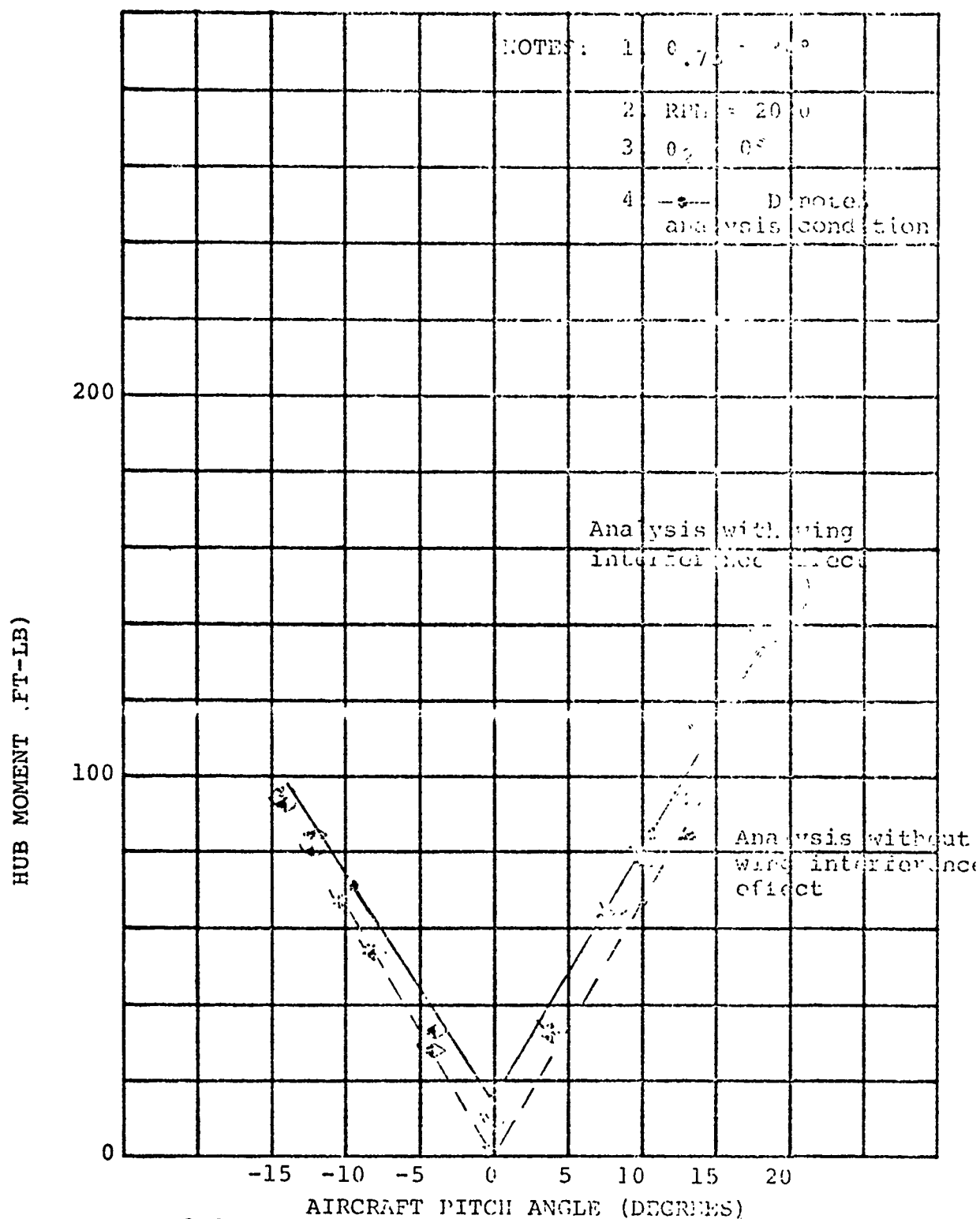


FIGURE 6-6

COMPARISON BETWEEN MEASURED AND CALCULATED STEADY HUB MOMENT VS. AIRCRAFT ANGLE OF ATTACK FOR $i_N = 0$ DEG, AND $V = 226$ FPS

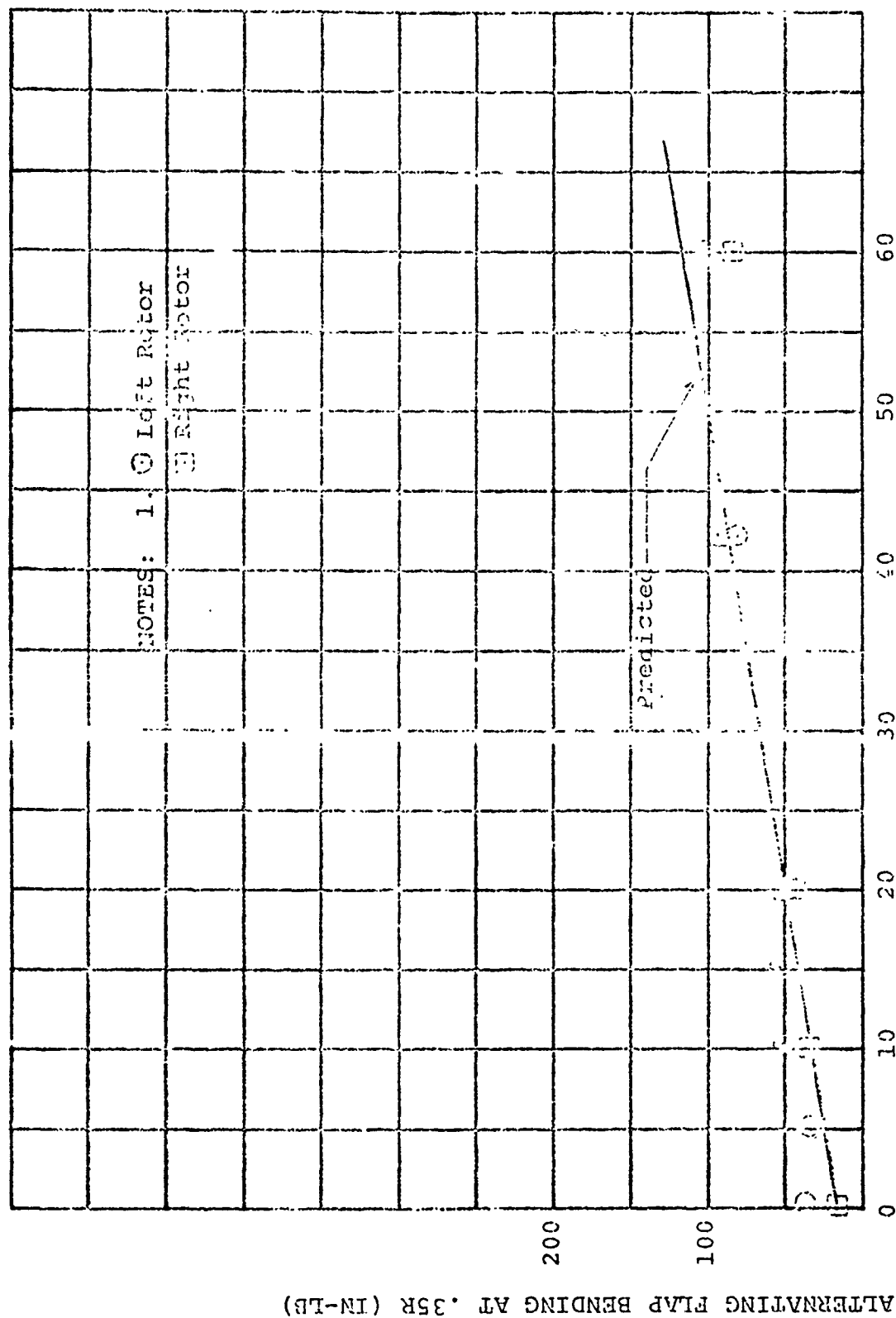


FIGURE 6-7. MEASURED AND PREDICTED ALTERNATING FLAP BENDING PRODUCED BY WING FLAP INCIDENCE IN CRUISE AT $\theta_{75} = 30^\circ$, $V_{TIP} = 570$ FPS, $V_{TUNNEL} = 220$ FPS AND $\alpha = 0$

6.1 BLADE FREQUENCY SUBSTANTIATION

The primary blade loads objective was to determine the first flap and first lag rotating frequencies for hover collective and correlate the results with a coupled blade frequency analysis. Test results show good agreement with analysis and substantiate the predicted first flap and first lag modes for the test RPM range. Blade torsion data was also obtained and the results show good agreement with the predicted first torsional mode.

Substantiation of the first two rotating blade frequencies can be accomplished if integer values of frequency ratios at various RPM's can be determined by test. If a forcing function is provided with the same frequency as a bending mode, the blade bending moments will respond predominantly at that frequency. Baffles were placed under the rotor disc plane in the hover position to provide a 1, 2, 3 and 4 per rev excitation. The baffles excite the blades by restricting the downwash as each blade passes over a baffle. Since the rotor wake is subsonic, any downwash restriction in the wake will immediately influence the flow field in the disc plane. A description of the baffle arrangement is shown on Page 17 in Section 3.

The baffle arrangement was induced a 1, 2, 3 or 4 per rev disturbance. Alternating blade bending moments showed amplification when the rotor RPM was such that the excitation frequency of the baffles was close to a predicted first flap bending or first lag bending frequency. Harmonic analyses of the right rotor data show that a RPM's corresponding to local blade bending moment amplification, the largest harmonic component was the blade natural frequency at that RPM.

6.1.1 First Flap Mode

Left and right rotor alternating flap and chord bending moments for each baffle run are shown in Figures 6-9 through 6-15 and 6-20 through 6-26. Harmonic analyses of the right rotor flap and chord bending data are shown in Figures 6-16 through 6-19 and 6-27 through 6-30. A summary of the baffle test results for the first flap and lag modes is presented in Figure 6-8. In a number of cases a graph is shown of the harmonic responses of the blade to the one-per-rev baffle for the right rotor but the overall response of the blade is missing. Those data were lost and are not retrievable.

Due to the small amount of data points, the 3P and 4P frequency crossings for the first flap mode were difficult to determine accurately. Amplification of alternating flap bending moments near the predicted 3P and 4P frequencies were small and in one case was misleading. For the 3P baffle configuration the right rotor alternating flap bending in Figure 6-14 showed a peak at 750 RPM. Harmonic analysis of the data in Figure 6-18 showed that the 3rd flap bending harmonic peaked at 650 RPM and the flap bending at 750 RPM was predominantly 2/rev. Since no data was taken below 650 RPM, this RPM was taken as the 3P flap frequency crossing due to the peak in 3rd harmonic flap moment.

Since harmonic analysis was not available for the left rotor, frequency crossings had to be determined by alternating bending moment values. Figure 6-11 shows a local alt. flap moment peak at 750 RPM for the 3 baffle configuration and Figure 6-12 shows a local peak at 430 RPM for the 4 baffle configuration.

Determination of the 2P frequency crossing for the first flapping mode was difficult due to flap bending response to a 4P lag frequency crossing. Left and right rotor alternating flap bending moments for the 2/rev baffle are presented in Figures 6-10 and 6-13, respectively, and show a local maximum at 1500 RPM. Harmonic analysis of the right rotor for the 2/rev baffle in Figure 6-17 shows a high 2/rev component from 1380 to 1570 RPM and a high 4/rev component at 1500 RPM. The 4/rev component is due to a first lag mode 4P frequency crossing at 1500 RPM. The close proximity of the lag mode 4P frequency crossing to the flap mode 2P crossing causes the blade to respond with high second and fourth harmonics and amplification of the blade flap bending response to the 2P frequency cannot be distinguished from the response to the lag mode 4P frequency crossing. Blade flap bending response to the 4P lag mode frequency would be expected since the aerodynamic damping in the lag mode contributes to the measured flap bending moment.

The local maximum of the right rotor second harmonic flap bending at 1380 RPM was taken to the 2P flap frequency crossing. The 2P flap frequency crossing for the left rotor was not determined since harmonic analysis was not available. Harmonic analysis is required to separate response to the 2P flap mode crossing from response to the 4P lag mode crossing. Alternating flap bending data shows a maximum of 1500 RPM but the waveform was predominantly 4/rev.

6.1.2 First Lag Mode

The 3P and 4P frequency crossings for the first lag mode were clearly recognized due to high amplification of the alternating chord bending as shown in Figures 6-22 and 6-23 for the left rotor and Figures 6-25 and 6-26 for the right rotor. The local maximums at 1500 RPM and 2050 RPM agree well with the predicted 4P and 3P lag mode frequency crossings, respectively. Harmonic analysis of the right rotor chord bending for the 3 and 4 baffle configurations in Figures 6-29 and 6-30 show the third harmonic response dominates the alternating chord bending at 2100 RPM and the fourth harmonic is dominant at 1500 RPM.

The good agreement with prediction of the 3P and 4P lag mode frequency crossings indicate the blade elastic stiffness properties have been correctly represented in the frequency analysis since the first lag frequency is highly dependent on elastic stiffness.

6.1.3 First Torsional Mode

Determination of the blade first torsional mode was not expected since the torsional frequency was predicted to be higher than the 4/rev baffle excitation frequency at limiting RPM. Harmonic analysis of the right rotor blade torsion data indicates that the rotor is oscillating in torsion at its torsional natural frequency regardless of the baffle excitation frequency. Alternating blade torsional moments for the right rotor are shown in Figures 6-33 through 6-35. Harmonic analysis of the right rotor data is shown in Figures 6-36 through 6-39.

Figure 6-31 summarizes the test results for the first torsional mode and shows good agreement with the uncoupled torsional frequency analysis. Operation of the blade at its torsional natural frequency is probably due to the nature of the baffle forcing function. The baffle arrangement used induced a 1, 2, 3 or 4 per rev impulsive disturbance rather than a 1, 2, 3 or 4 per rev sinusoidal disturbance. An impulsive disturbance would tend to force the blade at its torsional natural frequency and indicated in Reference 12. Figure 6-32 shows the waveform of the blade torsion response to the 2/rev baffle at 1100 RPM. The waveform shows the torsional response to the disturbance and decay during a rotor revolution.

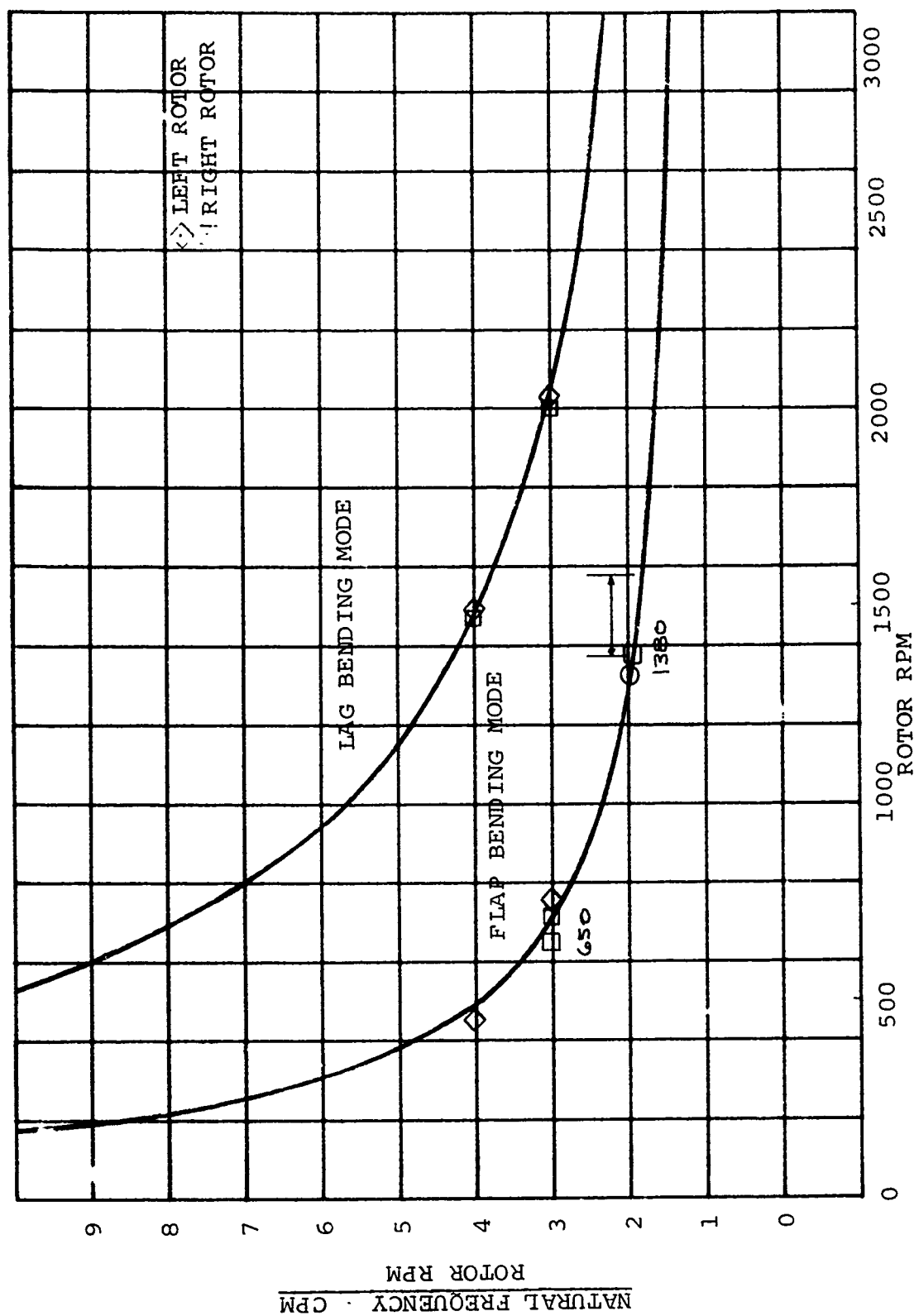


FIGURE 6-8. PREDICTED AND MEASURED ROTOR BLADE NATURAL FREQUENCIES FOR $\gamma = 15^\circ$

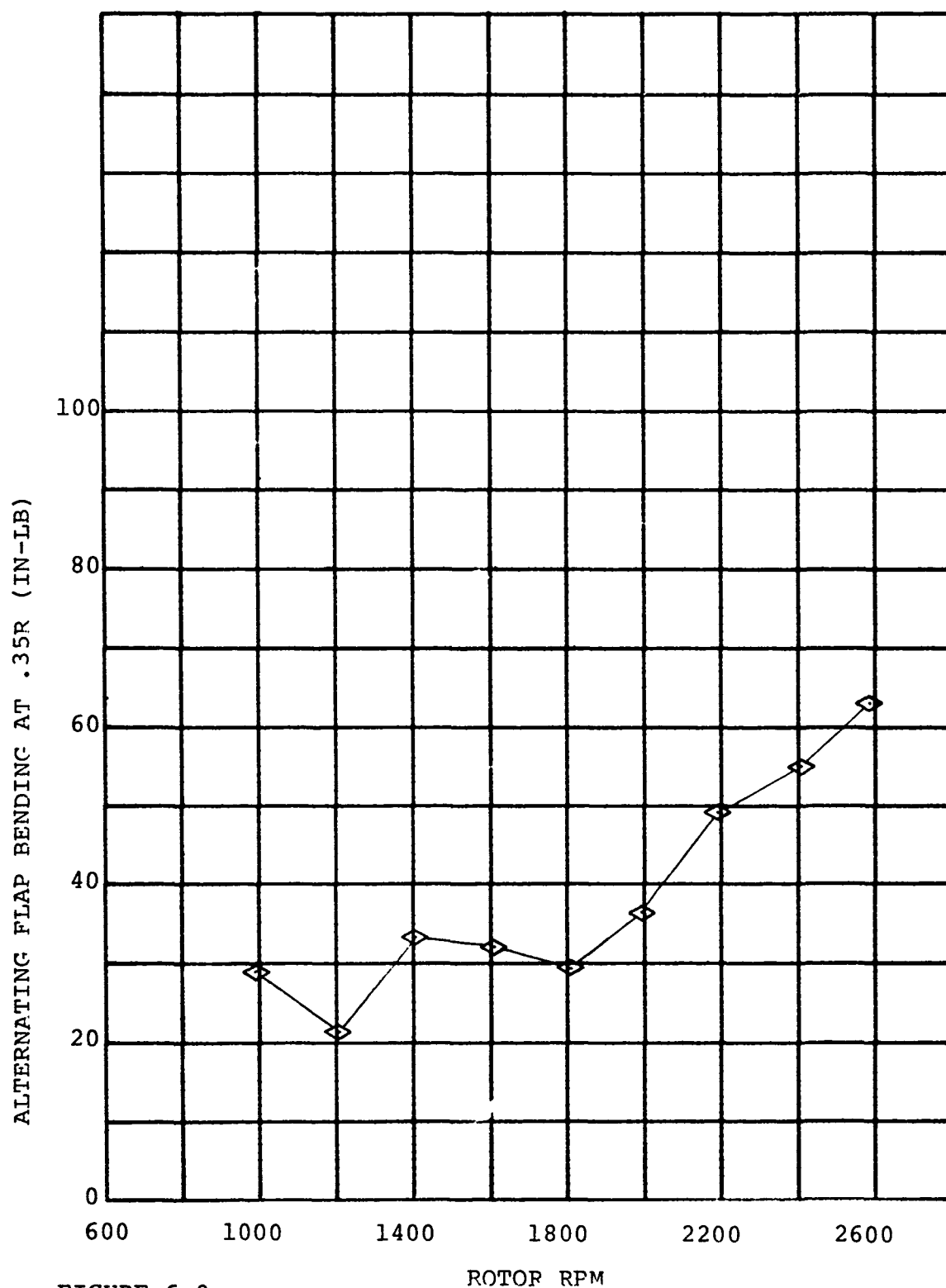


FIGURE 6-9

LEFT-HAND BLADE FLAP BENDING RESPONSE TO ONE-PER-REV BAFFLE FOR TEN DEGREES COLLECTIVE PITCH

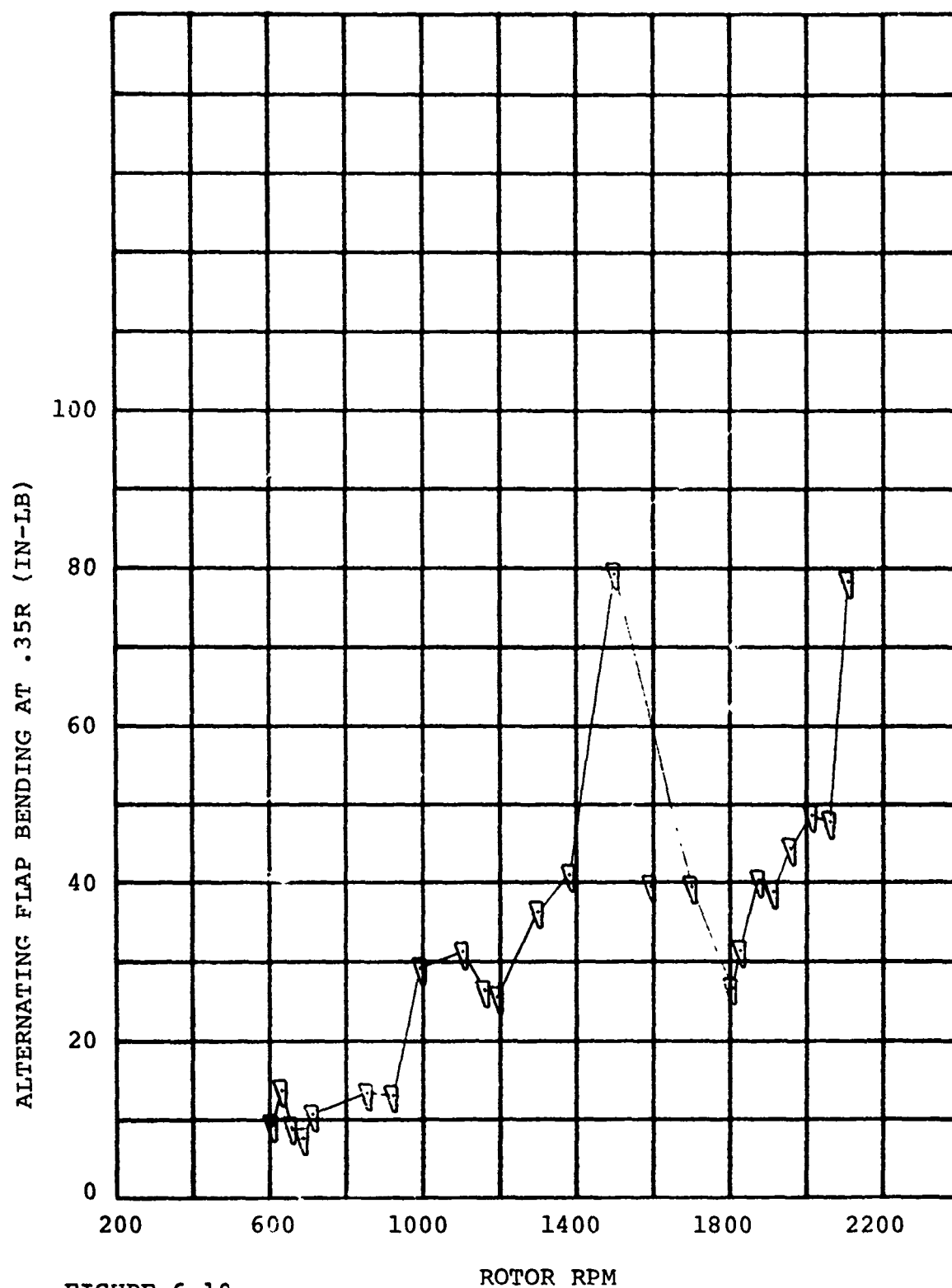


FIGURE 6-10

LEFT-HAND BLADE FLAP BENDING RESPONSE TO TWO-PER-REV BAFFLE FOR TEN DEGREES COLLECTIVE PITCH

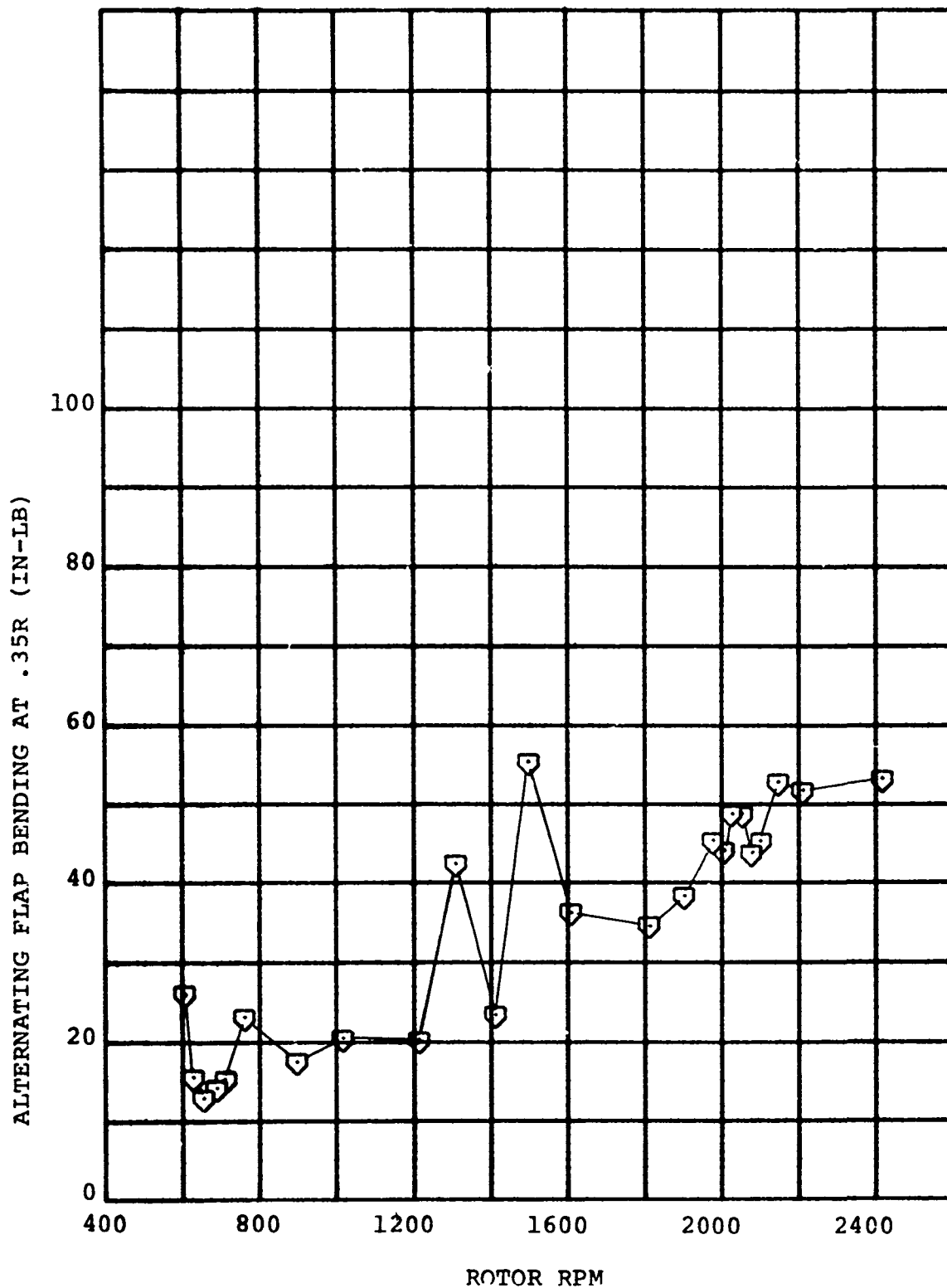


FIGURE 6-11
LEFT-HAND BLADE FLAP BENDING RESPONSE TO THREE-
PER-REV BAFFLE FOR TEN DEGREES COLLECTIVE PITCH

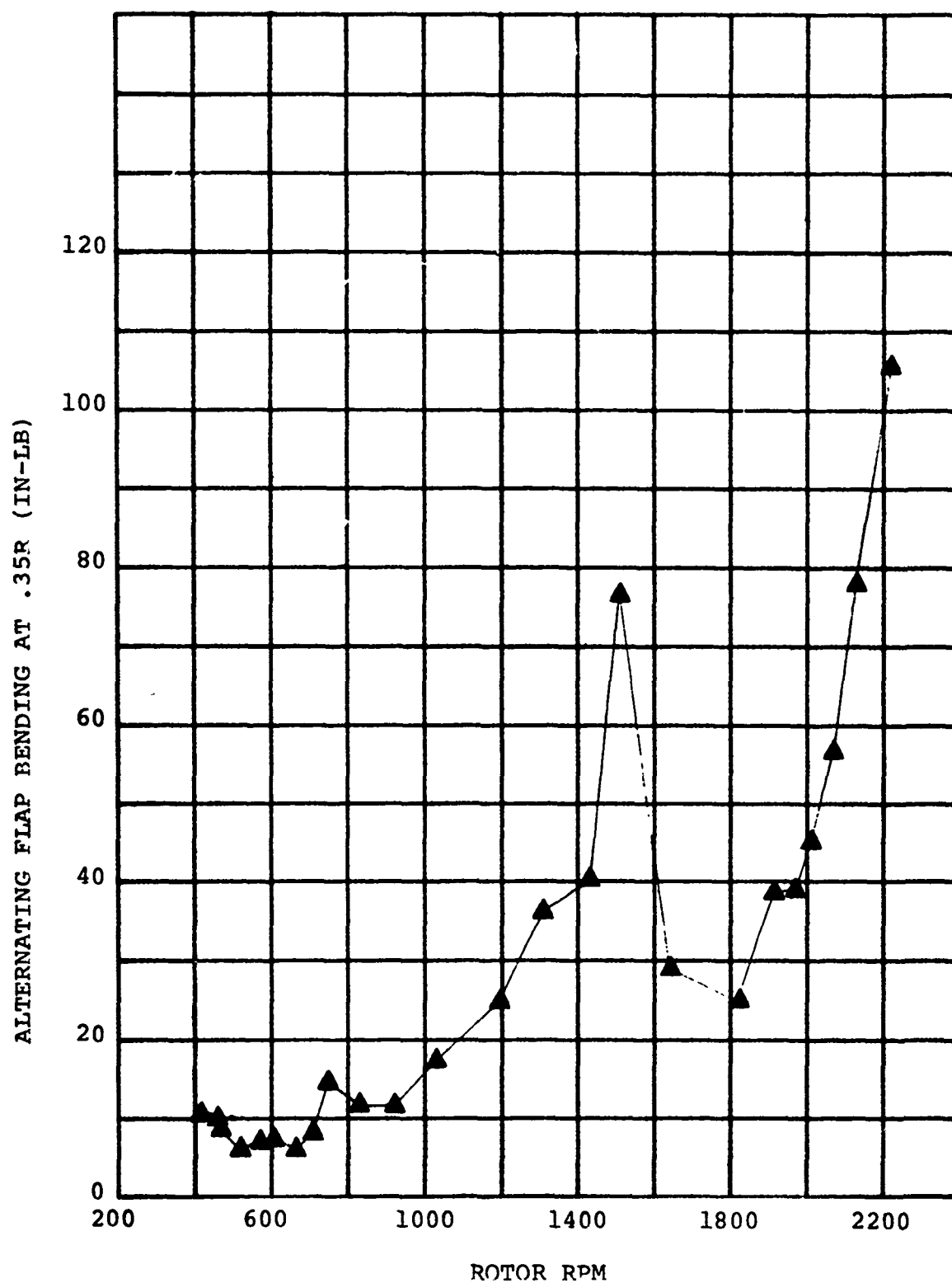


FIGURE 6-12
LEFT-HAND BLADE FLAP BENDING RESPONSE TO FOUR-
PER-REV BAFFLE FOR TEN DEGREES COLLECTIVE PITCH

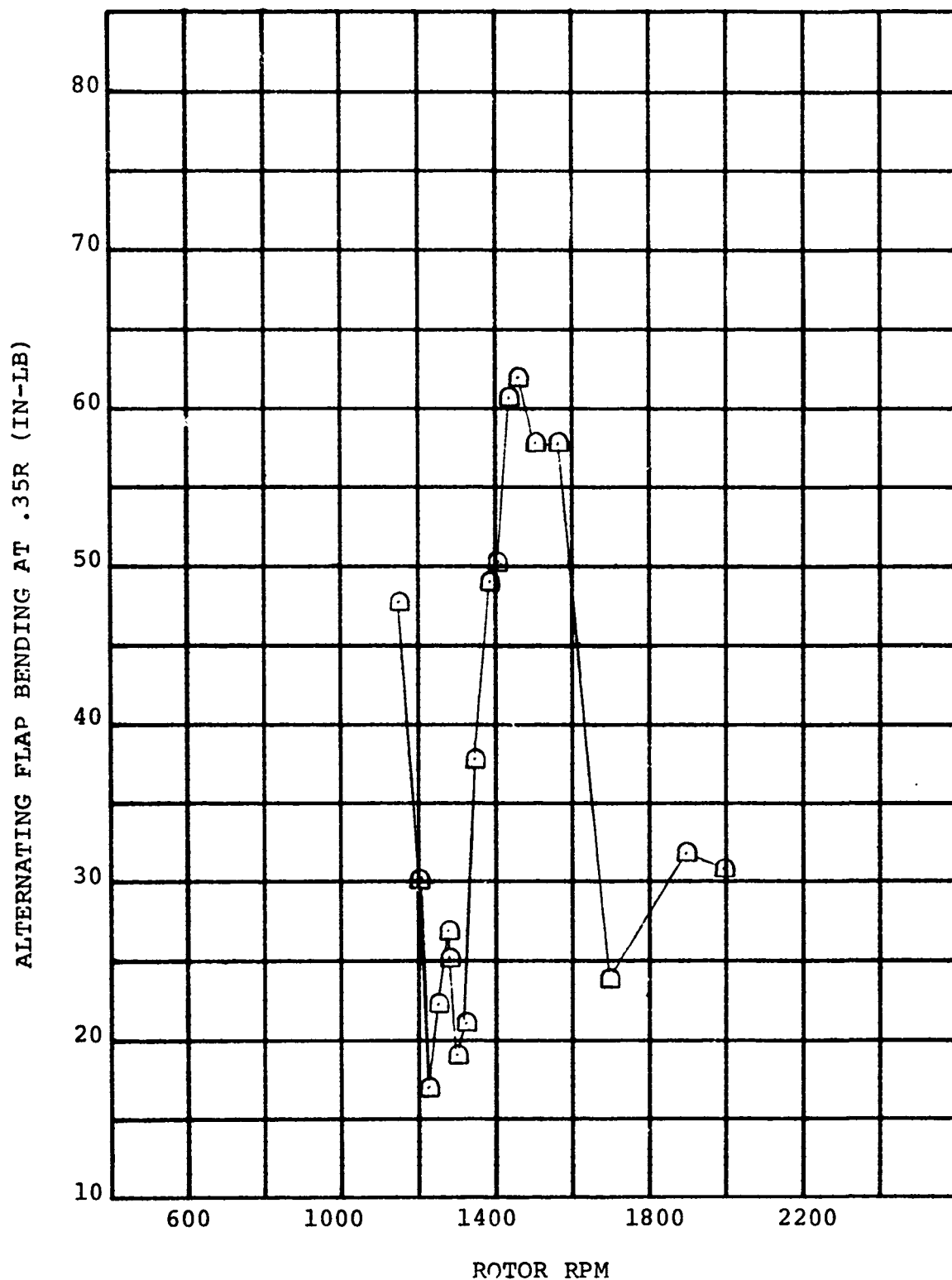


FIGURE 6-13

RIGHT-HAND BLADE FLAP BENDING RESPONSE TO TWO-PER-REV BAFFLE FOR TEN DEGREES COLLECTIVE PITCH

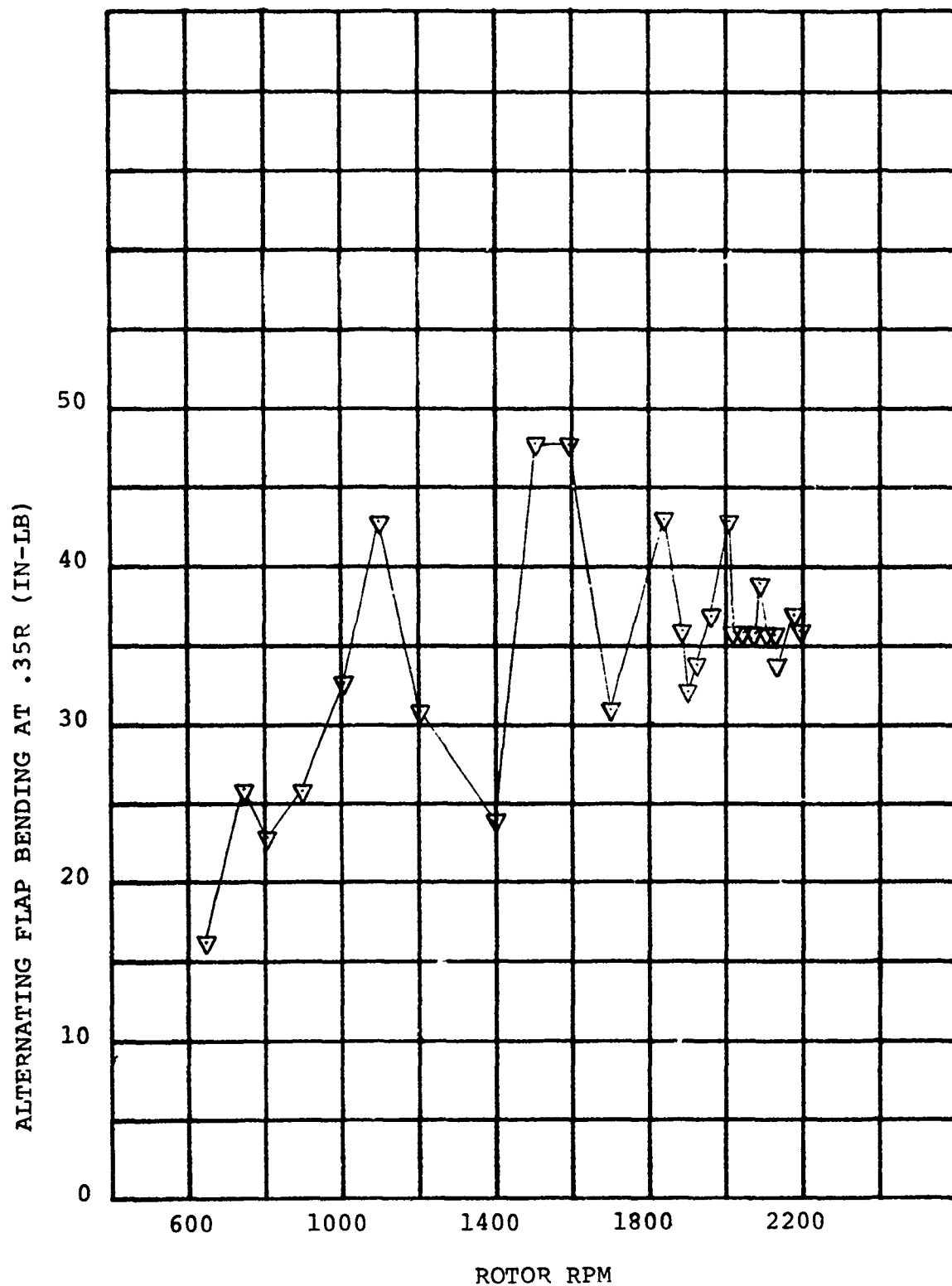


FIGURE 6-14
RIGHT-HAND BLADE FLAP BENDING RESPONSE TO THREE-
PER-REV BAFFLE FOR TEN DEGREES COLLECTIVE PITCH

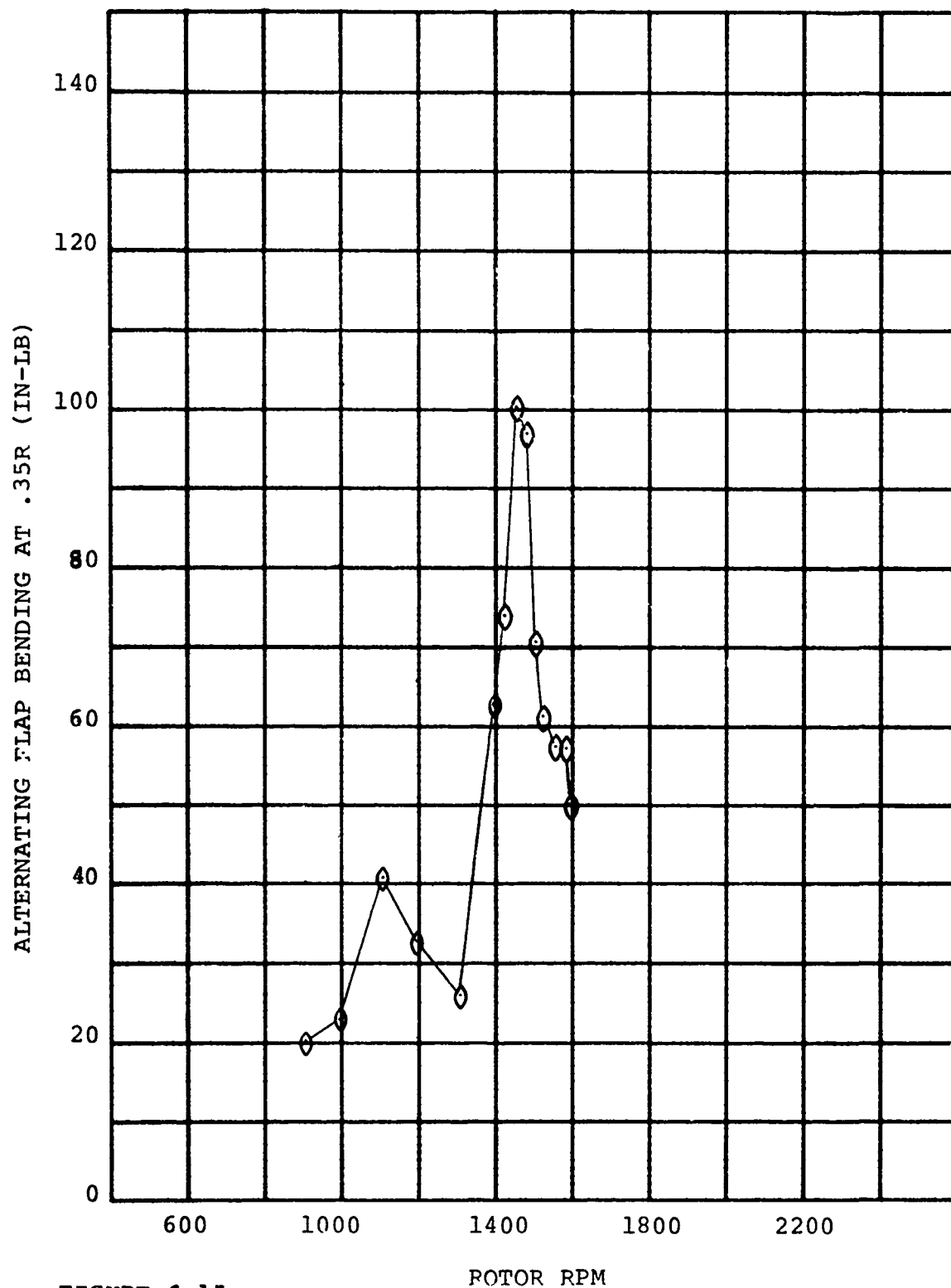


FIGURE 6-15

RIGHT-HAND BLADE FLAP BENDING RESPONSE TO FOUR-PER-REV BAFFLE FOR TEN DEGREES COLLECTIVE PITCH

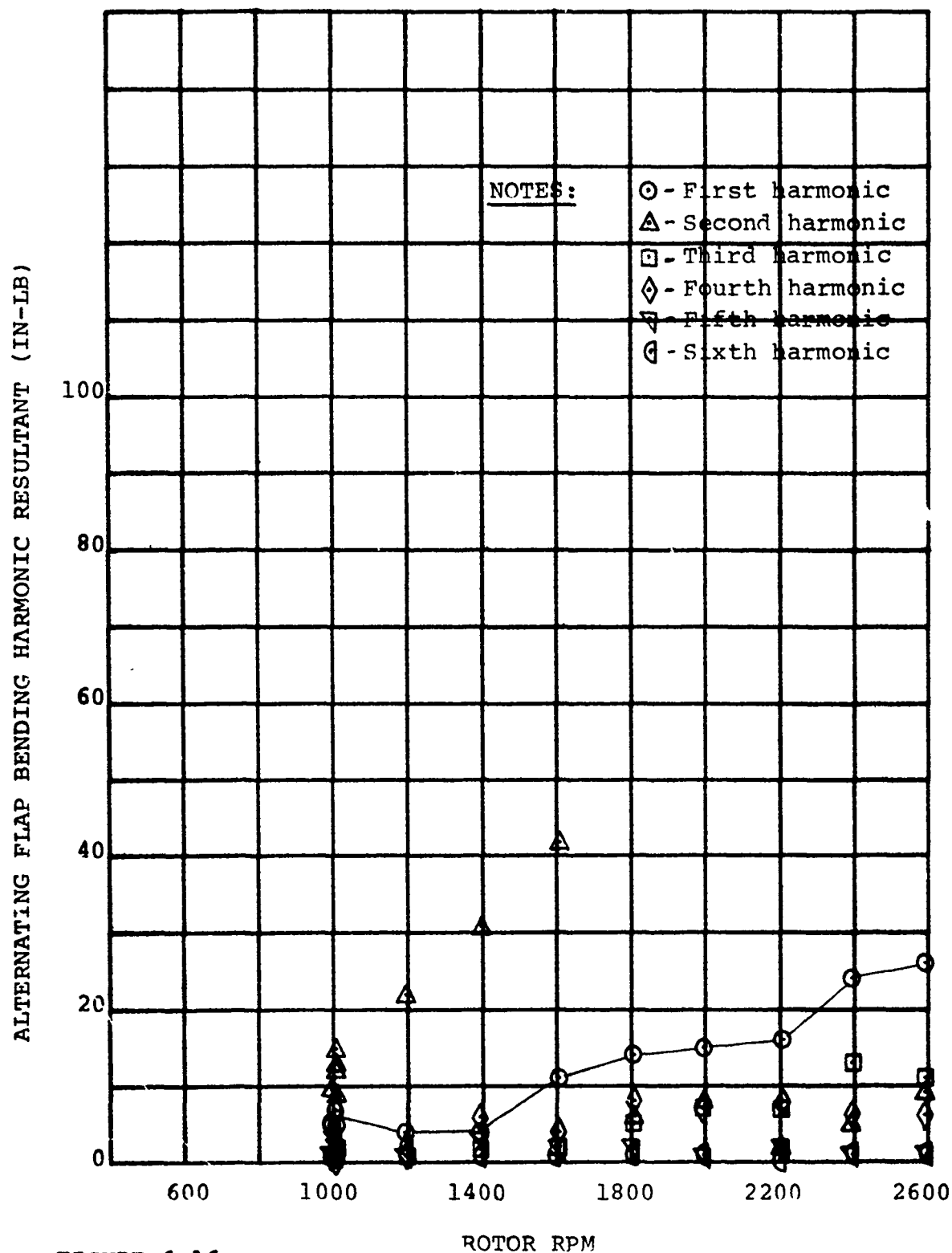


FIGURE 6-16

RIGHT-HAND BLADE FLAP BENDING HARMONIC RESPONSE TO ONE-PER-REV BAFFLE FOR TEN DEGREES COLLECTIVE PITCH

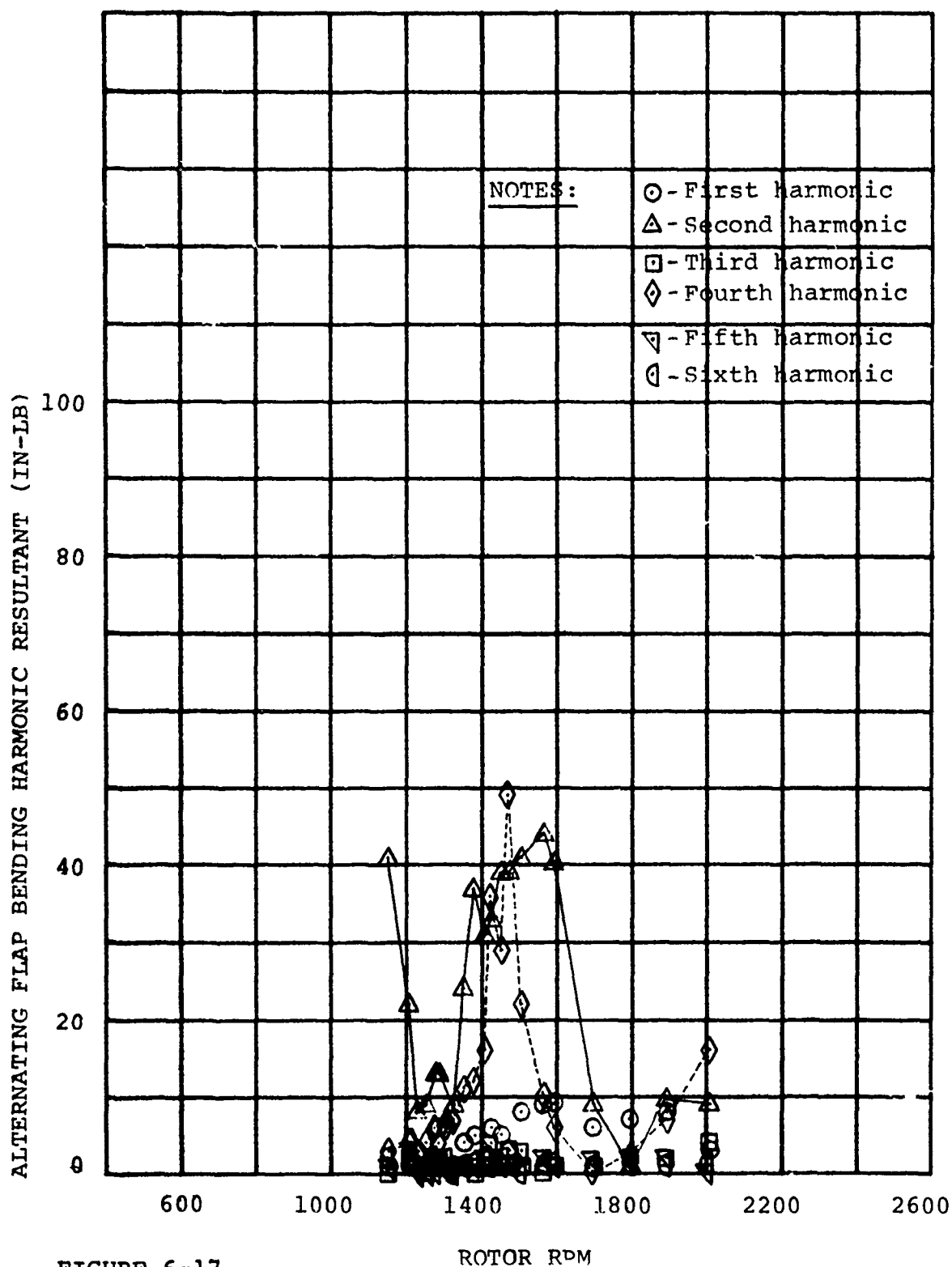


FIGURE 6-17

RIGHT-HAND BLADE FLAP BENDING HARMONIC RESPONSE TO TWO-PER-REV BAFFLE FOR TEN DEGREES COLLECTIVE PITCH

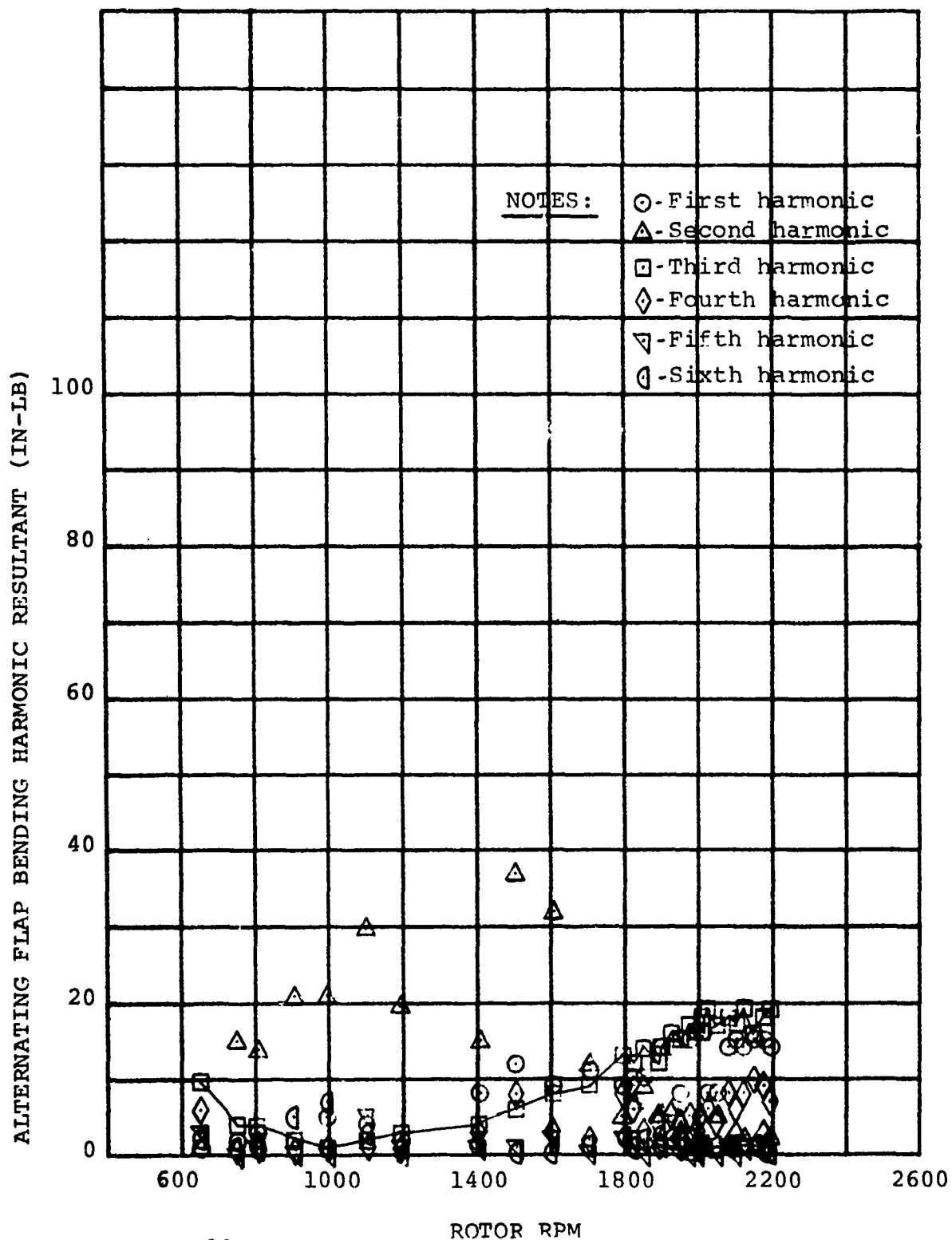


FIGURE 6-18

RIGHT-HAND BLADE FLAP BENDING HARMONIC RESPONSE TO
THREE-PER-REV BAFFLE FOR TEN DEGREES COLLECTIVE PITCH

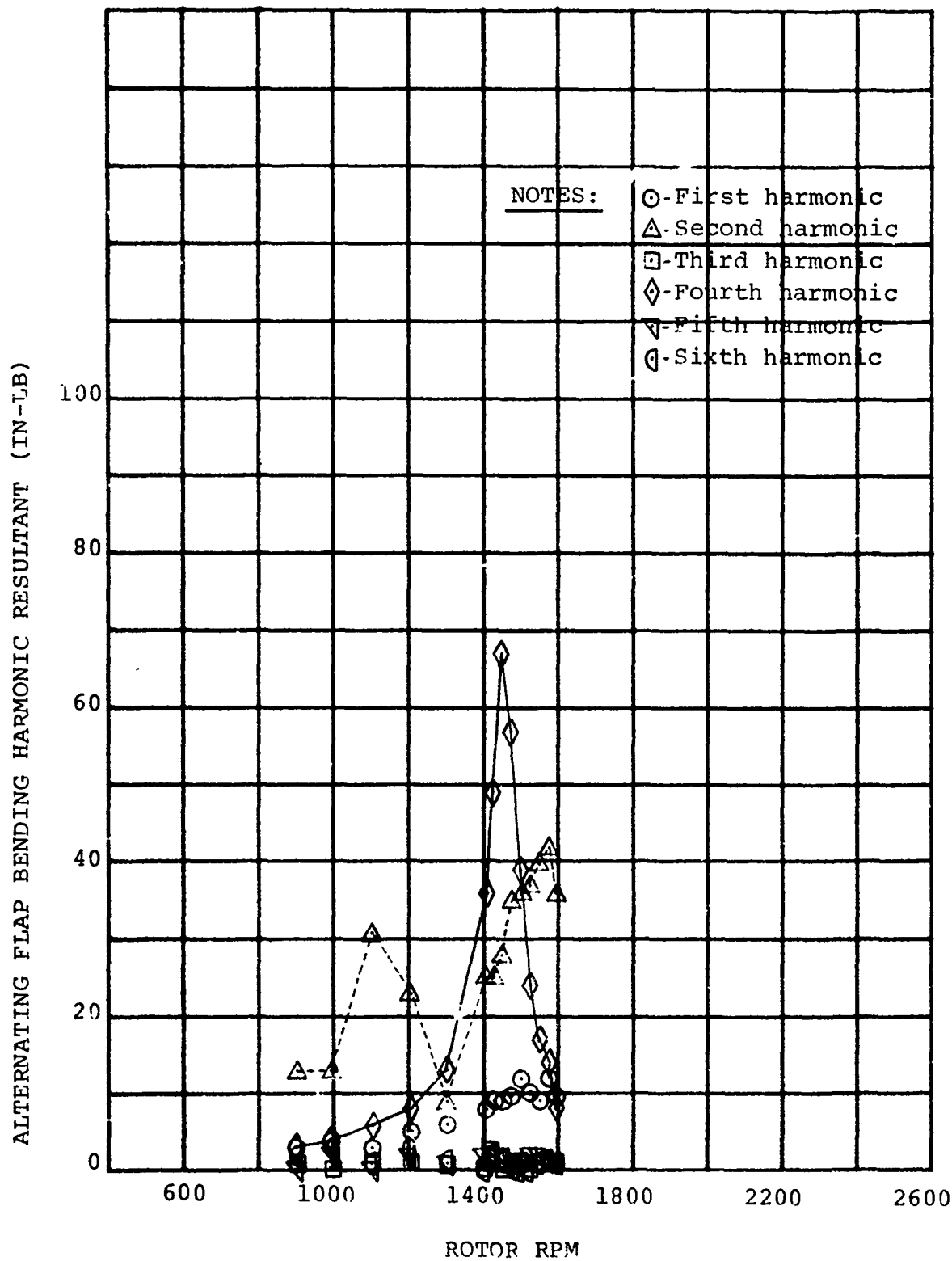


FIGURE 6-19

RIGHT-HAND BLADE FLAP BENDING HARMONIC RESPONSES TO
FOUR-PER-REV BAFFLE FOR TEN DEGREES COLLECTIVE PITCH

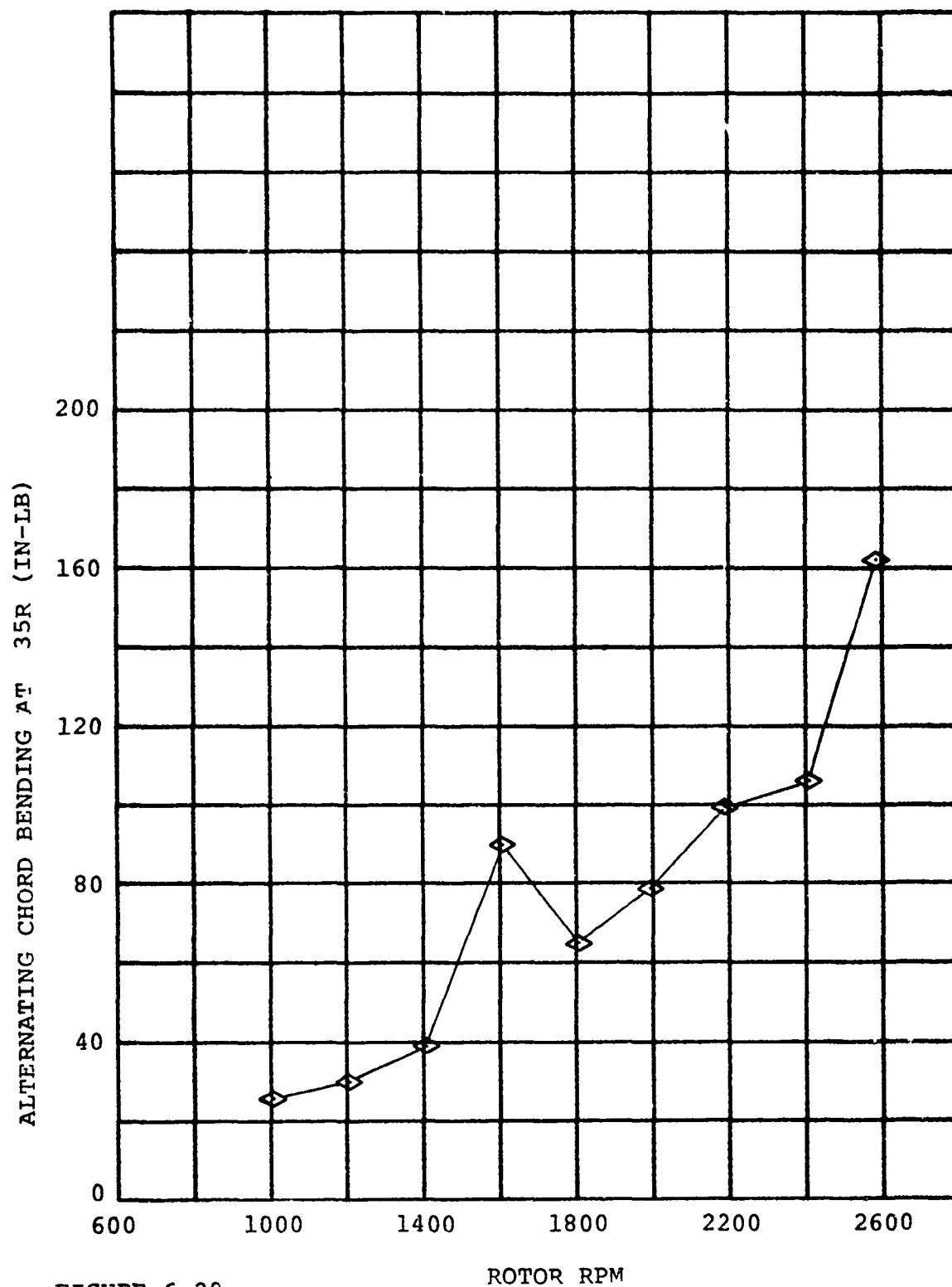


FIGURE 6-20

LEFT-HAND BLADE CHORD BENDING RESPONSE TO ONE-
PER-REV BAFFLE FOR TEN DEGREES COLLECTIVE PITCH

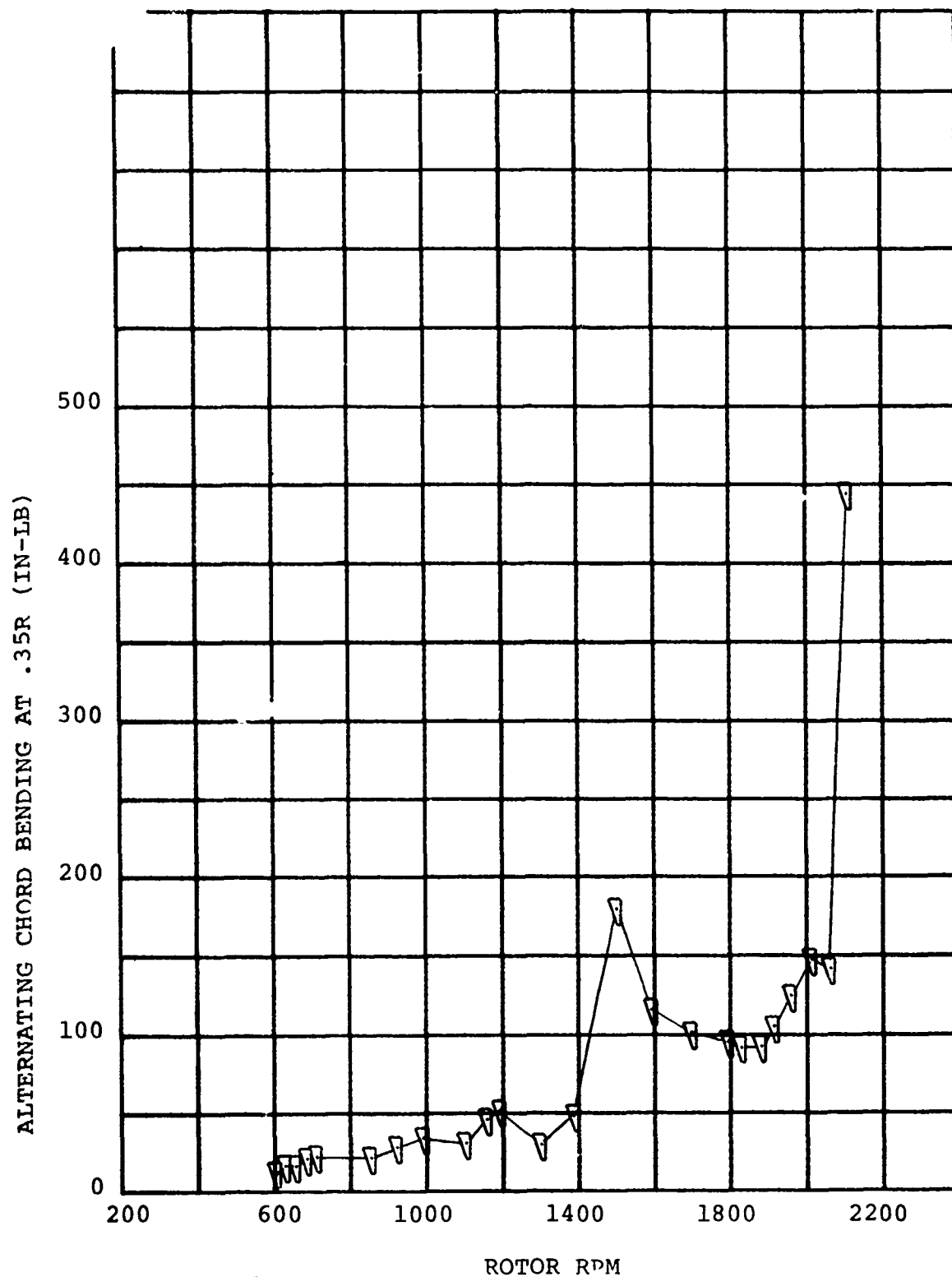


FIGURE 6-21

LEFT-HAND BLADE CHORD BENDING RESPONSE TO TWO-
PER-REV BAFFLE FOR TEN DEGREES COLLECTIVE PITCH

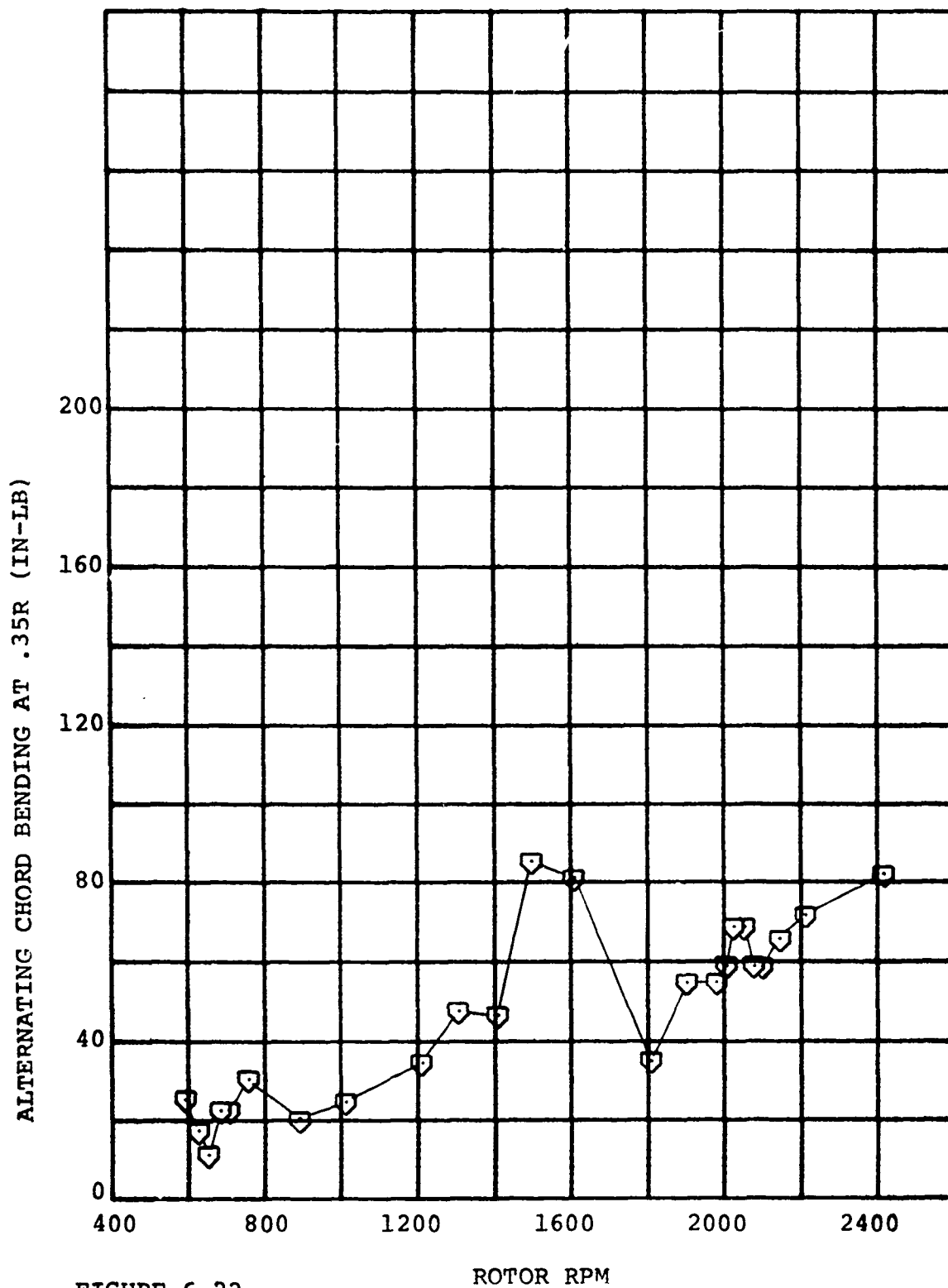


FIGURE 6-22

LEFT-HAND BLADE CHORD BENDING RESPONSE TO THREE-
PER-REV BAFFLE FOR TEN DEGREES COLLECTIVE PITCH

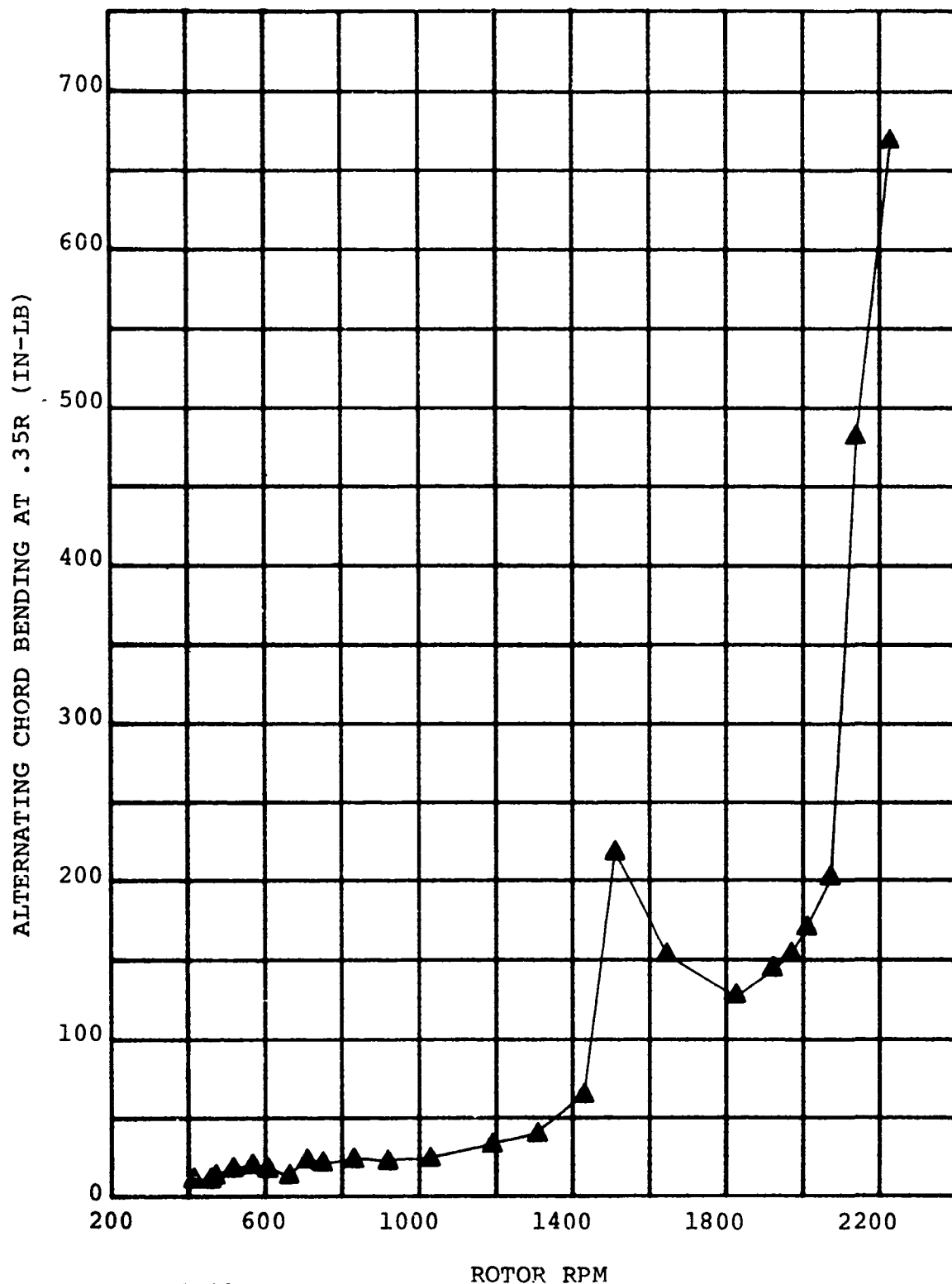


FIGURE 6-23

LEFT-HAND BLADE CHORD BENDING RESPONSE TO FOUR-
PER-REV BAFFLE FOR TEN DEGREES COLLECTIVE PITCH

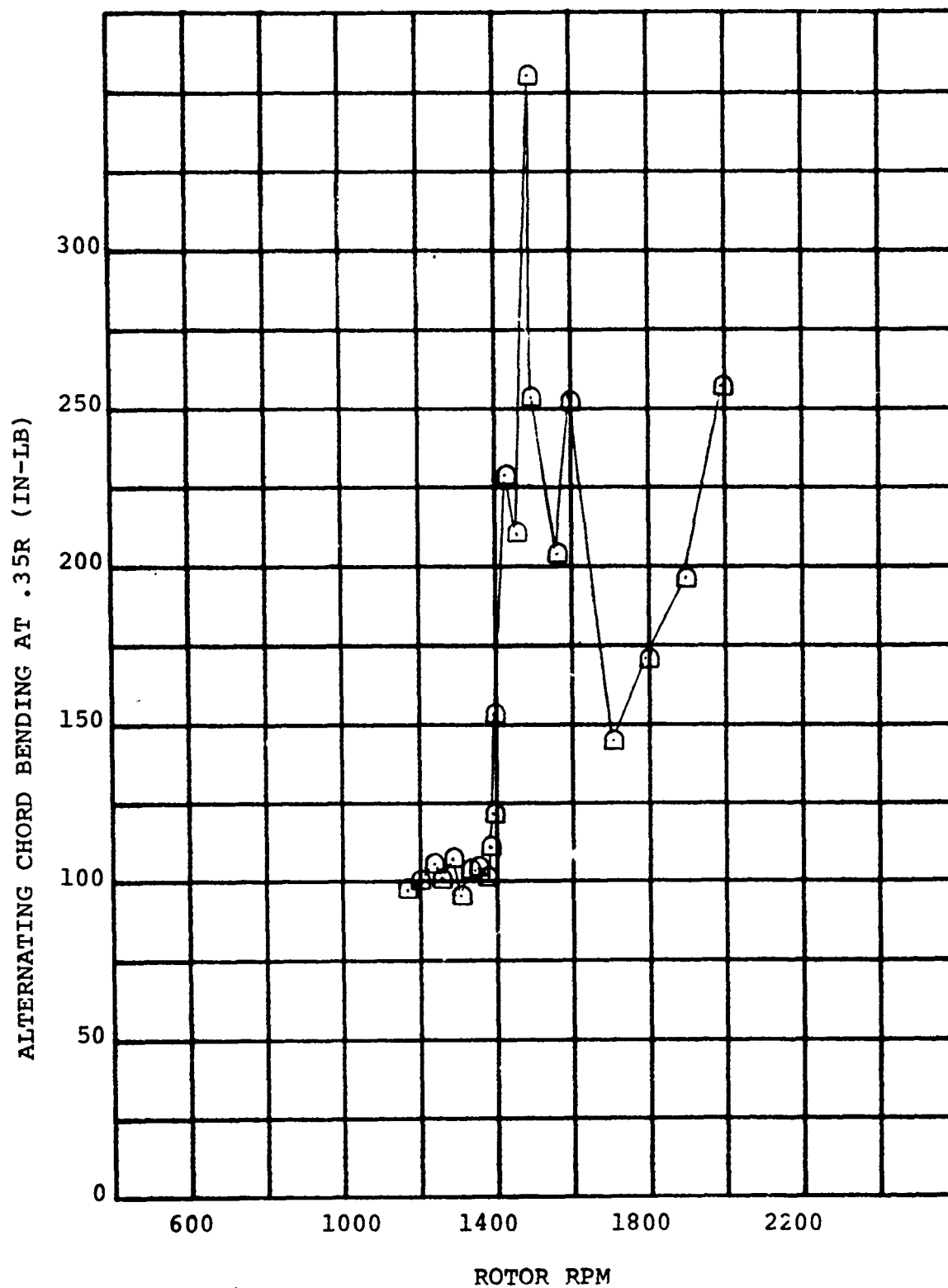


FIGURE 6-24

RIGHT-HAND BLADE CHORD BENDING RESPONSE TO TWO-PER-REV BAFFLE FOR TEN DEGREES COLLECTIVE PITCH

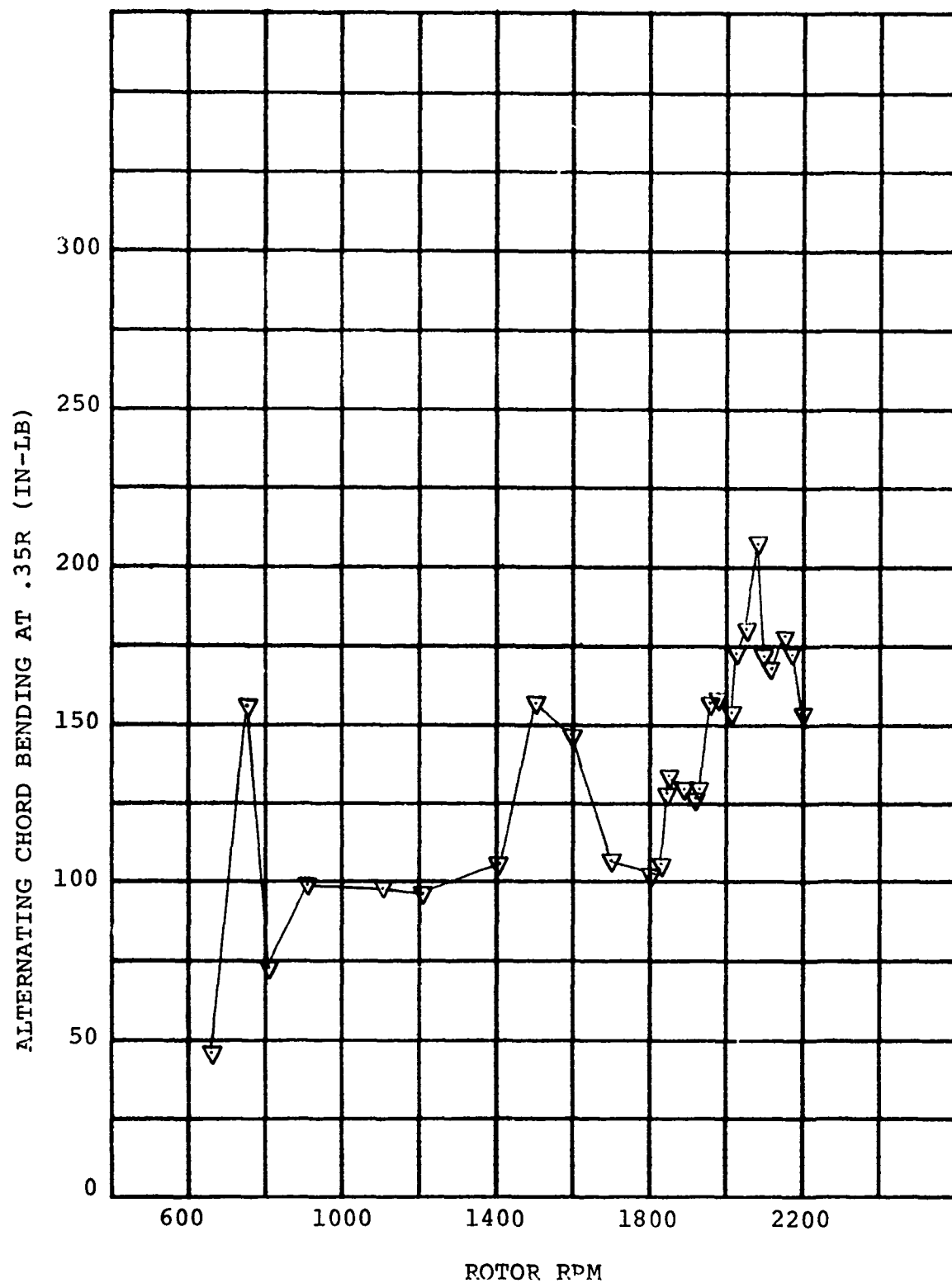


FIGURE 6-25
RIGHT-HAND BLADE CHORD BENDING RESPONSE TO THREE-
PER-REV BAFFLE FOR TEN DEGREES COLLECTIVE PITCH

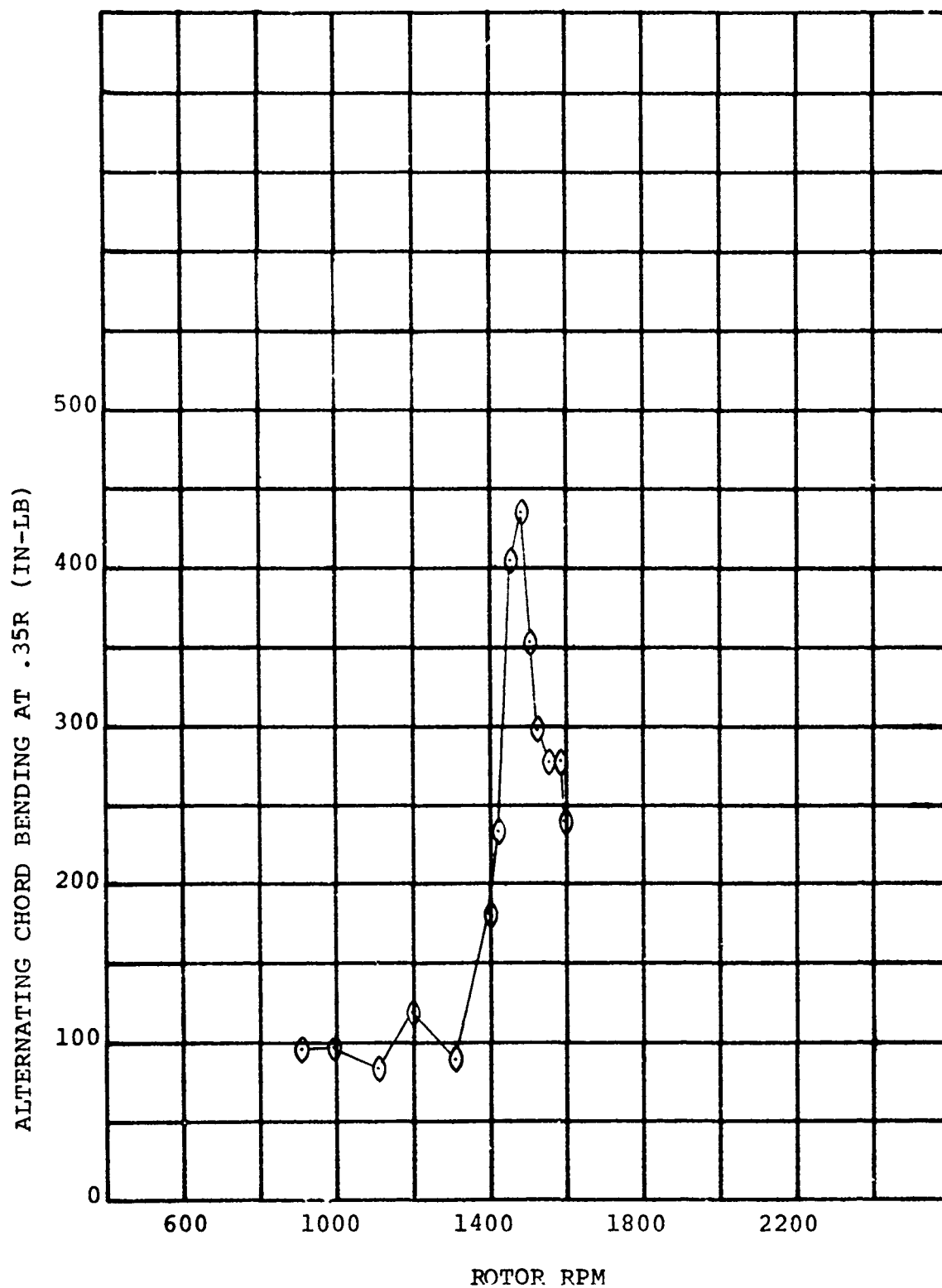


FIGURE 6-26
RIGHT-HAND BLADE CHORD BENDING RESPONSE TO FOUR-
PER-REV PAFFLE FOR TEN DEGREES COLLECTIVE PITCH

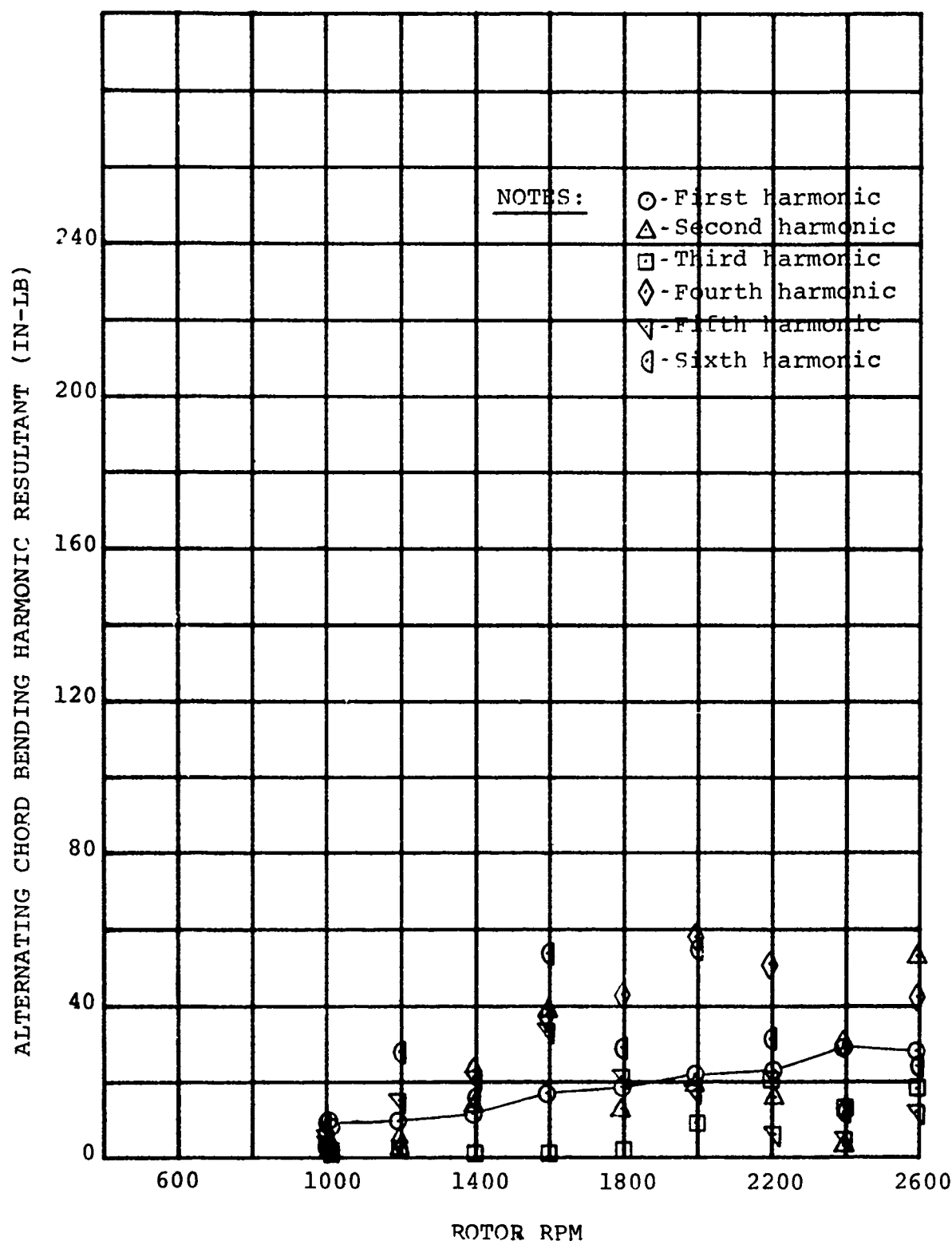


FIGURE 6-27

RIGHT-HAND BLADE CHORD BENDING HARMONIC RESPONSES TO ONE-PER-REV BAFFLE FOR TEN DEGREES COLLECTIVE PITCH

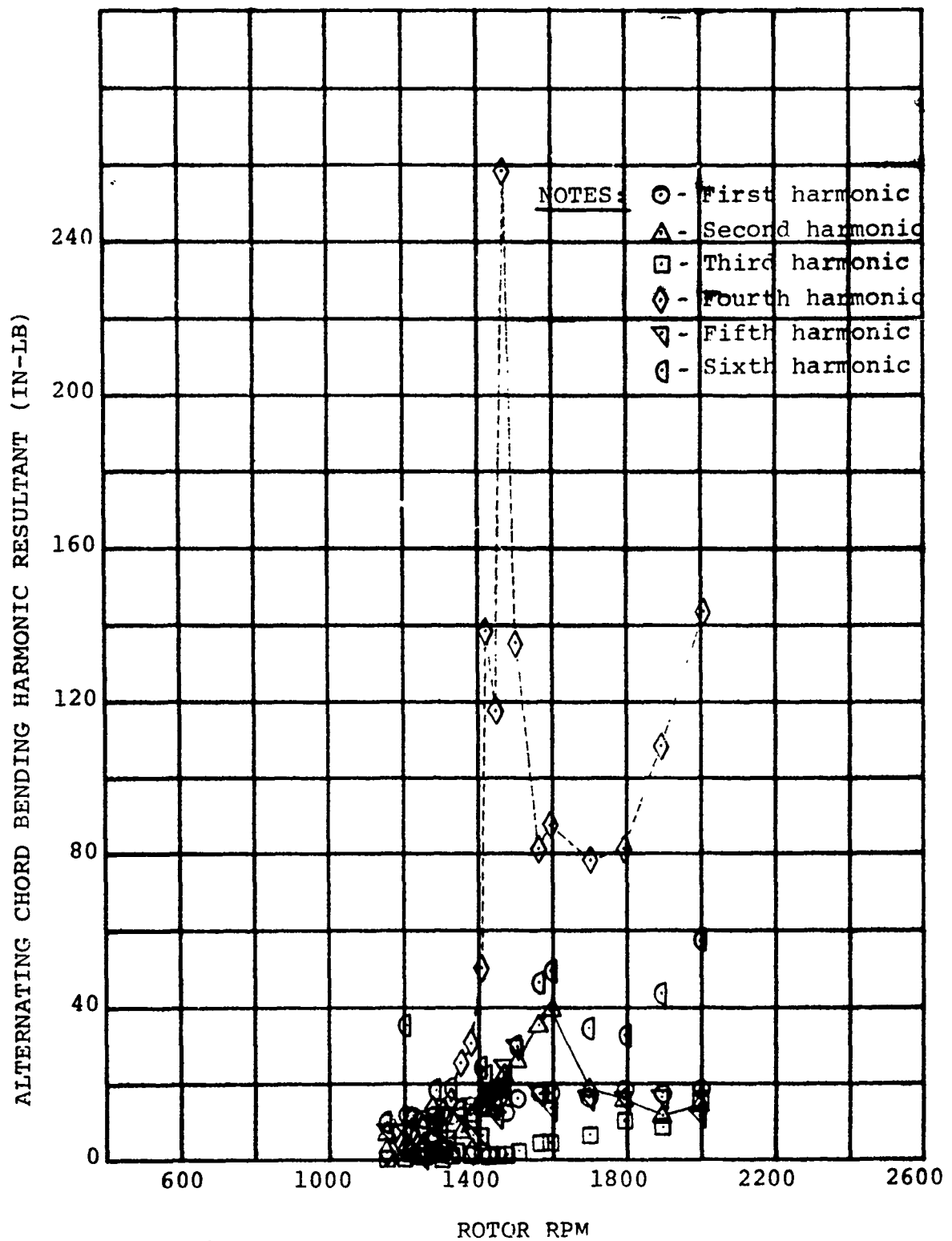


FIGURE 6-28

RIGHT-HAND BLADE CHORD BENDING HARMONIC RESPONSE TO TWO-PER-REV BAFFLE FOR TEN DEGREES COLLECTIVE PITCH

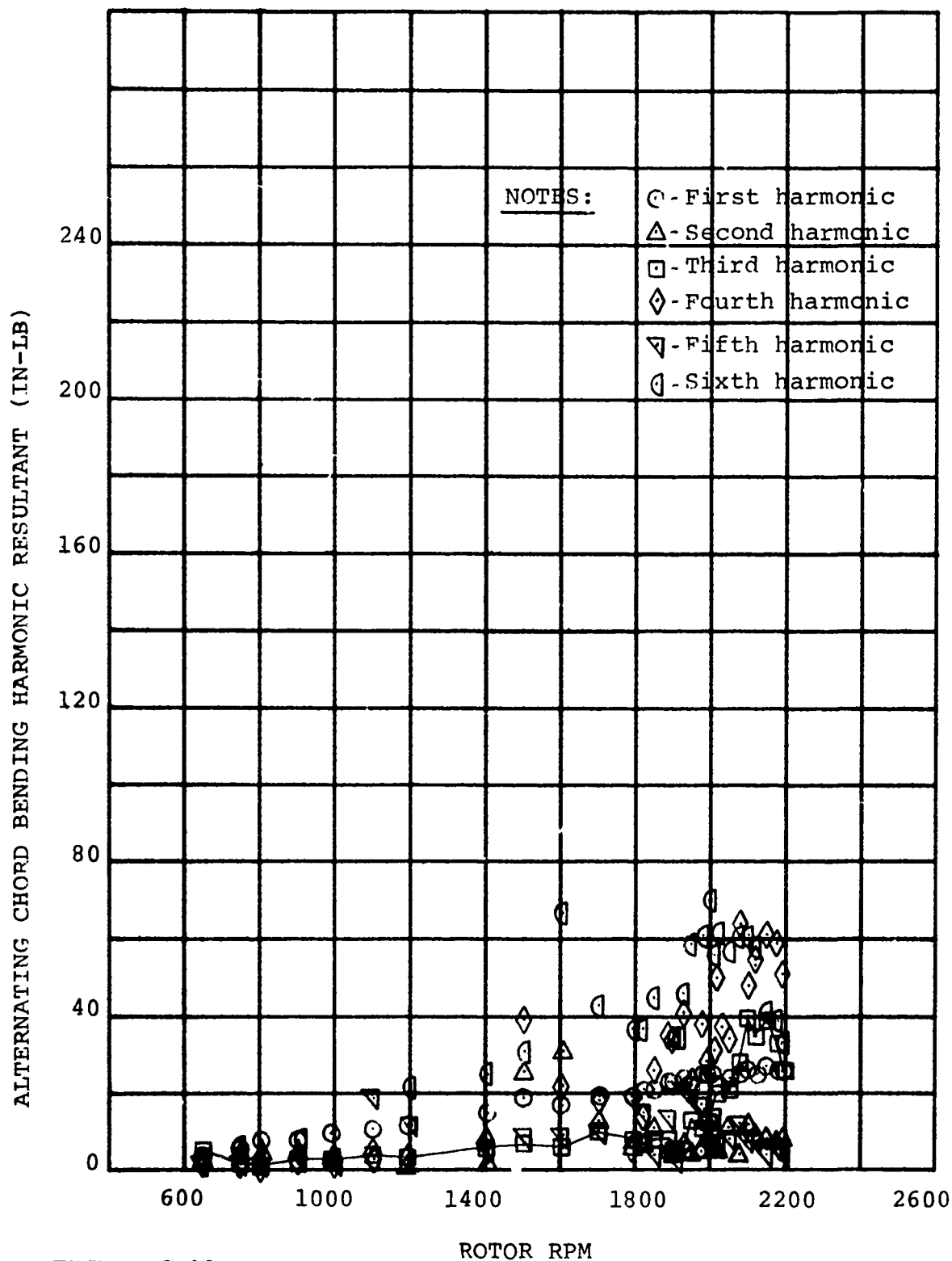


FIGURE 6-29

RIGHT-HAND BLADE CHORD BENDING HARMONIC RESPONSE TO THREE-PER-REV BAFFLE FOR TEN DEGREES COLLECTIVE PITCH

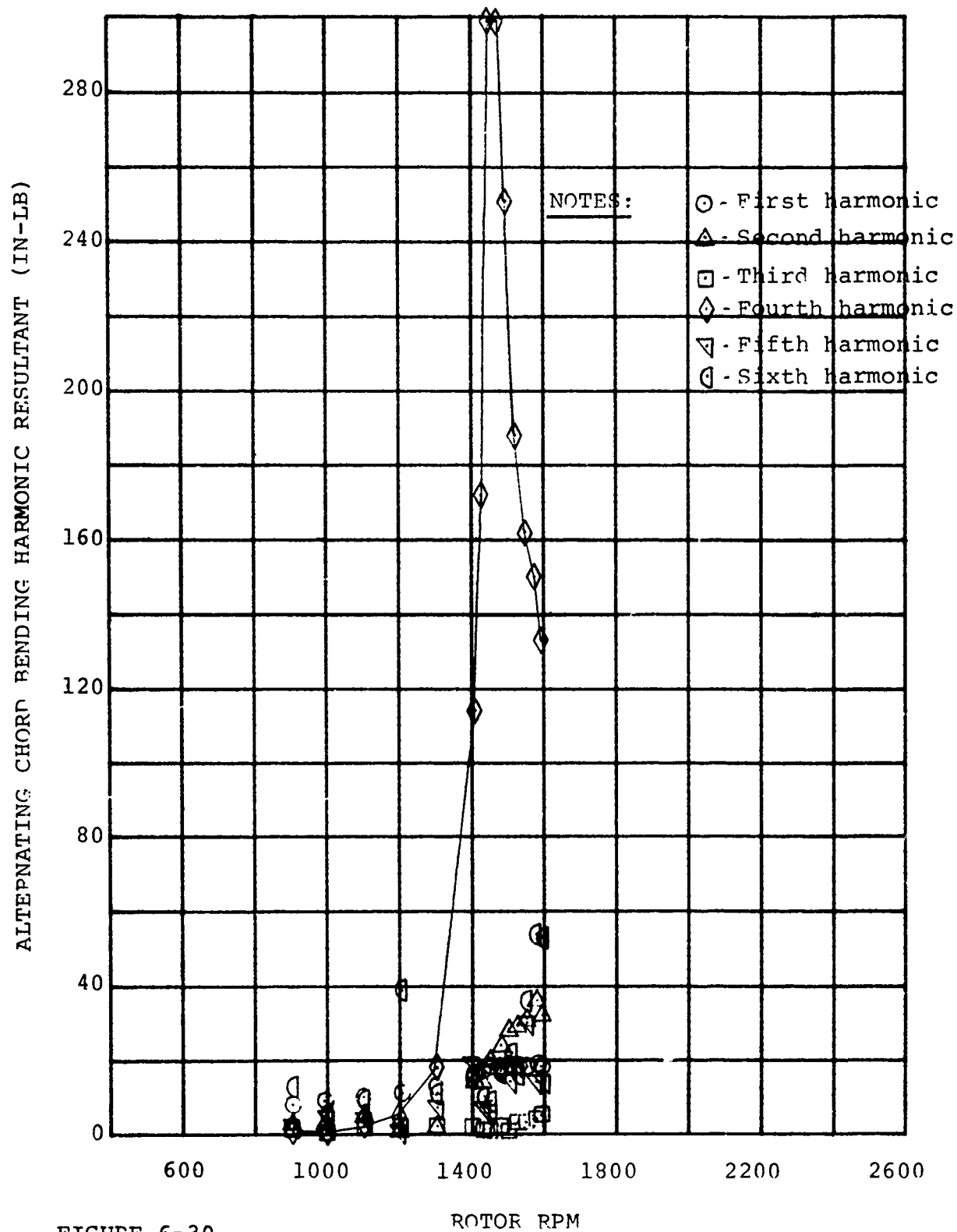


FIGURE 6-30

RIGHT-HAND BLADE CHORD BENDING HARMONIC RESPONSE TO
FOUR-PER-REV BAFFLE FOR TEN DEGREES COLLECTIVE PITCH

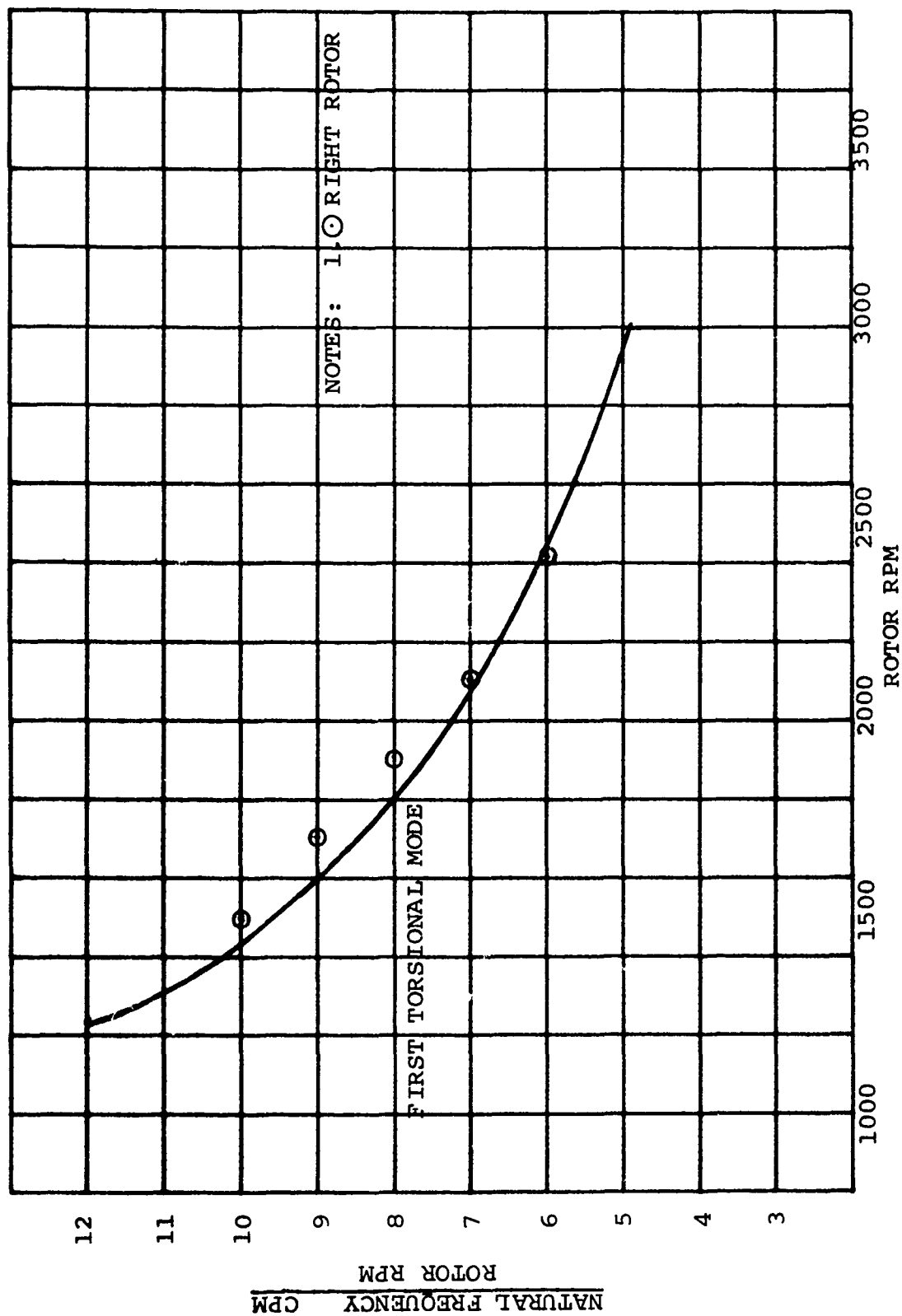


FIGURE 6-31. PREDICTED AND MEASURED ROTOR BLADE TORSIONAL NATURAL FREQUENCY

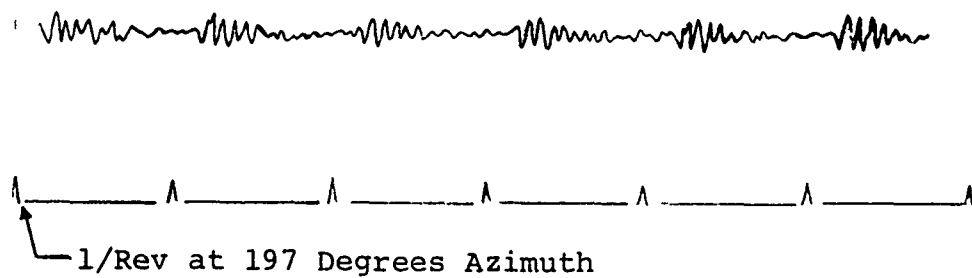


FIGURE 6-32

LEFT ROTOR BLADE TORSIONAL RESPONSE
TO TWO-PER-REV BAFFLE AT 1100 RPM

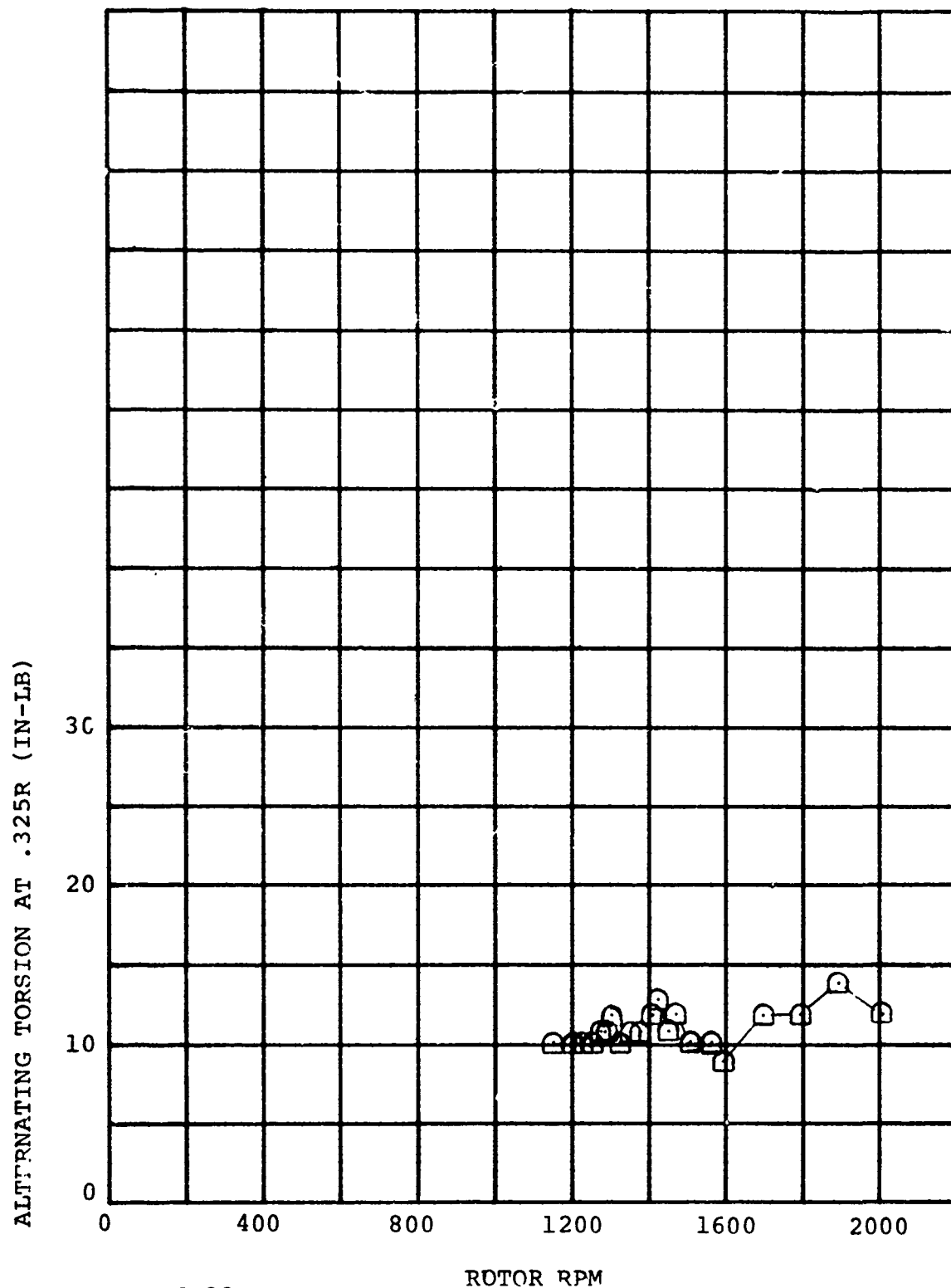


FIGURE 6-33

RIGHT-HAND BLADE TORSIONAL RESPONSE TO TWO-
PER-REV BAFFLE FOR TEN DEGREES COLLECTIVE PITCH

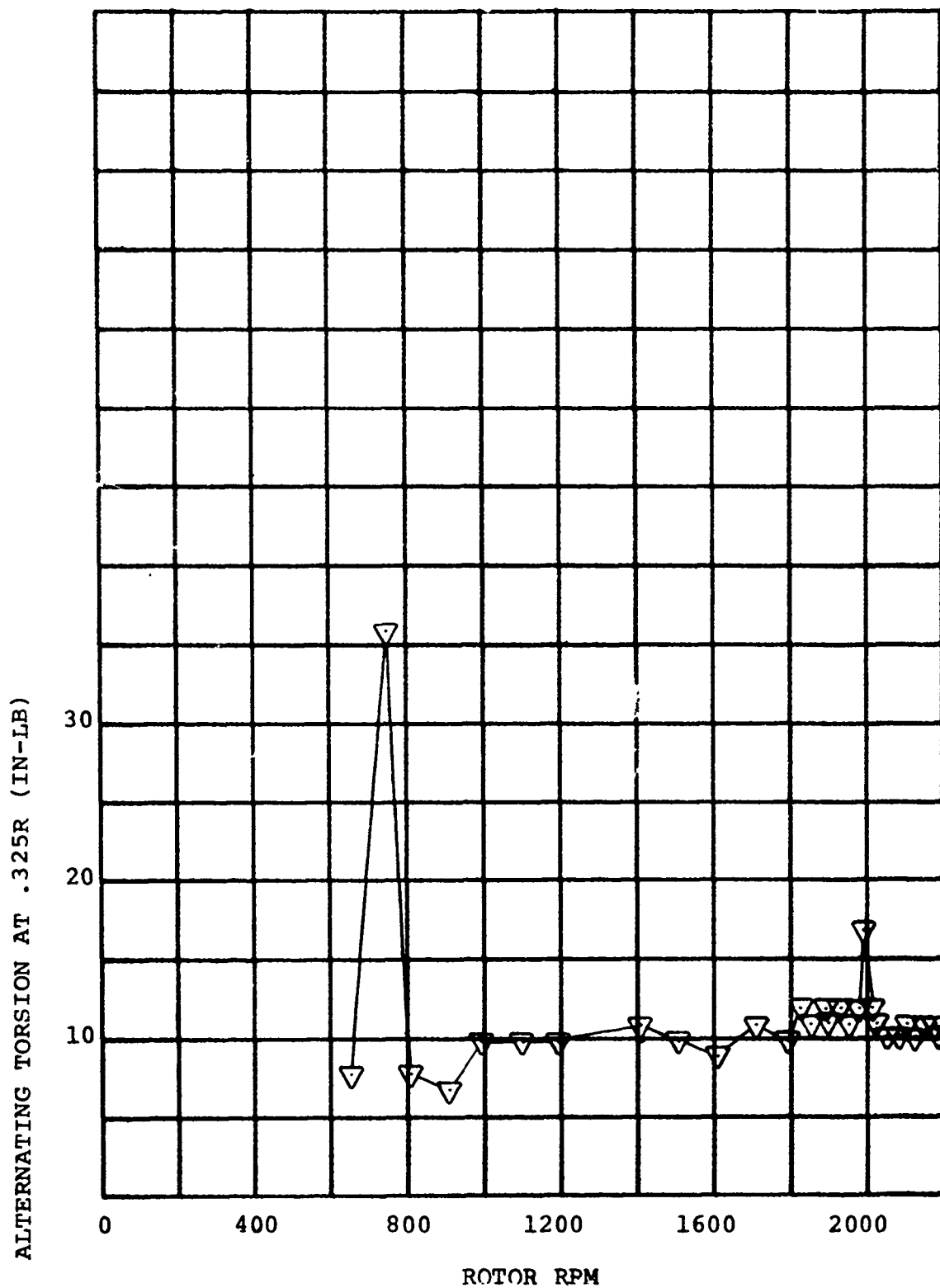


FIGURE 6-34
RIGHT-HAND BLADE TORSIONAL RESPONSE TO THREE-
PER-REV BAFFLE FOR TEN DEGREES COLLECTIVE PITCH

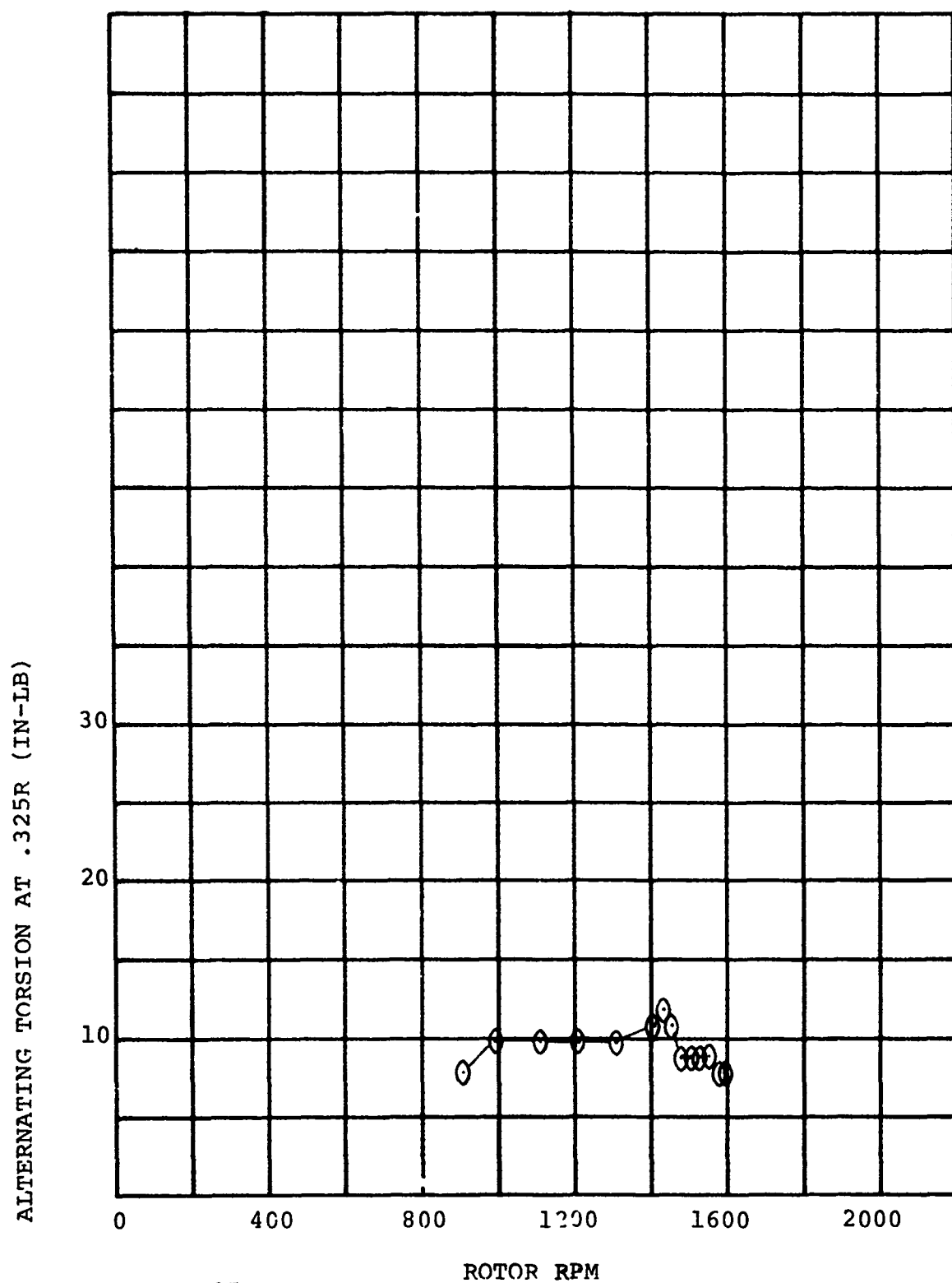


FIGURE 6-35
RIGHT-HAND BLADE TORSIONAL RESPONSE TO FOUR-
PER-REV BAFFLE FOR TEN DEGREES COLLECTIVE PITCH

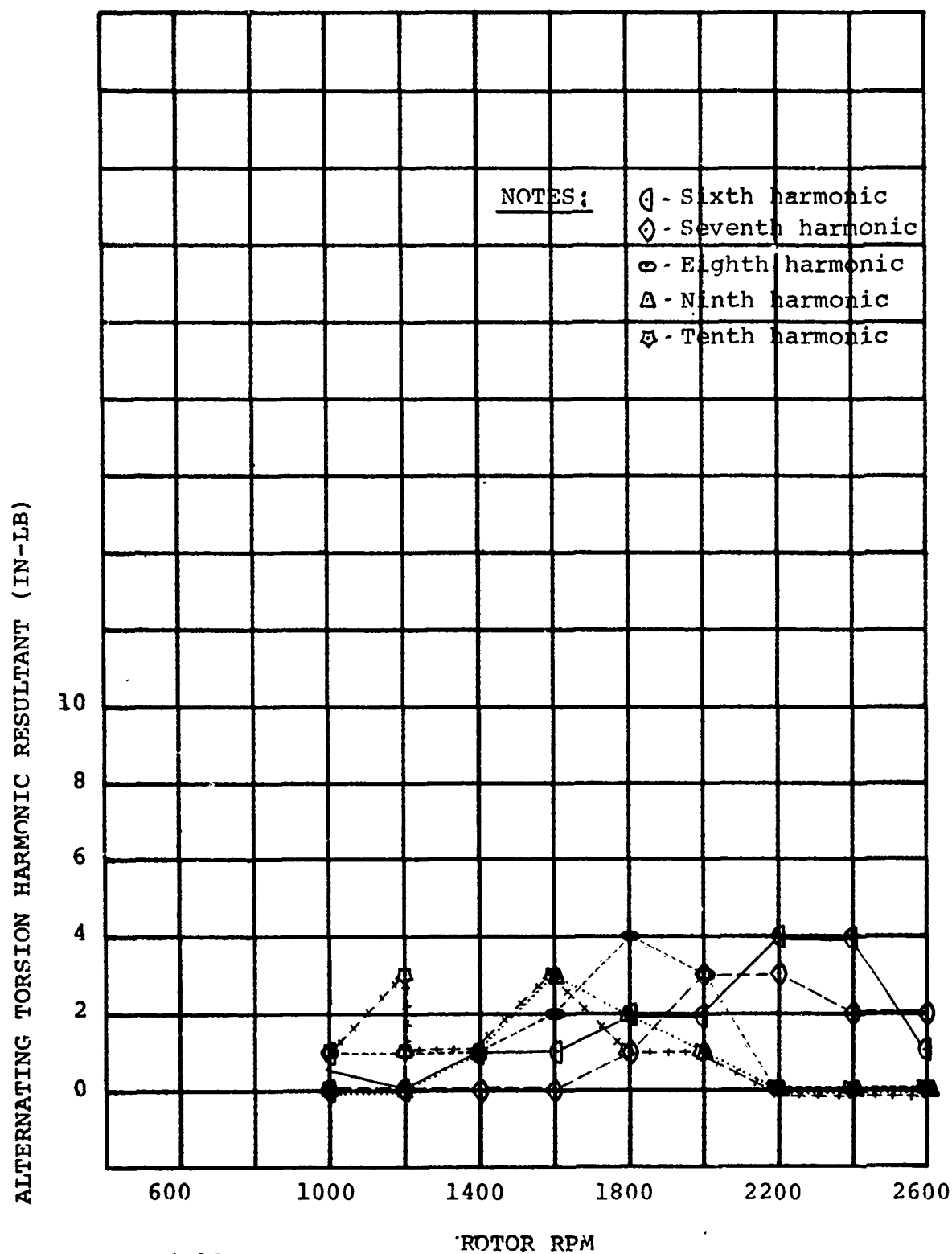


FIGURE 6-36

RIGHT-HAND BLADE TORSIONAL HARMONIC RESPONSE TO
ONE-PER-REV BAFFLE FOR TEN DEGREES COLLECTIVE PITCH

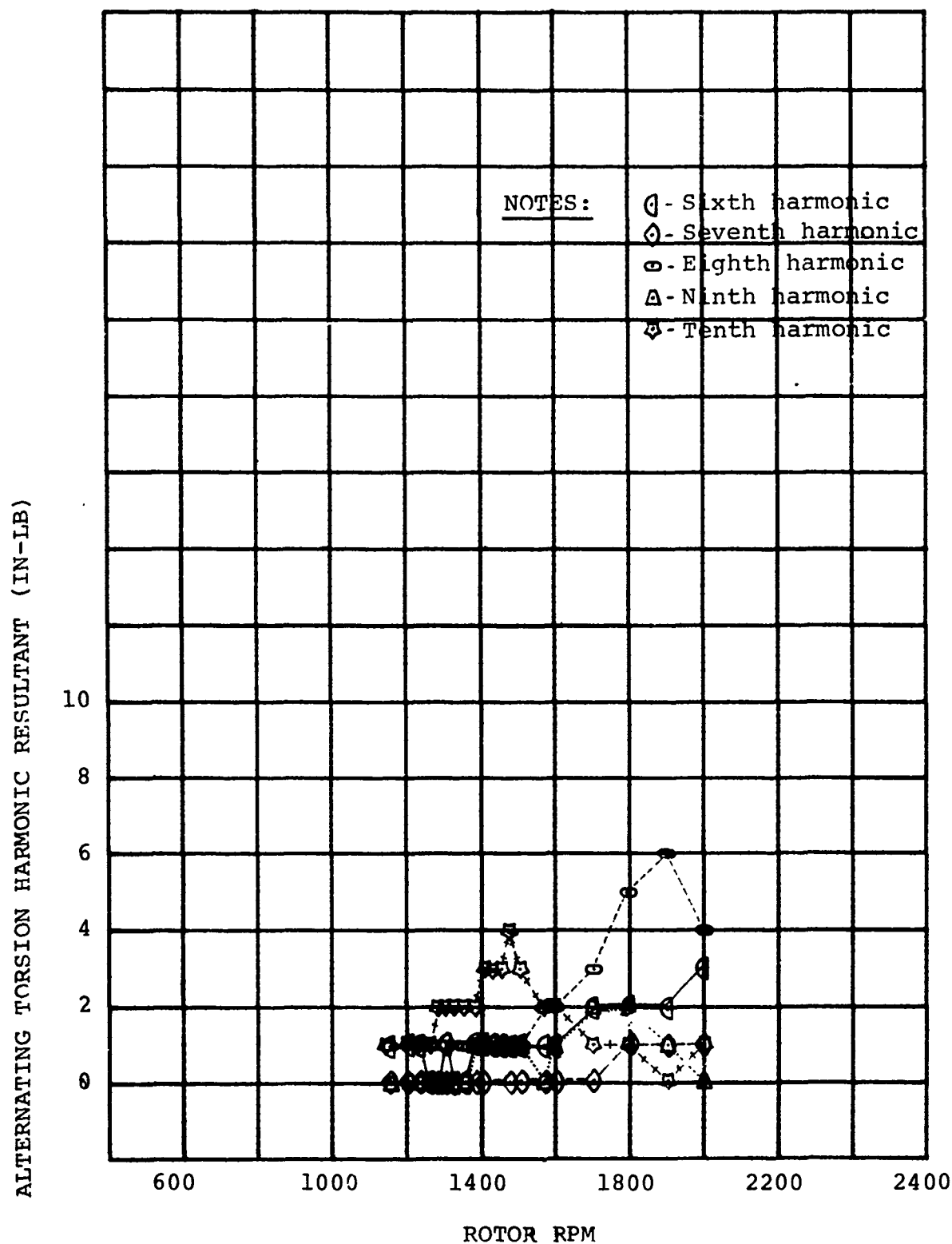


FIGURE 6-37
RIGHT-HAND BLADE TORSIONAL HARMONIC RESPONSE TO
TWO-PER-REV BAFFLE FOR TEN DEGREES COLLECTIVE PITCH

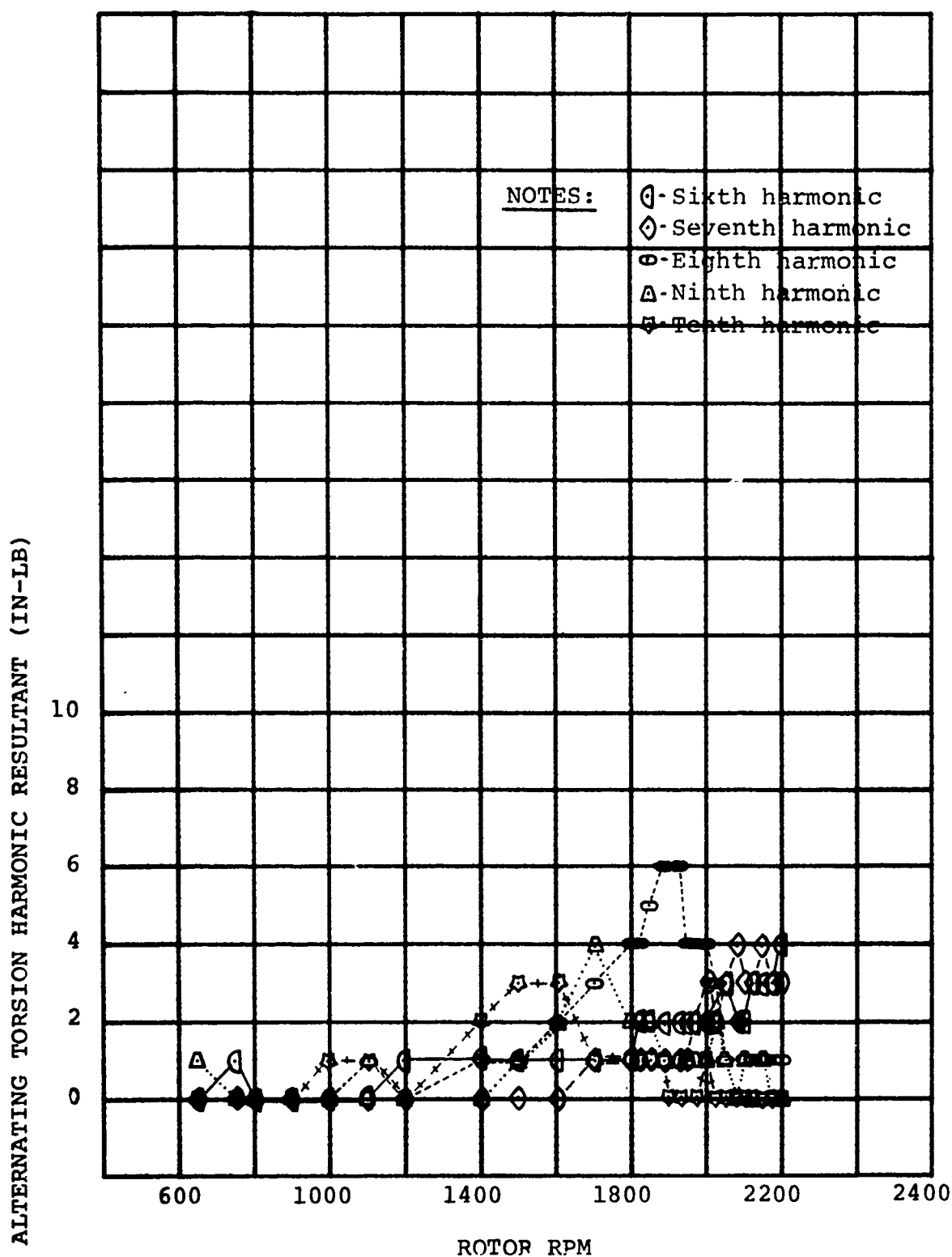


FIGURE 6-38

RIGHT-HAND BLADE TORSIONAL HARMONIC RESPONSE TO
THREE-PER-REV BAFFLE FOR TEN DEGREES COLLECTIVE PITCH

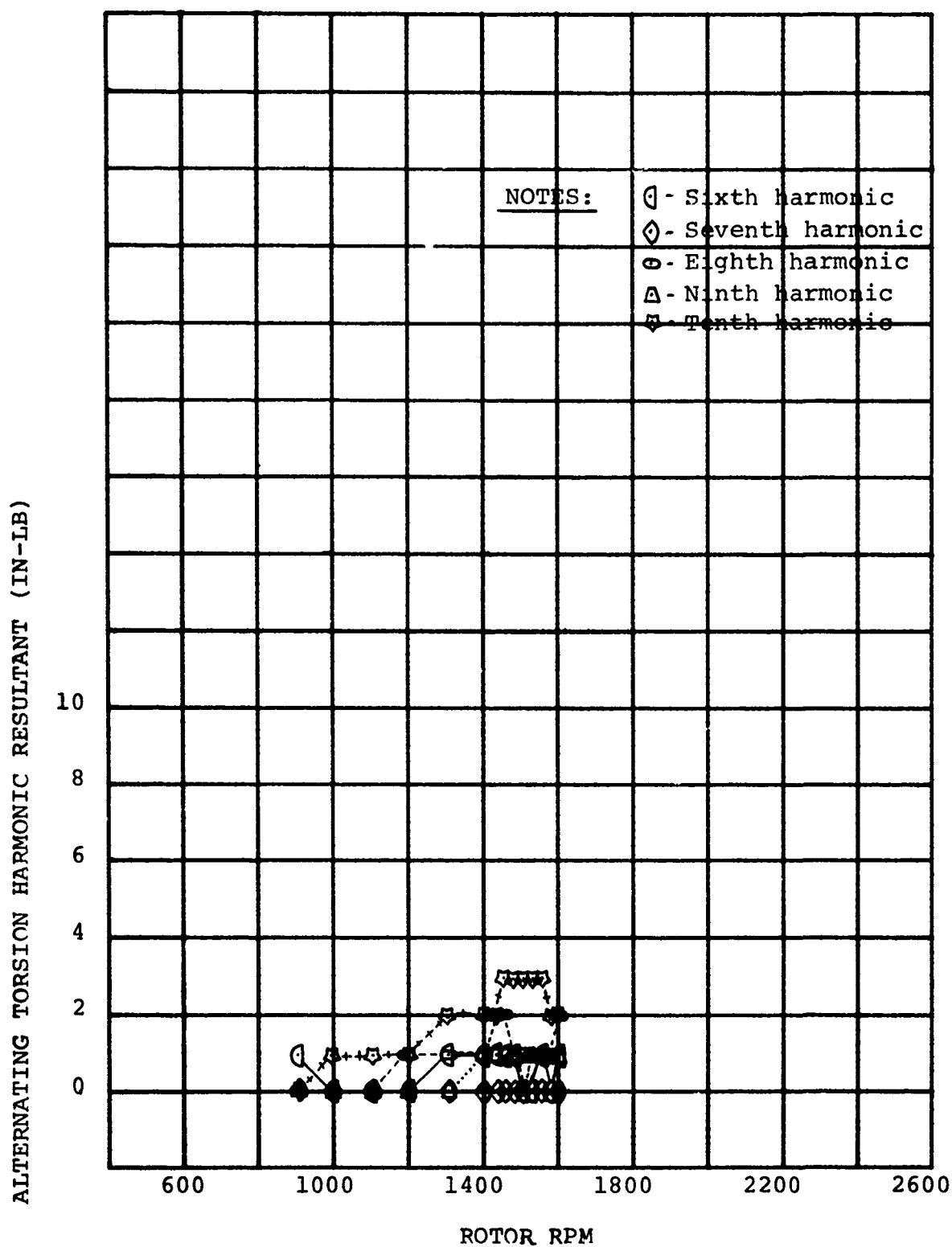


FIGURE 6-39
RIGHT-HAND BLADE TORSIONAL HARMONIC RESPONSE TO
FOUR-PER-REV BAFFLE FOR TEN DEGREES COLLECTIVE PITCH

6.2 HOVER BLADE LOADS

Primary blade loads objectives in hover were to determine the effect of cyclic pitch on alternating blade bending moments and to determine the effect of stall flutter on alternating blade torsion. Test data were obtained to answer these objectives and the results show that cyclic pitch substantially increases flap bending loads but has little effect on chord bending. Investigation for stall flutter shows that for the conditions tested, stall flutter did not occur. Additional data were obtained in hover to show the effects of aircraft height rotor-rotor interference and low forward speed on blade loads.

6.2.1 Effect of Cyclic Pitch

The effect of cyclic pitch on alternating blade bending moments is shown in Figures 6-40, 41 and 6-42. Flap bending moments due to cyclic shown in Figure 6-40 increase with RPM and are mostly first harmonic due to one-per-rev flapping. The zero cyclic loads shown in the same figure are due to configuration effects. The downwash is restricted by the wing and causes first harmonic as well as higher harmonic bending moments. Rotor height is shown to have little effect on flap bending moments with and without cyclic pitch. Operation of the rotor with cyclic in the cruise position to minimize wing blockage is also shown to have little effect on alternating flap bending moments.

Chord bending moments due to cyclic are shown in Figure 6-41. These data show no difference between blade loads with and without cyclic. Ground proximity and configuration do not affect these blade loads since the data show that operating in or out of ground effect or operating the rotor in the cruise position does not change the blade chord bending. The source of these loads are not known but blade dynamics and model mounting are likely to be involved.

Alternating blade torsion due to cyclic pitch is shown in Figure 6-42. These data show an increase with RPM and no effect of rotor height.

A semi-empirical approach was taken to predict blade loads in hover due to cyclic pitch. Blade loads due to ground proximity and configuration effects were predicted from past test data obtained from the model for hovering conditions without cyclic pitch. A coupled flap-pitch uncoupled lag rotor loads analysis was used to predict hover blade loads due to cyclic pitch.

The empirical contribution due to ground proximity and configuration effects and the theoretical contribution due to cyclic pitch were assumed additive and the sum represented the blade loads prediction for hover cyclic conditions. The empirical prediction was made for both rotors operating simultaneously while test data for 3 degrees of cyclic pitch were taken with the right rotor operating due to motor problems on the left rotor. A comparison of test data and prediction for $h/D=.39$ is shown in Figure 6-43. Flap blade bending moment data for zero cyclic and both rotors operating agree with the empirical prediction and the chord bending data for the same condition are 16% lower than predicted. The good agreement of the predicted and measured slopes of flap and chord bending moments with cyclic shows that the uncoupled rotor analysis accurately predicts hover blade loads due to cyclic pitch, since the constant difference between predicted loads for twin rotor operation and the measured loads for single rotor operation are due to configuration effects. Figure 6-44 shows a comparison of prediction and measured data for hover cyclic at $h/D=1.82$. Measured alternating flap bending for both rotors operating with zero cyclic is 50% (50 in-lb) lower than predicted and chord bending is 8% (20 in-lb) higher than predicted. The measured slope of flap and chord bending with cyclic agrees well with the predicted slope. This is further evidence that the uncoupled analysis accurately predicts blade loads due to cyclic pitch and also indicates that the configuration effects of twin rotor operation on blade loads are significant.

6.2.2 Stall Flutter

The criteria used to determine stall flutter inception in hover were that a large increase in alternating blade torsion would result and the predominant harmonic of the torsion would correspond to the first mode torsional frequency. Using these criteria, stall flutter inception could be found by the intersection of the slopes of alternating torsion versus RPM before and after inception. A collective pitch of 14 degrees was expected to provide thrust coefficients for sustained stall flutter and the results are shown in Figures 6-45 through 6-48. There was no sudden increase in alternating torsion and stall flutter did not occur for the RPM range tested.

The torsional loads shown in Figures 6-45 thru 6-48 are due to the wing acting as a baffle and restricting the downwash. This results in a small impulsive once-per-rev change in blade angle and alternating blade torsion responds at its first mode torsional frequency. A typical waveform of blade torsion in Figure 6-45 shows that it is operating at its natural frequency. To determine the effect of ground proximity and rotor-rotor interference

on stall flutter inception, testing on one rotor was done in and out-of-ground effect and both rotors were operated out-of-ground effect. As shown in Figures 6-46, 47, 48, neither ground proximity nor rotor-rotor interference caused stall flutter inception.

An empirical approach was taken to predict stall flutter inception in hover. Past test data for stall flutter inception on helicopter blades and prop/rotors were used. The range of test for stall flutter is compared with the prediction of flutter inception in Figure 6-49. Since stall flutter did not occur the prediction is shown to be conservative for this rotor.

6.2.3 Rotor Height

Additional data were obtained in hover to show the effect of rotor height on blade loads. Out-of-ground-effect blade loads are caused by wing blockage of the downwash and also rotor-rotor interference. In-ground-effect blade loads are caused by distortion of the downwash due to ground proximity. The effect of rotor height on alternating flap and chord bending and alternating torsion is shown in Figures 6-50 through 6-60. Alternating flap bending moments at aircraft touchdown ($h/D=.39$) are nearly double those when operating out-of-ground effect at $h/D=1.82$ and are approximately half of the flap bending loads due to 3 degrees of cyclic pitch. Distortion of the downwash due to ground proximity when operating in-ground effect has a large effect on flap bending than configuration effects when operating out-of-ground effect.

Alternating blade chord bending data decrease with increased rotor height and are comparable in magnitude to chord bending loads for 3 degrees cyclic pitch. The source of the chord bending loads is not known but disturbance of the velocity flow field in the disc plane is shown to affect chord bending.

Alternating blade torsion data decrease slightly with increased rotor height and are approximately half of the blade torsion loads due to 3 degrees cyclic pitch.

6.2.4 Rotor-Rotor Interference

Rotor-rotor interference results when the downwash of one rotor disturbs the velocity flow in the disc plane of the other rotor. Rotor-rotor interference is therefore dependent upon collective pitch and rotor RPM and is also dependent upon rotor height since ground proximity affects rotor thrust. Figures 6-61 and 6-62 show rotor-rotor interference data for rotor heights corresponding to aircraft touchdown ($h/D=0.39$). Right-hand rotor alternating blade bending moments are shown for single rotor operation and

for both rotors operating when the left-hand rotor RPM was maintained at 2000 RPM. At an h/D of 0.39, flap and chord bending moments are nearly constant with RPM for single rotor operation. The rotor wake for this condition is similar to that for an isolated rotor IGE where the downwash translates radially away from the rotor. When both rotors are operating and the left-hand rotor RPM is constant, right rotor bending moments increase with RPM and reach a maximum magnitude at 2200 RPM.

The local maximum in bending moments at 2200 RPM is due to distortion of the rotor downwash near the wing. As discussed in 6.2.3 the rotor wake is restrained from traveling under the fuselage by the ground and by the downwash of the other rotor. This condition is stable until the differential rotor thrust and resulting differential downwash is large enough so that the downwash from the rotor with the largest thrust overcomes the downwash restriction of the other rotor and travels under the fuselage. The wake from the rotor with the largest thrust is then similar to an isolated rotor OGE and this condition is stable as long as the minimum required differential thrust is maintained. Transformation of the downwash from the restricted wake to the isolated rotor wake is unstable and increased downwash distortion results. The unstable downwash condition causes blade loads which are larger than those caused by either the restricted wake or isolated rotor wake condition.

Rotor-rotor interference data out-of-ground effect at $h/D=1.82$ are shown in Figures 6-63 and 6-64. These data show a small increase in right-hand rotor bending moments when the left rotor is operating at 2000 RPM. Since the rotor is out-of-ground effect, there is no restriction on the downwash from each rotor and the downwash is not distorted regardless of the differential thrust. Out-of-ground effect rotor-rotor interference is limited to the vorticity of one rotor influencing the flow field of the other rotor. A comparison of the data at the two rotor heights shows that rotor-rotor interference effects on blade loads are largest when operating in-ground effect.

6.2.5 Low Forward Speed

Blade loads data were obtained in low-speed flight near the ground to determine the effect of low q on blade loads. Blade moment waveforms shown in Figure 6-65 are nearly sinusoidal and show no impulsive response to blade-tip vortex intersections. Blade-tip vortex intersections have occurred in helicopter practice for low-speed flight conditions near the ground and are due to the forward airspeed forcing tip vortices to travel in close proximity to the rotor before translating vertically away from the disc plane. The increased nacelle tilt from edgewise

flight ($i_N=70^\circ$) and the high disc loading for these test conditions were beneficial in reacting airspeed effects on the tip vortex trajectory since increased nacelle tilt decreases the in-plane component of the forward velocity and the large downwash velocity adds to the forward velocity out-of-plane component. The resulting distance between the tip vortex trajectory and the disc plane is sufficiently large so that blade tip vortex intersections do not occur.

Alternating blade moments are shown in Figures 6-66 through 6-67 for two aircraft heights. These data show that blade loads increase with increased airspeed in and out-of-ground effect. Blade loads for these conditions are due to a sinusoidal inflow variation which causes a once-per-rev change in local blade angle of attack. Since the change in blade angle is a sinusoidal once-per-rev change, cyclic pitch can be used to decrease blade loads in low-speed flight.

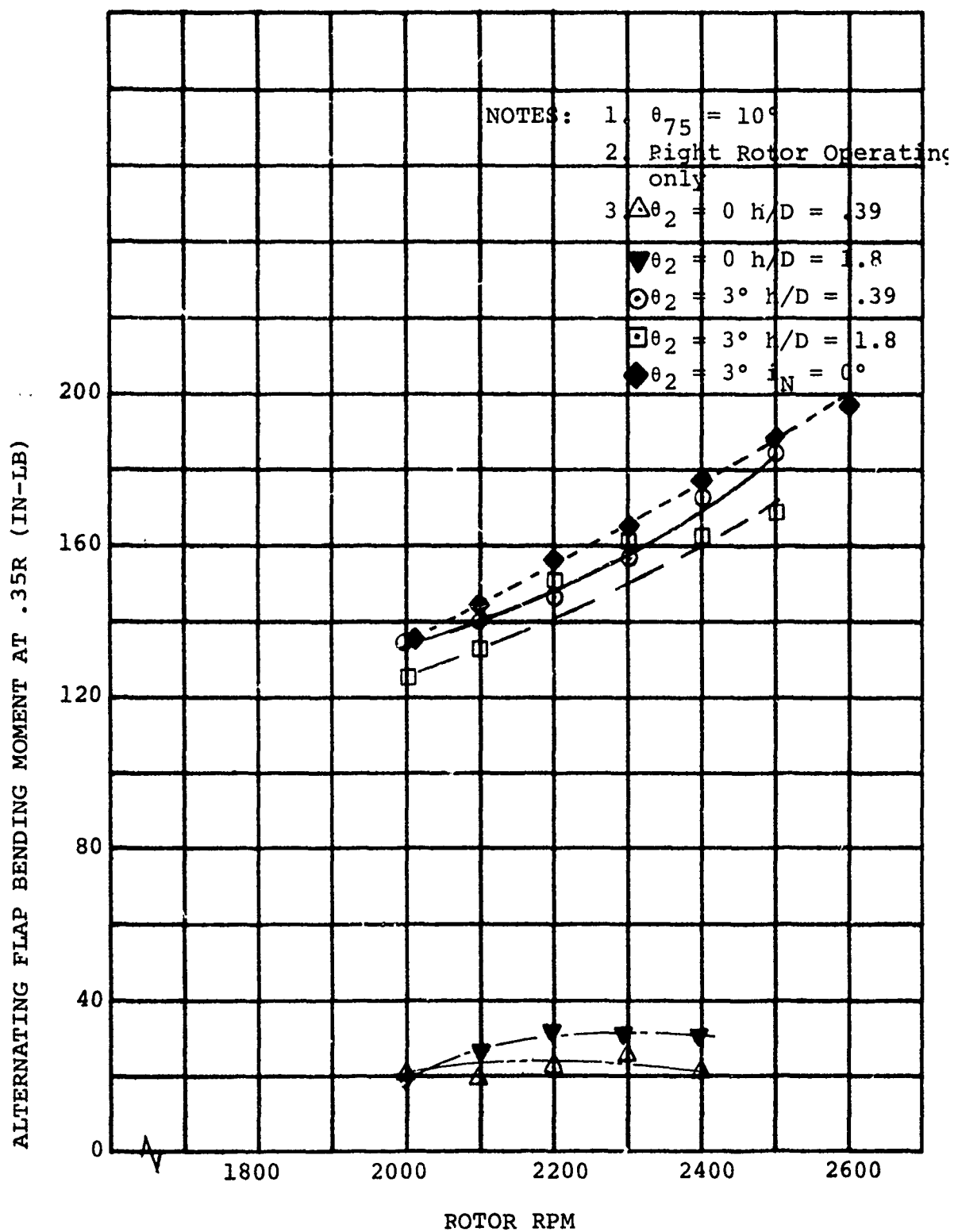


FIGURE 6-40

ALTERNATING BLADE FLAP BENDING VS.
 ROTOR RPM IN HOVER

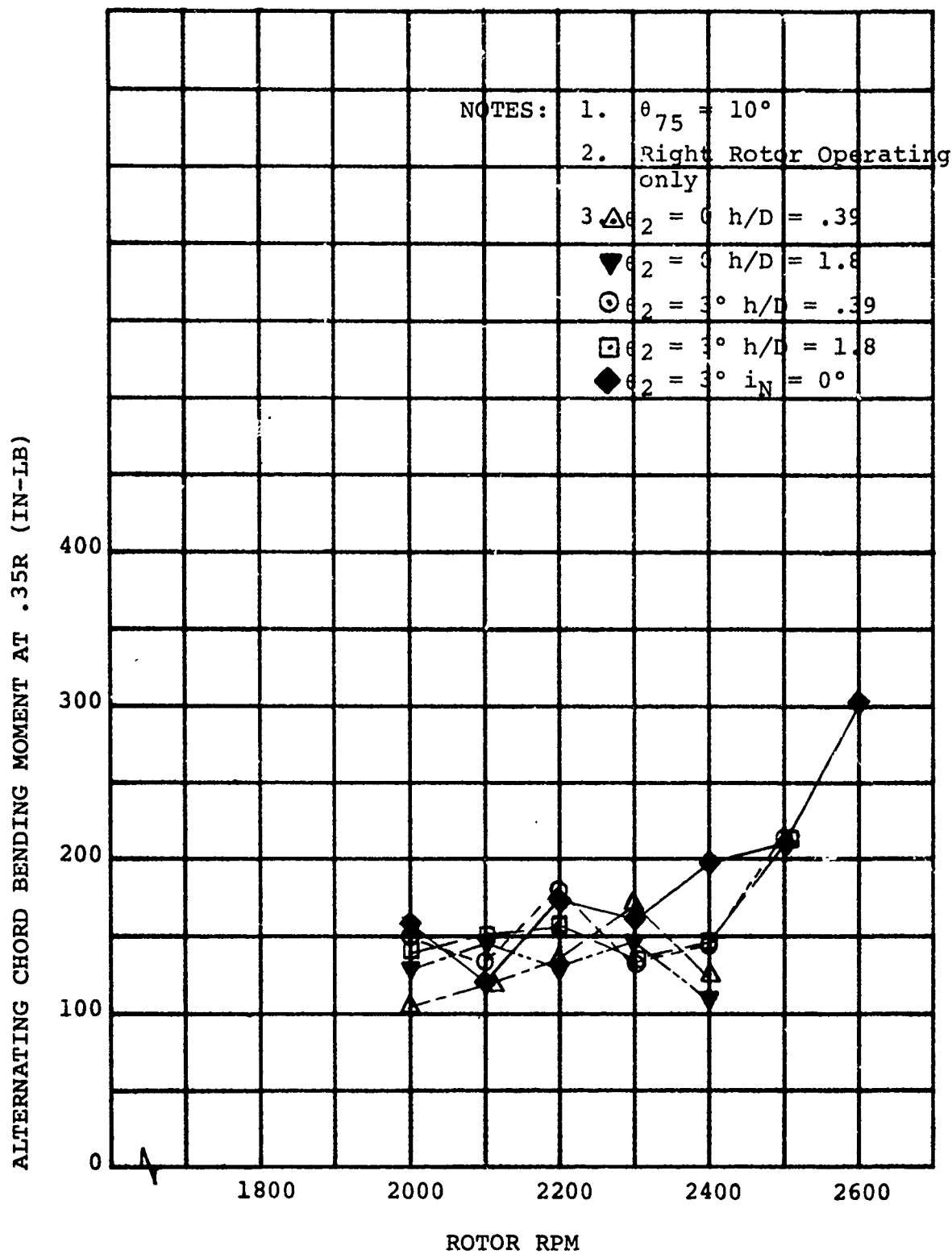


FIGURE 6-41

ALTERNATING BLADE CHORD BENDING VS.
ROTOR RPM IN HOVER

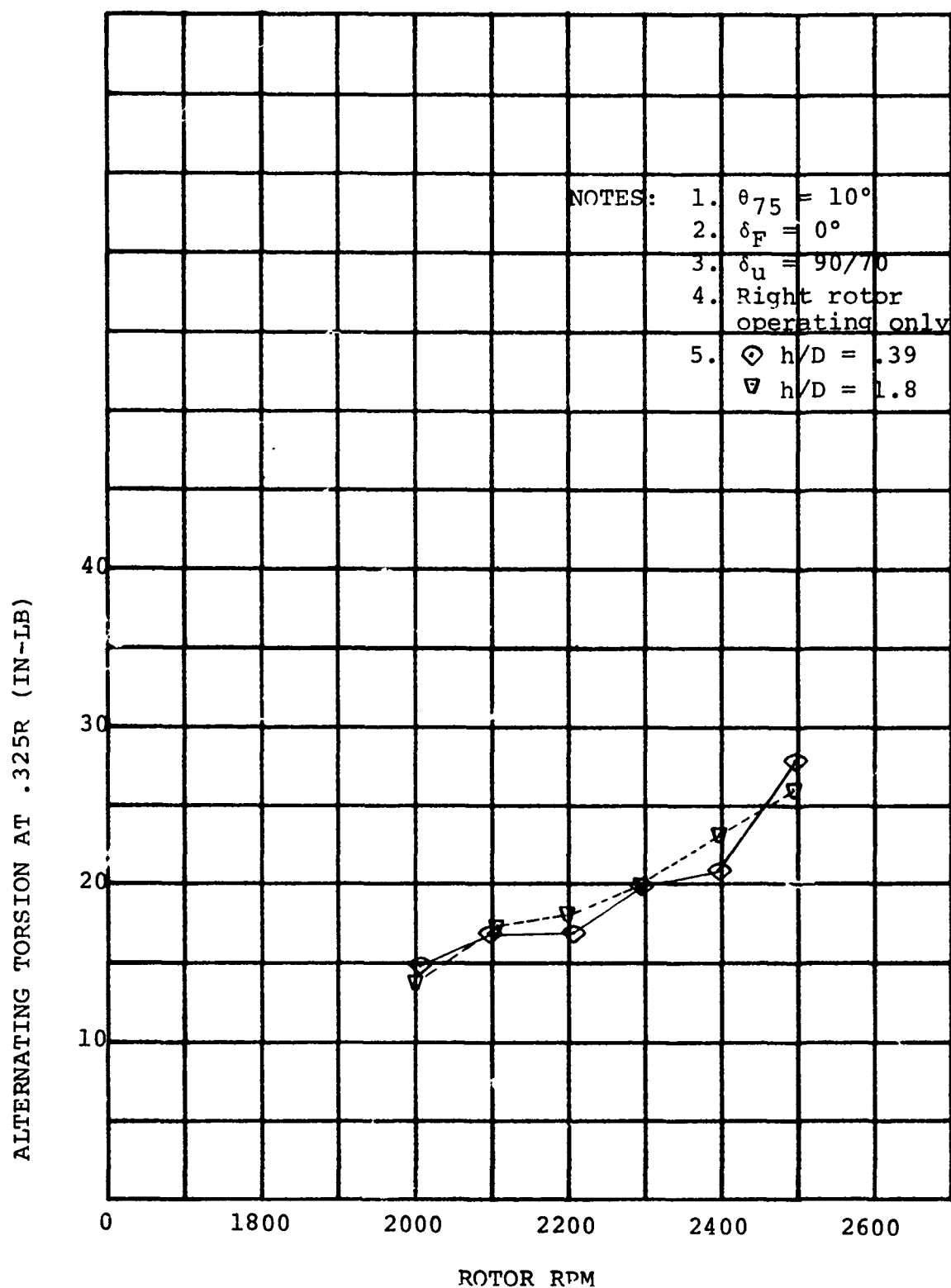


FIGURE
6-42

ALTERNATING BLADE TORSION VS. RPM FOR
 $i_N = 90^\circ$ DEG, $\theta_2 = 3^\circ$ DEG, AND $h/D = .39, 1.8$

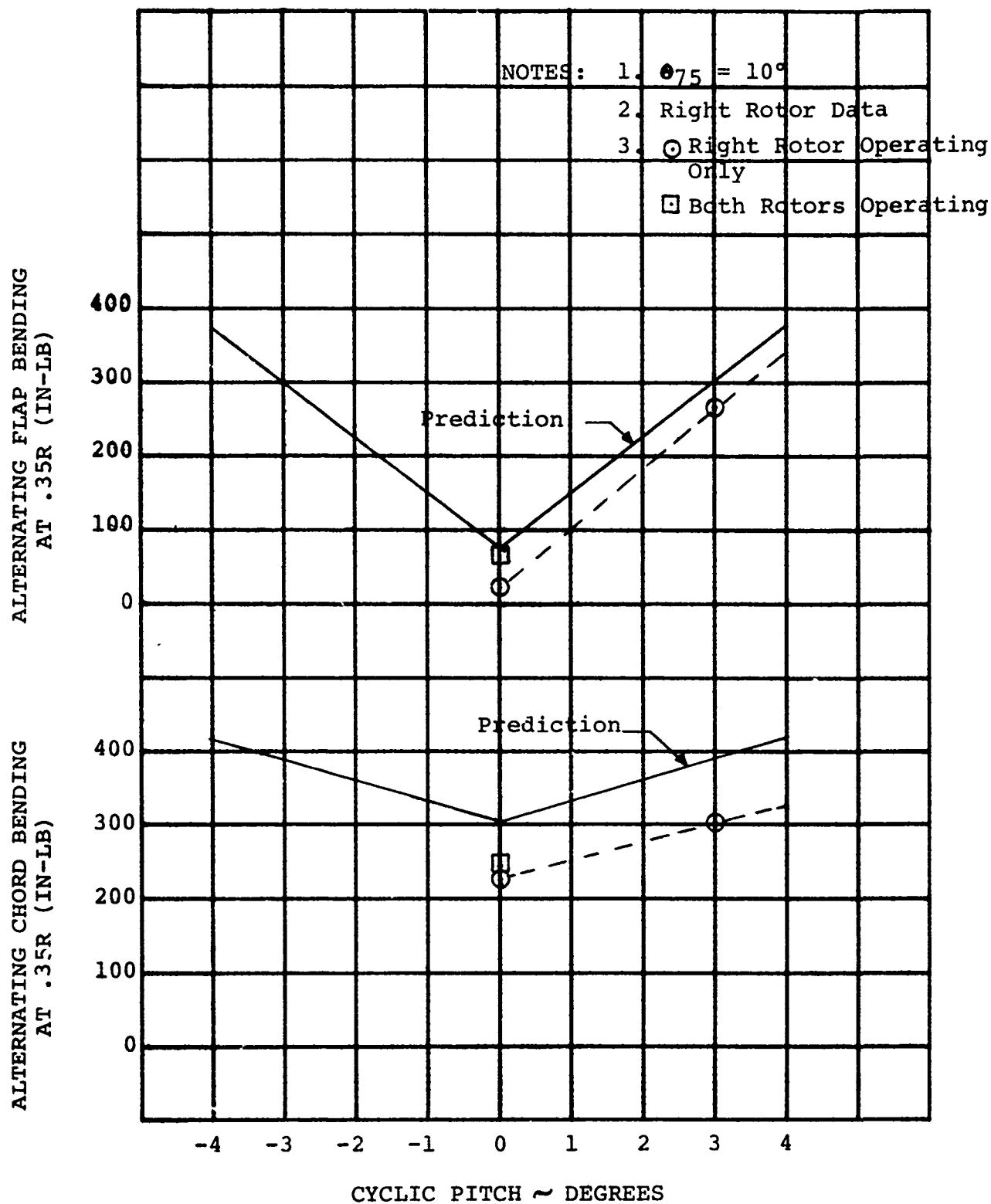


FIGURE 6-43

MEASURED AND PREDICTED BLADE LOADS PRODUCED BY CYCLIC PITCH IN HOVER AT $V_{TIP} = 750$ FPS AND $h/D = .39$

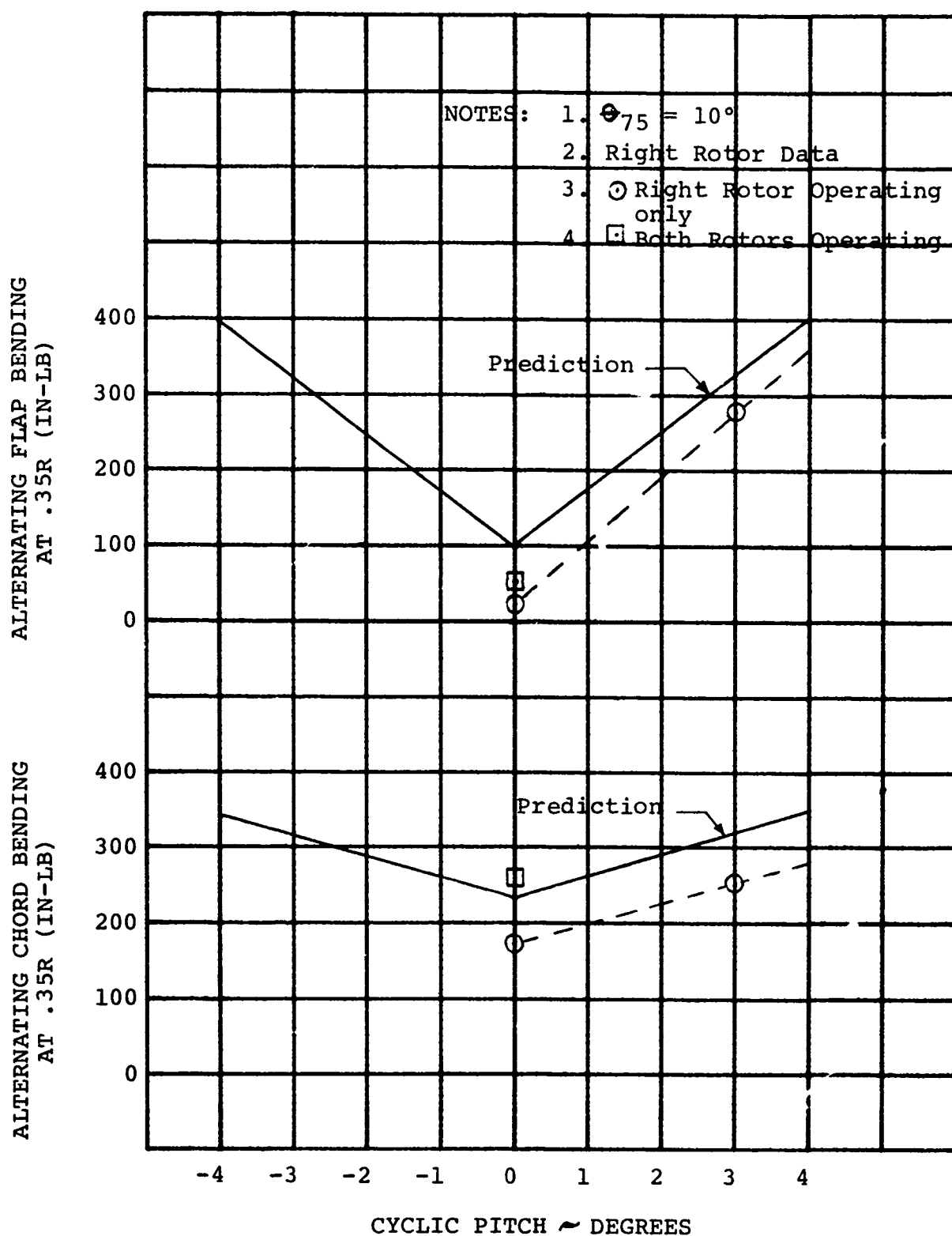


FIGURE 6-44

MEASURED AND PREDICTED BLADE LOADS PRODUCED BY CYCLIC PITCH IN HOVER AT $V_{TIP} = 750$ FPS AND $h/D = 1.8$

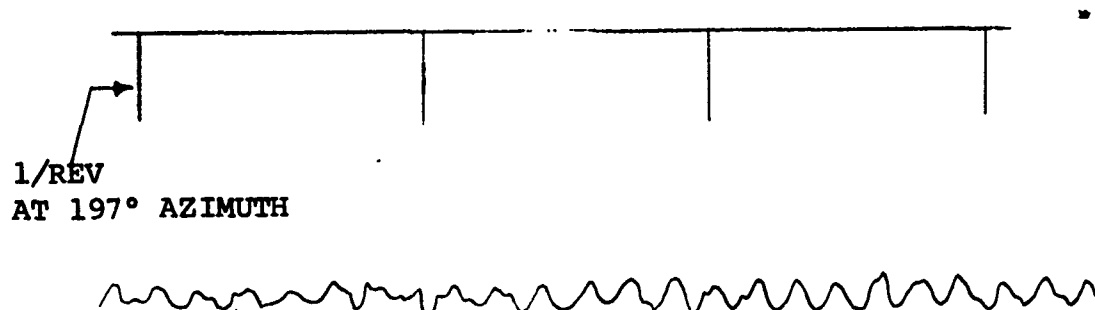


FIGURE 6-45 LEFT ROTOR BLADE TORSIONAL WAVEFORM
FOR $\theta_{75} = 14^\circ$, 2300 RPM AND $\frac{\omega_{\theta}}{\Omega} = 6.4$

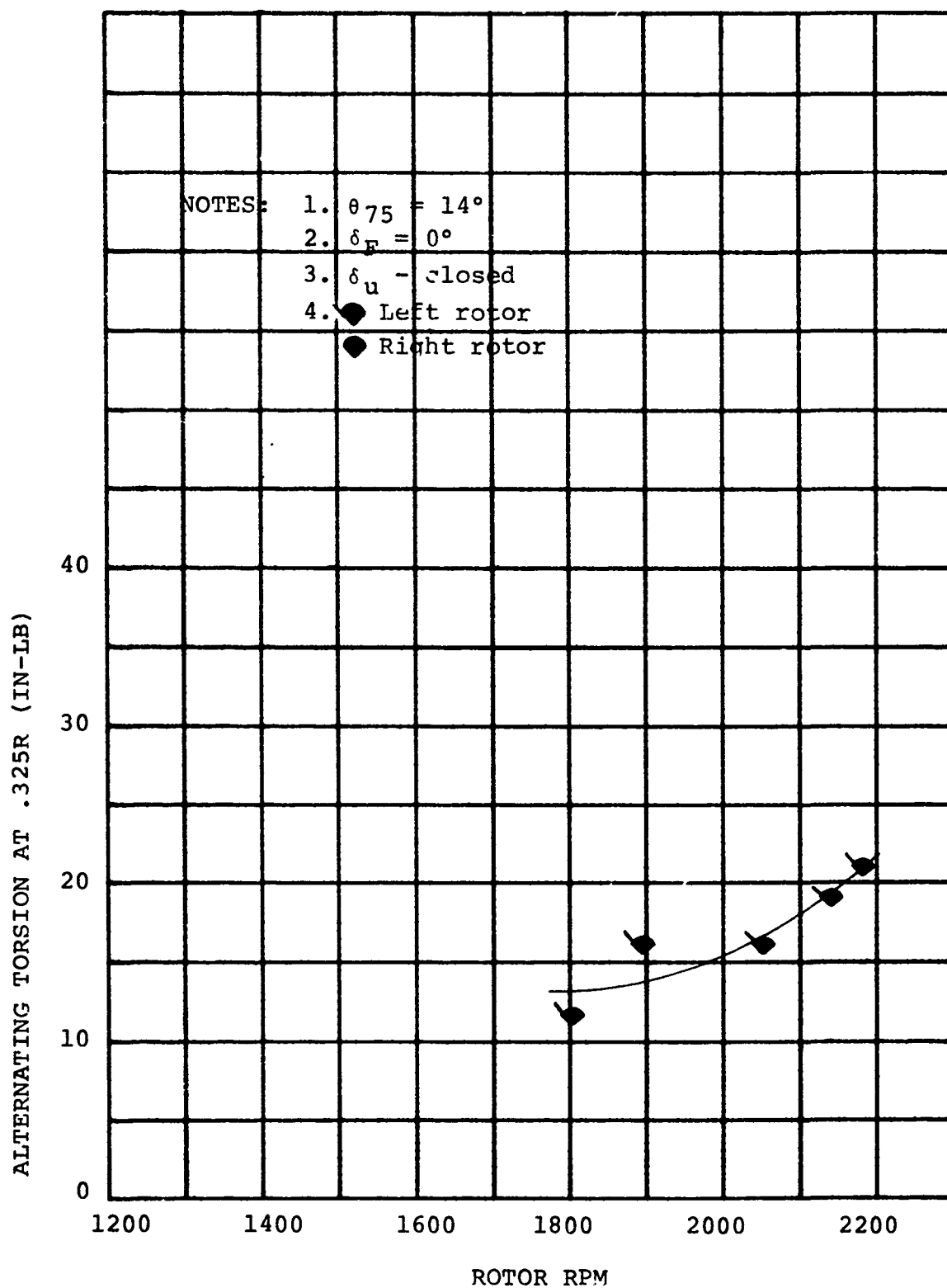


FIGURE 6-46

ALTERNATING BLADE TORSION VS. RPM
 FOR $i_N = 70^\circ$ AND $h/D = 1.8$

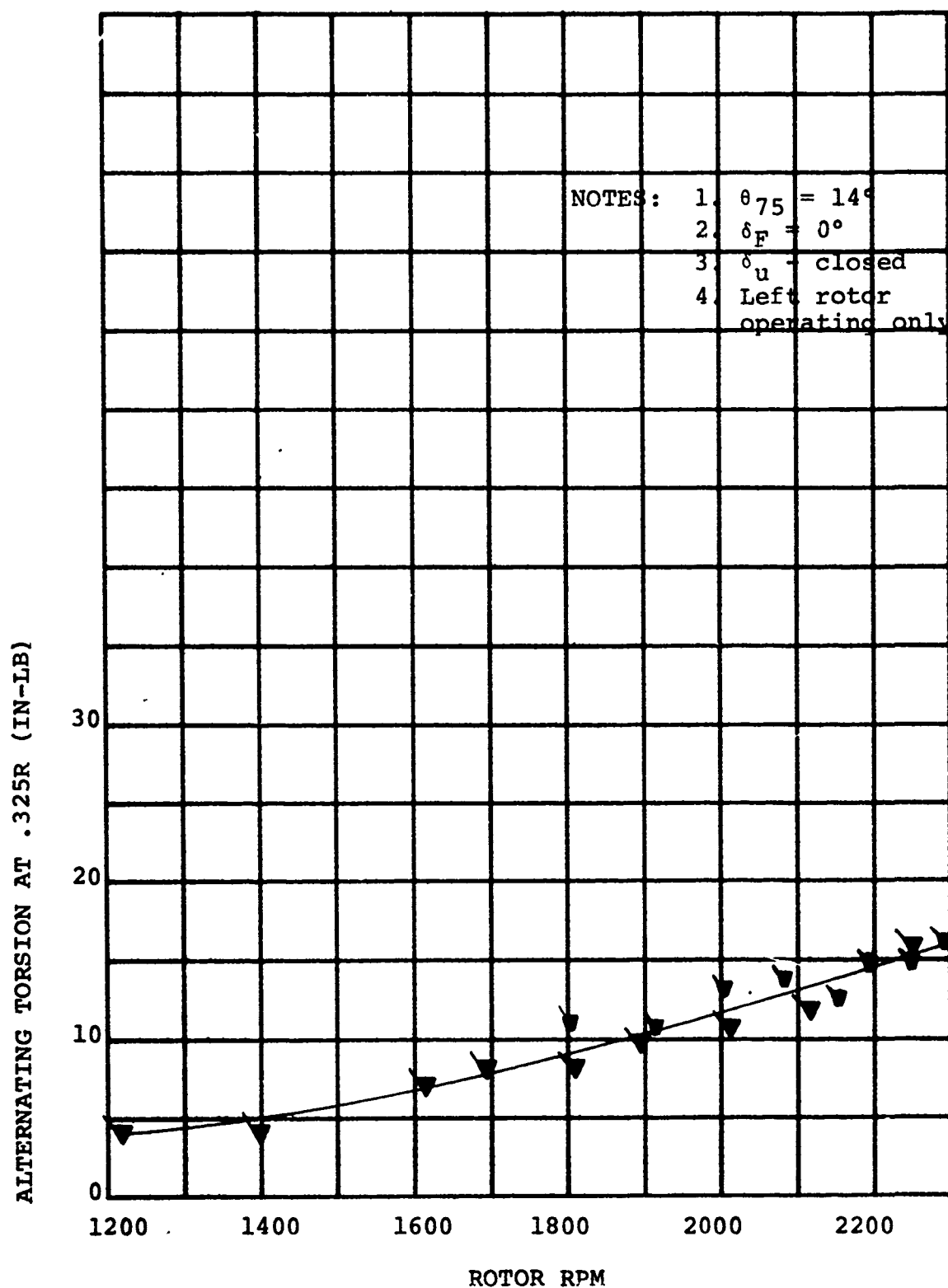


FIGURE 6-47

ALTERNATING BLADE TORSION VS. RPM
 FOR $i_N = 70^\circ$, AND $h/D = 1.8$

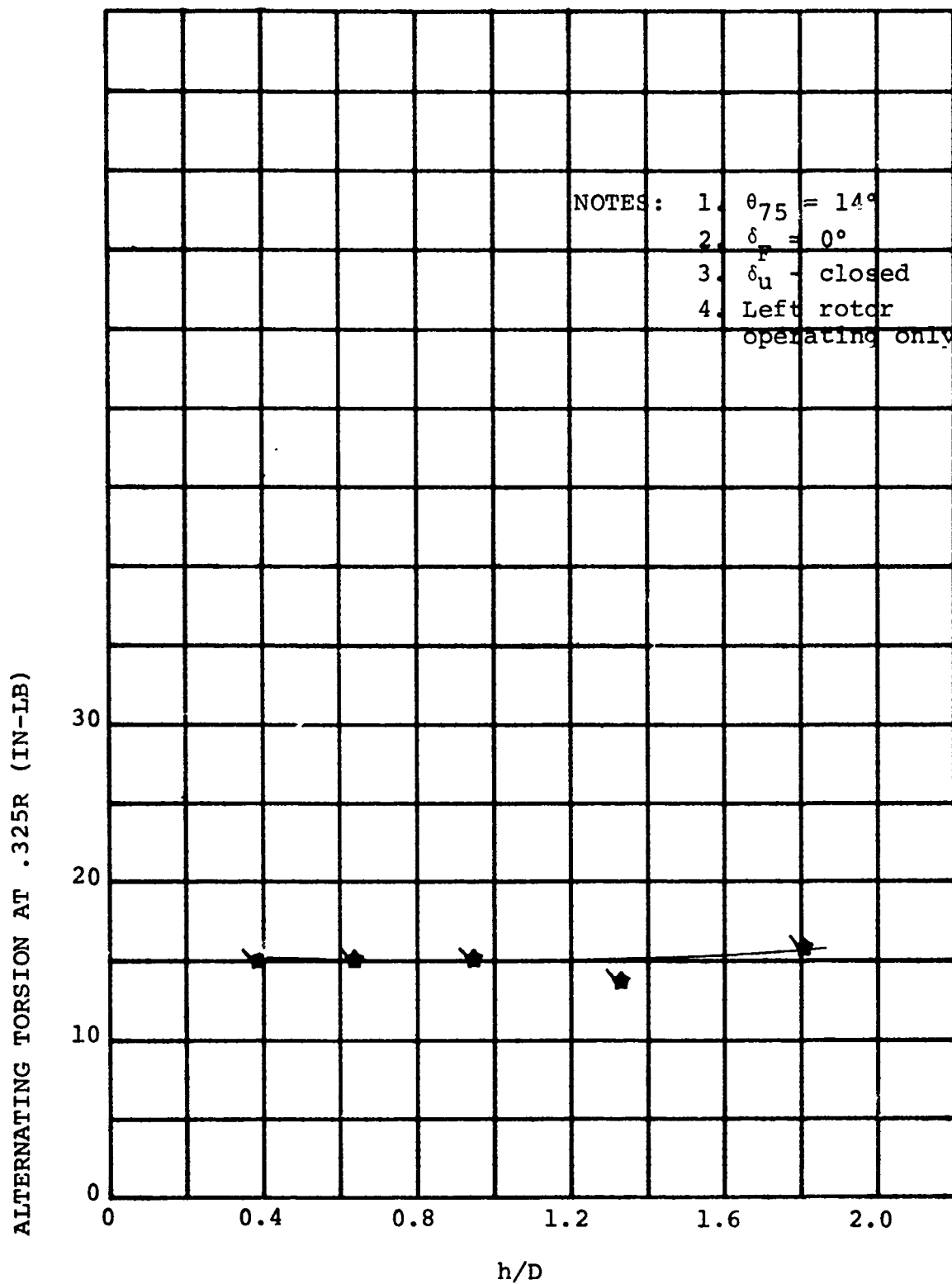


FIGURE 6-48 ALTERNATING BLADE TORSION VS. ROTOR HEIGHT FOR $i_N = 70^\circ$ AND 2180 RPM

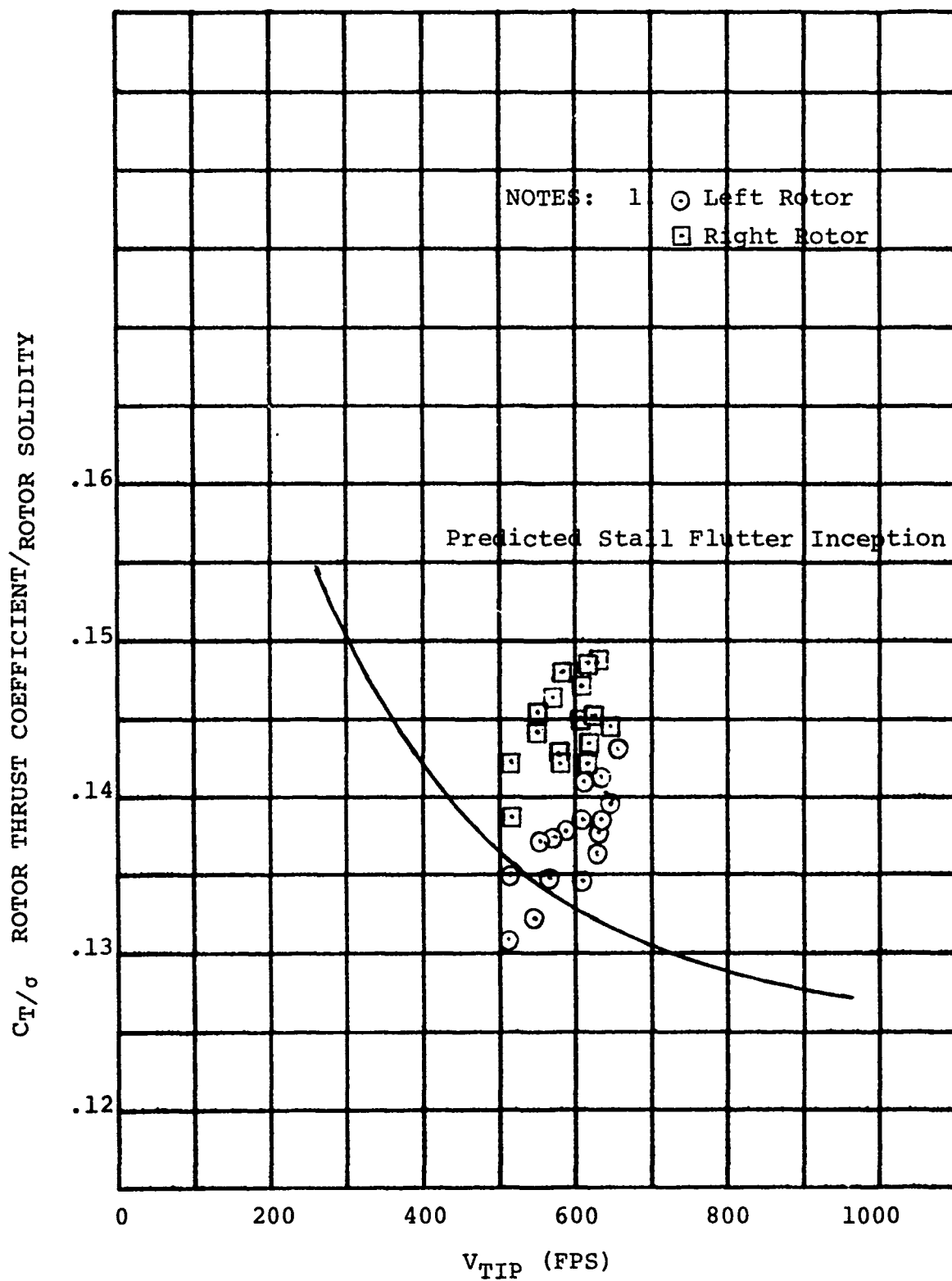


FIGURE 6-49

RANGE OF ROTOR THRUST AND TIP SPEED
WHERE STALL FLUTTER DID NOT OCCUR

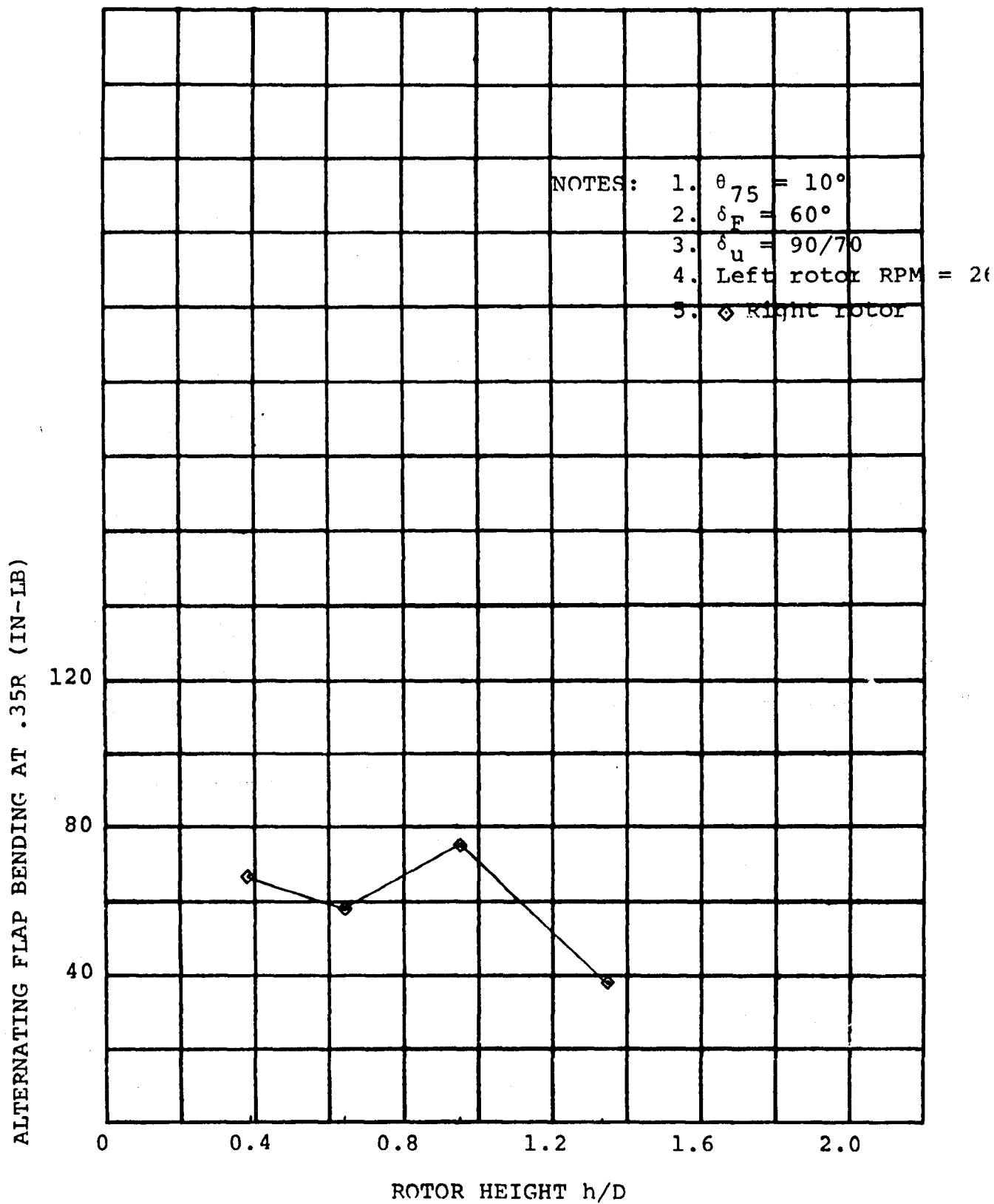


FIGURE 6-50 ALTERNATING BLADE FLAP BENDING
 VS. h/D FOR $i_N = 90^\circ$

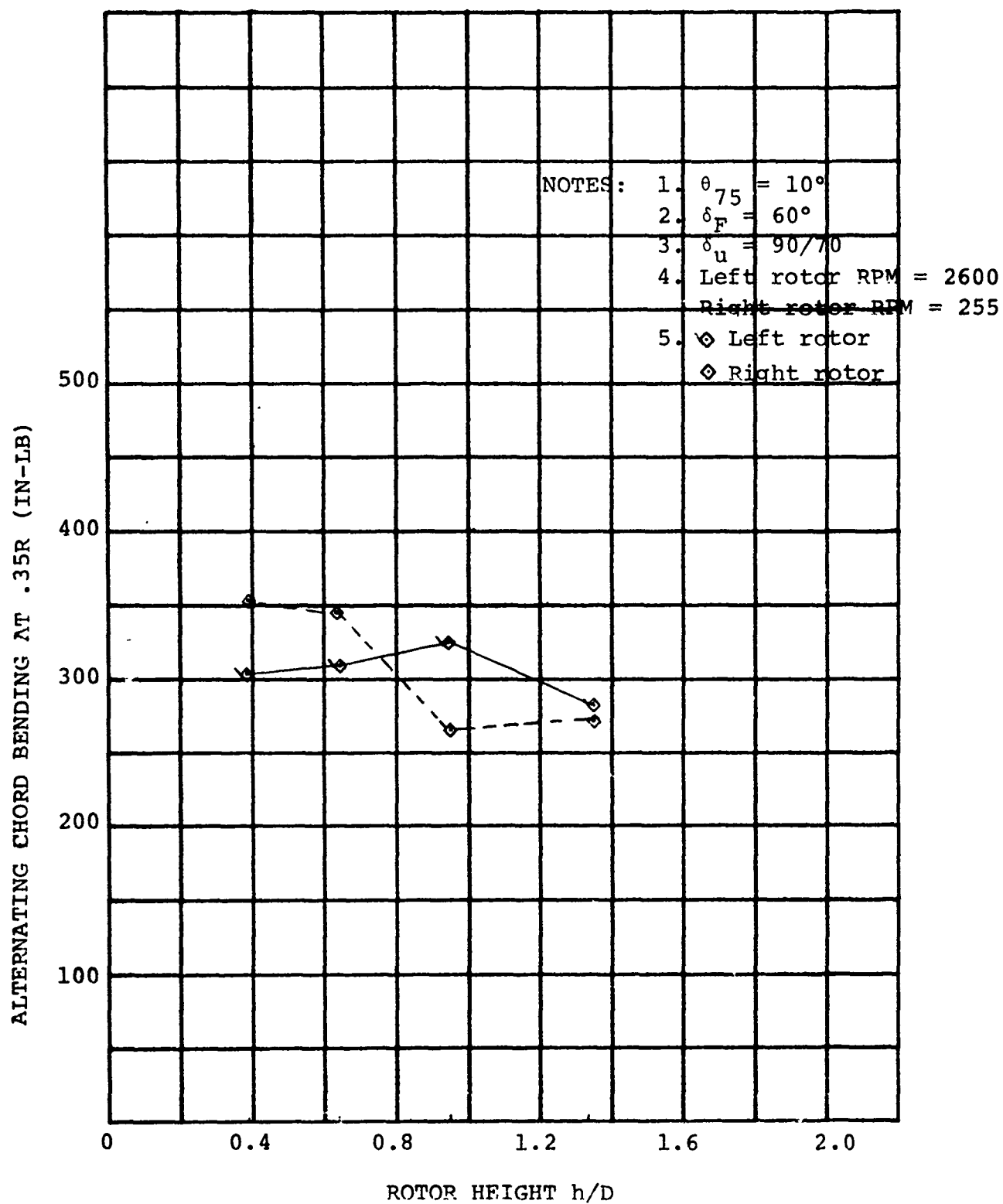


FIGURE 6-51 ALTERNATING BLADE CHORD BENDING
 VS. h/D FOR $i_N = 90$ DEG

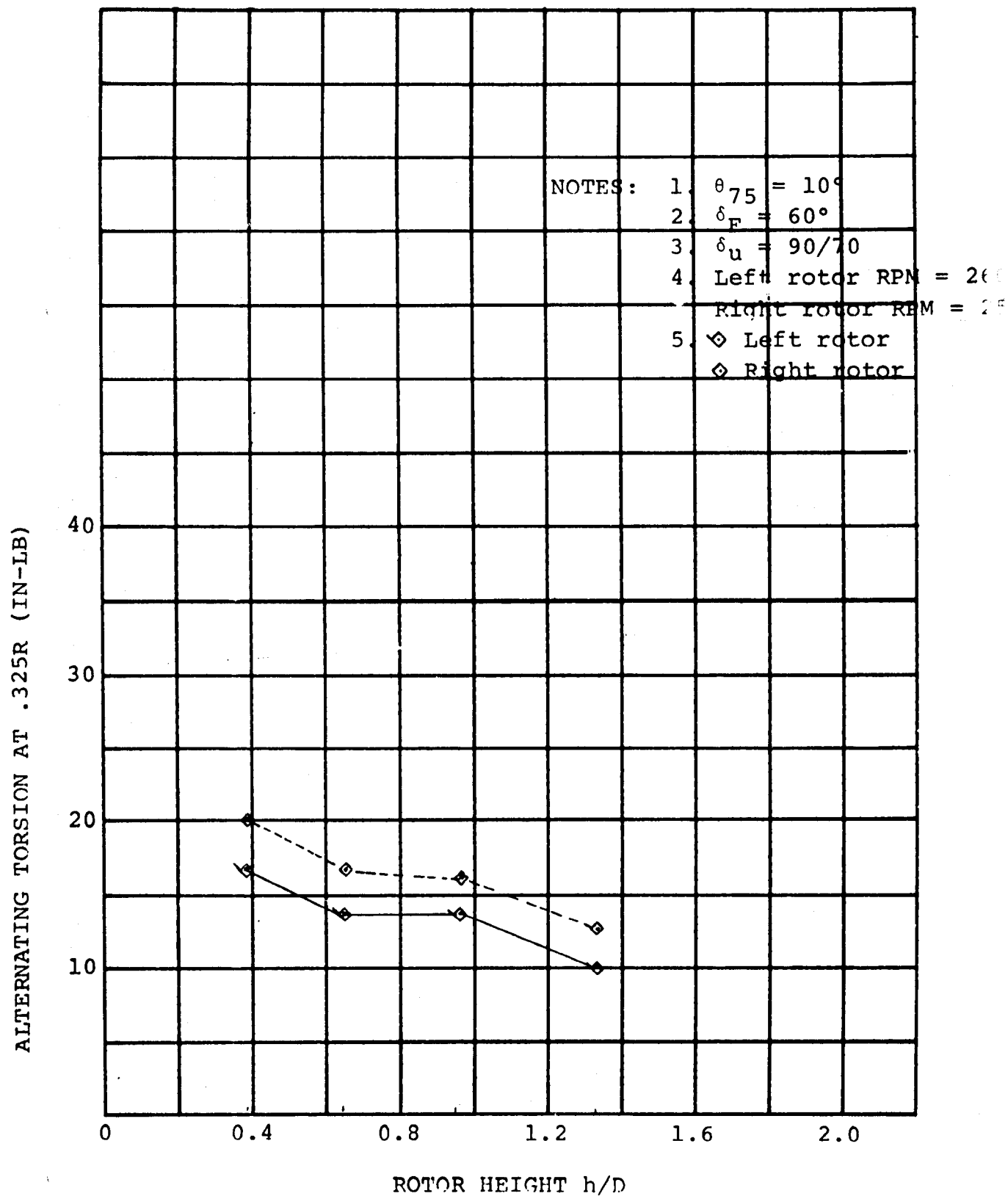


FIGURE 6-52 ALTERNATING BLADE TORSION VS.
 RPM FOR $i_N = 90$ DEG

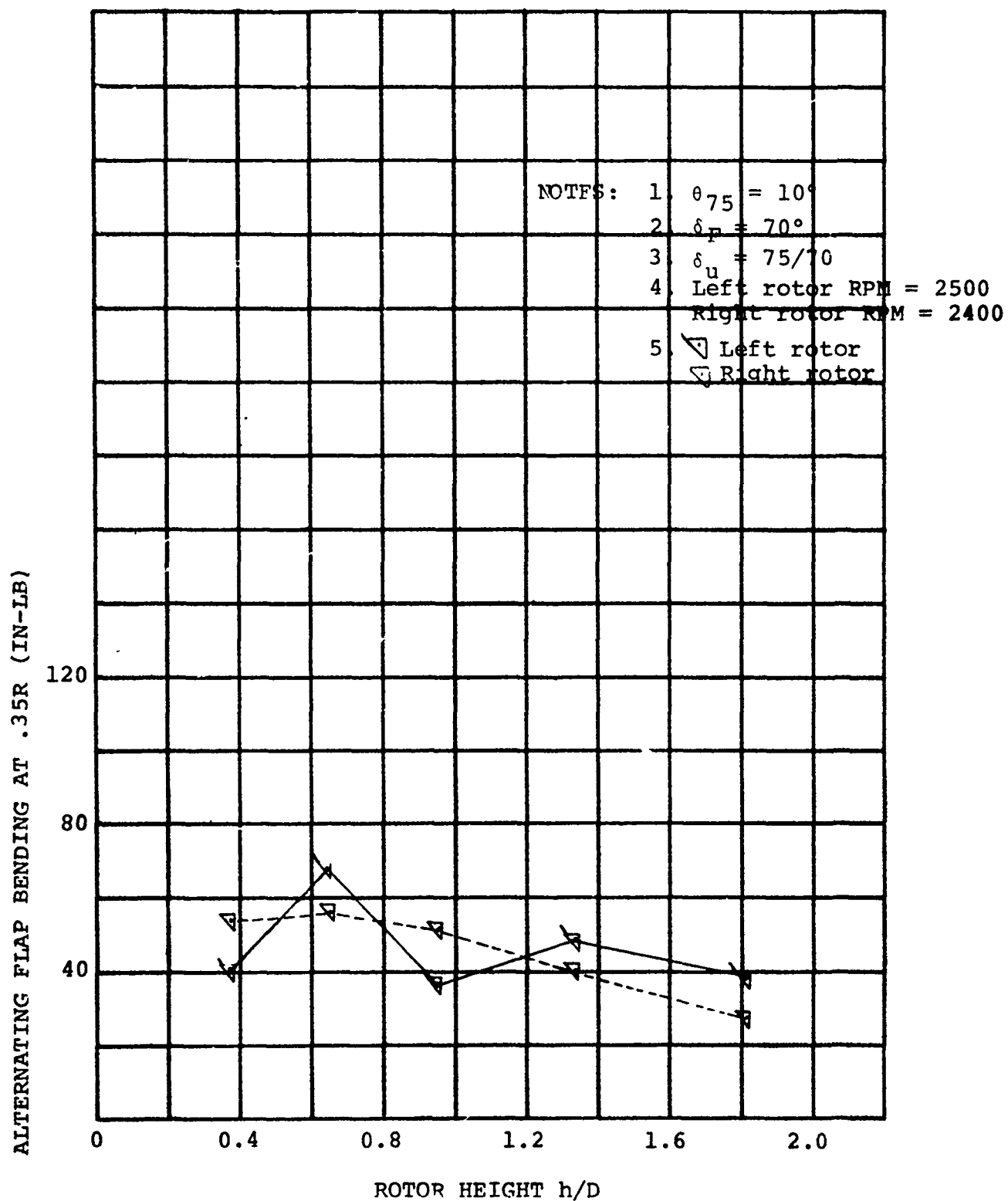


FIGURE 6-53

ALTERNATING BLADE FLAP BENDING
 VS. h/D FOR $i_N = 90^\circ$

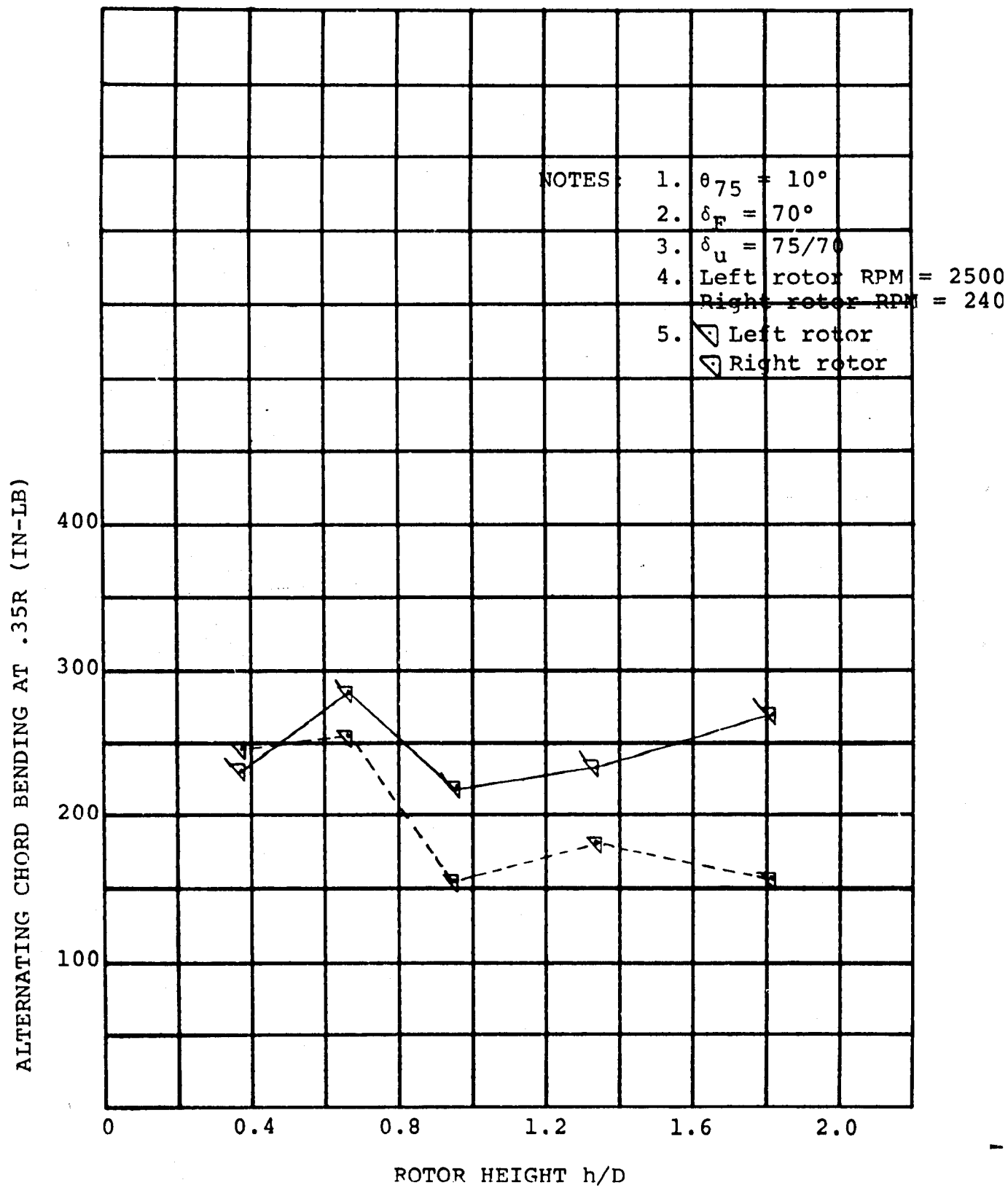


FIGURE 6-54

ALTERNATING BLADE CHORD BENDING
VS. h/D FOR $i_N = 90$ DEG

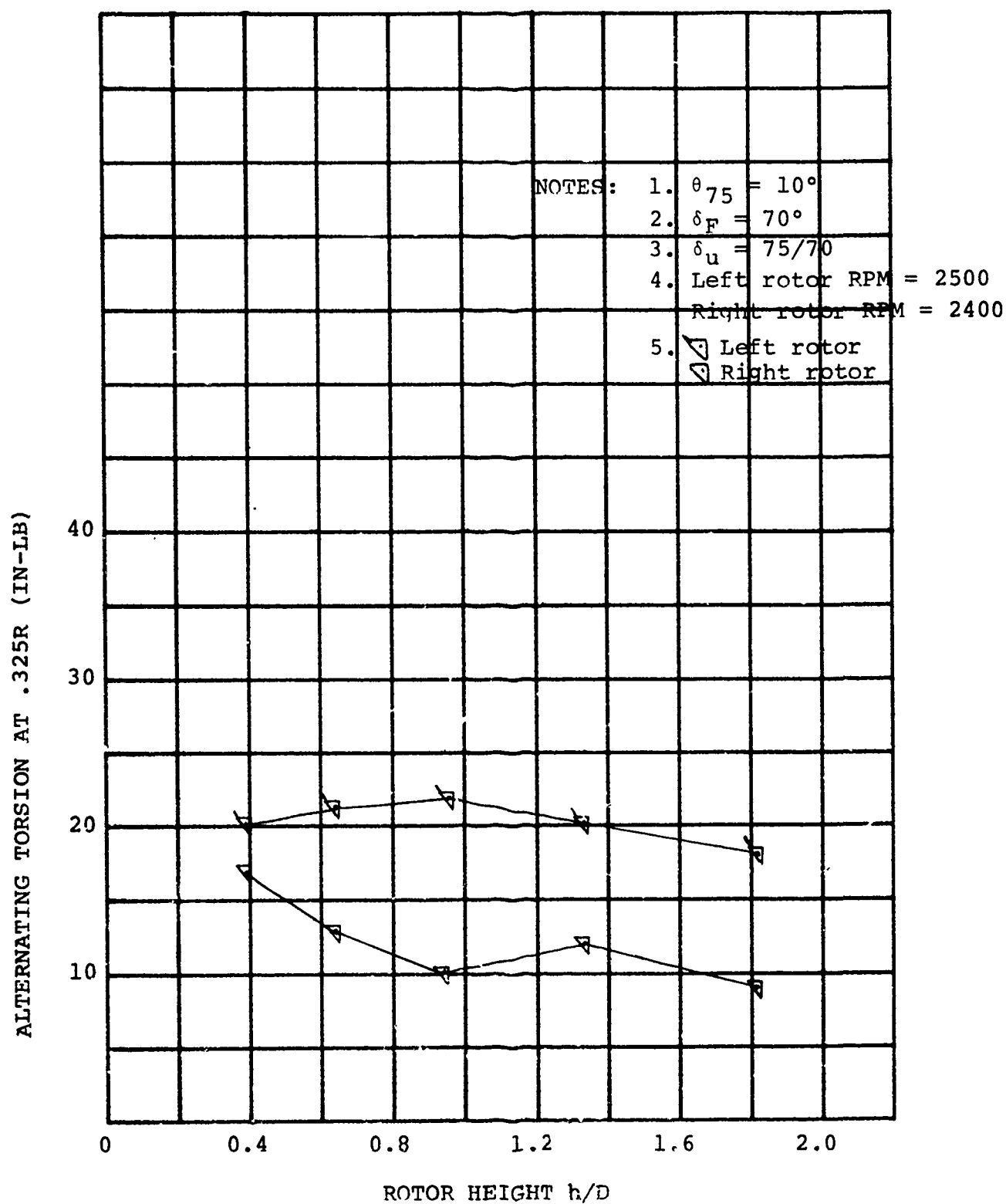


FIGURE 6-55

ALTERNATING BLADE TORSION
 VS. h/D FOP $i_N = 90^\circ$

ALTERNATING FLAP BENDING AT .35R (IN-LB)

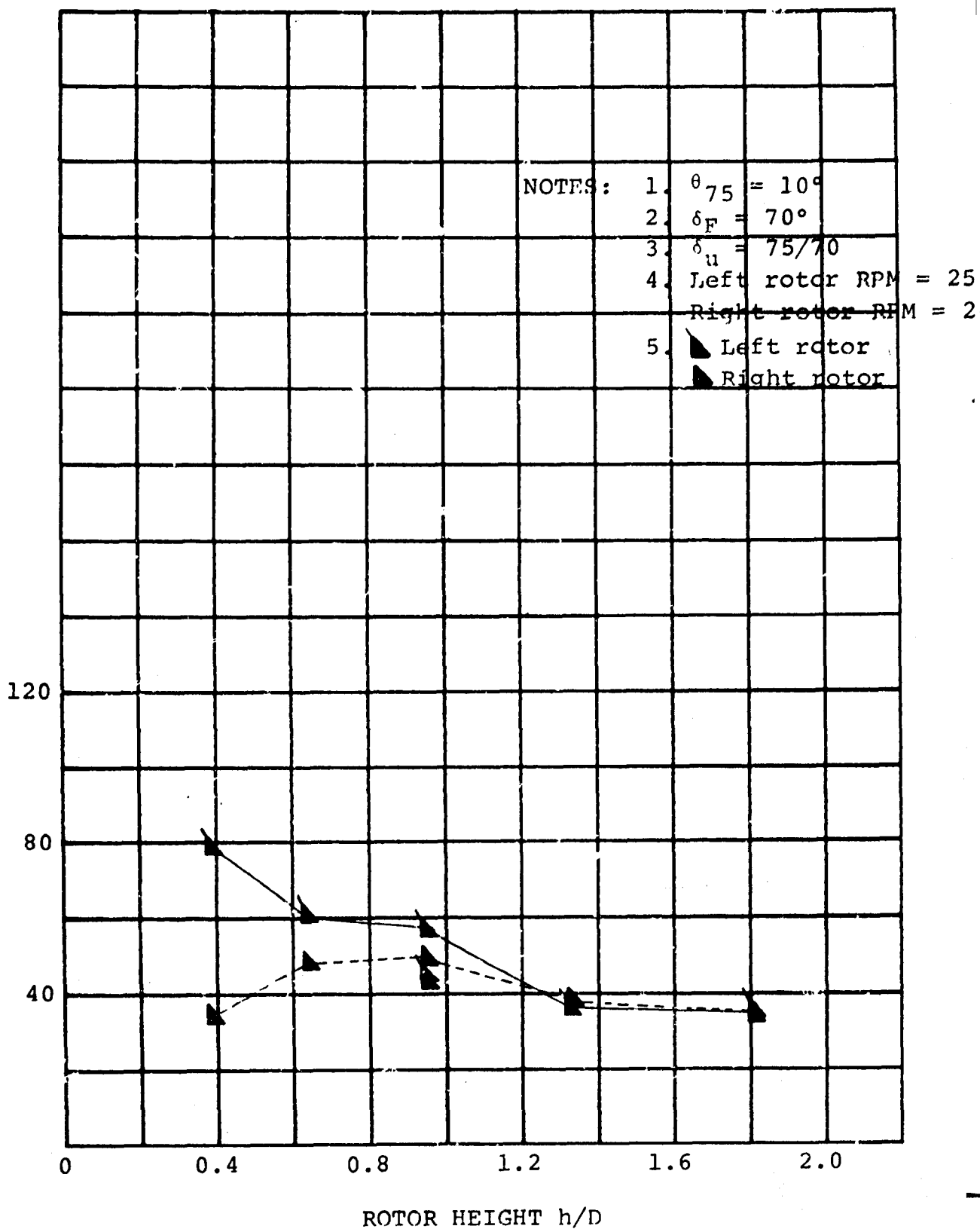


FIGURE 6-56 ALTERNATING BLADE FLAP BENDING VS.
 h/D FOR $i_N = 90$ DEG

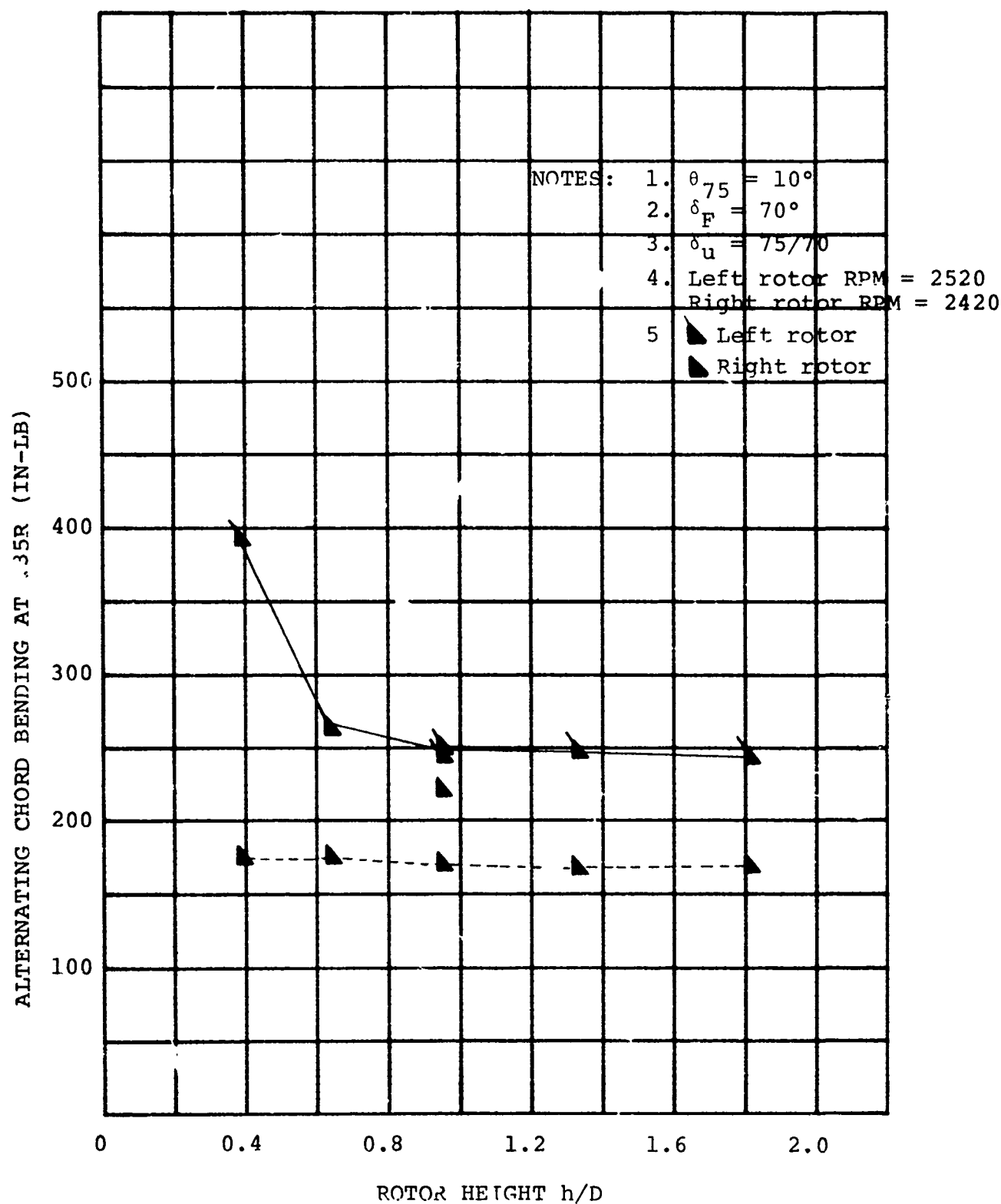


FIGURE 6-57 ALTERNATING BLADE CHORD BENDING
 VS. h/D FOR $i_N = 90$ DEG

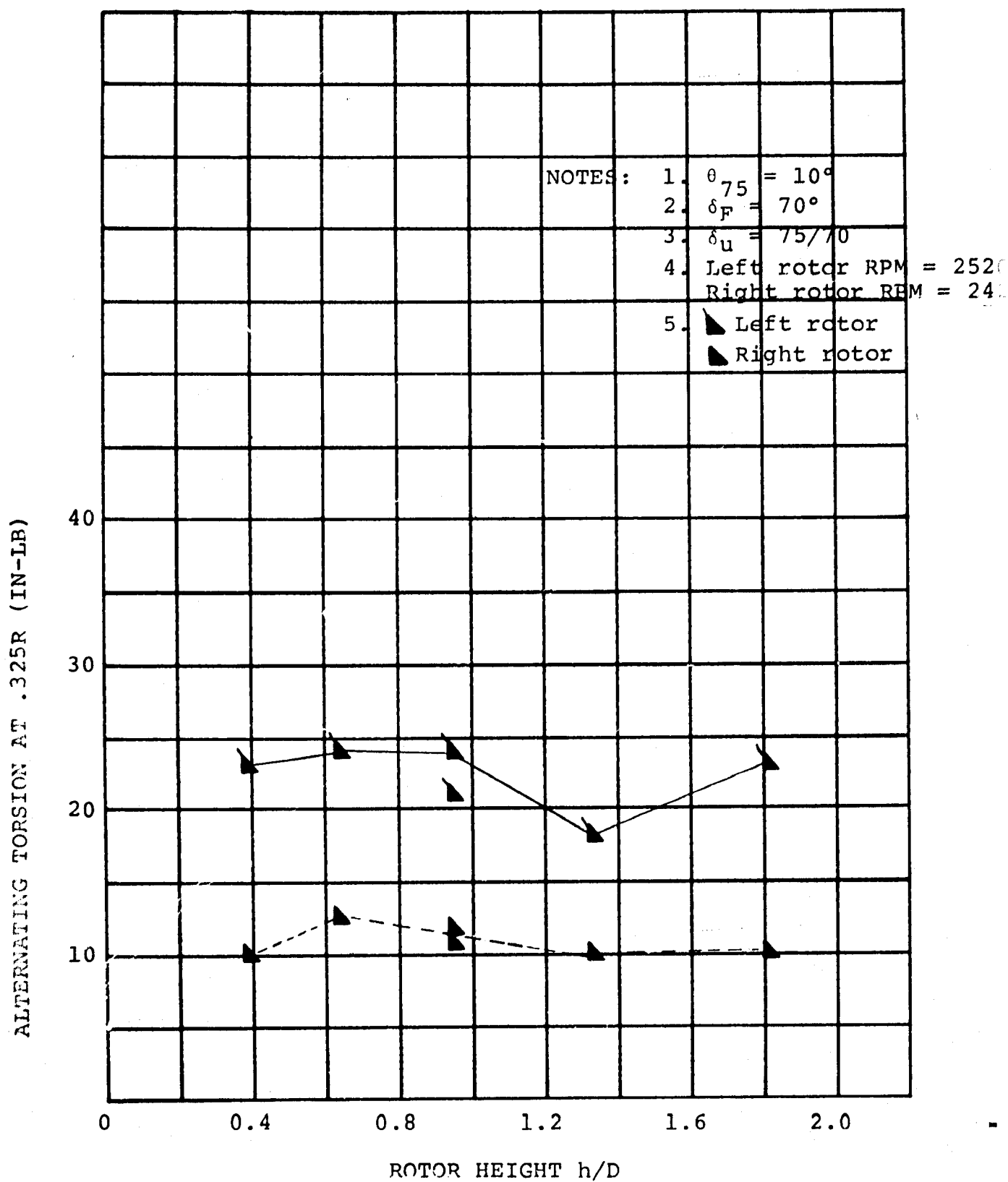


FIGURE 6-58

ALTERNATING BLADE TORSION VS.
 h/D FOR $i_N = 90^\circ$

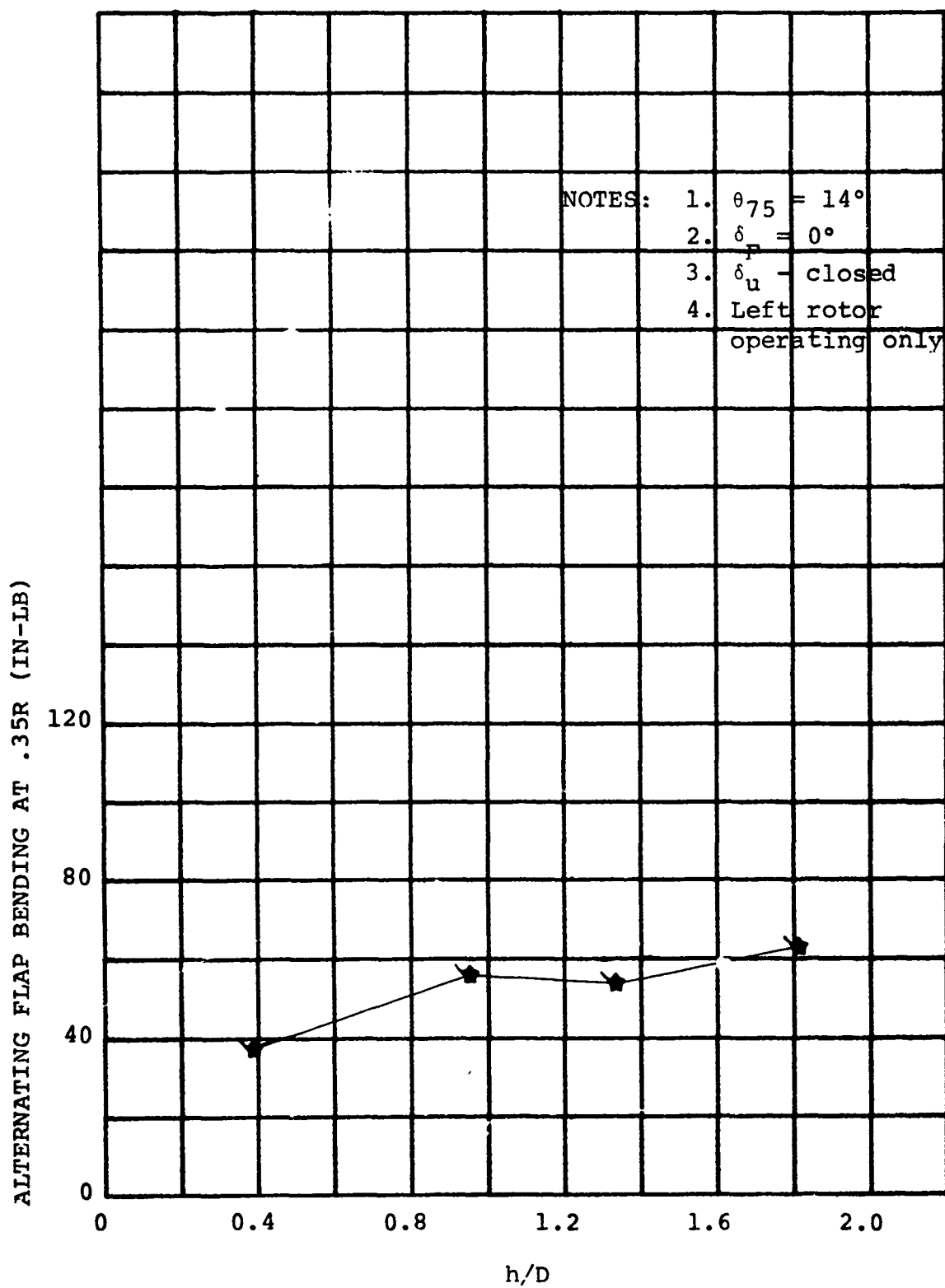


FIGURE 6-59 ALTERNATING BLADE FLAP BENDING VS.
 ROTOR HEIGHT FOR $i_N = 70^\circ$ AND 2180 RPM

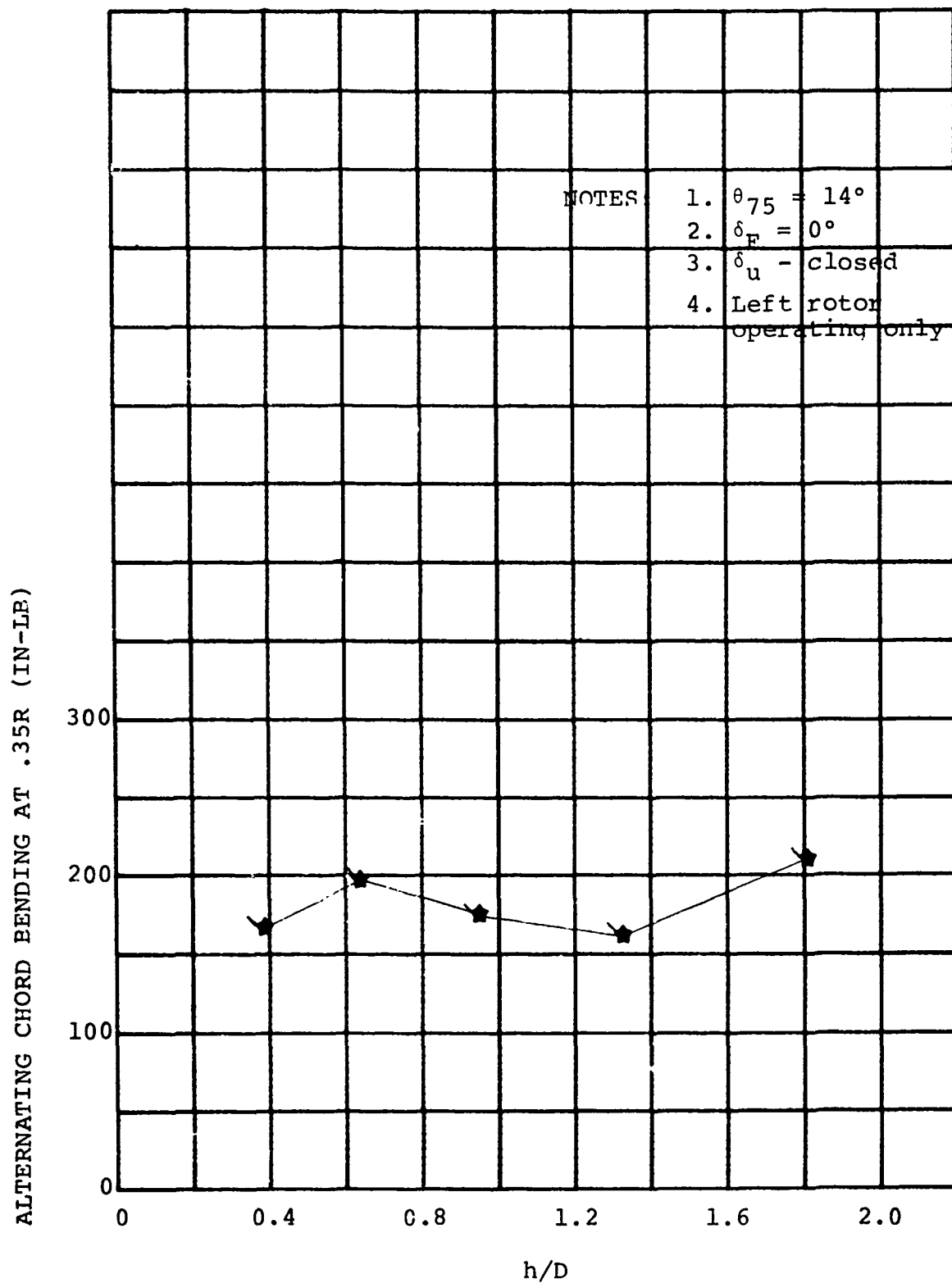


FIGURE 6-60 ALTERNATING BLADE CHORD BENDING VS. ROTOR HEIGHT FOR $i_N = 70^\circ$ AND 2180 RPM

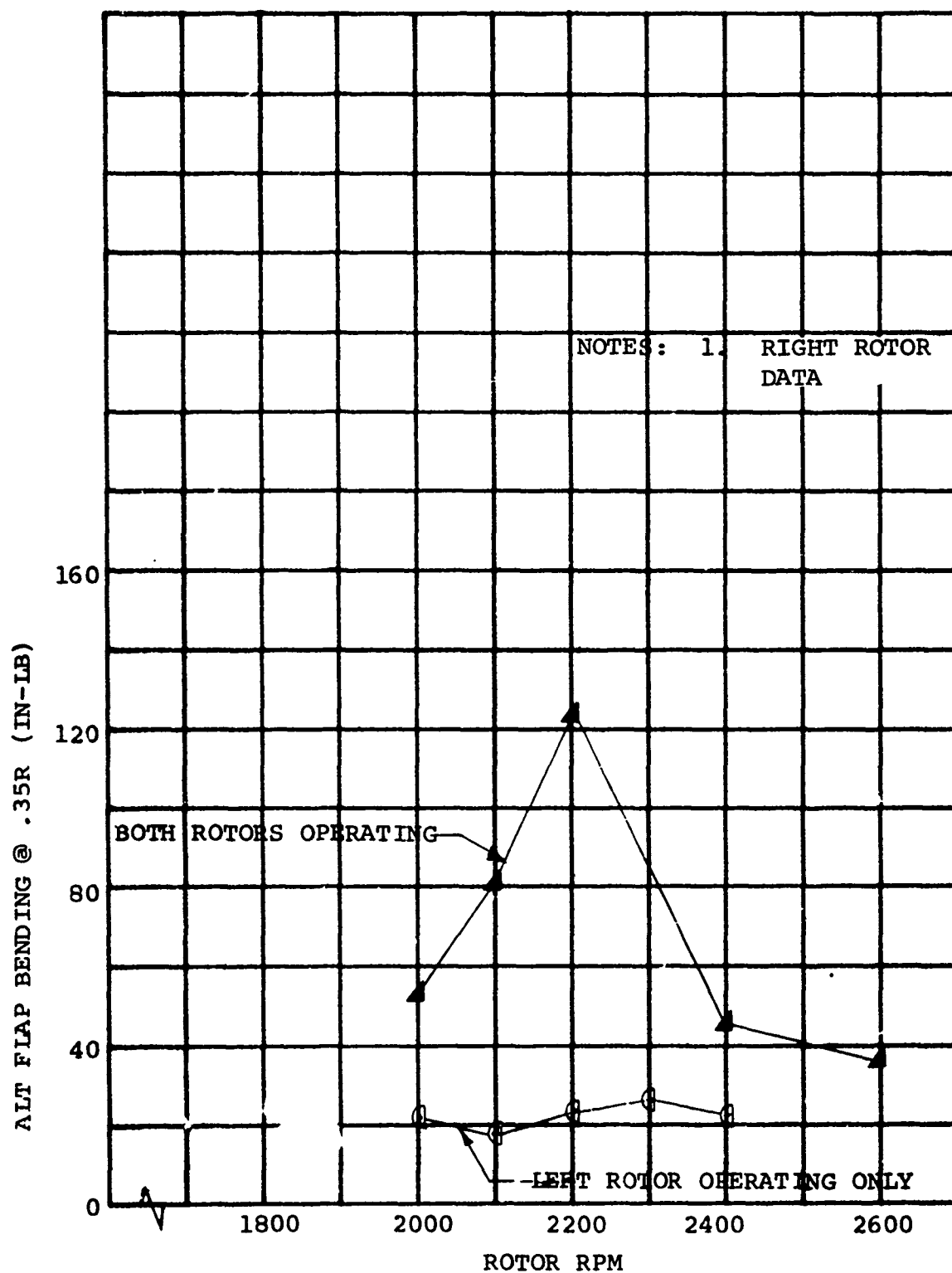


FIGURE 6-61. ALT FLAP BENDING VS RPM FOR $i_N = 90^\circ$, $\Theta_{75} = 10^\circ$ AND $h/d = .39$

LEFT ROTOR OPERATING ONLY

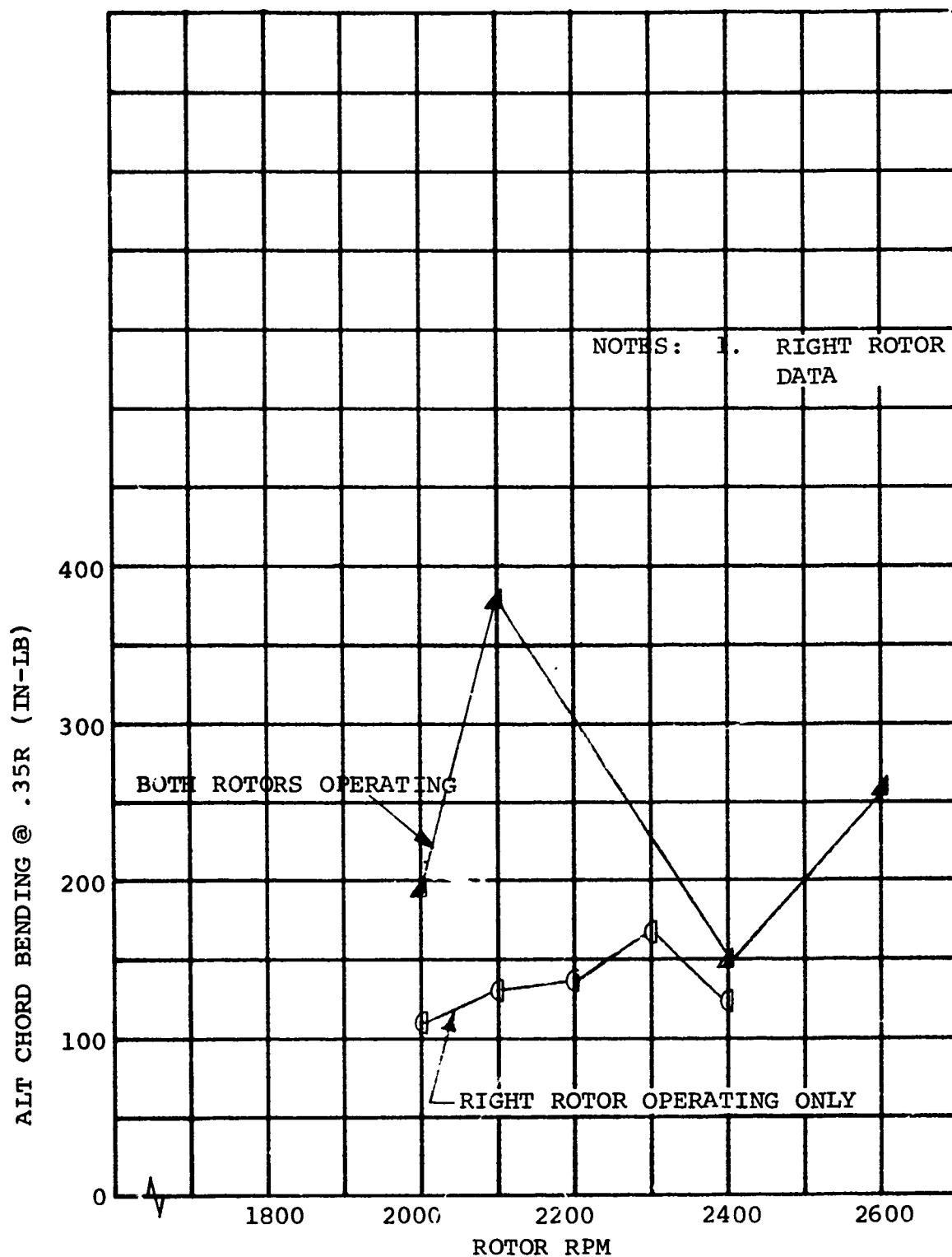


FIGURE 6-62. ALT CHORD BENDING VS RPM FOR $i_N = 90^\circ$, $\Theta_{75} = 10^\circ$ AND $h/D = .39$

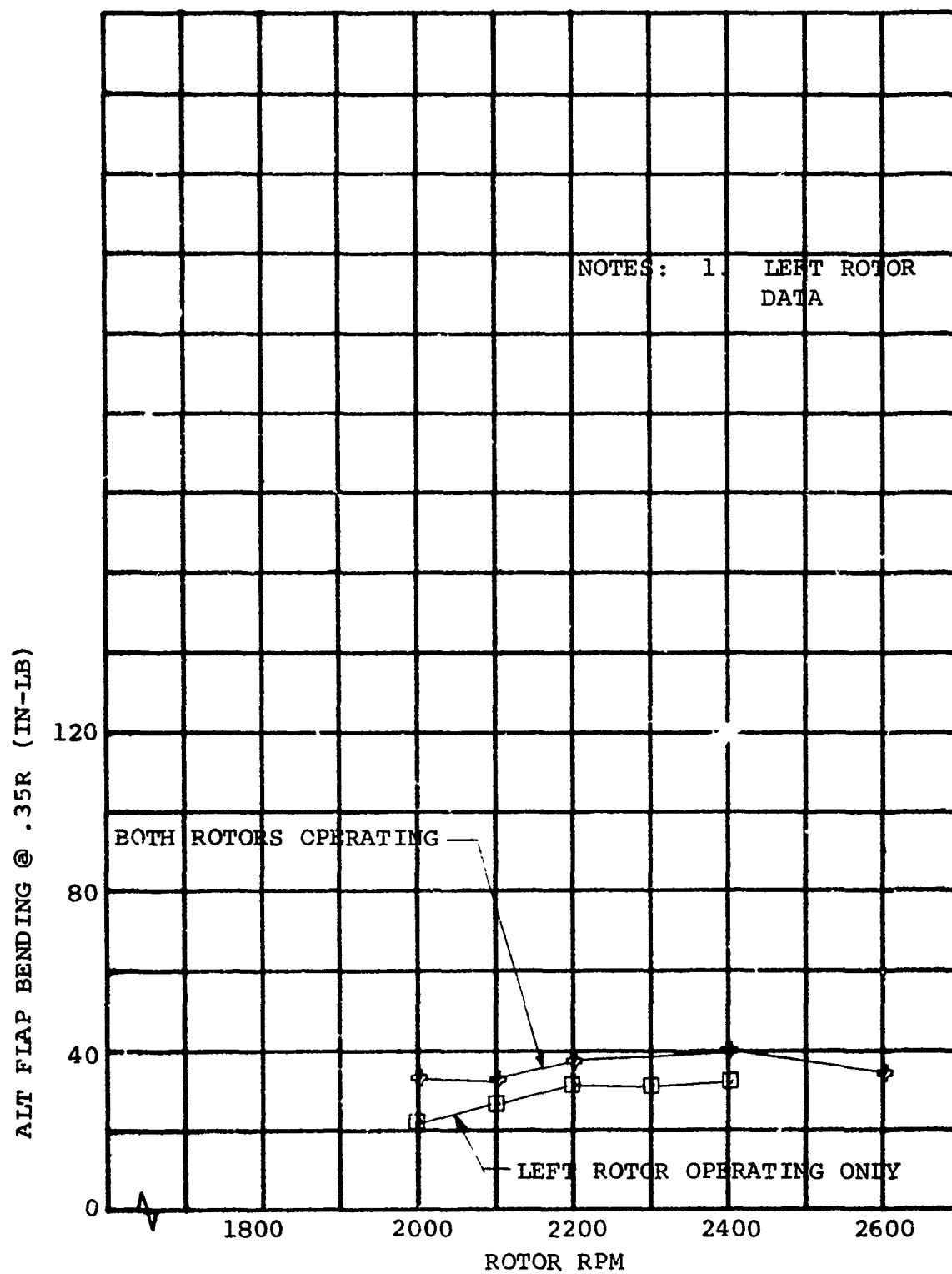


FIGURE 6-63. ALT FLAP BENDING VS RPM FOR $i_N = 90^\circ$, $\Theta_{75} = 10^\circ$ AND $h/D = 1.8$

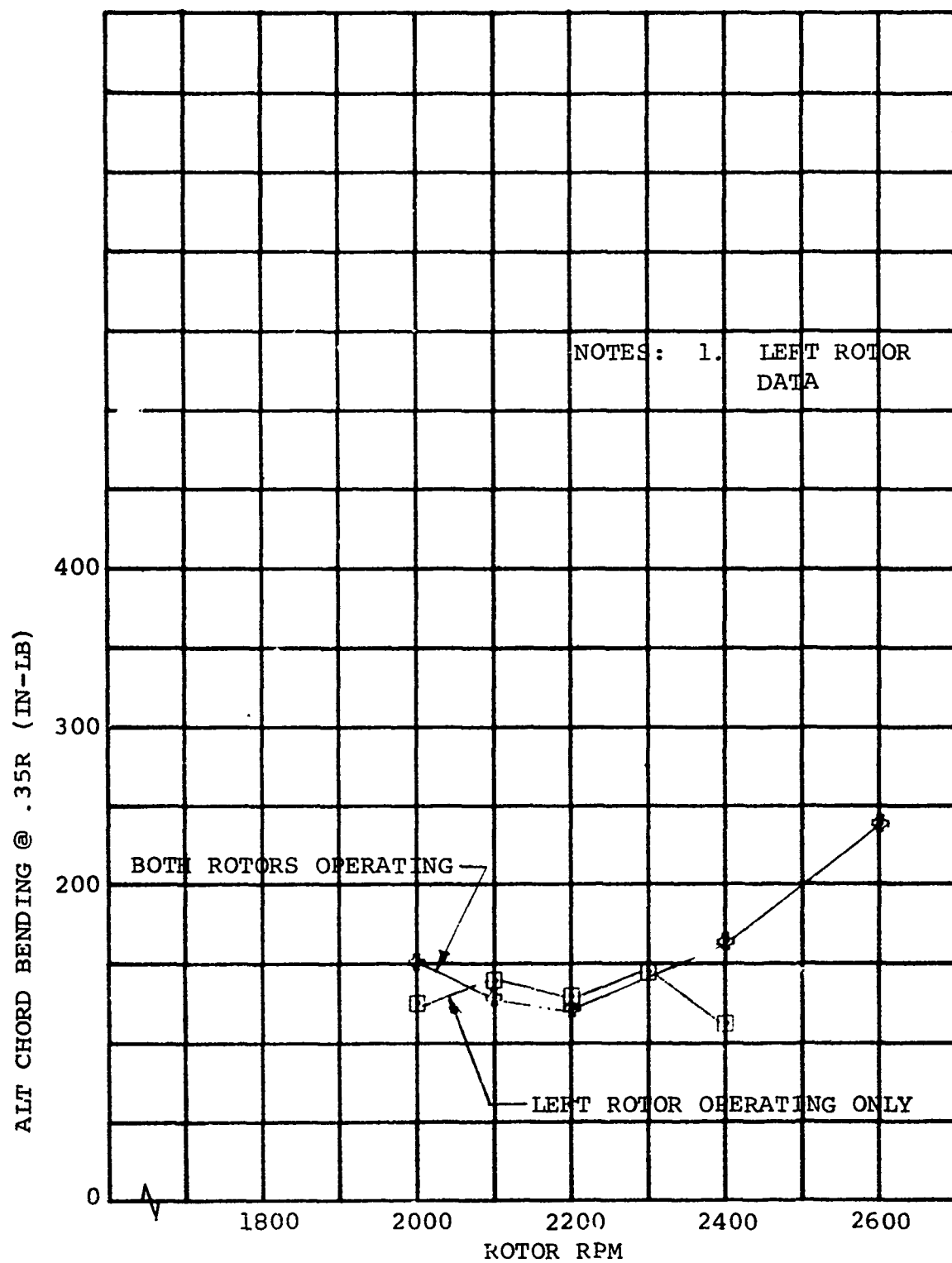


FIGURE 6-64. ALT CHORD BENDING VS RPM FOR $i_N = 90^\circ$, $\Theta_{75} = 10^\circ$ AND $h/D = 1.8$

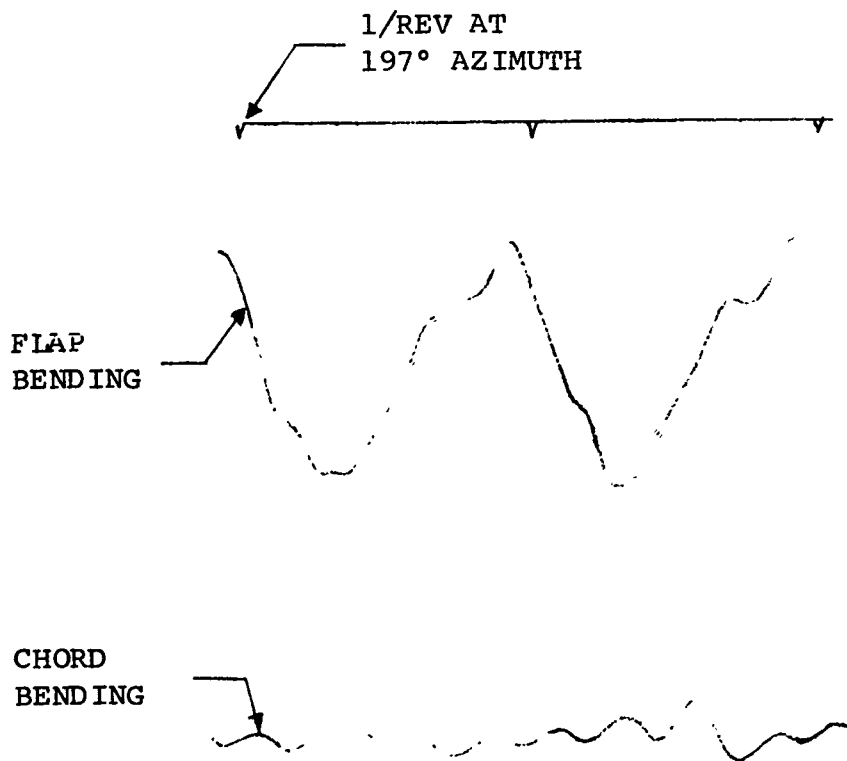


FIGURE 6-65

LEFT ROTOR MOMENT WAVEFORMS FOR $i_N = 70^\circ$, $V = 60$ FPS
 $\theta_{75} = 14^\circ$, RPM = 2180 AND $h/D = 0.39$

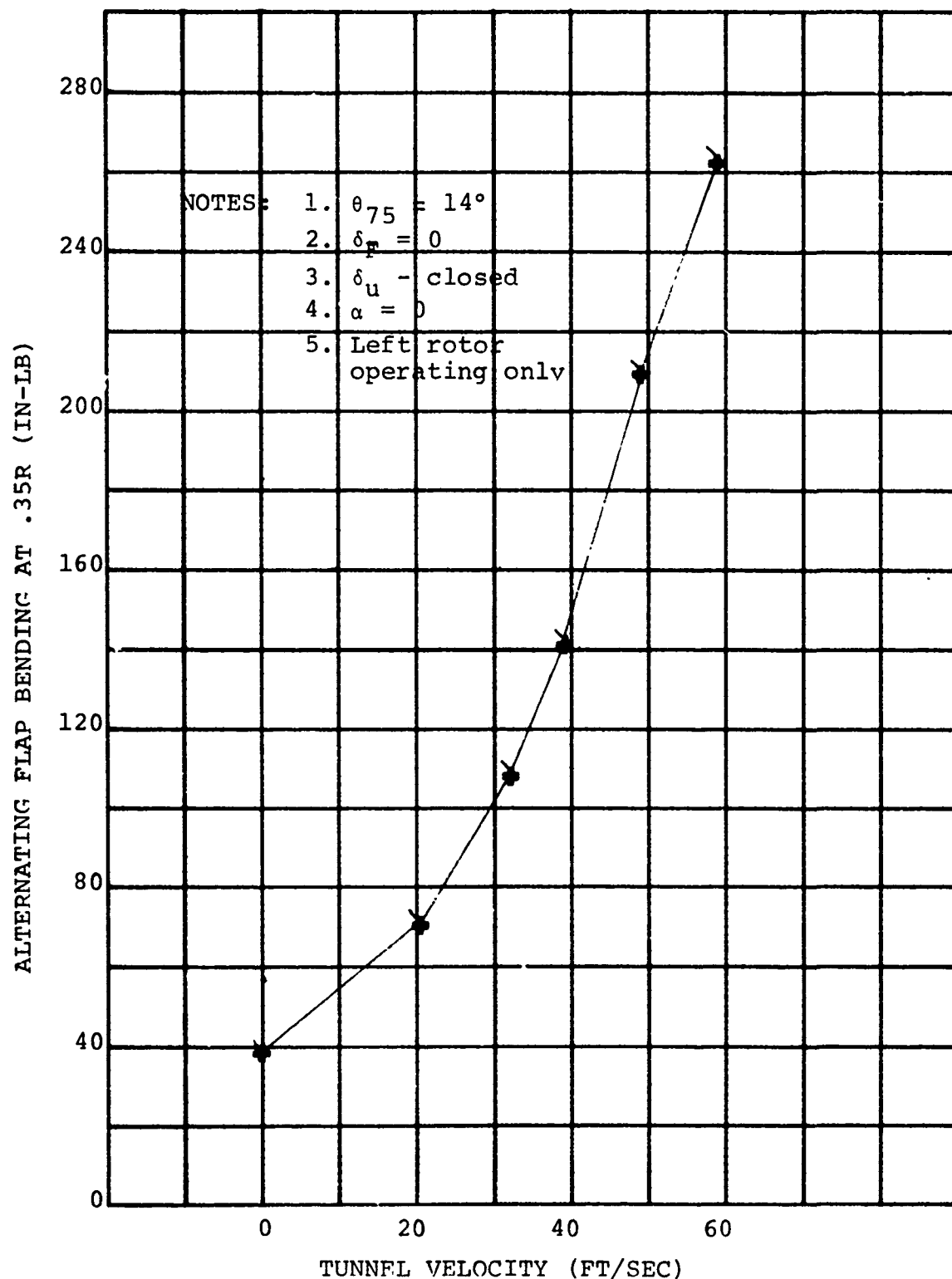


FIGURE 6-66

ALTERNATING BLADE FLAP BENDING VS. VELOCITY
FOR $i_N = 70$ DEG, $h/D = .39$ AND 2180 RPM

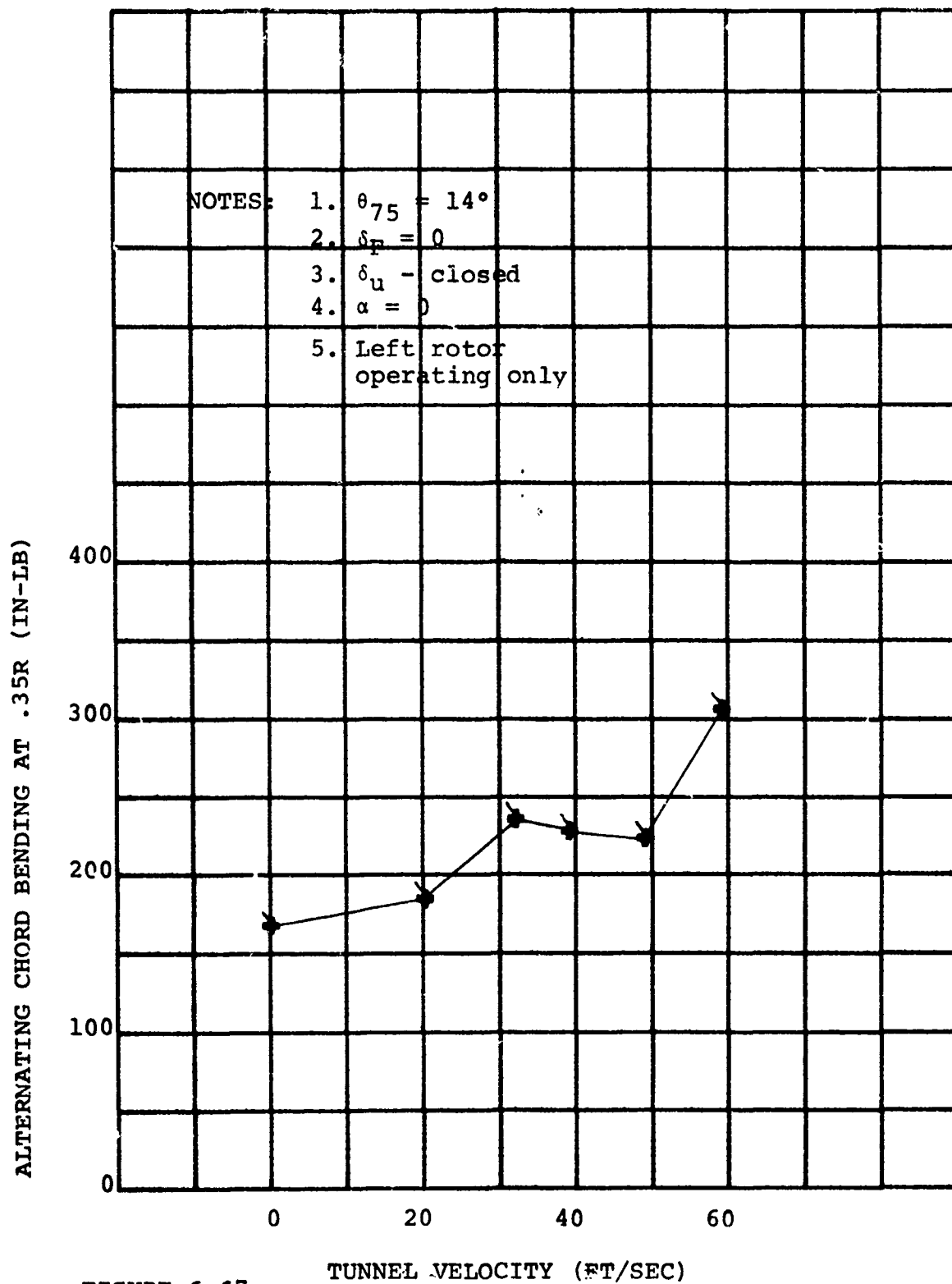


FIGURE 6-67

ALTERNATING BLADE CHORD BENDING VS. VELOCITY
 FOR $i_N = 70$ DEG. $h/D = .39$ AND 2180 RPM

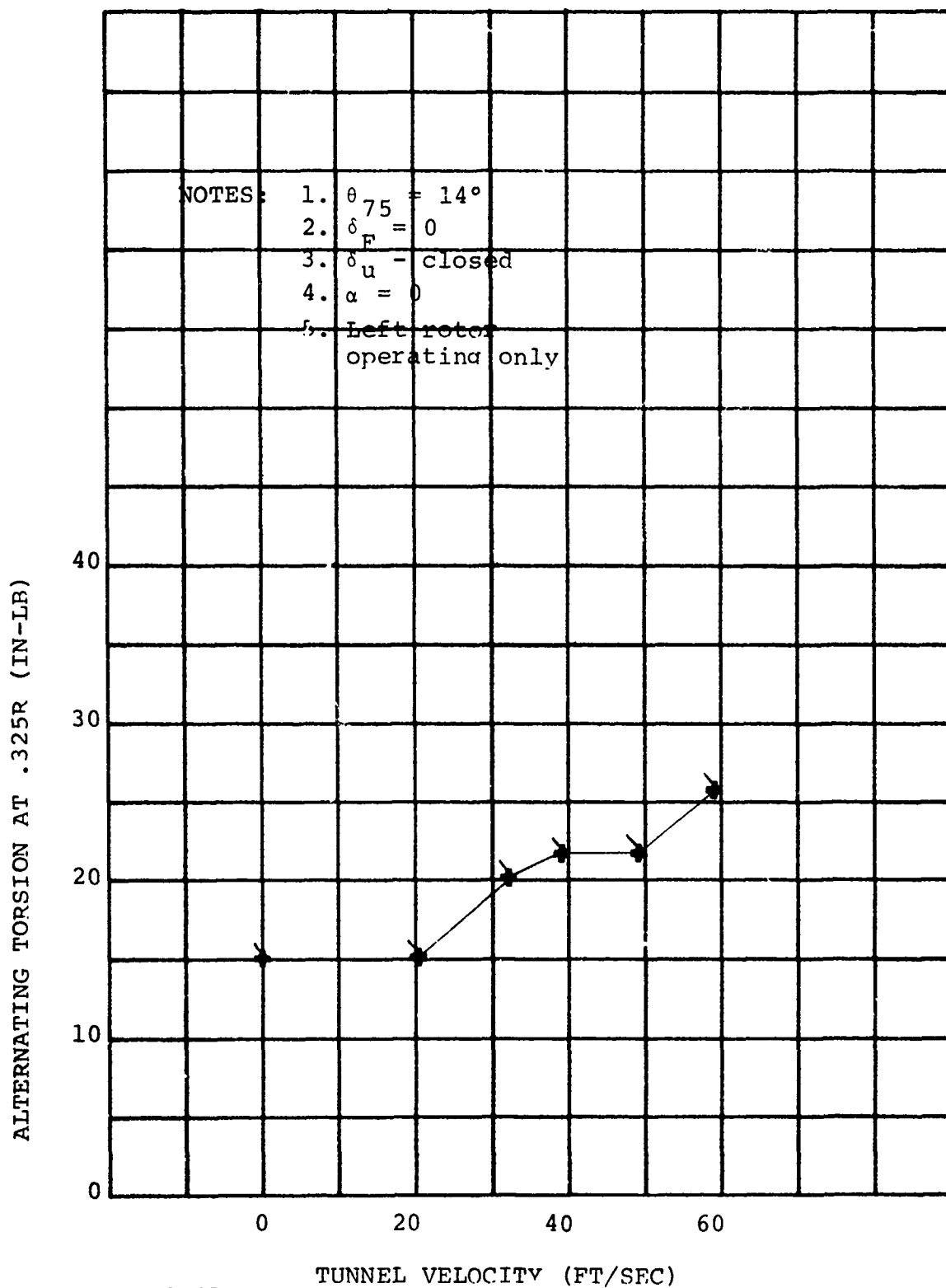


FIGURE 6-68

ALTERNATING BLADE TORSION VS. VELOCITY
 FOR $i_N = 70$ DEG, $h/D = .39$ AND 2180 RPM

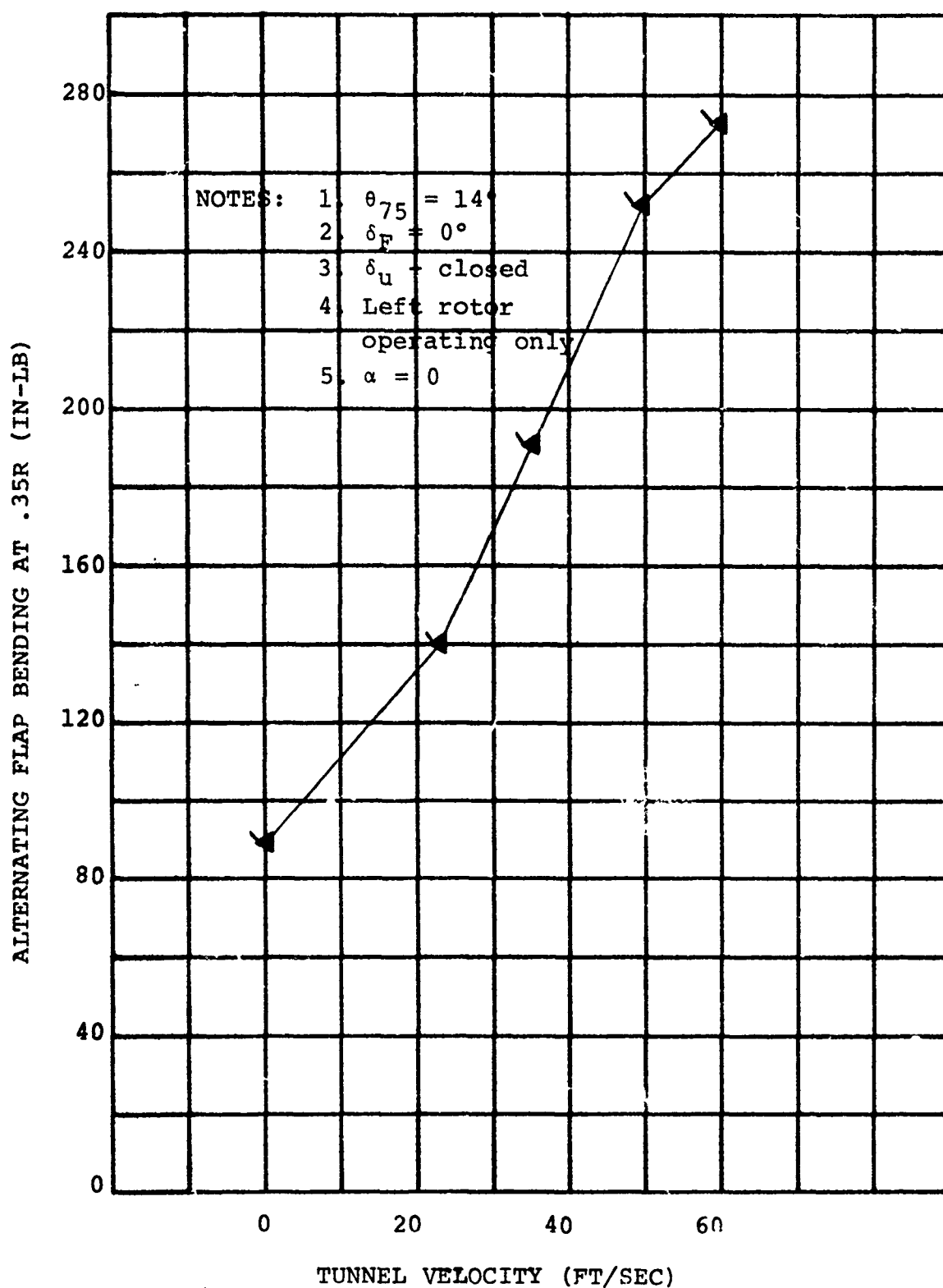


FIGURE 6-69

ALTERNATING BLADE FLAP BENDING VS. VELOCITY
 FOR $i_N = 70$ DEG, $h/D = 1.8$ AND 2180 RPM

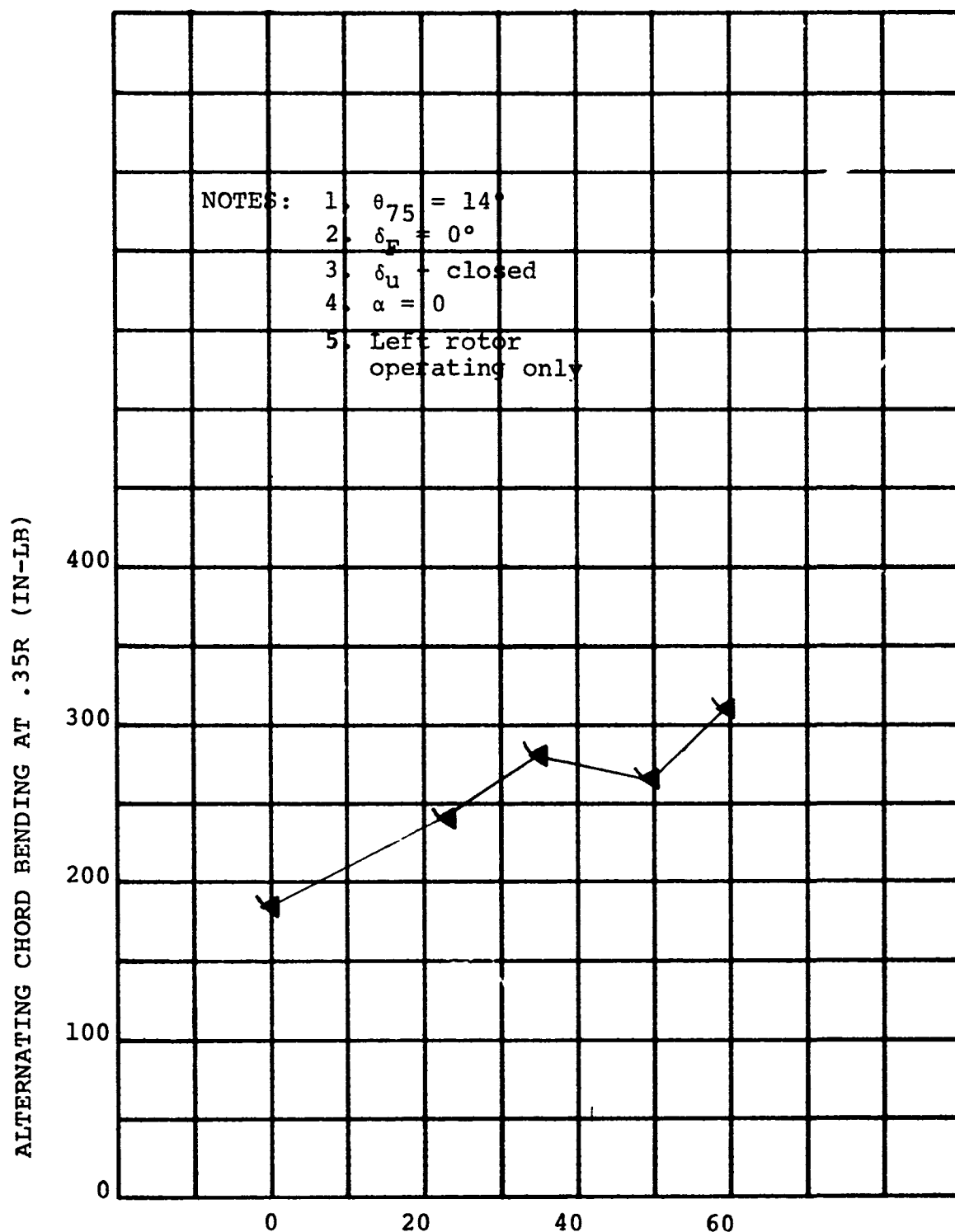


FIGURE 6-70 TUNNEL VELOCITY (FT/SEC)

ALTERNATING BLADE CHORD BENDING VS. VELOCITY
 FOR $i_N = 70$ DEG, $h/D = 1.8$ AND 2180 RPM

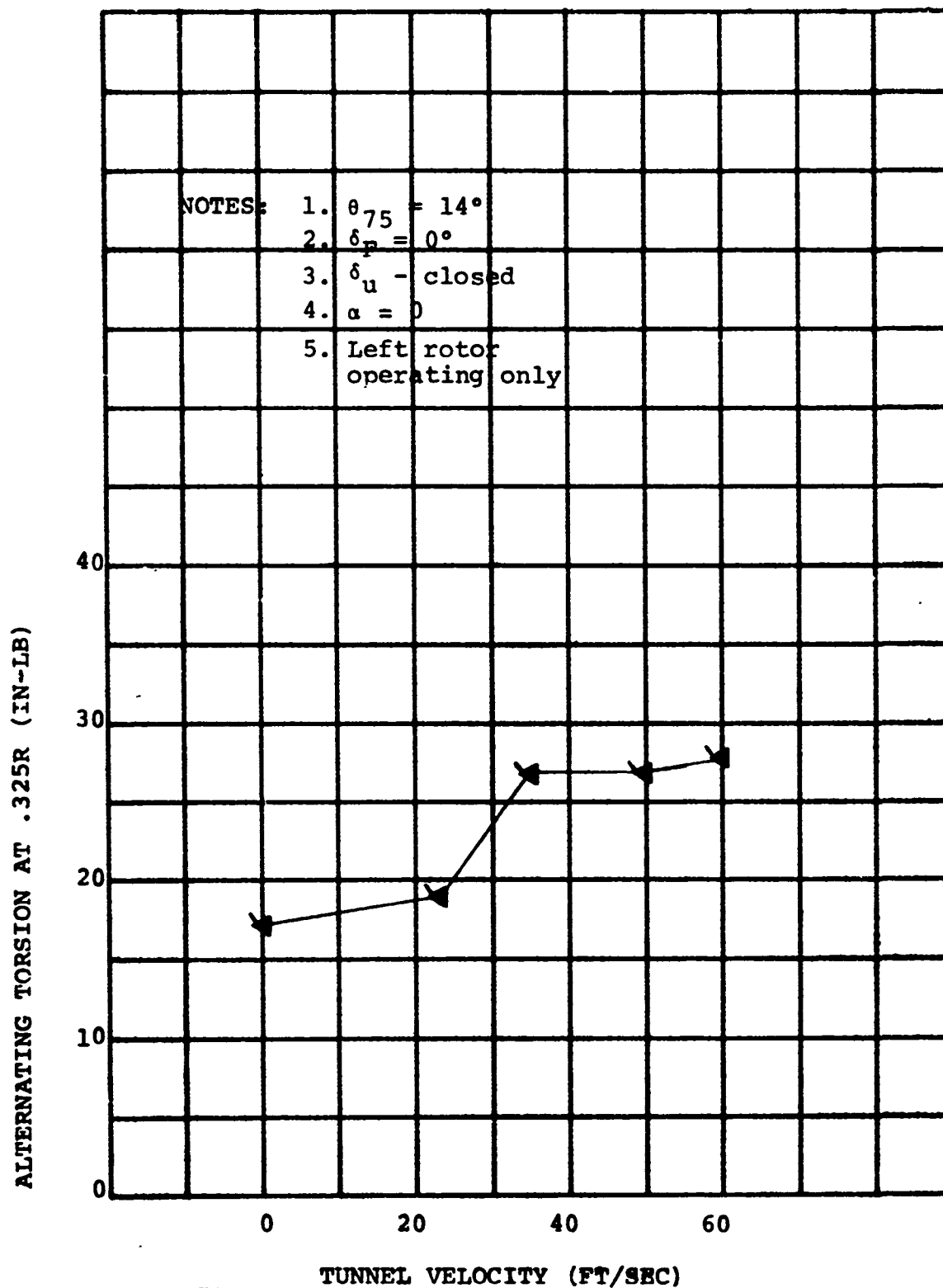


FIGURE 6-71

ALTERNATING BLADE TORSION VS. VELOCITY
 FOR $i_N = 70$ DEG, $h/D = 1.8$ AND 2180 RPM

6.3 HOVER HUB MOMENT

6.3.1 Effect of Cyclic Pitch

Rotor hub moment which results from one-per-revolution cyclic blade bending moment is practically zero for hover without blade cyclic pitch. Figure 6-72 shows hub moment versus rotor RPM with 3 degrees cyclic for two different h/D values with the nacelle in the hover position and also for 3 degrees cyclic with the nacelle in the cruise position. The forward velocity is zero for all three conditions. The data show that the height of the rotor above the ground and the presence of the wing in hover did not effect the hub moment.

The uncoupled rotor loads analysis was used to predict the rotor hub moment due to 3 degrees cyclic pitch in hover. A comparison of the predicted and measured hub moment is shown in Figure 6-73. The good agreement of the predicted and measured hub moment demonstrates that the hover blade flapping frequency has been correctly represented and the analysis accurately predicts hub moments in hover due to cyclic.

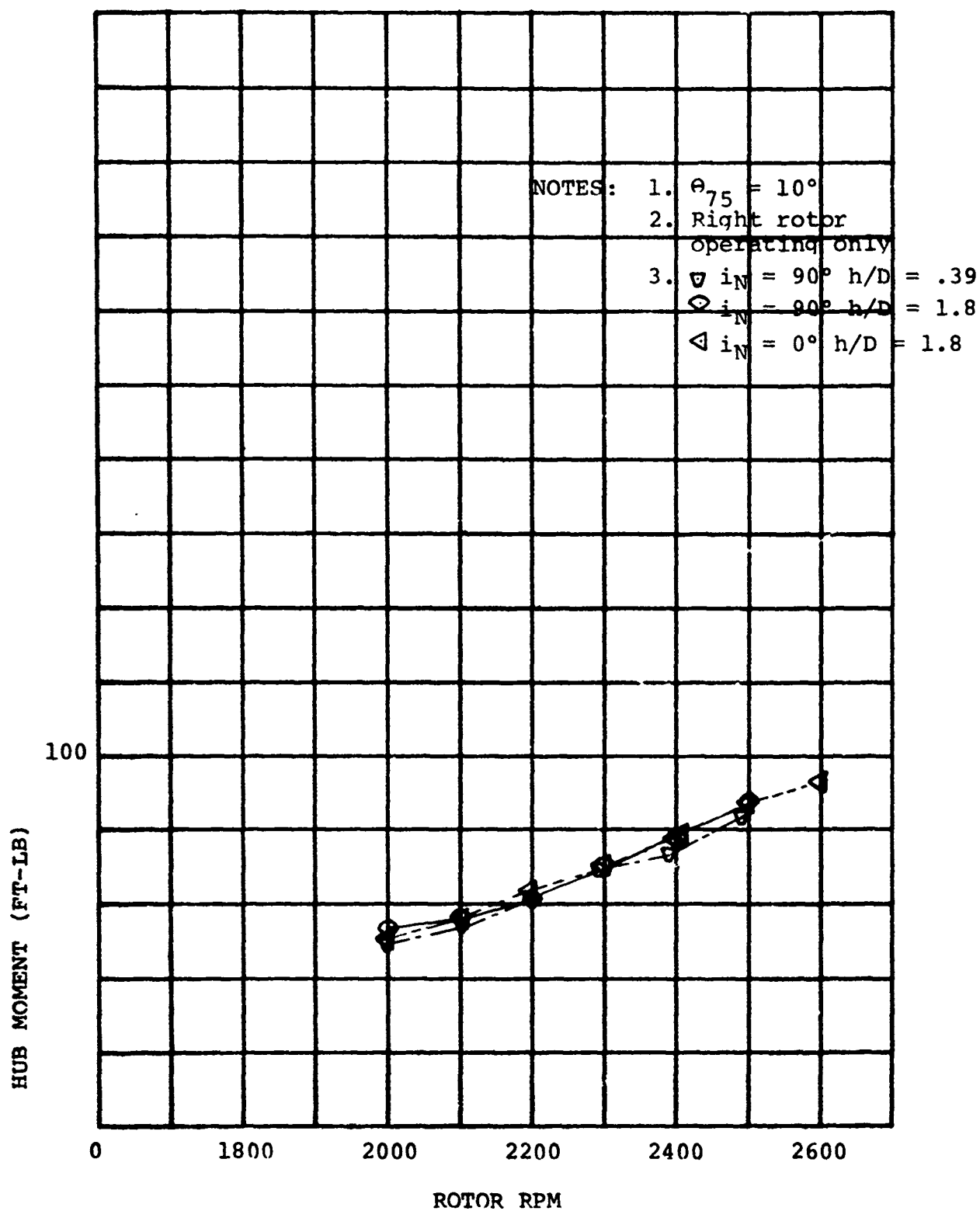


FIGURE 6-72

STEADY HUB MOMENT VS. RPM
 FOR 3° CYCLIC AND $V = 0$

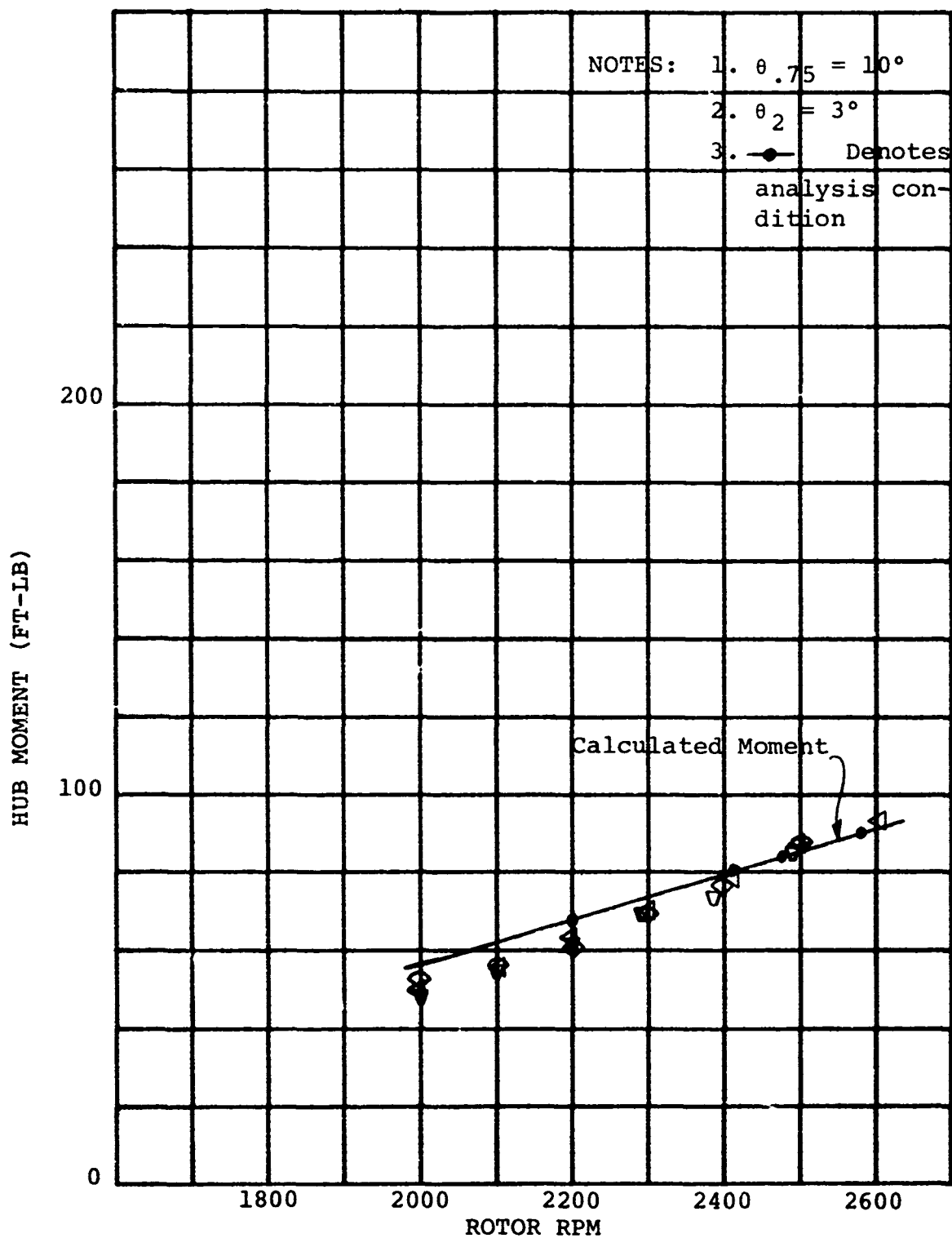


FIGURE 6-73
 COMPARISON BETWEEN MEASURED AND CALCULATED STEADY HUB
 MOMENT VS. RPM FOR 3° CYCLIC AND $V = 0$

6.4 TRANSITION BLADE LOADS

Blade loads data were obtained in transition flight to show the effects of aircraft angle of attack, cyclic pitch and aircraft yaw. Results of these data show that blade loads increase with aircraft angle of attack. Nose-down cyclic pitch decreases blade loads and nose-up cyclic increases blades loads. Aircraft yaw has little effect on blade loads.

6.4.1 Attitude Effects

Blade loads data presented in Figures 6-74 thru 6-77 show the effect of aircraft angle of attack on alternating flap and chord bending. The increase of flap and chord loads with angle of attack is due to rotor inflow and wing interference.

Blade loads data presented in Figures 6-78 and 6-79 show the effect of aircraft yaw on blade flap and chord bending. Aircraft yaw has little effect on blade loads. Increased blade loads for yawed conditions are due to rotor inflow since wing lift remains nearly constant. The results of these data show that increased rotor inflow due to aircraft yaw in transition has little effect on blade loads. The change in local blade angle due to rotor inflow for yawed conditions in transition is smaller than that due to the same yaw angle in cruise flight since nacelle tilt decreases the rotor inflow when all other conditions are kept constant. For 90 degrees nacelle tilt (edgewise flight), no rotor inflow occurs for yawed conditions.

6.4.2 Effect of Cyclic Pitch

Blade loads data presented in Figures 6-80 through 6-82 show the effect of cyclic pitch when the aircraft is pitched or yawed. These data show that 3 degrees nose-up cyclic increases and nose-down cyclic decreases alternating flap bending when the aircraft is pitched. Phasing of lateral and longitudinal cyclic was set for a pure rotor pitching moment in hover and therefore, the phasing for transition is not optimized to decrease blade loads. The correct phasing for minimum blade loads would be set to minimize the once-per-rev change in local blade angle due to rotor inflow. Therefore, for correct cyclic phasing, blade loads with angle of attack would be smaller for 3 degrees nose-down cyclic than those shown on Figure 6-80. The effect of cyclic on blade loads when the aircraft is yawed is shown in Figures 6-81 and 6-82. Nose-up cyclic increases and nose-down cyclic decreases flap and chord bending. Since cyclic phasing was not optimized for decreased blade loads, the correct phasing, which would be 90 degrees less than for aircraft pitch, would minimize blade loads for the same value of cyclic for these test conditions.

6.4.3 Stall Flutter

Stall flutter was experienced in transition flight at a nacelle tilt of 70 degrees and advance ratio of 0.21. The effect of stall flutter in transition on alternating blade torsion is shown in Figure 6-83. Blade torsion increases sharply when the angle of attack is increased above zero degrees. Figure 6-84 shows that alternating torsion is predominantly a one and eight-per-rev response. As discussed in Section 4.3.2, blade stall at the blade tip is evident at -5 degrees angle of attack since first harmonic flapping decreases and as shown in Figure 6-84, first harmonic torsion also decreases. The blade first torsional natural frequency is nearly eight per rev at 1970 RPM and as shown in Figure 6-84, the torsional eighth harmonic increases rapidly as the angle of attack is increased above 5 degrees. Five degrees angle of attack is the stall flutter inception point and torsional wave-forms before and after stall flutter inception are shown in Figure 6-85. At stall flutter inception, alternating torsion is 1.15 times that for 3 degrees of cyclic in hover at 750 FPS tip speed. At 12.5 degrees angle of attack, alternating torsion is 2.28 times that for 3 degrees of hover cyclic.

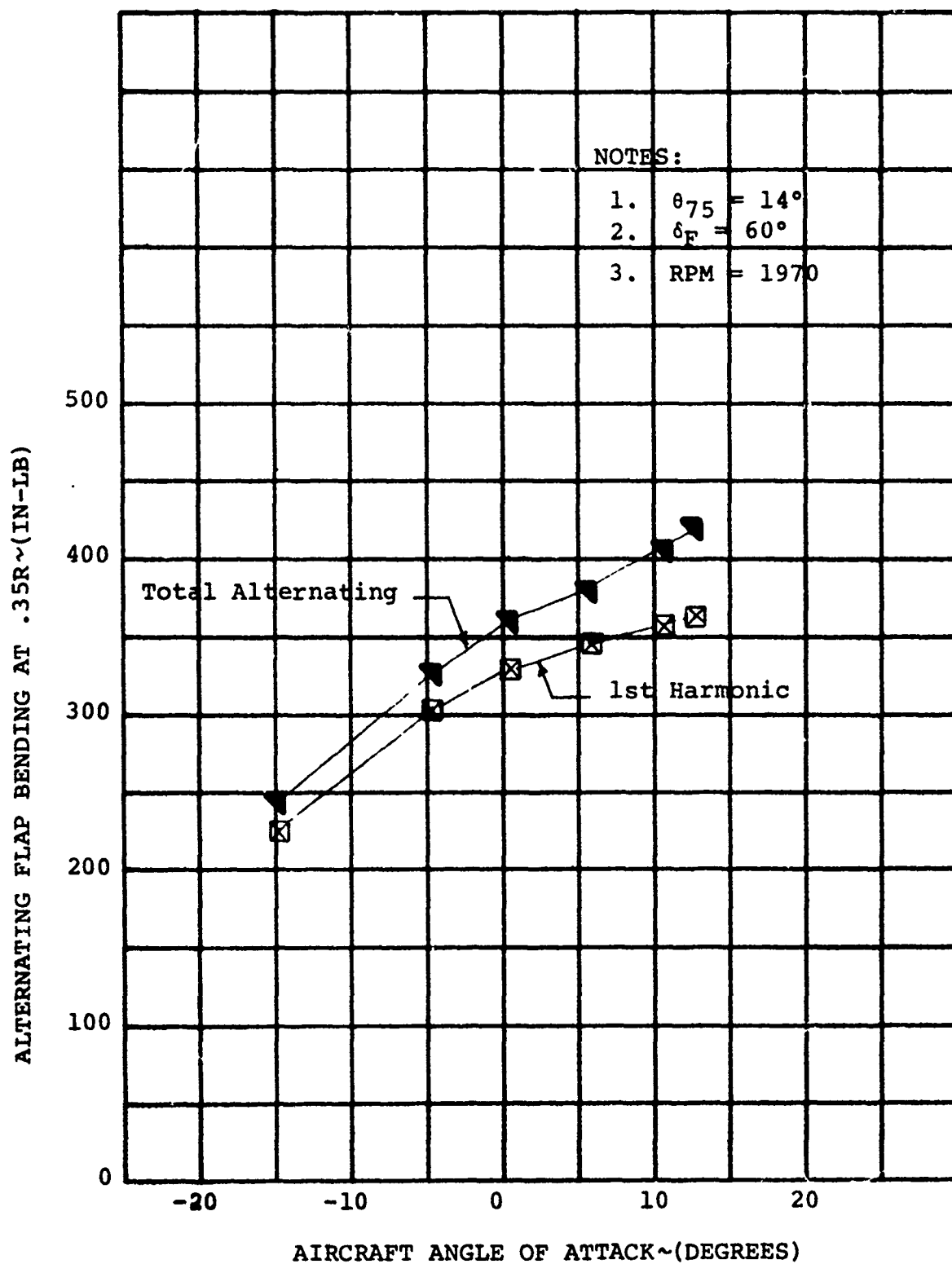


FIGURE 6-74

LEFT ROTOR ALTERNATING FLAP BENDING VS.
AIRCRAFT ANGLE OF ATTACK FOR $i_N = 70$
DEG AND $V = 116$ FPS

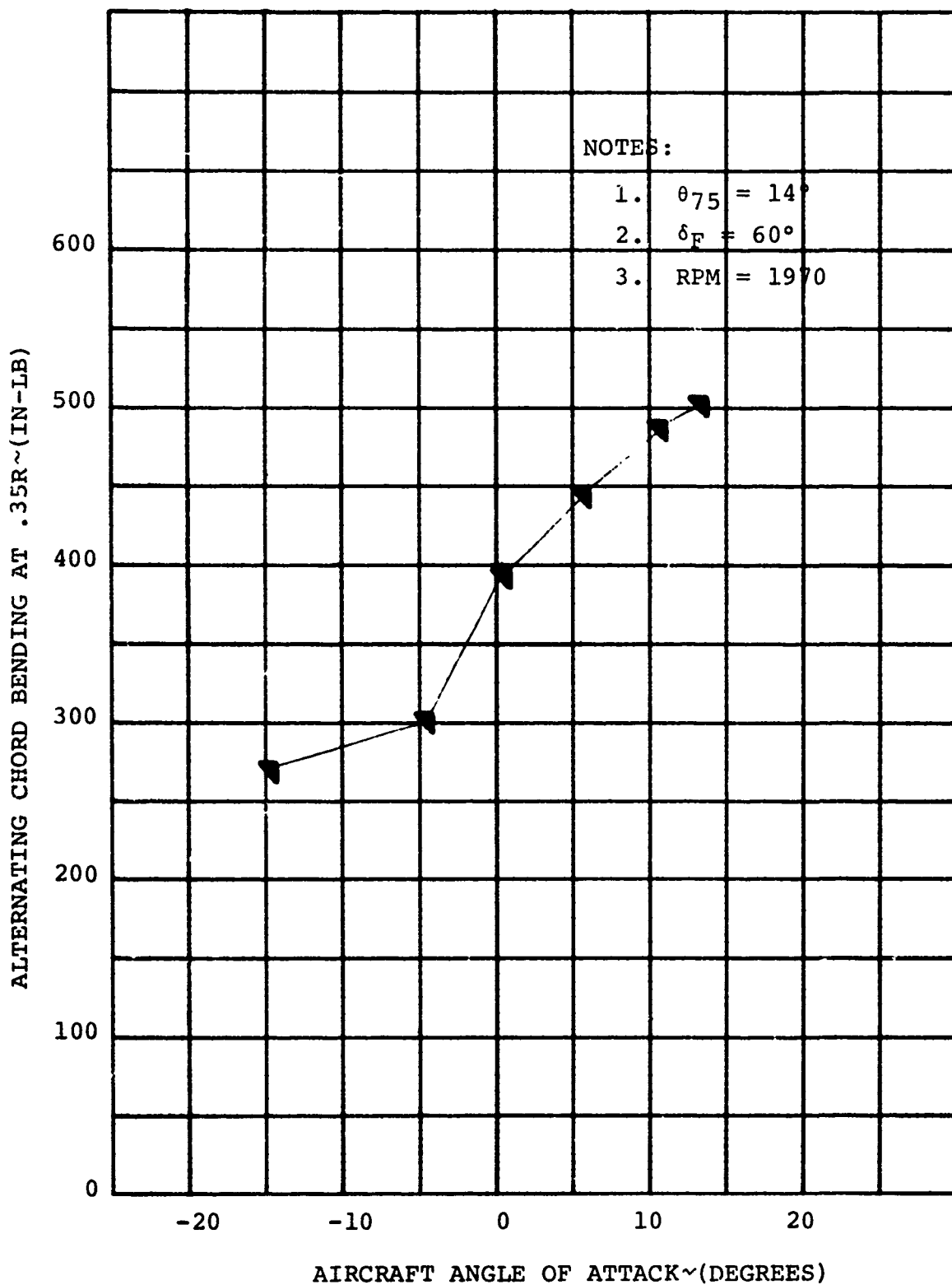


FIGURE 6-75

LEFT ROTOR ALTERNATING CHORD BENDING
VS. AIRCRAFT ANGLE OF ATTACK FOR $i_N = 70$ DEG, AND $V = 116$ FPS

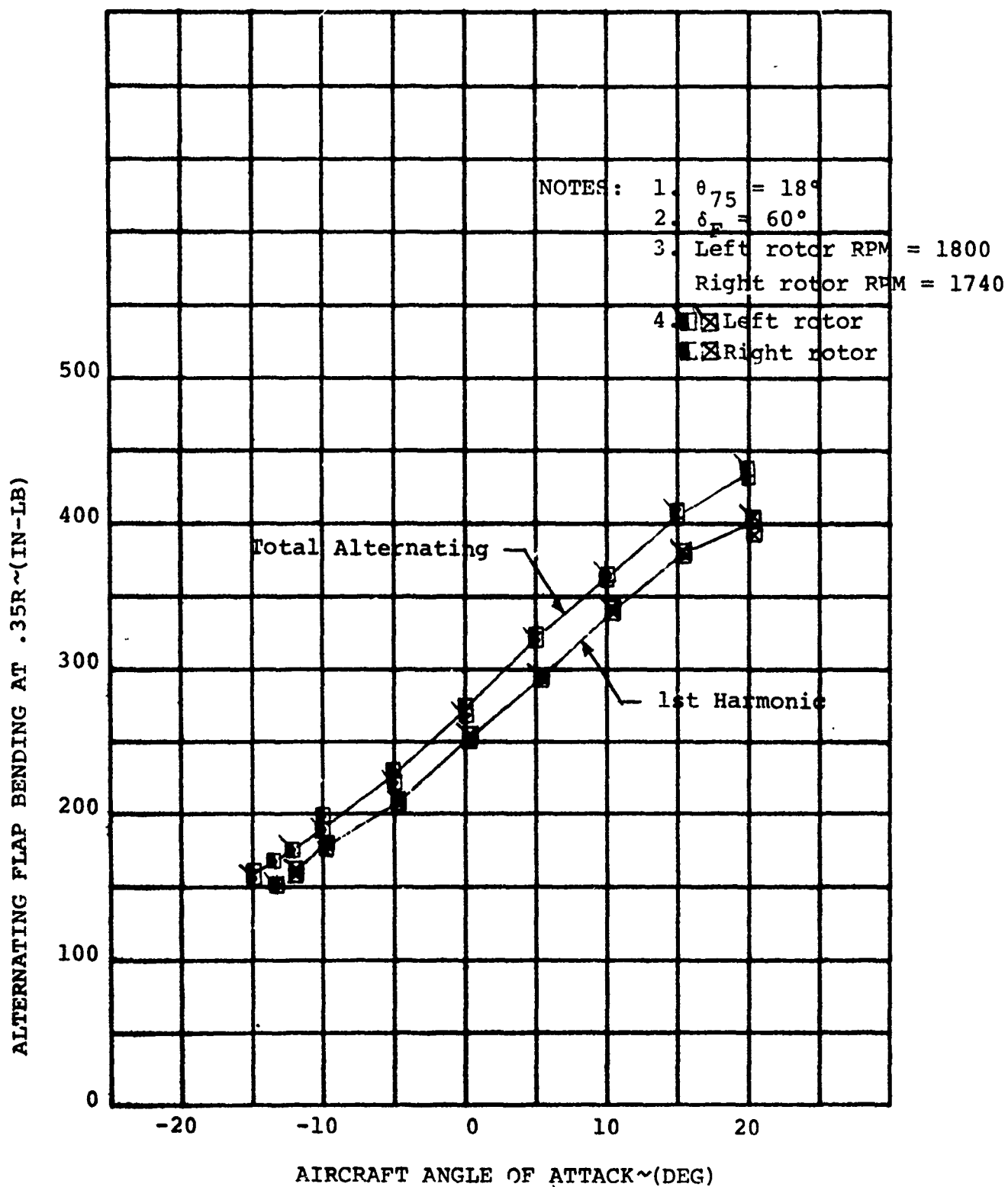


FIGURE 6-76 ALTERNATING BLADE FLAP BENDING VS. AIRCRAFT ANGLE OF ATTACK FOR $i_N = 45^\circ$, $V = 132$ FPS

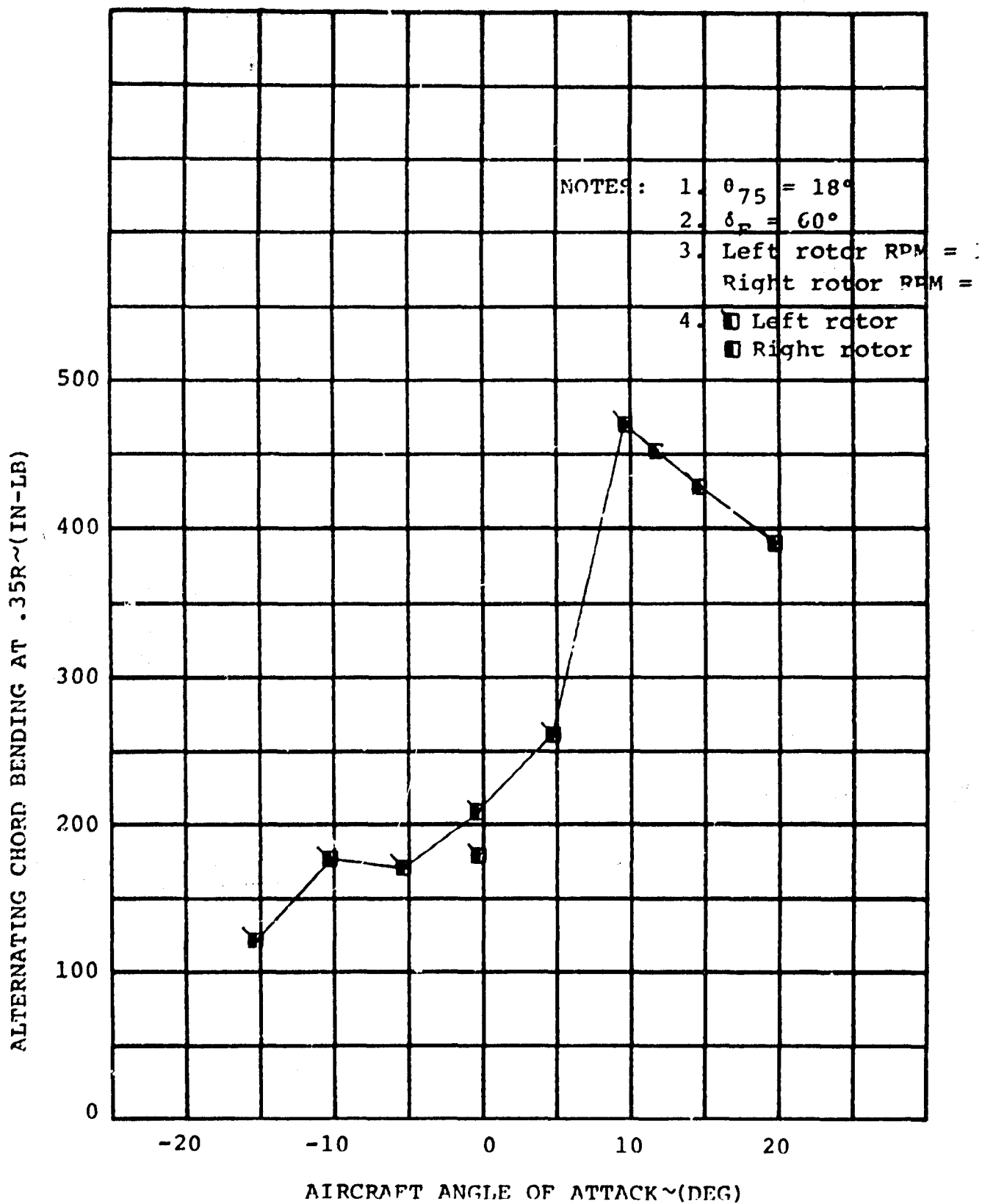


FIGURE
6-77

ALTERNATING BLADE CHORD BENDING VS. AIRCRAFT
 ANGLE OF ATTACK FOR $i_N = 45^\circ$, $V = 132$ FT

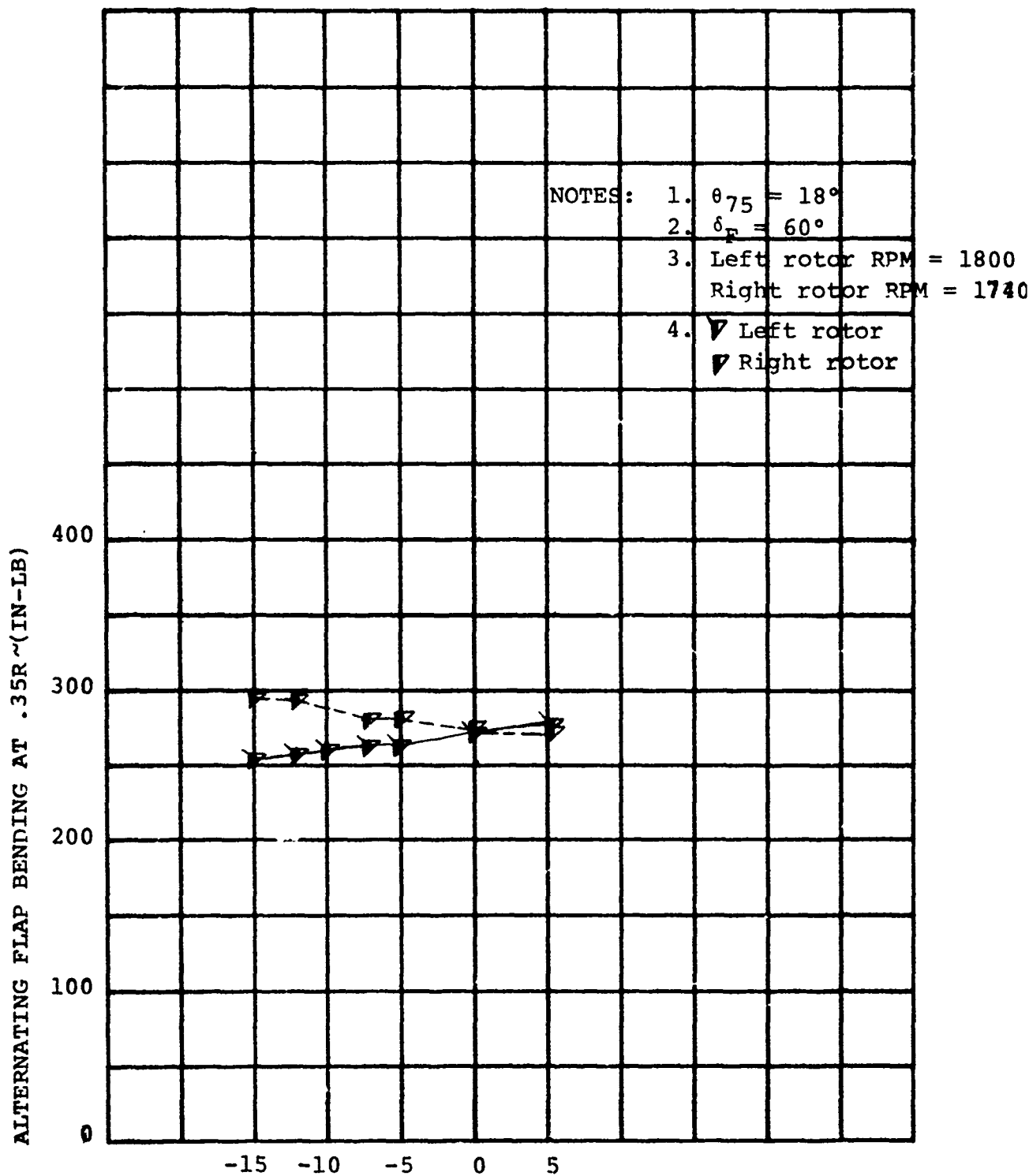


FIGURE 6-78

AIRCRAFT YAW~(DEG)

ALTERNATING BLADE FLAP BENDING VS. AIRCRAFT YAW ANGLE
 FOR $i_N = 45$ DEG, $V = 132$ FPS, AND $\alpha = 0$ DEG

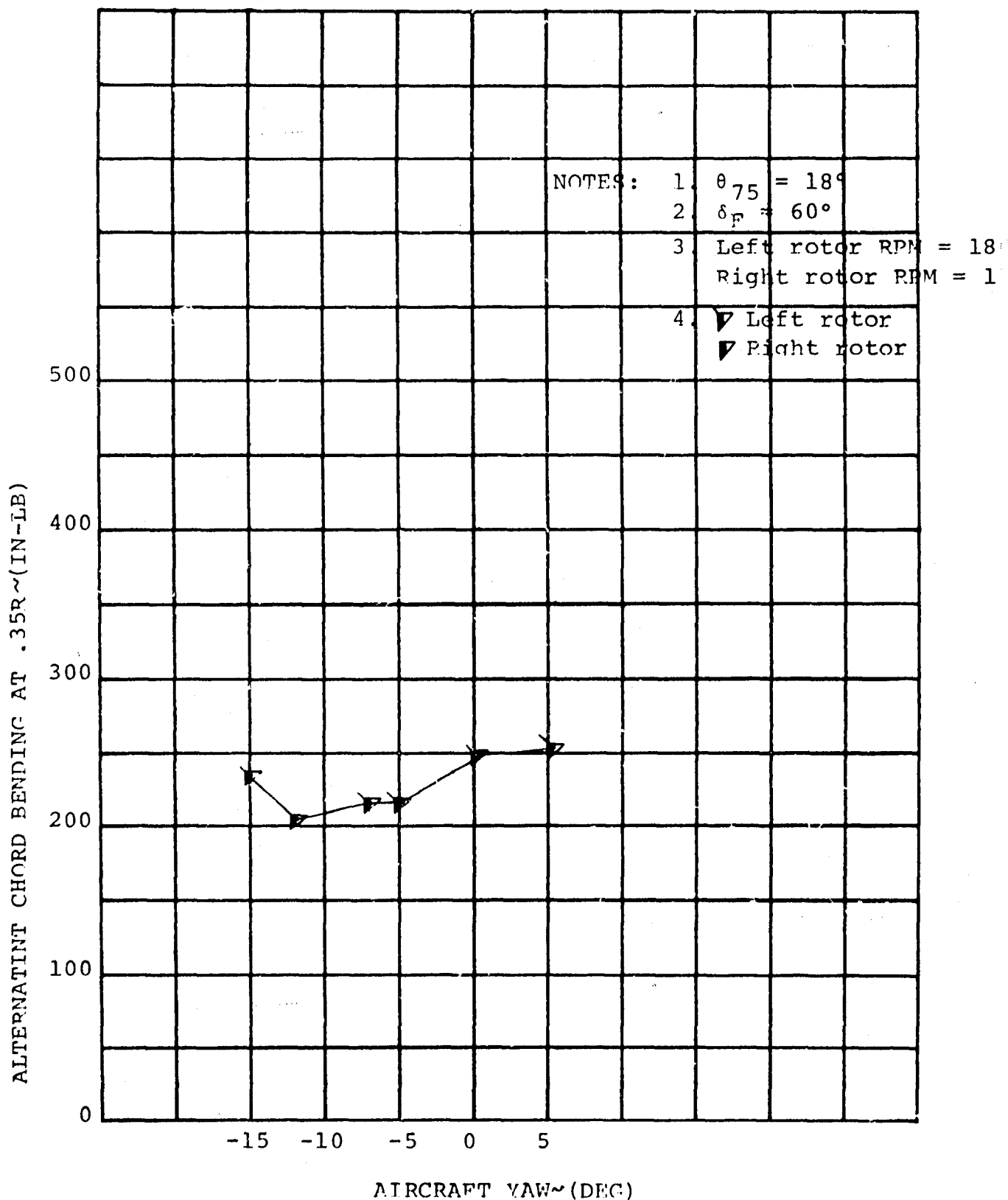


FIGURE 6-79

ALTERNATING BLADE CHORD BENDING VS. AIRCRAFT YAW
 ANGLE FOR $i_N = 45$ DEG, $V = 132$ FPS, AND $\alpha = 0$ DEG

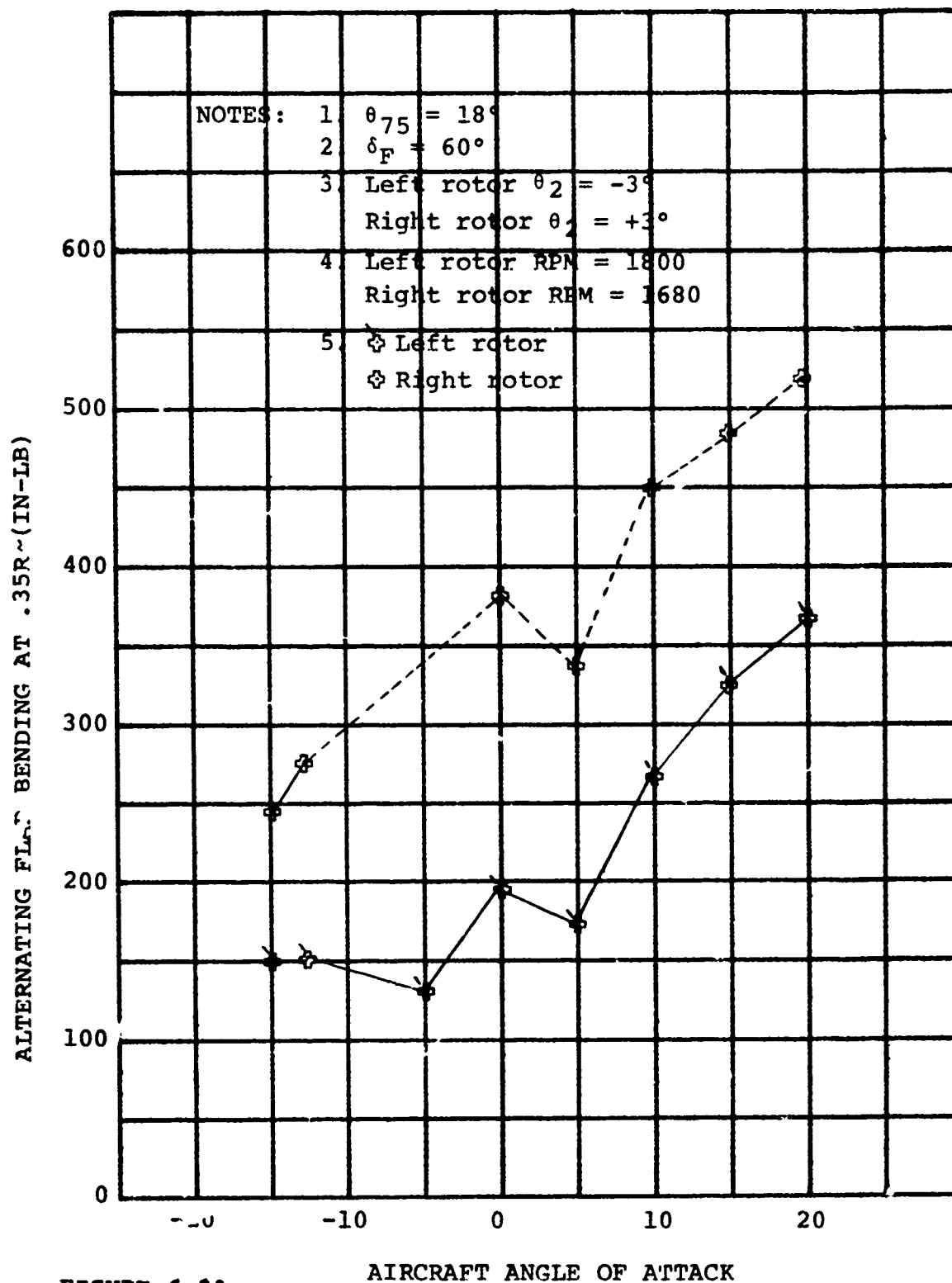


FIGURE 6-80

ALTERNATING BLADE FLAP BENDING VS. AIRCRAFT ANGLE OF ATTACK FOR $i_N = 45$ DEG, $V = 132$ FPS, AND $+3$ DEG CYCLIC

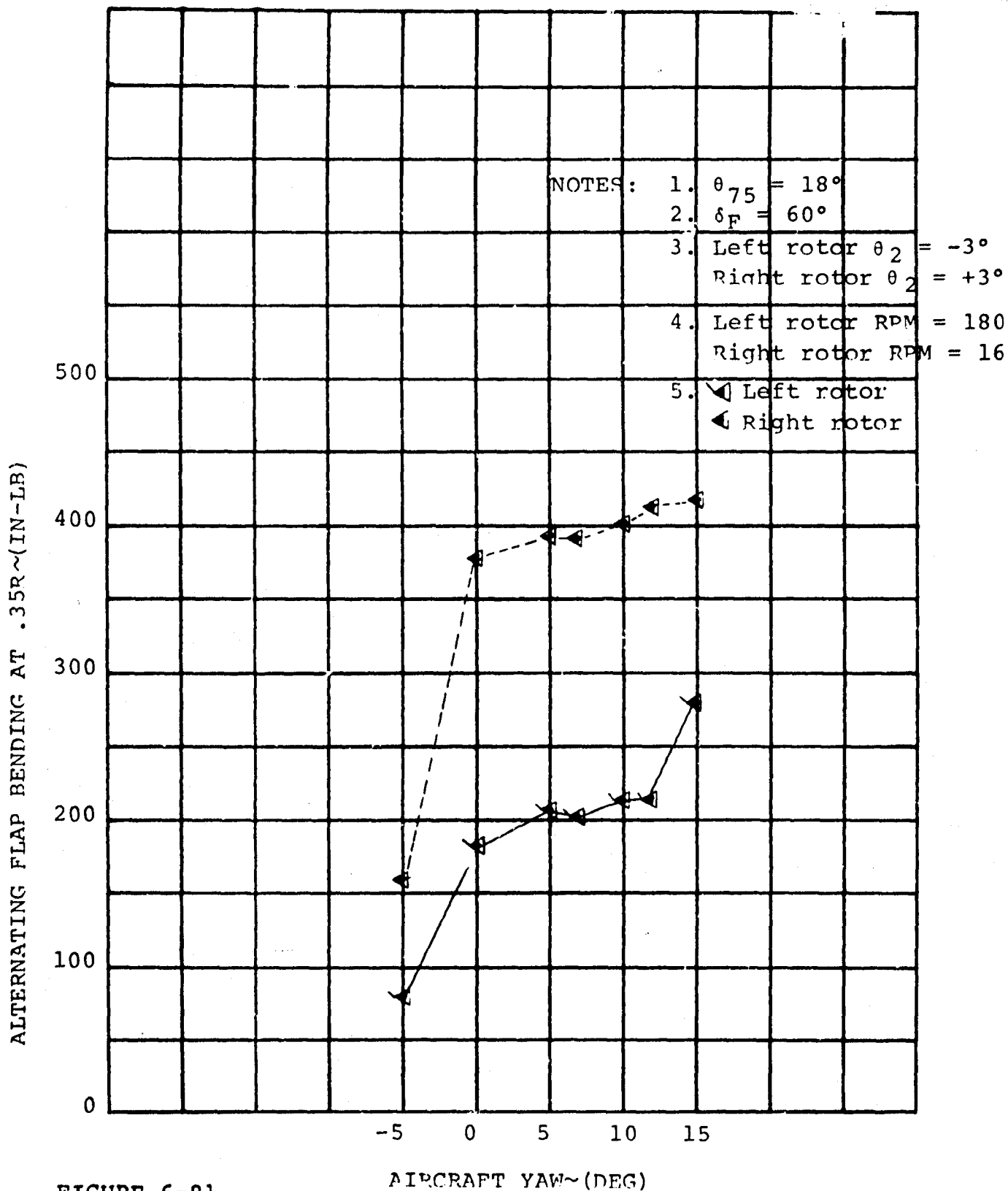


FIGURE 6-81

ALTERNATING BLADE FLAP BENDING VS. AIRCRAFT YAW ANGLE
 FOR $i_N = 45$ DEG, $V = 132$ FPS, $\alpha = 0$ DEG, AND ± 3 DEG CYCLIC

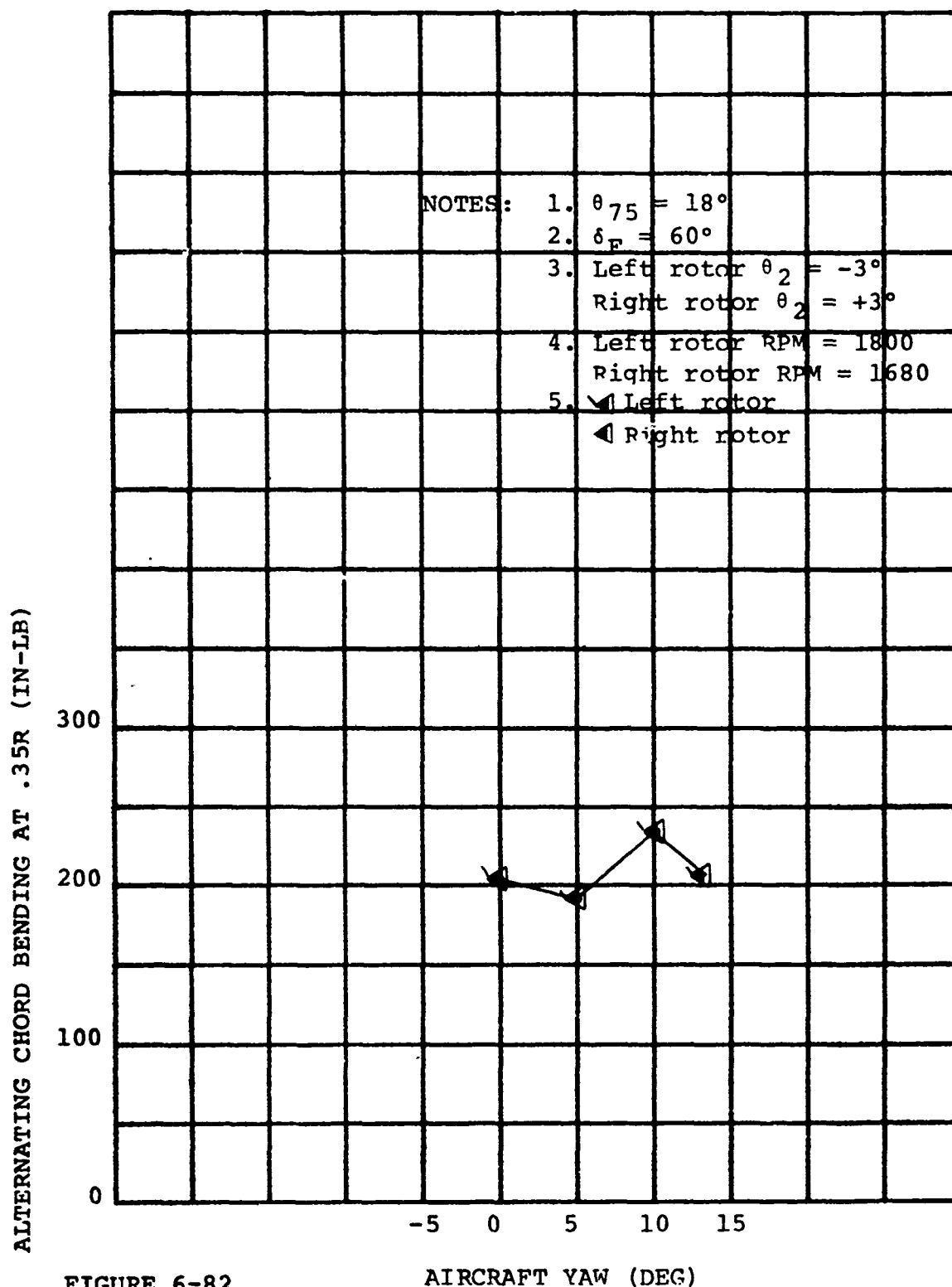


FIGURE 6-82

AIRCRAFT YAW (DEG)

ALTERNATING BLADE CHORD BENDING VS. AIRCRAFT YAW ANGLE FOR
 $i_N = 45^\circ$, $V = 132$ FPS, $\alpha = 0^\circ$, AND $\pm 3^\circ$ CYCLIC

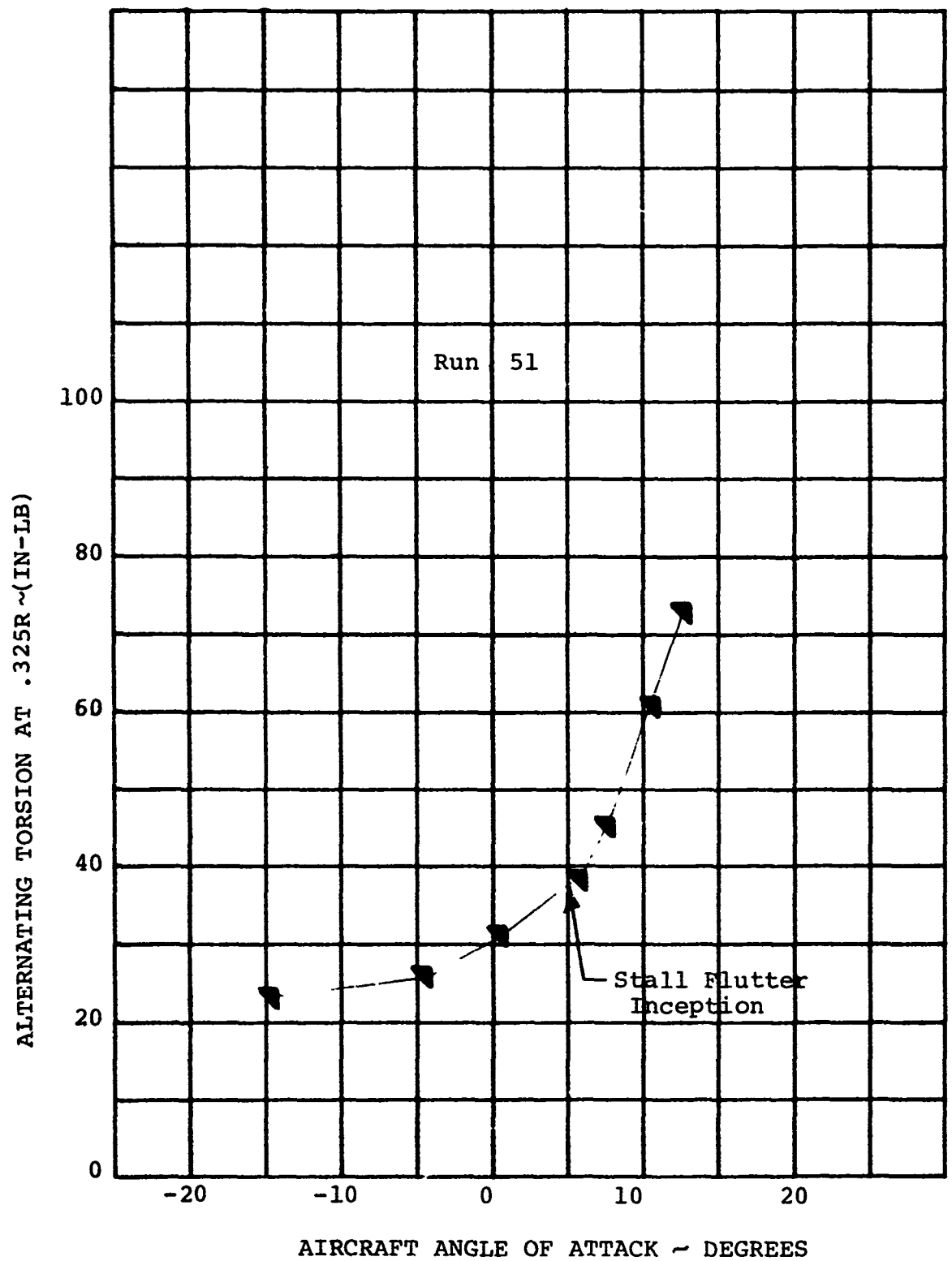


FIGURE 6-83

LIFT ROTOR ALTERNATING TORSION IN TRANSITION DUE TO STALL FLUTTER FOR $i_N = 70$ DEG, $\theta_{75} = 14$ DEG, $V_{TUNNEL} = 116$ FPS, 1970 RPM

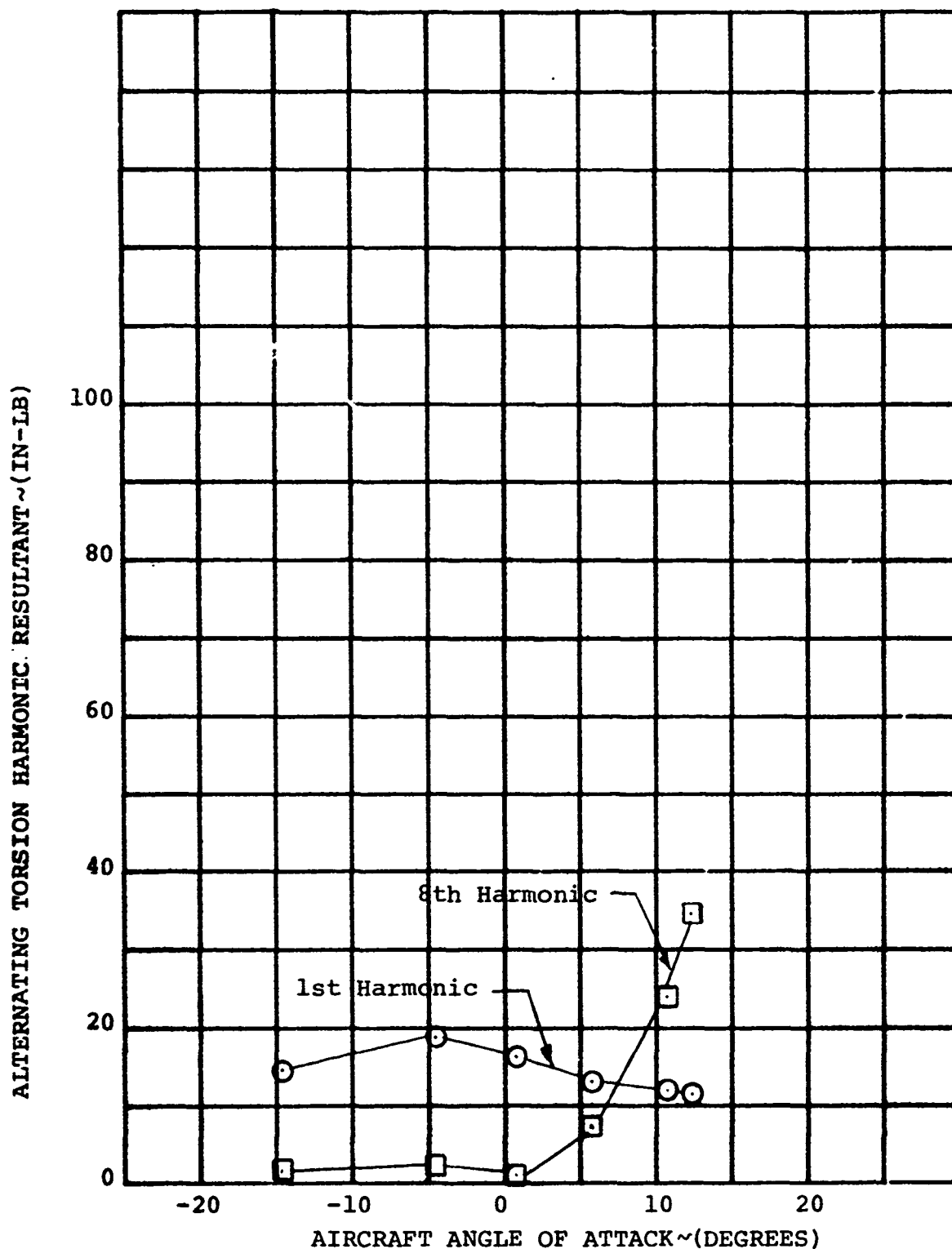
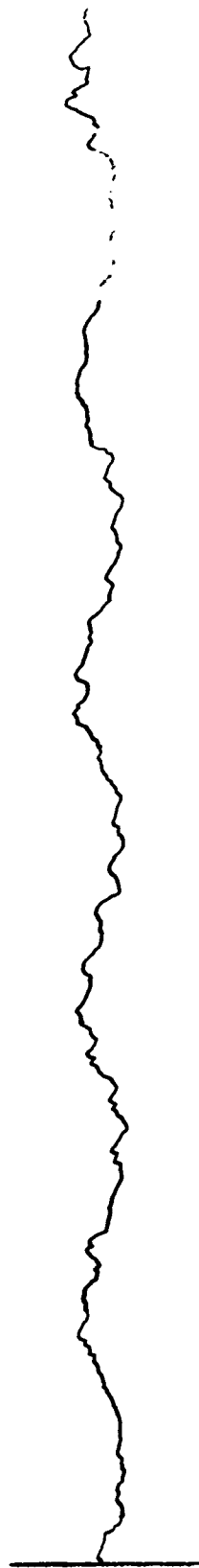


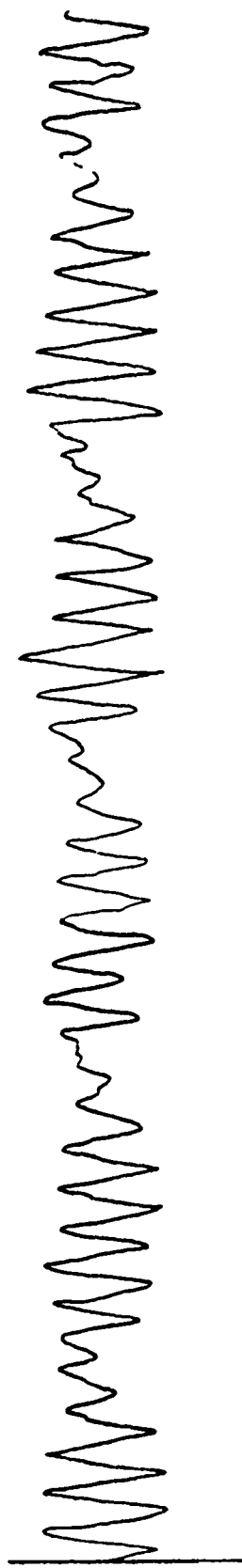
FIGURE 6-84

LEFT ROTOR TORSIONAL FIRST AND EIGHTH HARMONICS IN TRANSITION FOR $i_N = 70$ DEG, $\theta_{75} = 14$ DEG, $V_{TUNNEL} = 116$ FPS, 1970 RPM

$\alpha = -4.5$ DEGREES



$\alpha = 12.7$ DEGREES



1/REV AT 197 DEGREES AZIMUTH



FIGURE 6-85 LEFT BLADE TORSIONAL WAVEFORM BEFORE AND AFTER STALL FLUTTER INCEPTION FOR $i_N = 70$ DEG, $\theta_{75} = 14$ DEG, $V_{TUNNEL} = 116$ FPS AND 1970 RPM

6.5 TRANSITION HUB MOMENTS

6.5.1 Attitude Effects

Rotor hub moment for the transition flight mode (with nacelle angle equal to 45 degrees) resulting from aircraft pitch angle variation is shown in Figure 6-86. As for the cruise mode, the right and left rotors are identical and the hub moment is caused by the A_q condition and by wing interference.

6.5.2 Effect of Cyclic Pitch

Cyclic pitch will be considered as a means of reducing blade bending loads and hub moments in the transition flight mode. Figure 6-87 shows rotor hub moment for the same conditions as Figure 6-86 except that the cyclic pitch for each rotor is 3 degrees. Nose down cyclic pitch decreases blade flapping due to A_q and therefore decreases the hub moment.

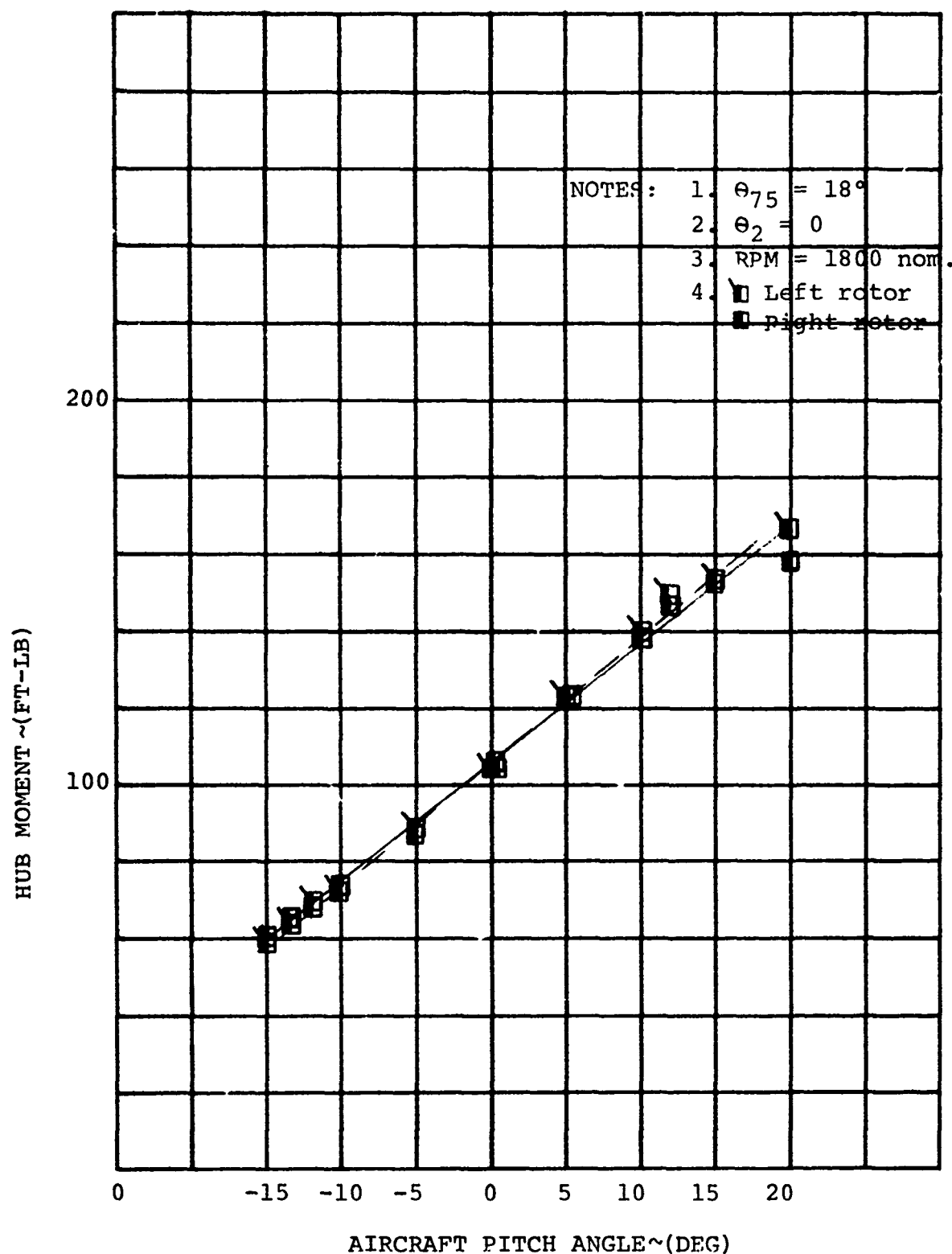


FIGURE 6-86 STEADY HUB MOMENT VS. AIRCRAFT ANGLE OF ATTACK FOR $i_N = 45$ DEG, AND $V = 132$ FPS

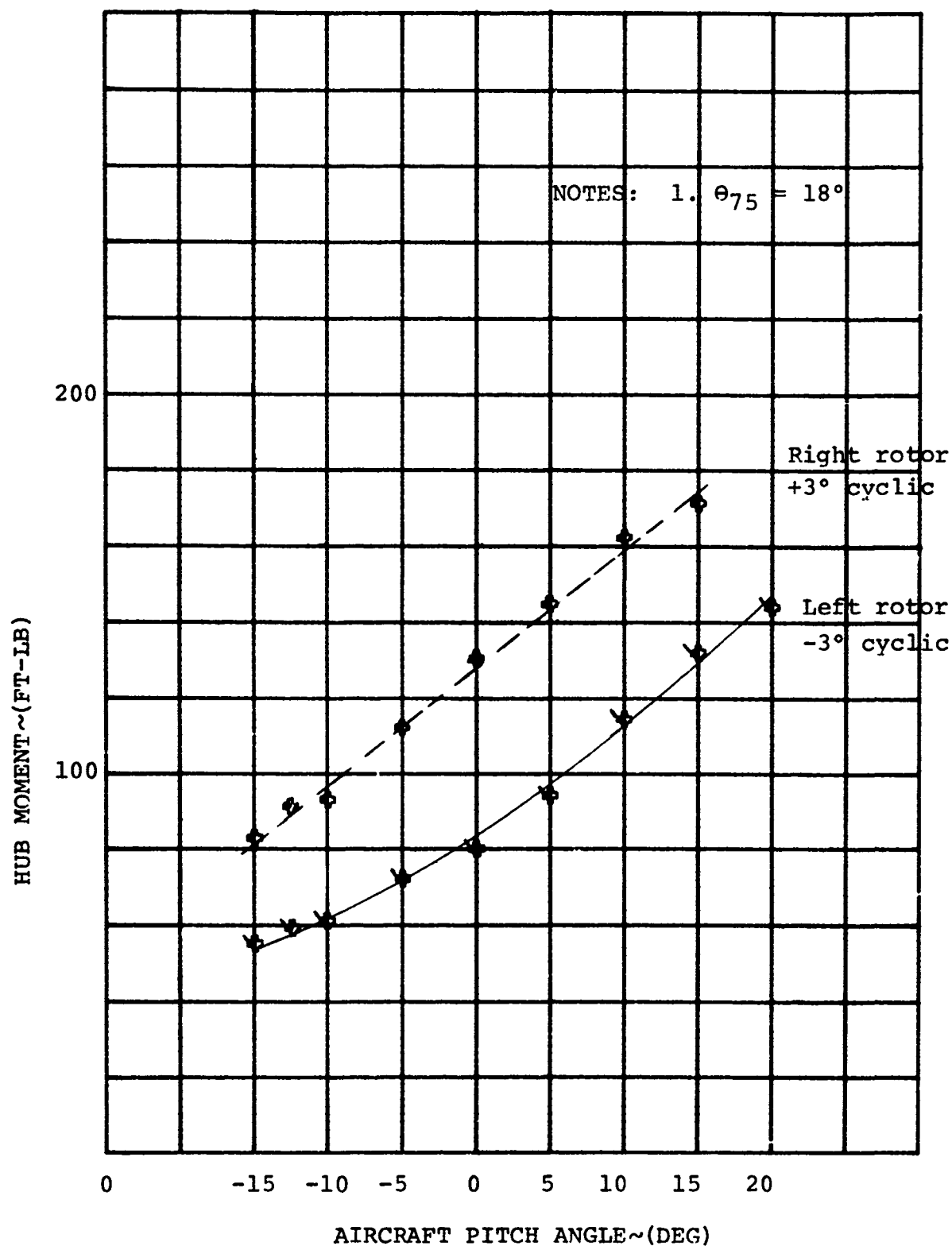


FIGURE 6-87

STEADY HUB MOMENT VS. AIRCRAFT ANGLE OF
ATTACK FOR $i_N = 45$ DEG, AND $V = 133$ FPS

6.6 CRUISE BLADE LOADS

The blade loads objectives in cruise were to determine the effects of aircraft angle of attack, wing flap incidence and aircraft yaw on alternating blade bending moments. Substantial data were obtained to answer the blade loads objectives and the results show that blade loads in cruise are affected by rotor inflow due to aircraft angle of attack and aircraft yaw, and wing circulation due to aircraft angle of attack and wing flap incidence. Wing interference effects cause approximately 20 percent of the alternating flap bending moments when the aircraft is pitched 10 degrees and have no effect on alternating flap bending when the aircraft is yawed.

6.6.1 Attitude Effects

The effect of angle of attack on blade flap and chord bending and blade torsion is shown in Figures 6-88 through 6-100. These data show a near-linear increase in blade loads as the aircraft angle of attack is varied from zero. This trend is expected since a change in rotor angle of attack from zero increases the rotor inflow and results in a once-per-rev sinusoidal variation of blade section angle of attack around the azimuth. Wing circulation also affects alternating blade moments when the aircraft angle of attack is such that the wing is producing lift. The downwash from the wing due to wing lift alters the velocity flowfield in the rotor disc plane and this results in a change in blade section angle of attack around the azimuth. The change in local blade angle due to wing interference is not sinusoidal but it is additive to the once-per-rev change in blade angle due to inflow. Rotor inflow and wing circulation both increase the blade angle on the advancing side of disc when the aircraft angle of attack is increased from zero. Rotor inflow and wing circulation effects on blade loads are also additive when the aircraft angle of attack is negative and the wing is producing negative lift since rotor inflow and wing circulation decrease the blade angle on the advancing side of the disc.

The uncoupled rotor loads analysis was used to predict the combined effect of rotor inflow due to rotor angle of attack and wing interference due to aircraft angle of attack on blade loads in cruise. The velocity flowfield in the disc plane due to wing circulation was input into the analysis and a comparison of the predicted and measured alternating flap bending moments is shown in Figure 6-101. The prediction is in good agreement with the test data and demonstrates that the uncoupled analysis can predict the effects of wing circulation and rotor inflow on blade flap bending in cruise. A comparison of the predicted and measured flap bending waveform for 10 degrees angle of attack is shown in Figure 6-102. Good agreement of the measured and predicted phase angle of the flap bending one-per-rev response shows that the first out-of-plane frequency has been correctly represented in the analysis.

Figure 6-103 is a comparison of predicted and measured alternating chord bending due to wing circulation and rotor inflow. Correlation of the chord bending with prediction is not as good as the flap bending correlation.

Representation of the blade lag properties in the uncoupled analysis is suspected to be the source of error. The blade lag mode frequency is highly dependent upon elastic stiffness and a small error in the lag mode frequency can result in large errors in blade loads predictions.

The effect of aircraft yaw on blade loads in cruise are shown in Figures 6-104 through 6-111. These data show the same trend, but increase less per degree change in angle, when the aircraft was pitched. Less sensitivity of blade loads to yaw angle changes than to pitch angle changes is expected since wing interference effects do not increase when the aircraft is yawed.

6.6.2 Effect of Wing Flap Deflection

To determine the effect of wing circulation on blade loads in cruise, the wing flap was varied at zero aircraft angle of attack. A summary of wing interference effects on cruise blade loads is presented in Figures 6-112 and 6-113 and shows that large changes in wing flap incidence (up to 60 degrees) result in small changes in alternating blade moments. Changing wing lift by flap deflection isolated wing interference effects and allowed a comparison of inflow effects and wing interference effects to be made. For a wing flap deflection of 24 degrees at zero aircraft angle of attack, the aircraft lift ($C_L=1.039$) is equivalent to a 10-degree aircraft angle of attack and zero flap incidence condition and therefore, wing interference would have the same effect on alternating blade flap bending for both conditions. From Figure 6-112, alternating flap bending is 55 in-lb at 24 degrees flap incidence and from Figure 6-94, alternating flap bending is 260 in-lb at 10 degrees angle of attack. Wing interference effects cause 55 in-lb (21 percent) of the total alternating flap bending at 10 degrees angle of attack.

The effect of wing circulation due to flap deflection was predicted in cruise with the uncoupled analysis. A comparison of predicted and measured alternating flap and chord bending is shown in Figures 6-114 and 6-115. Flap bending prediction agrees well with the measured data and demonstrates that the isolated effect of wing interference on blade flap bending in cruise can be predicted. Chord bending prediction does not agree with the measured data as well as the flap bending. Chord bending prediction shows more sensitivity to flow field disturbances in the disc plane.

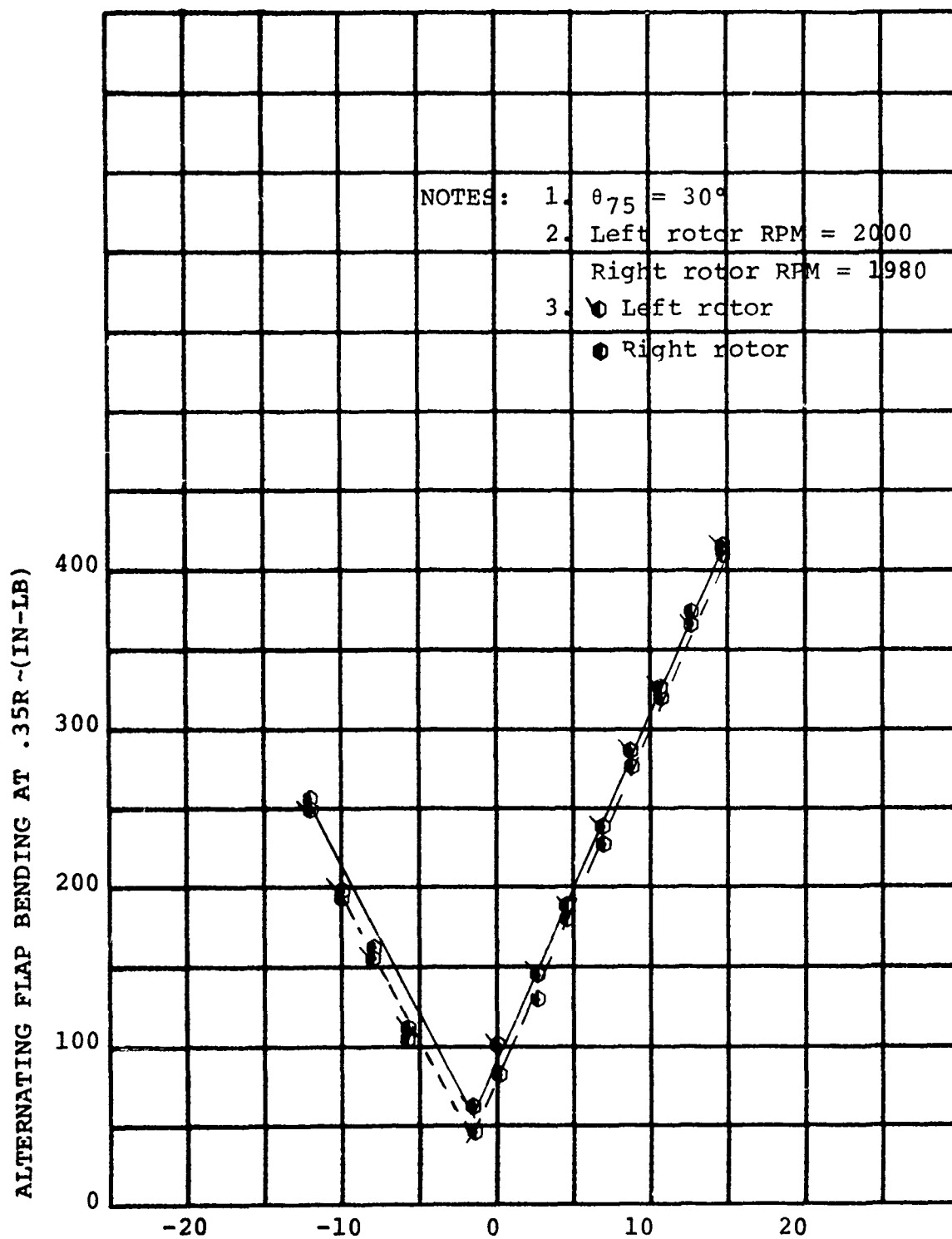


FIGURE 6-88 AIRCRAFT ANGLE OF ATTACK~(DEG)

ALTERNATING BLADE FLAP BENDING VS. AIRCRAFT ANGLE OF ATTACK
 FOR $i_N = 0$ DEG, $V = 224$ FPS, AND 60 DEG WING FLAP INCIDENCE

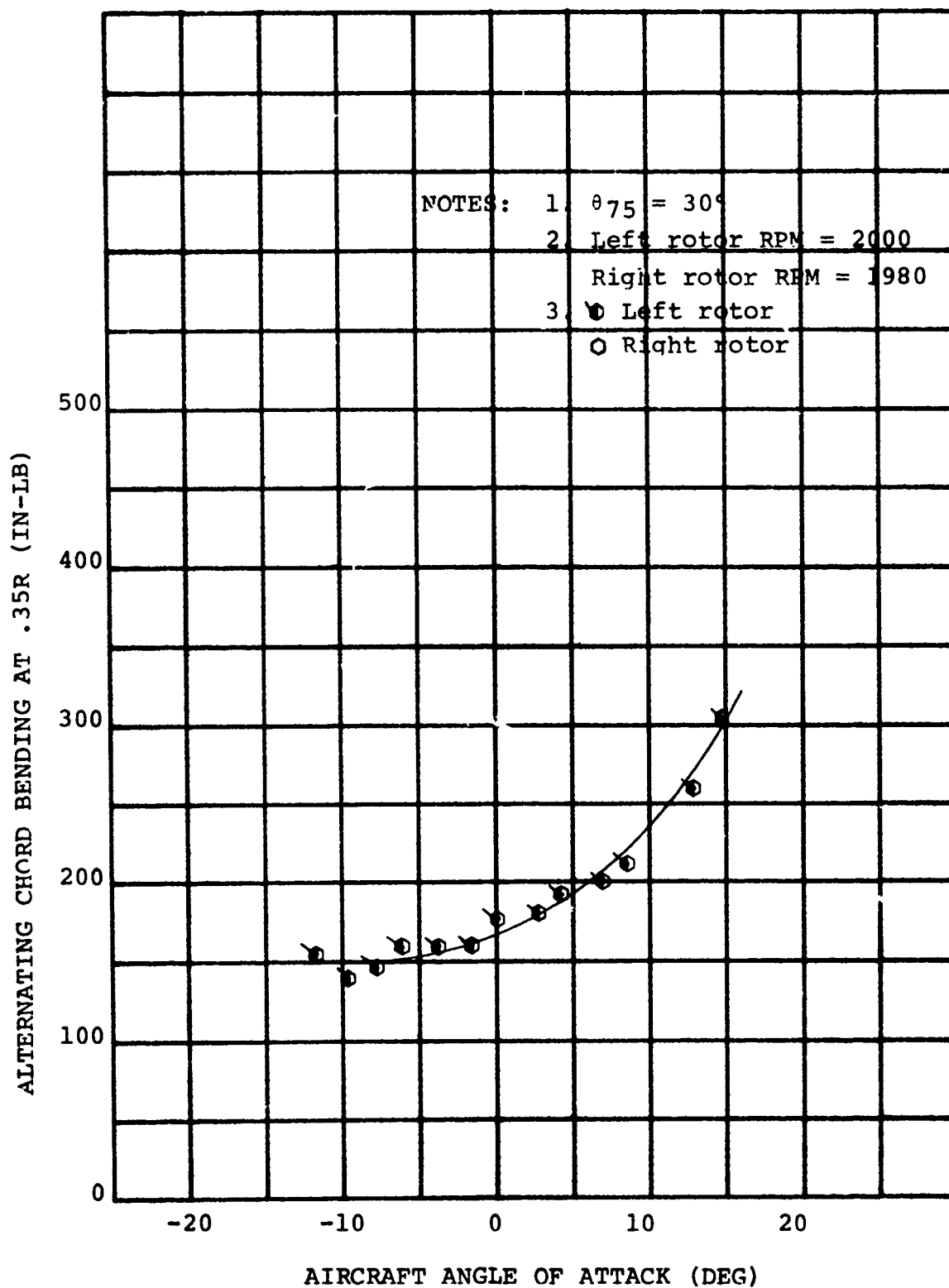


FIGURE 6-89
 ALTERNATING BLADE CHORD BENDING VS. AIRCRAFT ANGLE OF ATTACK
 FOR $i_N = 0$ DEG, $V = 224$ FPS, AND 60 DEG WING FLAP INCIDENCE

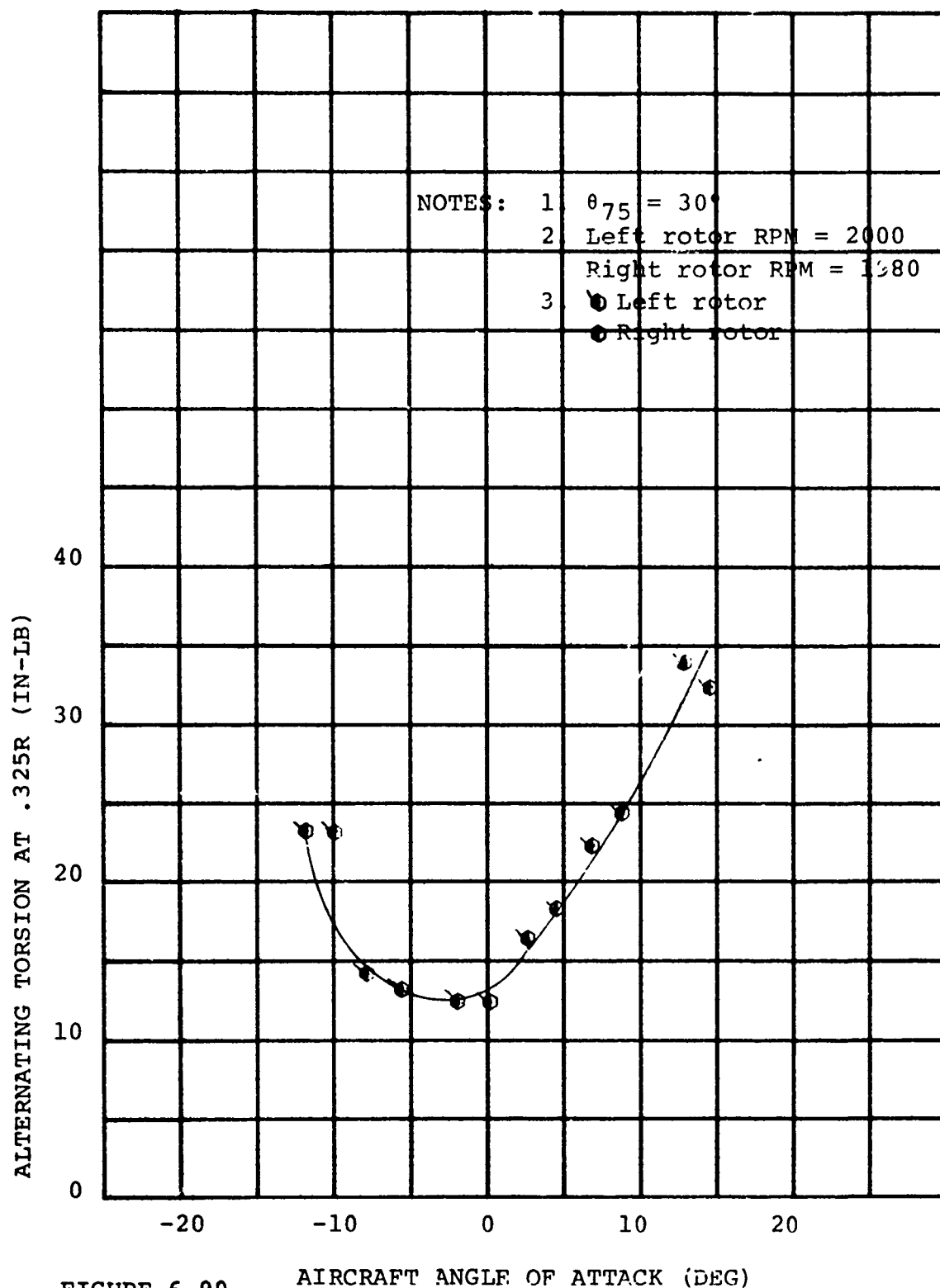


FIGURE 6-90 AIRCRAFT ANGLE OF ATTACK (DEG)

ALTERNATING BLADE TORSION VS. AIRCRAFT ANGLE OF ATTACK FOR $i_N = 0$ DEG, $V = 224$ FPS, AND 60 DEG WING FLAP INCIDENCE

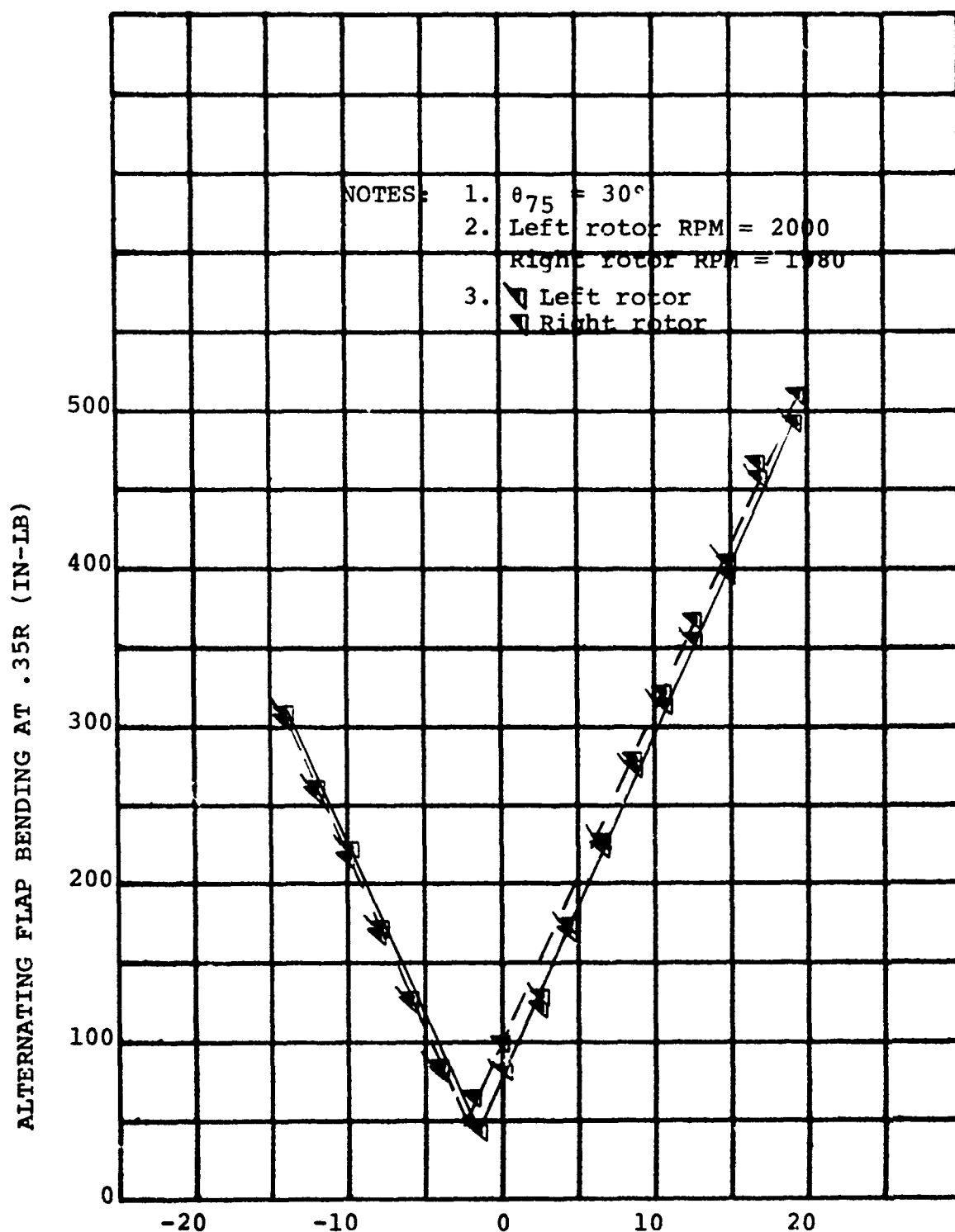


FIGURE 6-91 AIRCRAFT ANGLE OF ATTACK (DEG)

ALTERNATING BLADE FLAP BENDING VS. AIRCRAFT ANGLE OF ATTACK
 FOR $i_N = 0$ DEG, $V = 225$ FPS, AND 45 DEG WING FLAP INCIDENCE

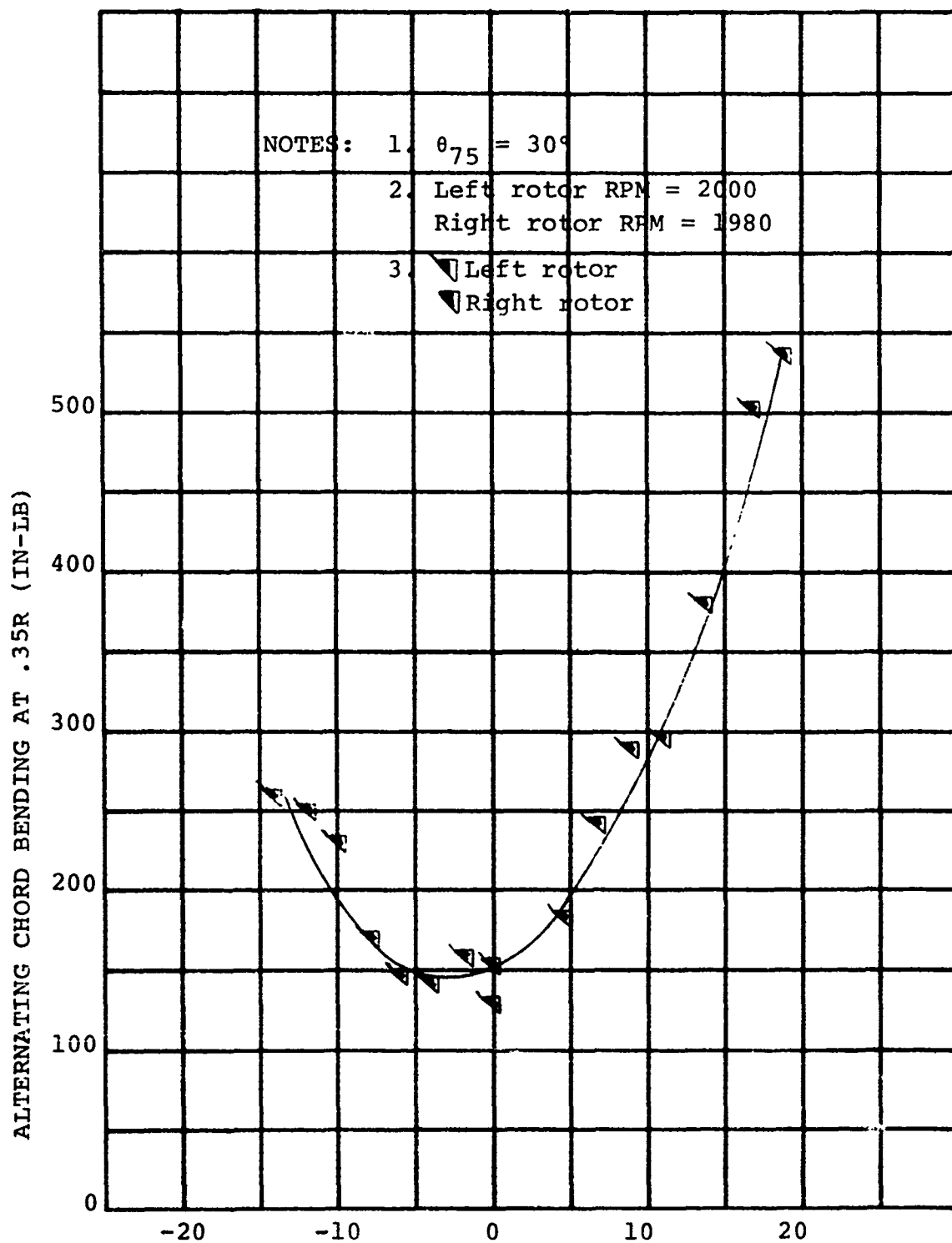


FIGURE 6-92 AIRCRAFT ANGLE OF ATTACK (DEG)
 ALTERNATING BLADE CHORD BENDING VS. AIRCRAFT ANGLE OF ATTACK
 FOR $i_N = 0$ DEG, $V = 225$ FPS, AND 45 DEG WING FLAP INCIDENCE

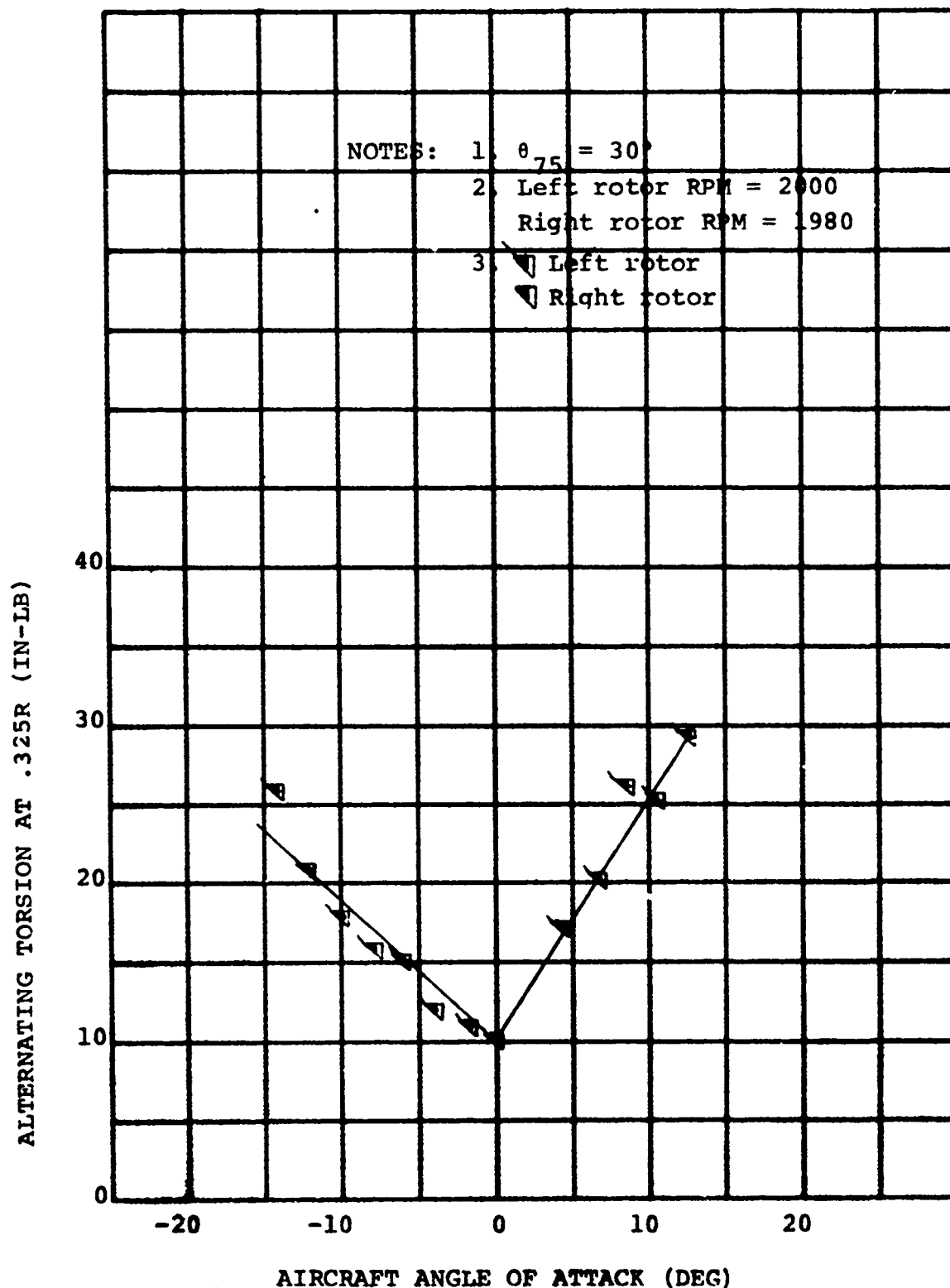


FIGURE 6-93

ALTERNATING BLADE TORSION VS. AIRCRAFT ANGLE OF ATTACK FOR
 $i_N = 0$ DEG, $V = 225$ FPS, AND 45 DEG WING FLAP INCIDENCE

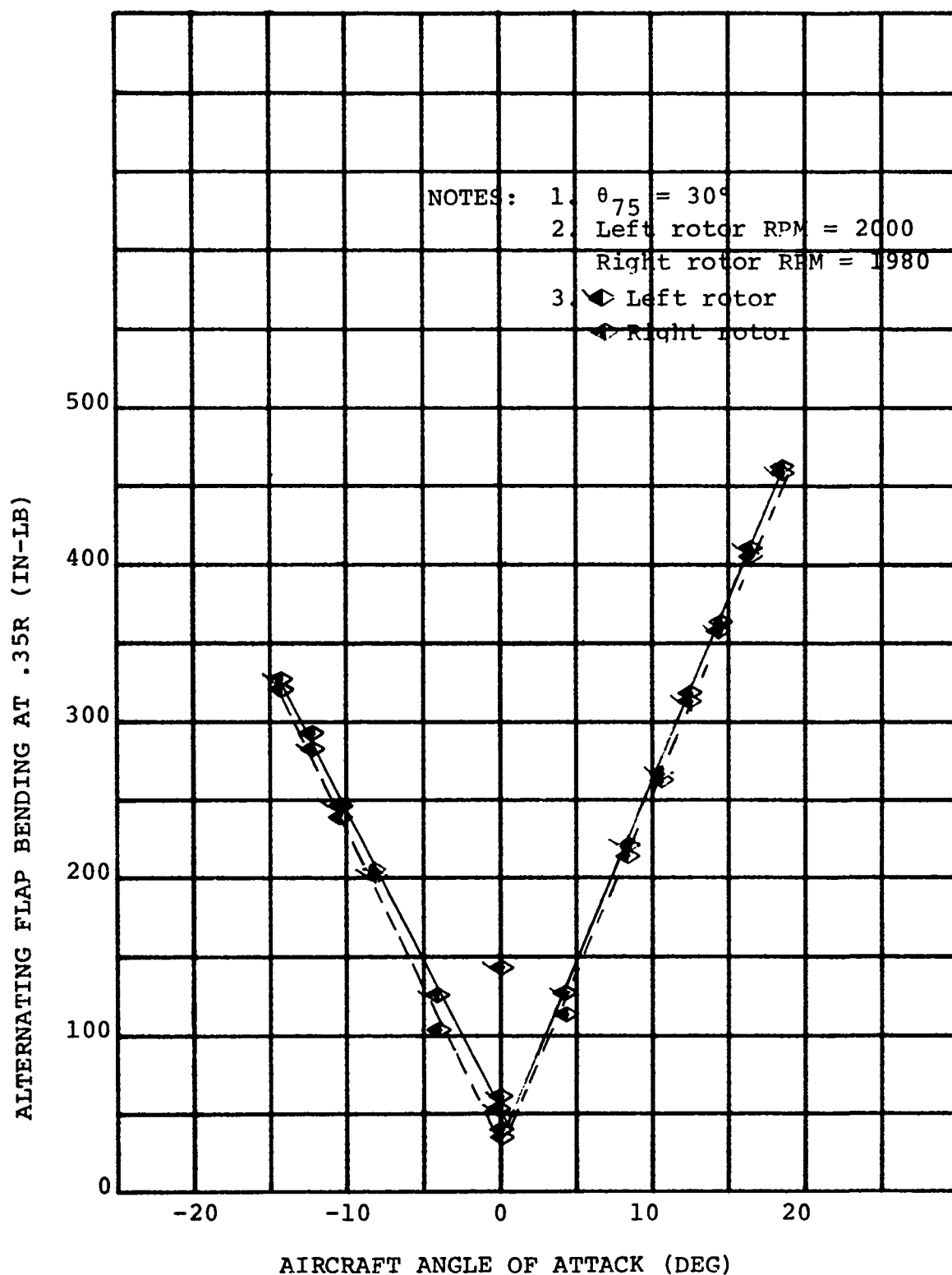


FIGURE 6-94
 ALTERNATING BLADE FLAP BENDING VS. AIRCRAFT ANGLE OF ATTACK
 FOR $i_N = 0$ DEG, $V = 226$ FPS, AND 0 DEG WING FLAP INCIDENCE

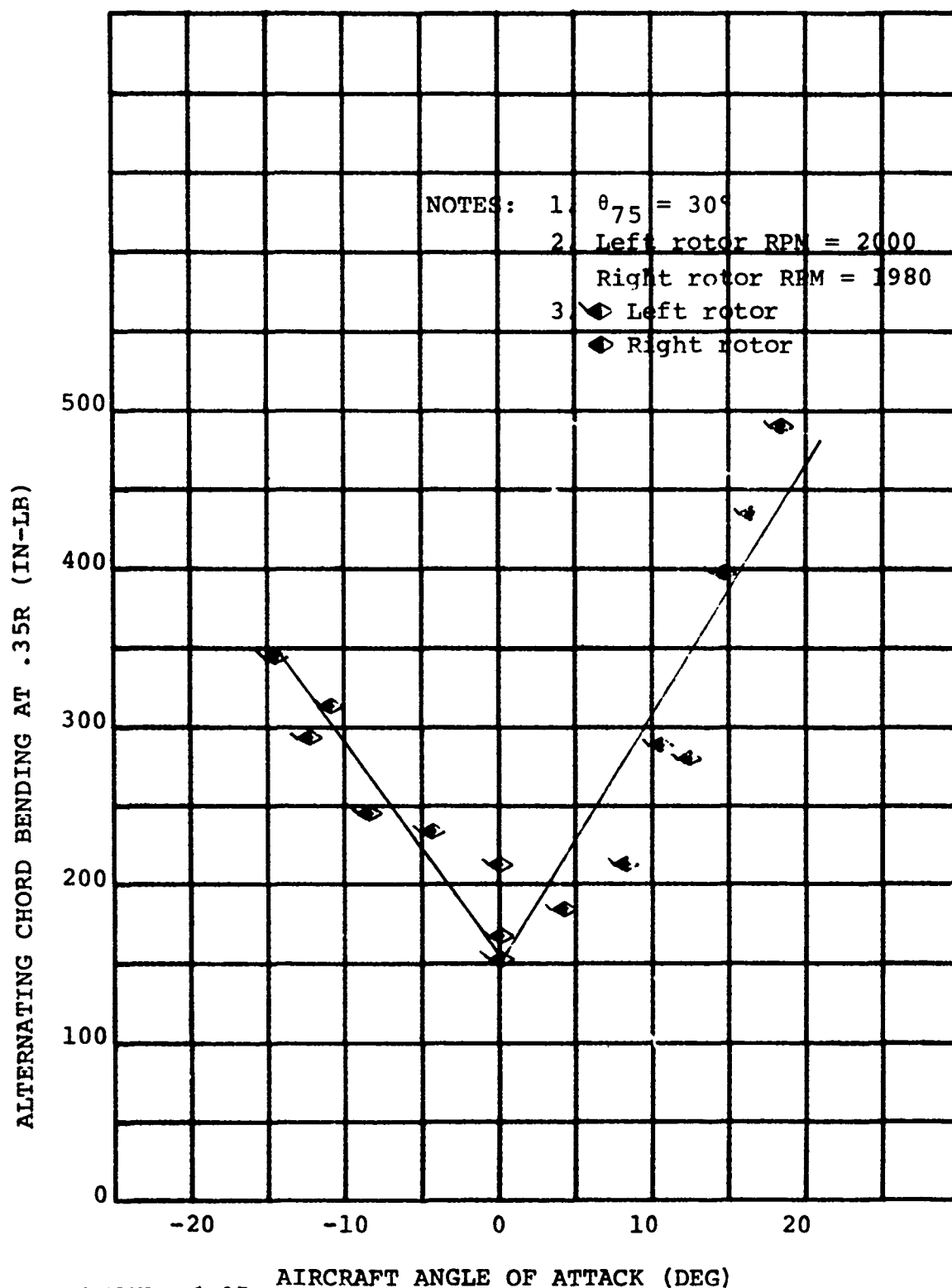


FIGURE 6-95 AIRCRAFT ANGLE OF ATTACK (DEG)
 ALTERNATING BLADE CHORD BENDING VS. AIRCRAFT ANGLE OF ATTACK
 FOR $i_N = 0$ DEG, $V = 226$ FPS, AND 0 DEG WING FLAP INCIDENCE

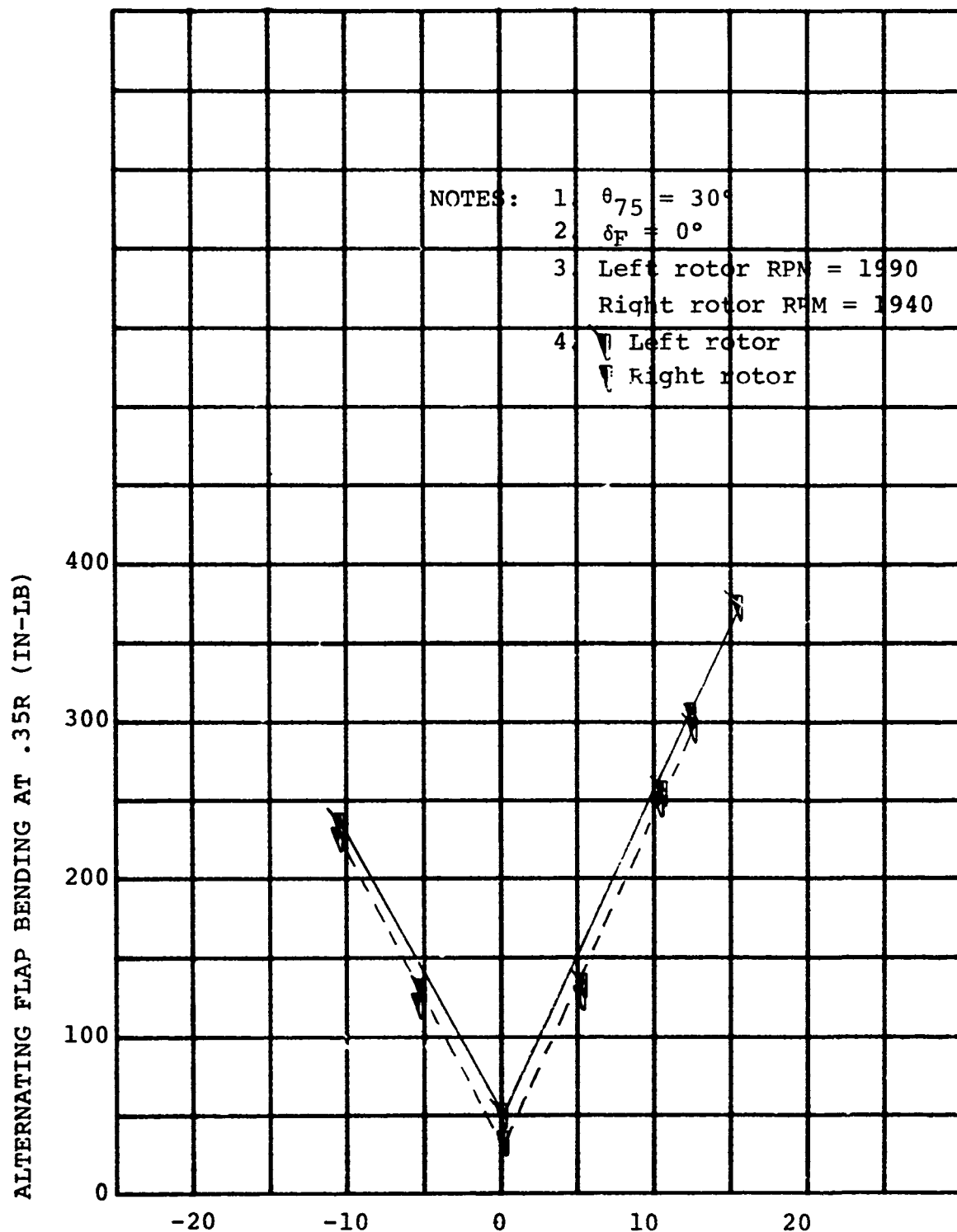


FIGURE 6-96 AIRCRAFT ANGLE OF ATTACK (DEG)

ALTERNATING BLADE FLAP BENDING VS. AIRCRAFT
 ANGLE OF ATTACK FOR $i_N = 0$ DEG, $V = 216$ FPS

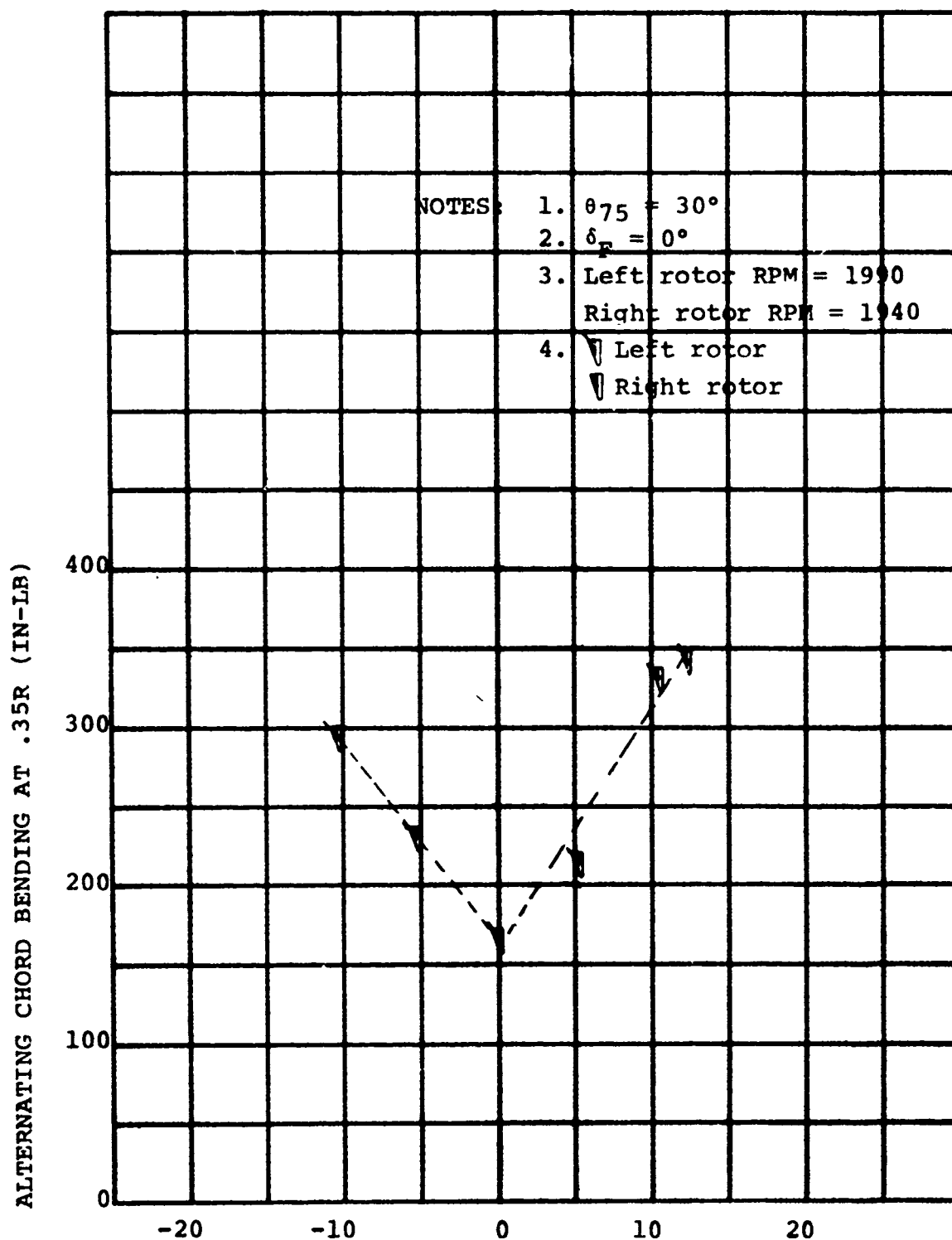


FIGURE 6-97 AIRCRAFT ANGLE OF ATTACK (DEG)

ALTERNATING BLADE CHORD BENDING VS. AIRCRAFT
ANGLE OF ATTACK FOR $i_N = 0$ DEG, $V = 216$ FPS

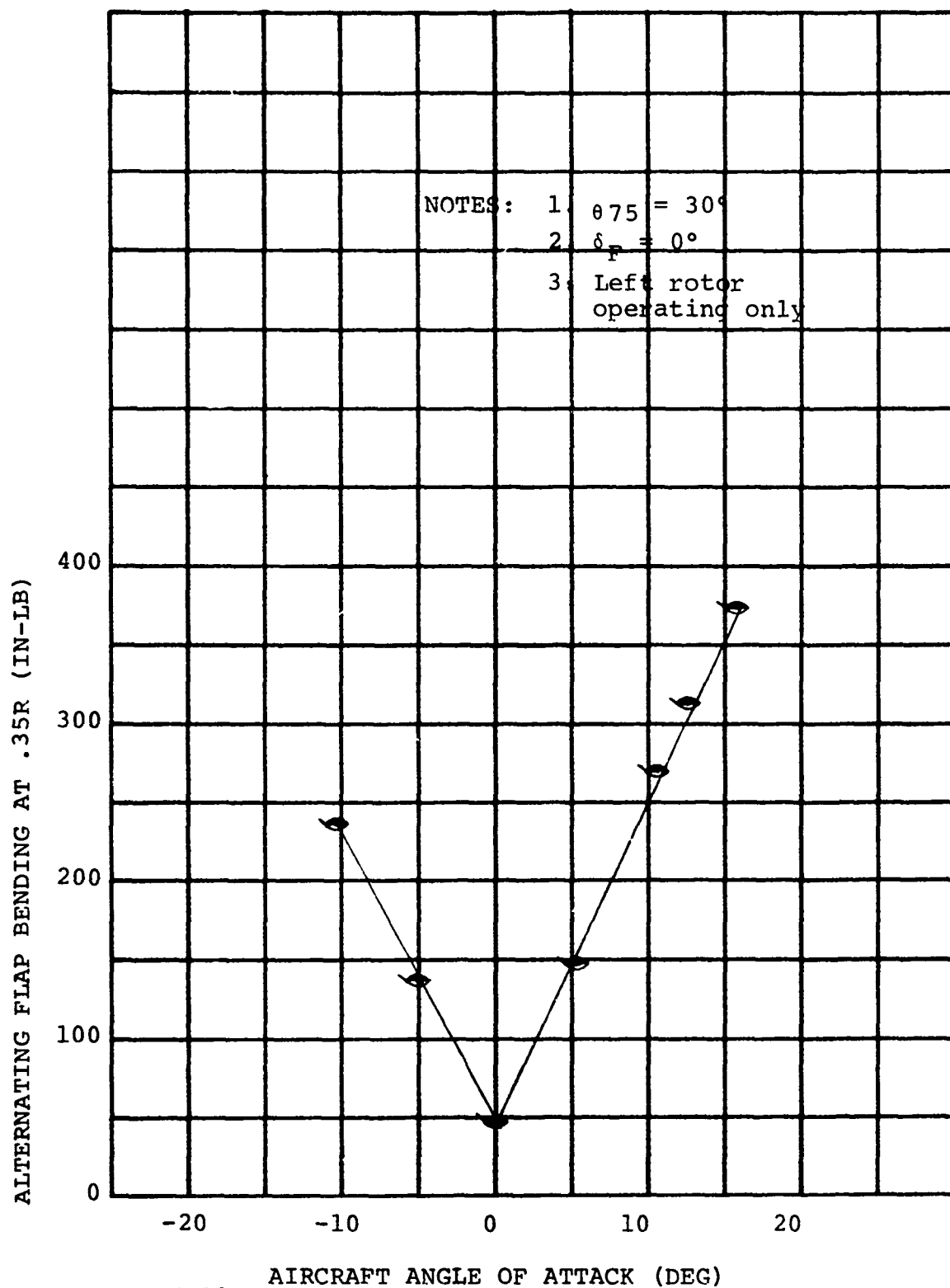


FIGURE 6-98

ALTERNATING BLADE FLAP BENDING VS. AIRCRAFT ANGLE OF ATTACK FOR $i_N = 0^\circ$, $V = 226$ FPS, AND 2030 RPM

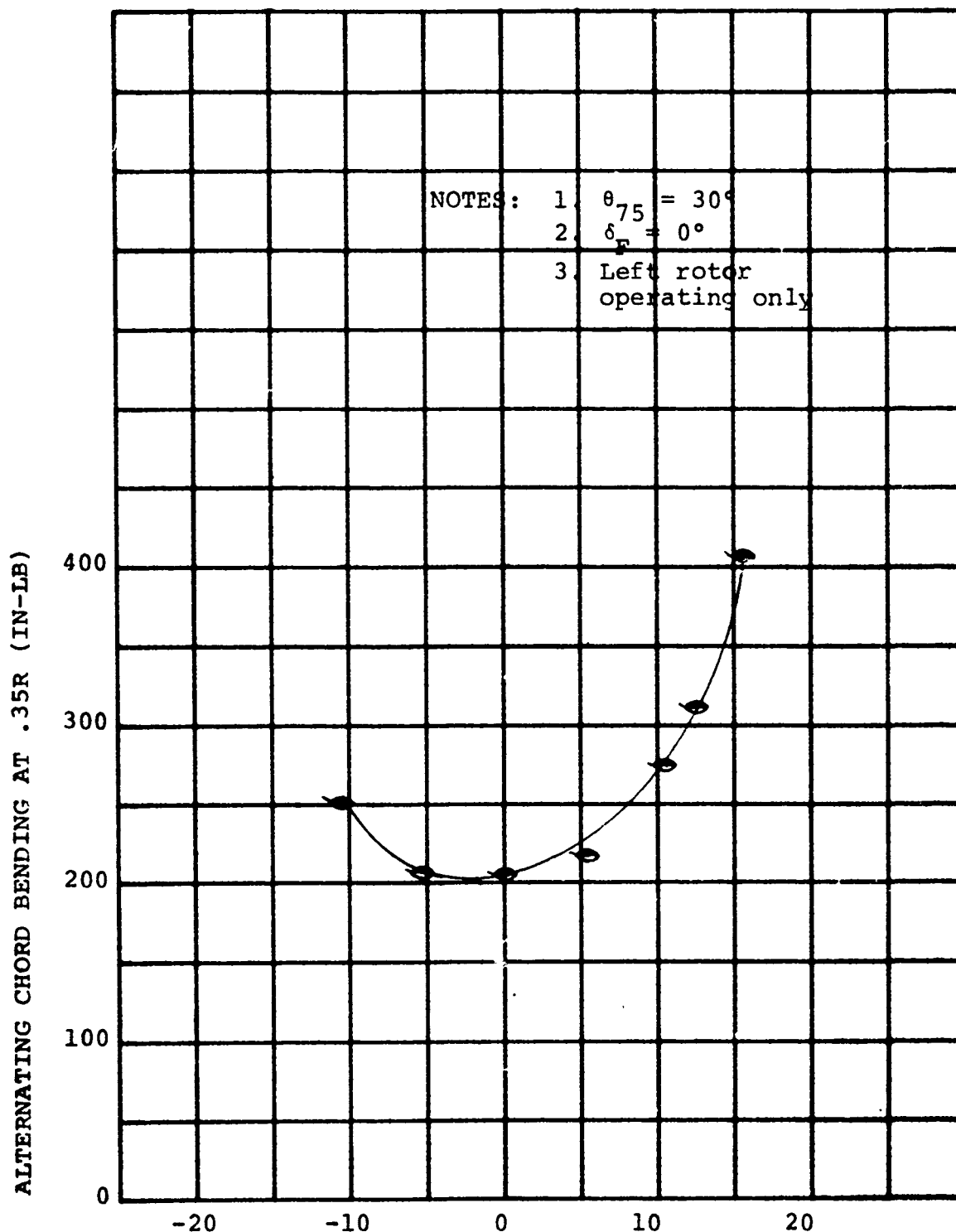


FIGURE 6-99

ALTERNATING BLADE CHORD BENDING VS. AIRCRAFT ANGLE OF ATTACK FOR $i_N = 0^\circ$, $V = 226$ FPS, AND 2030 RPM

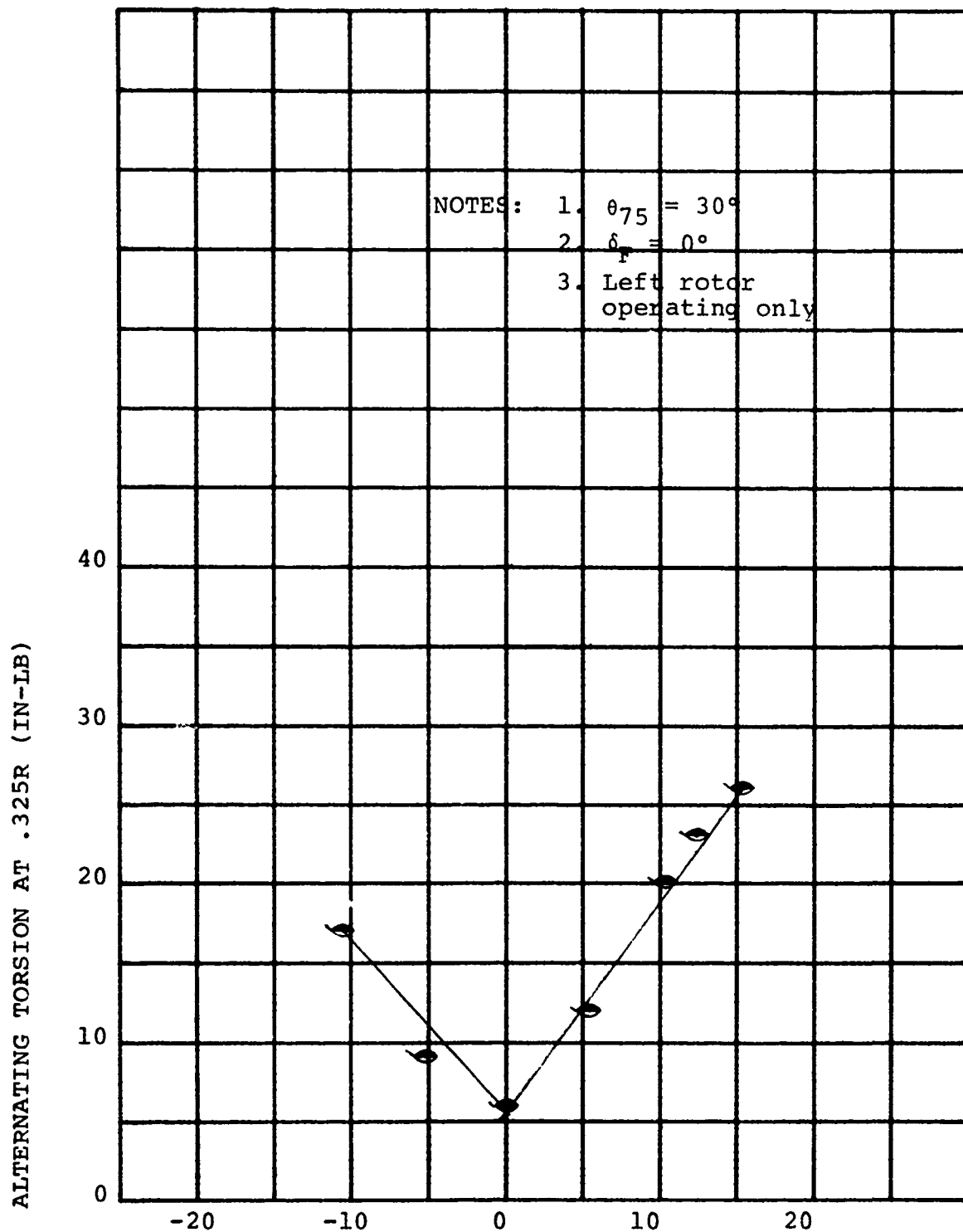


FIGURE 6-100 AIRCRAFT ANGLE OF ATTACK (DEG)

ALTERNATING BLADE TORSION VS. AIRCRAFT ANGLE OF
 ATTACK FOR $i_N = 0^\circ$, $V = 226$ FPS, AND 2030 RPM

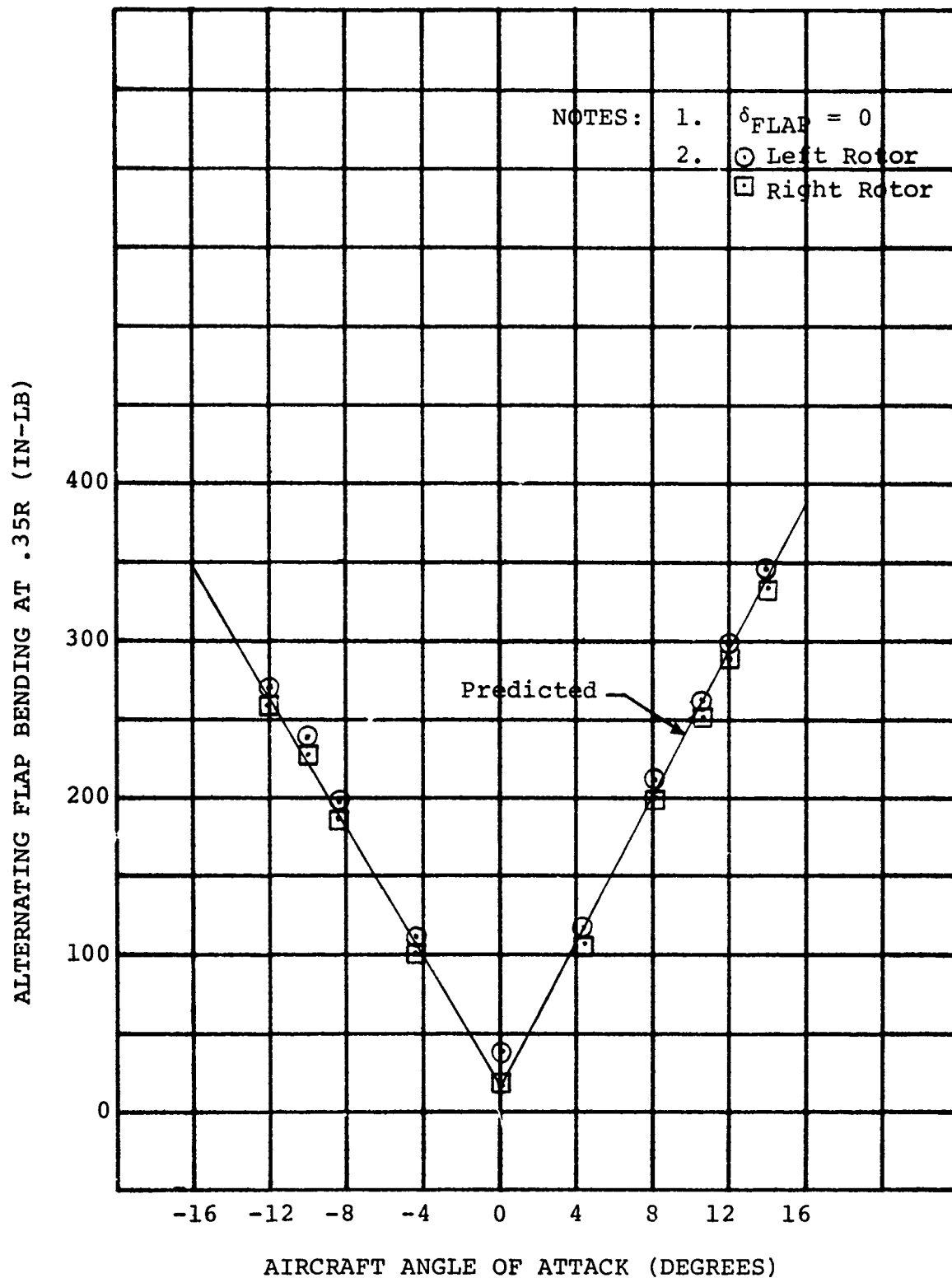


FIGURE 6-101

MEASURED AND PREDICTED ALTERNATING FLAP BENDING PRODUCED BY AIRCRAFT ANGLE OF ATTACK IN CRUISE AT $\Theta_{75} = 30^\circ$, $V_{TIP} = 570$ FPS AND $V_{TUNNEL} = 220$ FPS

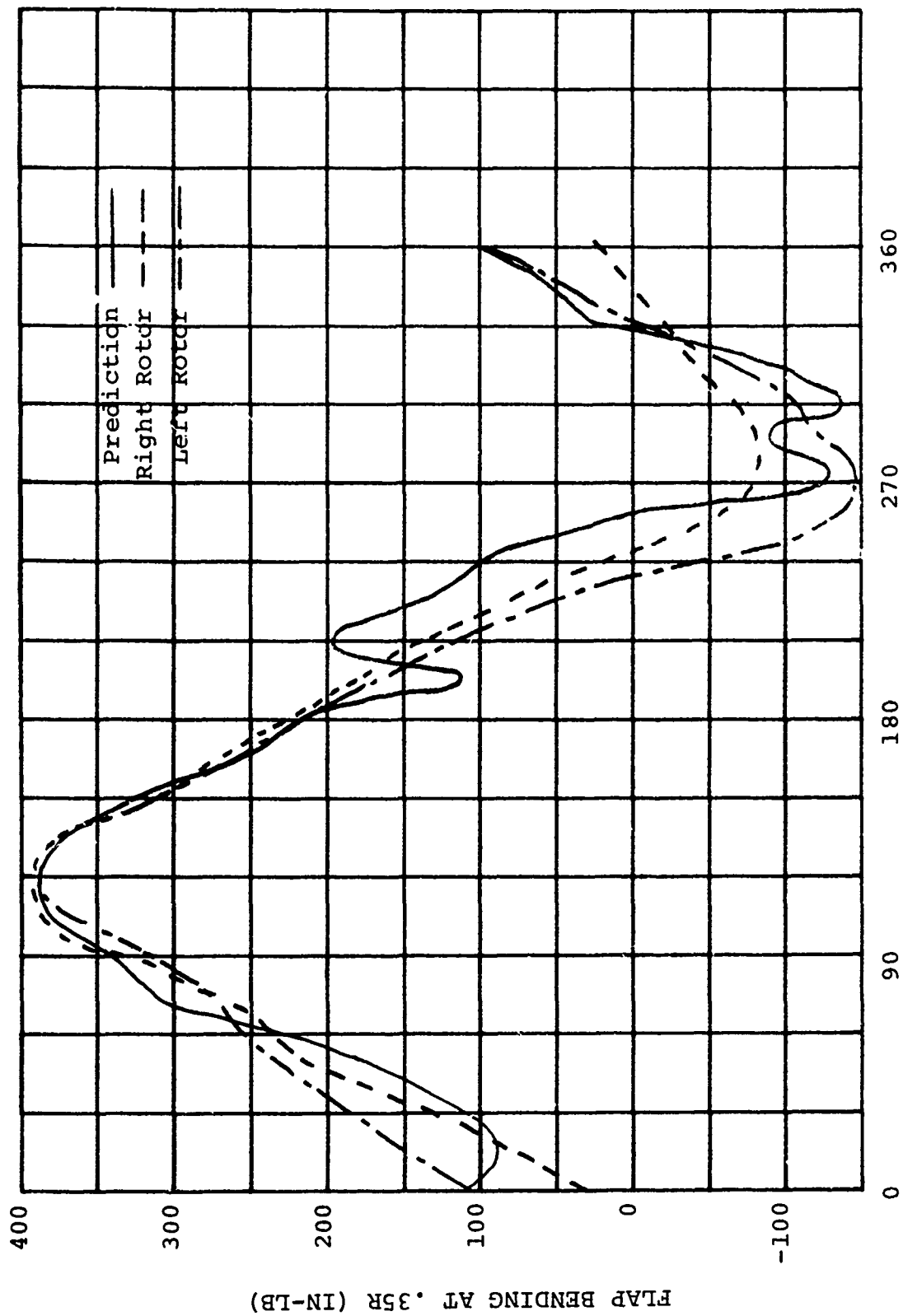


FIGURE 6-102
MEASURED AND PREDICTED BLADE FLAP BENDING IN CRUISE
FOR $\alpha = 10^\circ$, $75 = 30^\circ$, $V_{TIP} = 570$ FPS AND V_{TUNNEL}
220 FPS

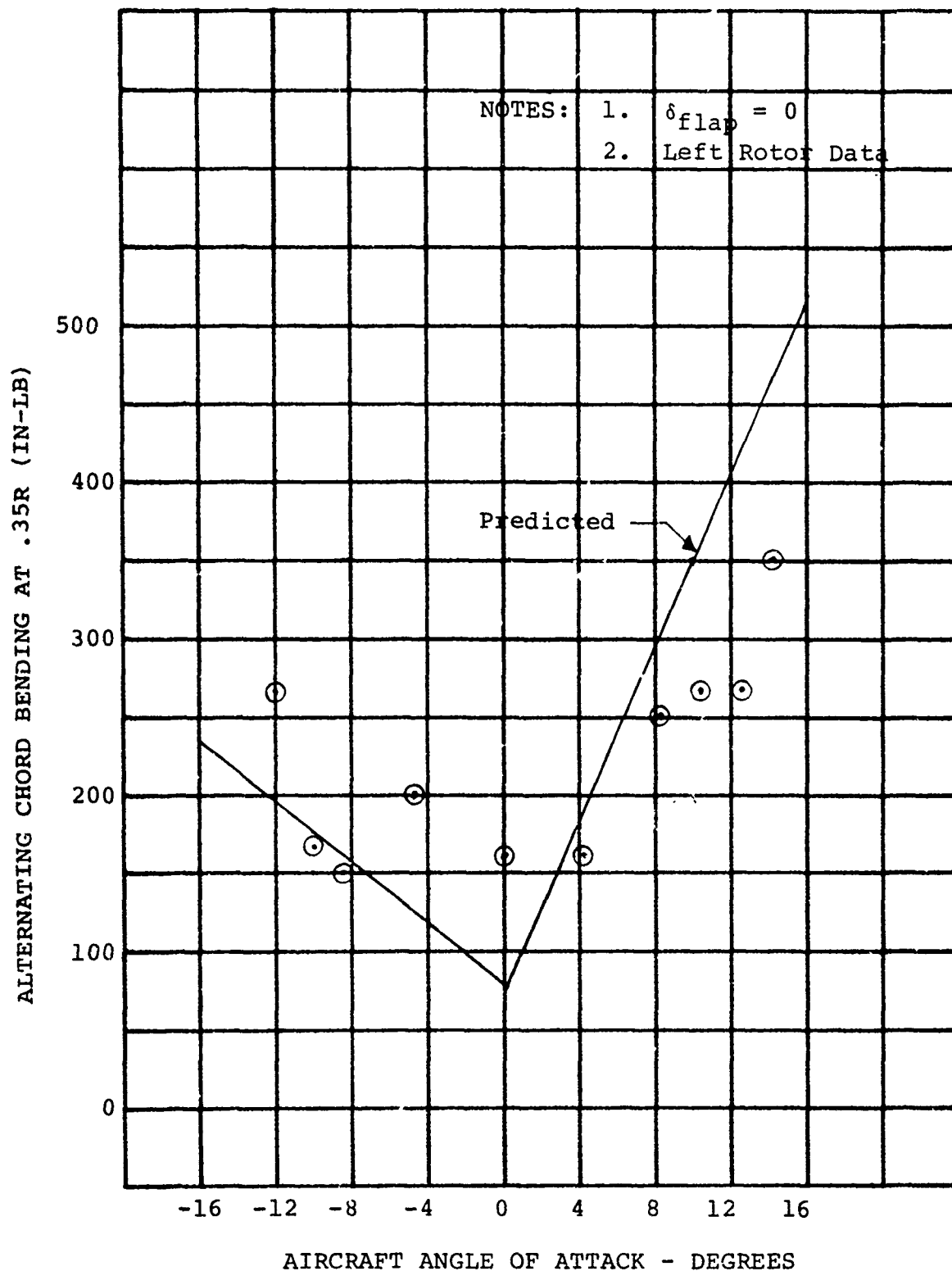


FIGURE 6-103

MEASURED AND PREDICTED ALTERNATING CHORD BENDING PRODUCED BY AIRCRAFT ANGLE OF ATTACK IN CRUISE AT $\theta_{75} = 30^\circ$, $V_{TIP} = 570$ FPS AND $V_{TUNNEL} = 220$ FPS

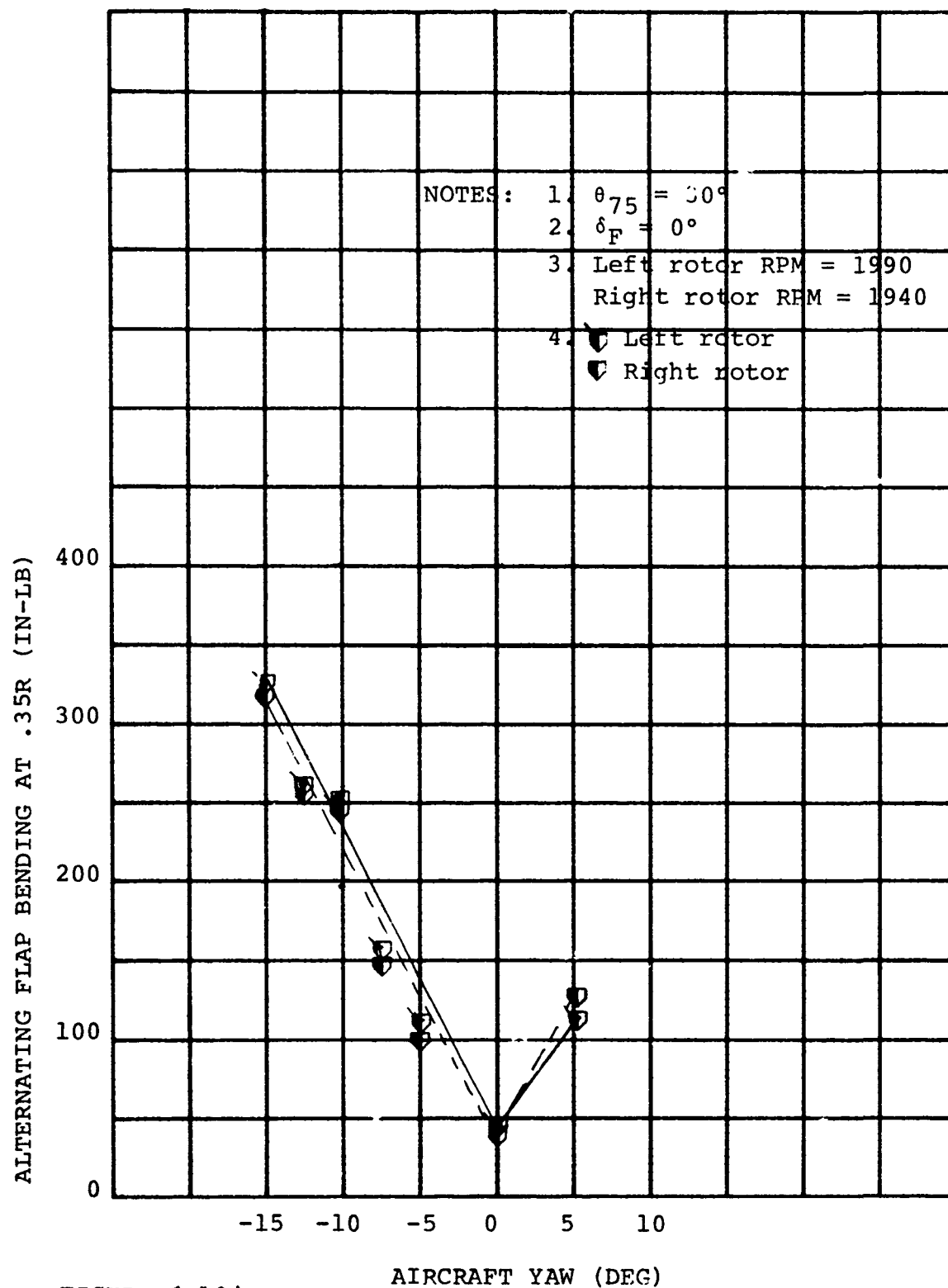


FIGURE 6-104

ALTERNATING BLADE FLAP BENDING VS. AIRCRAFT YAW
 ANGLE FOR $i_N = 0^\circ$, $V = 215$ FPS, AND $\alpha = 0$ DEG

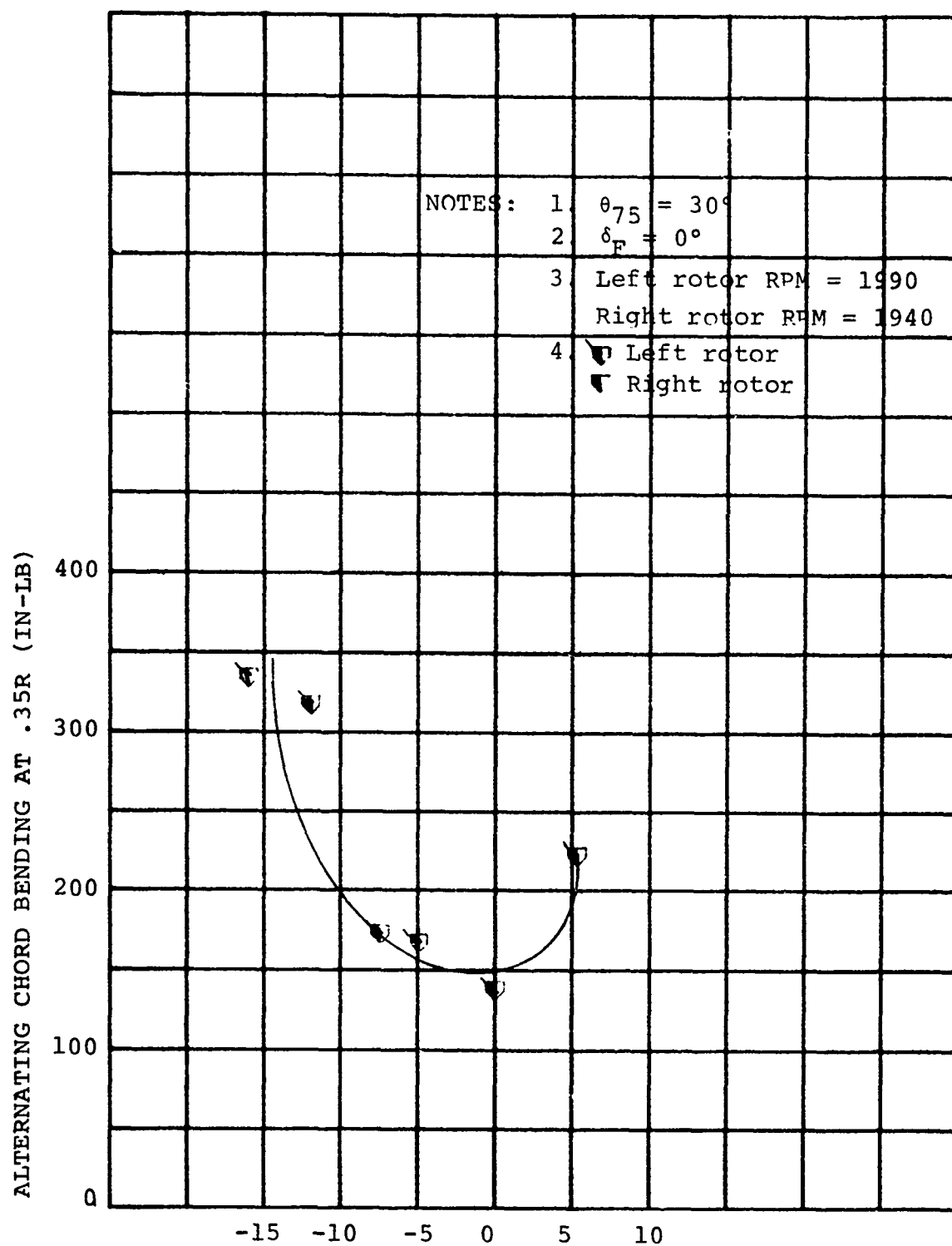


FIGURE 6-105

AIRCRAFT YAW (DEG)

ALTERNATING BLADE CHORD BENDING VS. AIRCRAFT YAW
 ANGLE FOR $i_N = 0^\circ$, $V = 215$ FPS, AND $\alpha = 0$ DEG

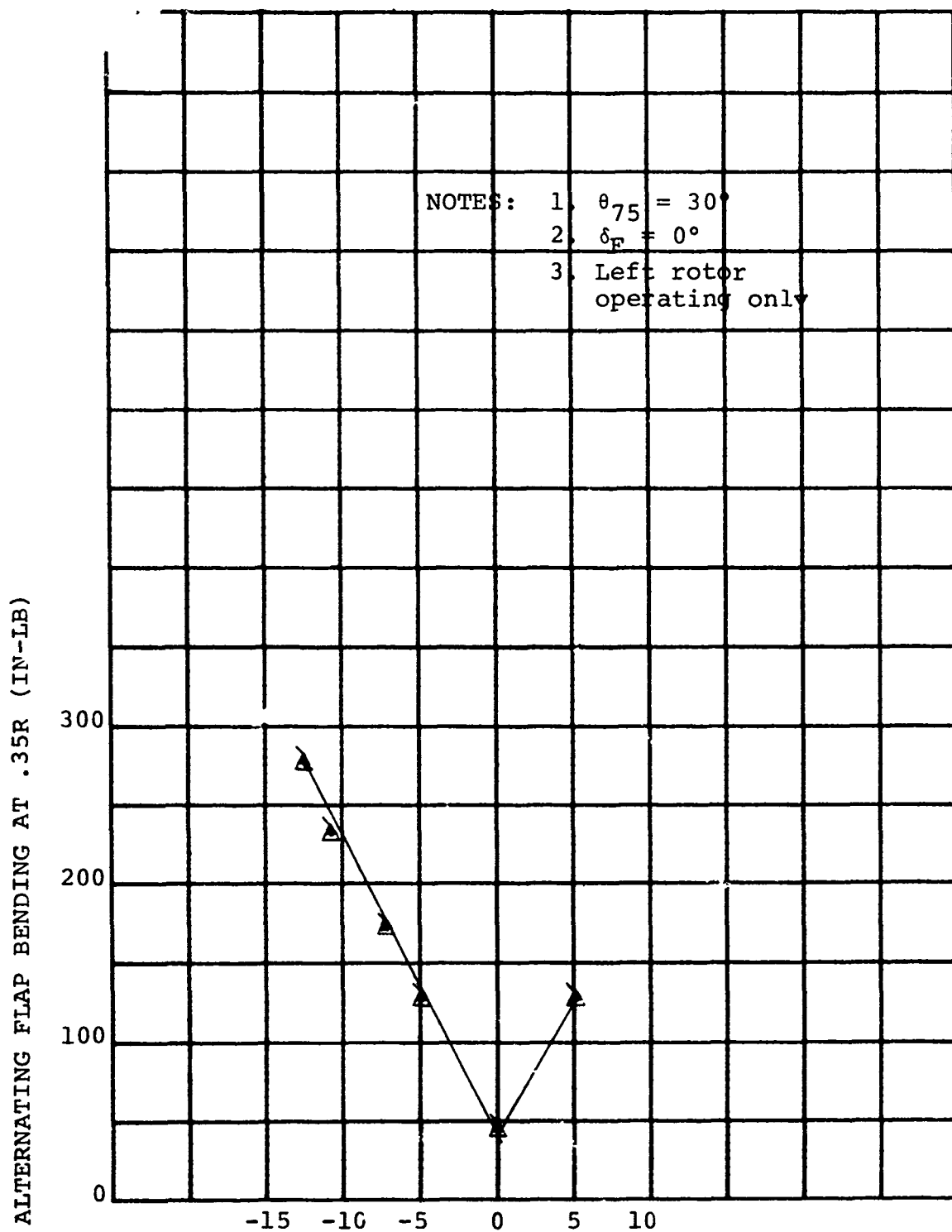


FIGURE 6-106 AIRCRAFT YAW (DEG)

ALTERNATING BLADE FLAP BENDING VS. AIRCRAFT YAW ANGLE
 FOR $i_N = 0^\circ$, $V = 226$ FPS, $\alpha = 0$ DEG, AND 2030 RPM

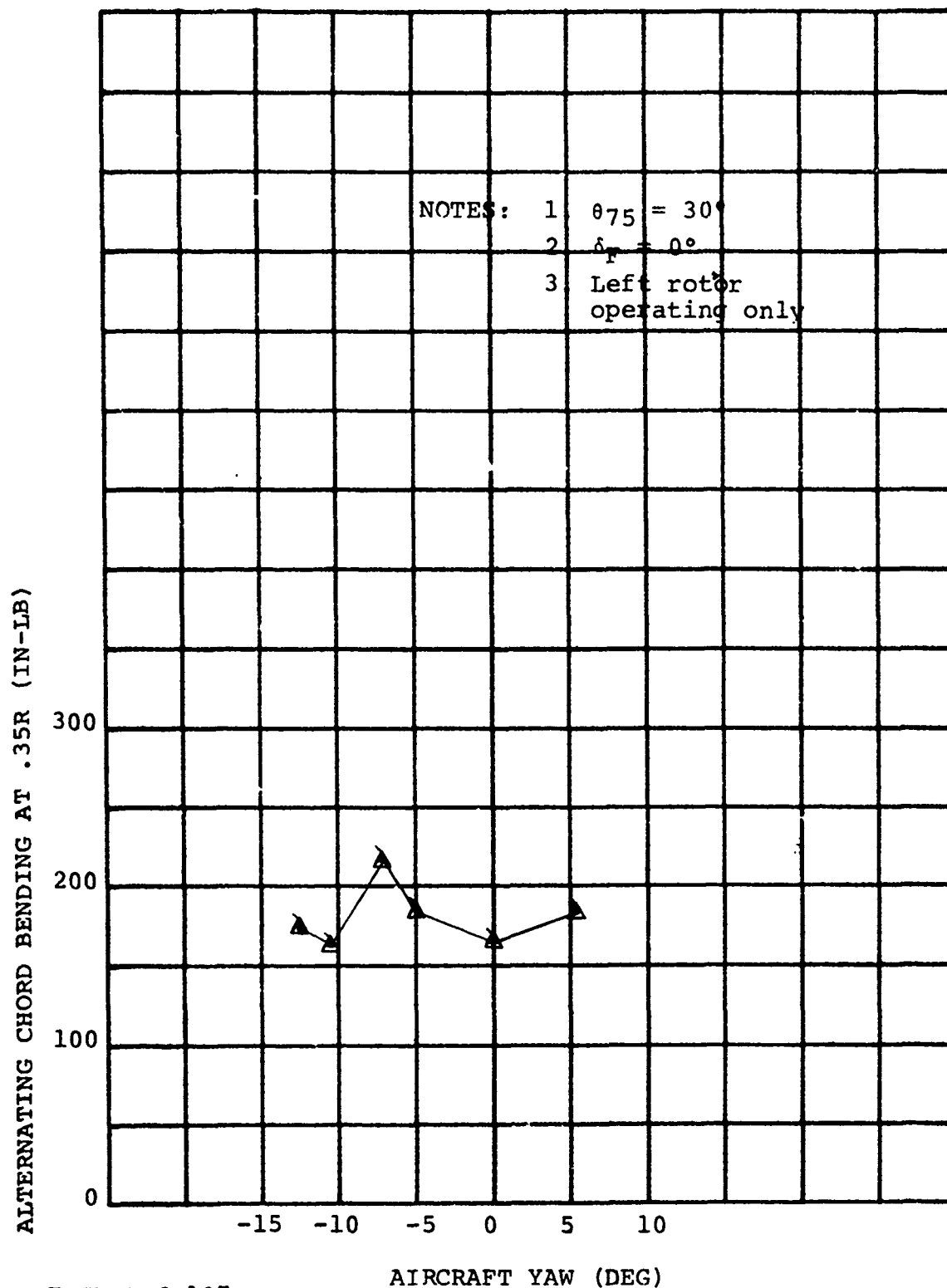


FIGURE 6-107

ALTERNATING BLADE CHORD BENDING VS. AIRCRAFT YAW ANGLE
 FOR $i_N = 0^\circ$, $V = 226$ FPS, $\alpha = 0$ DEG, AND 2030 RPM

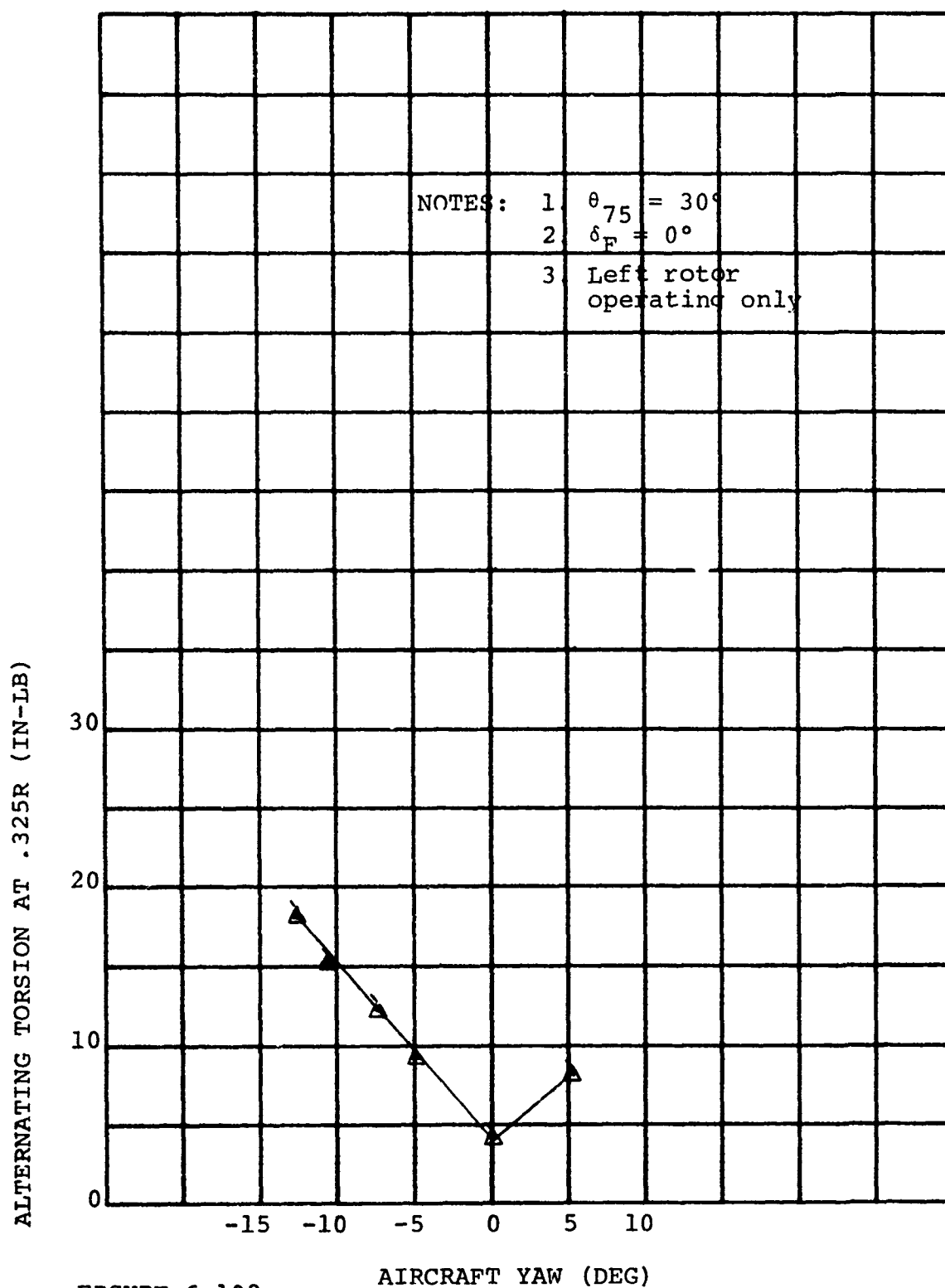


FIGURE 6-108

ALTERNATING BLADE TORSION VS. AIRCRAFT YAW ANGLE FOR
 $i_N = 0^\circ$, $V = 226$ FPS, $\alpha = 0$ DEG, AND 2030 RPM

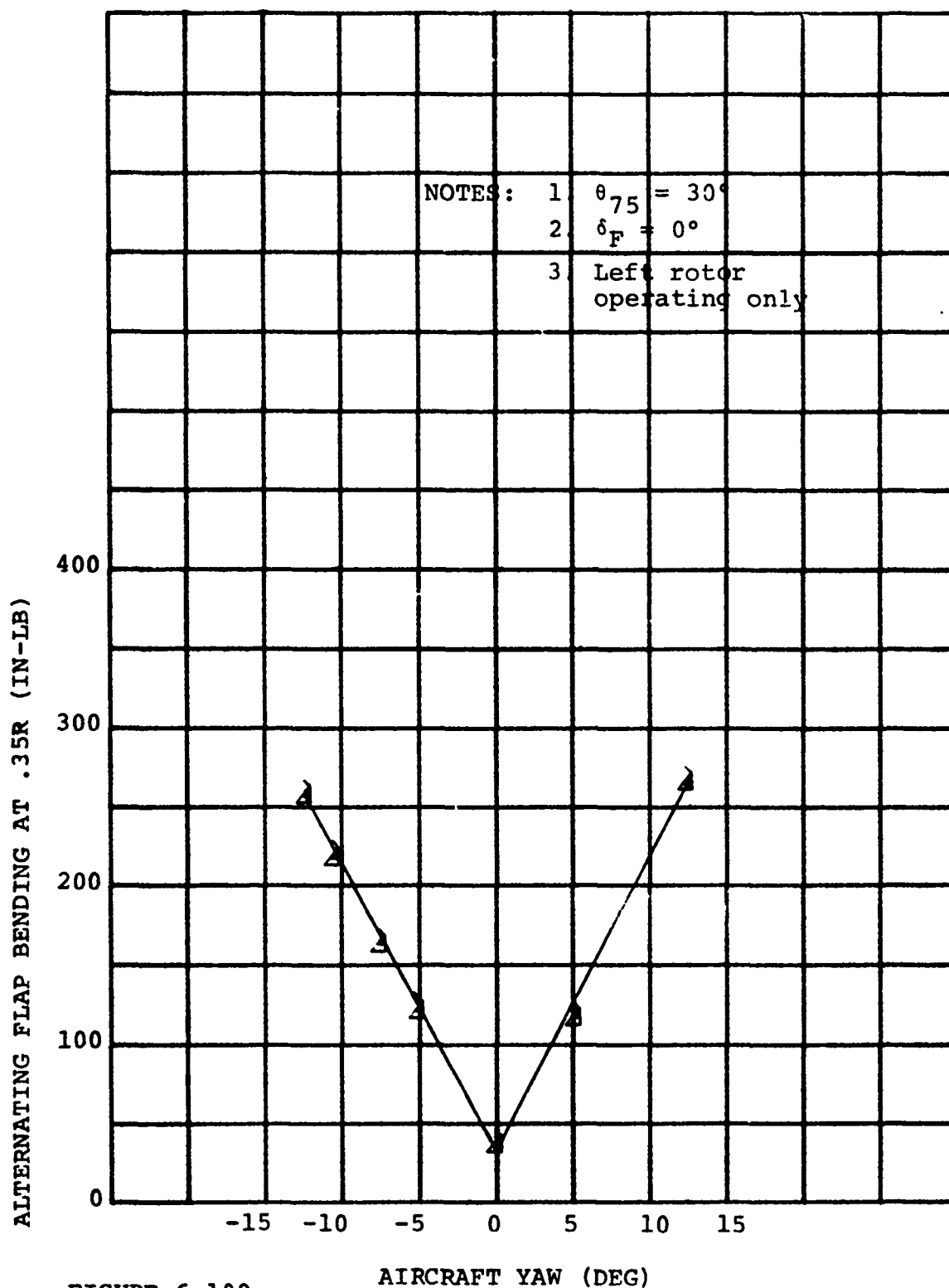


FIGURE 6-109

ALTERNATING BLADE FLAP BENDING VS. AIRCRAFT YAW ANGLE
 FOR $i_N = 0^\circ$, $V = 226$ FPS, $\alpha = 0$ DEG, AND 2040 RPM

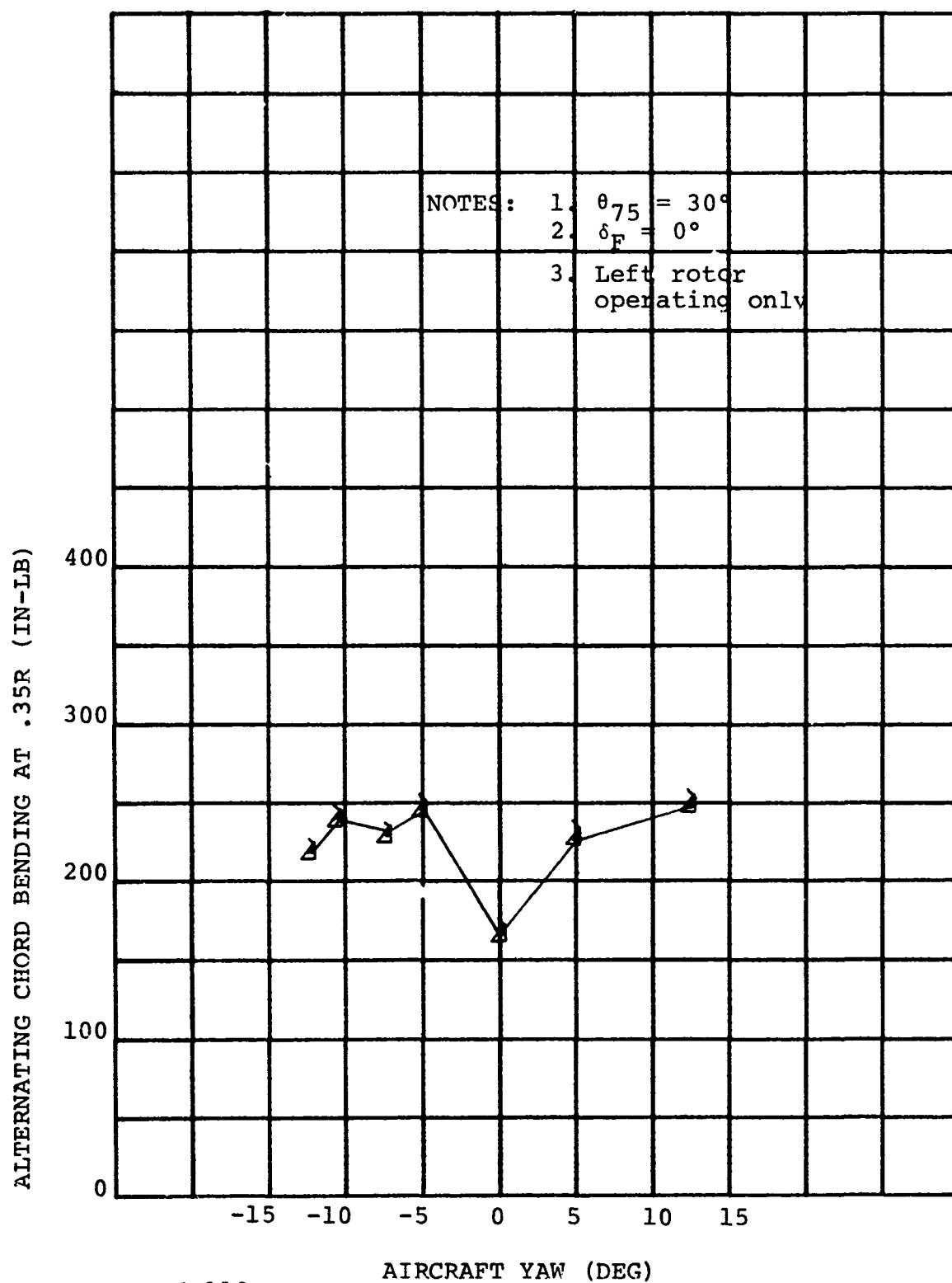


FIGURE 6-110

ALTERNATING BLADE CHORD BENDING VS. AIRCRAFT YAW ANGLE
FOR $i_N = 0^\circ$, $V = 226$ FPS, $\alpha = 0$ DEG, AND 2040 RPM

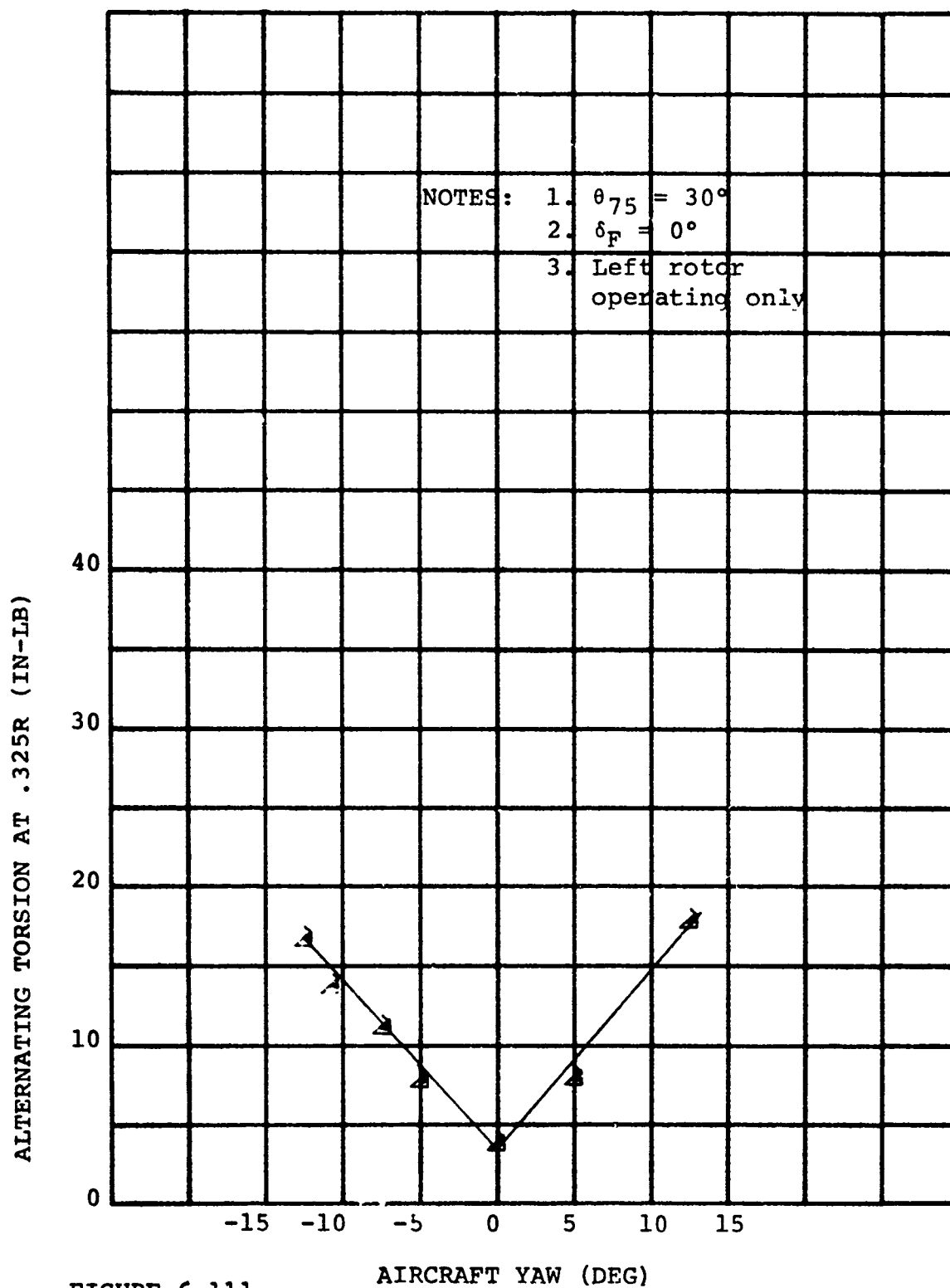


FIGURE 6-111

ALTERNATING BLADE TORSION VS. AIRCRAFT YAW ANGLE
 FOR $i_N = 0^\circ$, $V = 226$ FPS, $\alpha = 0$ DEG, AND 2040 RPM

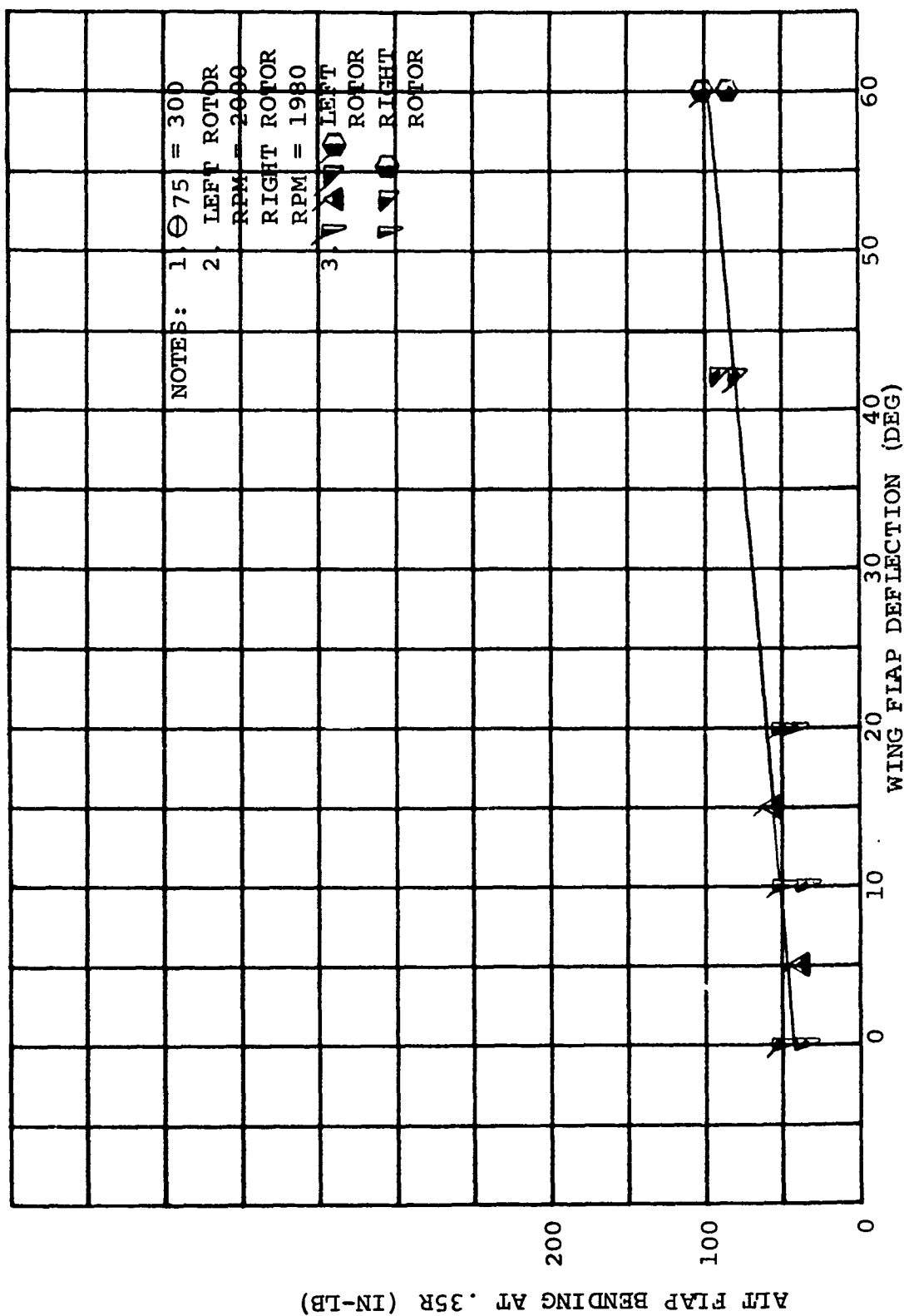


FIGURE 6-112. ALTERNATING BLADE FLAP BENDING VS WING FLAP DEFLECTION FOR $i_N=0$ DEG, $V=226$ FPS AND $\alpha=0$ DEG

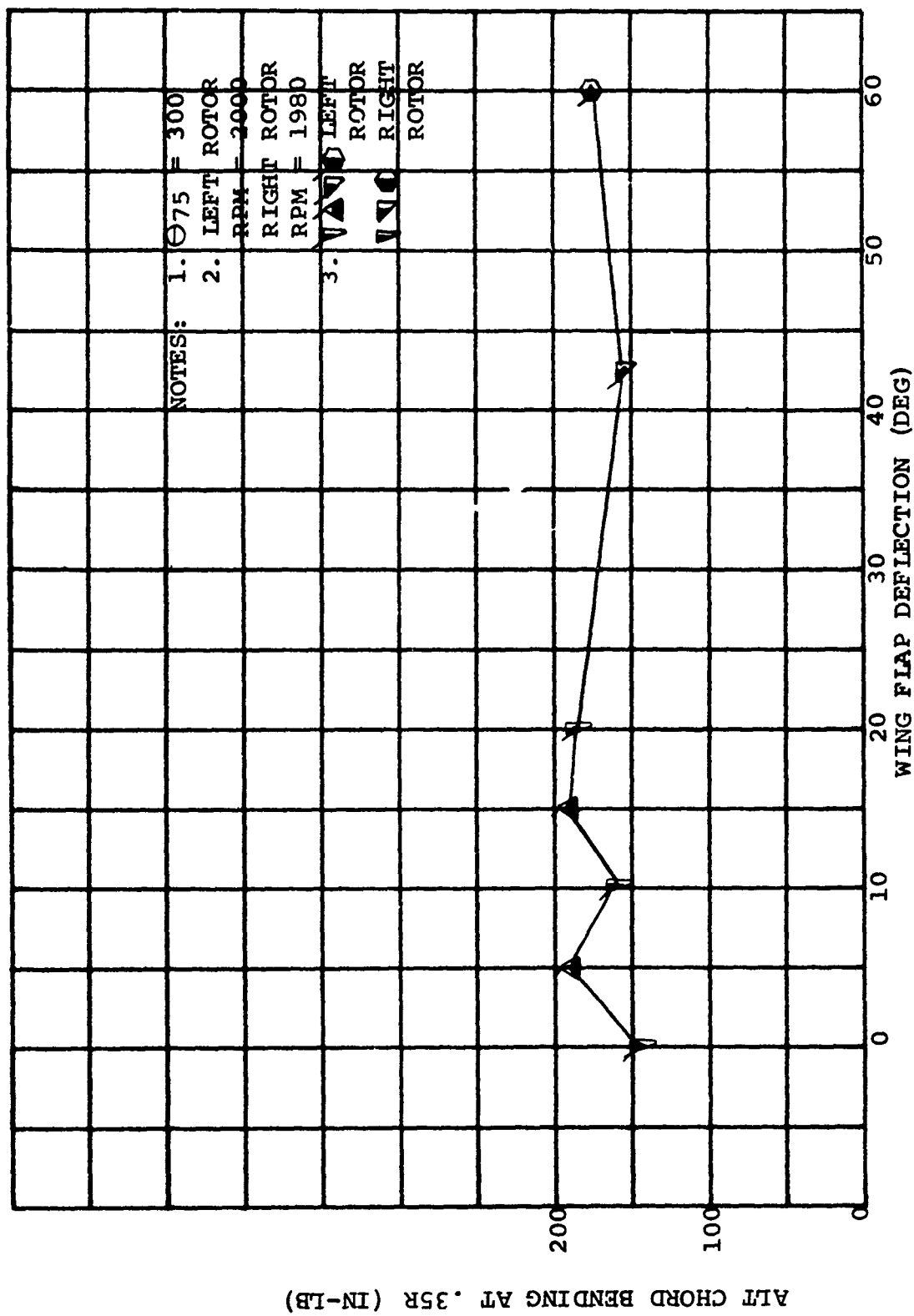


FIGURE 6-113. ALTERNATING BLADE CHORD BENDING VS WING FLAP DEFLECTION FOR $i_N=0$ DEG, $V=226$ FPS AND $\alpha=0$ DEG

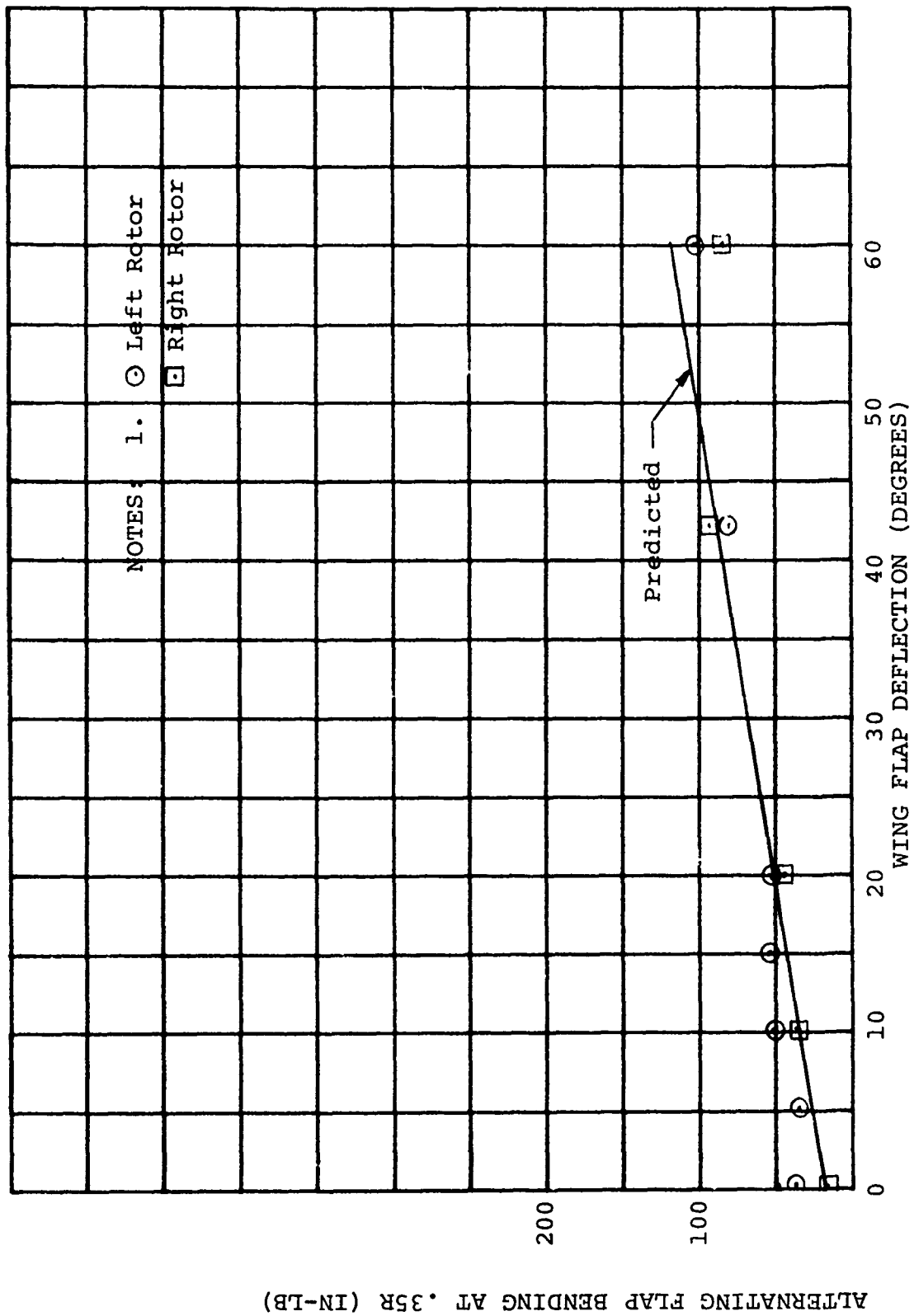


FIGURE 6-114 MEASURED AND PREDICTED ALTERNATING FLAP BENDING PRODUCED BY WING FLAP INCIDENCE IN CRUISE AT $\theta_{75} = 30^\circ$, $V_{TIP} = 570$ FPS, $V_{TUNNEL} = 220$ FPS AND $\alpha = 0$

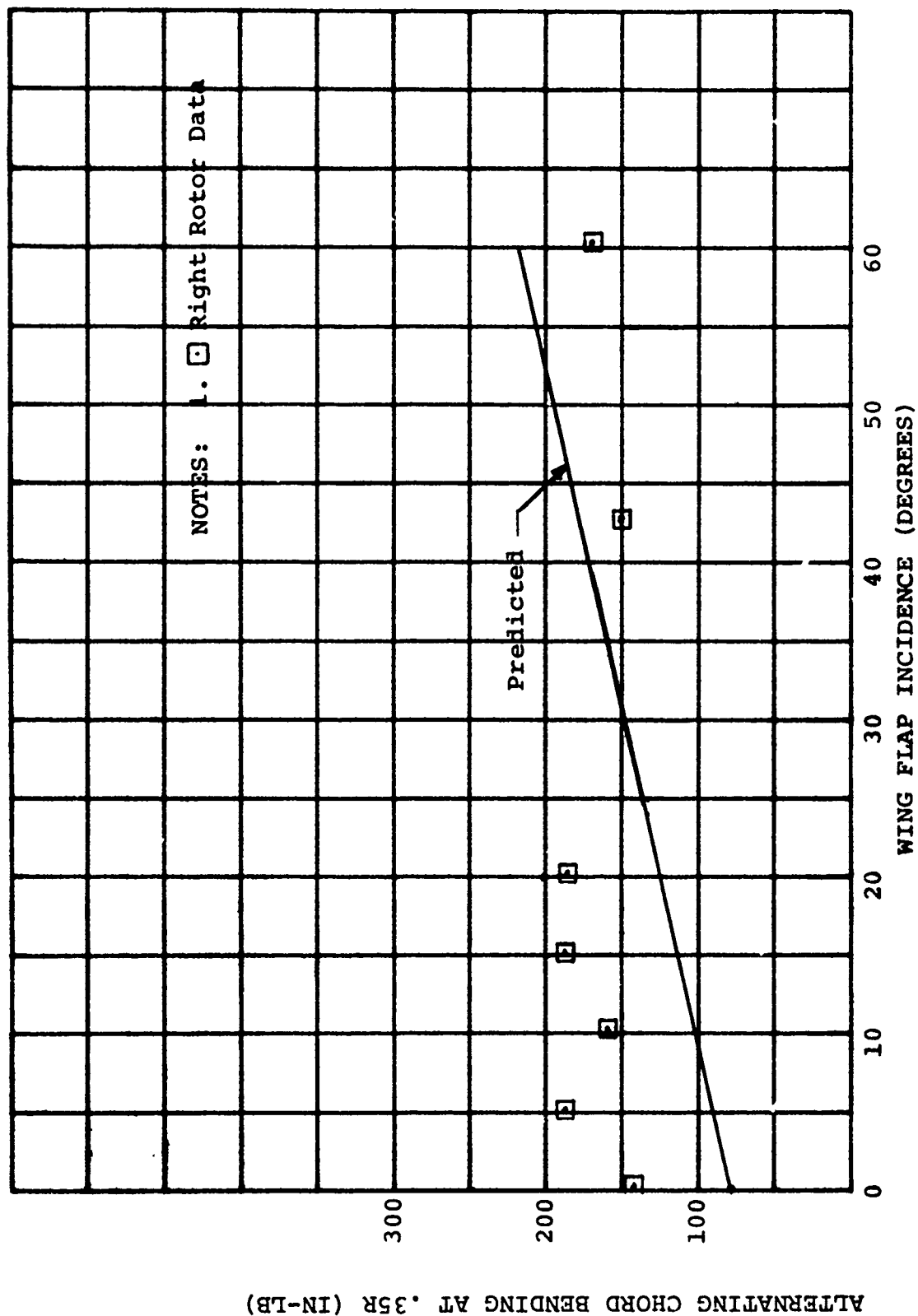


FIGURE 6-115 MEASURED AND PREDICTED ALTERNATING FLAP BENDING PRODUCED BY WING FLAP INCIDENCE IN CRUISE AT $\theta_{75} = 30^\circ$, $V_{TIP} = 570$ FPS, $V_{TUNNEL} = 220$ FPS AND $\alpha = 0$

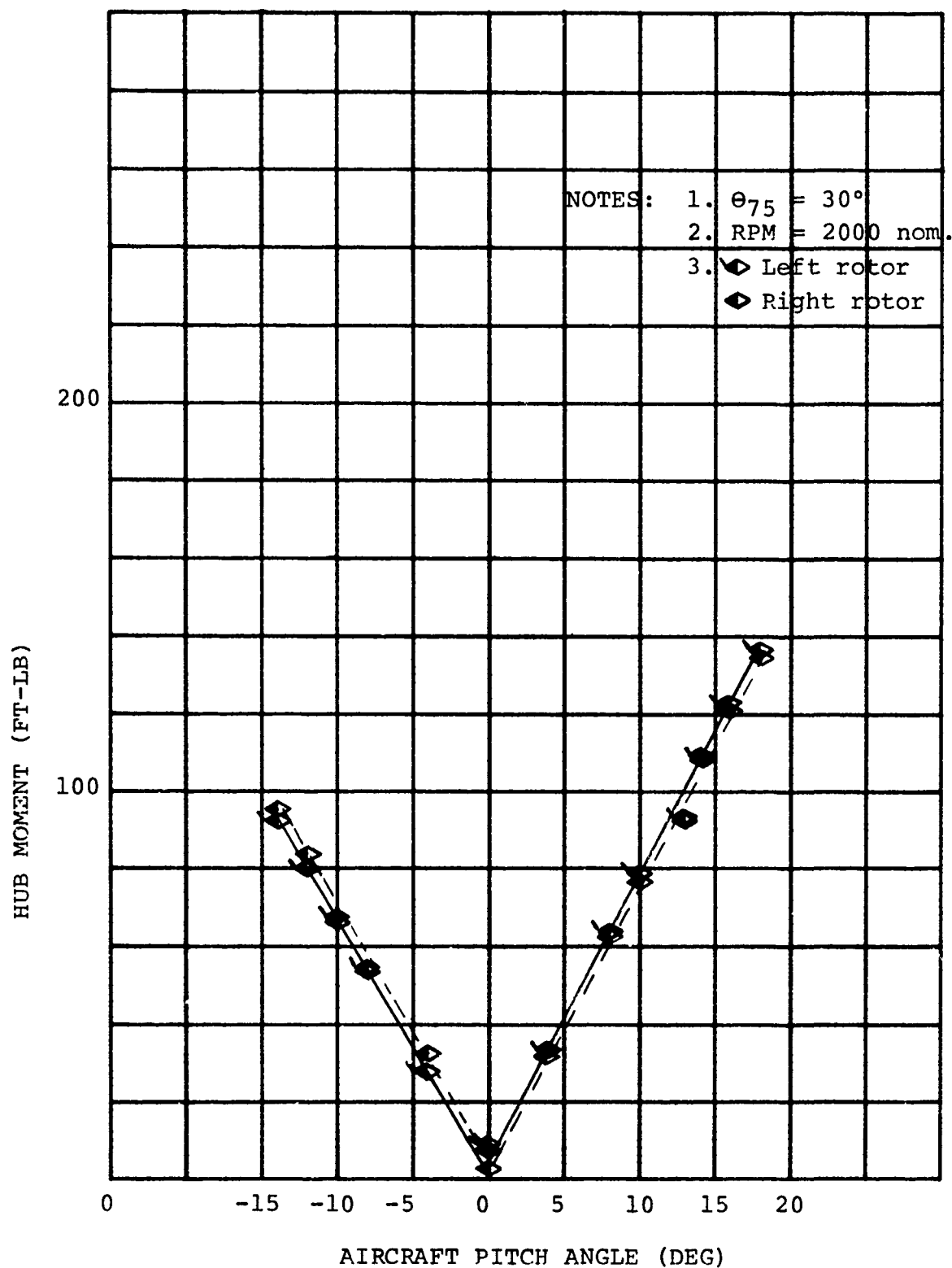


FIGURE 6-116

STEADY HUB MOMENT VS. AIRCRAFT ANGLE OF
 ATTACK FOR $i_N = 0$ DEG, AND $V = 226$ FPS

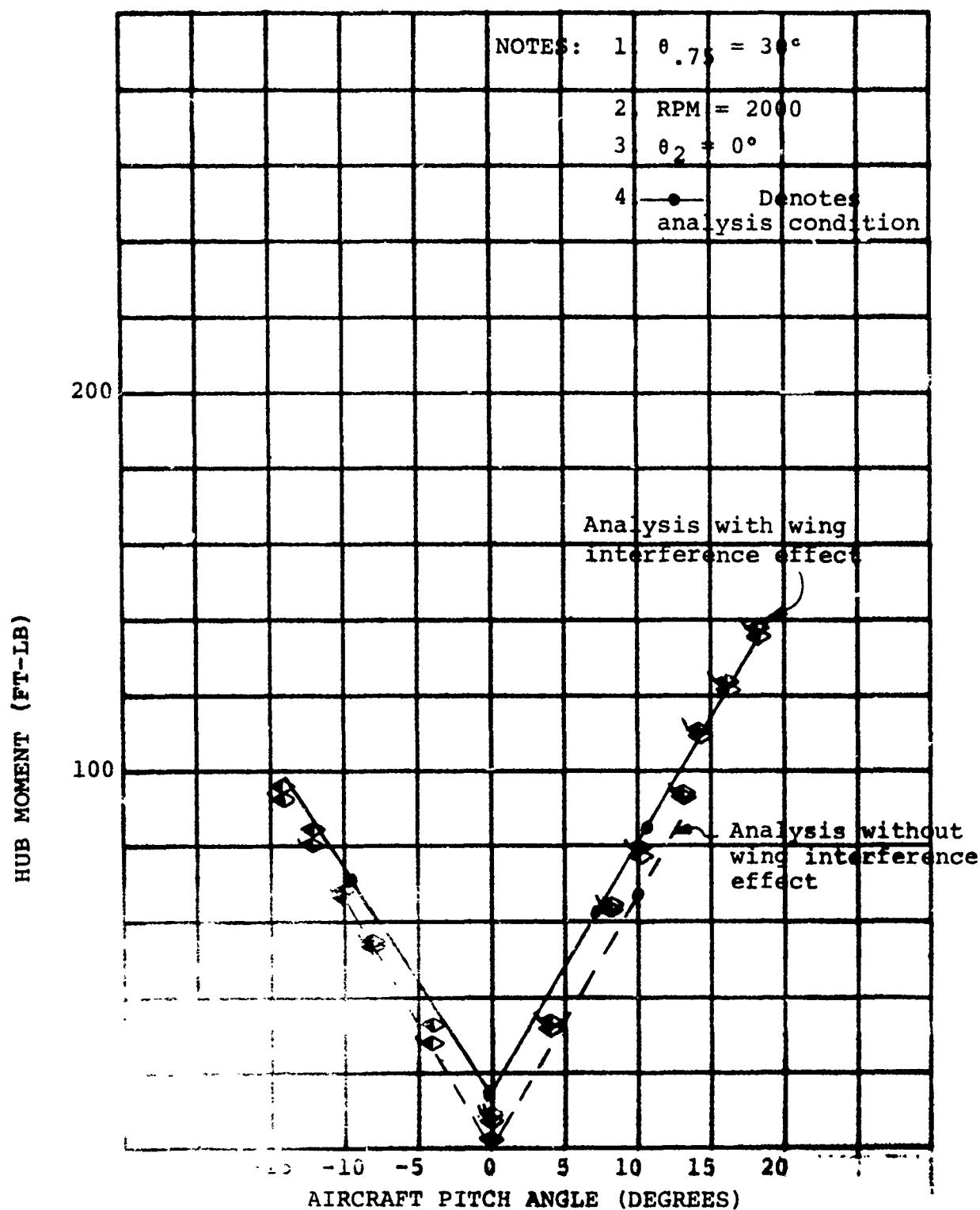


FIGURE 6-117
 COMPARISON BETWEEN MEASURED AND CALCULATED STEADY
 HUB MOMENT VS. AIRCRAFT ANGLE OF ATTACK FOR
 $\alpha_N = 0$ DEG. AND $V = 226$ FPS

6.7 CRUISE HUB MOMENTS

6.7.1 Attitude Effects

Rotor hub moment for the cruise flight mode resulting from aircraft pitch angle variation is shown in Figure 6-116. The right and left rotor hub moments are shown to be identical. The hub moment is caused by the Aq condition and by wing interference effects.

The effect of rotor inflow and wing circulation on hub moments in cruise was predicted by the uncoupled rotor loads analysis and a comparison of predicted and measured hub moments is shown in Figure 6-117. The analysis accurately predicts hub moments with angle of attack. Results of the analysis without wing interference show that 17 percent of the hub moment is due to wing interference at 10 degrees angle of attack.

Rotor hub moment for the cruise flight mode resulting from aircraft yaw angle variation is shown in Figure 6-118. The hub moment is caused by the Aq condition only. For a yaw angle of 10 degrees, the hub moment is 65 ft-lb. From Figure 6-116, the hub moment for 10 degrees of pitch angle is 78 ft-lb. The difference between these two values is 13 ft-lb. This indicates that the wing interference effect accounts for 17 percent of the hub moment due to aircraft pitch angle.

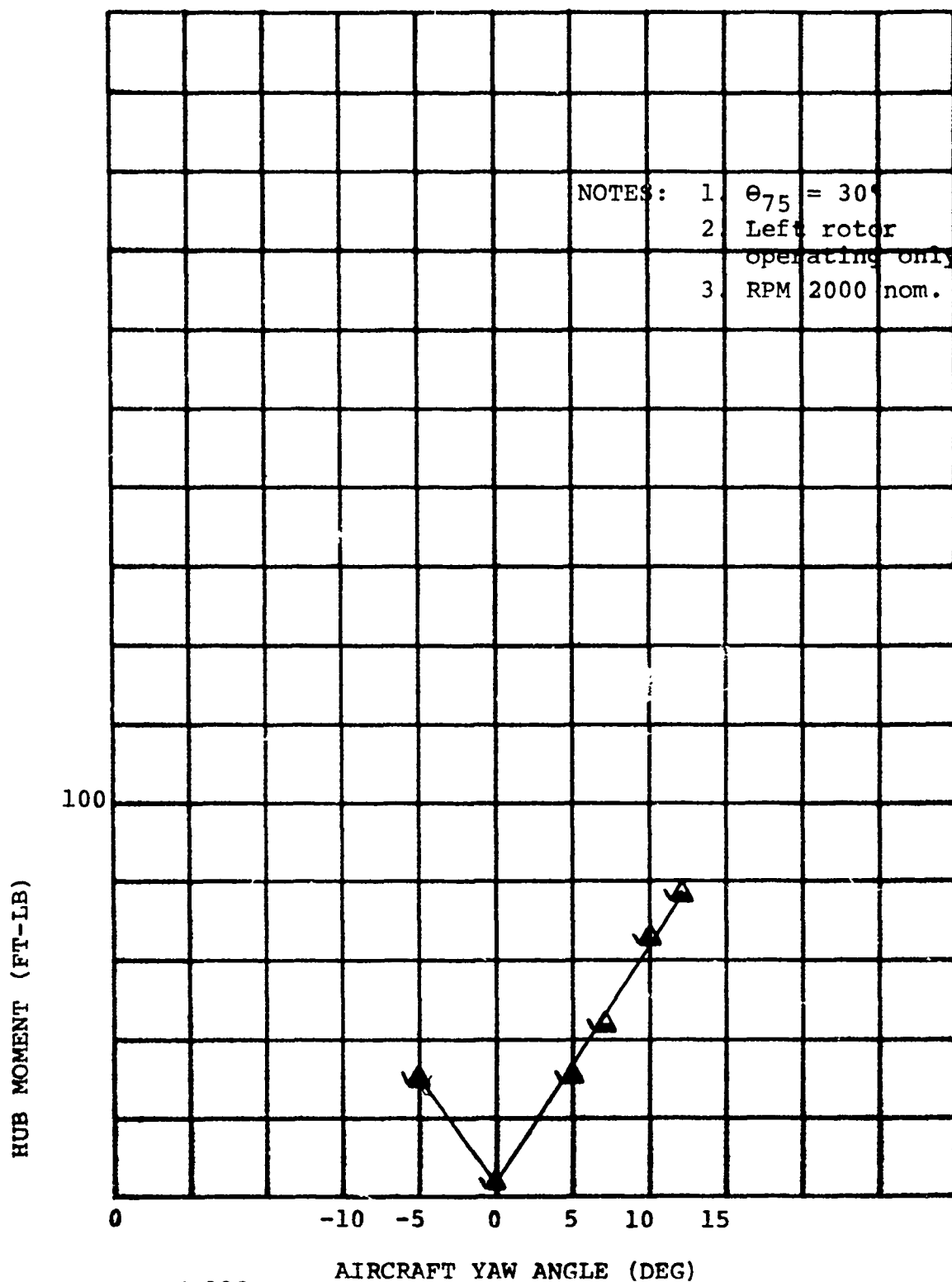


FIGURE 6-118

STEADY HUB MOMENT VS. AIRCRAFT ANGLE OF ATTACK
 FOR $i_N = 0$ DEG, AND $V = 226$ FPS

6.8 CONCLUSIONS - ROTOR LOADS

Analysis of the rotor loads test data presented here allows the following conclusions:

1. The baffle test can be used to measure rotating blade natural frequencies and verifies analysis.
2. Blade loads data in hover due to cyclic are correctly predicted using the uncoupled flap-lag analysis.
3. Stall flutter did not occur up to blade loadings in excess of expected inception loadings.
4. Wing interference increases rotor blade loads as much as 21 percent in cruise and these effects are correctly predicted by analysis.
5. Hub moments are correctly predicted by blade loads analysis in hover, due to cyclic, and in cruise, due to angle of attack.

7.0 DYNAMICS

Pre-test predictions of the modal frequencies and dampings were made prior to the 1/10-scale performance model wind tunnel test to insure structural integrity of the model during the test. The analyses used accounted for the dynamic interactions produced by rotor airframe coupling effects. During the test, baffles were used to determine blade frequencies at discrete rotor speeds. Measured blade flap and blade lag frequencies for given rotor speeds are presented in Figure 20 along with the predictions. The measured blade flap frequencies are in excellent agreement with the predictions and the blade lag frequencies are slightly higher than predicted.

Step aircraft angles of attack were input into the model in cruise, transition and hover flight modes to determine the aircraft's susceptibility in whirl flutter modes to forcing functions of this type. Results of the test show the aircraft to be insensitive to this type of forcing function.

7.1 FREQUENCIES AND MODAL DAMPING

Pretest predictions of the modal frequencies and dampings versus rotor speed for hover and modal frequencies and dampings versus equivalent forward speed in the cruise mode were made prior to the wind tunnel test for the 1/10-scale performance model (Figures 7-1 to 7-4). Positive (stabilizing) damping was predicted (Figures 7-2 and 7-4) for all modes; thus no instabilities were expected during hover or cruise testing and none were re-countered during the test.

During the test, baffles were placed under the rotor disc plane in the hover position to provide a 1,2,3 and 4-per-rev excitation. The response of the blades to these excitations was measured. Blade frequencies as a function of rotor speed were determined from peak responses. Measured blade flap and blade lag frequencies for given rotor speeds were plotted in Figure 7-1. The measured blade flap frequencies are in excellent agreement with the predictions. The measured blade-lag frequencies are slightly higher than predicted.

7.2 RESPONSE TO STEP ANGLE OF AIRCRAFT ATTACK

Step aircraft angles of attack were input into the model during the test to determine the aircraft's susceptibility in whirl flutter modes to forcing functions of this type, and, if susceptible, to measure the modal damping. Results of the test show the aircraft to be insensitive to this type of forcing function. Examination of oscillograph records at the completion of the step inputs in the cruise, transition and hover flight modes shows no amplitude of response decrease with time. Emphasis was placed on the blade flap response, as any significant whirl flutter response should include increased blade flap motion.

The insensitivity of the aircraft model is additionally emphasized by Figures 7-5 to 7-7. Peak-to-peak blade flap bending during continuous aircraft model angle of attack change is shown for cruise, transition and hover. For cruise and 45-degree transition, peak-to-peak blade flap bending at discrete aircraft angles of attack is superimposed. Note that there is no tendency for higher responses due to the step input (forcing function) nature of the aircraft model attack angle.

7.3 INFLUENCE OF FUSELAGE ANGLE OF ATTACK

The aircraft lift coefficient (with the nacelle in the cruise position) as a function of fuselage angle of attack for a wing trailing edge flap incidence (δ_F) of 45° and 0° is shown by Figures 5-130 and 5-131. For both a wing flap 45° and 0° incidence, the break in the $dC_L/d\alpha$ line (indicating onset of stall) occurs at a fuselage angle of attack near 8 degrees. Figures 7-8 and 7-9 show nondimensional fuselage balance moments as a function of fuselage angle of attack. A sharp increase in the yaw response occurs near 10° for a δ_F of 45° and near 8° for a δ_F of 0°. This could indicate some response increase due to buffeting produced by the wing stall; however, the yaw response in each case is just as great for fuselage negative angles of attack where there is no wing stall.

7.4 CONCLUSIONS - DYNAMICS

Analysis of the dynamics data presented here allows the following conclusions to be made:

1. The predicted modal frequencies and damping variation with rotor RPM show good agreement with test data.
2. Test results show the model to be insensitive in hover, transition and cruise flight modes to step angle of attack inputs.
3. All airframe moments were shown to be sensitive to fuselage angles of attack greater than $\pm 10^\circ$.

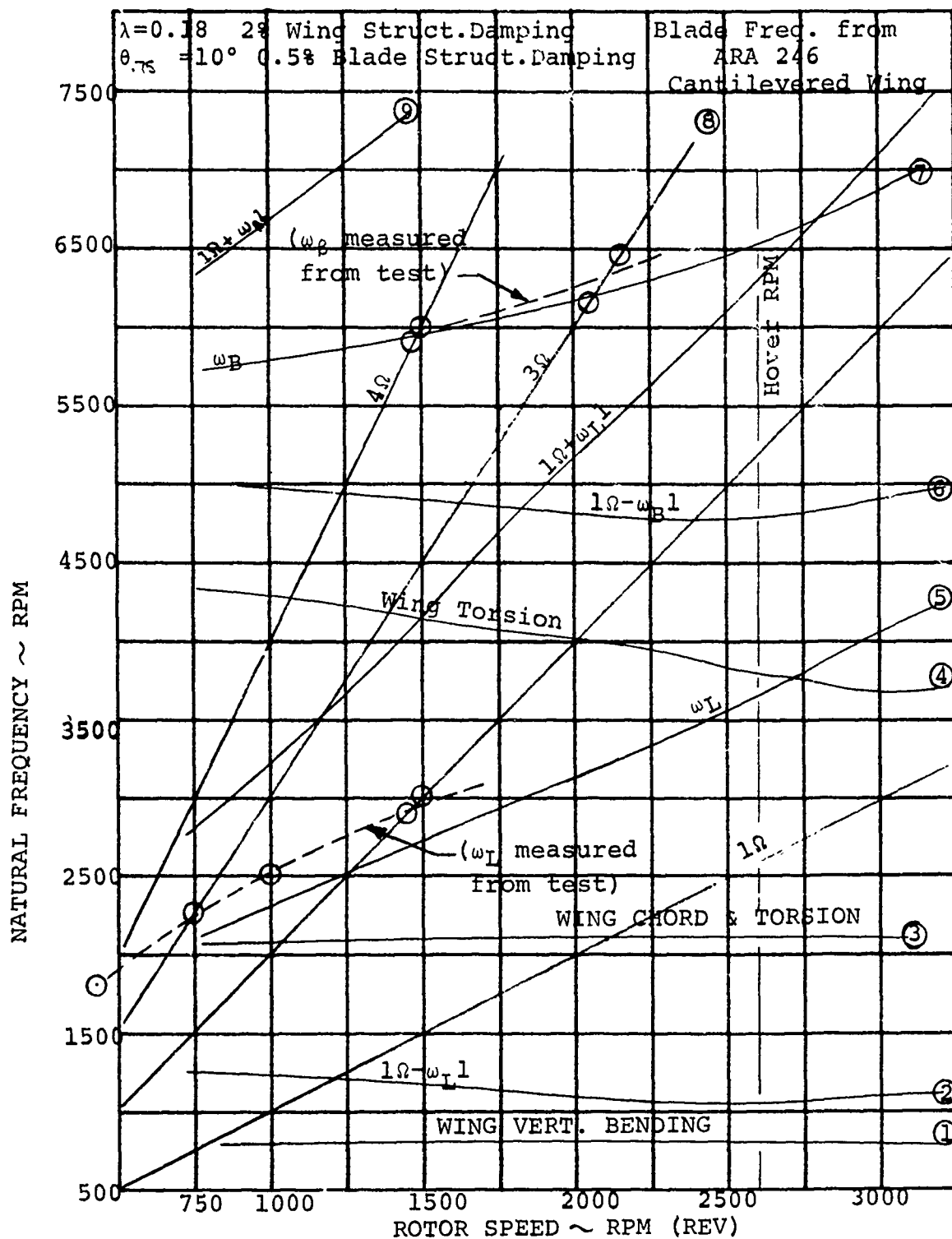


FIGURE 7-1 PREDICTED MODAL FREQUENCIES VS ROTOR SPEED (HOVER)

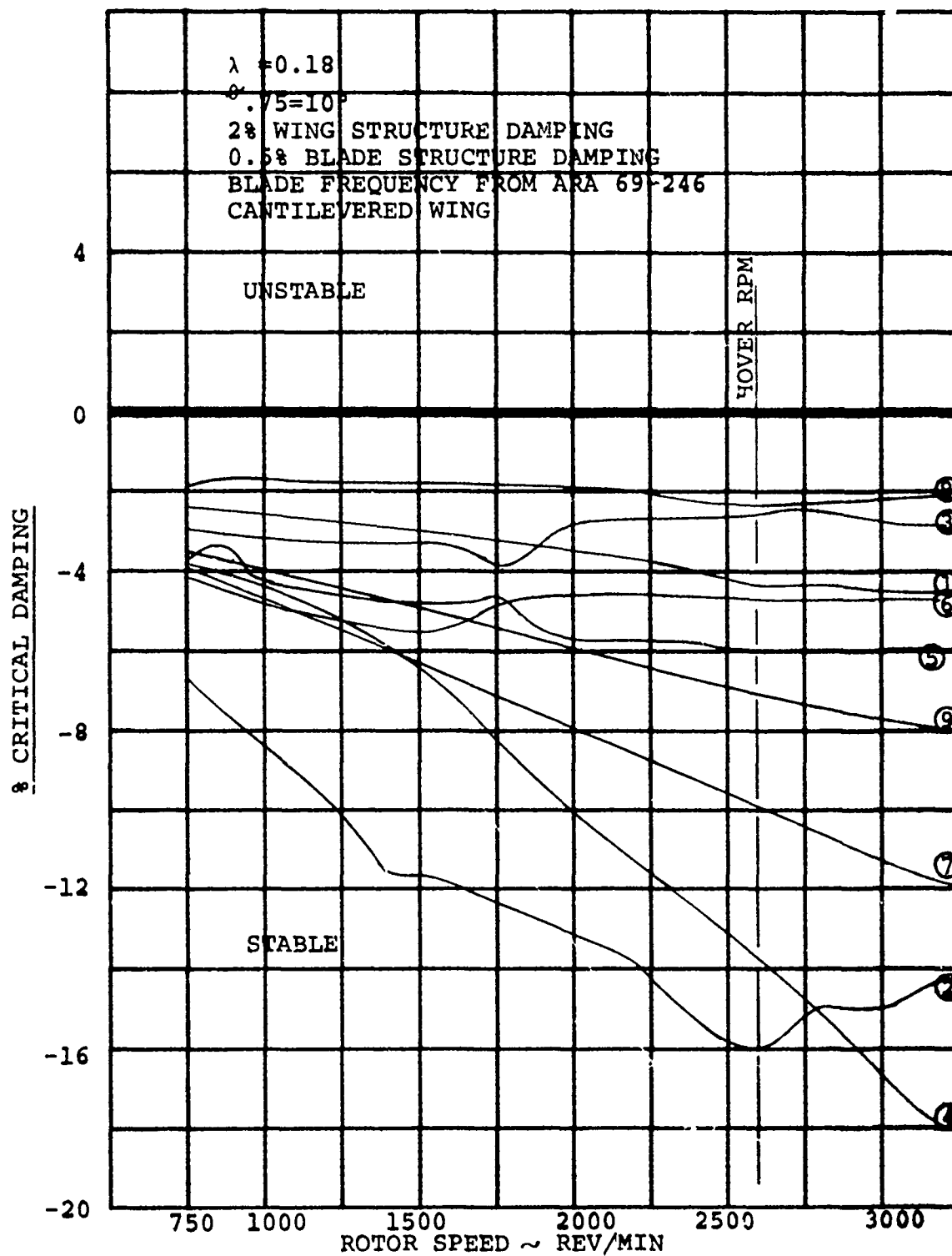


FIGURE 7-2 PREDICTED MODAL DAMPING VS ROTOR SPEED (HOVER)

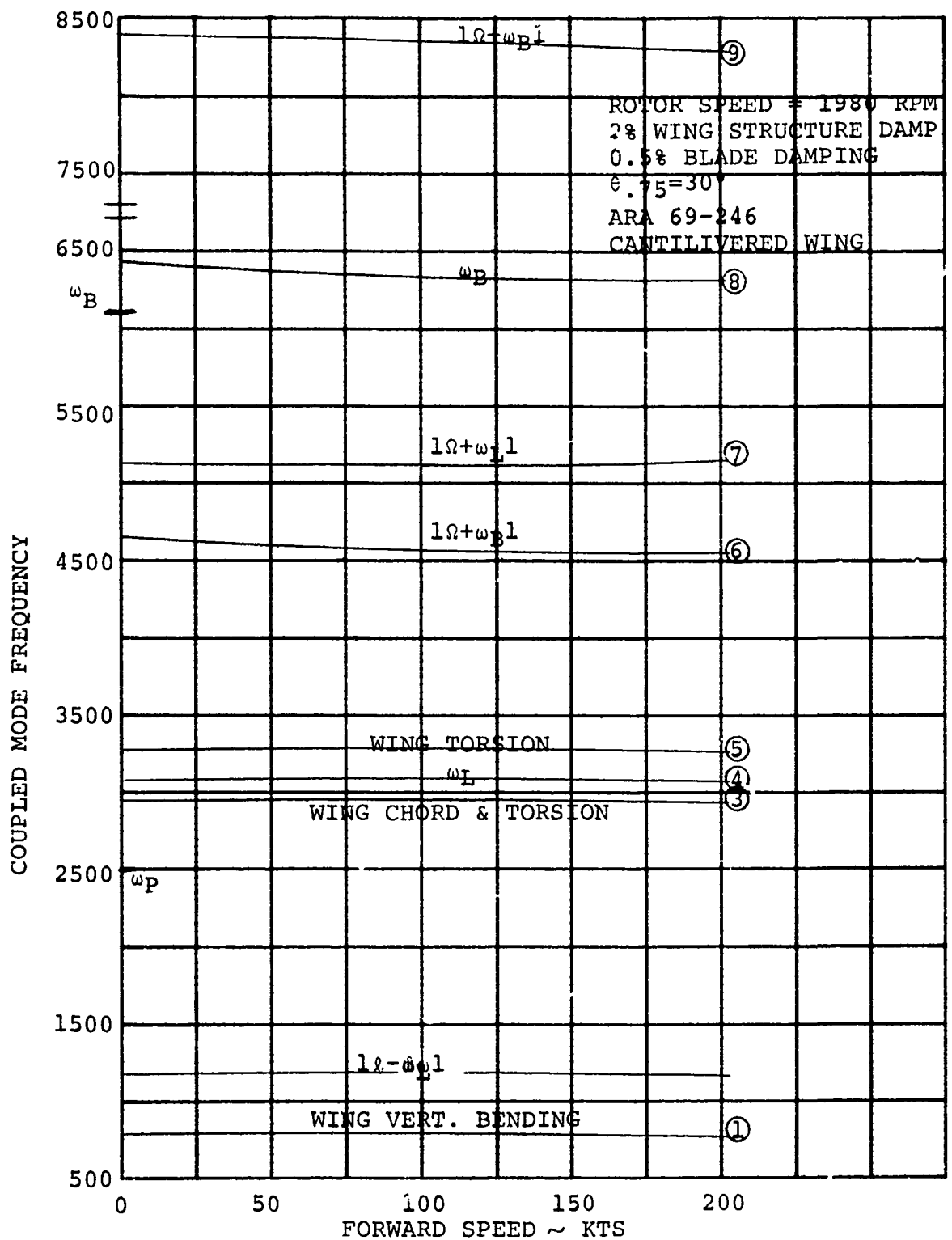


FIGURE 7-3 PREDICTED MODAL FREQUENCIES VS EQUIVALENT FORWARD SPEED (CRUISE)

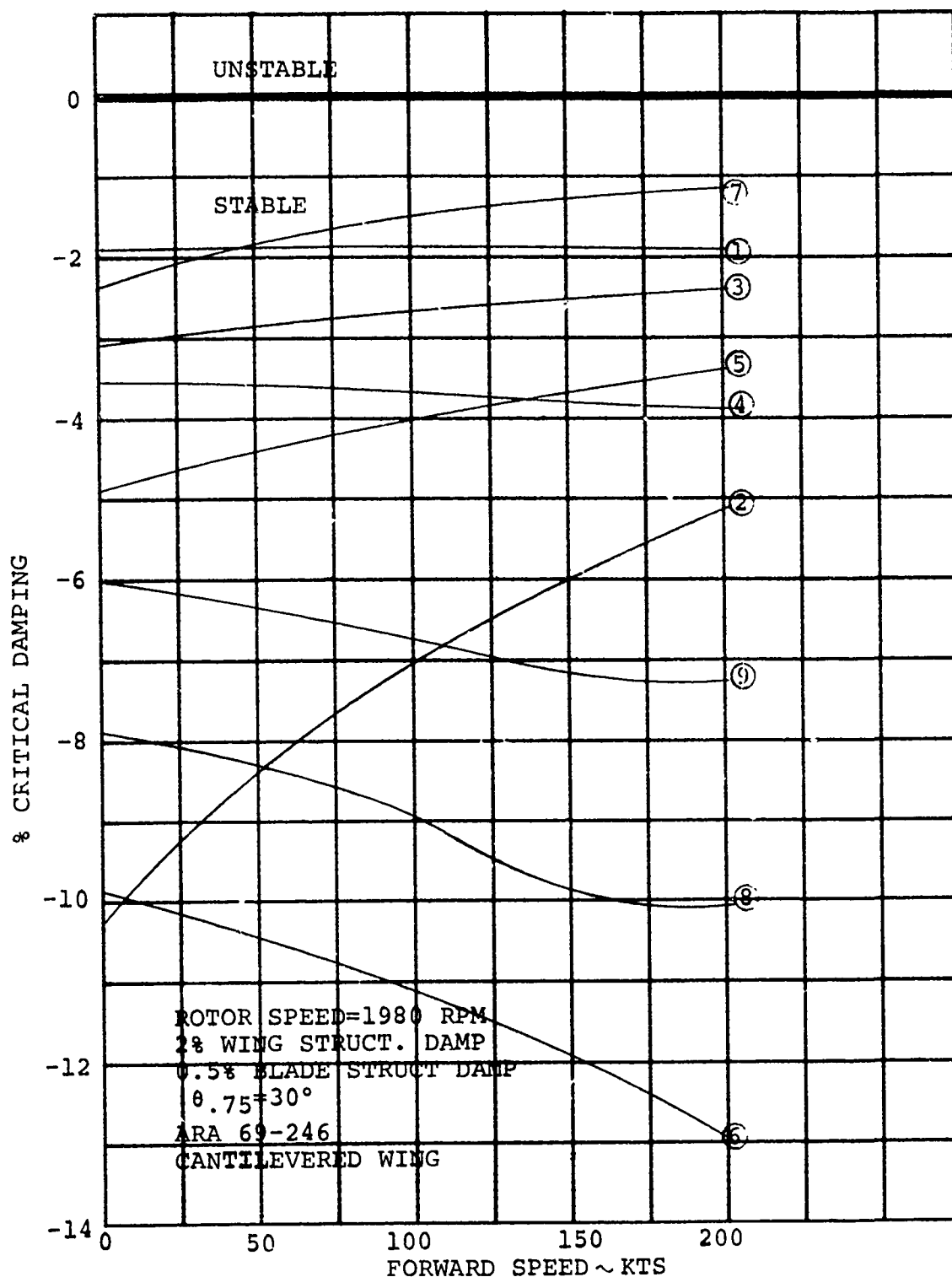


FIGURE 7-4 PREDICTED MODAL DAMPING VS EQUIVALENT FORWARD SPEED (CRUISE)

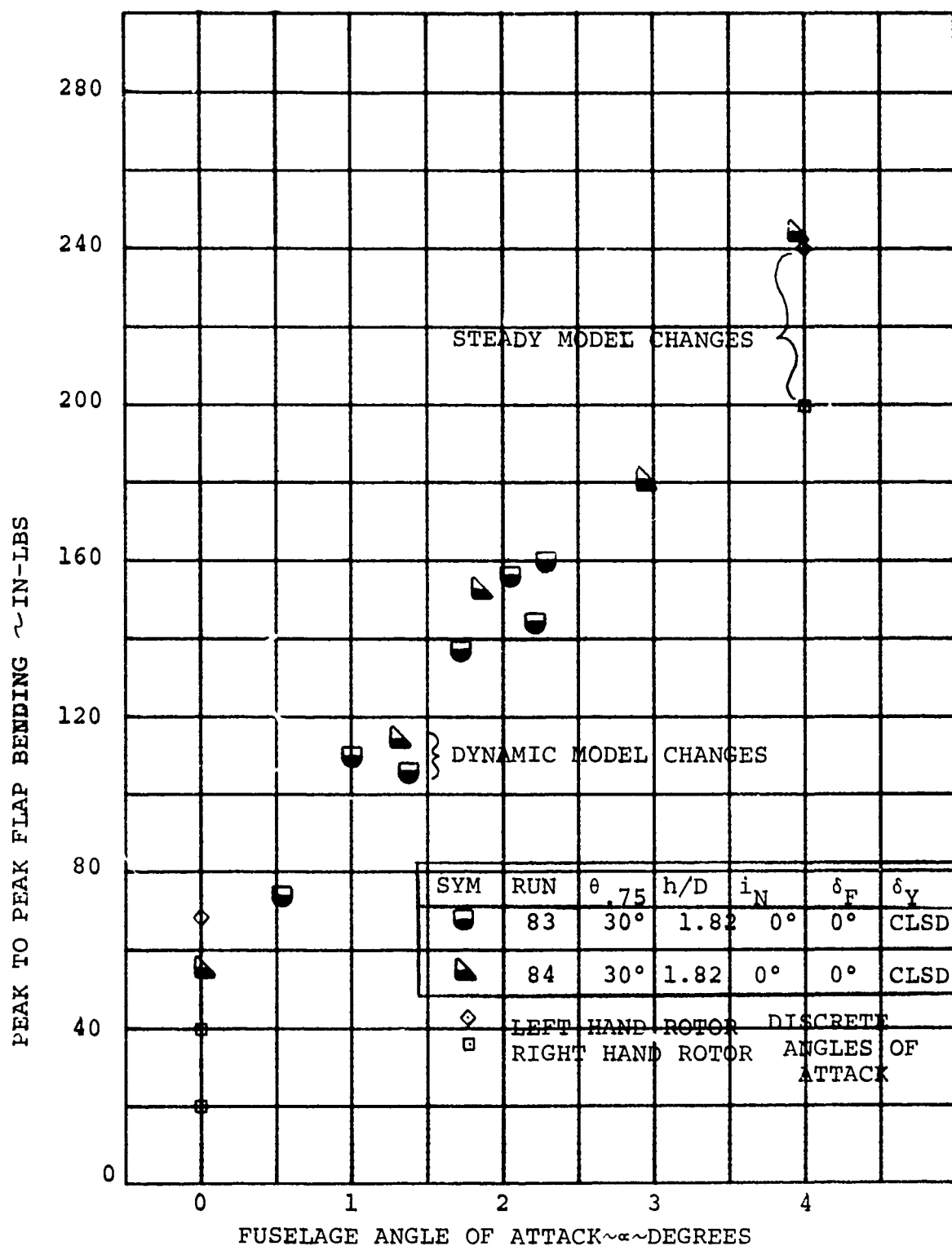


FIGURE 7-5. STEP ANGLE OF ATTACK INPUT DURING CRUISE

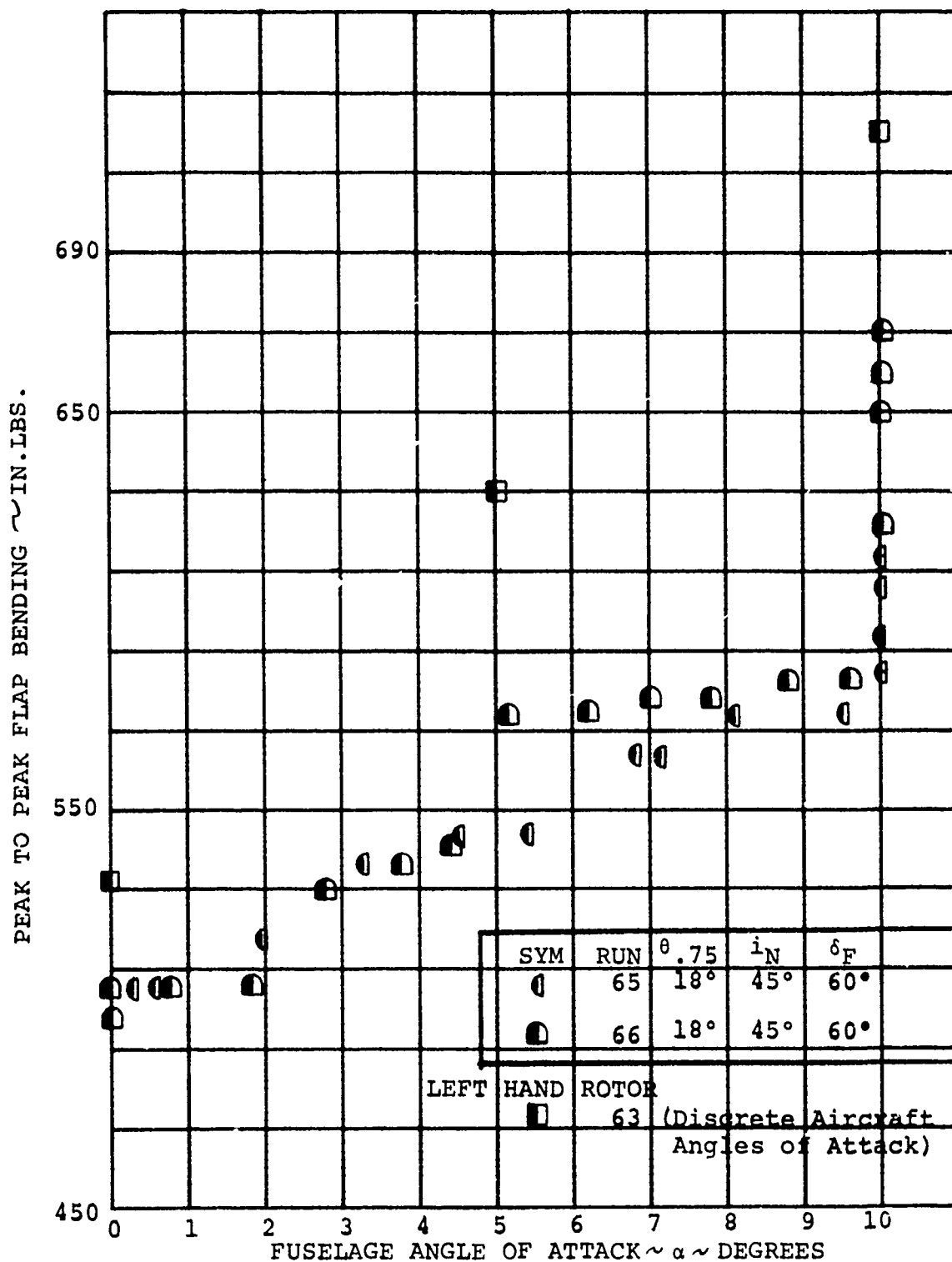


FIGURE 7-6. STEP ANGLE OF ATTACK INPUT DURING 45° TRANSITION

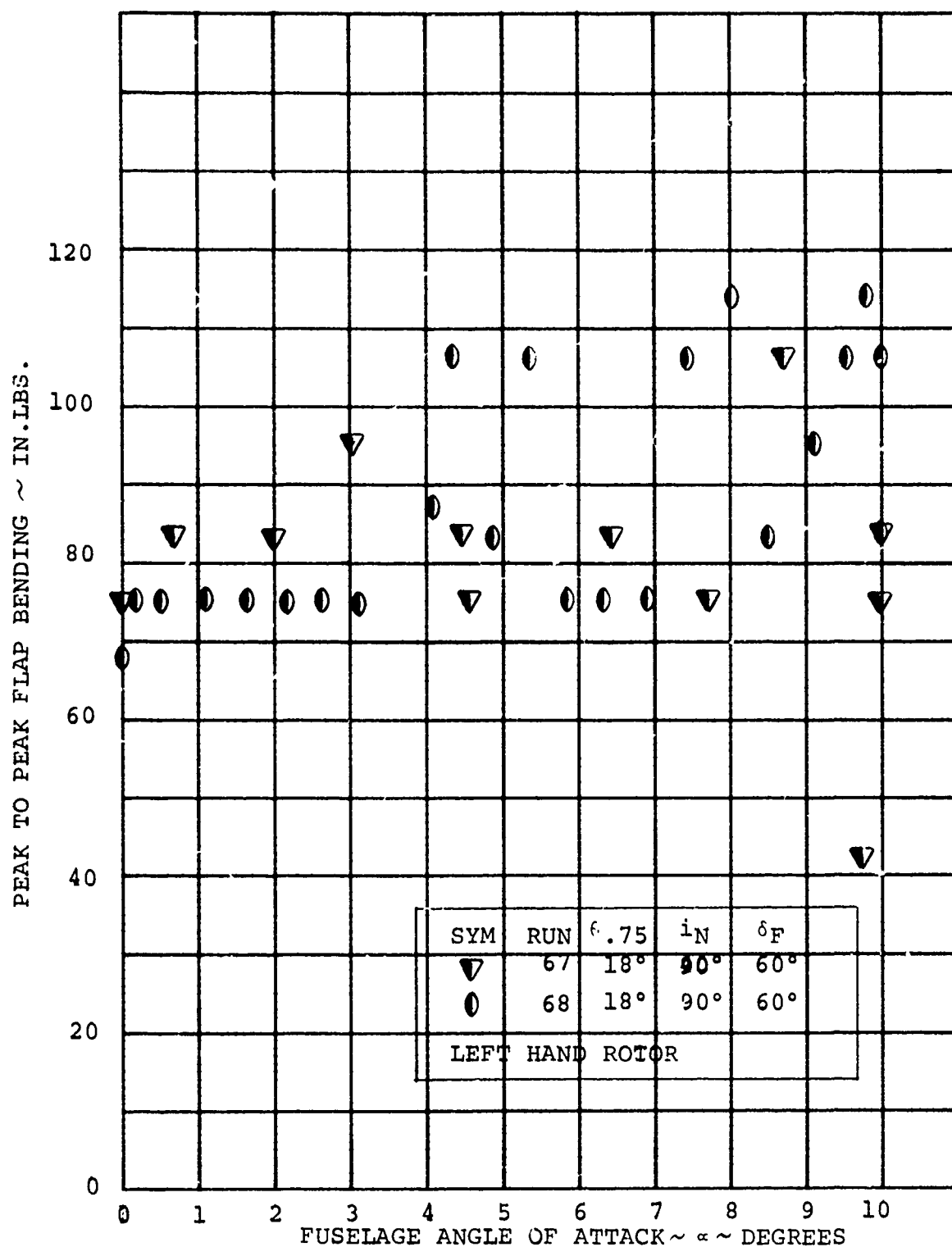


FIGURE 7-7. STEP ANGLE OF ATTACK INPUT DURING HOVER

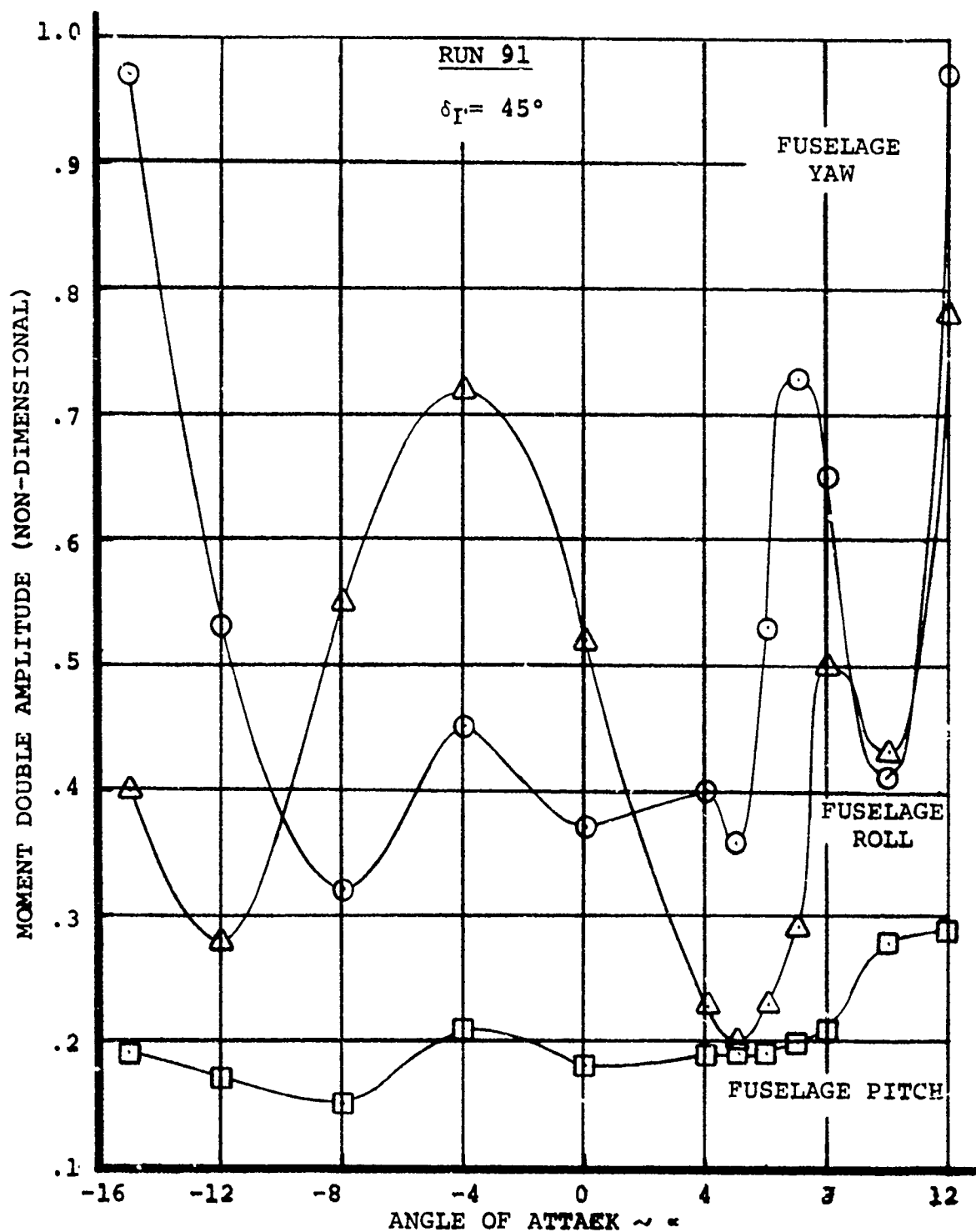


FIGURE 7-8. FUSELAGE BALANCE MOMENTS VS FUSELAGE ANGLE OF ATTACK

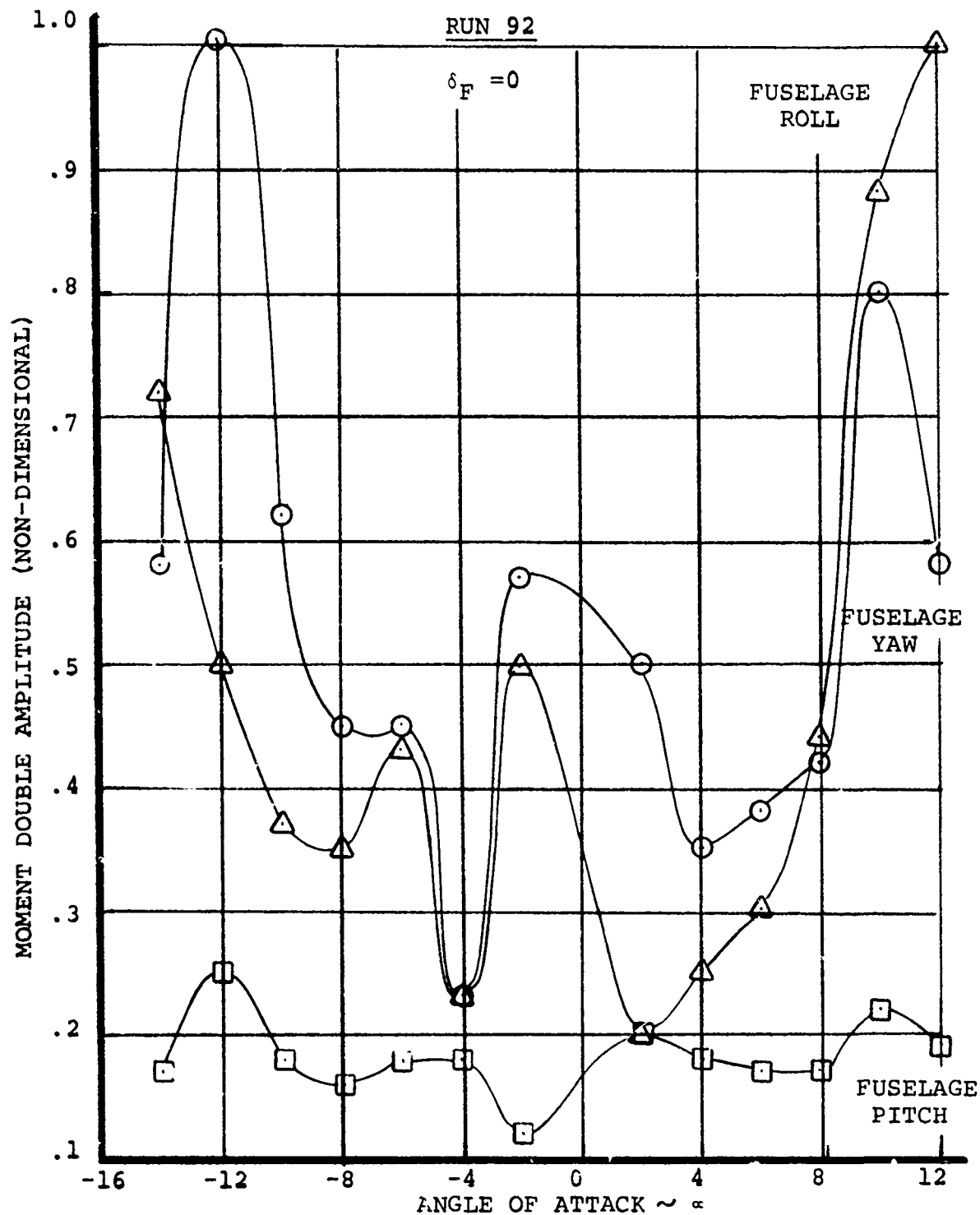


FIGURE 7-9. FUSELAGE BALANCE MOMENTS VS FUSELAGE ANGLE OF ATTACK

8.0 CONCLUSIONS

Test data were obtained to meet 90 percent of the stated objectives of the test including 100 percent of the contractual obligations. Analysis of the test data allows the following general conclusions to be made:

1. Minimum download was achieved in hover with a flap setting of 70 degrees and umbrella flaps set at $75^{\circ}/70^{\circ}$. The download out of ground is less than 5 percent of the aircraft thrust.
2. Flap setting and umbrella angle has no effect on rotor performance.
3. The minimum download configuration produces the best total aircraft performance.
4. The maximum lift loss due to rotor airframe interference is 3 percent of the total lift available in STOL operation.
5. The total aircraft maximum lift occurs at an angle of attack of 20 degrees in mid-transition.
6. The rotor performance and stability data cannot be scaled up and be representative of the full scale aircraft but is adequate for the correlation with theory for the contract final report.
7. Hover, pitch, roll and yaw control powers measured are sufficient to meet the specifications of Level 1 flying qualities of Reference 8.
8. The rotor has a large destabilizing effect on the aircraft in transition and cruise.
9. Rotor stall limits the destabilizing effects of the model rotor in transition.
10. Roll and yaw control moments can be obtained in transition using differential thrust with differential cyclic used as a decoupler.
11. The wing lift interference effect increases the rotor pitching moment derivative by 50 percent in cruise.
12. Predictions of isolated rotor derivatives agree well with data at zero wing lift.

13. Correlation of theory and test rotor stability derivatives provides confidence that the full-scale design aircraft will be stable as predicted.
14. The baffle test can be used to measure rotating blade natural frequencies and verifies analysis.
15. Blade loads data in hover due to cyclic are correctly predicted using the uncoupled flap-lag analysis.
16. Stall flutter did not occur up to blade loadings in excess of expected inception loadings.
17. Wing interference increases rotor blade loads as much as 21 percent in cruise and these effects are correctly predicted by analysis.
18. Hub moments are correctly predicted by blade loads analysis in hover, due to cyclic, and in cruise, due to angle of attack.
19. The predicted modal frequencies and damping variation with rotor RPM show good agreement with test data.
20. Test results show the model to be insensitive in hover, transition and cruise flight modes to step angle of attack inputs.
21. All airframe moments were shown to be sensitive to fuselage angles of attack greater than $\pm 10^\circ$.

9.0 RECOMMENDATIONS

1. Conduct additional tests, using the dynamic model, to define the apparent rotor mutual interference effect on rotor efficiency and blade loads.
2. Conduct tests in transition at various flap settings to determine the magnitude of wing rotor interference on the rotor force and moment derivatives.
3. Conduct tests in ground effect with two rotors to define the effects of ground proximity on control moments due to cyclic.
4. The representation of the blade lag properties in cruise should be modified in current prediction technique to more accurately represent the blade lag frequency so that rotor inflow and wing interference effects on alternating chord bending can be more accurately predicted.
5. The unsteady aerodynamics capability of Program D-88 should be utilized to predict stall flutter inception in hover and resulting blade torsional moments.
6. Conduct additional testing on the performance model in hover with additional damping provided to determine if any non-linearities or random variations in aircraft stability.

10.0 REFERENCES

1. Design Studies and Model Tests of Stowed Tilt-Rotor Concept, R&D Interim Report of Phase I; Contract No. F33615-69-C-1577, Fry, B.L., The Boeing Company (Vertol Division).

Volume 1 - Parametric Design Studies
Volume 2 - Component Design Studies
Volume 3 - Performance Data for Parametric Study Aircraft
2. The Prediction of Stability Derivatives of Large Flexible Prop/Rotors by a Simplified Analysis; Magee, J.P. and Pruyn, R.R., American Helicopter Society, Preprint No. 443, June 1970.
3. Flight Test Development of XV-1 Convertiplane; Marks, M.D. Journal of AHS, Volume 2, No.1, January 1957.
4. Phase II: Flight Evaluation (Evaluation of the XV-1) Putnam, V.F. and Eggert, W.W., AFFTC-TR-56-35, ASTIA Document No. AD-112423, February 1957.
5. Handling Qualities Experience with Several VTOL Research Aircraft; Reeder, J.P., NASA TN D-735, March 1961.
6. ARDC XV-3: Limited Flight Evaluation of the XV-3 Aircraft, Decker, W.H. and Ferry, R.G., AFFTC-TR-60-4, May 1960.
7. An Analysis of Results from Army-Sponsored VTOL Research Aircraft; U.S. Army Trec. Tech. Report 61-3, January 1961.
8. Flying Qualities of Piloted V/STOL Aircraft; Military Specification, July 1970 Proposed Document.
9. Wind Tunnel Tests of a Powered Aerodynamic 1/10 Scale Model of the Model 160 Tilt Rotor Aircraft in the Hover, Transition and Cruise Modes; Taylor, R. and Soule, V. D160-10014-1, January 8, 1971.
10. Configuration Design Analysis of a Prop/Rotor Aircraft, D. A. Richardson, Jaan Luva et al, AFFDL TR-70-44, April 1970
11. USAF Stability and Control DATCOM, D. E. Ellison, August 1968 Revision.
12. Mechanical Vibrations, J. P. Den Hartog

APPENDIX A

ROTOR BLADE PHYSICAL PROPERTIES

Table A-1 presents the rotor blade physical properties. A comparison of the design and measured blade twist is shown in Figure A-1. The predicted blade natural frequency spectrum is shown in Figures A-2 and A-3. Figure A-4 presents the first mode bending normal to the rotor disc and is used to define the virtual flap hinge and also Lock number. Included herein is a discussion of the test program conducted to define the shear center and elastic coupling of the 1/10 scale blade.

Blade Shear Center and Elastic Coupling Test Results

A bench test was conducted in February 1970 to determine the shear center and elastic coupling of the Model 160, 5.5' diameter stiff in-plane rotors. The deflections at .75R on one left-hand and one right-hand blade were measured. The major results of the test were as follows:

- a. The blade shear centers as measured at 3/4 radius were at 37.5% chord for the left-hand blade and 48% chord for the right-hand blade. The predicted value was 25% chord.
- b. The relationship between flap and chord bending moments and elastic change in twist at 3/4 radius does not vary between left and right-hand blades.
- c. The elastic coupling of blade pitch and blade flapping exhibited a positive δ_3 effect. As blade flapping angle increased, the angle of attack at 3/4 radius decreased.
- d. The horizontal deflection of the blades increased opposite in direction to the applied chord bending moment (tension in trailing edge). As the chord bending moment was increased further, the change in horizontal deflection became zero and then decreased.
- e. For chord bending moments at .35R greater than 100 in-lbs, the coupling of elastic twist angle at 3/4 radius and blade lead-lag is such that an increase in lag angle is accompanied by an increase in blade pitch.

A static blade deflection test was performed on the Model 160, 5.5' diameter, stiff in-plane prop/rotor. The purpose of the test was to determine the blade shear center at 3/4 radius and the elastic couplings between blade elastic twist angle, blade flapping, and blade lag at 3/4 radius.

The test set-up is shown in Figure A-5. Loads were applied at the blade tip and linear and angular deflections were measured at 3/4 radius. During testing for shear center, loads of 5, 10, 15 pounds were applied perpendicular to the 3/4 radius chord-line. The chordwise position of the load application point was varied and the loading repeated. During testing for blade elastic coupling, the load application point was set at the measured shear center location and the direction of loading was varied from vertical to nearly horizontal with the blade angle at 3/4 radius nominally zero. The load was resolved into flapwise and chordwise bending moments at .35 radius. This is the radius location where the model blade is strain-gauged for flapwise and chordwise bending during wind tunnel testing. Under rotating conditions, the model blades operate in the quadrant of tension in the lower surface and tension in the leading edge. The test was conducted with tension in the lower surface and tension in the trailing edge to avoid buckling of the trailing edge. A summary of the test data is presented in Table A-2.

The results of the test for shear center are shown in Figures A-6 and A-7. The shear center at 3/4 radius for the left-hand blade was determined to be .375 chord \pm .01 chord. The shear center for the right-hand blade at 3/4 radius was determined to be .48 chord \pm .01 chord. Predicted shear center location for both blades was .25 chord. The large variation between predicted and measured shear center location is difficult to understand since the measured values are considered accurate within the stated tolerance. It is suspected that the crossply outer wrap contributes more than calculated for prediction. Also, the large variation in measured shear center location for the left and right-hand blades suggests that small differences in blade layup such as resin content contribute significantly to shear center location. This effect is not limited to differences between left and right-hand blades. Variation in resin content could also occur between the three blades on either rotor.

Figures A-8 and A-9 show the change in elastic twist angle at $3/4$ radius with applied flap and chord bending moments. A comparison of Figures A-8 and A-9 indicates that there is little difference in elastic twist change between the left and right-hand blades under the same loading conditions. The data in the quadrant of tension in the lower surface and tension in the leading edge was extrapolated from the test data. Typical wind tunnel test data for the subject blades are shown in Figure A-8. The arrow indicates the general direction of alternating flap and chord bending for that condition. For the hover condition with 3° cyclic pitch, the change of angle of attack at $3/4$ radius oscillates $+0^\circ$, -4° from an average of $+1.6^\circ$. As the cyclic pitch increases to its maximum value, there is no elastic contribution to angle of attack change. As the cyclic pitch decreases to its minimum value, there is an additional decrease of -1.4° due to elastic coupling. For the hover condition without cyclic, the change in angle of attack due to elastic coupling varies $+1.4^\circ$, -1.5° from an average value of $+1.3^\circ$. As the blade flaps up and lags, the angle of attack increases; and as the blade flaps down and leads, the angle of attack decreases. Although the range of alternating flap and chord bending moments are smaller for this case than for the hover case with 3° cyclic, the oscillatory change in angle of attack at $3/4$ radius due to elastic coupling is twice as large. It can be concluded that the aerodynamic forcing function acting on the rotor governs to a large extent the effect of elastic coupling on oscillatory change in angle of attack due to elastic coupling whereas wing-rotor interference or a random forcing function seems to maximize the gradient of elastic angle of attack change.

Elastic pitch-flap coupling results are shown in Figures A-10 and A-11. The data illustrates that the blades have a positive elastic δ_3 effect. As the flapping angle increases, the elastic twist angle at $3/4$ radius decreases. A comparison of Figures A-10 and A-11 indicates that elastic pitch-flap coupling is the same for left and right-hand blades.

Figures A-12 and A-13 show the effect of applied moments on blade lag angle at $3/4$ radius. Loading the blade to produce tension in the lower surface and tension in the trailing edge caused the blade to deflect in a positive lag direction. As the loading was increased, the lagging deflection became zero. For chord bending moments above 100 in-lbs, the blade deflected forward (negative lag). Deflection of the blade opposite in direction to the load is difficult to understand. The high twist and high in-plane stiffness probably contribute significantly to this effect.

Figures A-14 and A-15 show the elastic pitch-lag coupling results. As the loading increases, the ratio of elastic twist angle at $3/4$ radius to elastic lag angle at $3/4$ radius increases. This effect is caused by a negative increase in pitch angle and a decrease in lag angle with increased loading even though the sign of the lag angle is positive.

Conclusions and Recommendations

- a. The blade deflection test served to give insight into the elastic couplings of highly twisted prop/rotors. It is emphasized that the test blades were stiff in-plane and that conclusions concerning soft in-plane rotors should not be drawn from the data presented. An elastic coupling test on a soft in-plane rotor is presently in progress and the data should serve as a comparison with the stiff in-plane data presented.
- b. The analytical determination of shear center location should be reviewed to ascertain the difference between predicted and measured values.
- c. Differences in resin content and resin flow should be carefully considered during fiberglass blade construction.
- d. Any further tests of blade elastic couplings should employ the use of strain gauges to measure bending moments. This method would reduce test time, ease data reduction and eliminate errors in extrapolation of bending moments between two spanwise stations. Further tests should also include more spanwise stations to determine the dependence of elastic coupling on blade station.

Sta r/R	C Chord Distr.	θ Twist in Degr.	P.A. S.C.		C.C. From L.E.	#/in Wt Per Inch	$EI_{\xi} \times 10^6$		I_p		I_p^*		$GJ \times 10^6$ Tor. Stif.
			Pitch Axis About L.E.	Shear Cent. About L.E.			(Flap)	(Chord)	Lb In ² In	Lb In ² In	Lb In ² In	Lb In ² In	
1.00	2.31	-10°	.576	.576	.517	.01194	.001286	.15255	.0040	.0039	.0039	.0039	.0039
.90	2.5594	-5.7°	.639	.639	.604	.01312	.001628	.20875	.0054	.0053	.0053	.0053	.0040
.80	2.8088	-1.6°	.704	.704	.667	.01578	.00353	.316751	.0081	.0079	.0079	.0079	.00460
.70	3.0582	1.6°	.765	.765	.722	.01886	.008001	.403241	.0102	.0099	.0099	.0099	.00473
.60	3.3077	4.8°	.826	.826	.812	.02491	.014912	.645071	.0418	.0144	.0144	.0144	.00825
.50	3.5571	8.14°	.889	.889	.841	.02997	.028518	1.047901	.0255	.0248	.0248	.0248	.01040
.40	3.803	11.8°	.951	.951	.896	.03727	.0648	2.2097	.0378	.0361	.0361	.0361	.01970
.30	4.0559	15.7°	1.016	1.016	1.23628	.04181	.114735	3.37158	.0499	.0471	.0471	.0471	.0290
.2575	4.1500	18.5°	1.05	1.05	1.471376	.14912	.3127	4.2347	.0832	.0785	.0785	.0785	.62
.22	4.2450	21.5°	1.1	1.1	1.593	.1637	.4100	4.6986	.0672	.0588	.0588	.0588	.79
.17	4.3750	27.0°	1.12	1.12	1.12	.283	1.155	3.04	.0302	.0291	.0291	.0291	1.435
.14	Round Shaft					.283	3.66	3.66					
.10	Hub					∞	∞	∞					

$K_{\theta} = K_{\xi} = 250,000 \frac{\text{in-lb}}{\text{rad}}$ at 14% (elas. brg.)

TABLE A-1 1/10 SCALE MODEL 160 CYCLIC BLADE
PHYSICAL PROPERTIES

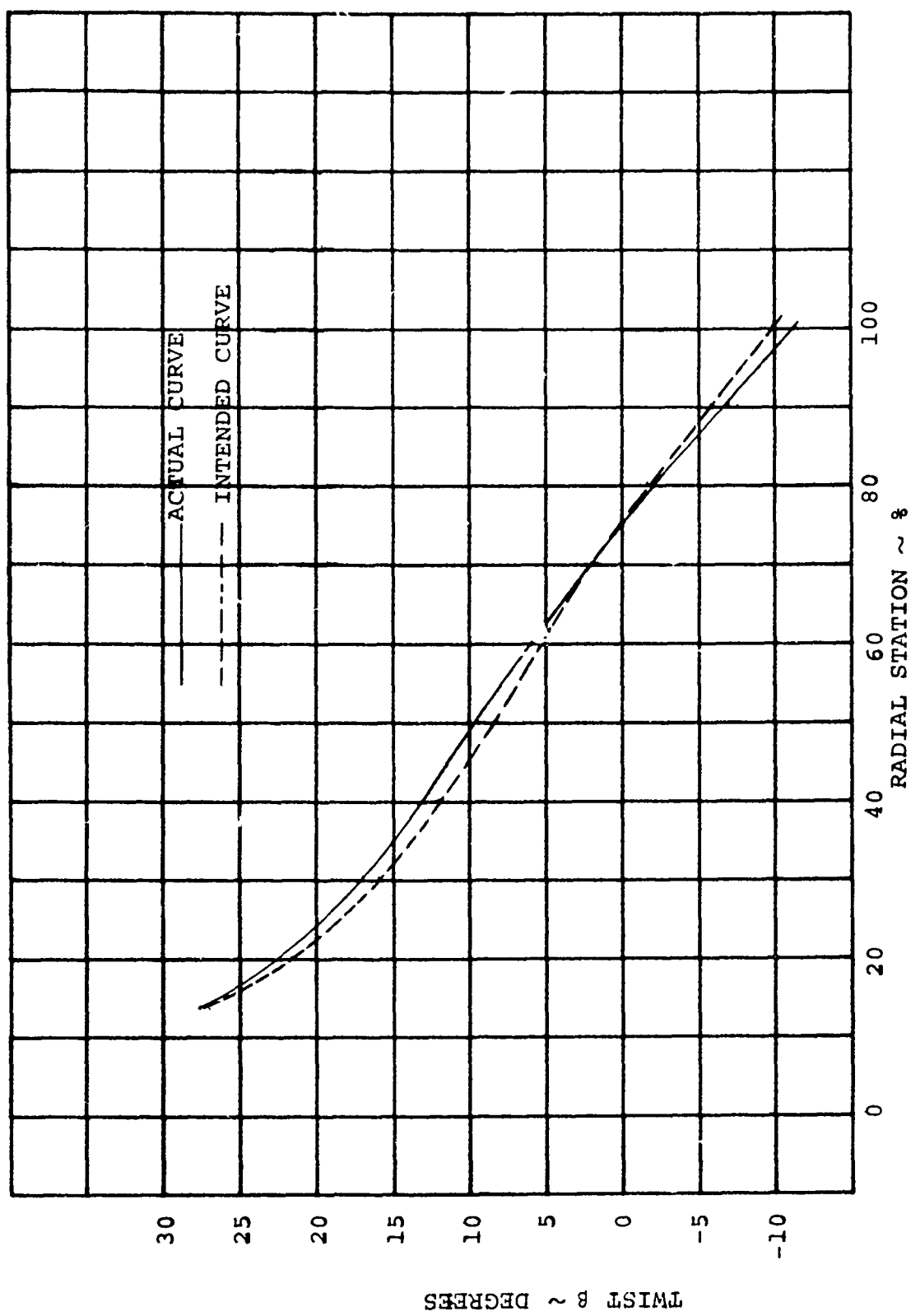


FIGURE A-1 MODEL 160 ATKINS & MERRILL BLADE TWIST

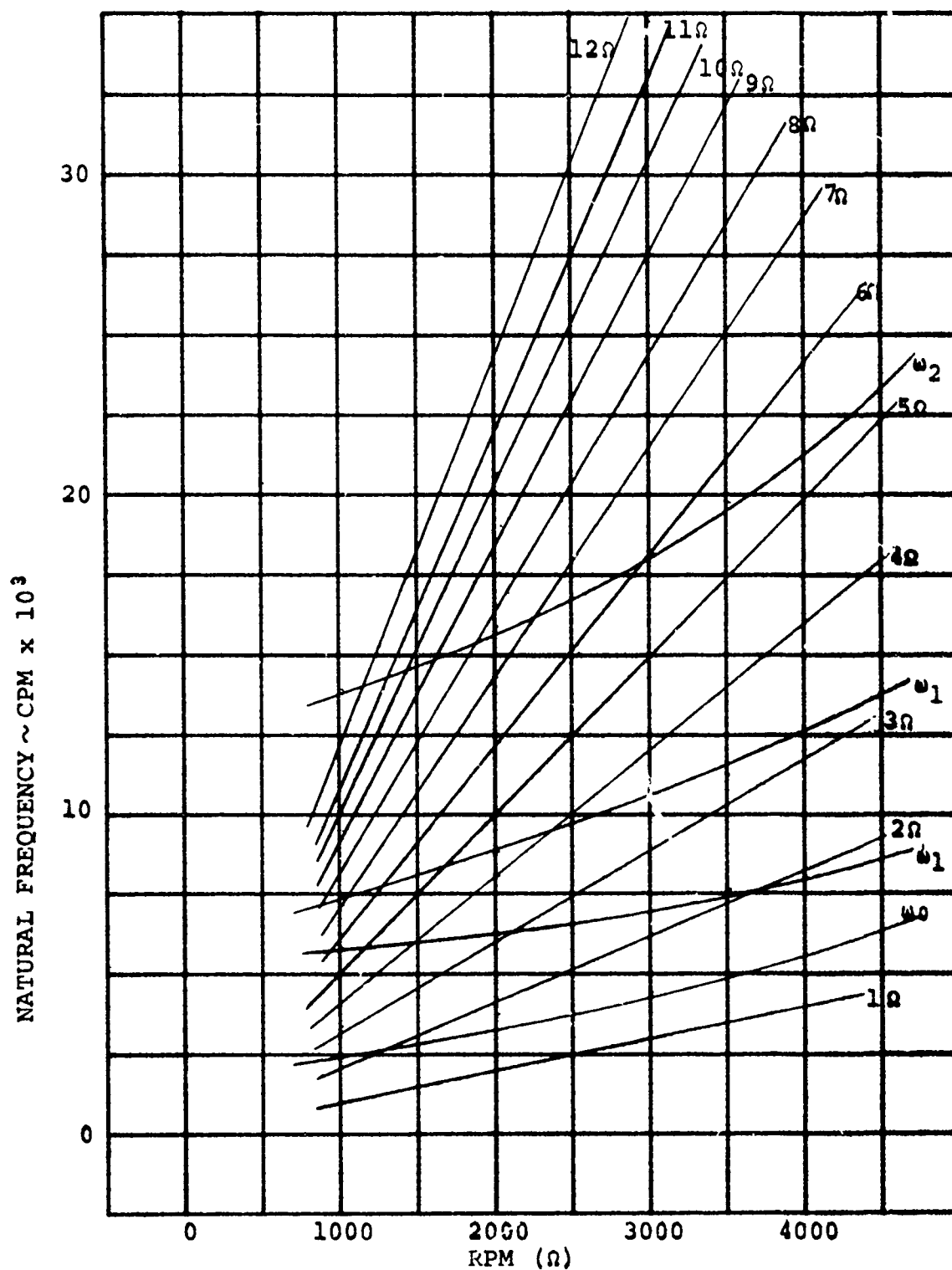


FIGURE A-2 1/10 SCALE MODEL 160 CYCLIC PROP BLADE
COUPLED FLAP AND CHORD NATURAL FREQUENCIES
 $K_B = K_\delta = 250 \times 10^3$

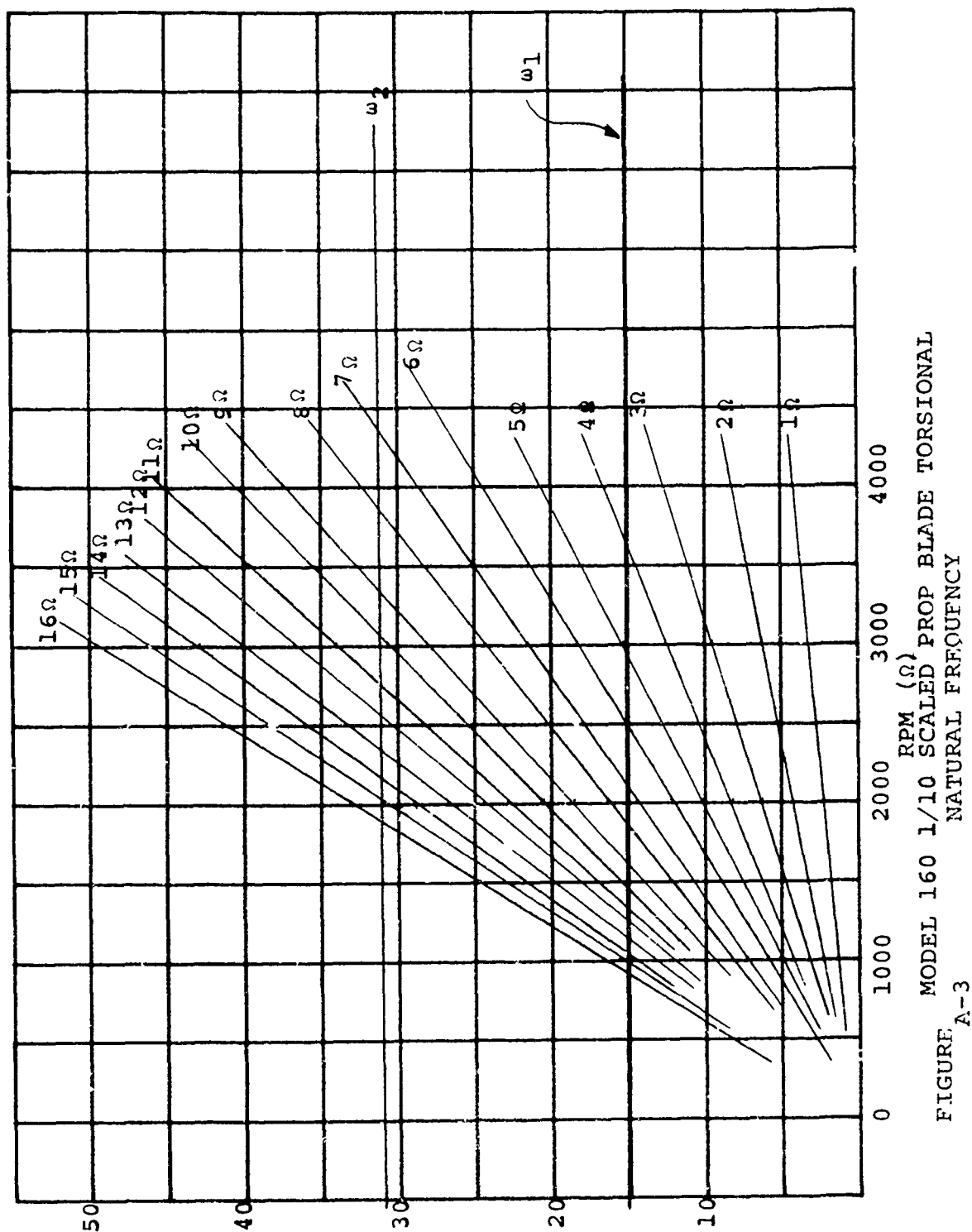


FIGURE A-3
MODEL 160 1/10 SCALED PROP BLADE TORSIONAL
NATURAL FREQUENCY

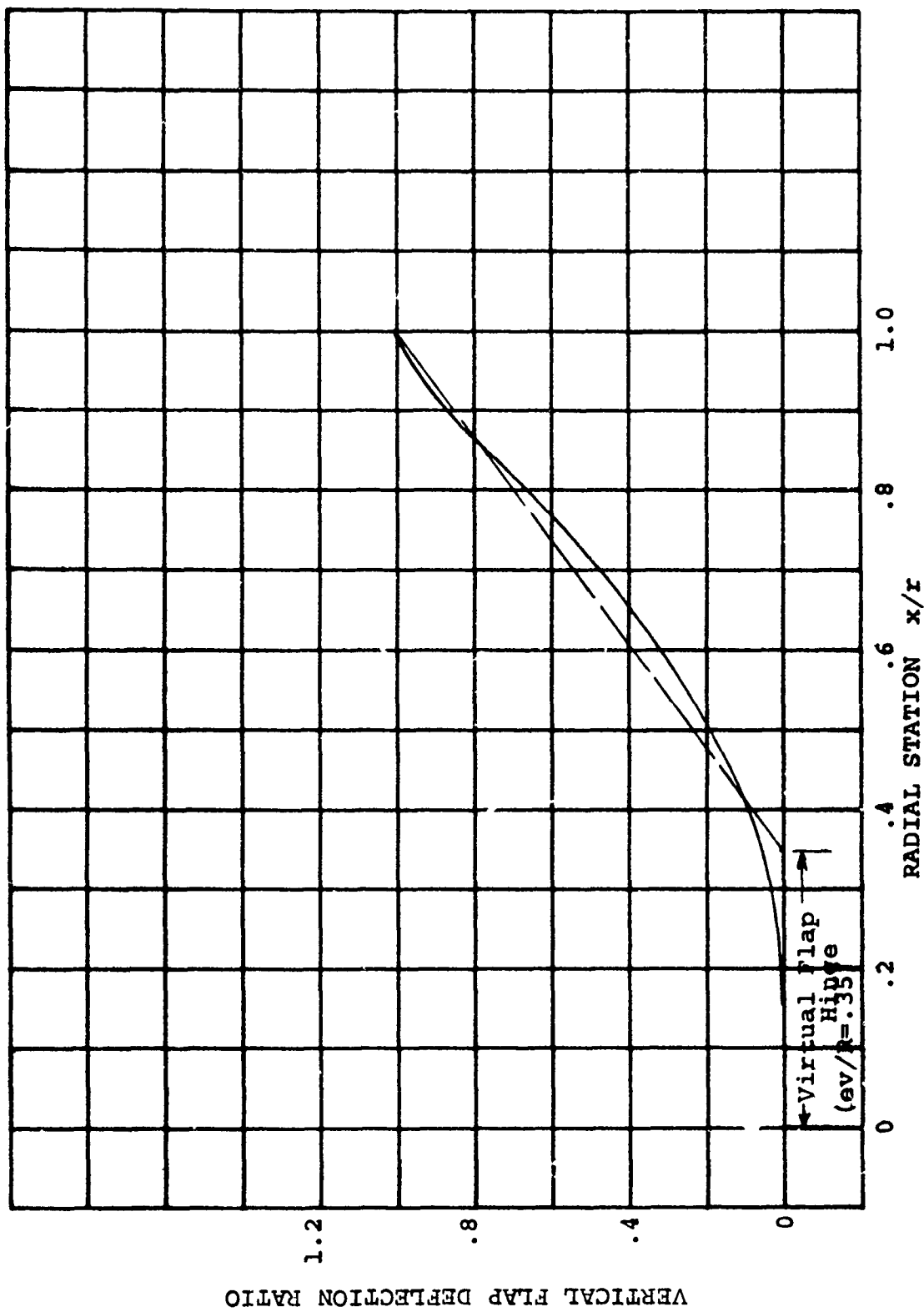
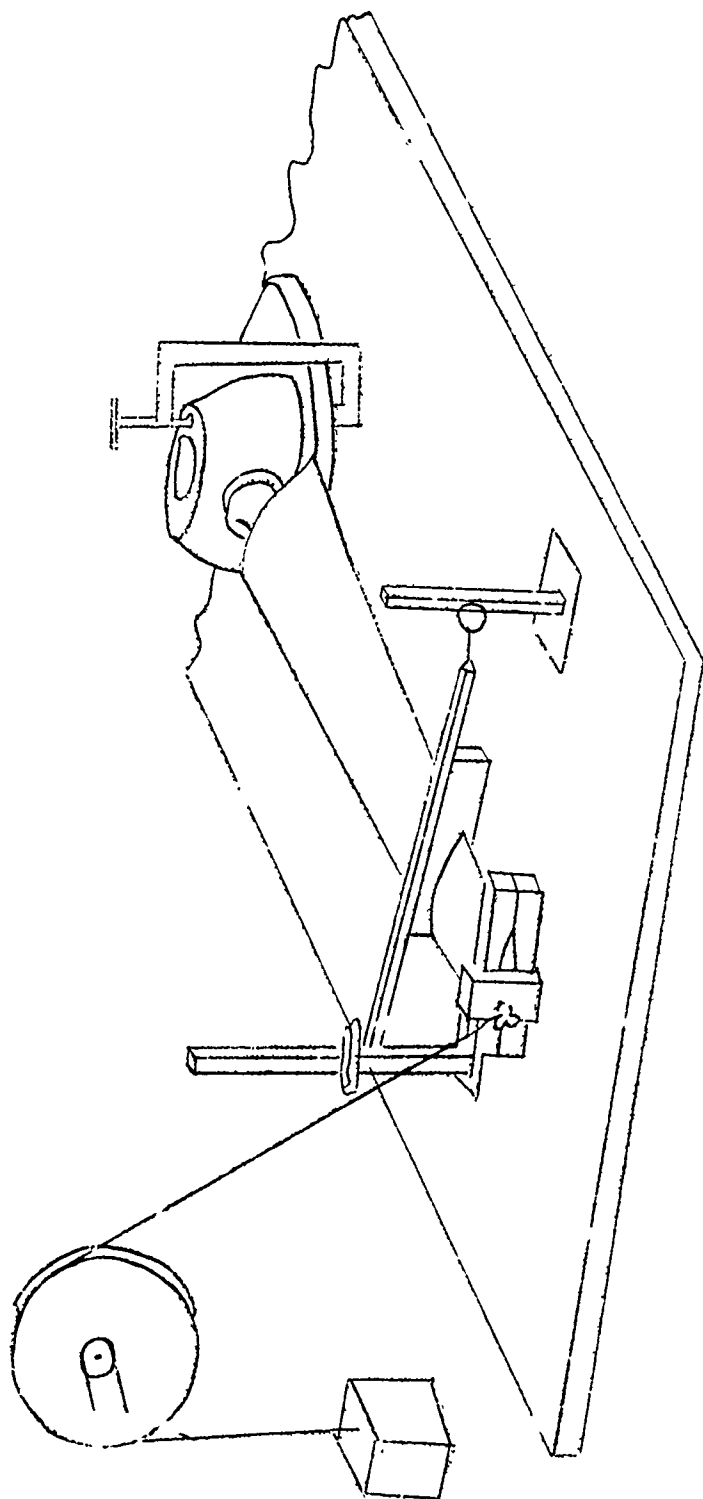


FIGURE A-4. FIRST MODE BENDING - DEFINITION OF VIRTUAL FLAP HINGE



STATIC BLADE DEFLECTION
TEST SETUP

FIGURE A-3

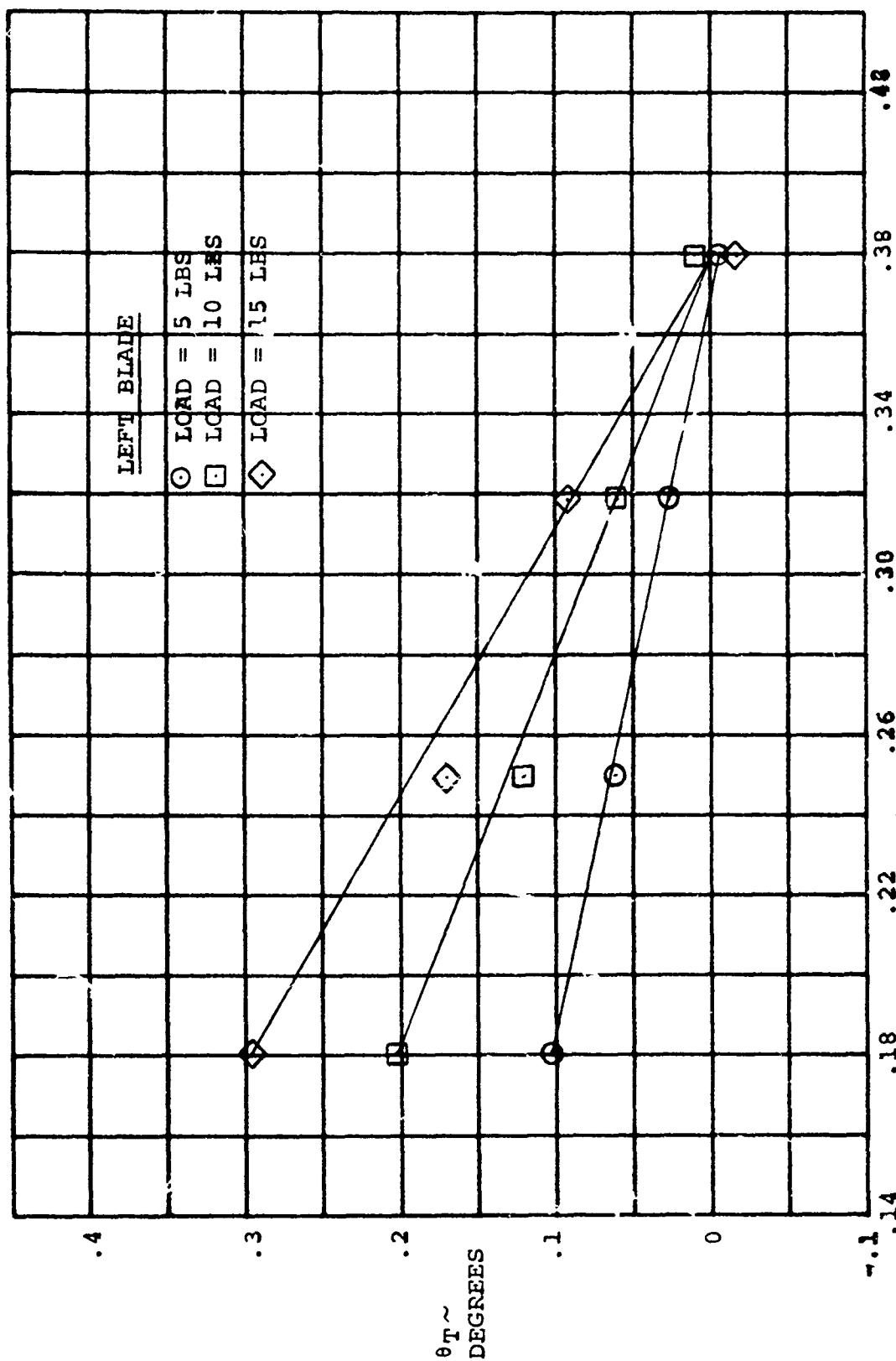


FIGURE A-6 LEFT HAND BLADE SHEAR CENTER DETERMINATION

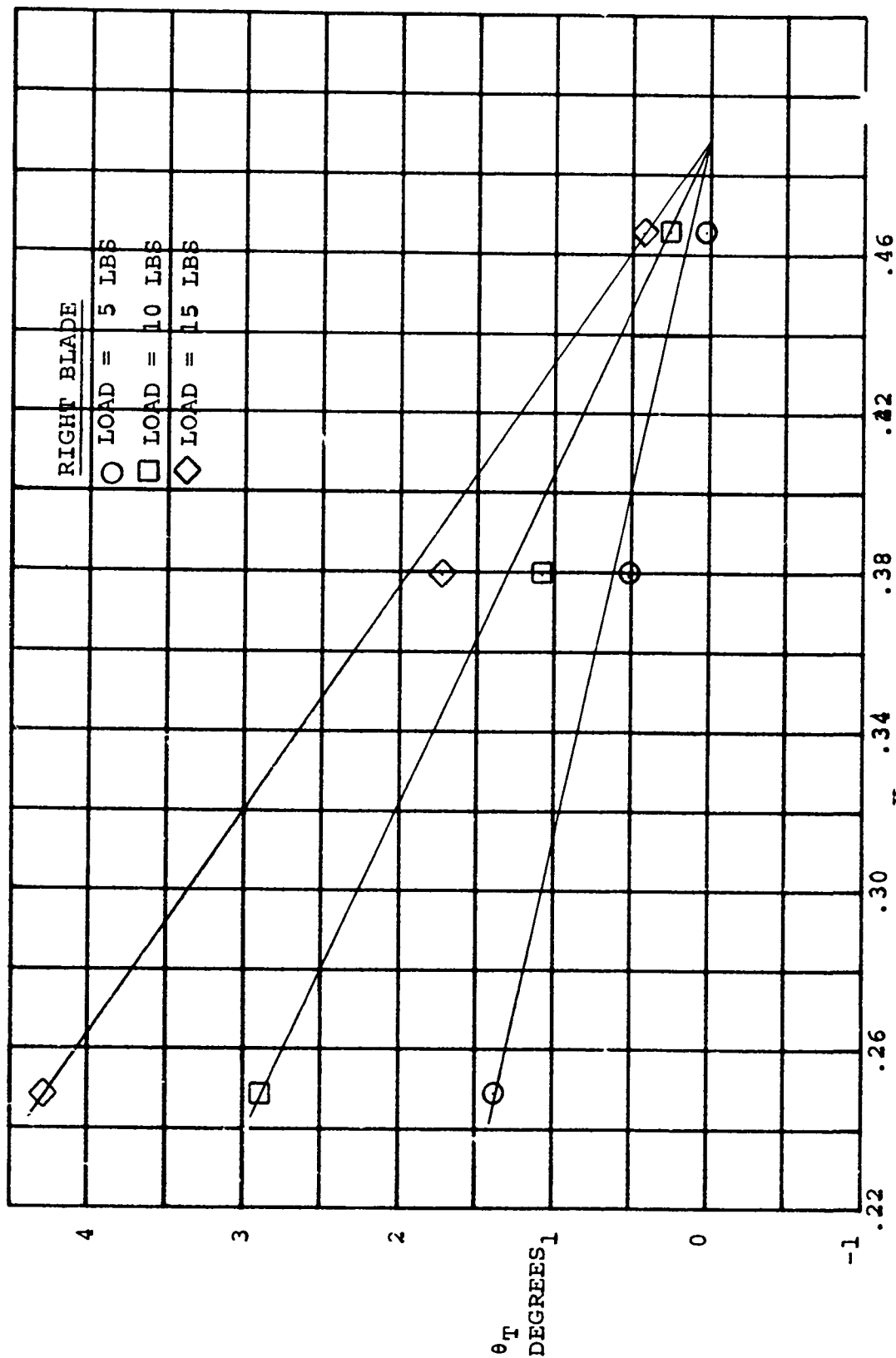


FIGURE A-7 RIGHT HAND BLADE CHORD AT .75R
DETERMINATION

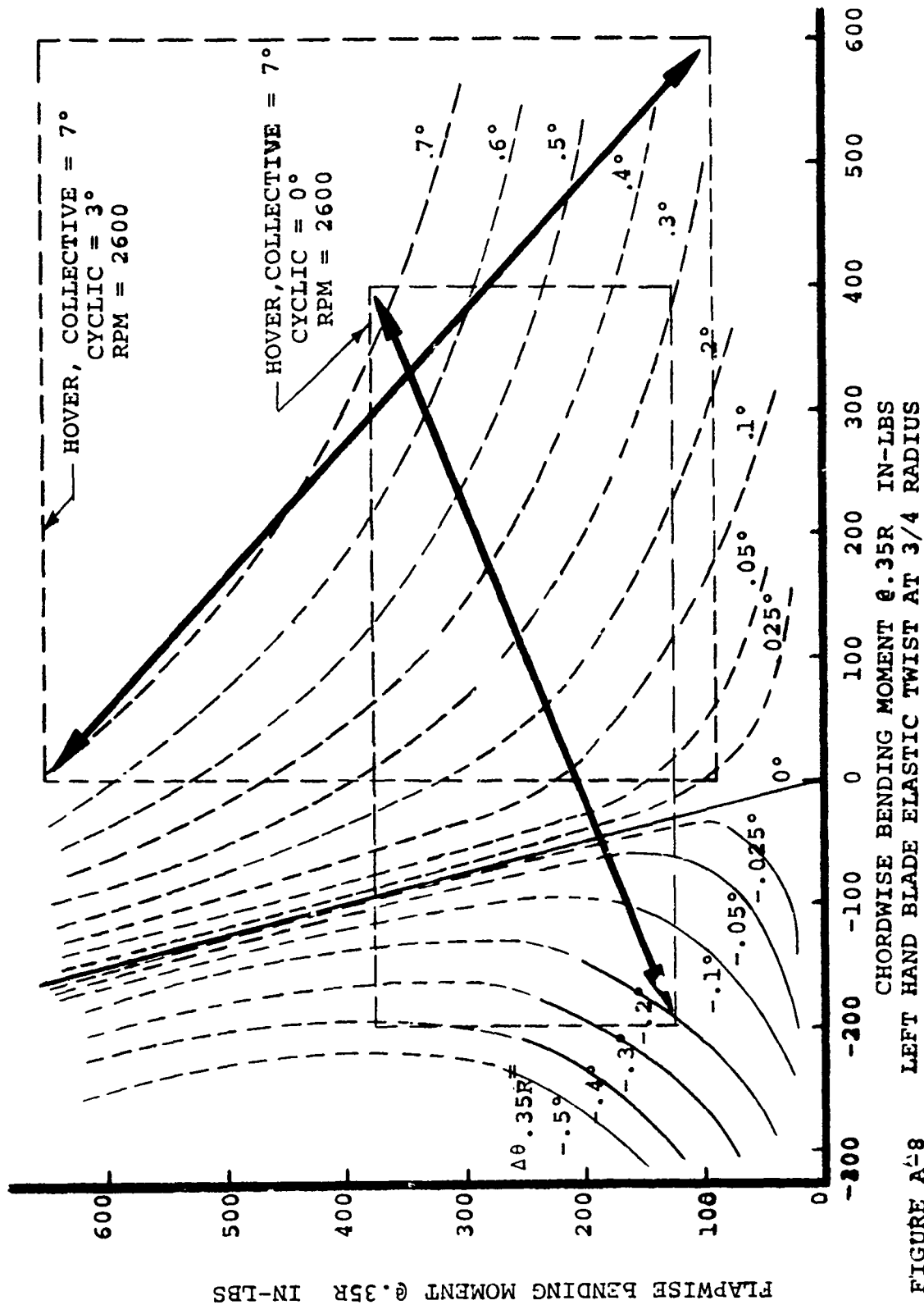


FIGURE A-8

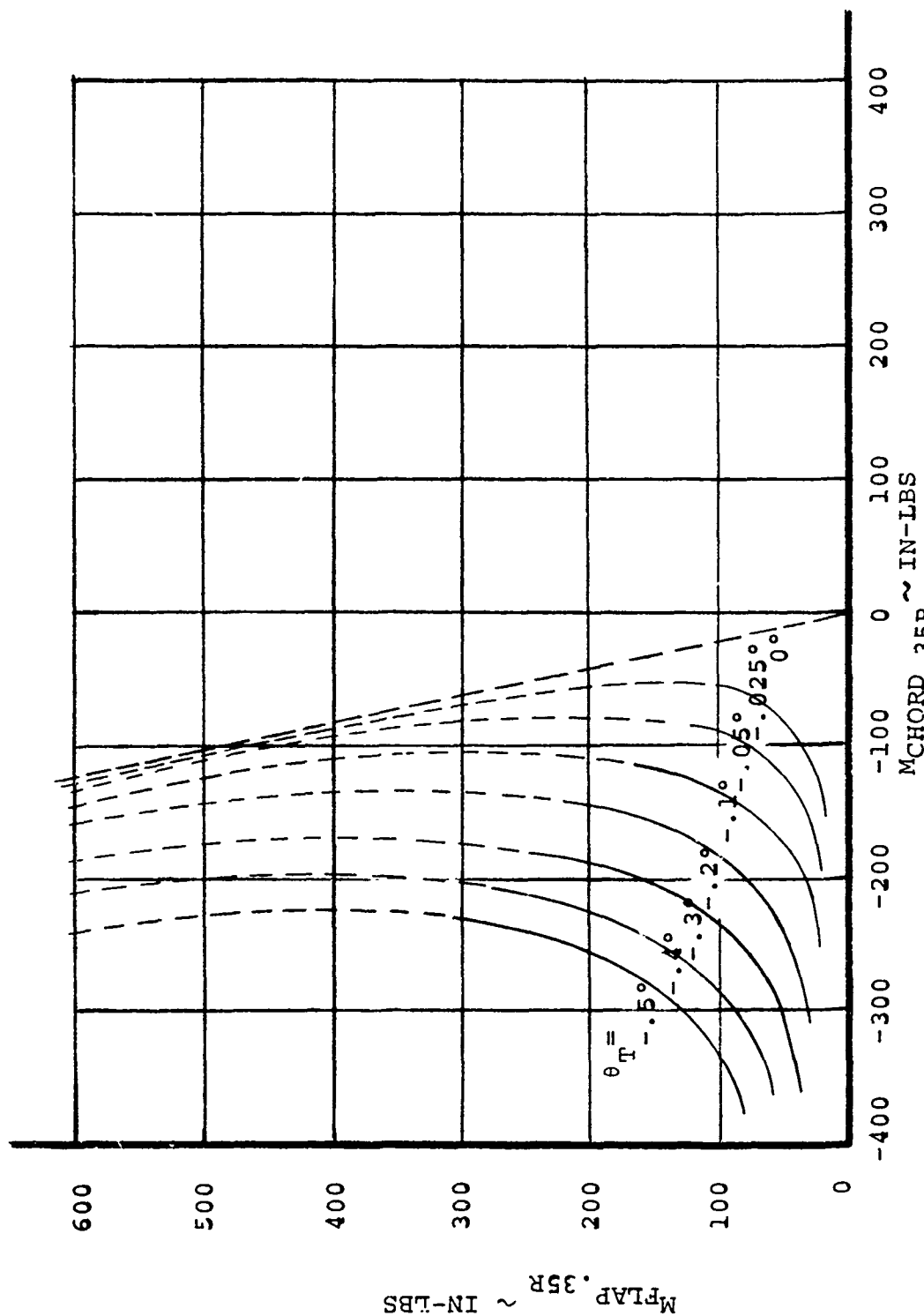


FIGURE A-9 RIGHT HAND BLADE ELASTIC TWIST AT 3/4 RADIUS

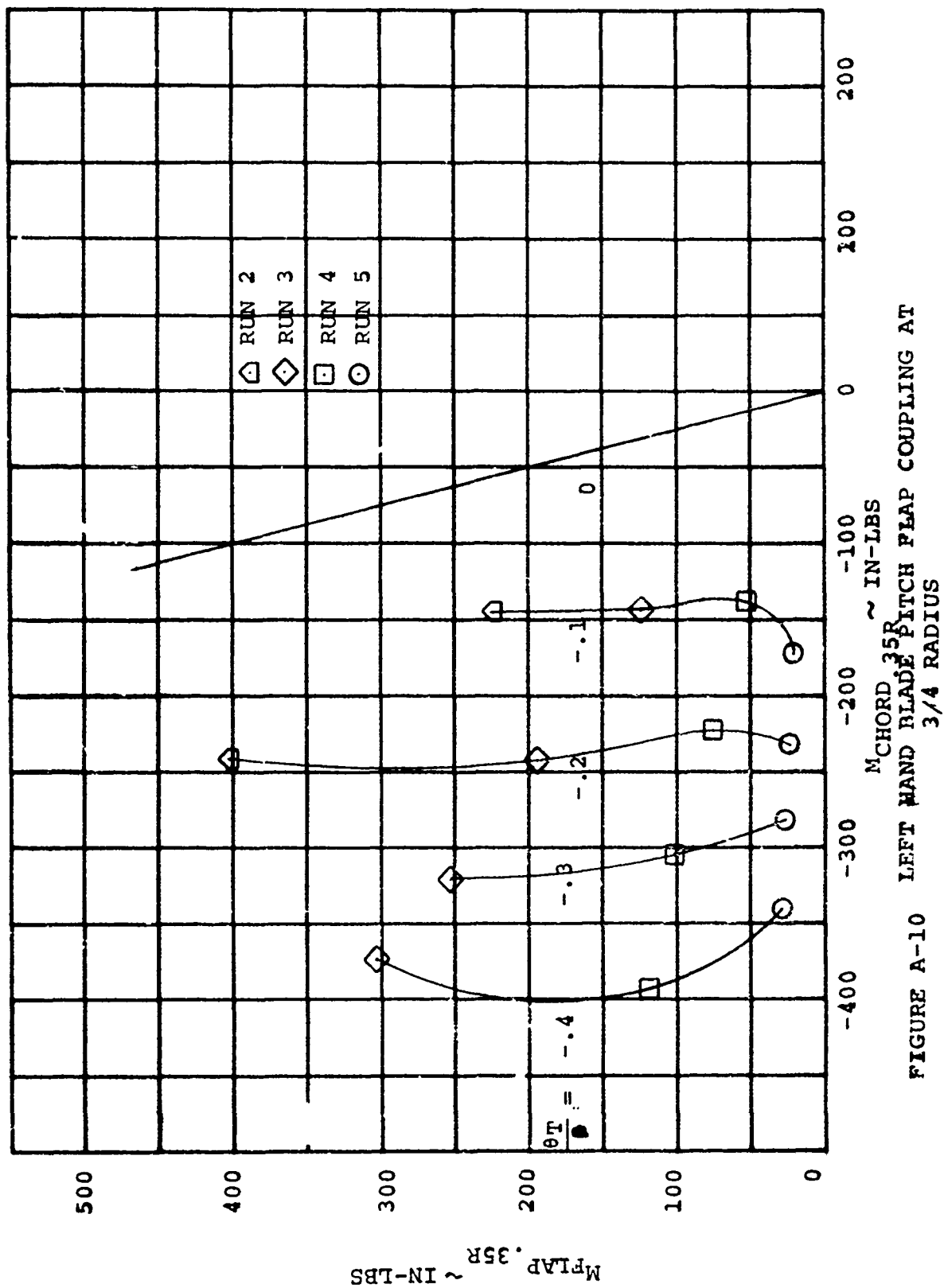


FIGURE A-10 LEFT HAND BLADE PITCH FLAP COUPLING AT $\frac{3}{4}$ RADIUS

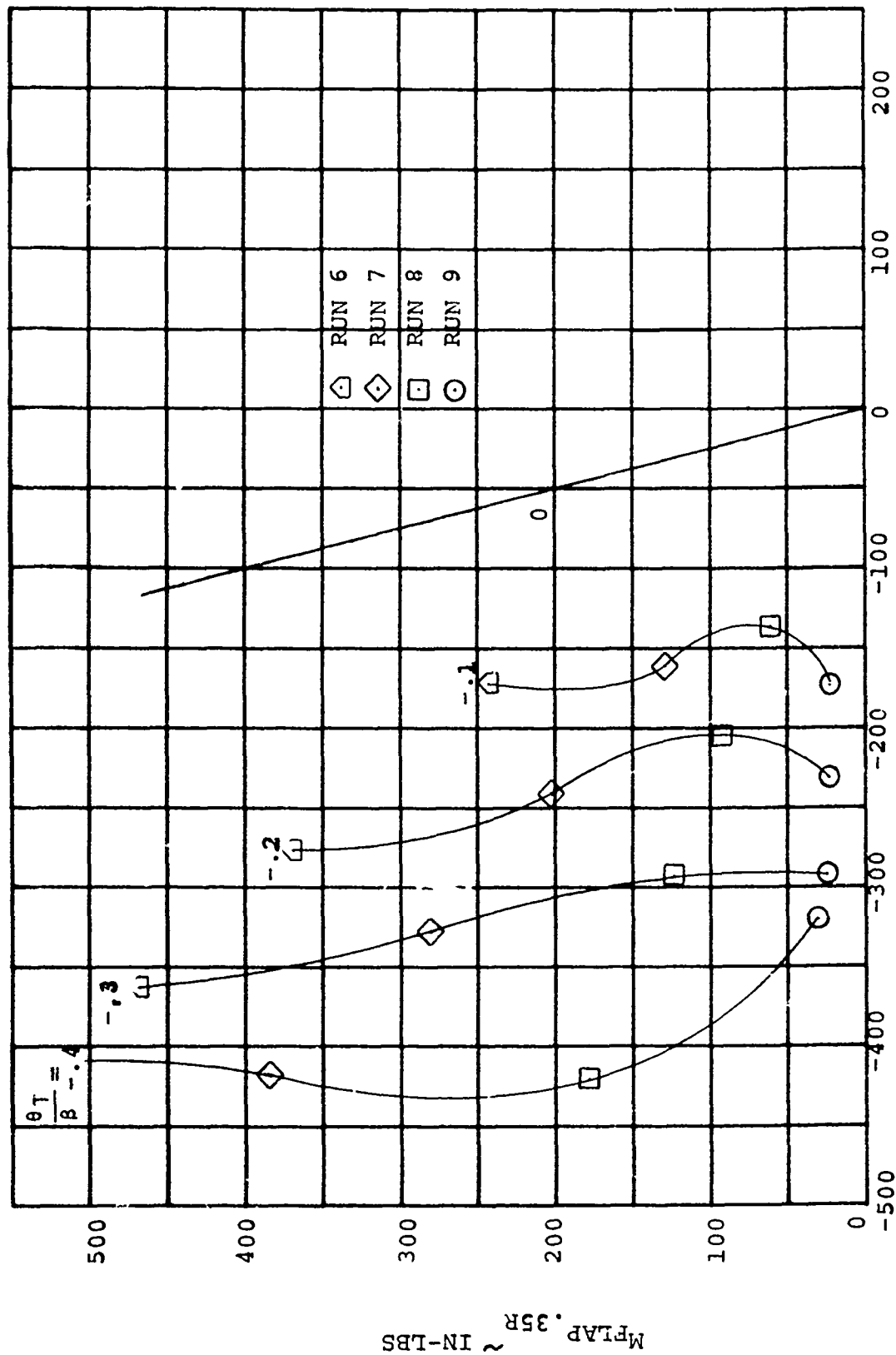


FIGURE A-11
RIGHT-HAND BLADE PITCH FLAP COUPLING
AT $3/4$ RADIUS
MCHORD.35R ~ IN-LBS

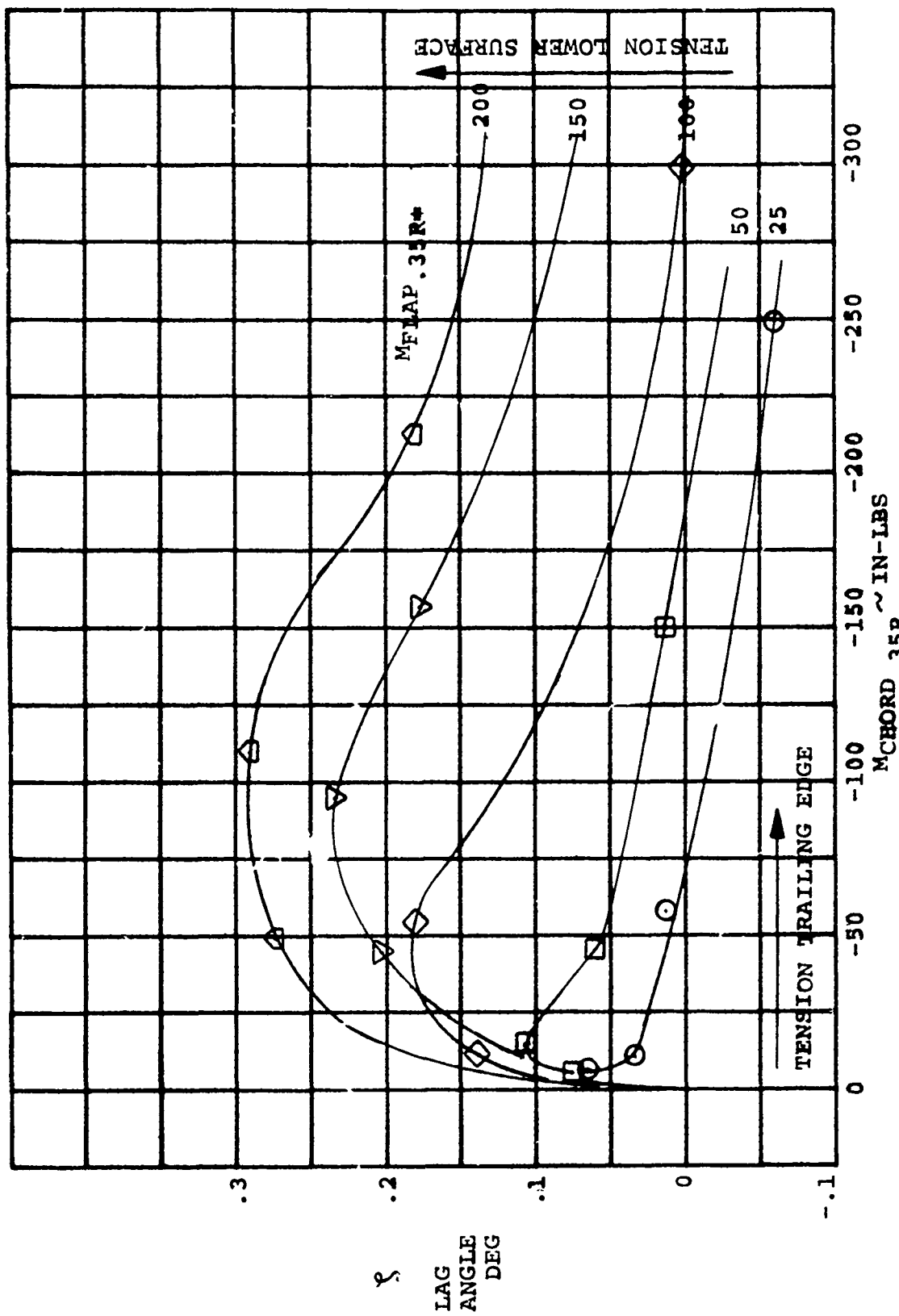


FIGURE A-12 LEFT HAND BLADE LAG ANGLE

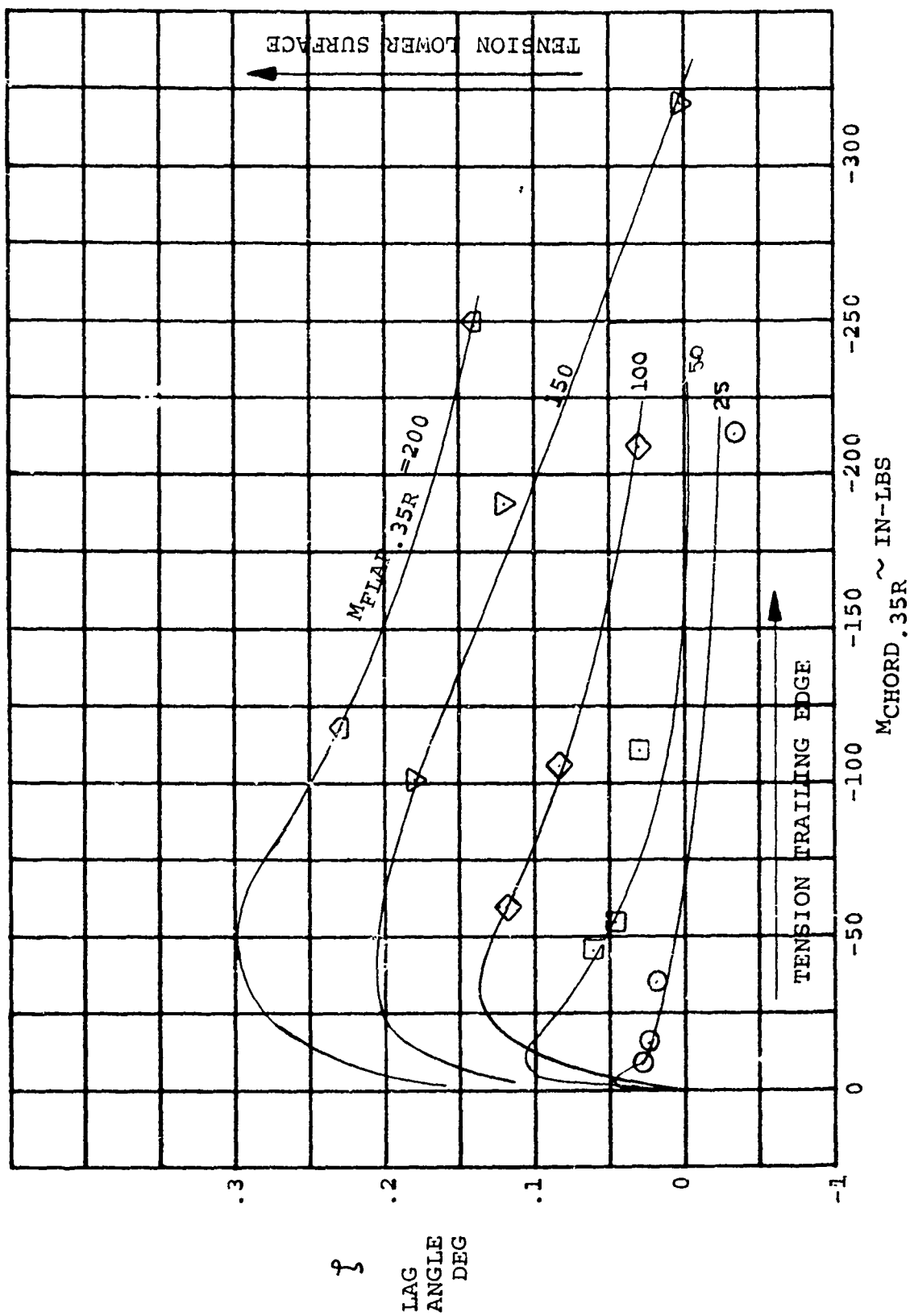


FIGURE A-13 RIGHT HAND BLADE LAG ANGLE

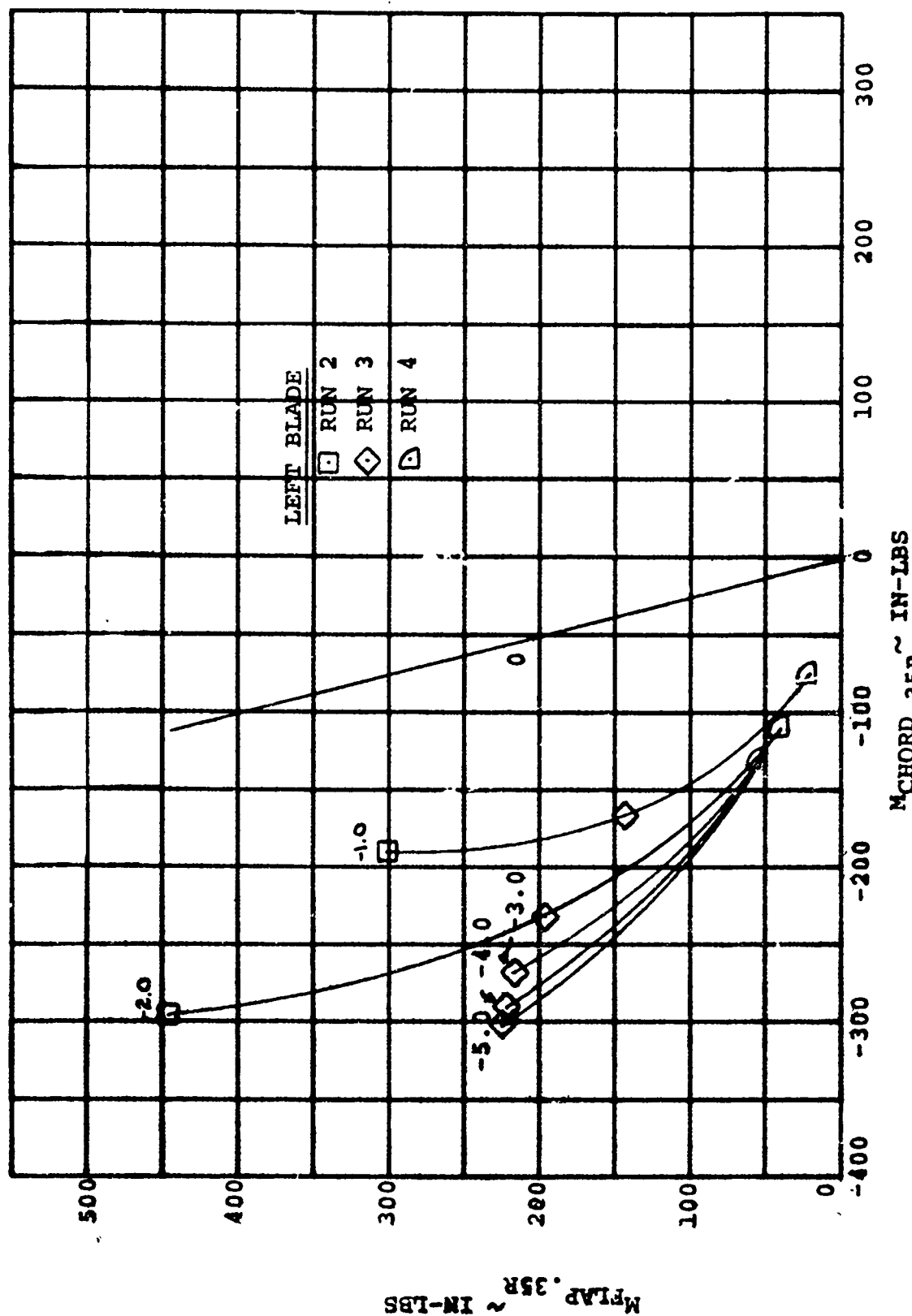


FIGURE A-14 LEFT HAND BLADE PITCH LAG COUPLING AT 3/4 RADIUS

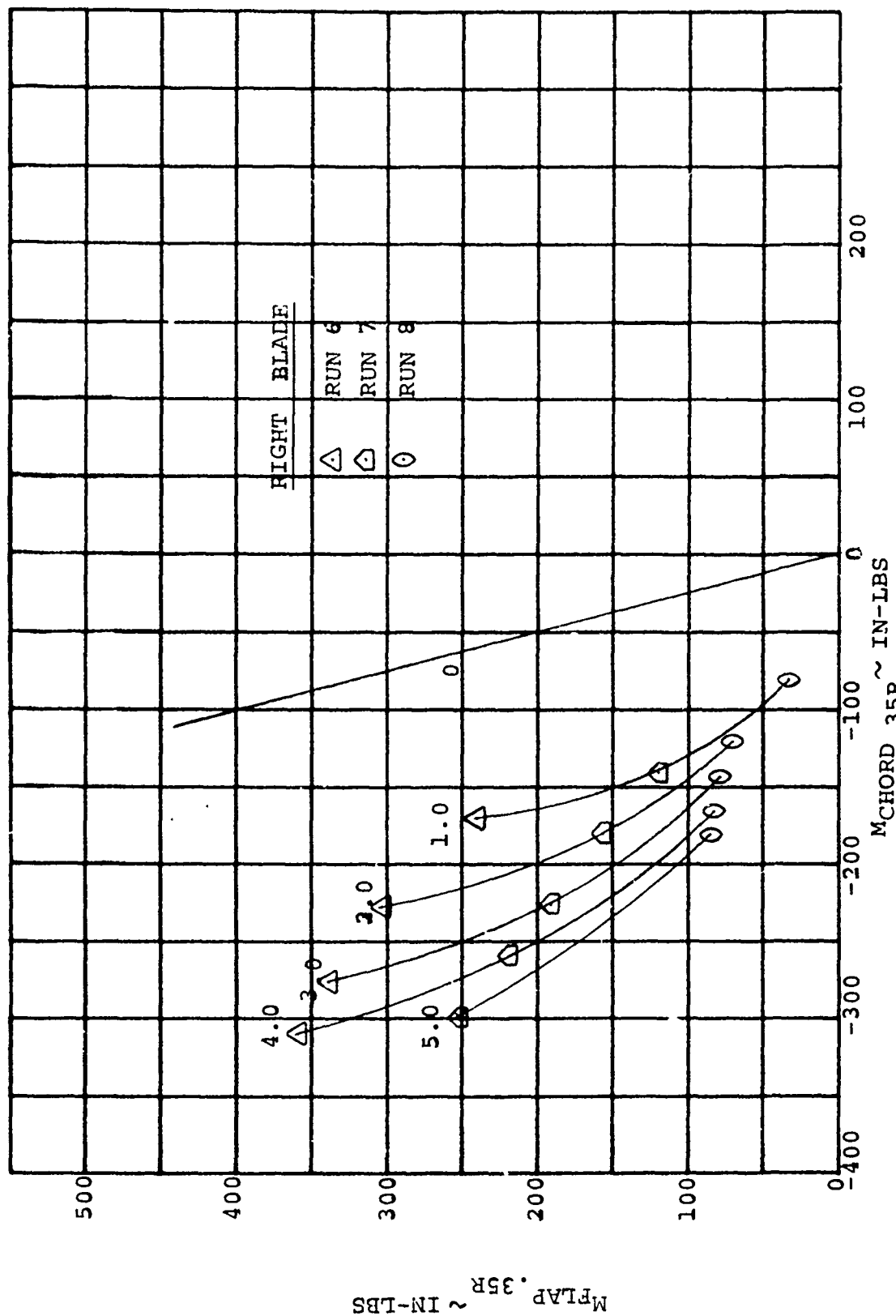


FIGURE A-15 RIGHT HAND BLADE PITCH HAG COUPLING AT $\frac{3}{4}$ RADIUS

BLADE	RUN NO.	M FLAP .75 R. (IN-LBS)	M CHORD .75 R. (IN-LBS)	M FLAP .35 R. (IN-LBS)	M CHORD .35 R. (IN-LBS)	δ LAG (IN.)	TAN δ LAG (DEGREES)	θ (DEGREES)	$\frac{\theta}{f}$	δ FLAP (IN)	β TAN-1 FLAP 17.16	$\frac{\theta}{\beta}$
LEFT HAND	1	47.49	-0.37	110.13	-27.46	+0.51	+1.543	-0.023	-0.149	.321	1.017	.0182
		95.00	-0.97	220.25	-54.95	+0.95	+2.2674	.0029	+0.101	.631	2.1089	.0014
		142.50	-0.88	330.37	-82.42	+1.17	+4.447	.0029	+0.065	.931	3.1055	.0007
	2	45.48	-13.70	97.82	-57.55	+0.60	+1.815	-0.0332	-0.1829	.295	.9847	.0337
		90.65	-28.42	194.35	-117.27	+0.94	+2.844	-0.1455	-0.5116	.572	1.9092	.0162
		35.45	-44.30	289.36	-179.50	+1.127	+3.872	-0.3581	-0.9321	.827	2.7591	.1299
	3	38.54	-27.77	78.19	-68.43	+0.31	+0.933	-0.0406	-0.4328	.233	.7119	.0522
		76.00	-57.01	144.16	-175.35	+0.58	+1.755	-0.1839	-1.0479	.447	1.4922	.1132
		113.09	-26.72	213.45	-265.30	+0.55	+1.664	-0.4770	-2.9988	.654	2.1876	.1286
	4	25.25	-39.85	37.45	-107.14	+0.05	+0.151	-0.0309	-2.0464	.137	.4574	.0676
		50.96	-80.17	72.94	-214.96	+0.05	+0.151	-0.1741	-1.5298	.267	.8914	.1253
		75.74	-120.70	107.52	-333.06	-0.005	-0.051	-0.4205	-27.8477	.384	1.2819	.3280
RIGHT HAND	5	16.27	-44.63	12.51	-112.81	-0.005	-0.0151	-0.0074	+0.4901	.064	.2137	.0319
		32.13	-89.40	23.99	-225.73	-0.019	-0.0575	-0.0813	+1.4139	.126	.4207	.032
		46.81	-134.60	32.50	-338.95	-0.032	-0.0968	-0.2389	+2.4660	.180	.6010	.3978
	6	44.11	-16.21	93.81	-62.99	+0.35	+1.059	-0.0287	-0.2710	.323	1.0783	.0266
		87.72	-33.77	185.68	-128.84	+0.75	+2.269	-0.1341	-0.5910	.627	2.0946	.0641
		130.75	-52.79	275.35	-197.76	+0.86	+2.602	-0.3702	-1.4228	.912	3.0442	.1216
	7	38.62	-26.79	74.95	-84.56	+0.22	+0.666	-0.0143	-0.2147	.265	.8347	.0162
		76.15	-55.12	146.48	-172.10	+0.39	+1.180	-0.2005	-1.6992	.519	1.7324	.1157
		113.23	-84.02	216.63	-260.73	+0.46	+1.392	-0.5536	-3.9770	.753	2.5126	.1253
	8	28.95	-37.02	46.54	-102.97	+0.09	+0.272	-0.0401	-1.4743	.187	.6244	.0642
		57.51	-74.35	92.01	-206.41	+0.11	+0.333	-0.2435	-7.3123	.359	1.1825	.1252
		85.57	-112.06	136.06	-310.48	+0.05	+0.151	-0.5467	-36.2054	.520	1.7357	.1250
9		16.13	-44.14	12.54	-112.30	-0.010	-0.0303	.0046	-0.1518	.078	.2604	.0177
		31.76	-88.47	23.81	-224.73	-0.020	-0.0605	-0.0911	+1.5058	.146	.4875	.1869
		47.07	-132.91	34.27	-337.28	-0.037	-0.1119	-0.2578	+2.3038	.204	.6811	.3785

TABLE A-2 TEST DATA SUMMARY FOR BLADE SHEAR AND ELASTIC COUPLING TEST

APPENDIX B

STATIC DISTURBANCE TESTS

Background

The static natural frequencies and damping of the model on its balance and also the influence of the sting mounting are required in order to analyze oscillatory phenomena such as long-period forces and moments measured in hover. The blade tweek data provide the natural frequencies of the rotor blades at zero RPM and are correlated against blade predictions.

Test Technique

The model was caused to oscillate at its natural frequency by a sharp rap with a rubber mallet so as to produce as pure a response as practically possible in the desired direction. The response was measured using CEC traces enabling the frequency and damping to be obtained. This procedure was performed for all six components of the fuselage balance. Blade tweeks were performed by deflecting the blade tip in flapwise, chordwise and torsion directions relative to 35% radius station. Blade strain gauges were used to record the blade response. These tests were performed at intervals throughout the test program.

Further disturbance tests were performed to excite the sting deflection modes where the excitation was applied aft of the model. The difference between these tests and the model disturbance tests is shown schematically in Figure B-1.

Test Data

The frequencies and damping for the uninstrumented blades obtained from the static disturbance tests are given in Tables B-1 and B-2 and compared with the pretest calculated frequencies. The natural frequencies and damping of the model on its balances excited as shown in Figure B-1 are given in Tables B-3 and B-4. The data obtained when the excitation was applied to the sting are given in Tables B-5 and B-6, and the nacelle balance data are tabulated in Table B-7.

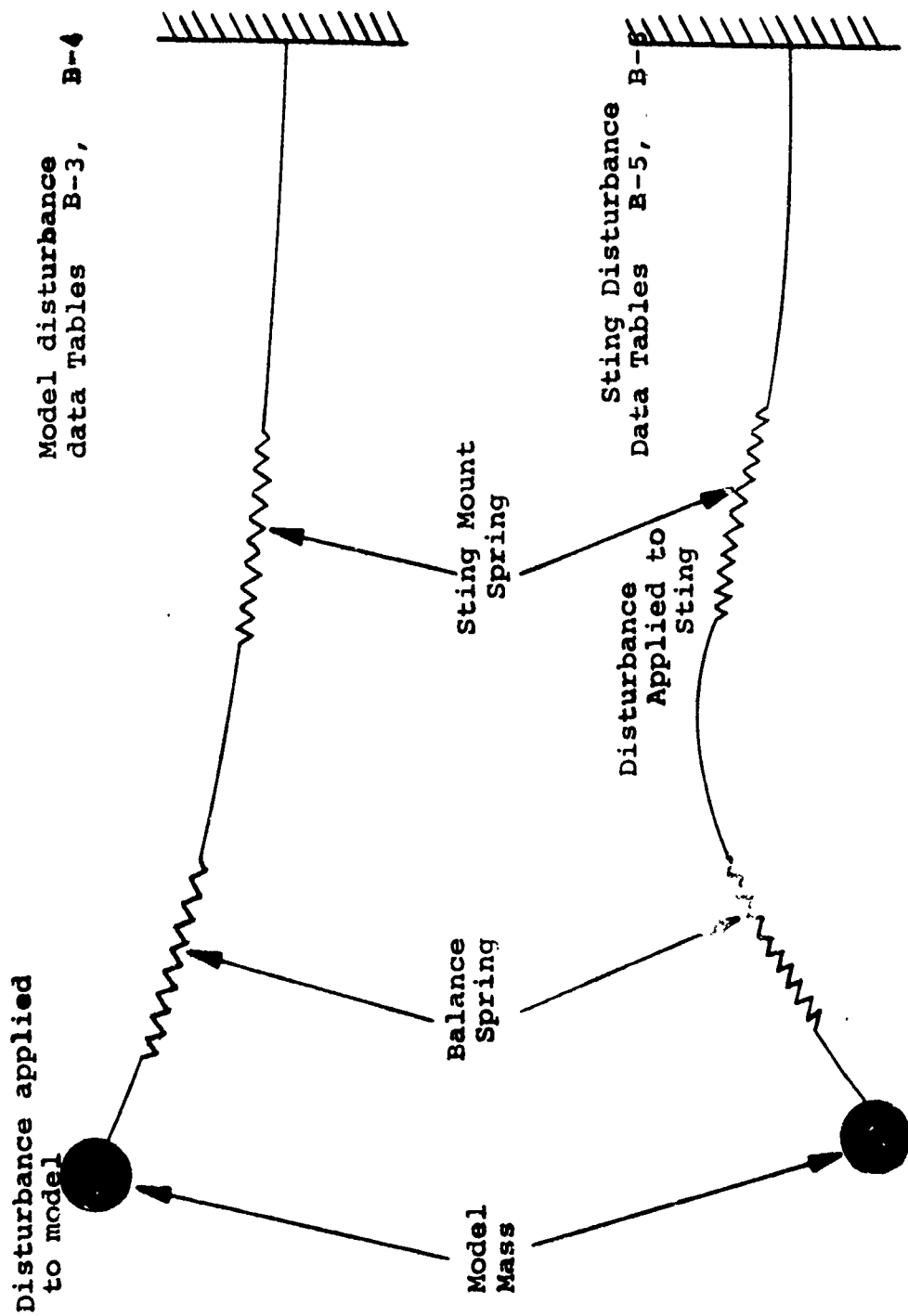


FIGURE B-1 SCHEMATIC OF MODEL-STING MODES

DATE	RUN NO.	FLAP BENDING		CHORD BENDING		TORSION	
		FREQ.	DAMPING	FREQ.	DAMPING	FREQ.	DAMPING
8/20	PRE-TEST	24.5	1.42	81.0	0.34	258	0.32
8/26	0	24.5	0.842	86.6	0.56	259	0.22
8/27	2	24.6	1.295	82.0	0.44	256	0.234
8/29	14	23.9	0.85	84.0	-	264	0.289
9/2	56	24.2	1.24	81.0	0.265	262	0.241
Predicted		30.0	-	86.0	-	250	-

- NOTES: 1. Response data obtained from strain gauges at $r/R = 0.35$
2. Frequencies in hertz, damping % critical

TABLE B-1

STATIC DISTURBANCE DATA -
RIGHT-HAND ROTOR BLADE DATA

DATE	RUN NO.	FLAP BENDING		CHORD BENDING		TORSION	
		FREQ.	DAMPING	FREQ.	DAMPING	FREQ.	DAMPING
8/26	2	25.5	0.63	94.0	1.1	264	-
9/2	56	25.7	0.925	91.0	0.33	278	.251
9/3	72	25.2	0.99	89.0	-	268	.366
Predicted		30.0	-	86.0	-	250	-

- NOTES: 1. Data obtained from strain gauge
at $r/R = .35$
2. Frequencies are in hertz damping
% critical

TABLE B-2

STATIC DISTURBANCE DATA -
LEFT-HAND ROTOR BLADE DATA

DATE	RUN NO.	PITCH MOMENT		YAW MOMENT		ROLL MOMENT		COMMENTS
		FREQ.	DAMPING	FREQ.	DAMPING	FREQ.	DAMPING	
8/27	2	22.9	0.6	7.03	1.15	5.1	0.61	Hover Mode Fairings Re- moved (30 Lbs)
8/29	14	23.6	0.89	7.9	1.11	6.2	0.53	Left-Hand Rotor and Motor Missing Baffle on Right Wing
9/2	56	16.3	1.08	7.5	1.22	5.09	1.22	Tail off in = 70°, Both Rotors On
9/3	76	19.8	0.82	7.3	0.83	5.1	1.25	Complete Model Cruise Mode
9/4	89	21.4	1.07	7.5	1.42	5.5	1.01	No Rotors Cruise Mode

NOTES: 1. Frequencies in Hertz
2. Damping in % Critical
3. Disturbance Applied to Model

TABLE B-3 FUSELAGE BALANCE MOMENT STATIC DISTURBANCE DATA

DATE	RUN NO.	NORMAL FORCE		AXIAL FORCE		SIDE FORCE		COMMENTS
		FREQ.	DAMPING	FREQ.	DAMPING	FREQ.	DAMPING	
8/27	2	103	1.36	110.0	1.17	94.5	1.153	Hover Mode Fairings Re- moved (30 Lbs)
8/29	14	99	1.44	89.5	0.585	93.5	1.66	Left-Hand Rotor and Motor Missing Baffle on Right Wing
9/2	56	100	1.51	111.0	0.615	91.2	0.97	Tail Off $i_N = 70^\circ$
9/3	76	101	1.58	89.0	0.71	89.0	1.26	Cruise Mode
9/4	89	111	1.6	95.3	1.19	85.5	0.985	No Rotors Cruise Mode

NOTES: 1. Frequencies in Hertz
2. Damping % Critical
3. Disturbance Applied to Model

TABLE B-4 FUSELAGE BALANCE FORCE STATIC DISTURBANCE DATA

DATE	RUN NO.	PITCH MOMENT		YAW MOMENT		ROLL MOMENT		COMMENTS
		FREQ.	DAMPING	FREQ.	DAMPING	FREQ.	DAMPING	
	2	4.11	1.6	4.23	1.41	4.25	1.461	Same as Table A2-3
8/29	14	4.3	3.2	4.09	-	2.28	2.4	

NOTES: 1. Frequencies are in Hertz

2. Damping & Critical

3. Sting Disturbance Test

DATE	RUN NO.	NORMAL FORCE		AXIAL FORCE		SIDE FORCE		COMMENTS
		FREQ.	DAMPING	FREQ.	DAMPING	FREQ.	DAMPING	
	2	4.2	2.27	-	-	2.15	2.5	Same as Table A2-3
8/29	14	4.13	2.72	-	-	2.33	1.71	

NOTES: 1. Frequencies in Hertz
2. Damping % Critical
3. Sting Disturbance Test

TABLE B-6 FUSELAGE BALANCE STATIC DISTURBANCE DATA

RIGHT-HAND NACELLE BALANCE NATURAL FREQUENCIES

STATIC DISTURBANCE DATA

Normal Force	12.92 Hertz
Sideforce	18.7
Axial Force	- Not Recorded
Yaw Moment	18.1
Pitch Moment	11.8
Roll Moment	19.6

Rotor Blades ON

TABLE B-7

NACELLE BALANCE STATIC DISTURBANCE DATA

APPENDIX C

Deflection Test

The rotor hub calibration fixtures were used to apply loads to the rotor hub in the normal force, side force, pitch moment and yawing moment. The resulting deflections of the sting, model fuselage, wing and nacelle, defined in Figures C-1 and C-2, are tabulated in Tables C-1 to C-5. These data provide a means of establishing the effect of model deflection on the stability and performance data measured and these effects are discussed in Section 5.1.5.

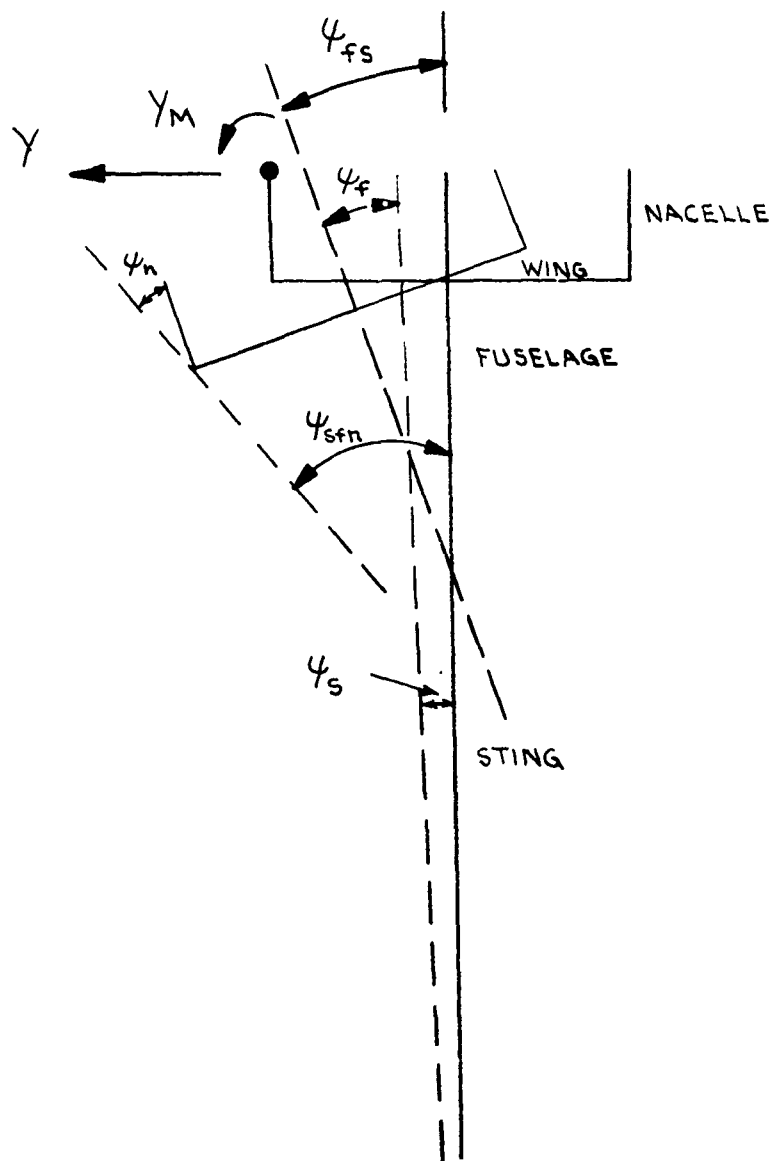


FIGURE C-1

DEFINITION OF YAW DEFLECTION ANGLES DUE TO SIDEFORCE AND YAWING MOMENT LOADINGS

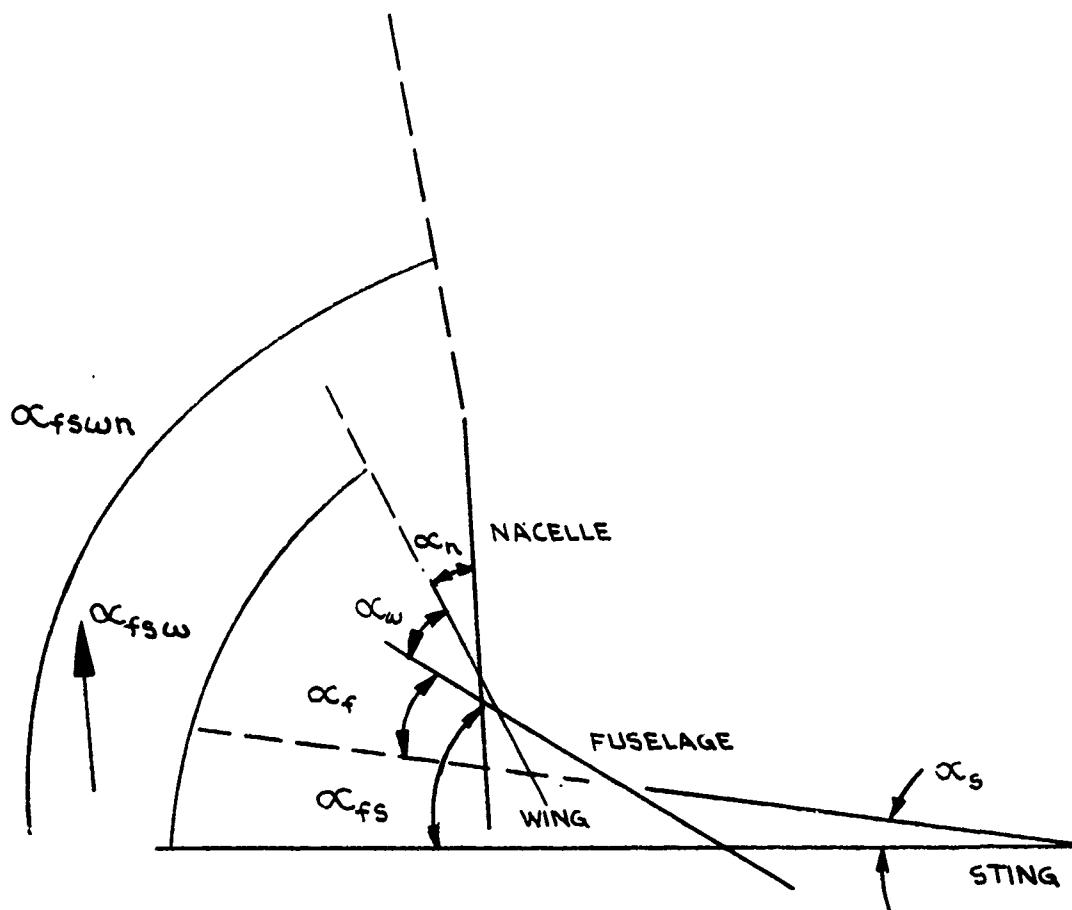


FIGURE C-2

DEFINITION OF PITCH DEFLECTION ANGLES FOR
NORMAL FORCE AND PITCH MOMENT LOADINGS

Sting Deflection ψ_s	= 0.0004125°/lb Y
---------------------------	-------------------

Sting and Fuse Deflection ψ_{sf}	= 0.00074599°/lb Y
---------------------------------------	--------------------

Fuselage Deflection ψ_f	= 0.0003335 °/lb Y
------------------------------	--------------------

Nacelle, Sting and Fuse ψ_{sfn}	= 0.002055°/lb Y
--------------------------------------	------------------

Rotorshaft Deflection ψ_n	= 0.001309°/lb Y
--------------------------------	------------------

Fuselage-Balance Yaw Stiffness	= 2.06 x 10 ³ ft-lbs/°
--------------------------------	-----------------------------------

Nacelle-Balance Yaw Stiffness	= 0.523 x 10 ³ ft-lbs/°
-------------------------------	------------------------------------

TABLE C-1

YAW DEFLECTIONS DUE TO SIDEFORCE APPLIED
AT ROTOR HUB

Sting Deflection ψ_s	=	0.0000752°/ft lb
Sting and Fuse Deflection ψ_s	=	-0.000425°/ft lb
Fuselage ψ_f	=	-0.0005002°/ft lb
Nacelle, Sting and Fuse ψ_{sfn}	=	.001345°/ft lb
Rotorshaft Deflection ψ_n	=	0.00177°/ft lb

Fuse Balance Yaw Stiffness	=	2.0 x 10 ³ ft-lbs/°
Nacelle Balance Stiffness	=	0.562 x 10 ³ ft-lbs/°

TABLE C-2

YAW DEFLECTIONS DUE TO PURE YAW MOMENT
APPLIED AT THE ROTOR HUB

$$\alpha_n = .001038 \text{ }^\circ/\text{lb}$$

$$\alpha_w = .001015 \text{ }^\circ/\text{lb}$$

$$\alpha_f = .000665 \text{ }^\circ/\text{lb}$$

$$\alpha_{wfs} = .00168 \text{ }^\circ/\text{lb}$$

$$\alpha_{sf} = .000665 \text{ }^\circ/\text{lb}$$

$$\alpha_{nfs} = .002718 \text{ }^\circ/\text{lb}$$

$$\text{Fuselage Balance Pitch Stiffness} = 2.21 \times 10^3 \text{ ft-lbs/}^\circ$$

$$\text{Nacelle Balance Pitch Stiffness} = 0.66 \times 10^3 \text{ ft-lbs/}^\circ$$

TABLE C-3

PITCH DEFLECTIONS DUE TO NORMAL FORCE
LOADING AT THE ROTOR HUB

$$\alpha_f = .000417 \text{ }^\circ/\text{ft lb}$$

$$\alpha_{fs} = .000417 \text{ }^\circ/\text{ft lb}$$

$$\alpha_{wfs} = .000734 \text{ }^\circ/\text{ft lb}$$

$$\alpha_w = .000317 \text{ }^\circ/\text{ft lb}$$

$$\alpha_{nfs} = .00225 \text{ }^\circ/\text{ft lb}$$

$$\alpha_n = .001516 \text{ }^\circ/\text{ft lb}$$

$$\text{Fuse Balance Pitch Stiffness} = 2.4 \times 10^3 \text{ ft-lbs/}^\circ$$

$$\text{Nacelle Balance Pitch Stiffness} = 0.66 \times 10^3 \text{ ft-lbs/}^\circ$$

$$\text{Wing Torsional Stiffness} = 3.13 \times 10^3 \text{ ft-lbs/}^\circ$$

TABLE C-4

PITCH DEFLECTIONS DUE TO A PURE PITCHING MOMENT APPLIED AT ROTOR HUB

Roll Deflection = 0.0701 °/ft lb

Balance Stiffness = 0.0143×10^3 ft-lbs/°

TABLE C-5

ROLL DEFLECTIONS

APPENDIX D

Test Run Log

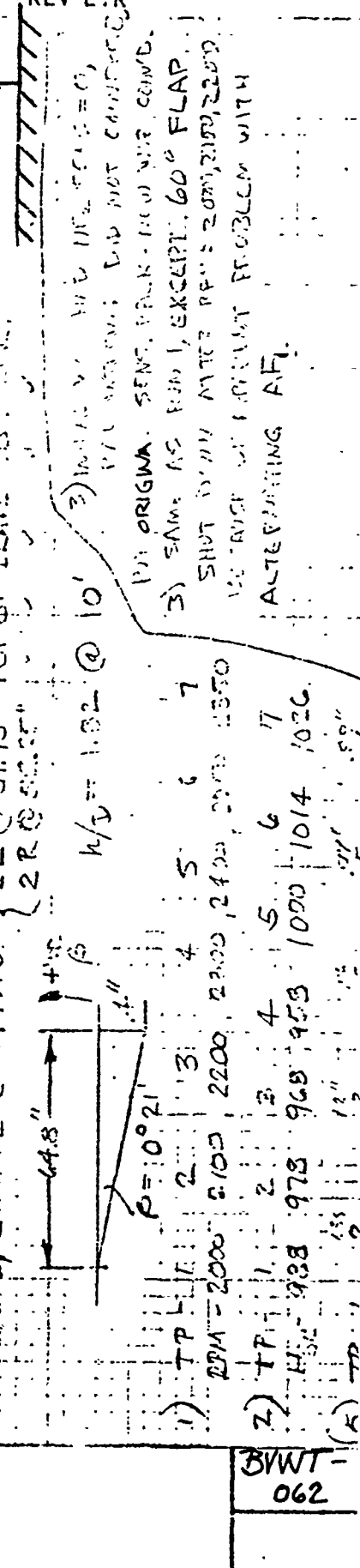
Enclosed is a copy of the on line test run log that describes the model configuration for each test run and any additional notes required to define the test conditions.

VR-044Q BVWT-062 CONFIGURATION	DP/ CBP	TYPE OF RUN	WT. TARE RUN	PT PSF	RPM	α_F	ρ_F	J/ μ	i_2/i_3	θ_{75}	δ_2/δ_3	δ_F/δ_H	δ_{sum}/H_1	DATE / TIME
1 B, W, T, R ₂ , R ₃	7/7	✓	✓	0	2400	0	0	7/2	7/10	10	0/0	0/0	100%	27 Nov 59 0624
2 ✓	7/7	✓	✓	✓	2400	✓	✓	✓	✓	✓	✓	✓	✓	27 Nov 59 0625
3 ✓	7/7	✓	✓	✓	2400	✓	✓	✓	✓	✓	✓	✓	✓	27 Nov 59 0626
4 ✓	7/7	✓	✓	✓	2400	✓	✓	✓	✓	✓	✓	✓	✓	27 Nov 59 0627
5 ✓	7/7	✓	✓	✓	2400	✓	✓	✓	✓	✓	✓	✓	✓	27 Nov 59 0628
6														
7														
8														
9														
10														

3 - FUSELAGE
W - WING
T - T-tail

R₂ - L.H. Rotor (1/2 in)
R₃ - R.H. Rotor (1/2 in)
H₁ - DIM. 10 FT. FROM TAIL OF EXISTING (51.96)
H₂ = 10' 7.35' 5.23' 3.55' 2.15' W/ SURFACE @ 977.96 OR -14.00
H₃ = 10' 7.35' 5.23' 3.55' 2.15' W/ SURFACE @ 977.96 OR -14.00
H₄ = 10' 7.35' 5.23' 3.55' 2.15' W/ SURFACE @ 977.96 OR -14.00
H₅ = 10' 7.35' 5.23' 3.55' 2.15' W/ SURFACE @ 977.96 OR -14.00
H/D = 1.32 1.34 1.35 1.36 1.37

1) MODEL 0° 10' NOSE UP W/ GILMORE AT -13.83, USED -14.05 DE-RENS α
W/ GILMORE @ 977.96 { 2L @ 51.75" TOP OF ELASE TO TAIL
2R @ 51.75" TOP OF ELASE TO TAIL



TEST RUN LOG
VR-044Q
RUNS 1-5

BVWT
062

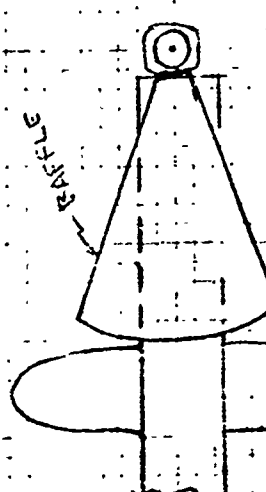
NOTE: UPPER SURFACE OF
BAFFLE 4-5 IN. FROM BLADE TIP

DATE / TIME	S	EF	0 ₂	0 ₇₅	0 ₇	βF	αF	RPM	FT	WT. TARE RUN	TYPE OF RUN	CDP	CONFIGURATION	RUN NO.
28 AUG 0413	1.1	4.1	0.0	10	1.90	0	0	VAR	0	6	✓	2.44	B, W, T, R ₂ R ₃	6
0405	1.1	✓	✓	✓	✓	✓	✓	1200	✓	✓	✓	6.20	✓	7
0414	1.1	✓	✓	✓	✓	✓	✓	1200	✓	✓	✓	7.57	B, W, T, R ₃ - R.H. BARRON	8
0416	1.1	✓	✓	✓	✓	✓	✓	1200	✓	✓	✓	6.63	✓	9
0418	1.1	✓	✓	✓	✓	✓	✓	1200	✓	✓	✓	6.67	B, W, T, R ₂ R ₃ - BOTH ROTORS	10
0419	1.1	✓	✓	✓	✓	✓	✓	1200	✓	✓	✓	6.63	B, W, T, R ₃ + KEV BATTLE (REV)	11

12	13	14	15	16	17	18	19
2600	2500	2400	2300	2200	2100	2000	1900
2600	2500	2400	2300	2200	2100	2000	1900

U.H. JACKET
LUBRICATION TEMP. AMP SURVEY ON L.H. MOTOR ABOUT 2000 RPM
COMING DOWN FROM 2600 ON 2100

8 RPM = 90/70



1) L.H. MOTOR HUB OFF, ONE BAFFLE ON R.H. WINGS, GILLMORE HT 989.2 - TOOK ONE DP - NO DATA
SHUT DOWN TO FIX RPM PROBLEM.

PREP. CHK. J.E. LaCase 8 Sept. 70 APPR. REVISED DATE

TEST RUN LOG
VK-044Q
RUNS 6-11

TEST RUN LOG
VIR-044Q
RUNS 12-17

NOT REPRODUCIBLE

4/22/2016 12:10:00 PM

BANS TLT ON RM BLADE, PACELE, MAIN BRN. POST RUN 14-

(51) $\Sigma_{\text{syn}} = 90/70$

BVWT-062

0098-2600
Small Group Unit

THE **BOEING** COMPANYNUMBER
REV LTR

PREP.	CHK.	APPR.	REVISED	DATE	RUN NO.	CONFIGURATION	DP/CDP	TYPE OF RUN	WT. TARE RUN	9T PSF	RPM	α_F	β_F	J/μ	L_2/L_3	θ_7	γ_2/γ_3	δ_F/δ_H	δ_{umb}/H_1	DATE / TIME
					18	B, W, T, R, R ₂	18/213	HOVER	6	0	VARY	0	0	0	0	0	10	0	0	31 AUG 0520
					19	✓	19/221	✓	✓	✓	✓	✓	✓	✓	✓	✓	✓	✓	✓	0546
					20	✓	20/230	✓	✓	✓	✓	✓	✓	✓	✓	✓	✓	✓	✓	0655
					21	✓	21/237	✓	✓	✓	✓	✓	✓	✓	✓	✓	✓	✓	✓	0700
					22	✓	22/243	✓	✓	✓	✓	✓	✓	✓	✓	✓	✓	✓	✓	0710
					23	✓	23/248	✓	✓	✓	VARY	✓	✓	✓	✓	✓	✓	✓	✓	0800
					24	✓	24/254	✓	✓	✓	✓	✓	✓	✓	✓	✓	✓	✓	✓	0814
					25	✓ + 1/REV Baffle (LH)	25/265	✓	✓	✓	VARY	✓	✓	✓	✓	✓	✓	✓	✓	0857
					26	✓ + 2/REV Baffle (LH)	26/276	✓	✓	✓	VARY +3	✓	✓	✓	✓	✓	✓	✓	✓	1016
					27	✓ + 3/REV Baffle (LH)	27/286	✓	✓	✓	✓	✓	✓	✓	✓	✓	✓	✓	✓	1108
					18	1ST 2 DP - LH ONLY TO CHK OPERATING	18/213	✓	✓	✓	✓	✓	✓	✓	✓	✓	✓	✓	✓	1208
					19	2ND 2 DP - LH ONLY TO CHK OPERATING	19/221	✓	✓	✓	✓	✓	✓	✓	✓	✓	✓	✓	✓	1312
					20	3RD 2 DP - LH ONLY TO CHK OPERATING	20/230	✓	✓	✓	✓	✓	✓	✓	✓	✓	✓	✓	✓	1312
					21	4TH 2 DP - LH ONLY TO CHK OPERATING	21/237	✓	✓	✓	✓	✓	✓	✓	✓	✓	✓	✓	✓	1312
					22	5TH 2 DP - LH ONLY TO CHK OPERATING	22/243	✓	✓	✓	✓	✓	✓	✓	✓	✓	✓	✓	✓	1312
					23	6TH 2 DP - LH ONLY TO CHK OPERATING	23/248	✓	✓	✓	✓	✓	✓	✓	✓	✓	✓	✓	✓	1312
					24	7TH 2 DP - LH ONLY TO CHK OPERATING	24/254	✓	✓	✓	✓	✓	✓	✓	✓	✓	✓	✓	✓	1312
					25	8TH 2 DP - LH ONLY TO CHK OPERATING	25/265	✓	✓	✓	✓	✓	✓	✓	✓	✓	✓	✓	✓	1312
					26	9TH 2 DP - LH ONLY TO CHK OPERATING	26/276	✓	✓	✓	✓	✓	✓	✓	✓	✓	✓	✓	✓	1312
					27	10TH 2 DP - LH ONLY TO CHK OPERATING	27/286	✓	✓	✓	✓	✓	✓	✓	✓	✓	✓	✓	✓	1312

NOTE: L.H. E.P. NG FOR RYNG 17

19) DP 2 3 4 5 6 7 8 9 10 11 12 13 14 15 16 17

20) DP 2 3 4 5 6 7 8 9 10 11 12 13 14 15 16 17

21) DP 2 3 4 5 6 7 8 9 10 11 12 13 14 15 16 17

22) DP 2 3 4 5 6 7 8 9 10 11 12 13 14 15 16 17

23) DP 2 3 4 5 6 7 8 9 10 11 12 13 14 15 16 17

24) DP 2 3 4 5 6 7 8 9 10 11 12 13 14 15 16 17

25) DP 2 3 4 5 6 7 8 9 10 11 12 13 14 15 16 17

26) DP 2 3 4 5 6 7 8 9 10 11 12 13 14 15 16 17

27) DP 2 3 4 5 6 7 8 9 10 11 12 13 14 15 16 17

AT END OF RUN, BLADE WIRING OBSERVED TO BE COMING LOOSE FROM BLADE. TESTING STOPPED TO BOND WIRING BACK TO BLADE.

* RUNS 25-27 RIGHT HAND BLADES WERE ON THE MODEL BUT NOT RUNNING. GILLMORE HT. 973.50

PREP.	CHK.	APPR.	REVISED	DATE	RUN NO.	CONFIGURATION	DP/CDG	TYPE OF RUN	WT. TARE RUN	QT RF	RPM	ΔF	βF	γ/μ	i_2/i_3	θ_{YS}	k_2/i_3	δF	Sum	DATE / TIME
					28	B, W, T, R ₂ R ₃ + KEY BATTLE	6/25	H.A.	6	0	VARY	+3	0	-	90/100	10	0%	0/10	-1.1	1522 1504
					29	B, W, T, R ₂ R ₃ + TUFT RIG	6/25	H.A.	✓	✓	2500	VAR	✓	✓	✓	✓	✓	10/0	✓	1504 0103
					30	✓ +	6/25	✓	✓	✓	✓	0	✓	✓	✓	✓	✓	✓	✓	0103 0112
					31	✓ +	6/25	✓	✓	✓	VERY	✓	✓	✓	✓	✓	✓	✓	✓	0112 0121
					32	B, W, T, R ₂ R ₃	6/25	✓	✓	✓	✓	✓	✓	✓	✓	✓	✓	✓	✓	0121 0130
					33	✓	6/25	✓	✓	✓	✓	✓	✓	✓	✓	✓	✓	✓	✓	0130 0140
					34	B, W, T, R ₂ R ₃ - $\phi = 20^\circ$	6/25	✓	✓	✓	2500	VAR	✓	✓	✓	✓	✓	✓	✓	0140 0150
					35	B, W, R ₂ R ₃ - TAIL OFF	6/25	✓	35	✓	✓	✓	✓	✓	✓	✓	✓	✓	✓	0150 0200
					36	✓ - RAIL = 0°	6/25	✓	✓	✓	✓	✓	✓	✓	✓	✓	✓	✓	✓	0200 0210
					37	B, W, T, R ₂ R ₃	6/25	✓	6	✓	✓	0	✓	✓	✓	✓	✓	✓	✓	0210 0220

28) RH BLADES ON MODEL BUT NOT RUNNING. LOST WOODEN WEDGE SUPPORTING. BATTLE PARD ON WING @ 2400. SHUT DOWN. END OF RUN.
GILLMORE HIT. 27.35

29) ORANGE TUFTS ABOVE WING, WHITE TUFTS BELOW & FWD, ORANGE TUFTS BELOW & AFT

NOT REPRODUCIBLE

30) LTP 1 2 3 / 4, 5, 6, 7, 8, 9, 10
H 215 3.55 5.23 / 6.23 7.35 8.45 9.55 10.10
ADJ. CAMBER & LIGHTS

31) RPM 2100 2200 2300 2400 2500 2600

32) RPM 2000 → 2600; 2100 RH / 2600 → 2600; 2100 L.H. / 2600 → 2100 MATCHED TH

33) RPM AS RUN 30

34) MODEL ROLLED - 2.167° $\alpha F = 0, +2, +4, -2, -4$
35) A.S. 134- $\alpha F = 0, +2, +4, -2, -4, 0$

GENERAL NOTE: * J1.53 MISUSEFUL RM, INSTEAD OF YM.

TEST RUN LOG
VR-044Q
RUNS 28-37

BVWT-062

TEST RUN LOG
VR-044Q
RUNS 38-46

BVWT-062

NOT REPRODUCIBLE

RUN NO.	CONFIGURATION	DP/CTP	TYPE OF RUN	WT. TARE RUN	GT. TARE	RPM	α_F	β_F	J/ μ	L_2/L_1	θ_{75}	δ_2/δ_1	δ_F/L_1	SUNY/ H_1	DATE / TIME
47	B ₁ W ₁ T ₁ R ₂ R ₃	11/51A	TP15	6	VR1	VR1	0	0	VR1	17/15	1.1	0/0	68/0	25/15	04:20
48	✓	9/51A	V	✓	VR1	VR1	✓	✓	VR1	✓	✓	✓	✓	✓	2:57:17
49	✓	6/52F	✓	✓	VR1	VR1	✓	✓	VR1	✓	✓	✓	✓	✓	05:45
50	✓	7/52F	✓	✓	VR1	VR1	✓	✓	VR1	✓	✓	✓	✓	✓	05:31
51	✓	11/51A	✓	51	✓	VR1	✓	0	VR1	✓	✓	✓	✓	✓	05:31
52	✓	7/51A	✓	✓	2.1/1	✓	✓	✓	✓	✓	✓	✓	✓	✓	05:42
53	✓	8/52F	✓	✓	✓	✓	0	✓	VR1	✓	✓	✓	✓	✓	06:15
54	✓	5/52F	✓	✓	✓	✓	+6	✓	✓	✓	✓	✓	✓	✓	07:04
55	✓	5/52F	✓	✓	✓	VR1	0	0	✓	✓	✓	✓	✓	✓	07:17
56	B ₁ W ₁ R ₂ R ₃ - T ₁ 11.05F	6/51A	✓	56	✓	VR1	0	VR1	✓	✓	✓	✓	✓	✓	08:16

NOT REPRODUCIBLE															
47)	g - 0 → 60; 45														
48)	TP	1	2	3	4	5	6	7	8						
49)	B	0	-5	0	+5	10	15	12.5	7.5						
49)	TP	1	2	3	4	5	6								
50)	H ₁ W02	2.15	355	5.23	7.55	10.00									
50)	TP	1	2	3	4	5	6	7	8	9					
51)	B	0	-5	0	+5	+7.5	10.0	12.5	15.0	W02					
51)	TP	1	2	3	4	5	6	7	8	9	11				
52)	α _F W02	0	-15	0	-15	-10	-5	0	5	10	12.5				
52)	TP	1	2	3	4	5	6	7							
52)	α _F	0	-15	-10	-5	+5	+10	12.5							
53)	TP	1	2	3	4	5	6	7	8						
53)	B	-	0	-5	+5	7.5	10	12.5	15						
54)	TP	1	2	3	4	5									
54)	B	0	-5	+5	7.5	10									
X _{max} = +9° @ δ _{max} = 60°															

TEST RUN LOG

VR-044Q

RUNS 47-56

BWV

062

FORM 48510 (3/70)

PREP.	CHK.	APPR.	RUN NO.	CONFIGURATION	DP / COR	TYPE OF RUN	WT. TARE RUN	QPM	α	β_c	γ / μ	δ_1 / δ_2	$\theta_{1.5} / \theta_{1.2}$	δ_1 / δ_2	SUM	DATE / TIME
			67	B, W, T, R ₂ R ₃ (TAILON)	1/68	α CONT	—	0	1300	0	—	—	18"	4/40	4/11	3 SEPT 0325
			68	✓	1/68	α CONT	—	✓	0	✓	—	✓	✓	✓	✓	✓
			69	✓	5/104	1200	01	VACY	0	✓	—	5/15	✓	✓	✓	✓
			70	✓	1/68	✓	✓	37	VACY	✓	—	✓	✓	✓	✓	✓
			71	✓	8/681	✓	✓	20	1800	0	—	✓	✓	✓	✓	✓
			72	✓	9/681	✓	✓	✓	VACY	0	—	✓	✓	✓	✓	✓
			73	B, W, R ₂ R ₃ - (TAIL OFF)	1/68	✓	5)	✓	0	VACY	—	✓	✓	✓	✓	✓
			74	✓	1/68	✓	✓	✓	VACY	0	—	✓	✓	✓	✓	✓
			75	B, W, T, R ₂ R ₃ - (TAILON)	3/115	✓	6-1	VACY	2200	✓	—	9/0	✓	✓	✓	✓
			76	✓	3/115	✓	6	25	VACY	✓	—	✓	✓	✓	✓	✓

NOT REPRODUCIBLE

67 } DEC 21 11 00 AM '4

	TP	1	2	3	4	5	6	7	8	9	10	11	12	13	14	15	16	17	18	19	20
70) A)	TP	1	2	3	4	5	6	7	8	9	10	11	12	13	14	15	16	17	18	19	20
71) B)	TP	1	2	3	4	5	6	7	8	9	10	11	12	13	14	15	16	17	18	19	20
72) C)	TP	1	2	3	4	5	6	7	8	9	10	11	12	13	14	15	16	17	18	19	20
73) D)	TP	1	2	3	4	5	6	7	8	9	10	11	12	13	14	15	16	17	18	19	20
74) E)	TP	1	2	3	4	5	6	7	8	9	10	11	12	13	14	15	16	17	18	19	20
75) F)	TP	1	2	3	4	5	6	7	8	9	10	11	12	13	14	15	16	17	18	19	20
76) G)	TP	1	2	3	4	5	6	7	8	9	10	11	12	13	14	15	16	17	18	19	20

TEST RUN LOG
VR-044Q
RUNS 67-76

3VWT-
062

PREP.	CHK.	APPR.	REVISED	DATE	TEST RUN LOG	BRWT -
	J.C. LaCasse		8 Sept. 70		VR-044Q	062
					RUNS 77-86	

RUN NO.	CONFIGURATION	DP/COI	TYPE OF RUN	WT. TAKE RUN	Q.P.F.	PRM	α_F	β_F	J/M	$\frac{R_2}{R_1}$	$\frac{R_2}{R_1}$	$\frac{\delta_F}{\gamma_F}$	SURE	DATE / TIME
77	B, W, T, R ₂ , R ₃ - (TAIL ON)	18/18	CRUISE	77	55	1980	1184	0	0.00	0.00	0.00	0.00	✓	2.00.27.27
78	✓ - - ✓	20/18	✓	✓	✓	✓	✓	✓	✓	✓	✓	✓	✓	2.00.27.27
79	✓ - - ✓	18/18	✓	✓	✓	✓	✓	✓	✓	✓	✓	✓	✓	2.00.27.27
80	✓ - - ✓	8/18	✓	✓	50	✓	✓	✓	✓	✓	✓	✓	✓	4.51.17.01.17
81	✓ - - ✓	7/18	✓	✓	✓	✓	0	VAR4	✓	✓	✓	✓	✓	0.11.20.01.30
82	B, W, T, R ₂ (R ₃ HUB ONLY) - ✓	7/18	✓	✓	✓	2030	✓	✓	✓	✓	✓	✓	✓	0.13.20.01.30
83	✓ - - ✓	1/18	OC COUNT	✓	✓	✓	12°	0	✓	✓	✓	✓	✓	0.00.17.01.17
84	✓ - - ✓	1/18	✓	✓	✓	✓	14°	0	✓	✓	✓	✓	✓	0.03.11.01.17
85	B, W, T, R ₂ (R ₃ HUB ONLY) - TAIL OFF - ✓	8/18	✓	25	✓	✓	VAR4	✓	✓	✓	✓	✓	✓	0.04.17.01.17
86	✓ - - ✓	8/18	✓	✓	✓	✓	0	VAR4	✓	✓	✓	✓	✓	0.04.17.01.17

77) TP 1 2 3 4 5 6 7 8 9 10 11 12 13 14 15 16 17 18 19 20 21 22 23 24 25 26 27 28 29 30 31 32 33 34 35 36 37 38 39 40 41 42 43 44 45 46 47 48 49 50 51 52 53 54 55 56 57 58 59 60 61 62 63 64 65 66 67 68 69 70 71 72 73 74 75 76 77 78 79 80 81 82 83 84 85 86 87 88 89 90 91 92 93 94 95 96 97 98 99 100

78) TP 1 2 3 4 5 6 7 8 9 10 11 12 13 14 15 16 17 18 19 20 21 22 23 24 25 26 27 28 29 30 31 32 33 34 35 36 37 38 39 40 41 42 43 44 45 46 47 48 49 50 51 52 53 54 55 56 57 58 59 60 61 62 63 64 65 66 67 68 69 70 71 72 73 74 75 76 77 78 79 80 81 82 83 84 85 86 87 88 89 90 91 92 93 94 95 96 97 98 99 100

79) TP 1 2 3 4 5 6 7 8 9 10 11 12 13 14 15 16 17 18 19 20 21 22 23 24 25 26 27 28 29 30 31 32 33 34 35 36 37 38 39 40 41 42 43 44 45 46 47 48 49 50 51 52 53 54 55 56 57 58 59 60 61 62 63 64 65 66 67 68 69 70 71 72 73 74 75 76 77 78 79 80 81 82 83 84 85 86 87 88 89 90 91 92 93 94 95 96 97 98 99 100

80) TP 1 2 3 4 5 6 7 8 9 10 11 12 13 14 15 16 17 18 19 20 21 22 23 24 25 26 27 28 29 30 31 32 33 34 35 36 37 38 39 40 41 42 43 44 45 46 47 48 49 50 51 52 53 54 55 56 57 58 59 60 61 62 63 64 65 66 67 68 69 70 71 72 73 74 75 76 77 78 79 80 81 82 83 84 85 86 87 88 89 90 91 92 93 94 95 96 97 98 99 100

81) TP 1 2 3 4 5 6 7 8 9 10 11 12 13 14 15 16 17 18 19 20 21 22 23 24 25 26 27 28 29 30 31 32 33 34 35 36 37 38 39 40 41 42 43 44 45 46 47 48 49 50 51 52 53 54 55 56 57 58 59 60 61 62 63 64 65 66 67 68 69 70 71 72 73 74 75 76 77 78 79 80 81 82 83 84 85 86 87 88 89 90 91 92 93 94 95 96 97 98 99 100

82) TP 1 2 3 4 5 6 7 8 9 10 11 12 13 14 15 16 17 18 19 20 21 22 23 24 25 26 27 28 29 30 31 32 33 34 35 36 37 38 39 40 41 42 43 44 45 46 47 48 49 50 51 52 53 54 55 56 57 58 59 60 61 62 63 64 65 66 67 68 69 70 71 72 73 74 75 76 77 78 79 80 81 82 83 84 85 86 87 88 89 90 91 92 93 94 95 96 97 98 99 100

83) CEC DATA ONLY

84) CEC DATA ONLY

85) TP 1 2 3 4 5 6 7 8 9 10 11 12 13 14 15 16 17 18 19 20 21 22 23 24 25 26 27 28 29 30 31 32 33 34 35 36 37 38 39 40 41 42 43 44 45 46 47 48 49 50 51 52 53 54 55 56 57 58 59 60 61 62 63 64 65 66 67 68 69 70 71 72 73 74 75 76 77 78 79 80 81 82 83 84 85 86 87 88 89 90 91 92 93 94 95 96 97 98 99 100

86) TP 1 2 3 4 5 6 7 8 9 10 11 12 13 14 15 16 17 18 19 20 21 22 23 24 25 26 27 28 29 30 31 32 33 34 35 36 37 38 39 40 41 42 43 44 45 46 47 48 49 50 51 52 53 54 55 56 57 58 59 60 61 62 63 64 65 66 67 68 69 70 71 72 73 74 75 76 77 78 79 80 81 82 83 84 85 86 87 88 89 90 91 92 93 94 95 96 97 98 99 100

RUN NO.	CONFIGURATION	PP	TYPE OF RUN	WT. TARE RUN	WT. TARE RUN	RPM	RF	J/μ	W/L	Q ₁₅	Q ₂ /Q ₁	DATE / TIME
87	B ₁ W ₁ R ₂ (R ₃ HUB ONLY) - TAIL OFF	✓	✓	✓	✓	1916	0	✓	✓	✓	✓	45 FT 5000
88	B ₁ W ₁ T ₁ - HUBS ONLY	✓	✓	✓	✓	1916	0	✓	✓	✓	✓	45 FT 5000
89	B ₁ W ₁ T ₁ - HUBS ONLY	✓	✓	✓	✓	1916	0	✓	✓	✓	✓	45 FT 5000
90	B ₁ W ₁ T ₁ - HUBS ONLY	✓	✓	✓	✓	1916	0	✓	✓	✓	✓	45 FT 5000
91	B ₁ W ₁ T ₁ - HUBS ONLY	✓	✓	✓	✓	1916	0	✓	✓	✓	✓	45 FT 5000
92	B ₁ W ₁ T ₁ - HUBS ONLY	✓	✓	✓	✓	1916	0	✓	✓	✓	✓	45 FT 5000
93	B ₁ W ₁ T ₁ - HUBS ONLY	✓	✓	✓	✓	1916	0	✓	✓	✓	✓	45 FT 5000
94	B ₁ W ₁ T ₁ - HUBS ONLY - TAIL OFF	✓	✓	✓	✓	1916	0	✓	✓	✓	✓	45 FT 5000
95	B ₁ W ₁ T ₁ - HUBS ONLY	✓	✓	✓	✓	1916	0	✓	✓	✓	✓	45 FT 5000
96	B ₁ W ₁ T ₁ - HUBS ONLY	✓	✓	✓	✓	1916	0	✓	✓	✓	✓	45 FT 5000

87) TP	1	2	3	4	5	6	7	8	9	10	11	12	13	14	15	16	17	18	19	20	21
OC	W02	0	4	2	0	0	0	0	0	0	0	0	0	0	0	0	0	0	0	0	0
88) SMALL FL WTER ATTACH - COULD NOT GET HIGH ENOUGH - W/ JESU SINGING	TP	1	2	3	4	5	6	7	8	9	10	11	12	13	14	15	16	17	18	19	20
89) TP	1	2	3	4	5	6	7	8	9	10	11	12	13	14	15	16	17	18	19	20	21
90) TP	1	2	3	4	5	6	7	8	9	10	11	12	13	14	15	16	17	18	19	20	21
91) TP	1	2	3	4	5	6	7	8	9	10	11	12	13	14	15	16	17	18	19	20	21
92) TP	1	2	3	4	5	6	7	8	9	10	11	12	13	14	15	16	17	18	19	20	21
93) TP	1	2	3	4	5	6	7	8	9	10	11	12	13	14	15	16	17	18	19	20	21
94) TP	1	2	3	4	5	6	7	8	9	10	11	12	13	14	15	16	17	18	19	20	21
95) TP	1	2	3	4	5	6	7	8	9	10	11	12	13	14	15	16	17	18	19	20	21

TEST RUN LOG
VR-044 Q
RUNS 87-96

BVWT
062

PREP.	CHK.	APPR.	RUN NO.	CONFIGURATION	DR / CDP	TYPE OF RUN	WT. TARE RUN	9-T	RPM	α_F	β_F	γ / μ	δ / δ_3	δ_2 / δ_3	θ_{75}	DATE / TIME
			97	B, W, - HUBS ONLY - TAIL OFF	10/30	SCISE	94	55	—	VARY	0	—	—	—	—	4 SEP 2153
			98	✓ - ✓ - ✓	10/30	TRANS	98	20	—	✓	0	—	—	—	—	4 SEP 2306
			99	✓ - ✓ - ✓	8/54	✓	✓	✓	—	0	VARY	—	—	—	—	4 SEP 2316
			100	B, W, T, - HUBS ONLY	8/62	✓	100	✓	—	✓	✓	—	—	—	—	4 SEP 2323
			101	✓ - ✓ - ✓	10/30	✓	✓	✓	—	VARY	0	—	—	—	—	4 SEP 2340
			102	✓ - ✓ - ✓	10/30	✓	102	15.5	—	✓	0	—	—	—	—	4 SEP 2350
			103	✓ - ✓ - ✓	8/54	✓	✓	✓	—	0	VARY	—	—	—	—	4 SEP 2417
			104	✓ - ✓ - ✓	5/45	✓	✓	✓	—	0	0	—	—	—	—	4 SEP 0022
			105	✓ - ✓ - ✓	8/54	✓	✓	✓	—	✓	VARY	—	—	—	—	4 SEP 0033
			106	B, W, - HUBS ONLY - TAIL OFF	10/30	✓	106	✓	—	VARY	0	—	—	—	—	4 SEP 0106

97) $\alpha_F = -15 + 16, A 4^\circ$
 98) $\alpha_F = AS RUN 97$
 99) $\beta_F = -8 + 16, A 4^\circ$
 100) $\beta_F = AS RUN 97$
 101) $\alpha_F = AS RUN 97$
 102) $\alpha_F = AS RUN 97$
 103) $\beta_F = AS RUN 97$
 104) $H_1 = 10.735 5.23 3.55 2.15$
 105) $\beta_F = AS RUN 97$
 106) $\alpha_F = AS RUN 97$

TEST RUN LOG
 VR-044 G
 RUNS 97-106

BVWT-
 062

[illegible]